International VLBI Service for Geodesy and Astrometry

MEASURING THE FUTURE

Proceedings of the Fifth IVS General Meeting

Andrey Finkelstein and Dirk Behrend, Editors

Saint Petersburg
«Nauka»
2008

УДК 521
ББК 22.61
И32

«Измеряя будущее», Труды 5-ой Генеральной ассамблеи международной РСДБ-службы по геодезии и астрометрии, / под ред. А. Финкельштейна и Д. Беренда. — СПб.: Наука, 2008, 487 с.

ISBN 978-5-02-025332-2

В сборнике представлены материалы 5-ой Генеральной ассамблеи международной РСДБ-службы по геодезии и астрометрии, проходившей с 3 по 6 марта 2008 г. в Институте прикладной астрономии Российской академии наук в Санкт-Петербурге. На конференции обсуждался вклад радиоинтерферометрии со сверхдлинными базами в развитие глобальной наблюдательной системы. РСДБ позволяет проводить мониторинг полного набора параметров вращения Земли, состоящего из координат земного и небесного полюсов и поправки Всемирного времени UT1, что делает ее ключевой технологией для построения глобальных систем координат и наблюдения за их изменениями. Однако необходимый уровень точности и высокая стабильность на больших интервалах времени могут быть гарантированы только при своевременной модернизации РСДБ-систем.

Сборник рассчитан на специалистов в области радиоинтерферометрии, радиоастрономии, геодезии, астрометрии и наук о Земле.

«Measuring the Future», Proceedings of the Fifth IVS General Meeting, A. Finkelstein, D. Behrend (Eds.).

This volume contains the proceedings of the fifth General Meeting of the International VLBI Service for Geodesy and Astrometry (IVS) held in St. Petersburg, Russia, March 3-6, 2008. The fifth General Meeting was held at the Institute of Applied Astronomy of the Russian Academy of Sciences. The keynote of the 5th General Meeting was the vital contribution of VLBI to the future of global observing systems under the theme of "Measuring the Future". VLBI is a key technique for realizing the global reference frames and studying global change by monitoring the full set of Earth orientation parameters (polar motion, dUT1, celestial pole). Required accuracy levels and long-term stability can only be guaranteed with a rejuvenated VLBI system. The content of the meeting is of interest to the broad spectrum of IVS members as well as to the wider VLBI and Earth science community who have interests in the various applications and research fields of VLBI such as geodesy, astrometry, Earth sciences, and related fields.

ISBN 978-5-02-025332-2
© Институт прикладной астрономии РАН, 2008
© Издательство «Наука», 2008

Contents

Welcome Address of Professor Alexander Viktorov, the Minister of Science and Education of Saint Petersburg Government XIII

Welcome Address of Professor Andrey Finkelstein, the Director of the Institute of Applied Astronomy XIV

Welcome Address of Professor Harald Schuh, the IVS Chair XV

Part 1. VLBI — A Vital Player in Global Observing Systems 1

Harald Schuh, Dirk Behrend. **IVS Plans and Perspectives** 3

Daniela Thaller, Volker Tesmer, Rolf Dach, Manuela Krügel, Markus Rothacher, Peter Steigenberger. **Combining VLBI Intensive with GPS Rapid Solutions for Deriving a Stable UT Time Series** ... 8

Johannes Boehm, Paulo Jorge Mendes Cerveira, Sigrid Englich, Harald Schuh. **Atmosphere Angular Momentum Time Series for CONT05** 14

Paulo Jorge Mendes Cerveira, Sigrid Englich, Harald Schuh, Thomas Klügel, Aleksander Velikoseltsev, Ulrich Schreiber. **How Can the Wettzell "G" Ring Laser Improve VLBI Measurements of Subdiurnal Earth Rotation Variations?** 19

Géraldine Bourda, Patrick Charlot, Richard Porcas, Simon Garrington. **Multi-Step VLBI Observations of Weak Extragalactic Radio Sources to Align the ICRF and the Future GAIA Frame** 25

Igor Molotov, Maria Nechaeva, Igor Falkovich, Alexander Konovalenko, Vladimir Agapov, Gino Tuccari, Giuseppe Pupillo, Stelio Montebugnoli, Gennadiy Kharlamov, Lance Benner, Viacheslav Fateev, Yuriy Burtsev, Alexander Volvach, Xiang Liu, Vasiliy Oreshko, Ivars Shmelds, Pietro Bolli, Alexander Dementiev, Alexander Antipenko, Nikolay Dugin, Vladimir Jazykov, Dmitriy Bezrukov. **Astrometry of the Solar System Bodies with VLBI Radar** 30

Part 2. Network Stations, Operation Centers, Correlators 37

Andrey Finkelstein, Alexander Ipatov, Sergey Smolentsev. **The Network "Quasar": 2008–2011** *(invited)* 39

Kerry Kingham, David Hall. **Equipment Failures, Chronic Station Problems, and RFI: Their Effects on Geodetic VLBI Data** 47

Alessandra Bertarini, Walter Alef, Brian Corey, Axel Nothnagel, Craig Walker. **Effects on the Geodetic-VLBI Observables Due to Polarization Leakage in the Receivers** *(invited)* 53

Axel Nothnagel, Alessandra Bertarini, Christian Dulfer, Thomas Artz, Jan Wagner, Guifre Molera, Jouko Ritakari. **Comparisons of Correlations Using Disk-Transfer and e–VLBI-Transfer** 63

Shigeru Matsuzaka, Hiromi Shigematsu, Shinobu Kurihara, Morito Machida, Kensuke Kokado, Daisuke Tanimoto. **Ultra Rapid UT1 Experiment with e–VLBI** 68

Mikhail Kharinov, Andrey Mikhailov. **Single Dish Radiometric Observations of Geodetic Sources on Radio Telescopes of the QUASAR Network** 72

Dmitriy Ivanov, Aleksandr Vytnov. **Automatic System for Monitoring Hydrogen Masers in QUASAR VLBI Network** 77

Iskander Gayazov, Elena Skurikhina. **Local Ties between Co-located Space Geodetic Instruments at QUASAR Network Observatories** 82

Roberto Lanotte, Mauro Pirri, Giuseppe Bianco. **Matera Site Survey and VLBI Invariant Point Determination** 87

Susana Garcia-Espada, Rüdiger Haas, Francisco Colomer. **Space Geodesy at Yebes: Station Motion from VLBI and GPS** 93

Shigeru Matsuzaka, Kojin Wada, Etsuro Iwata, Hiromi Shigematsu, Shinobu Kurihara, Machida Morito, Kensuke Kokado, Daisuke Tanimoto, Kentaro Nozawa. **VLBI Activities of Tsukuba 32-m Station and Tsukuba Correlator** 98

Shigeru Matsuzaka, Kozin Wada, Etsurou Iwata, Hiromi Shigematsu, Shinobu Kurihara, Morito Machida, Kensuke Kokado, Daisuke Tanimoto. **The Past Decade of Tsukuba 32-m VLBI Station** 104

Hayo Hase, Reiner Dassing, Gerhard Kronschnabl, Wolfgang Schlüter, Walter Schwarz, Richard Kilger, Pierre Lauber, Alexander Neidhardt, Konrad Pausch, Willi Göldi. **Twin Telescope Wettzell — a VLBI2010 Radio Telescope Project** 109

Oleg Titov, Sergei Gulyaev, Jim Lovell, John Dickey. **Australian — New Zealand Geodetic VLBI Network Project** 114

Robert Campbell, Arpad Szomoru. **The EVN Mark IV Data Processor at JIVE and e–VLBI Developments in the EVN** 119

Igor Surkis, Vladimir Zimovsky, Alexey Melnikov, Violetta Shantyr, Artemiy Fateev, Andrey Bogdanov. **The IAA RAS 6-station VLBI Correlator** 124

Zheng Weimin, Luo Wuchao. **CVN Software Correlator Development and Applications in Chinese Lunar Exploration Mission** . 129

Part 3. VLBI Data Structure, Analysis Strategies and Software 137

Yuri Gnedin. **VLBI as a Tool to Connect Astrometry and Astrophysics** *(invited)* 139

John Gipson. **IVS Working Group 4 on VLBI Data Structures** . 143

Thomas Hobiger, Yasuhiro Koyama, Tetsuro Kondo. **MK3TOOLS — Seamless Interfaces for the Creation of VLBI Databases from Post-Correlation Output** 153

John Gipson, Daniel MacMillan, Leonid Petrov. **Improved Estimation in VLBI through Better Modeling and Analysis** 157

Volkmar Thorandt, Gerald Engelhardt, Dieter Ullrich. **Data Analysis at BKG in the Frame of IVS** 163

Ichikawa Ryuichi, Thomas Hobiger, Yasuhiro Koyama, Tetsuro Kondo. **Real-Time Ray-Tracing through Numerical Weather Models for Space Geodesy** 168

Kamil Teke, Robert Heinkelmann, Johannes Boehm, Harald Schuh. **VLBI Baseline Length Repeatability Tests of IVS-R1 and -R4 Session Types** 173

Zinovy Malkin. **Influence of Elevation-Dependent Weighting on Parameter Estimates: A Case of CONT05** 178

Zinovy Malkin, Oleg Titov. **Optical Characteristics of Astrometric Radio Sources** 183

Robert Heinkelmann, Johannes Böhm, Harald Schuh. **Effects of Surface Pressure and Temperature on the VLBI Reference Frames** 188

Jinling Li. **The Contribution of CVN to the CE-1 Mission** 193

Christian Bizouard, Oliver Becker. **WEB Tools and WEB Service of the IERS Earth Orientation Centre** 199

Sébastien Lambert, Florent Deleflie, Anne-Marie Gontier, Philippe Berio, Christopher Barache. **The Astronomical Virtual Observatory and Application to Earth's Sciences** 203

Part 4. Interpretation of VLBI Results in Geodesy, Astrometry and Geophysics 209

George Krasinsky. **Secular Decrease of the Earth's Ellipticity from the Analysis of VLBI Data of 1984–2006, and the Long-term Systematic Errors of the Precession-Nutation Models IAU 2000 and IAU 2006** *(invited)* 211

Nicole Capitaine, P.M. Mathews, Véronique Dehant, Patrick Wallace, Sébastien Lambert. **Comparisons of Precession-Nutation Models** *(invited)* 221

Vadim Gubanov. **The Phase Variations of Retrograde Free Core Nutation** 231

Sergey Pasynok. **Comparison of the Prediction Force of the Nutation Theories IAU2000 and ERA-2005** 236

Maria Kudryashova, Kristýna Šnajdrová, Robert Weber, Robert Heinkelmann, Harald Schuh. **Combination of Nutation Time Series Derived from VLBI and GNSS** 240

Séverine Rosat, Sébastien Lambert. **Earth's Interior from VLBI and Superconducting Gravimeter Data** 246

Chopo Ma, David Gordon, Daniel MacMillan, Leonid Petrov. **Some Challenges in Developing the Second ICRF** 251

Zinovy Malkin. **On Construction of ICRF-2** 256

David Gordon, Chopo Ma, John Gipson, Leonid Petrov, Daniel MacMillan. **On Selection of "Defining" Sources for ICRF-2** 261

Oleg Titov. **Systematic Effects in Apparent Proper Motion of Radio Sources** 265

Sergei Bolotin, Svitlana Lytvyn. **Comparison of Radio Source Positions from Individual Solutions** 270

Julia Sokolova, Zinovy Malkin. **Comparison and Combination of CRF Catalogs** 275

Sergey Kurdubov, Elena Skurikhina. **Source Selection for NNR Constraints from Source Position Time Series** 279

Christopher Jacobs, Ojars Sovers. **Extending the ICRF above S/X-band: X/Ka-band Global Astrometric Results** 284

Gabor Lanyi, David Boboltz, Patrick Charlot, Alan Fey, Ed Fomalont, Barry Geldzahler, David Gordon, Christopher Jacobs, Chopo Ma, Charles Naudet, Jonathan Romney, Ojars Sovers, Liwei Zhang. **Astrometry from VLBA Observations at 24 and 43 GHz** 289

Takaaki Jike, Seiji Manabe, Yoshiaki Tamura. **Result from K-band Geodetic VLBI Using VERA** 293

Jean Souchay, Alexandre Andrei, Christophe Barache, Sébastien Bouquillon, Anne-Marie Gontier, Sébastien Lambert, Christophe Le Poncin-Lafitte, François Taris, Elisa Felicitas Arias, Daniel Suchet, Mathieu Baudin. **The Large Quasar Astrometric Catalog and the Radio-Optical Link** 297

Natalia Miller, Zinovy Malkin. **Using Singular Spectrum Analysis for the Investigation of Troposphere Parameters** 302

Volker Tesmer, Johannes Boehm, Barbara Meisel, Markus Rothacher, Peter Steigenberger. **Atmospheric Loading Coefficients Determined from Homogeneously Reprocessed GPS and VLBI Height Time Series** 307

Sigrid Englich, Robert Heinkelmann, Harald Schuh. **Re-assessment of Ocean Tidal Terms in High-Frequency Earth Rotation Variations Observed by VLBI** 314

Andrey Finkelstein, Elena Skurikhina, Igor Surkis, Alexander Ipatov, Ismail Rahimov, Sergey Smolentsev. **QUASAR National Programs of EOP Determinations** 319

Thomas Artz, Sarah Böckmann, Axel Nothnagel, Volker Tesmer. **Comparison and Validation of VLBI Derived Polar Motion Estimates** 324

Sarah Böckmann, Axel Nothnagel. **The Variance Component Approach in the IVS Combination** 329

Robert Heinkelmann, Jeffrey Freymueller, Harald Schuh. **A Postseismic Relaxation Model for the 2002 Denali Earthquake from GPS Deformation Analysis Applied to VLBI Data** 335

Sébastien Lambert, Christophe Le Poncin-Lafitte. **Measuring the Relativistic Parameter γ Using the Current Geodetic VLBI Data Set** 341

Patrick Charlot. **Astrophysical Stability of Radio Sources and Implication for the Realization of the Next ICRF** *(invited)* 345

Part 5. Progress in Technology Development and the Next Generation VLBI System 359

Tobias Nilsson, Rüdiger Haas. **Modeling Tropospheric Delays with Atmospheric Turbulence Models** *(invited)* 361

Dean Chalmers, Gordon Lacy, Peter Dewdney, William Petrachenko, Gary Hovey. **Composite Applications for Radio Telescopes** 371

Gino Tuccari, Walter Alef, Alessandra Bertarini, Salvatore Buttaccio, Dave Graham, Gaetano Nicotra, Alan Roy, Michael Wunderlich. **DBBC Development Status** 376

Xiuzhong Zhang, Wenren Wei, Ying Xiang, Bin Li, Fengchun Shu, Renjie Zhu, Zhijun Xu, Zhong Chen, Weihua Wang, Weimin Zheng, Zhuhe Xue, Q. Ling, R. Zhao, Jingling Wang, Qingyuan Fan, Yusufu Aili, Huihua Li, Y. Wu, L. Chen, J. Luo. **Progress of Wideband VLBI Digital System Development at SHAO** 381

Dan Smythe. **Mark 5 Disk Drive Performance and Reliability** ... 386

Alan Whitney. **The Mark 5C VLBI Data System** 390

Chester Ruszczyk. **Mark 5C Software Development Program** 395

Ichikawa Ryuichi, Ishii Atsutoshi, Takiguchi Hiroshi, Kuboki Hiromitsu, Kimura Moritaka, Nakajima Junichi, Koyama Yasuhiro, Kondo Tetsuro, Machida Morito, Kurihara Shinobu, Kokado Kensuke, Matsuzaka Shigeru. **Development of a Compact VLBI System for Providing over 10-km Baseline Calibration** 400

Yasuhiro Koyama, Mamoru Sekido, Thomas Hobiger, Hiroshi Takiguchi, Tetsuro Kondo. **Developments of Automated Data Processing System for Ultra Rapid dUT1 e–VLBI Sessions** 405

Bill Petrachenko, Johannes Boehm, Daniel MacMillan, Arthur Niell, Andrea Pany, Anthony Searle, Joerg Wresnik. **VLBI2010 Antenna Slew Rate Study** 410

Daniel MacMillan. **Simulation Analysis of the Geodetic Performance of Networks of VLBI2010 Stations** 416

Joerg Wresnik, Johannes Boehm, Andrea Pany, Harald Schuh. **VLBI2010 Simulations at IGG Vienna** 421

Andrea Pany, Jörg Wresnik, Johannes Böhm, Harald Schuh. **Vienna VLBI2010 PPP Simulations** 427

Arnaud Collioud, Patrick Charlot. **Imaging Capabilities of the Next Generation VLBI System** 433

Vincenza Tornatore, Gino Tuccari, Erhu Wei. **First Considerations on the Feasibility of GNSS Observations by the VLBI Technique** . 439

Hideo Hanada, Takahiro Iwata, Nobuyuki Kawano, Noriyuki Namiki, Kazuyoshi Asari, Yoshiaki Ishihara, Toshiaki Ishikawa, Fuyuhiko Kikuchi, Qinghui Liu, Koji Matsumoto, Hirotomo Noda, Seiitsu Tsuruta, Sander Goossens, Natalia Petrova, Sho Sasaki, Kenzaburo Iwadate, Takaaki Jike, Osamu Kameya, Katsunori Shibata, Yoshiaki Tamura, Xiaoyu Hong, Jinsong Ping, Yusufu Aili, Simon Ellingsen, Wolfgang Schlüter. **VLBI Observation of SELENE (KAGUYA) by VERA and an International Network** 445

Vladimir Zharov, Leonid Matveenko. **VLBI and Precise Space Navigation** 450

Erhu Wei, Jingnan Liu, Vincenza Tornatore, Chuang Shi, Wei Yan. **On the Space VLBI Mathematical Model with Nutation Parameters** 455

Splinter Meeting Report 463

Axel Nothnagel. **Notes of the 9th IVS Analysis Workshop** 465

Program Committee

Behrend Dirk, Charlot Patrick, Finkelstein Andrey, Himwich Ed, Koyama Yasuhiro, Li Jinling, Malkin Zinovy, Nothnagel Axel, Petrachenko William, Schuh Harald, Titov Oleg, Whitney Alan

Local Organizing Committee

Finkelstein Andrey, Ipatov Alexander, Shuygina Nadia, Skurikhina Elena, Smolentsev Sergey

Welcome Addresses

Welcome Address of Professor Alexander Viktorov, the Minister of Science and Education of Saint Petersburg Government

Dear participants
of the 5th IVS General Meeting!

On behalf of Saint Petersburg Government and of the Saint Petersburg Governor Valentina Matvienko I am pleased to welcome you in our city. The fifth General Meeting is carried out by Institute of Applied Astronomy of Russian Academy of Sciences, one of the biggest astronomical institutes of Russia, which in this year celebrates its 20-year anniversary. IAA is the creator of "Quasar" VLBI Network, the largest Russian astronomical project of the last two to three decades. This system is used for solution of a lot of fundamental astrometrical and astrophysical problems and unites scientists from different academician and applied institutions of Russia. I am pleased that the "Quasar" system operates in close cooperation with the radio telescopes of the IVS VLBI Network.

The main goals of this meeting are to unite efforts of representatives of different institutions which are working under the umbrella of IVS, to sum up the basic scientific results of the VLBI community and to discuss new ideas and plans for the next two years. The IVS meeting is a good chance to strengthen world cooperation in astrometry, geodynamics, and space geodesy. For Russia this meeting plays an important role in the connection with the development of the technology of global navigation satellite systems and, first of all, the GLONASS system, the basic system of time-positioning and navigation service of Russia.

I would like to wish you a successful work and a pleasant stay in our remarkable city.

Thank you for your attention!

Welcome Address of Professor Andrey Finkelstein, the Director of the Institute of Applied Astronomy

Dear Minister Professor
Alexander Viktorov!
Dear IVS Chair Professor
Harald Schuh!
Dear colleagues and friends!

I am happy to welcome you in our institute. It is a great pleasure for me to host the fifth General Meeting of the IVS. I am very glad that the General Meeting coincides with the 20-year anniversary of the Institute of Applied Astronomy. Twenty years ago, twenty young scientists and engineers were united in a new institute designing and creating the Russian dedicated VLBI Network "Quasar". Now "Quasar" is fully operational and regularly participates in the IVS observational programs.

Our American colleagues from NASA played a very important role in the development of the "Quasar" Network. First of all, it concerned our first observatory "Svetloe", which was equipped with a Mark 3 system owned by our American friends. I have to express my sincere thanks. I am very glad to see some of them here—Chopo Ma, Brian Corey, Alan Whitney—and I am sad that some of them could not come.

In the next three–four years, we will have to develop "Quasar" Network in three main directions. We will unite the three "Quasar" observatories with the 70-meter radio telescope in the far east of Russia, will install there the new generation of satellite laser ranging systems and will connect all four observatories by optical fiber lines and equip theirs with corresponding facilities for the realization of e–VLBI mode. We count on the help of the IVS community and the exchange of ideas and advice is very important for us.

Local committee together with program committee intensively prepared the General Meeting and we will try to provide you the comfortable conditions for work and rest. In this connection I would like to introduce you to Dr. Nadia Shuygina. She is the head and heart of organization in our local committee, and she personally and her team will be able to answer any questions and solve any problems.

Now I want to give the floor to my boss in the IVS Directing Board Prof. Harald Schuh for his Welcome Address.

Thank you!

Welcome Address of Professor Harald Schuh, the IVS Chair

Honorable Authorities,
Distinguished Guests,
Dear Colleagues,
Dear IVS Family!

It is a great pleasure for me to welcome you in St. Petersburg to our 5th IVS General Meeting and thank you, Professor Viktorov and Professor Finkelstein, for the warm welcome words. I would like to express my gratitude that this General Meeting is held here in Russia, hosted by the Institute of Applied Astronomy. As the General Meeting is held every two years in the period January to March, the weather very much depends on the hemisphere where the conference takes place. Two years ago in Concepcion, Chile, it was summer and it was warm. This year we expect weather much colder than in Chile and maybe even with some snow or rain. But knowing the hospitality of the Russian hosts, I am sure our meeting will be very warm and pleasant again.

More than 120 participants from 18 countries and from 77 different institutions have registered for this conference and a high number of IVS components have sent their representatives. Considering that IVS has about 270 Associated Members, the large attendance in the General Meeting is highly encouraging and shows that the IVS is an active and vital international organization.

The General Meeting of the IVS is the important meeting for all the various components. During the conference experiences will be exchanged and new results will be reported. One of the goals of this meeting is to strengthen cooperation and to build bridges between the various components for a better understanding and for improvements. These goals were considered by the Program Committee.

I express my thanks to Dirk Behrend, Director of the IVS Coordinating Center, who coordinated the Program Committee, and also to its members: Patrick Charlot (France), Andrey Finkelstein (Russia), Ed Himwich (USA), Yasuhiro Koyama (Japan), Jinling Li (China), Zinovy Malkin (Russia), Axel Nothnagel (Germany), Bill Petrachenko (Canada), Oleg Titov (Australia), and Alan Whitney (USA), and Harald Schuh (Austria) was also in the Program Committee.

Just to give you an idea about the organization of the program: one week before the deadline for submission there were just 2 papers, two days before deadline we had 9, one day before deadline 17 papers and until the deadline (which was on December 21st) we have received 35 abstracts, only. Then the

deadline was extended till January and finally we ended up with 112 submissions. Thus, the Program Committee had to be very flexible and several presentations had to be changed from oral to poster to keep the limited time that we have.

Now, the Program Committee has set up a very interesting program for the next two and a half days. With the excursion on Thursday and the various splinter meetings on Monday, Wednesday, Friday, and Saturday we will have a tough week with a very tight schedule. I am looking forward to fruitful discussions and expect a very successful meeting.

For the organization of the conference we employed Web-based technology, which is a very efficient tool. In addition many things still had to be organized "manually". I would like to thank the groups involved in the organization for their excellent work. In particular I would like to thank Dirk Behrend for the great job he did during the past months.

The Local Organizing Committee has done an outstanding job in preparing the meeting, and I would like to express my gratitude to Prof. Andrey Finkelstein (chair of the LOC), and to the members of the Local Organizing Committee: Alexander Ipatov, Sergey Smolentsev, Nadia Shuygina, and Elena Skurikhina for their work, guaranteeing a pleasant stay in St. Petersburg.

The success of the fifth General Meeting will depend on the contributions of the participants. Highly interesting and important contributions will be provided as oral presentations, as posters, and during discussions. I thank all the speakers, the session chairpersons, and the authors in advance for their excellent presentations. The value of the conference is maintained by providing your papers to be printed shortly after the conference in the Proceedings. Thanks to all—let us keep up the momentum and finish the Proceedings in time.

The General Meeting will show results of VLBI at the state-of-the-art and will place emphasis on VLBI2010. The plans for future developments within the IVS and the transition to the next generation VLBI system are of great importance and need coordination in order to make best use of the international resources. With the VLBI2010 Committee, chaired by Bill Petrachenko, we have an excellent basis for developing our future. VLBI2010 will be a challenge not only until 2010 but for many more years to come.

I am certain that the meeting will be very successful and will stimulate our work. I wish all attendants to enjoy the conference and the splinter meetings—as well as the Russian hospitality.

Thank you!

Part 1. VLBI — A Vital Player in Global Observing Systems

The 5th IVS General Meeting Proceedings, 2008, p. 3–7

IVS Plans and Perspectives

Harald Schuh [1], *Dirk Behrend* [2]

[1] *Institute of Geodesy and Geophysics, Vienna University of Technology, Austria*
[2] *NVI, Inc./GSFC, USA*

Abstract. Plans and future perspectives of the IVS are presented and discussed. This includes ongoing activities within VLBI2010 but also future technological developments, new tasks and goals, and the general strategies of the Service. Its role with respect to GGOS is also described.

1. Role of the IVS w.r.t. GGOS

In the past several years the International Association of Geodesy (IAG) has established the Global Geodetic Observing System (GGOS) as one of its main components. GGOS works with all other IAG components to provide the geodetic infrastructure necessary for monitoring the Earth system and for global change research. GGOS is the IAG contribution to the realization of GEOSS (Global Earth Observation System of Systems) which aims at integrating Earth observations in order to better serve users in a number of societal benefit areas, including disaster prevention and mitigation. Thus, GGOS can be seen in the frame of the scientific and political activities of the intergovernmental Group on Earth Observations (GEO).

The major scientific and technological challenges for GGOS are consistency across the three areas of geodesy (geometry, gravity, and rotation) and consistency between observations and models. The structure of GGOS is shown in Fig. 1 and, being one of the key IAG Services, the IVS plays a critical role within GGOS, because several of the geodetic parameters are uniquely provided by VLBI (Tabl. 1). Further information about GGOS can be obtained on the web sites http://geodesy.unr.edu/ggos/ and http://www.ggos.org/.

Recently, at the GGOS Unified Analysis Workshop in Monterey, CA (Dec. 5–7, 2007) consistent models and parameterization for the various space geodetic techniques and also for gravity analyses were thoroughly discussed by representatives of all Services, e.g. models of pole tide and of reference pressure and temperature, and finally 27 action items were defined (see the aforementioned web sites).

Table 1. Geodetic parameters provided by the various space geodetic techniques

Parameter Type	VLBI	GNSS	DORIS	SLR	LLR	Altimetry
ICRF	X					
Nutation	X	(X)		(X)	X	
Polar Motion	X	X	X	X	X	
UT1	X					
Length of Day	(X)	X	X	X	X	
ITRF (Stations)	X	X	X	X	X	(X)
Geocenter		X	X	X		X
Gravity Field		X	X	X	(X)	X
Orbits		X	X	X	X	X
LEO Orbits		X	X	X		X
Ionosphere	X	X	X			X
Troposphere	X	X	X			X
Time Freq./Clocks	(X)	X		(X)		

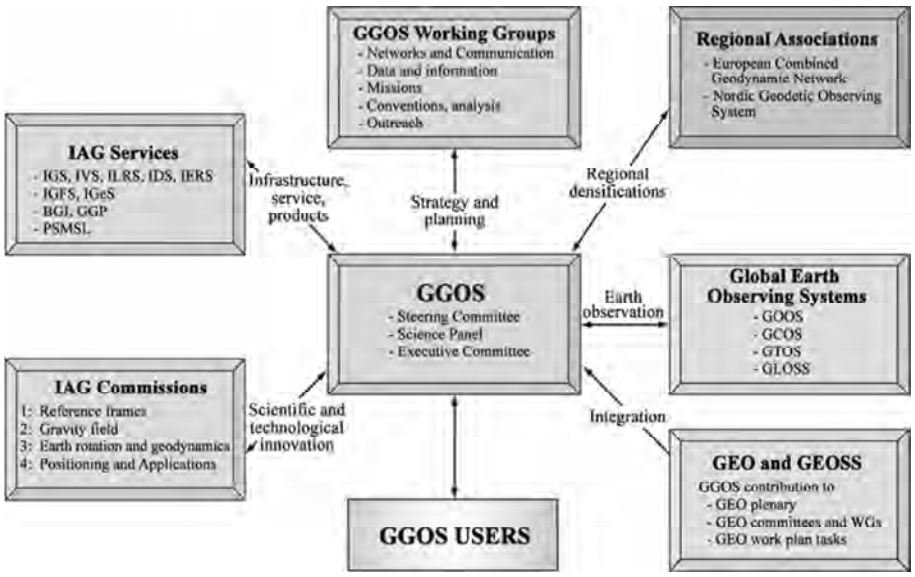

Figure 1. Structure of GGOS, the Global Geodetic Observing System of the IAG

2. Status of the IVS Network of Radio Telescopes

In spite of the cessation of the VLBI operations of the Algonquin radio telescope in Canada in 2007, the worldwide number of stations available for geodetic VLBI is increasing and there are several very promising plans for new

radio telescopes in countries such as:

- Germany (Twin Telescope at Wettzell station, funded by the German BKG);
- Korea (Korean VLBI Network, KVN, with three antennas; plus another one to be operated by the National Geographic Information Institute, NGII);
- Australia/New Zealand (Australian Geodetic VLBI Network Project of Geoscience Australia with three new antennas and New Zealand with one new site);
- USA (Fairbanks, possible installation of a new antenna by NASA/GSFC);
- India, Turkey, Saudi Arabia (plans).

3. Working Groups within the IVS

Since its start the following Working Groups have been established within the IVS which very successfully provided valuable results that usually have been summarized in published reports:

- WG 1: Phase Center Mapping (2001/2002);
- WG 2: IVS Product Specification and Observing Programs (2001/2002);
- WG 3: VLBI2010 (2003-2005);
- IERS/IVS Working Group: Second Realization of the ICRF (since 2006);
- WG 4: VLBI Data Structures (Chair: J. Gipson) (since 2007).

4. Realization of the VLBI2010 Concept

Based on the recommendations for the next generation VLBI system defined by IVS Working Group 3 (http://ivscc.gsfc.nasa.gov/about/wg/wg3/index.html), the VLBI2010 Committee (V2C) has intensively worked on the realization of the new VLBI system since 2005. A large number of simulations have been carried out and the results have shown that a VLBI system with about the following technical specifications:

- broadband observations from 2 to 15 GHz (or 18 GHz),
- small (12-m) antennas,
- slew speeds larger than 7.5 °/sec,
- recording rates 8-16 Gbps,
- new feeds.

will be able to provide the required accuracy of 1 mm for position and 0.1 mm/y for velocity of a station.

5. e–VLBI and Software Correlation

Today, high-speed optical fiber connections exist worldwide which will soon allow the application of VLBI in near real-time. As an e–VLBI example we present the ultra-rapid e–Intensives between Europe and Japan (baselines Onsala-Tsukuba and Metsähovi-Kashima) that have successfully proven to provide UT1 estimates within 3 min 45 sec after the observation had been taken (Fig. 2) [1].

Another promising development are software correlators that already exist e.g. in Kashima and Bonn [2].

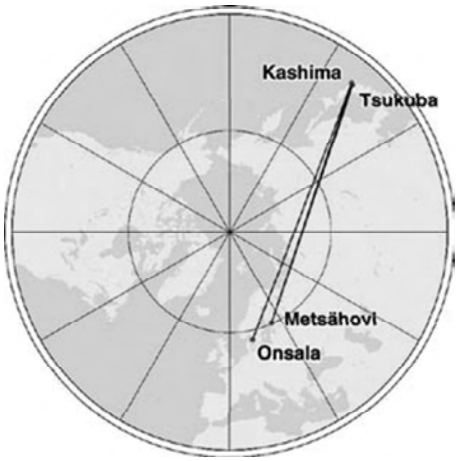

Figure 2. Baselines of ultra-rapid e–Intensives between Europe and Japan

6. CONT08 Campaign

An upcoming highlight for the IVS will be the CONT08 campaign to be observed over 15 continuous days in the second half of August 2008. In total, 11 stations will participate. It is planned to encourage other space geodetic techniques to join with their best efforts and after having carefully analyzed the CONT08 data and combined with other measurements a special issue of Journal of Geodesy will be published.

7. Visions for VLBI in the Next Decades

One of the goals that might be realized with the VLBI2010 system are phase delay solutions that will provide a significantly higher precision of the observables than current group delay measurements. Another task that requests a lot of additional research is the link of the quasi-inertial celestial reference frame

(CRF) realized by VLBI to dynamical reference frames.

Finally, we would like to mention frequency dissemination by optical fiber that will be feasible applying the so-called frequency comb technique (Fig. 3) for which Theodor Walter Hänsch was awarded the Physics Nobel Prize 2005. It can be assumed that in a few years optical clocks will outperform microwave clocks and that frequency dissemination by optical fiber can be done with unprecedented stability (various publications by H. Schnatz, G. Grosche, N.R. Newburry, and many others).

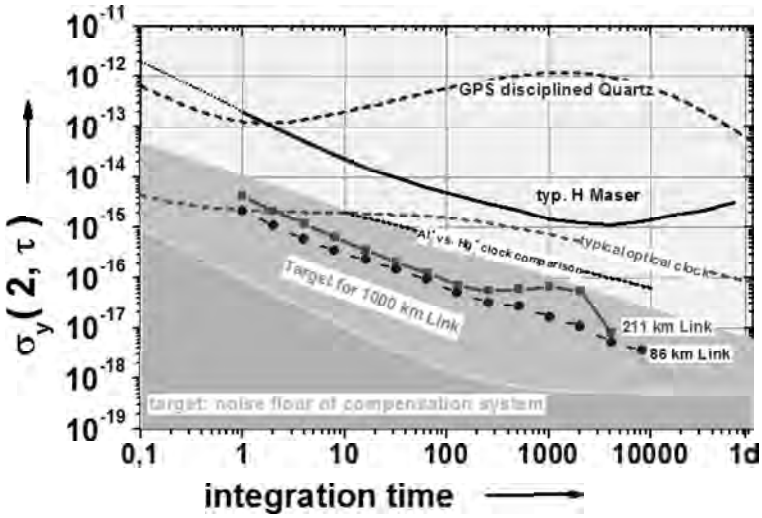

Figure 3. Stability of clocks and target performance of optical links (courtesy of H. Schnatz, PTB Braunschweig, Germany)

References

[1] Koyama, Y., M. Sekido, T. Hobiger, et al. Developments of Automated Data Processing System for Ultra Rapid dUT1 e–VLBI Sessions. This volume.

[2] Sekido, M., et al. Publications of NICT, 2008.

The 5th IVS General Meeting Proceedings, 2008, p. 8–13

Combining VLBI Intensive with GPS Rapid Solutions for Deriving a Stable UT Time Series

Daniela Thaller [1], *Volker Tesmer* [2], *Rolf Dach* [3], *Manuela Krügel* [2], *Markus Rothacher* [1], *Peter Steigenberger* [4]

[1)] *GeoForschungsZentrum Potsdam, Germany*

[2)] *Deutsches Geodätisches Forschungsinstitut, Germany*

[3)] *Astronomisches Institut, Universität Bern, Switzerland*

[4)] *Institut für Astronomische und Physikalische Geodäsie, Germany*

Abstract. Two different applications of the SINEX files for the intensive sessions will be shown in this contribution. In the first part, we demonstrate the benefit for the UT estimates if the intensive session is combined with the rapid GPS solution of the corresponding day. Secondly, we show their importance for deriving a combined long-time series of UT at daily intervals.

1. Introduction

In standard solutions for the intensive sessions, all parameters except for universal time (UT), one troposphere zenith delay per site and one clock parameter are fixed on their a priori values. The most critical parameters among the fixed parameters are polar motion (PM) and nutation [1]: as PM estimates often are not available in due time, they have to be fixed on predicted values. The nutation is fixed on the IAU2000 values so that the free core nutation is neglected. Recently, the IVS started to provide SINEX files for the intensive sessions, containing station coordinates, PM, UT and length of day (LOD), allowing for a rigorous combination with other data in order to have more reliable information than the predictions for PM. We assess the benefit of such a combination using normal equations derived from rapid GPS analysis. In general, if a combination of GPS- and VLBI-derived UT and LOD should be performed, the intensive sessions play a very important role as they fill many gaps between the 24-h sessions.

2. Daily Rapid ERP Combination

As the main intention of the intensive sessions is to have UT estimates with a very short latency, the rapid solutions from the International GNSS Service (IGS) are suitable for a combination. We use the normal equations from the rapid analysis at the CODE analysis center, containing station coordinates, PM, PM rates, UT1-UTC and LOD.

2.1. Impact of Fixed a Priori Pole Coordinates on UT

According to the Rapid Service and Prediction center of the IERS, the predicted values for PM have an accuracy of about 2.0 mas. In order to assess the impact of fixing pole coordinates that are wrong by this order of magnitude, we shifted the IERS-C04 series by 2.0 mas and estimated UT for the intensive sessions by fixing these falsified pole coordinates (one solution for shifting the x-pole only and a second solution for shifting the y-pole only). Additionally, we estimated UT for the same sessions by fixing PM on the original values of the IERS-C04 series. Comparing both resulting time series of UT (see Fig. 1 for the impact of the x- and y-pole, respectively), we see that the impact on UT is twofold: a mean bias and annual variations. However, the mean bias as well as the annual variation differ between the individual baselines. We can conclude that uncertainties in the y-pole have nearly no effect on UT derived from the baseline Wettzell-Tsukuba (XK-sessions), i.e., a bias of only 1.8 μs and almost no annual variation (i.e., 4.0 μs in terms of an RMS of unbiased residuals). But a wrong x-pole for this baseline will cause a large bias of about 64.3 μs in UT and only a small annual variation (RMS of 11.0 μs). The same is true for the impact of the y-pole for the baseline Wettzell-Kokee (XU-sessions) with a bias of 27.0 μs and an RMS of 5.3 μs. The largest variation in UT is visible for an error in x-pole in case of the baseline Wettzell-Kokee, resulting in a bias of 21.0 μs and an annual variation with an RMS of 16.2 μs. These results are in good agreement with the analysis carried out by [1]. It is clear that the predicted values for PM often are not as bad as 2 mas, and they are not wrong systematically as we assumed for our tests. However, the errors in the a priori PM have an impact on UT that should not be neglected.

2.2. Combination Results

For the last 16 months (November 2006 until February 2008), each normal equation of the intensive sessions is combined with the normal equation of the GPS rapid analysis of the corresponding day. Altogether, 287 XU sessions (Wettzell-Kokee) and 144 XK sessions (Wettzell-Tsukuba) are available. The combination is done in two steps: In a first step, only those parameters are combined that have to be fixed in a standard VLBI-only intensive solution, i.e., station coordinates and PM. In a second step, the contributions of GPS and VLBI to UT/LOD are combined additionally.

One pre-condition for the combination is that a co-located GPS site is

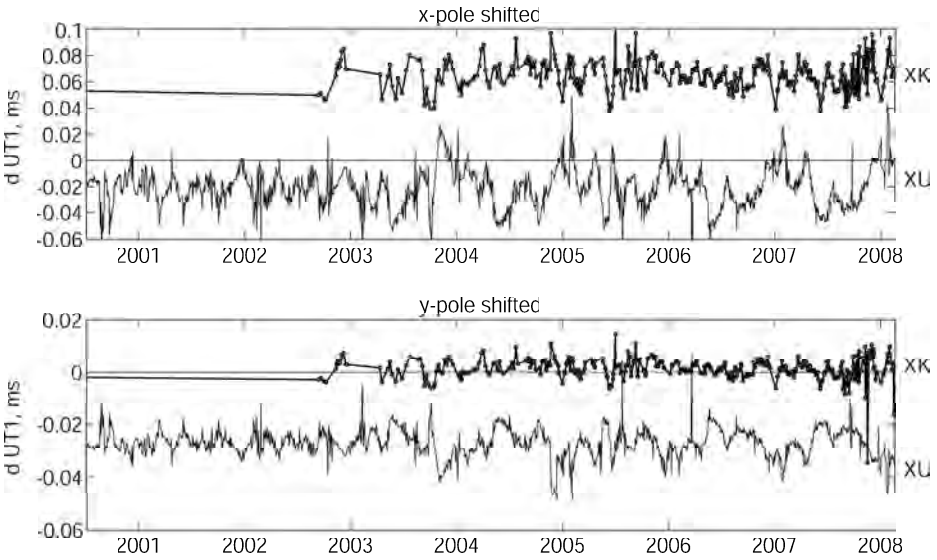

Figure 1. Impact on UT if pole coordinates shifted by 2.0 mas are fixed (XU: Wettzell-Kokee; XK: Wettzell-Tsukuba)

needed for both VLBI sites. However, the station priorities in the rapid GPS analysis did not yet consider the needs for the VLBI intensive sessions. Therefore, the site Tsukuba is often missing so that only 44 out of 144 XK sessions remain for the combination studies. The situation is much better for the XU sessions: 276 out of 287 sessions are usable. Another remark should be added regarding the GPS site at Wettzell. Normally, the site WTZR is included in the rapid solution, but due to the request for tracking GLONASS satellites, the site WTZZ was included (instead of WTZR) from July 2007 until mid of November 2007.

In order to assess the benefit of a combination, we first computed a VLBI-only solution for each intensive session by fixing the station coordinates to ITRF2005 and PM to the IERS-C04 series. The resulting VLBI-only time series is shown in Fig. 2. When combining station coordinates and PM, the resulting UT estimates are shown in Fig. 2 as well. The scatter of the residuals to IERS-C04 is reduced from 22.3 μs for the VLBI-only solution to 18.9 μs for the combined solution, demonstrating the benefit of a combination with GPS rapid solutions. However, the time series between July and November 2007 is striking. This is exactly the time span where the GPS site WTZZ instead of WTZR is included in the GPS rapid solution (see above). In an ideal case, this change should not have any impact on the results. However, as the solution heavily depends on the local tie information that is introduced, we can conclude from the results that there is a discrepancy between the local tie connecting VLBI with WTZR and that connecting VLBI with WTZZ. If

we consider only those combined sessions that are tied to WTZR, the RMS of the unbiased residuals is reduced to only 15.6 μs. The combined solution

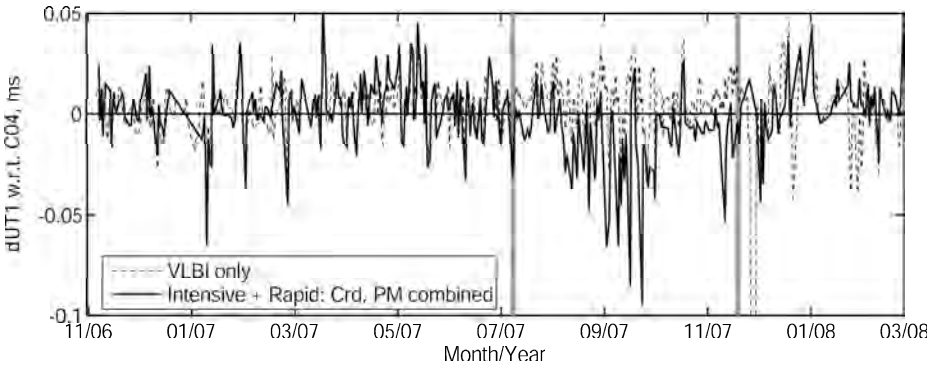

Figure 2. Differences of the UT1-UTC estimates compared to IERS-C04 for daily solutions. The two vertical lines delimit the time span with the site WTZZ

of the second step is not shown here because the results look similar to those of the first step (with identical RMS value). Thus, it can be concluded that the inclusion of the GPS-derived information about UT/LOD does not have a large impact, neither positive nor negative.

3. Combined Continuous Time Series of UT

In an ideal case, a time series of Earth orientation parameters (EOPs) contains estimates at equidistant epochs. This is problematic in the case of UT because VLBI does not have continuous observations but it is the only technique to determine UT in an absolute sense. Although the intensive sessions have no importance for the other EOPs, they are essential for UT. In order to show their importance, we combine normal equations for GPS and 24-h VLBI sessions generated within the project GGOS-D, and normal equations for the intensive sessions provided by BKG. All normal equations are combined into one full solution by estimating daily EOPs, station coordinates and velocities.

As our basic parameterization of the EOPs is a daily piece-wise linear polygon with functional values at epochs 00:00 UTC, we include the VLBI contribution by linearly transforming offset and drift given at the mean epoch of the session into two functional values at 00:00 UTC and 24:00 UTC of the corresponding day.

Considering the year 2004, we have only 129 24-h sessions, i.e., about two third of the daily UT values are derived solely from GPS and, thus, suffer from the systematic drifts induced when integrating GPS-derived LOD (Fig. 3, left plot). If we use the intensive sessions additionally, altogether 283 epochs in 2004 have a contribution by VLBI (Fig. 3, right plot). Comparing both figures,

it becomes clear that the intensive sessions fill many gaps between the 24-h sessions with valuable information. However, there are still about 80 epochs left that are determined solely by GPS. Tabl. 1 summarizes the RMS of the residuals compared to the IERS-C04 series. The benefit of combining the 24-h sessions with GPS can be clearly seen. The inclusion of the intensive sessions improves the full time series only slightly, but may be that the weighting still has to be optimized.

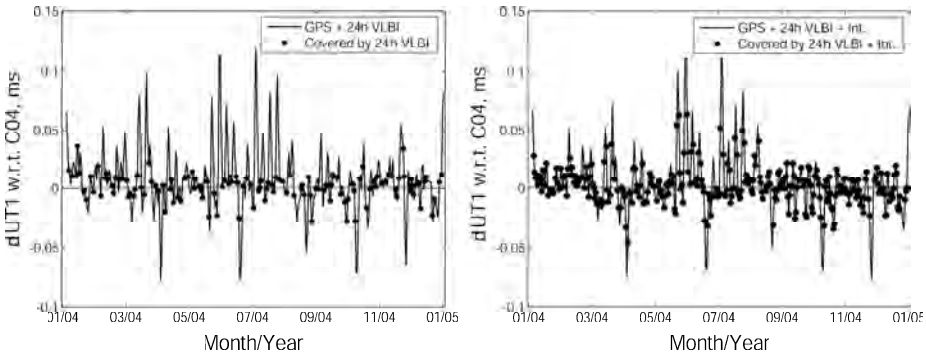

Figure 3. Combined time-series of UT at daily intervals (dots mark the epochs with a contribution of VLBI)

Table 1. RMS of UT residuals compared to IERS-C04 for the year 2004

Time series	RMS VLBI epochs	RMS all epochs
24-h VLBI	16.9 μs (129 epochs)	–
GPS + 24-h VLBI	10.8 μs (129 epochs)	26.4 μs
GPS + 24-h VLBI + Intensives	15.7 μs (283 epochs)	25.4 μs

4. Conclusions and Outlook

The impact of wrong fixed pole coordinates on UT for the VLBI intensive sessions has been demonstrated. An improvement compared to the VLBI-only solution can be seen if a combination with GPS is performed. However, it must be emphasized that the VLBI-only solution used here as a reference was computed with very good a priori PM (IERS-C04) instead of predicted values. Thus, we assume that the benefit of a rapid daily combination is even larger for the estimated UT values than it turned out in the studies presented here.

As regards GPS, the combination with VLBI intensive sessions will allow to derive daily rapid solutions with a correct alignment of UT. However, the benefit still has to be investigated.

The importance of the intensive sessions for a combined time series of UT at daily intervals has been shown for the year 2004. However, the combination should be extended to the whole time span where SINEX files are available.

Acknowledgements

We want to thank the VLBI group at BKG and the GGOS-D partners for providing SINEX files for the intensive and 24-h VLBI sessions, respectively.

References

[1] Nothnagel, A., D. Schnell. The impact of errors in polar motion and nutation on UT1 determinations from VLBI Intensive observations. J. Geod., DOI 10.1007/s00190-008-0212-2, 2008.

The 5th IVS General Meeting Proceedings, 2008, p. 14–18

Atmosphere Angular Momentum Time Series for CONT05

Johannes Boehm, Paulo Jorge Mendes Cerveira, Sigrid Englich, Harald Schuh

Institute of Geodesy and Geophysics, Vienna University of Technology, Austria

Abstract. We compare four atmosphere angular momentum time series for the time span of CONT05, a 15 days period in the second half of September 2005. Two series are based on analysis data from the European Centre for Medium-Range Weather Forecasts (ECMWF) (with different horizontal resolutions), the third series was derived from 3 and 6 hours forecast and boundary condition data of the ECMWF, and the fourth series from data of the National Centers for Environmental Prediction (NCEP) was provided by the Special Bureau of the Atmosphere (SBA). As expected, both series from ECMWF analysis data agree at the level of 10^{23} kg·m^2/s or better, except for the mass terms when inverted-barometer (IB) correction is applied where the selection of the land-sea mask is a critical factor. Six hours forecast values from the ECMWF agree at the level of 10^{24} kg·m^2/s or better with the analysis data. The motion terms from NCEP as provided by the SBA deviate from the other series because wind fields are only applied up to 10 hPa.

1. Introduction

The components of the inertia tensor c_{13}, c_{23}, and c_{33} in kg·m^2 (mass terms) and of the relative angular momentum l_1, l_2, and l_3 in kg·m^2/s (motion terms) due to the atmosphere can be determined with (1), (2) and (3), (4), respectively [1]. The abbreviations in these equations are: r radius, g gravity, p_S surface pressure, φ latitude, λ longitude, u eastward and v northward velocity component of the wind.

$$c_{13} + i \cdot c_{23} = -\int\int \frac{1}{g} \cdot r^4 \cdot p_S \cdot sin\varphi \cdot cos^2\varphi \cdot e^{i\lambda} \cdot d\lambda \cdot d\varphi, \tag{1}$$

$$c_{33} = \int\int \frac{1}{g} \cdot r^4 \cdot p_S \cdot cos^3\varphi \cdot d\lambda \cdot d\varphi, \tag{2}$$

$$l_1 + i \cdot l_2 = -\int\int\int \frac{1}{g} \cdot r^3 \cdot (u \cdot sin\varphi + i \cdot v) \cdot cos\varphi \cdot e^{i\lambda} \cdot d\lambda \cdot d\varphi \cdot dp, \tag{3}$$

$$l_3 = \int\int\int \frac{1}{g} \cdot r^3 \cdot u \cdot cos^2\varphi \cdot d\lambda \cdot d\varphi \cdot dp. \quad (4)$$

The European Centre for Medium-Range Weather Forecasts (ECMWF) is archiving analysis data (AN) every 6 hours, i.e. at 0, 6, 12, and 18 UT. Furthermore, it is providing forecast data (FC, initialized at 0 and 12 UT) and boundary condition data (BC, initialized at 6 and 18 UT). FC and BC data are available with a time resolution of 3 hours. To create a continuous 3-hours time series, which is based on forecast steps as short as possible, we concatenate the 3 and 6 hour steps from FC and BC data, respectively (Tabl. 1).

Table 1. Forecast data (FC) and Boundary Condition data (BC) from the ECMWF are concatenated to create continuous 3-hours series with forecast steps as short as possible (3 and 6 hours)

Time (UT)	Type	Initialized (UT)	Step (hours)
0	BC	18	6
3	FC	0	3
6	FC	0	6
9	BC	6	3
12	BC	6	6
15	FC	12	3
...			

2. Comparison of Mass and Motion Terms During CONT05

We compare four different series of (relative) angular momentum contributions during the time span of the continuous VLBI campaign CONT05 (second half of September 2005):

- 1° ECMWF analysis data as determined in Vienna (vie-an),
- 1° ECMWF FC plus BC data as determined in Vienna (vie-fc),
- 1.825^o ECMWF analysis data as determined by the GeoForschungsZentrum Potsdam (gfz),
- 2.5^o NCEP reanalysis data as determined by the Special Bureau of the Atmosphere (sba) [2].

Fig. 1 and 2 and Tabl. 2 and 3 show the differences and standard deviations of the mass terms for the equatorial and axial components, respectively. Fig. 3 and Tabl. 4 illustrate the comparison of the motion terms.

Table 2. Standard deviations for c_{13} (left) and c_{23} (right) with inverted barometer (lower left triangles) and non-inverted barometer (upper right triangles) correction expressed as angular momentum in 10^{23} kg·m^2/s

–	vie-an	vie-fc	gfz	sba	vie-an	vie-fc	gfz	sba
vie-an	–	2.5	0.1	2.2	–	2.2	0.1	2.3
vie-fc	0.9	–	2.5	3.7	1.3	–	2.2	3.3
gfz	1.2	1.3	–	2.3	1.1	1.5	–	2.3
sba	0.8	1.4	1.3	–	1.3	2.1	1.9	–

Table 3. Standard deviations for c_{33} with inverted barometer (lower left triangle) and non-inverted barometer (upper right triangle) correction expressed as angular momentum in 10^{23} kg·m^2/s

–	vie-an	vie-fc	gfz	sba
vie-an	–	6.1	0.2	4.5
vie-fc	3.7	–	6.1	6.1
gfz	18.9	18.9	–	4.5
sba	4.4	5.1	19.0	–

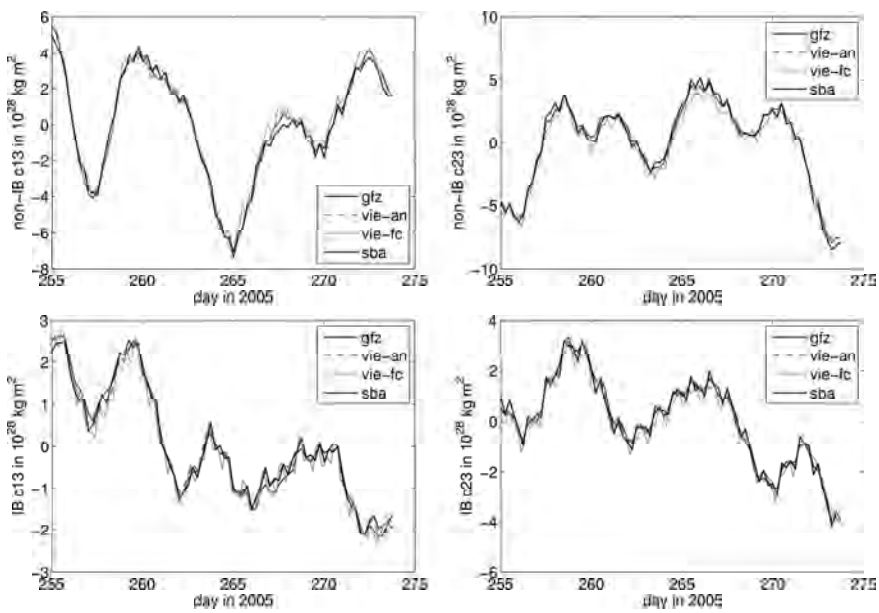

Figure 1. Components of the inertia tensor. Upper left: non-IB c_{13}, upper right: non-IB c_{23}, lower left: IB c_{13}, lower right: IB c_{23}

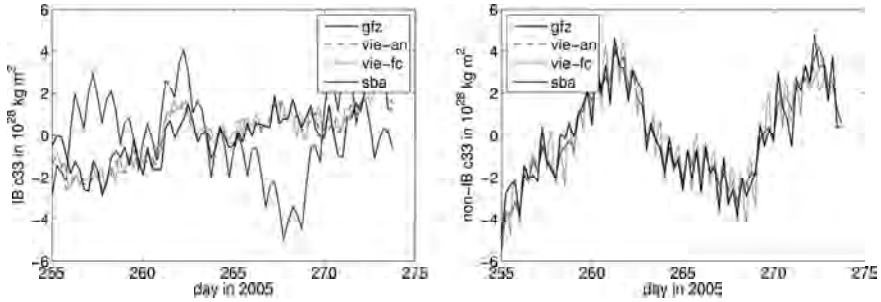

Figure 2. Components of the inertia tensor. Left: IB c_{33}, right: non-IB c_{33}

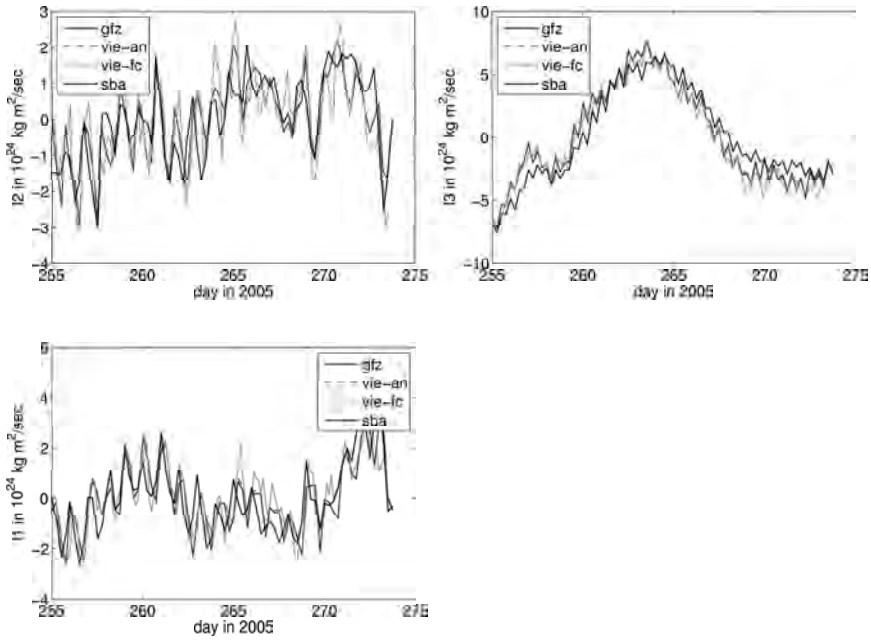

Figure 3. Components of the relative angular momentum. Upper left: l_2, upper right: l_3, lower left: l_1

The following conclusions can be drawn from the comparisons:

- As expected, the non-IB mass and motion terms from ECMWF analysis data determined in Vienna and Potsdam agree on average to better than 0.2 and $1.0{\cdot}10^{23}$ kg·m^2/s, respectively, as the horizontal resolution is not a critical factor for the determination of the angular momentum functions. The differences are larger by a factor of 10 for the IB mass terms because of the differences in the land-sea mask (Tabl. 2).

Table 4. Standard deviations for l_1 (lower left triangle) and l_2 (upper right triangle of left part) and for l_3 (right side) in 10^{23} kg·m^2/s

–	vie-an	vie-fc	gfz	sba	vie-an	vie-fc	gfz	sba
vie-an	–	6.3	0.7	8.5	–	7.5	1.0	12.4
vie-fc	6.2	–	6.4	8.7		–	7.5	12.8
gfz	0.4	6.2	–	8.4			–	11.6
sba	7.2	9.5	7.2	–				–

- The deviation of the c_{33} (IB) inertia tensor component is too large; thus, further investigations need to be carried out (Tabl. 3).
- ECMWF 6-hours forecast data agrees at a level of 10^{24} kg·m^2/s or better with the time series from analysis data, in terms of angular momentum.
- For the motion terms, the deviation is largest for the NCEP time series from the SBA, because wind fields were only used up to 10 hPa (unlike the ECMWF series where wind fields up to 1 hPa are used).

Acknowledgements

We would like to thank Maik Thomas and Andre Grötzsch from the GeoForschungsZentrum Potsdam and David Salstein from the Special Bureau of the Atmosphere for providing the atmosphere angular momentum functions.

References

[1] Schuh, H., et al. Erdrotation und globale dynamische Prozesse. Mitteilungen des Bundesamtes für Kartographie und Geodäsie, Band 32, 2003.

[2] Salstein, D.A., D.M. Kann, A.J. Miller, et al. The Sub-bureau for Atmospheric Angular Momentum of the International Earth Rotation Service: A Meteorological Data Center with Geodetic Applications. Bulletin of American Meteorological Society, v. 74, 1993.

The 5th IVS General Meeting Proceedings, 2008, p. 19–24

How Can the Wettzell "G" Ring Laser Improve VLBI Measurements of Subdiurnal Earth Rotation Variations?

Paulo Jorge Mendes Cerveira [1], *Sigrid Englich* [1], *Harald Schuh* [1], *Thomas Klügel* [2], *Aleksander Velikoseltsev* [2], *Ulrich Schreiber* [3]

[1)] *Institute of Geodesy and Geophysics (IGG), Vienna University of Technology, Austria*

[2)] *Bundesamt für Kartographie und Geodäsie, Geodätisches Observatorium Wettzell, Germany*

[3)] *Forschungseinrichtung Satellitengeodäsie der Technischen Universität München, Geodätisches Observatorium Wettzell, Germany*

Abstract. The orientation of the Earth in space and on the Earth, and the rotational speed change unpredictably in a rapid and irregular manner. The Wettzell "G" ring laser is about to sense the signatures of the ocean tidal effect on polar motion (and possibly length of day). We therefore analysed two Wettzell "G" ring laser data sets for detecting ocean tidal effects. Several amplitudes could be detected in the diurnal and semidiurnal tidal band. However, in order to validate the detection of ocean tidal effects upon the Wettzell "G" ring laser data, we need first to split up the model of the ocean tidal effect on polar motion of the celestial intermediate pole into its retrograde and prograde contributions, prior to applying the conversion to the polar motion of the instantaneous rotation pole. One major question needs to be resolved: what causes the high amplitude in the O1 tidal period of the ring laser residuals? A Kalman filter, which takes as input estimates of the Earth rotation based on Very Long Baseline Interferometry (VLBI) and Wettzell "G" ring laser, could be particularly useful for application to spacecraft navigation, reduction of geodetic data, and research into geophysical causes.

1. Introduction

In 1884, Küstner discovered the variation of latitude, and in 1891, Chandler explained it as polar motion. Until the mid-1960s, optical astrometry was the only source of Earth rotation information. At present, Very Long Baseline Interferometry (VLBI) technique provides the most complete high-accuracy observations for monitoring the rotation of the Earth, i.e., the motion of the

Celestial Intermediate Pole (CIP) w.r.t. both a Conventional Celestial Reference Frame (CCRF) and a Conventional Terrestrial Reference Frame (CTRF), in addition to Universal Time (UT1) variations w.r.t. the Universal Time Coordinated (UTC). For near real time considerations, electronic VLBI (e–VLBI) is nowadays able to provide UT1 with a time delay of less than one hour [5]). Since a few years, an emerging and more "exotic" instrument, the Wettzell "G" ring laser proved its ability in sensing variations in the Earth rotation [9]. Unlike VLBI, the Wettzell "G" ring laser responds directly to the instantaneous Earth rotation vector (ERV). In the case of VLBI, the latter is only a by-product, which is not required for geophysical interpretation: geophysical angular momentum functions are related to the polar motion of the CIP, and excess length of day (LOD). However, the Wettzell "G" ring laser generates observables with a temporal resolution of 30 minutes, which give access to the rate of change of precession-nutation (PN) of the CIP, to LOD variations, polar motion (PM) of the CIP and its rate of change [7]. The main contribution of the ring laser for the five Earth Orientation Parameters (EOP) lies in the spectrum from 1 to 48 hours. In terms of competitiveness, the question remains: how much does the Wettzell "G" ring laser sense considering Earth rotation signatures?

2. Ring Laser: Basic Equations Relating Observations to Earth Rotation

Fig. 1 gives a schematic overview of the PM of the CIP, the instantaneous rotation pole (IRP), and the geophysical pole G, which conveys the geophysical external torque-free equatorial part of Earth rotation.

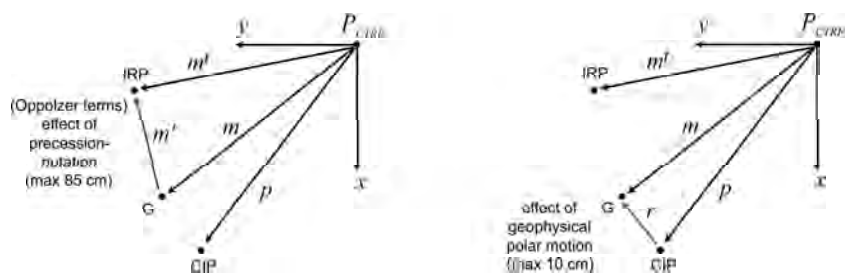

Figure 1. Schematic representation in a CTRF between the PM of the CIP p vs. PM of the IRP m^t, including the geophysical pole G, as well as the pole of the CTRF

The ERV w.r.t. a CTRF is given as:

$$\vec{\omega} = (\omega_1, \omega_2, \omega_3)^T = \omega_0 \cdot \left(m_1^t, m_2^t, 1 + m_3^t\right)^T, \tag{1}$$

where ω_0 is the mean angular speed of the sidereal rotation of the Earth, i.e.,

$7.2921150(1) \cdot 10^{-5}$ rad/s. The quantities m_1^t, m_2^t, and m_3^t represent the total terrestrial PM and axial motion of the IRP, respectively.

The total terrestrial PM of the IRP sums up as:

$$m^t = m + m' = m_1^t + i \cdot m_2^t, \tag{2}$$

where $i = \sqrt{-1}$, $m = m_1 + i \cdot m_2$ represents PM of the geophysical pole G, and $m' = m_1' + i \cdot m_2'$ being a function of the geodetic PN of the CIP. The geodetic PM of the CIP is denoted by $p = p_x - i \cdot p_y$.

The PM of the geophysical pole G was derived by Gross [4] and Brzezinski and Capitaine [2]:

$$m = p - i \cdot \frac{\dot{p}}{\omega_0} = p + r. \tag{3}$$

The quantity m' was derived by Eubanks [3] and Brzezinski and Capitaine [2]:

$$m' = i \cdot \frac{\dot{N}}{\omega_0} \cdot e^{-i \cdot \theta}, \tag{4}$$

where the geodetic PN of the CIP reads

$$N = \delta\psi \cdot \sin\epsilon_0 + i \cdot \delta\epsilon = X + i \cdot Y, \tag{5}$$

and X, Y are the celestial coordinates of the CIP, $\delta\psi, \delta\epsilon$ being the corresponding geodetic PN angles, ϵ_0 the mean obliquity at epoch J2000.0, and θ the sidereal rotation angle.

Let us now turn our attention to the ring laser. For the most up-to-date description of the Wettzell "G" ring laser, we refer to [10]. The basic relation between the relative change in the Sagnac frequency [8], corrected for latitudinal tilt variations due to local effects, and the perturbation of the ERV, i.e., m_1^t, m_2^t, and m_3^t has been summarized [6]:

$$\Delta S_{RLG} = \cot\phi_0 \cdot \left[-m_1^t \cdot \cos\lambda_0 + m_2^t \cdot \sin\lambda_0\right] + m_3^t, \tag{6}$$

where ϕ_0 and λ_0 are the nominal latitude and longitude of Wettzell, respectively, and m_1^t, m_2^t, and m_3^t being expressed as:

$$m_1^t = \frac{1}{\omega_0} \cdot \left[\omega_0 \cdot p_x - \dot{p}_y + \dot{X}\sin\theta - \dot{Y}\cos\theta\right], \tag{7}$$

$$m_2^t = \frac{-1}{\omega_0} \cdot \left[\omega_0 \cdot p_y + \dot{p}_x - \dot{X}\cos\theta - \dot{Y}\sin\theta\right], \tag{8}$$

$$m_3^t = \frac{-\delta LOD}{T_0} = \frac{\partial(UT1 - UTC)}{\partial t}. \tag{9}$$

3. Results

In order to study the tidal signatures, possibly of oceanic origin, we analysed two Wettzell "G" ring laser data sets: the first one covered 40 days since Sep. 17, 2002 (MJD 52534), while the second included 144 days since Sep. 22, 2006 (MJD 54000), both having a temporal resolution of half an hour given in the time scale of UTC. In a first step, both data sets were corrected for local deformations induced by the solid Earth tides at station Wettzell, following the formalism described by Mendes Cerveira et al. [6]. Then the effect of the Oppolzer terms, denoted by the quantity $m^{\cdot}$, were reduced using the model of Brzezinski [1]. A program for removing jumps and breaks was applied, and then a high-pass smoothing filter of two days was applied to get rid of low frequency signals. In Fig. 2 the effect of the Oppolzer terms was restored for visualization purposes.

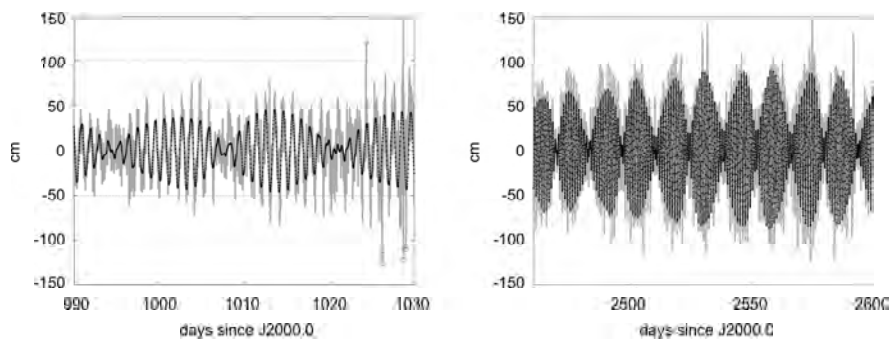

Figure 2. Pre-processed relative Sagnac frequency ring laser data (grey), and transformed model of Brzezinski [1] (black), both being projected to Earth's surface. Black circles are outliers. The ring laser data covers 40 days since Sep. 17, 2002 (MJD 52534), and 144 days since Sep. 22, 2006 (MJD 54000)

The next largest signatures in the ring laser data are the effect of ocean tides on PM and LOD, followed by the minor effect of tidal gravitation on PM for a non-rigid Earth. For this reason, we performed a least squares adjustment for the 71 waves included in the current correction of ocean tides on PM of the CIP (and LOD) to the residual relative Sagnac frequency variation. In addition, amplitudes of three further periods (8.28, 8.00, and 6.00 hours) were estimated, in order to check if the M3 tidal wave as well as both overtones could be detected. The standard deviation of unity weight of the complete adjustment is 13.7 cm. No significant amplitude ($\sim$ 6 mm) could be detected at the latter three periods. Amplitudes of such a magnitude can simply be generated by the noise level of 13.7 cm. Some constraints had to be applied, proportional to the

ratio of the respective coefficients in the tidal potential, in order to separate all tidal waves, due to the short time span of the ring laser data. Tabl. 1 shows the residual amplitudes (processed ring laser obervations minus model by Brzezinski) of the most prominent tidal waves having an amplitude larger than 8 mm. An amplitude of ~ 4 cm pops up for the O1 tidal wave: this is far too high to be explained solely by tidal oceanic effects and tidal gravitation. The next largest amplitude appears at the S2 tidal wave with ~ 2 cm. Other significant amplitudes in the diurnal and semidiurnal band exist, e.g., for the P1 or M2 tidal waves.

A next step should therefore split up the model of ocean tidal effect on PM of the CIP into the retrograde and prograde contributions prior to apply the conversion to the PM of the IRP, and then apply this model as a correction to the Wettzell "G" ring laser data.

Table 1. Difference in amplitude between the CIP and the IRP and the model of Brzezinski. Temporal reference for the phase is J2000.0. Asin and Acos represent the amplitudes in the sine and cosine components, respectively. Mean solar day is denoted by msd, and the standard deviation of the amplitude by sA

Name *Doodson*	Period, hours	Period, msd	Asin, mm	Acos, mm	A, mm	sA, mm
SIG1	27.848	1.1603	−2.5	8.2	8.6	2.3
Q1	26.868	1.1195	−8.8	1.0	8.9	2.3
RO1	26.723	1.1134	10.1	3.2	10.6	2.3
	25.823	1.0759	5.2	6.4	8.2	0.6
O1	25.819	1.0758	26.5	35.2	44.0	2.4
TAU1	25.668	1.0695	11.8	7.9	14.2	2.2
	24.974	1.0406	3.4	9.2	9.8	2.3
P1	24.065	1.0027	−12.4	−8.8	15.2	3.1
SO1	22.420	0.9341	10.6	3.9	11.3	2.2
OO1	22.306	0.9294	13.5	5.6	14.7	2.7
	22.303	0.9292	8.6	3.6	9.3	1.7
V1	21.578	0.8990	−12.1	−12.3	17.3	2.2
	21.575	0.8989	−7.7	−7.9	11.0	1.4
NI2	12.626	0.5260	−0.8	8.4	8.5	2.0
M2	12.420	0.5175	1.8	8.9	9.1	2.7
S2	12.000	0.5000	7.1	17.2	18.6	2.1
ETA2	11.754	0.4897	−7.2	4.6	8.5	2.3

4. Discussion and Conclusions

A dynamical model, i.e., the Euler-Liouville equation, is available for Earth rotation. VLBI delivers EOP with a certain time delay. The Wettzell "G" ring laser produces integrated 30 minutes observables, and apparently senses the effects of ocean tides on PM. For this reason, a software based on the Kalman filter approach will be developed for monitoring and predicting Earth rotation for near real time applications from VLBI and ring laser observations. But first, the high amplitude in the O1 tidal wave in the residuals of the Wettzell "G" ring laser data should be elucidated.

Acknowledgements

The first author is indebted to the Fonds National de la Recherche (FNR) of the Luxembourg Government for financing the participation at the IVS GM 2008 by grant FNR/08/MA2/01. The German Science Foundation (DFG, Deutsche ForschungsGemeinschaft) is highly acknowledged for funding this work within the Research Unit FOR584 "Earth Rotation and Global Dynamic Processes".

References

[1] Brzezinski A. Contribution to the theory of polar motion for an elastic earth with liquid core. Manuscripta Geodaetica, v. 11, 226–241, 1986.

[2] Brzezinski A., N. Capitaine. The use of the precise observations of the Celestial Ephemeris Pole in the analysis of geophysical excitation of Earth rotation. J. Geophys. Res., v. 98 (B4), 6667–6675, 1993.

[3] Eubanks T.M., Variations in the Orientation of the Earth. Geodynamic Series, v. 24, 1–54, 1993.

[4] Gross R.S., Correspondence between theory and observations of polar motion. Geophys. J. Int., v. 109, 162–170, 1992.

[5] Haas R., J. Wagner, J. Ritakari, et al. Report on the Fennoscandian-Japanese Project for Near real-time UT1-Observations with e–VLBI. Submitted to Proc. Journées Systèmes de Référence Spatio-Temporels 2007, 2008.

[6] Mendes Cerveira P.J., H. Spicakova, H. Schuh, et al. Earth rotation parameters from Very Long Baseline Interferometry and ring laser observables. Accepted to Advances in Geosciences, 2008.

[7] Mendes Cerveira P.J., J. Böhm, H. Schuh, et al. Using Very Long Baseline Interferometry and Ring Laser for Monitoring Earth Rotation. Submitted to Journal of Geodesy, 2008.

[8] Post E.J. Sagnac Effect. Reviews of Modern Physics, v. 39 (2), 475–493, 1967.

[9] Schreiber K.U., A. Velikoseltsev, M. Rothacher, et al. Direct measurement of diurnal polar motion by ring laser gyroscopes. J. Geophys. Res., v. 109 (B06405), DOI 10.1029/2003JB002803, 2004.

[10] Schreiber K.U., T. Klügel, A. Velikoseltsev, et al. The Large ring laser G for Continuous Earth Rotation Monitoring. Submitted to Journal of Geodesy, 2008.

The 5th IVS General Meeting Proceedings, 2008, p. 25–29

Multi-Step VLBI Observations of Weak Extragalactic Radio Sources to Align the ICRF and the Future GAIA Frame

Géraldine Bourda [1], *Patrick Charlot* [1], *Richard Porcas* [2], *Simon Garrington* [3]

[1)] *Laboratoire d'Astrophysique de Bordeaux, Université Bordeaux 1, France*

[2)] *Max Planck Institute for Radio Astronomy, Germany*

[3)] *Jodrell Bank Observatory, The University of Manchester, UK*

Abstract. The space astrometry mission GAIA will construct a dense optical QSO-based celestial reference frame. For consistency between optical and radio positions, it will be important to align the GAIA frame and the International Celestial Reference Frame (ICRF) with the highest accuracy. Currently, it is found that only 10% of the ICRF sources are suitable to establish this link, either because they are not bright enough at optical wavelengths or because they have significant extended radio emission which precludes reaching the highest astrometric accuracy. In order to improve the situation, we have initiated a VLBI survey dedicated to finding additional suitable radio sources for aligning the two frames. The sample consists of about 450 sources, typically 20 times weaker than the current ICRF sources (down to the 20 mJy flux level), which have been selected by cross-correlating optical and radio catalogues. This paper presents the observing strategy to detect, image, and measure accurate positions for these sources. It will also provide results about the VLBI detectability of the sources, as derived from initial observations with the European VLBI Network in June and October 2007. Based on these observations, an excellent detection rate of 89% is found, which is very promising for the continuation of this project.

1. Context

The ICRF (International Celestial Reference Frame [1, 2]) is the fundamental celestial reference frame adopted by the International Astronomical Union (IAU) in August 1997. It is currently based on the VLBI (Very Long Baseline Interferometry) positions of 717 extragalactic radio sources, estimated from dual-frequency S/X (2.3 and 8.6 GHz) observations. The European space astrometry mission GAIA, to be launched by 2011, will survey about one billion stars in our Galaxy and 500 000 Quasi Stellar Objects (QSOs) brighter than

magnitude 20 [3]. Unlike Hipparcos, GAIA will construct a dense optical celestial reference frame directly at optical bands, based on the QSOs with the most accurate positions (i.e. those with optical apparent magnitude $V \leq 18$ [4]). In the future, the alignment of the ICRF and the GAIA frame will be crucial, in particular for ensuring consistency between measured radio and optical positions. This alignment, to be determined with the highest accuracy, requires hundreds of sources in common, with a uniform sky coverage and very accurate radio and optical positions. Obtaining such accurate positions implies that the link sources must have $V \leq 18$ and no extended VLBI structures.

In a previous study, we investigated the current status of this link based on the present list of ICRF sources [5]. We found that although about 30% of the ICRF sources have an optical counterpart with $V \leq 18$, only one third of these are compact enough on VLBI scales for the highest astrometric accuracy. Overall, only 10% of the current ICRF sources (70 sources) are thus available for the alignment with the GAIA frame. This highlights the need to identify additional suitable radio sources, which is the purpose of the project described here.

2. Strategy to Identify New Link Radio Sources

Searching for additional radio sources suitable for aligning accurately the ICRF and the GAIA frame could rely on the VLBA Calibrator Survey (VCS; [9] and references therein), the catalogue of more than 3000 extragalactic radio sources observed with the VLBA (Very Long Baseline Array; the american VLBI network), which is currently underway. Another possibility is to search for new VLBI sources, which implies going to weaker radio sources with flux densities typically below 100 mJy. This can now be realized owing to recent increases in the VLBI network sensitivity (e.g. recording now possible at 1Gbps) and by using a network comprising large antennas like the European VLBI Network (EVN).

A sample of about 450 radio sources, for which there are no published VLBI observations, was selected for this purpose by cross-identifying the NRAO VLA Sky Survey (NVSS) [6], a deep radio survey (complete to the 2.5 mJy level) which covers the entire sky north of $-40°$, with the Véron & Véron (2006) optical catalogue [7]. This sample is based on the following criteria: $V \leq 18$ (to ensure very accurate positions with GAIA), $\delta \geq -10°$ (for possible observing with northern VLBI arrays), and NVSS flux density ≥ 20 mJy (for possible VLBI detection).

The observing strategy to identify the most appropriate link sources from this sample includes three successive steps to detect, image and measure accurate positions for these sources: (i) to determine the VLBI detectability of these weak radio sources; (ii) to image the sources detected in the first step, in order to identify the most point-like sources; and (iii) to determine an accurate astrometric position for the most compact sources of the sample.

3. Initial VLBI Results

Initial VLBI observations for this project were carried out in June and October 2007 (during two 48-hours experiments, named EC025A and EC025B, respectively), with a network of four EVN telescopes (Effelsberg, Medicina, Noto, Onsala; and the 70 m Robledo telescope for part of the time in EC025B). The purpose of these two experiments was to determine the VLBI detectability of the 447 weak radio sources in our sample based on snapshot observations.

Our results indicate excellent detection rates of 97% at X band and 89% at S band, with 432 sources and 399 sources detected at X and S bands, respectively (the individual results for EC025A and EC025B are detailed separately in Tabl. 1). This detection rate is in agreement with that reported in [8] (80%) for quasars from the Sloan Digital Sky Survey. The overall mean correlated flux densities (i.e. for each source and band, the mean over all scans and baselines detected) have a median value of 26 mJy at X band and 46 mJy at S band (see Fig. 1) with the weakest sources at the level of 1 mJy at X band and 8 mJy at S band. A comparison between the X-band flux density distribution for our sources, those from the VCS and the ICRF sources shows that the sources of our sample are indeed much weaker. On average, they are 27 times weaker than the ICRF sources and 8 times weaker than the VCS sources.

The spectral index α (defined as $S \propto \nu^{\alpha}$, where S is the source flux density and ν is the frequency) was also investigated. In this definition, the sources with a compact core are expected to have $\alpha > -0.5$. Fig. 2 shows the spectral index distribution for the 398 radio sources detected at both frequencies in EC025A and EC025B. The corresponding distribution for the sources which also belong to the CLASS catalogue [10], well known to be composed of compact sources, is also plotted and no major differences are noticed. The median value of α is -0.34 and about 70% of the sources have $\alpha > -0.5$, hence indicating that they must have a dominating core component, which is very promising for the future stages of this project.

Table 1. VLBI detection rate for the 447 weak extragalactic radio sources observed during EC025A and EC025B

	Sources observed	X-band detection	S-band detection	S and X detection
EC025A	218	216 sources 99%	211 sources 96%	211 sources 96%
EC025B	229	216 sources 94%	188 sources 82%	187 sources 82%
Overall	447	432 sources 97%	399 sources 89%	398 sources 89%

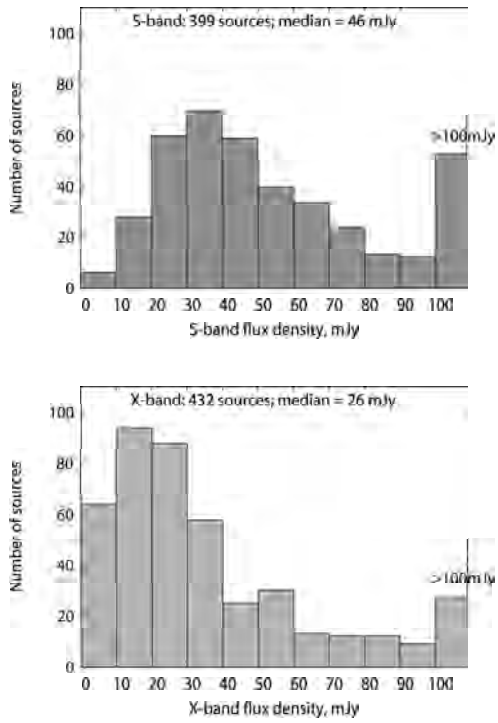

Figure 1. Mean correlated flux density distribution (units in mJy), at S band and X band, for the sources detected in EC025A and EC025B, conducted respectively in June and October 2007

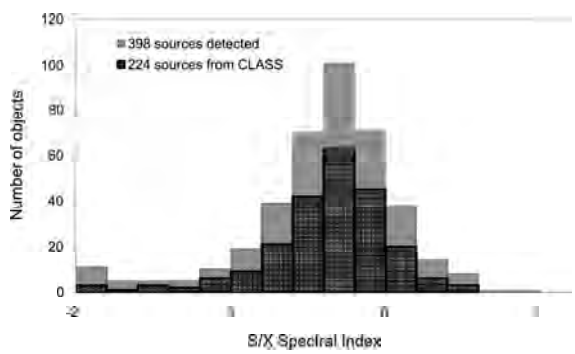

Figure 2. S/X spectral index distribution for the 398 weak extragalactic radio sources detected at both S and X bands during the experiments EC025A and EC025B. Additionally, the S/X spectral index distribution for the sources also belonging to the CLASS catalogue is plotted (in black)

4. Summary

Based on observations with the European VLBI Network, we identified 398 new VLBI sources which are potential candidates to align the ICRF and the future GAIA frame. On average, these sources are 27 times weaker than the ICRF sources. Overall, this multiplies by a factor of 6 the current number of potential ICRF–GAIA link sources (awaiting for the potential candidates identified from the VCS catalogue). The excellent detection rate inferred from the observations may suggest that our initial VLBI detection step is unnecessary for such radio sources having an optical counterpart with magnitude brighter than 18. Future steps will be targeted at imaging the 398 sources that we have detected at both frequencies by using the global VLBI network (EVN+VLBA), in order to identify the most point-like sources and therefore the most suitable ones for the ICRF–GAIA link.

Acknowledgements

The authors wish to thank Dave Graham for assistance with the correlation in Bonn, John Gipson for advice when scheduling the observations, and Alexander Andrei for providing improved optical positions. This work has benefited from research funding from the European Community's sixth Framework Programme under RadioNet R113CT 2003 5058187. The EVN is a joint facility of European, Chinese, South African and other radio astronomy institutes funded by their national research councils.

References

[1] Ma, C., E. Arias, T. Eubanks, et al. A.J., v. 116, 516–546, 1998.

[2] Fey, A., C. Ma, E. Arias, et al. A.J., v. 127, 3587–3608, 2004.

[3] Perryman, M., K. de Boer, G. Gilmore, et al. Astron. Astrophys., v. 369, 339–363, 2001.

[4] Mignard, F. IAU 25 Joint Discussion 16, 133–140, 2003.

[5] Bourda, G., P. Charlot, J.-F. Le Campion. Submitted to Astron. Astrophys, 2008.

[6] Condon, J., W. Cotton, E. Greisen, et al. A.J., v. 115, 1693–1716, 1998.

[7] Véron-Cetty, M.-P., P. Véron. Astron. Astrophys., v. 455, 773–777, 2006.

[8] Frey, S., L. Gurvits, Z. Paragi, et al. Astron. Astrophys., v. 477, 781–787, 2008.

[9] Petrov, L., Y. Kovalev, E. Fomalont, et al. Submitted to A.J., 2008 (ArXiv:0801.3895).

[10] Myers, S., N. Jackson, I. Browne, et al. MNRAS, v. 341, 1–12, 2003.

The 5th IVS General Meeting Proceedings, 2008, p. 30–34

Astrometry of the Solar System Bodies with VLBI Radar

Igor Molotov [1], *Maria Nechaeva* [2], *Igor Falkovich* [3], *Alexander Konovalenko* [3], *Vladimir Agapov* [4], *Gino Tuccari* [5], *Giuseppe Pupillo* [6], *Stelio Montebugnoli* [5], *Gennadiy Kharlamov* [7], *Lance Benner* [8], *Viacheslav Fateev* [9], *Yuriy Burtsev* [9], *Alexander Volvach* [10], *Xiang Liu* [11], *Vasiliy Oreshko* [12], *Ivars Shmelds* [13], *Pietro Bolli* [5], *Alexander Dementiev* [2], *Alexander Antipenko* [2], *Nikolay Dugin* [2], *Vladimir Jazykov* [1], *Dmitriy Bezrukov* [13]

1) *Central Astronomical Observatory at Pulkovo, Russia*
2) *Radiophysical Research Institute, Russia*
3) *Institute of Radio Astronomy, Ukraine*
4) *Keldysh Institute of Applied Mathematics, Russia*
5) *Istituto di Radioastronomia, Italy*
6) *Osservatorio Astronomico di Torino, Italy*
7) *Special Research Bureau, Russia*
8) *Jet Propulsion Laboratory, USA*
9) *International Vimpel Corporation, Russia*
10) *Crimean Astrophysical Observatory, Ukraine*
11) *Urumqi Astronomical Observatory, China*
12) *Pushchino Radio Astronomy Observatory, Russia*
13) *Institute of Astronomy, Latvia*

Abstract. Three VLBI sessions of Low Frequency VLBI Network (LFVN) were carried out in 2006–2007 (VLBR06.1, VLBR07.1, VLBR07.2) having the main goal to adjust the application of the VLBI radar method for astrometry of the solar system bodies. The transmitter of Evpatoria RT-70 provided the radio sounding of planets, asteroids and space debris objects at 6-cm wavelengths. Also LFVN joined to the radar experiments of Goldstone RT-70 at 3.6 wavelengths for NEA during VLBR06.1 and VLBR07.1 sessions. The echo-signals were recorded by array of the radio telescopes in Russia, Ukraine, Italy, China and Latvia using NRTV, Mk5 and Mk2 terminals. The number of experimental results is presented in the paper.

1. Introduction

The project of the Low Frequency VLBI Network (LFVN) was started in 1996 in order to arrange the international VLBI cooperation with participation of former USSR radio telescopes [1]. One of the LFVN goals is developments of the VLBI radar (VLBR) for the investigations of the Solar system bodies. LFVN arranges VLBR experiments since 1999 with the help of the C-band transmitter of Evpatoria RT-70. The VLBR combines the radar sounding of space objects with a powerful transmitter and the receiving of radar echoes by an array of radio telescopes in VLBI mode. VLBR is a scientific instrument for 3-D measurements: the radar has the high resolution for range and radial velocity, and the VLBI provides the angle and angular rate. VLBR allows to measure the variations of proper rotation of the Earth group planets and determine the trajectories of planets and asteroids in the Radio Reference Frame. VLBR program of research of new promising space debris problem was started in 2001 [2]. The main tasks were the VLBI measurements of the Doppler shifts and fringe rates of echoes from the space debris objects and determination of the object rotation period and orientation of rotation axis, as well as the estimation of the objects size and their basic constructions [3].

The efforts of three LFVN sessions during 2006-2007 were concentrated on the adjustment of the VLBR method for the planets, asteroids, and small fragments of space debris in geostationary orbit. Also complimentary work was carried out, which included the development of an e–VLBI technique with dedicated Near-Real-Time-VLBI (NRTV) terminal, improvement of the correlation center of the Radiophysical Research Institute (RRI) in Nizhnij Novgorod, elaboration of the new data processing center of the International Vimpel Corporation in Moscow (for Mk5 format VLBI data) and testing of the Ventspils RT-32 in Latvia with new equipment (a new C-band receiver, feed-horn and digital BBC).

2. Observations and Results

VLBR06.1 (Jul. 3–9, 2006), VLBR07.1 (Jul. 28 – Aug. 3, 2007) and VLBR07.2 (Nov. 10–14, 2007) experiments were carried out with participations of Evpatoria RT-70 and Simeiz RT-22 in Ukraine, Kalyazin RT-64 and Zelenchuckskaya RT-32 (06.1) in Russia, Noto RT-32 and Medicina RT-32 (07.1 & 07.2) in Italy, Urumqi RT-25 (06.1 & 07.1) in China, and Ventspils RT-32 (07.2) in Latvia. Twice (06.1 & 07.1) JPL joined the asteroid radar experiments LFVN with the Goldstone RT-70 in USA at X-band. The recorded VLBI data was partially received on videocassettes and partially downloaded through Internet, converted into uniform format and processed at the RRI correlation center. Vimpel processing center was used for the primary autocorrelation of VLBR data and for Mk5 data extraction. In the course of the data processing the correlation of the transmitter signal model and the echo signal, obtained at each receiving point, was performed. Then a spectral analysis of the correlation

signal was done for further calculation of frequencies. The measurement of the frequency of the maximum spectral response allows to evaluate the Doppler frequency shift, conditioned by the object radial velocity.

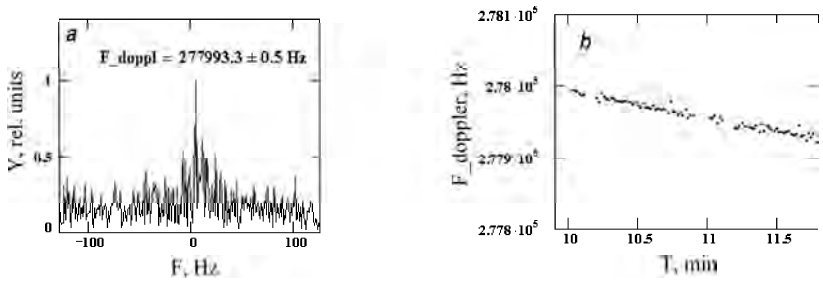

Figure 1. The cross-spectra of echo from Venus, received in Kalyazin RT-64 in 08:11:25 UT and the time dependence of Doppler shift frequency (Experiment VLBR07.1, Jul. 31, 2007, 08:10:00 UT)

One of the tasks of the VLBR sessions was research of the orbital parameters of Earth's group planets. During July 2007 Venus was at a comparatively small distance from the Earth (about 0.3 AU), that allowed to successfully implement the cross-correlation of transmitted signal of Evpatoria radar and received signal at station Evpatoria (the radio telescope in Evpatoria was switched to receive mode in the period ~ 5 minute before the end of each scan) and Kalyazin. The signal spectrum, obtained as a result of the correlation between Evpatoria transmitter signal and echo from Venus, obtained at Kalyazin is presented in Fig. 1a. The estimation of Doppler shift frequencies F_doppl was made in result of spectral analyses according to the frequency of main maximum of the spectrum. Fig. 1b shows the Doppler shift frequencies as a function time.

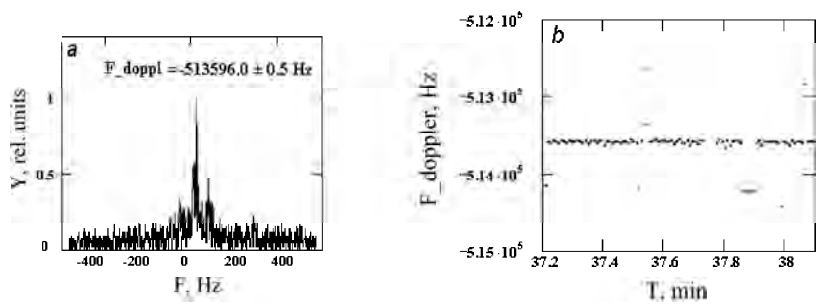

Figure 2. The cross-spectrum of echo from asteroid 2004XP14, received in Evpatoria RT-70 in 08:39:00 UT and the time dependence of Doppler shift frequency. The radar sounding provided with Goldstone RT-70 at X-band. (Experiment VLBR06.1, Jul. 3, 2007, 08:37 UT)

The successful radar detection of asteroid 2004 XP14 was carried out on Jul. 3, 2006, when the asteroid reached minimal distance to Earth (near 400000 km). The assumed diameter of the asteroid is 430 m. The radar of such large asteroid

on small distance did not carried out before. In session VLBR06.1 the radar sounding was provided in two frequency range: at 5010.024 MHz by Evpatoria RT-70 transmitter and at 8560.0 MHz by Goldstone RT-70 transmitter. The correlation and spectral analysis of data allowed to obtain the response from asteroids in both frequency ranges. The cross-correlation of model of transmitter signal and signal, reflected from asteroid, has been performed. The spectral response of Evpatoria on echo from asteroid at radar of Goldstone emission is on Fig. 2a. Evaluations of Doppler shift frequencies are carried out according main spectral maximum (Fig. 2b).

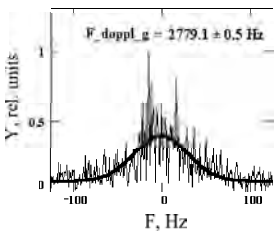

Figure 3. The cross-spectrum of echo from GEO object 95120, received in Noto (thin) and its approximation (solid). Experiment VLBR06, Jul. 6, 2006, 01:20:05.3 UT

Other goal of the sessions was improving of the measurement precision for the cases, when the spectra of space debris objects are widening up to hundreds of kilohertz. This effect is become especially apparent at large sizes and irregular shape of investigated objects and at radar of revolving objects. Besides, the main maximum may be essentially shifted from central frequency of spectrum (Fig. 3). To exclude the error in frequency Doppler shift determination, the procedure of spectrum approximation by Gauss function is applied. The solid line on Fig. 3 presents the Gaussian, which makes best fit the wide spectrum. The Doppler shift F_doppl_g, measured by frequency of Gaussian maximum, carries information about average radial velocity of space debris object.

Fig. 4 presents the time dependence of spectral maximum amplitude (Fig. 4a) and Doppler shift frequency (Fig. 4b) at radar of GEO debris fragment 95034 with size about 1 m. Analysis of temporal dynamics (Fig. 4a) of the frequency spectrum gives an additional possibility to obtain information on the general state of a spacecraft, including its rotation velocity, the presence of separate reflecting fragments on the object body, etc. Rotation period P for fragment 95034 is about 60 seconds. The Doppler shift frequency is linear dependence on Fig. 4b. The time intervals, where scattered signal is missed, may be excluded or changed by interpolated values. Fig. 5 demonstrates the results for GEO debris fragment 90032 with size about 50-cm that were discovered by International Scientific Optical Network (ISON) [3] in 2007.

3. Conclusions

The LFVN experiments of 2006-2007 provided a next step in the VLBR method development. The first VLBR results were obtained for the asteroid, Venus and the small space debris fragments. Also the procedure of spectrum approximation by Gauss function was proposed that allowed to improve the precision of Doppler shift and fringe rate frequency measurements. The pre-

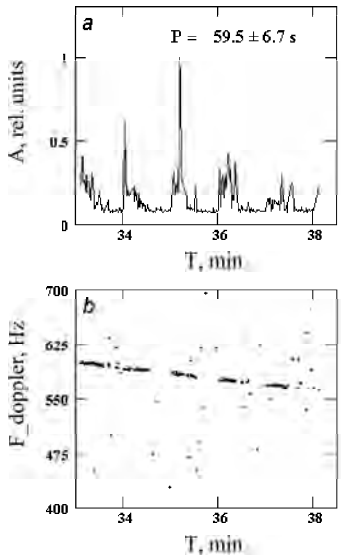

Figure 4. The time dependences of spectral maximum amplitude (a) and Doppler shift frequency (b), obtained from analysis of echo from fragment 95034, received in Urumqy. Experiment VLBR07.1, Aug. 4, 2007, 06:33 UT

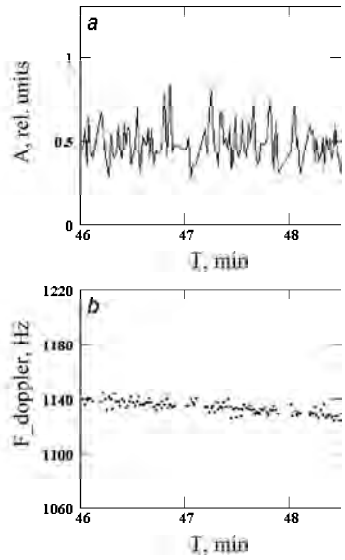

Figure 5. The time dependences of spectral maximum amplitude (a) and Doppler shift frequency (b), obtained from analysis of echo from object 90032, received in Kalyazin. Experiment VLBR07.1, Aug. 4, 2007, 02:46 UT

cise measurements of ephemeris of space debris fragments are important for the prognosis of the dangerous approaches with operational satellites. During VLBR08.1 (Sep. 3–12, 2008) it is planned to arrange the VLBR observations of the objects with high AMR recently discovered into international optical observing campaigns [3].

The authors thank the staff of radio telescopes for the participation in the experiments, ISON observatories for the ephemeris support, and JPL asteroid radar team for the collaboration.

References

[1] Molotov, I.E., S.F. Likhachev, A.A. Chuprikov, et al. Low Frequency VLBI Project. The Universe at Low Radio Frequencies, Proc. of IAU Symposium 199, Pune, India, 492–493, 2002.

[2] Molotov, I.E., M.B. Nechaeva, A.A. Konovalenko, et al. VLBI radar method development under LFVN project. Journal of the Central Astronomical Observatory in Pulkovo, v. 218, 402–414, 2006 (in Russian).

[3] Molotov, I.E., V. Agapov, V. Titenko, at al. International scientific optical network for space debris research. Advances in Space Research, v. 41, No 7, 1022–1028, 2008.

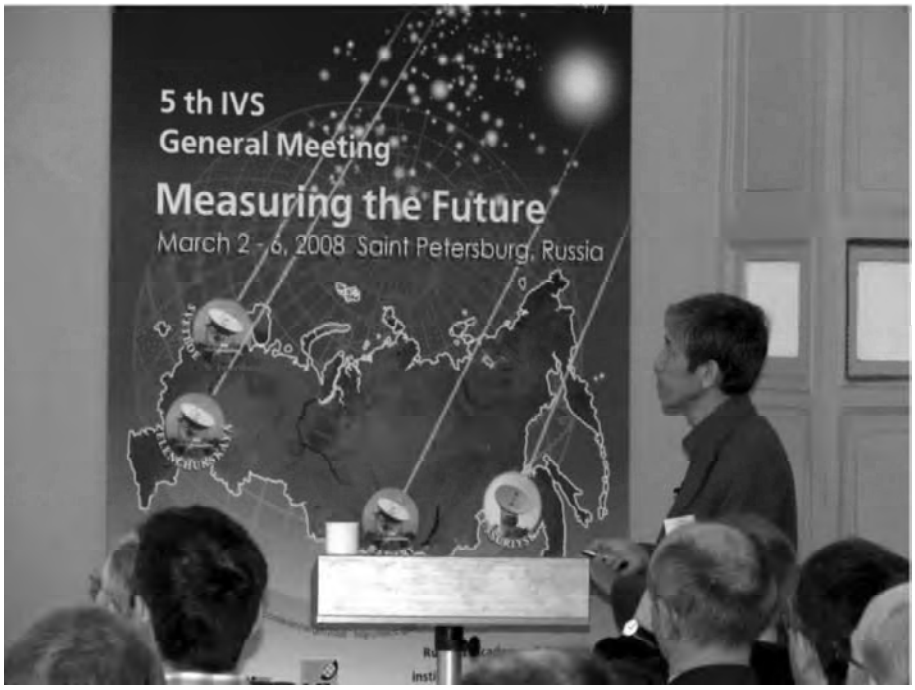
5 th IVS
General Meeting
Measuring the Future
March 2 - 6, 2008 Saint Petersburg, Russia

International VLBI Service for Geodesy and Astrometry
5 th IVS
General Meeting
Measuring the Future
March 2 - 6, 2008 Saint Petersburg, Russia

Part 2. Network Stations, Operation Centers, Correlators

The 5th IVS General Meeting Proceedings, 2008, p. 39–46

The Network "Quasar": 2008–2011

Andrey Finkelstein, Alexander Ipatov, Sergey Smolentsev

Institute of Applied Astronomy, Russian Academy of Sciences, Russia

Abstract. The paper gives the description of the current status of Russian VLBI Network "Quasar", geometry of the network and its equipment. Modern international and domestic observational programs are described in details. A brief review of upgrade and development of the VLBI Network "Quasar" up to 2011 year is presented.

1. "Quasar" — 2007

In 2005 three radio astronomical observatories of the VLBI Network "Quasar" were put into service (Fig. 1). As a result the three-element VLBI Network with baselines of about $2015 \times 4282 \times 4404$ km connected to the Control and Processing center in St. Petersburg was established (Fig. 1). The Network geometry was chosen to proceed from the requirements of astrometric and geodynamical problems to have equatorial and polar components of baselines and sufficiently large mutual visibility of radio sources with different declinations.

The basic element of the each observatory is a fully steerable 32-meter radio telescope. The antenna was designed on the basis of a modified Cassegrain scheme with a main quasi-parabolic reflector with focal length of about 11.4 meters and the secondary quasi-hyperbolic mirror of 4 meters in diameter. The asymmetric secondary mirror focuses the emission of radio sources aside of the main dish axis and the focal point draws the circle during the rotation of the secondary reflector. It is this circle on which the horns for different wavelengths are located. Fast transfer from one wavelength to another is performed by the rotation of the secondary mirror to a given angle.

The radio telescope drivers allow the antenna to rotate along elevation and azimuth angles with slow and fast rates. There are two types of antenna rotations: low-speed regime for guiding the objects and high-speed regime for antenna changeover with the rates of about of $1.6°/s$ and of $1.0°/s$ along elevation and azimuth angles respectively.

The sensitivity of the telescope is provided by a low-noise multi-wave receiving SHF-system which consists of 1.35, 6, 18–21, 3.5, and 13 centimeter double-channels (left and right polarizations) cryogenic radiometers (Tabl. 1),

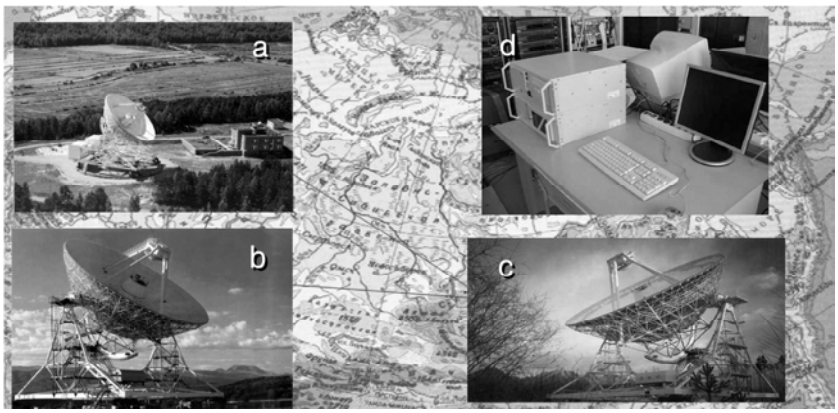

Figure 1. VLBI Network "Quasar" – 2007 (a — Observatory "Svetloe" ($\varphi = 60°32'$, $\lambda = 29°47'$, $h = 86$ m); b — Observatory "Zelenchukskaya" ($\varphi = 43°47'$, $\lambda = 41°34'$, $h = 1175$ m); c — Observatory "Badary" ($\varphi = 51°46'$, $\lambda = 102°$, $h = 813$ m), d — Correlator "MicroParsec" (Saint Petersburg))

Table 1. Parameters of the VLBI Network "Quasar" receivers

Wavelength, cm	Frequency band, GHz	T_r, K	T_{sys}, K	SEFD, Jy
21/18	1.38–1.72	8	43	240
13	2.15–2.50	10	48	330
6	4.60–5.10	8	27	140
3.5	8.18–9.08	11	34	200
1.35	22.02–22.52	20	80	710

the last two being used for joint reception in S/X range.

The time-keeping complex of each observatory is the unified system, which consists of a hydrogen maser with 3×10^{-15} stability for 1000 s time of averaging, site clock, and the GPS/GLONASS timing receivers for time synchronization with about 50 nanosecond accuracy. The synchronized SHF-local oscillators with 1.26, 2.02, 4.5, 8.08, 22.92 GHz as well as picoseconds impulses generator are included into the system.

The system of transforming, formatting, and receiving signal for radiometric and VLBI modes operates in the 100–1000 MHz basic range of intermediate frequencies. It permits to use the system with radio astronomical receivers of any type. The system consists of two main sub-systems of radiometric and VLBI units connected to the outputs of receivers by wideband coaxial link.

A radiometric unit allows to carry out radiometric observations in two frequency channels and two polarizations simultaneously [1]. This system is used for the Sun, galactic, and extragalactic radio sources observational programs [2–9].

Mark IV, VLBA4 and P1000 (developed by IAA [10]) data acquisition systems and the S2, Mark 4, Mark 5A, Mark 5B recording terminals are used for operation in VLBI-mode. This system is used for VLBI observations carried out according to both international and domestic astrometrical, geodynamical, and geodetic programs [11–16].

The observations, planning, testing and express analysis are accomplished by automatic control of facilities mentioned above. The program packages NASA SKED and NRAO SCHED are used for planning astrometrical and astrophysical VLBI programs, respectively. The program package IAA Sched Maker [17] is used for radiometric observations planning. The program systems NOVAS-C (USNO) and ERA (IAA) [18] are used for obtaining ephemeredes of Solar system bodies. Using these packages the control files are prepared and transmitted to main frame computer of each observatory where Mark IV Field System (FS) is installed. The special software is included in Mark IV FS for the control of radio telescope, time-keeping system, and DAS P1000.

There are two domestic programs: Ru-E — daily observations on the 3-baselines interferometer for determining all Earth orientation parameters, and Ru-U —observations of 8-hour duration for obtaining Universal Time. The 2-station correlator "MicroParsec" processes the VLBI observational data in S2 format transmitted from each station through the digital communication channels at 128 Mbps rate [19].

A brief review of upgrade and development of the VLBI Network "Quasar" up to 2011 year will be presented below.

2. "Quasar" — 2008–2009

In 2008 the VLBI Network "Quasar" will be upgraded to permit reliable 24-hours everyday operation. Fig. 2 shows the main features of the observatories hardware upgrade which has to be completed by the end of 2008. The main components of this upgrade are the following:

- Substitution of gear and pointing systems electronic (USUK "Salgir" is to be replaced by the USUK "Salgir-M") which allows to cut down the rack size, simplify power supply parameters (from 220 V and 400 Hz to 36 V and 50 Hz) and for increasing the system reliability.
- Upgrade of the frequency transformation block for receivers of S/X range on the basis of new generation chips, which improve amplitude-frequency characteristics and expanded dynamical range significantly.
- Replacement of the CH1-80 hydrogen maser by CH1-80 and CH1-75 ones to increase reliability characteristics and permits their remote control through the communication lines and Internet. It should be noted that the new generation hydrogen masers CH1-75 have higher stability (better then 10^{-15} for 24 hours) as compared with CH1-80 masers.
- Replacement of data acquisition systems DAS Mark 4, DAS VLBA4, and DAS P1000 to a digital DAS P1002 which consists of 16 absolutely

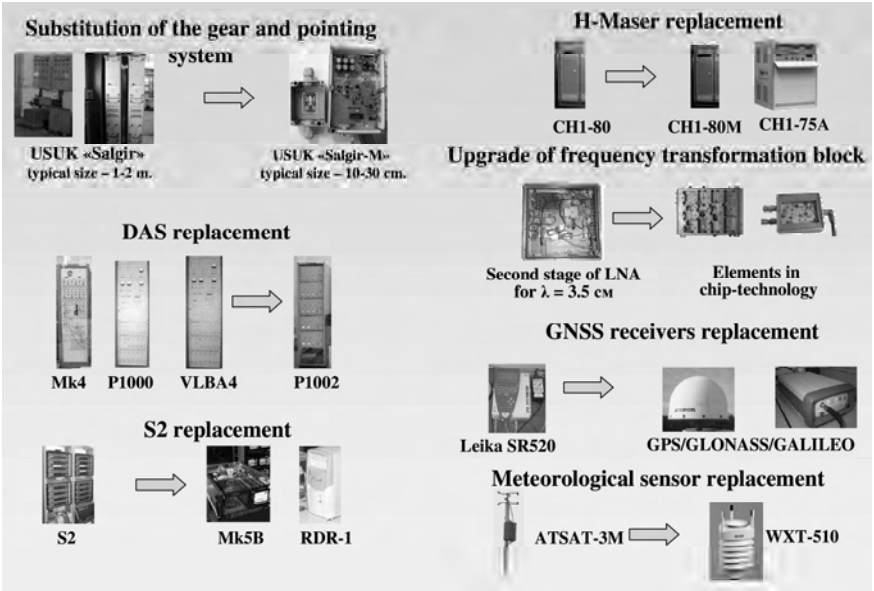

Figure 2. Upgrade and development of VLBI Network "Quasar"

identical frequency channels with high quality digital filters. This data acquisition system will be fully compatible with modern analog systems and makes it possible to over program the frequency bandwidths and keep phase-and-frequency channel characteristics.

- Replacement of S2 tape recorders to disk terminals Mark 5B and RDR-1 [20] recording signals in VSI-H and S2 modes correspondingly. Installation of the Mark 5B terminal makes it possible not only to record data flows on disks, but also to attach this device to the equipment required for e–VLBI mode of data transmission. The RDR-1 terminals will be used since 2009 in observation within the RADIOASTRON space mission.
- Replacement of geodetic GPS-receivers to three-system GPS/GLONASS/GALILEO receivers and Russian meteo-station ATSAT-3M to the more modern WXT-510.

In 2007 all observatories of the VLBI Network "Quasar" were linked by optical fiber lines (Fig. 3) to provide both e–VLBI mode for determining the Universal Time in intensive 1-hour sessions and real-time remote monitoring of each part of the Network. At present the observatories have data transmission channels to St. Petersburg at 2 Mbps rate. By the end of 2008 the observatories and the Control and Processing Center of the Network "Quasar" will be supplied by hardware and software providing VLBI data transmission rates of at least 100 Mbps.

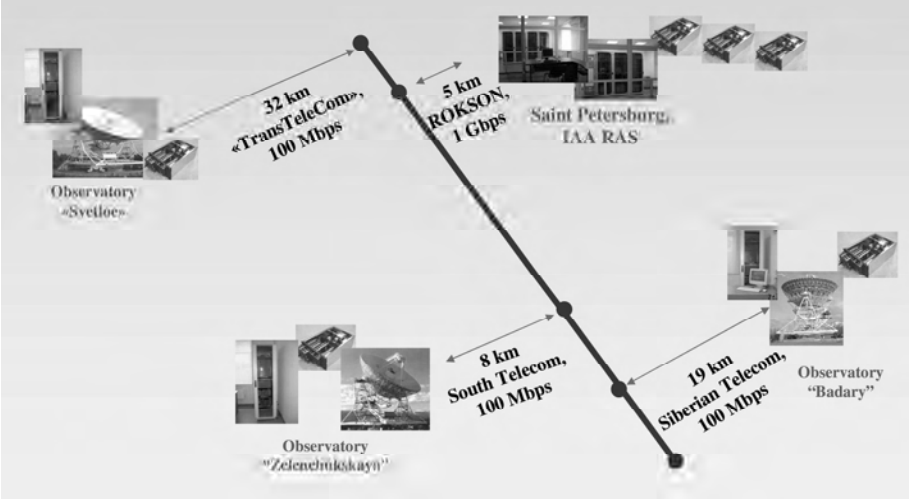

Figure 3. Optical Fiber Lines of VLBI Network "Quasar"

In 2008, IVS VLBI programs make use of Mark 5A and Mark 5B recording terminals. The domestic programs Ru-E and Ru-U are being carried out twice per month with S2 and Mark 5B terminals.

3. "Quasar" — 2009–2010

In 2009 the 6-station correlator ARC [21] will be put into action. It will provide processing data for 16 channels with 16 MHz bandwidth and two-byte sampling for each of 15 baselines. It will be used for processing once per week data of domestic Ru-E and Ru-U with Mark 5B terminals as well as data of IVS programs with Mark 5A and Mark 5B terminals.

At the same time Russian satellite laser ranging system "Sazhen-TM" will be mounted at the observatory "Svetloe" (Fig. 4). It makes possible to range satellites at 400–23000 km height. In 2010 the "Zelenchukskaya" and "Badary" observatories will be supplied by the same facilities. Co-location of VLBI with SLR and GPS/GLONASS/GALILEO facilities will decrease random and, what is the most important, systematic errors of determining Earth orientation parameters and dynamical celestial and terrestrial frames.

In 2010 two main problems will be solved:

- Mounting VLBI equipment on radio telescope RT-70 (Ussurijsk, Far East) with 70-meter dish and unification RT-70 (Fig. 5) with the Network "Quasar" for participation in astrometrical, geodetic, and deep space programs.
- Starting every day intensive sessions for UT-determination in e–VLBI mode.

Satellite heights	400–23000 km
Optical system diameter	25 cm
Laser pulse frequency	300 Hz
Pulse energy	2.5 mJ
Mass	120 kg
Normal points precision	1 cm
Angular precision	1–2”

Figure 4. Satellite Laser Ranging System “Sazhen-TM”

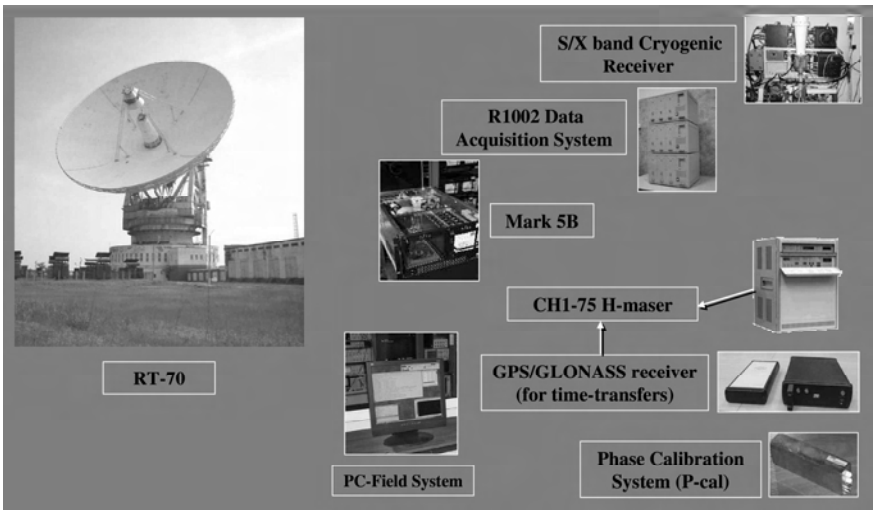

Figure 5. Upgrade of Radio Telescope RT-70 (Ussurijsk, Far East)

4. "Quasar" — 2011

Fig. 6 demonstrates the structure of the VLBI Network "Quasar" at the beginning of 2011.

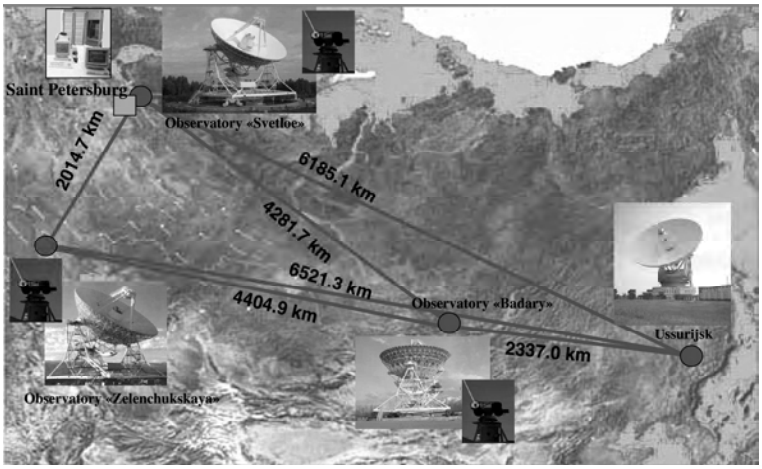

Figure 6. The VLBI Network "Quasar" — 2011

References

[1] Gornovesov, S., N. Kol'tsov, V. Tsarev. Digital system of measuring and recording radiometric signals. IAA RAS Transactions, v. 2. St. Petersburg, 1997, 11–123 (in Russian).

[2] Ahmedov, Sh., I. Ipatova, A. Ipatov, et al. Observations of the Solar Eclipse 11.08.1998 at the observatory "Svetloe". IAA RAS Transactions, v. 5. St. Petersburg, 2000, 5–14 (in Russian).

[3] Ivanov, V., I. Rahimov, S. Smolentsev, et al. Nonstability of radio luminosity of the remnant of supernova 1181 (3C 58). Astronomy Letters, v. 30, No 4, 240–246, 2004.

[4] Finkelstein, A.M., A.V. Ipatov, Yu.N. Gnedin, et al. Observations of Radio Emission from the Cosmic Gamma-Ray Burst GRB030329). Astronomy Letters, v. 30, No 6, 368–375, 2004.

[5] Finkelstein, A.M., A.V. Ipatov, M.A. Kharinov, et al. Supernovae and micro quasars: radio and infrared telescope observations of IAA RAS and CAO RAS. IAA RAS Transactions, v. 12. "Nauka", St. Petersburg, 2005, 36–52 (in Russian).

[6] Ivanov, V., Rahimov I., Smolentsev S., et al. 3C58 is the remnant of two supernovae explosions. IAA RAS Transactions, v. 12. "Nauka", St. Petersburg, 2005, 18–35 (in Russian).

[7] Ivanov, V., A. Ipatov, I. Rahimov, et al. Determination of the NIRFI flux-density scale for the current epoch. IAA RAS Transactions, v. 12. "Nauka", St. Petersburg, 2005, 12–17 (in Russian).

[8] Ivanov, V., A. Ipatov, I. Rahimov, et al. Calibration of radio sources with arcseconds angular size as a basis for modern radio astronomical flux scale. Preprint NIRFI, No 501. Nizhnij Novgorod, 2006, 16 p. (in Russian).

[9] Gnedin, Yu.N., A. Ipatov, M.Yu. Piotrovich, et al. Radio emission of the magnetar SGR 1806-20: evolution of the magnetic field in the region of the radio afterglow. Astronomy Reports, v. 51, No 10, 863–869, 2007.

[10] Fedotov, L.V., N.E. Kolstov. VLBI-terminals of the network "Quasar". IAA RAS Transactions, v. 17. "Nauka", St. Petersburg, 2007, 298–302 (in Russian).

[11] Finkelstein, A.M., V. Grachev, A. Ipatov, et al. The first results of VLBI observations at the Svetloe observatory in the framework of the IVS observing programs. Proceedings of Journees 2003 "Astrometry, Geodynamics and Solar System Dynamics: from Milliarcseconds to Microarcseconds". A. Finkelstein, N. Capitaine (eds.), St. Petersburg, 2003, 32–38.

[12] Finkelstein, A.M., A.V. Ipatov, S.G. Smolentsev, et al. Highly Accurate Determination of the Coordinates and the Earth's Rotation Parameters Involving the Svetloe VLBI Observatory. Astronomy Letters, v. 29, No 10, 667–673, 2003.

[13] Finkelstein, A.M., V. Grachev, A. Ipatov, et al. Some results of the first year of participation of the Svetloe observatory in IVS observing programs. IVS 2004 General Meeting Proceedings. NASA, GSFC, Ottawa, 2004, 128–132.

[14] Finkelstein, A.M., A.V. Ipatov, Z.M. Malkin, et al. Results of the First Two Years of VLBI Observations at the Svetloe Observatory within the Framework of International Geodynamical Programs, v. 32, No 2, 138–145, 2006.

[15] Finkelstein, A.M., E.A. Skurikhina, I.A. Rahimov, et al. CONT05 — preliminary results. IAA RAS Transactions, v. 14. "Nauka", St. Petersburg, 2006, 3–19 (in Russian).

[16] Finkelstein, A.M., E.A. Skurikhina, I.F. Surkis, Using the Quasar VLBI Network for the Fundamental Time-Positioning Service of GLONASS. Astronomy Letters, v. 34, No 1, 59–69, 2008.

[17] Kharinov, M.A. Software for scheduling single-dish observations Sched Maker v.2.06. IAA RAS Transactions, v. 15. "Nauka", St. Petersburg, 2006, 15–37 (in Russian).

[18] Krasinsky, G.A., M.V. Vasilyev. Universal programming system for ephemeris and dynamical astronomy. IAA RAS Transactions, v. 1. St. Petersburg, 1997, 228–248 (in Russian).

[19] Grachev, V.G., L.A. Kuptsov, I.F. Surkis. One board VLBI Correlator "MicroParsec". IAA Communications, v. 162. St. Petersburg, 2004, 22 p. (in Russian).

[20] Belousov, K.G., C.F. Likhachev. Digital processing of "RADIOASTRON" space mission data. Preprint PHIAN, No 34. Moscow, 2000, 16 p. (in Russian).

[21] Surkis, I., V. Zimovsky, A. Melnikov, et al. The IAA RAS 6-station VLBI correlator. This volume.

The 5th IVS General Meeting Proceedings, 2008, p. 47–52

Equipment Failures, Chronic Station Problems, and RFI: Their Effects on Geodetic VLBI Data

Kerry Kingham, David Hall

U.S. Naval Observatory, USA

Abstract. In the course of processing routine IVS sessions, several common station problems reoccur. Missing channels, spurious signals, and radio frequency interference (RFI) all make correlation a challenge. We present some of these problems as they are seen at the correlator, point out their deleterious effects on the integrity of the observations, and suggest mitigation actions.

1. Introduction

In the last few years, there has been an increase in problems at network stations that directly affect the IVS products. Most of these problems directly affect the basic observable of group delay through the contamination of the bandwidth–synthesis observables or calibrations.

2. Missing Channels in Frequency Bandwidth Synthesis

One of the most serious problems in geodetic VLBI is channels deleted due to RFI or signal path problems. While dropping one channel is not a large problem, it is an issue when two stations have different missing channels, the delay resolution function now suffers from two lost channels and the effects can be more severe.

Fig. 1 shows the response in delay space of the the R4 S-Band frequency sequence. This sequence is typical of the frequencies used in geodetic VLBI sessions. Fig. 2 shows the result of losing the top three frequencies (1/2 the total). The increased amplitude of the sub–ambiguity side–lobes make it much more likely that the delay solution will find a sub-ambiguity. This will occur if only one of the upper two frequencies is lost. The correlator processing can be tuned to remove sub-ambiguities from the final export, but there is a practical limit on the time resolution that can be applied. In the extreme case, the baseline might have to be deleted. Note also that the delay resolution is half that of the all–channels case.

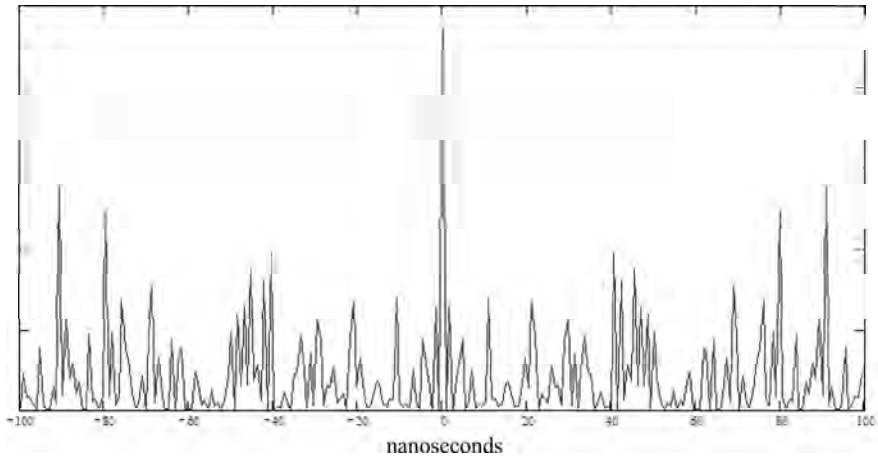

Figure 1. Delay resolution function with all S–Band channels present. The largest side–lobes at +/− 80 and +/− 90 ns are less than 60% of the main–lobe. The first ambiguity is at +/− 200 ns

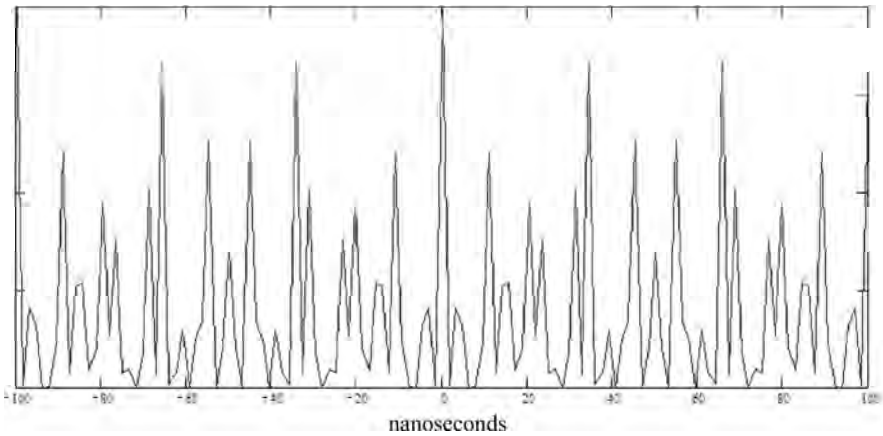

Figure 2. Delay resolution function with only the lowest 3 S–Band channels present. The first ambiguity is at +/−100 ns and the side–lobes are nearly 90% of the strength of the main–lobe

3. Spurious Signals

One of the most common problems with observations is spurious signals internal to the data acquisition rack that make it into the recorded data. It is particularly bad if these signals coincide with the phase calibration tones.

A spurious signal at a phase-cal frequency, locked to the maser (as are most of the rack–generated signals), will have a fixed phase at phase–cal extraction. The phase calibration tones will usually vary over 360° as the signal path changes over the course of an observing session. The resultant vector sum of the the two signals at different phase-cal phases is shown in Fig. 3. Note that the *amplitude* also changes with the phase–cal rotation. This results in a sine wave when the amplitude of the phase–cal signal is plotted by phase. In the left plot in Fig. 4, the case where there is no spurious signal, the amplitude is constant regardless of phase, but in the center plot of Fig. 4, there is the signature sine wave indicating a spurious tone at the phase–cal frequency. If the spurious signal is greater than −13 dB with respect to the phase cal tone, then an error in the phase cal of more than 1° of phase in that channel will result.

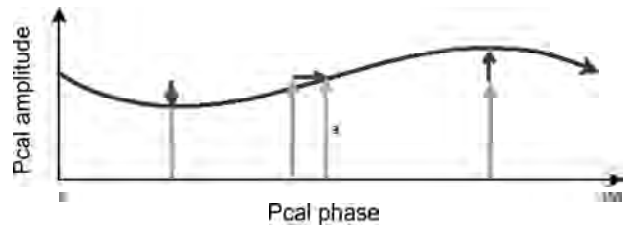

Figure 3. Vector diagram showing interaction between the phase–cal vector (big), and a spurious signal (small). Both the phase (displaced vector "a") and amplitude (sine curve) are affected

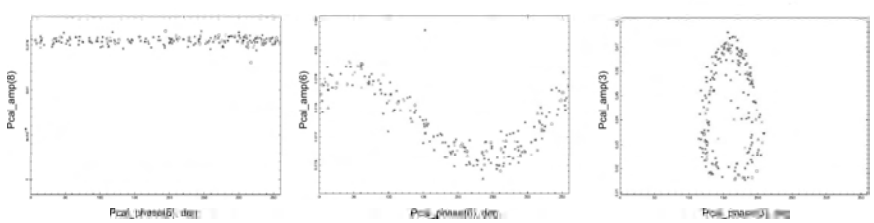

Figure 4. Three plots of amplitude versus phase for phase–cal with no spurious signals (left); a strong spurious signal (center); and a puzzling case discussed in the text (right). The center plot corresponds to the plot in Fig. 3

A rare case is shown in the right plot in Fig. 4. While initially puzzling, the diagram of Fig. 5 explains the plot. The spurious signal is stronger than the phase–cal tone, about twice the power. In this case manual phase–cal must be used.

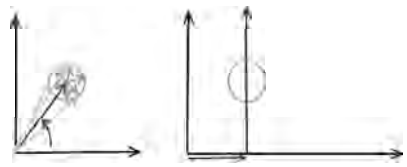

Figure 5. Vector diagram explaining the right plot in Fig. 4. In the left plot, the (dark) spurious signal, which is locked to the maser and does not rotate is stronger than the phase–cal (small and light vectors) which is rotating through 360°

4. External Radio Frequency Interference (RFI)

External Radio Frequency Interference (RFI), for our purposes, is defined as unwanted signals that are generated outside the Data Acquisition System and are not locked to the maser. These signals usually do not show up at phase cal tone frequencies. They are usually detected as low amplitude channels. This effect is shown in Fig. 6. Notice that channel "d" has a low cross–correlation amplitude and the phase has more scatter than the other channels. Low amplitude can be a diagnostic of a strong, unwanted signal in the channel. Often with external RFI, this effect can be time and/or direction dependent. Fig. 7 shows the same baseline a few minutes later. Note that the amplitude is close to average and the phase aligns with the other channels.

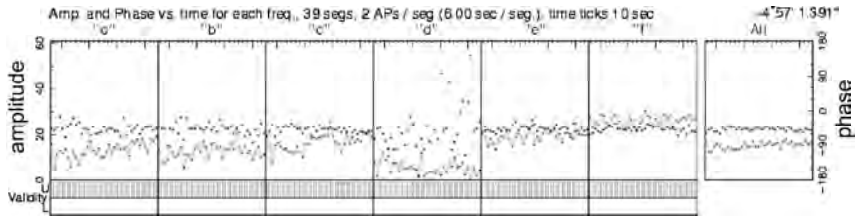

Figure 6. RFI in channel "d",which has low amplitude (line) and noisier phase (dots)

Fig. 8 shows autocorrelations of the channel bandwidth. The first plot has no RFI, the second plot is from the scan where the channel has below average amplitude and indeterminate phase. The third plot is from the second time period when the RFI did not appear serious, the interfering signal is weaker and has a different frequency.

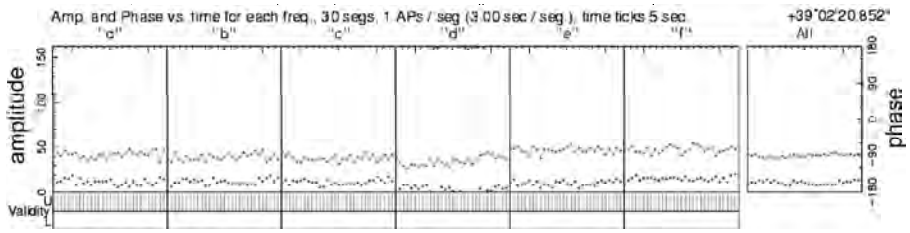

Figure 7. Same baseline and session as Fig. 6 a few minutes later. RFI is reduced

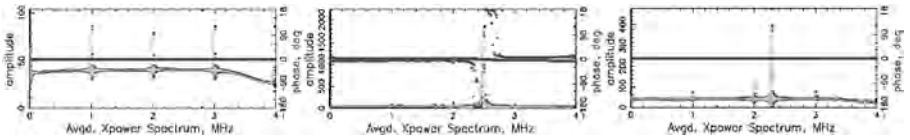

Figure 8. Three plots of Channel "d". The left plot has no RFI at all, with phase–cal tones every MHz. Middle plot is from the time period of Fig. 6, there is a signal at approximately 2.5 MHz. Right plot shows that during the time of Fig. 7 there still was a signal in the channel, but it has a lower amplitude and a shift in frequency

5. Very External RFI

The final category of interfering signal that we will consider in this paper is a very external Until recently, external sources of interference to the S-band & X-band regions used by geodetic VLBI were very rare. That situation is now changing. New services are filling the spectrum with signals. One of the worst, from the geodetic VLBI point of view, is the Direct Digital Audio Satellite service. Over North America, these services, called "XM" and "Sirius" have satellites that beam powerful S-Band signals directly at the radio telescopes. If the geodetic frequency sequence has a channel that includes a signal from these satellites, it makes the channel unusable. Examples of these signals, an out–of–passband and an in–passband example, are shown in Fig. 9. These strong, disrupting signals are also seen at Ny–Ålesund (Norway), Fortaleza (Brazil) and Kokee Park (Hawaii).

6. Discussion

None of the problems presented in this paper are new, although with the increase in recorded bandwidth over the last few years, there is more opportunity for interference to be a serious problem. There is no single solution. Stations need to be instructed in tracking down and eliminating internal spurious signals in the rack. The Technical Operations Workshops (TOW) are a good venue for this, but the station sponsors must be urged to send station

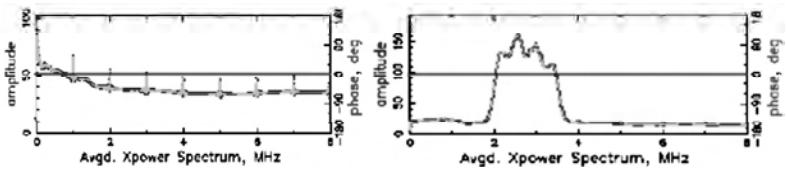

Figure 9. Autocorrelation plots of two S-Band channels. On the left, the XM signal is just off the lower edge in frequency than the passband of the channel leading to reduced phase–cal amplitudes and distorted continuum. On the right, the XM signal dominates the channel

personnel. The major external RFI sources must be mapped at each station so that rational decisions can be made concerning frequency sequences. And finally, schedulers may have to tailor frequency sequences flexibly, depending on which stations are in a session.

Acknowledgements

We would like to thank the staff of the other Mark 4 correlators for discussions about common problems, particularly Arno Müskens and Alessandra Bertarini at Bonn and Mike Titus and Brian Corey at Haystack. Brian Corey has written several memos that, put together, are a great resource in figuring out exactly what is going on with a station for a given correlator output.

The 5th IVS General Meeting Proceedings, 2008, p. 53–62

Effects on the Geodetic-VLBI Observables Due to Polarization Leakage in the Receivers

Alessandra Bertarini [1], *Walter Alef* [2], *Brian Corey* [3], *Axel Nothnagel* [1], *Craig Walker* [4]

[1] *Institute of Geodesy and Geoinformation, Bonn University, Germany*

[2] *Max Planck Institute for Radio Astronomy, Germany*

[3] *MIT Haystack Observatory, USA*

[4] *National Radio Astronomy Observatory, USA*

Abstract. Polarization leakage is one of the instrumental errors that decreases the precision of the geodetic and astrometric measurements. Its effect can be corrected in the data provided one knows the leakage characteristics. In this paper we present a project to measure the polarization leakage at some geodetic VLBI stations and at the VLBA. We describe the observation strategy used to measure the leakage, the correlation process, and some preliminary results.

1. Introduction

Polarization leakage is one of the biggest of the instrumental error sources remaining in the determination of multi-band delay (MBD) and hence in the determination of geodetic and astrometric parameters such as baseline length, Earth orientation parameters, and source positions. Leakage occurs primarily due to the electrical properties and shape of the polarizer and varies with frequency. Under certain assumptions about feed performance, Rogers [1] estimates a MBD error from polarization leakage of order 14 ps. An error term this large dominates the total error from all instrumental sources [1]. Typical MBD errors from leakage are expected to be smaller than 14 ps, and indeed the few values measured to date are typically in the range 2–9 ps at 8.4 GHz (X-band) [2]. Even at this level, the leakage error is still a major contributor, if not the dominant one, to the total instrumental error in geodetic VLBI. By solving for the intrinsic source polarization during data analysis, the rss error should further improve as reported by Rogers [1].

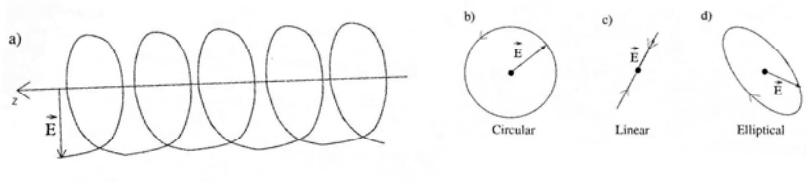

Figure 1. (a): cartoon of the electric field component of a plane monochromatic electromagnetic wave propagating along the z direction. Panels (b), (c) and (d): movement of the tip of the electric vector and representing respectively circular (b), linear (c) and elliptical (d) polarization states achieved by adjusting the phase difference between the x and y components of the wave. Taken from [5]

2. Background

2.1. Concept of Polarization

In free space, far enough from the source of the emitted radiation, an electromagnetic wave can be described as a plane propagating wave. Fig. 1a represents the projection onto two perpendicular axes, x and y, of the electric field component of a plane monochromatic electromagnetic wave propagating along the z direction.

If we consider the motion of the tip of the electric vector with time at a fixed position in space we see that the tip of $\vec{E}$ can describe a circle (Fig. 1b), a line (Fig. 1c), or an ellipse (Fig. 1d). More generally the orientation of the electric vector will change randomly with time and in this case the wave is unpolarized.

The radiation from radio astronomical sources is found to be either unpolarized or only weakly linearly polarized, which means that the radiation has either no statistical tendency or only weak statistical tendency to favour one of the two polarization states and, further, that its phase is random from one instant of time to the next.

2.2. Polarizers and Their Effects on the Geodetic Observables

VLBI, like most forms of interferometry, needs to preserve both the phase and the amplitude of the incoming radiation to perform a measurement [3]. In VLBI, the sky signal is typically collected by coupling the radiation into a waveguide through which both orthogonal polarization states can propagate. Radiation is coupled out of the waveguide into coaxial cables using electric dipole antennas, which respond to linear polarization [4]. The generally unpolarized incoming radiation (see 2.1) is a mixture of two incoherent polarization states. To maximize the signal-to-noise ratio (SNR) in the cross correlation between two antennas, one would like both antennas to select the same two

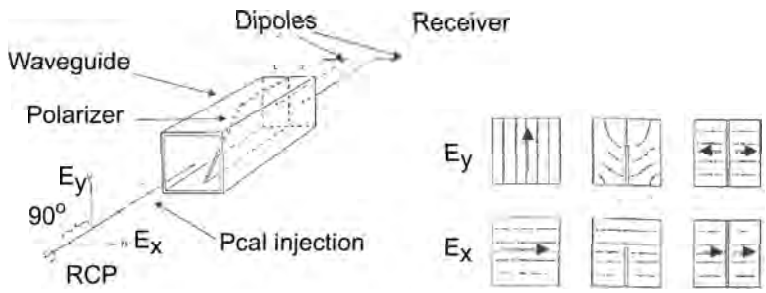

Figure 2. Left: schematic diagram of a septum polarizer. Right: the field pattern in cross section across the septum polarizer at the input, half way and at the output. Courtesy of S. Srikanth

polarization states out of the mixture. To make the selection one uses a device called a polarizer. In VLBI it is convenient to use circular polarization (CP) instead of linear polarization because the Earth is round, so antennas on different continents must point with different parallactic angles (that is the angle between the line joining the source to the north celestial pole and the line joining the source to the zenith at the antenna) and so linear feeds will not remain parallel throughout the array (unless the feeds can be rotated axially). Instead, using CP, the parallactic angle difference introduces simply a phase rotation of the fringe visibility, which can be removed in the post-correlation data analysis.

Here we describe one among the various kinds of polarizers in use in VLBI: the septum polarizer. We will, for simplicity, consider the incoming radiation as pure right circular polarization (RCP), thus having the same amplitude in the x and y directions and a 90° phase shift between the x and the y component of the wave. The wave encounters the septum polarizer, which contains a metal fin within the waveguide as shown in Fig. 2. The component of the electric field perpendicular to the fin (E_x) is divided, due to the boundary conditions on the conducting fin, in two electric field regions which have the same intensity and orientation as E_x. The component of the electric field parallel to the fin (E_y) is divided, due to the boundary conditions on the conducting fin, in two electric field regions which have the same intensity as E_y but the orientations are rotated into the horizontal plane in the clockwise direction in one region and in the counterclockwise direction in the other region. The phase velocities of the E_x and E_y components differ from each other while propagating from the polarizer input to the dipole because the septum divides the waveguide into regions that have different dimensions in the x and y directions (x is halved, y remains the same). These dimensions and the length of the septum are chosen to introduce a 90° phase shift between the E_x and E_y components. When those

fields (i.e. E_x and the rotated E_y fields with 90° phase shift) superimpose at the dipoles, they interfere constructively at one dipole and destructively at the other dipole. This logic can be repeated for pure left-circular polarization (LCP) and the output power will appear at the other dipole. The general case is a mixture of RCP and LCP input, which will be separated to produce outputs on both dipoles. In the real case, a band of frequencies is observed and the theoretical phase difference inserted by the polarizer between the two linear polarizations measured at one dipole output is an accurate 90° only at two frequencies. In this broad-band case, the septum polarizer will not separate the two polarization with perfect purity at most frequencies and some contamination from the unwanted polarization will add algebraically to the signal.

The effect of leakage is to perturb the visibility phase in one polarization with a small amount of signal leaking from the other polarization. The leakage and hence the phase perturbation is frequency dependent and so perturbs the delay and will not close around a triangle of baselines [8, 9].

2.3. Past Studies

That polarization leakage affects the VLBI measurements has been known for more than a decade and both the geodetic and astronomical communities have conducted some studies to either estimate or quantify the contamination of the observables due to the polarization leakage. Rogers [1] adopted a nominal value for polarization leakage of −15 dB (corresponding to a leakage of about 3% of the power from one polarization into the other) and estimated from it, for unpolarized radio sources, a MBD error of the order of 14 ps (4.2 mm) or less and for 10% polarized radio sources typically an extra 8 ps (2.4 mm) error assuming that the polarization leakage introduces a phase gradient over 360 MHz bandwidth. Corey & Titus [2] found that the VLBA antennas polarization leakage is less than −20 dB at 2.3 GHz (S-band) and 8.4 GHz (X-band), so the leakage is less than 1% of the power from one polarization into the other, and estimated from that a maximum of 1.0 ps (0.3 mm) MBD error at X-band and a maximum of 2.2 ps (0.7 mm) MBD error at S-band. At the geodetic sites, Corey & Titus [2] measured the polarization leakage to be typically greater than −20 dB, leading to MBD errors between 2 ps (0.6 mm) and 9 ps (2.7 mm) at X-band.

The variation of leakage amplitude with frequency has been measured for the European VLBI Network antennas by Massi et al. [9]. This amplitude change causes lower dynamic range (peak to rms ratio) in images made using these antennas compared to images made using the VLBA antennas.

The need for new measurements arose because in the previous studies only approximate values were established: the calibrators were assumed to be unpolarized, the sources were not imaged, the bandwidth spanned for the geodetic antennas was only 360 MHz of the 720 MHz available at X-band [2], and some stations upgraded the receivers since those measurements were made.

3. The New Project

In our study we assume that the observed sources can be polarized, therefore we will image them to determine the source structure and intrinsic polarization simultaneously with the leakage determination. We spanned the so called geodetic wide band that is from 8212 MHz to 8932 MHz at X-band and from 2225 MHZ to 2365 MHz at S-band. We will also measure the polarization leakage every 8 MHz for better interpolation of the leakage vectors across the whole bands and in case the geodetic frequency sequence is changed in the future. This study could be considered as a pilot project to establish the procedure for high quality measurements and corrections of the leakage. It is based upon a subset of antennas and later could be expanded to the whole geodetic network.

3.1. Strategy

Leakage is detected by the following procedure. In the absence of leakage the signals received in the LCP channel and RCP channel are uncorrelated gaussian noise processes and cross correlation between them will yield no coherence. If leakage is present then some of the signal in one polarization channel will add to the signal in the other polarization channel. By cross-correlating the contaminated RCP channel at one antenna and the contaminated LCP channel at the other antenna one will find coherence caused by the LCP in the LCP channel correlating against the LCP that leaked into the RCP channel. Geodetic stations mostly have only RCP, but measurements of the leakage for these stations are still possible if the antenna at the other end of the baseline has dual-polarization receivers. Therefore, we used the 10 VLBA antennas for their dual polarization capability plus 10 geodetic antennas. Correlation was performed between all possible combination of polarization (i.e. RCP against RCP, LCP against LCP, RCP against LCP and LCP against RCP). Data reduction is proceeding using AIPS (Astronomical Image Processing System), which is one of the most widely used interferometric data reduction packages for radio astronomy. In AIPS we measure the terms that represent the leakage, which in jargon are called D-terms ([5, 6]). Once the D-terms are available we will modify the post-correlator software to use the D-terms to correct the effects of the leakage and will perform validation tests.

3.2. Scheduling

To cover from 8212 MHz to 8932 MHz completely requires 720 MHz divided into 8 MHz per VC/BBC sideband, i.e. 15 setups observing three frequencies in X-band and one frequency in S-band simultaneously.

The production of the schedule file was made quite complicated by some tuning and patching constraints at both the VLBA and geodetic antennas. Whilst the geodetic stations have 14 video converters (VC), the VLBA antennas are limited to eight baseband converters (BBC) and we have paired those to

get both hands of polarization. Instead of using only four VCs at the geodetic stations, since they can observe only RCP, we used all 14 for simplicity of scheduling, providing redundant frequency coverage as backup in the case of a VC problem, though with the risk of increased crosstalk between VCs when many are set to the same local oscillator (LO) setting. The dichroic mirror that enables simultaneous S-band and X-band observing at the VLBA stations remains deployed only when at least one BBC is tuned to X-band and at least one BBC is tuned to S-band. Thus, we needed to observe with at least one BBC in each band at all times. The Mark IV data acquisition racks have three intermediate frequency (IF) inputs, each with their own band-limiting filters [12] that leave a gap between 8580 MHz and 8680 MHz that cannot be observed. To ease the work at the Mark IV stations we kept the standard geodetic patching, reducing the probability of false patching and consequent loss of one or more frequency setups, though increasing the complexity of the scheduling as described above.

We had 24 h of observing time on the IVS and VLBA antennas. We observed the first 12 h at 512 Mbps with 2 bit sampling switching among the 15 frequency setups. The second 12 h were observed using the rapid (R1) frequencies at 256 Mbps, 1 bit sampling switching among four frequency setups.

Target sources were OQ 208 and 3C 84 as they are known to be nearly unpolarized. We observed also some backup sources for calculating the polarization leakage and as calibrators.

3.3. Correlation

Correlation of the experiment started in October 2007 using the Bonn MPIfR/BKG Mark IV correlator and produced fringes to all the VLBA antennas except Hancock, which was down during the observation, and to most of the geodetic antennas. Unfortunately we lost Ny Alesund, due to manpower limitations and Kokee Park and Fortaleza due to technical reasons. Since the correlator has eight Mark 5A playback units and we had a total of 16 stations, we ran the correlation in six passes to form all the baselines. In December 2007 we fringe fitted and checked the quality of the data using the HOPS (Haystack Observatory Postprocessing System) package and found that most setups yielded good quality data but some were degraded by RFI, especially in S-band. One setup might require recorrelation due to a problem encountered in fringe fitting the data.

3.4. Data Reduction

Data reduction in AIPS started in January 2008. We reduced the data for the first frequency setup in S-band (i.e. 2225 MHz). The results are still preliminary and the setup will soon be reprocessed to understand some unresolved issues. For clarity we will present the data reduction step by step.

The data were imported into AIPS and a priori amplitude calibration was

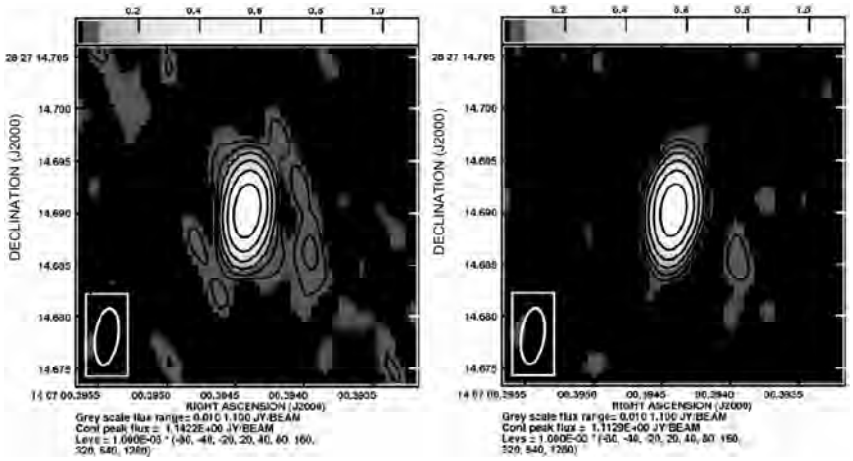

Figure 3. Image of OQ 208 at 2225 MHz with the VLBA and geodetic array with phase self calibration (left) and after amplitude self calibration (right)

performed based on the system temperature (T_{SYS}) and antenna sensitivity measured at the stations. The conversion factor between correlator amplitude and flux density in Jy is derived from T_{SYS} measurements in each polarization and the knowledge of the sensitivity of the antennas, possibly as a function of elevation for each polarization. The a priori amplitude calibration contained large systematic errors because the purely geodetic stations did not provide the elevation-dependent gain curves and many did not provide the system equivalent flux density (SEFD) and its variation with frequency. The remaining amplitude calibration errors could be corrected later by applying amplitude self calibration after imaging the source.

After a priori amplitude calibration we performed phase, delay and delay-rate calibration by fringe fitting the parallel hands of polarization (RCP-RCP and LCP-LCP) in AIPS.

The AIPS fringe fit algorithm is global, i.e. it uses constraints from all baselines to an antenna when determining a delay solution for that antenna and potentially gives better SNR compared to the baseline-based fringe fit algorithm used by HOPS.

After fringe fitting, we applied bandpass calibration for compensating the gain variation with frequency and to enable extraction of more than one leakage term within the 8 MHz bandwidth per BBC/VC.

To reduce further the calibration errors in phase and amplitude, we iteratively improved our model of the sky brightness distribution using self calibration [10]. Fig. 3 shows the before-and-after images after two cycles of phase self calibration and one of amplitude self calibration. The artifacts in the image were reduced by the improvement in the amplitude calibration.

At this point the total intensity calibration was complete and the polariza-

tion calibration began. The first step was to correct the delay offset between the two opposite hands of polarization due to differences in the electronic path length before calculating the leakage. The cross-hand (RCP-LCP and LCP-RCP) delay offset following the parallel hand fringe fit is the same for all the antennas since much of the antenna-based delay differences gets absorbed into the parallel hands delay solutions. Thus cross-hand fringe fit was performed between only two VLBA antennas. The cross-hand delays and phases were averaged to improve SNR, allowing for their sign inversion when the polarizations are swapped [13]. This procedure ties the RCP and LCP channels at all antennas, including the geodetic antennas although they have no LCP channels.

The derivation of leakage proceeded as follows. If the source is polarized, the LCP-RCP (and RCP-LCP) cross correlations are non zero. The RCP-LCP and LCP-RCP cross correlations contain also a contribution due to leakage between the polarization channels. The two contributions can be separated since the LCP-RCP phase due to source polarization rotates with the parallactic angle whereas the LCP-RCP phase due to leakage remains constant throughout an observation (and over much larger periods) [5]. This principle is illustrated in Fig. 4, which shows the LCP-RCP cross correlation real and imaginary components for OQ 208 throughout the observation. The data were corrected for the parallactic angle, which means that the visibility phases were rotated according to the parallactic angle, causing the LCP-RCP phase due to source polarization to remain constant and the LCP-RCP phase due to the leakage to rotate. Since OQ 208 is unpolarized, we see the rotating leakage vector centered at zero in the real/imaginary plane as shown in the left most two panels of Fig. 4. After deriving the D-terms and correcting the data for their effect, the leakage disappears as shown in the right most two panels of Fig. 4.

The amplitude of the leakage term in this first setup was found to vary from -40 dB (1% of voltage leakage of one polarization into the other) at Wettzell to -15 dB (17% of voltage leakage) at Westford. We checked with the HOPS package whether we could detect the signal produced by the leakage in the cross-correlation of the left circular feed at one VLBA antenna and the right circular feed at the Westford antenna and indeed had a detection.

The large leakage values derived above need not yet be of concern, since this analysis represents only one channel that lies at extreme edge of the band where the worst leakage is expected. The concern for the geodesist lies in the variation with frequency of both the phase and amplitude of the leakage. Additionally, geodesy is interested in the leakage correction to the parallel hands (i.e. RCP-RCP) whilst astronomy is not, since the contribution is small enough to be ignored for continuum imaging purposes. AIPS does not perform the parallel-hand correction, therefore we had to calculate it ourselves. We found that the leakage causes a difference in amplitude, ΔA, of 0.016 Jy and a difference in phase, $\Delta\phi$, of 1° for the baseline Pie-Town - Westford and source OQ 208 with 1.33 Jy in the the S-band channel we analyzed. If phase is constant across the 140 MHz band, then $\Delta\phi = 0$ and so $\Delta\tau = 0$, i.e. no change in delay would be

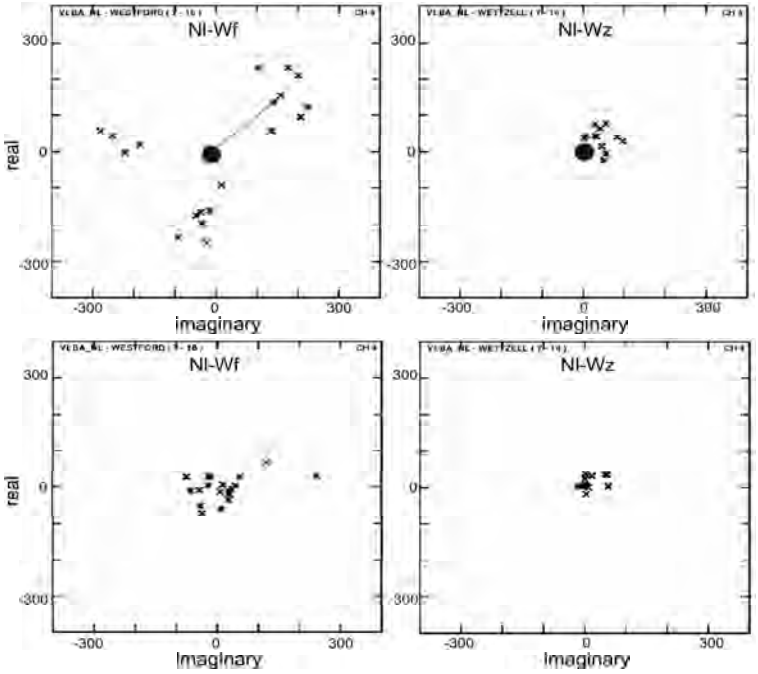

Figure 4. LCP-RCP visibility on the unpolarized source OQ 208 plotted in the imaginary vs real plane for the baseline North Liberty - Westford (first and third panels) and the baseline North Liberty - Wettzell (second and fourth panels). Visibilities are shown before (first and second panels) and after (third and fourth panel) the corrections for the instrumental polarization were applied. The big dot at the center of the images in the first and second panels is the origin of the axes and the crosses are the measured visibilities, which are seen to rotate due to the leakage vector. For clarity one of the vectors has been drawn in full for the baseline North Liberty - Westford. Third and fourth panels: same as first and second panels, but after having the D-term correction applied. The residual leakage vector has almost zero amplitude

caused by the polarization leakage. From the previous studies we know that this is not the case and if we assume a change of visibility phase of 2° across 140 MHz at S-band, then we have a change in delay of 37 ps (11 mm).

The data reduction for the other 14 frequency setups observed in the first 12 h and four setups observed in the second 12 h will lead to the measurement of the rate of change of the leakage phase across the bands.

The change of the leakage phase across the bands is not expected to change with time. Gomez et al. [11] found the leakage to be stable over a period of 1.3 years. Further, data from some VLBA monitoring programmes suggest that the leakages do not change much, unless station hardware is changed [11].

4. Summary

The polarization leakage is one of the major instrumental sources of error, is unavoidable and is frequency dependent since it occurs due to the electrical properties and shape of the polarizer. It cannot be absorbed in the clock model since it is baseline based and therefore it contaminates the delay measurements. The correction will yield a better accuracy of the delay observables and, thus, of the geodetic and astrometric parameters.

Acknowledgements

We thank Alan Roy for helping throughout the proposal, scheduling and data reduction.

References

[1] Rogers, A.E.E. Instrumentation Improvements to Achieve Millimeter Accuracy. Proceedings of the AGU Chapman Conference on Geodetic VLBI: Monitoring Global Change, NOAA Technical Report NOS 137, NGS 49, 1–6.

[2] Corey, B., M. Titus. Antenna Cross-Polarization Characteristics at Geodetic VLBI Stations. 4th IVS General Meeting Proceedings. Behrend, D. and Baver, K.D. (eds.), 2006.

[3] Thompson, A.R., J.M. Moran, G.W. Swenson. Interferometry and Synthesis in Radio Astronomy. John Wiley & Sons, Inc. (eds.), 2001.

[4] Hertz, H. Ueber Strahlen Electrischer Kraft Annalen der Physik und Chemie v. 36, Issue 4, 769–783, 1889.

[5] Cotton, W.D. Polarization in Interferometry. Synthesis Imaging in Radio Astronomy II. Taylor, G.B., Carilli, C.L., Perley, R.A. (eds.), 1999, 111–126.

[6] Sault, R.J., T.J. Cornwell. Hamaker-Bregman-Sault Measurement Equation. Synthesis Imaging in Radio Astronomy II. Taylor, G.B., Carilli, C.L., Perley, R.A. (eds.), 1999, 111–126.

[7] Rohlfs, K., T.L. Wilson. Tools of Radio Astronomy. Springer (eds.), 2004.

[8] Massi, M., S. Aaron. Stability of EVN D-terms, EVN Doc No 77., 1997.

[9] Massi, M., M. Rioja, D. Gabuzda, et al. Baseline errors in European VLBI Network measurements III. The dominant effect of instrumental polarization. Astron. Astrophys., v. 318, L32, 1997.

[10] Cornwell, T., E.B. Fomalont. Self-Calibration. Synthesis Imaging in Radio Astronomy II. Taylor, G.B., Carilli, C.L., Perley, R.A. (eds.), 1999, 187–199.

[11] Gomez, J.L., A.P. Marscher, A. Alberdi, et al. Polarization calibration of the VLBA using the D-terms. VLBA Scientific Memo No 30, 2002.

[12] Clark, T.A., A.E.E. Rogers. Mark III VLBI Data Acquisition Terminal. GSFC, NASA, 1982.

[13] Kemball, A.J. VLBI Polarimetry. Synthesis Imaging in Radio Astronomy II. Taylor, G.B., Carilli, C.L., Perley, R.A. (eds.), 1999, 187–199.

The 5th IVS General Meeting Proceedings, 2008, p. 63–67

Comparisons of Correlations Using Disk-Transfer and e–VLBI-Transfer

Axel Nothnagel [1], *Alessandra Bertarini* [1], *Christian Dulfer* [1], *Thomas Artz* [1], *Jan Wagner* [2], *Guifre Molera* [2], *Jouko Ritakari* [2]

[1)] *Institute of Geodesy and Geoinformation, University of Bonn, Germany*

[2)] *Metsähovi Observatory, Finland*

Abstract. In May 2007 in the EURO87 session, the station at Metsähovi recorded the VLBI data in parallel on a Mark 5A disk module and on a Linux RAID system (PCEVN). The Mark 5A disk module was shipped to the correlator and the data from the raid system were transferred to a Linux RAID system in Bonn by e–VLBI using the UDP-based protocol Tsunami. In Bonn the data were then copied onto a Mark 5A disk module for correlation. Both data streams were correlated as if they came from different sites. At S-band there are noticeable differences in the delay observables of up to 400 ps for which the origin is not yet discovered.

1. Introduction

For some time now, transfer of raw VLBI data via electronic data transmission and, in particular, via the Internet has become common, however not routine practice, e.g. [5, 3, 2]. Today, the main hurdle to take is that not all stations are yet capable of sustaining reasonable data rates (i.e. > 100 Mbps) for long periods of time. In order to evaluate the actual quality of the electronic transfer in the current Internet environment, a test has been carried out with the data of the Metsähovi Observatory observed within the Europe-87 VLBI session [1].

At Metsähovi, the digitized data from the sampler have been recorded simultaneously on a Mark 5A recording system and on a PCEVN [4] (Fig. 1). The Mark 5A disk module has been shipped to the Bonn MPIfR/BKG correlator by courier service while the data from the PCEVN system were electronically transferred to a Linux PC with a RAID (VIOLA) at the correlating facility using the UDP based protocol TSUNAMI. The average transfer rate was 605 Mbit/s and the 524 GB of data were succesfully transferred in about 1h 47m. Here, the data were copied using the EGAE (Experimental Guided Adaptive Endpoint Architecture) software to another Mark 5A system.

From this point onwards, the two data streams have been treated completely independently. For a better separation, the data which has been transported along the traditional path was assigned to the standard station name METSAHOV while for the data which was transferred electronically a new station name SUOMI was introduced.

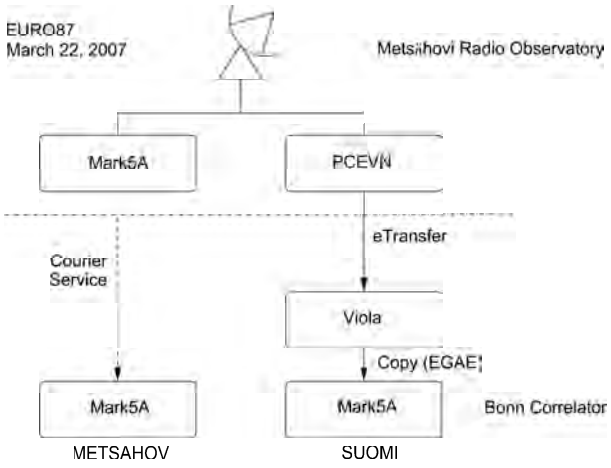

Figure 1. Data flow of Metsähovi VLBI data within test experiment

2. Data Processing

In the correlation process, the two data sources have been treated as two different stations with correlations being performed on all baselines of the network including those to SUOMI and even on the METSAHOV–SUOMI zero-length baseline. In this post correlation analysis we compare and discuss the differences of the delay observables which have been determined for METSAHOV and SUOMI to all other stations in the network.

The first fringe fitting process carried out using HOPS (Haystack Observatory Postprocessing Software) had been set up with slightly different sets of additive phase offsets of the individual channels for SUOMI and METSAHOV. While at X-band this oversight had hardly any effect on the resulting delay determinations, the S-band delays were affected quite significantly. The reason is that at S-band on some baselines only very few common channels, 3 - 4 out of 6, remained and the delay fit ($d\phi/dt$) reacted quite sensitively to these small phase offsets. Noticeable were the non-zero delays on the zero-length baseline SUOMI – METSAHOV (16 ps). By re-fringe fitting the session applying the same manual phase cal to both METSAHOV and SUOMI the problem disappeared.

In Fig. 2, the differences of the delay observables from the two different

Metsähovi data streams at S-band are depicted for all baselines versus epoch of observation. It becomes immediately obvious that in the first five hours of the session some peculiarities surface because the delay differences reach up to 400 ps in magnitude. Remarkable, though, is the fact that these large differences are not present at X-band where they are always below 5 ps with a hand-full exceptions of up to 13 ps.

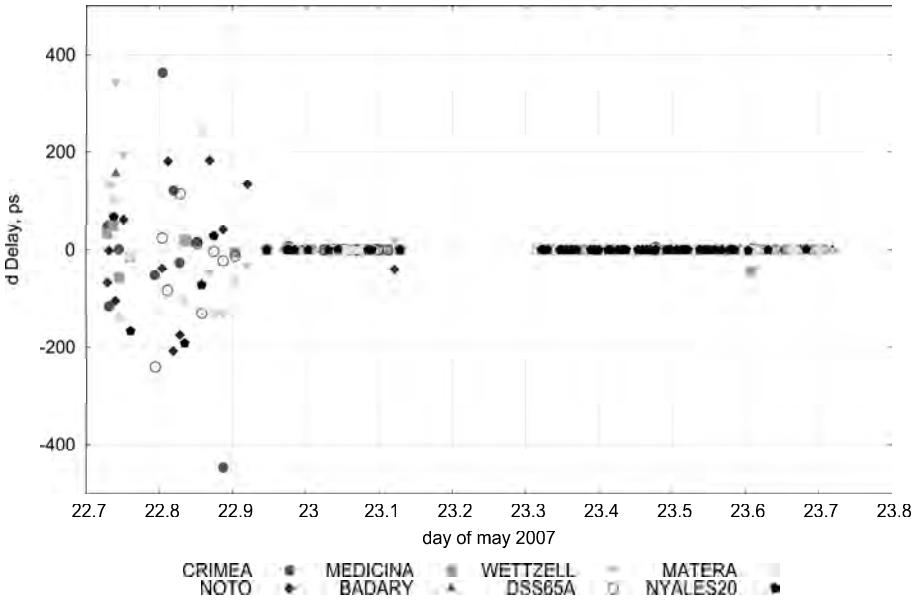

Figure 2. Delay differences versus time

In an attempt to figure out what may have caused these large discrepancies, we checked the number of samples (bits) which were used in the correlation process. It turned out that in the beginning of the session, i.e. when the large discrepancies actually happend, up to 200000 samples of roughly 20 million in each channel were missing. Fig. 1 depicts the delay differences versus percentage of difference in the correlated data for all baselines. In general, the integration times of the SUOMI data stream are slightly shorter by small fractions of a second because PCEVN starts recording at the edge of the one-pulse-per-second station synchronization signal, whereas the Mark 5A does not. This could explain some of the missing samples. However, this could not be proven yet. In addition, no further systematics could be detected.

In order to check whether a low level of SNR made the scans more prone to larger delay differences, we also looked at the delay differences versus SNR. As can be seen in Fig. 2 no clear systematic dependency of the delay differences from SNR can be found as well.

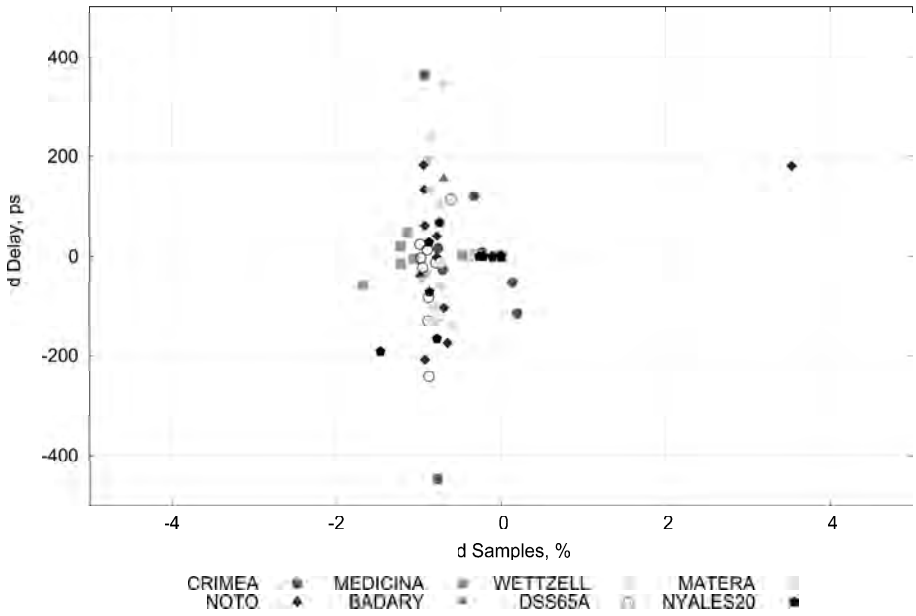

Figure 3. Delay differences versus sample differences in percent

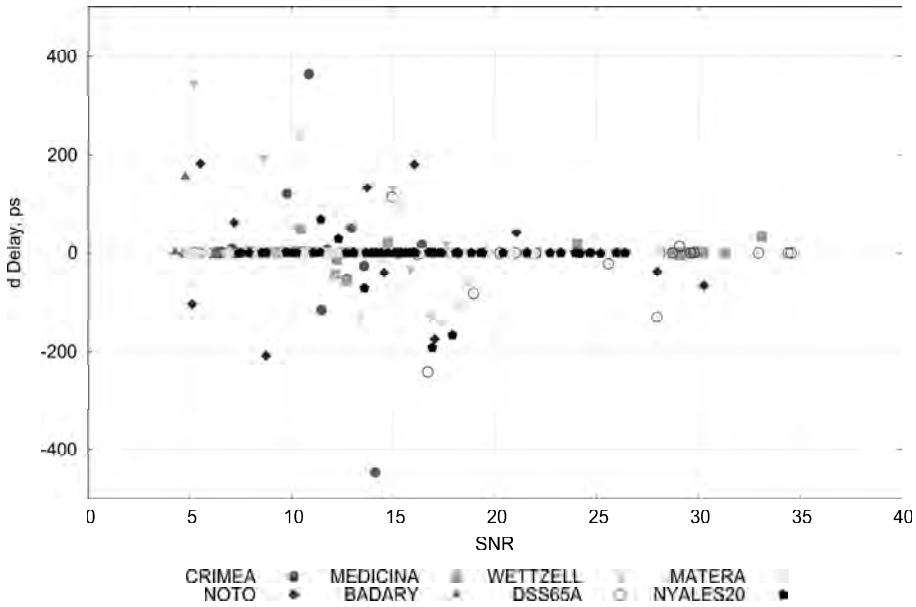

Figure 4. Delay differences versus SNR

3. Conclusions

So far, we were unable to find a clear reason for the delay differences and, thus, why the electronic transfer produced different delay results than the standard disk shipment procedure. The fact, that the discrepancies are only present at S-band but not at X-band casts some doubts on the assumption that the electronic transfer as such has caused the delays to change. Small differences in the integration times of less than 0.2 seconds should not cause such large changes in the delay determinations.

However, if the data had only been transferred electronically and processed in the normal way, the delay deviations had gone unnoticed and the ionosphere corrections had had serious deficiencies. For this reason these investigations are continued.

References

[1] Campbell, J., A. Nothnagel. European VLBI for crustal dynamics. Journal of Geodynamics, v. 30, 321–326, 2000.

[2] Koyama, Y., T. Kondo, M. Kimura, et al. e–VLBI Developments with the K5 VLBI System. International VLBI Service for Geodesy and Astrometry 2006 General Meeting Proceedings. Dirk Behrend and Karen Baver (eds.), NASA/CP-2006-214140, 2006, 216–220.

[3] Lapsley, D. A practical approach to e–VLBI over long fast networks. International VLBI Service for Geodesy and Astrometry 2006 General Meeting Proceedings. Dirk Behrend and Karen Baver (eds.), NASA/CP-2006-214140, 2006, 215–219.

[4] Parsley, S., S. Pogrebenko, A. Mujunen, et al. PCEVN, New Technologies in VLBI. ASP Conference Series, v. 306, 2003.

[5] Parsley, S. eVLBI Research in the European VLBI network. International VLBI Service for Geodesy and Astrometry 2006 General Meeting Proceedings. Dirk Behrend and Karen Baver (eds.), NASA/CP-2006-214140, 2006, 205–209.

The 5th IVS General Meeting Proceedings, 2008, p. 68–71

Ultra Rapid UT1 Experiment with e–VLBI

Shigeru Matsuzaka, Hiromi Shigematsu, Shinobu Kurihara, Morito Machida, Kensuke Kokado, Daisuke Tanimoto

Geographical Survey Institute, Japan

Abstract. Tsukuba 32 m performed intensive experiments for ultra rapid UT1 measurement. The purpose of the experiments is to obtain the UT1 result within 30 minutes after the end of the observing session. The stations that participated in the experiments are Tsukuba 32 m, Kashima 34 m, Onsala, and Metsahovi with high-speed network. One of the key factors to enable the ultra rapid UT1 measurement is to transfer and convert the data as fast as possible. Therefore, we established some systems, such as real time data transfer and automatic data conversion system. As a result, we succeeded in obtaining UT1 result within 4 minutes after the end of the observing session with Onsala on Feb. 21, 2008.

1. Introduction

The Earth Orientation Parameters (EOP) describe the relation between the Celestial Reference Frame (CRF) and Terrestrial Reference Frame. UT1 is one of the EOP, and it is the rotation angle of the earth. EOP parameter is necessary in orbit control of satellites for space exploration, such as Deep Impact mission and Mars Global Surveyor by NASA. Many analysts need a present and a future value of EOP. The prediction data of EOP for one year into the future is weekly published in IERS Bulletin-A from the Rapid Service and Prediction Center at USNO. However, the accuracy of the prediction value degrades rapidly with time. The error of the prediction value of UT1 becomes over 1 millisecond in 10 days. The rapid solution of EOP is produced by combined analysis with the latest available data (VLBI, GPS, AAM) and published with the prediction data in Bulletin-A. Therefore, obtaining the UT1 result rapidly will contribute to the improvement of the prediction value.

2. IVS Intensive VLBI Sessions

IVS schedules 3 intensive sessions which yield a UT1 measurement a day. From Monday through Friday, INT1 session is performed on the Kokee-Wettzell baseline; INT2 session is performed on the Wettzell–Tsukuba baseline on Satur-

Table 1. IVS Intensive VLBI Sessions (Kk–Kokee, Wz–Wettzell, Ts–Tsukuba, Ny–NyÅlesund, On–Onsala, Mh–Metsahovi)

Session	Sending data	Processing time	Stations	Correlator
INT1	Network	3–5 days	Kk, Wz	Washington
INT2	Network (BBFTP)	1–3 days	Ts, Wz	Tsukuba
INT3	Network (Tsunami)	Within 1 day	Ts, Wz, Ny	Bonn
Ultra Rapid	Network (Real-time)	Within 30 minutes	Ts, Kb, On, Mh	Tsukuba, Kashima

day and Sunday. INT3 is performed on Wettzell-Tsukuba-NyÅlesund network between INT1 and INT2 (Monday). The data of all intensive sessions are transferred from the observing stations to the correlator directly (INT2 and INT3). In the case of INT1, Wettzell data are transferred to a place near the correlator where the data is written to disk and picked up by the correlator, and Kokee data are sent as a disk by airmail. Tabl. 1 shows the data processing times of these sessions. Ultra rapid UT1 experiment enable us to obtain UT1 result far more rapidly than the other sessions.

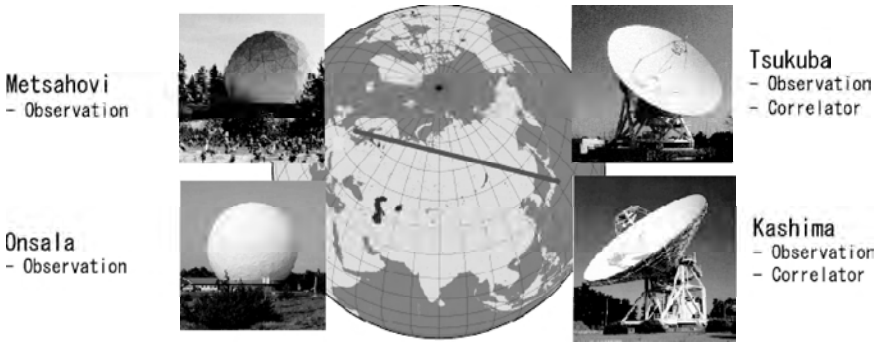

Figure 1. The Stations of Ultra Rapid UT1 Experiment

3. Ultra Rapid UT1 Experiment

The stations that participated in the experiment are showed in Fig. 1. All of the stations have a high-speed network. We have performed the experiments since July 2007. In the experiments, we performed a real-time data transfer and data conversion from Mark 5 format to K5 format. A high-speed network and UDP-based data transfer protocol “Tsunami” assisted the real-time data

transfer from Europe to Japan. After the data conversion, we performed a correlation and data analysis with OCCAM automatically. These automatic processes enable us to obtain the UT1 result within a few minutes after the end of the observing session.

The session's duration is 1 hour which is the same as existing IVS intensive sessions. Before the main session, we add 30 minutes observation for finding fringes, which is a procedure to detect the clock offset between two VLBI stations.

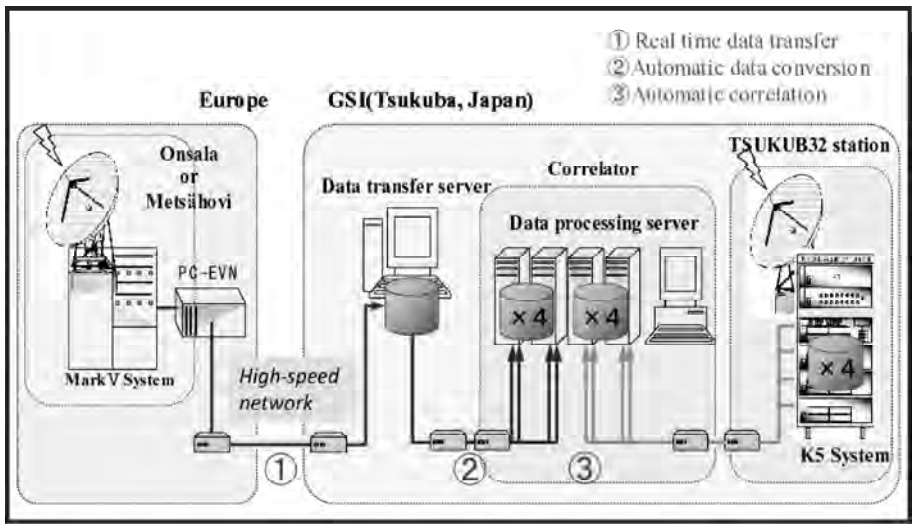

Figure 2. Data Processing of Ultra Rapid UT1 Experiment

4. Results of Ultra Rapid UT1 Experiments

The results of the experiments performed since July 2007 are showed in Tabl. 2. Since the environments of the automatic data processing were not completed in the early stage, we failed in the real-time data transfer and the data conversion. Therefore we improved these processes every time we failed in the experiments. Eventually we could obtain the UT1 result within 4 minutes after the end of the last scan of the session on Feb. 21, 2008.

Fig. 3 shows the comparison of the dUT1 estimated by ultra rapid UT1 experiment with the Rapid Service of Bulletin-A. The accuracy of the dUT1 measurement by ultra rapid UT1 experiment has the same accuracy with the Rapid Service, which is about a few tens of microseconds.

Table 2. Results of Ultra Rapid UT1 Experiments

	Date	Stations	Results
1st	Jul. 14, 2007	Ts, Kb, On	We confirmed how to perform the experiment. We failed in real-time data transfer.
2nd	Sep. 07, 2007	Ts, On, Mh	We failed in automatic data conversion.
3rd	Oct. 29, 2007	Ts, On	We succeeded in real-time data transfer and conversion, but we failed in finding fringes during the experiments.
4th	Nov. 22, 2007	Ts, On	We succeeded in all of the automatic processes, but the data conversion took more time than we thought. We could obtain UT1 result within 1 hour after the experiment.
5th	Feb. 21, 2008	Ts, On	We succeeded in obtaining UT1 result within 3 minutes 45 seconds after the experiment.

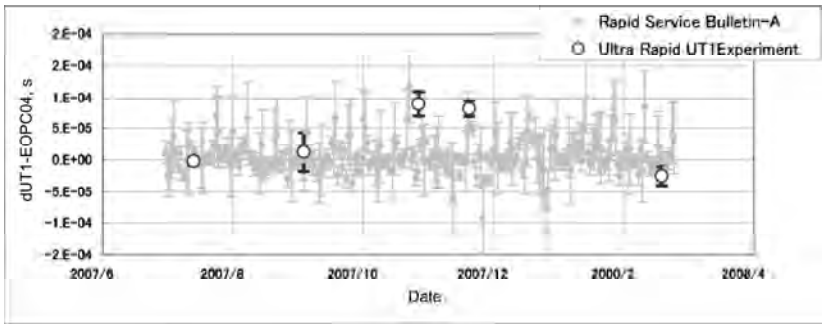

Figure 3. Comparison of the dUT1 Results with Rapid Service of Bulletin-A

5. Conclusion

We succeeded in obtaining the UT1 result within 4 minutes after the VLBI observation. This is based on several automatic processes, such as real time data transfer and automatic data conversion. The accuracy of the dUT1 measurement was the same level with Rapid Service of Bulletin-A. In the current situation, it is possible that we perform the ultra rapid UT1 experiment in 256 Mbps. However, we can not perform the experiment in over 512 Mbps, because we can not transfer the data faster than 500 Mbps. Therefore, we have to maintain the environment of the network at Tsukuba Correlator if we perform the experiment at over 512 Mbps. In the near future, we plan to introduce the system of ultra rapid UT1 experiment at steadily sessions scheduled by IVS.

The 5th IVS General Meeting Proceedings, 2008, p. 72–76

Single Dish Radiometric Observations of Geodetic Sources on Radio Telescopes of the QUASAR Network

Mikhail Kharinov, Andrey Mikhailov

Institute of Applied Astronomy, Russian Academy of Sciences, Russia

Abstract. The radio telescopes of the Quasar Network are equipped with control system integrated with Mark IV Field System (FS) software that is used for radio interferometric observations. A complex of software was developed at IAA RAS in order to perform single dish radiometric observations. This complex consists of FS extensions, scheduling, and data processing software packages. Different methods of antenna beam scanning required for single dish observations are implemented in the control system. A complete set of software support for radiometric registration devices used in IAA was developed. It provides device control, graphical visualization, and data recording in special compressed file format. All these capabilities are controlled by the commands added to the FS SNAP language. Two special software packages SchedMaker and Class Visual were developed for observation scheduling and radiometric data processing respectively. The scheduling uses SNAP language with additional non-standard commands. These observation facilities are used for regular monitoring of the flux density of the sources from the four lists, which are used in the following IVS programs: 1) Intensives INT1 and INT2, 2) CRF, 3) ICRF and 4) Geodesy (R1, R4, T2). The complete list of sources consists of 128 sources. The observations are carried out every month on X-band. Each time from 30 up to 50 sources are being observed. The program of monitoring was started in July 2005. There are 1782 single source sets observed during the period up to May 2007.

1. Introduction

The IVS carries out regular observations of radio sources in geodesy and astrometry programs: 1) Intensive (IVS-INT1, IVS-INT2); 2) CRF; 3) ICRF; 4) Geodesy programs (R1, R4, T2). The ICRF sources showing an appreciable increase of the flux density are to be included certainly into the VLBI observations. It is important to forecast the flux density changes of the radio sources at scheduling other IVS sessions as well. The validity of the forecast strongly depends on the quantity of information about the history of radio sources behavior.

Single dish radiometric monitoring of the required sources is able to pro-

vide additional data for a reasonable selection of sources when scheduling IVS sessions. The project of monitoring the flux density histories (FDH) based on single dish observations was begun on the QUASAR network radio telescopes of the IAA RAS. The measurements were made monthly between July 2005 and May 2007 on X-band. There are 1782 single source sets observed.

2. Observing Methods and Software

The radio telescopes of the Russian VLBI QUASAR network participate since 2003 in the regular international VLBI observations within IVS programs. These radio telescopes are equipped with a control system integrated with the Mark IV Field System (FS) software that is used for radio interferometric observations. A set of radiometric registration devices and software packages was developed at IAA RAS in order to perform single dish radiometric observations. The software consists of FS extensions, scheduling, and data processing software components.

The technique of single dish observations is essentially different from the one used for VLBI. In particular, there are various methods of antenna beam scanning required for single dish observations. Such methods are implemented in the antenna control program on the central computer.

The radiometric registration devices used in single dish observations are connected directly to the central control computer of the radio telescope. The control software supports several generations of such devices developed at IAA RAS. There are also the software units for real time graphical data visualization and for writing data into the files for the forthcoming processing. Data are saved into the files in a specially developed compressed format.

The QUASAR network is dedicated to VLBI and therefore FS is the key part of the radio telescope central control computer software. All extra single dish observation capabilities are controlled by the non-standard commands added to the FS SNAP language. There are two noticeable improvements in the FS architecture implemented for the QUASAR radio telescopes: 1) integration of "asynchronous" programs into FS structure, and 2) using more reliable method for interprocess communications.

Two special software packages, SchedMaker (SM) and Class Visual (CV), were developed for observation scheduling and radiometric data processing respectively. The scheduling uses the SNAP language with additional non-standard commands. Both packages support various methods of single dish observations used on the QUASAR network radio telescopes (on/off, linear and raster beam scanning).

The X-band RCP was chosen for single dish observations according to frequency band used for corresponding VLBI sessions. The full list of sources consists of 110 objects used in geodesy and astrometry sessions (Tabl. 1). The list was built in coordination with NVI, Inc./NASA Goddard Space Flight Center. The flux density values of these sources are in the range from several units up to tens of Jansky. Therefore they are strong enough to be registered with

the QUASAR network radio telescopes.

Table 1. Source list (only source names)

Stable or slightly variable					
0014+813	0106+013	0119+115	0201+113	0202+149	0229+131
0454+844	0458-020	0552+398	0556+238	0602+673	0642+449
0718+793	0743+259	0805+410	1004+141	1038+52A	1101+384
1117+146	1128+385	1150+812	1252+119	1345+125	1611+343
1741-038	1745+624	1803+784	1823+568	1923+210	2029+121
2113+293	2128-123	2134+00	2255-282	3C274	3C371
3C418	3C446	CTA26			
Variable					
0059+581	0133+476	0234+285	0235+164	0528+134	0536+145
0657+172	0722+145	0727-115	0748+126	0749+540	0804+499
0808+019	0823+033	0827+243	0917+449	0955+476	1044+719
1053+815	1300+580	1308+326	1334-127	1354+195	1357+769
1417+385	1726+455	1749+096	1849+670	2121+053	2318+049
OJ287	NRAO512				
Need more data					
0003-066	0048-097	0104-408	0111+021	0119+041	0434-188
0454-234	0607-157	0749+540	1034-293	1116+128	1124-186
1156+295	1219+044	1307+121	1351-018	1418+546	1538+149
1606+106	1622-253	1739+522	1908-201	1921-293	1954-388
1958-179	2126-158	2136+141	2145+067	2149+056	2201+315
2209+236	2234+282	2243-123	2356+385	4C39.25	DA426
OQ208	NGC6251	VR422201			

About 30–50 sources were observed during each session. To measure the flux density of VLBI sources a multiple elevation beam scan was used during 40 minutes for each source. Additionally, 15 minutes beam scanning of calibrators was carried out periodically. A telescope gain curve (including atmosphere attenuation) was determined for each session from measurement of calibrators in elevation range from 15 up to 75 degrees.

The data processing performed with CV package consists of the following steps: 1) Each scan was corrected for sky emission and different instrumental errors. 2) Multiple beam scans were averaged. 3) A Gaussian was fitted to average scan and the peak value of the Gaussian fit was taken as final result.

The flux densities of calibrators were taken from [1].

3. The Flux Density Histories (FDH) for IVS Sources

Single dish observations were carried out and processed at IAA RAS. Final results were sent to NVI, Inc./NASA Goddard Space Flight Center. Besides, at IAA RAS a database of FDH based on the results of single dish observations

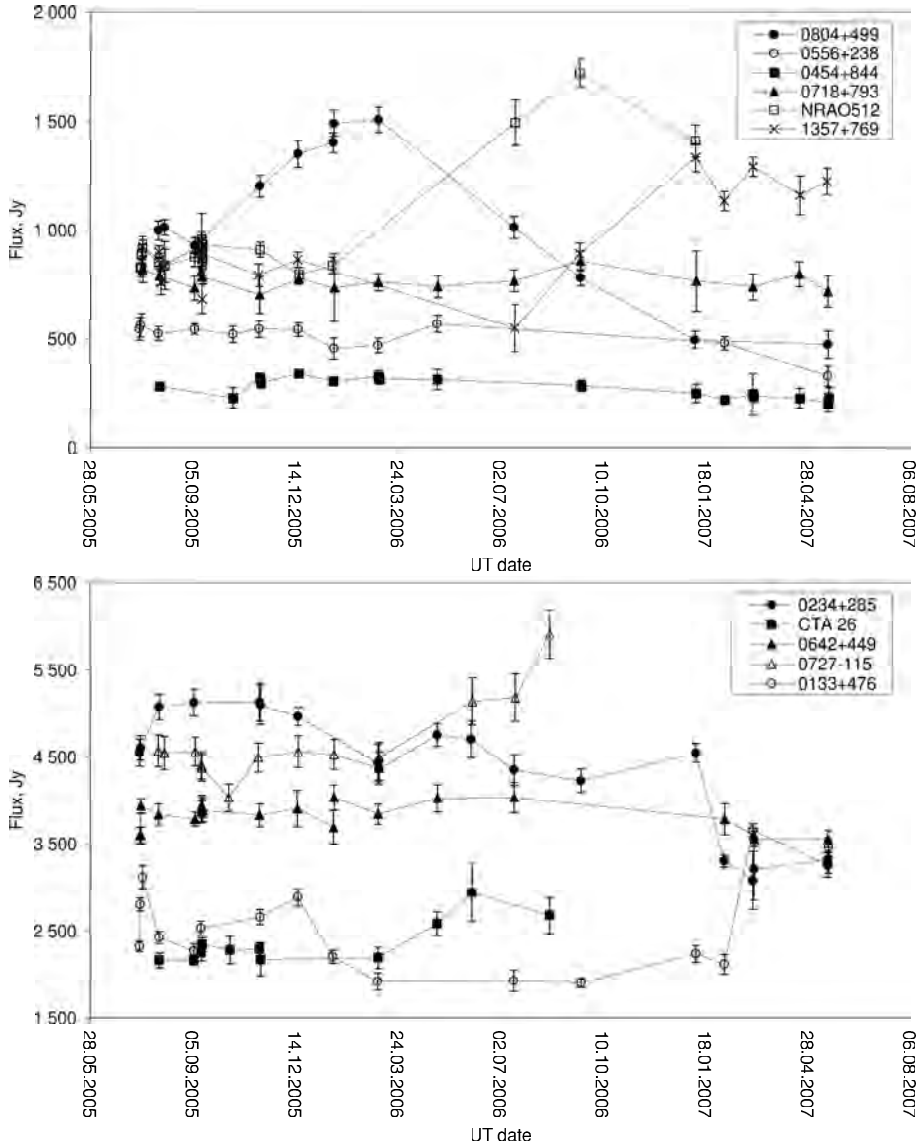

Figure 1. Flux density of the IVS sources 0133+476, 0234+285, 0454+844, 0556+238, 0642+449, 0718+793, 0727-115, 0804+499, 1357+769, CTA 26, and NRAO512

of IVS sources was created. All sources have different kinds of radiation variability: stable enough, with slow monotonous changes, and with fast bursts. As a result of database analysis, the general source list was divided into three parts (Tabl. 1):

"Stable or slight variable" — sources with stable enough flux density or with small variability;

"Variable" — sources with significant changes of flux density;

"Need more data" — for these sources more observations are needed to determine their behavior.

Several typical curves of brightness for sources from the first and second groups are presented in Fig. 1. As shown the sources 0454+844, 0556+238, 0642+499, 0718+793, and CTA26 belong to the first group. The sources 0234+285, 0727-115, 0133+476, 0804+499, and NRAO512 tend to have significant changes of their flux density and these sources at the moments of decline could be unwanted for VLBI sessions.

4. Summary

The complex methodology for automatic radiometric single dish observations was formed based on developed software for scheduling, carrying out and processing single dish observations. Operability of this methodology and of the software complex was tested and then used for observations of a list of geodetic and astrometric sources. A preliminary data base of the IVS sources flux density history (FDH) was formed as a result of the observations. The data base allows to evaluate the stability of the sources flux density and probability of their declines or bursts.

Acknowledgements

It is a pleasure to thank Daniel S. MacMillan (NVI, Inc./NASA Goddard Space Flight Center, USA) for concept approval and helpful discussions.

References

[1] Ott, M., A. Witzel, A. Quirrenbach, et al. An updated list of radio flux density calibrators. Astron. Astrophys. v. 284, 331–339, 1994.

The 5th IVS General Meeting Proceedings, 2008, p. 77–81

Automatic System for Monitoring Hydrogen Masers in QUASAR VLBI Network

Dmitriy Ivanov, Aleksandr Vytnov

Institute of Applied Astronomy, Russian Academy of Sciences, Russia

Abstract. The observatories of the QUASAR VLBI network are equipped with a set of hydrogen masers. For remote monitoring and testing of hydrogen masers a software and hardware system is developed at IAA.

1. Introduction

The accuracy of a VLBI network is substantially defined by the characteristics of hydrogen masers which provide the function of independent local oscillators to spatially separated radiotelescopes as a phase measurement radiosystem [1].

All observatories of the QUASAR VLBI network are equipped with a set of three active hydrogen masers CH1-80 (Fig. 1), manufactured at IEM "Kvartz" (Nizhniy Novgorod, Russia) [2–4].

The masers are widely spaced. The problem of definition of parameters of the separated masers will traditionally be solved in several stages: measurement of parameters, entering of data in a computer, data transmission, processing, and providing access to data. The delay of data acquisition can be several days, besides, mistakes of operators are added. Additional mistakes arise because of non-simultaneous registration of measurements on standards.

For VLBI network reliable functioning creation of the system, allowing to receive parameters hydrogen masers in real time without participation of operators is necessary.

2. The Automatic System

For remote monitoring and testing of hydrogen masers a software and hardware system is developed at IAA (Fig. 2).

This automatic system provides internal comparisons between hydrogen masers and external comparison of the basic standard by GPS/GLONASS signals. The data measured are transmitted in quasi-real time mode to the IAA

Figure 1. The set of active hydrogen standards CH1-80, observatory "Zelenchukskaya"

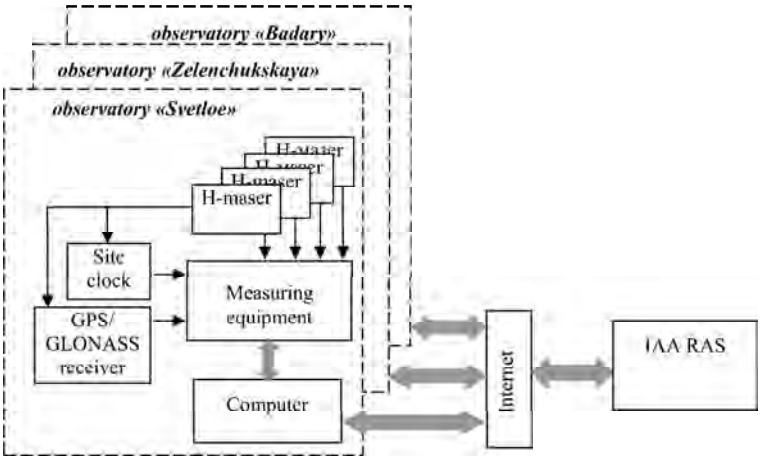

Figure 2. The automatic system for monitoring parameters of the removed standards of time and frequency

for processing and analysis. The adjustment of the frequency standards is made by the results of processing.

The block diagram of measuring equipment is presented in Fig. 3.

The commutation unit (Fig. 4) allows to switch inputs with a time delay of 0.1 nanoseconds. The special interface board for management of the commutation unit by a computer is developed.

The special software for automation of process of measurements is developed in "LabView" development software system [5]. This software allows to realize

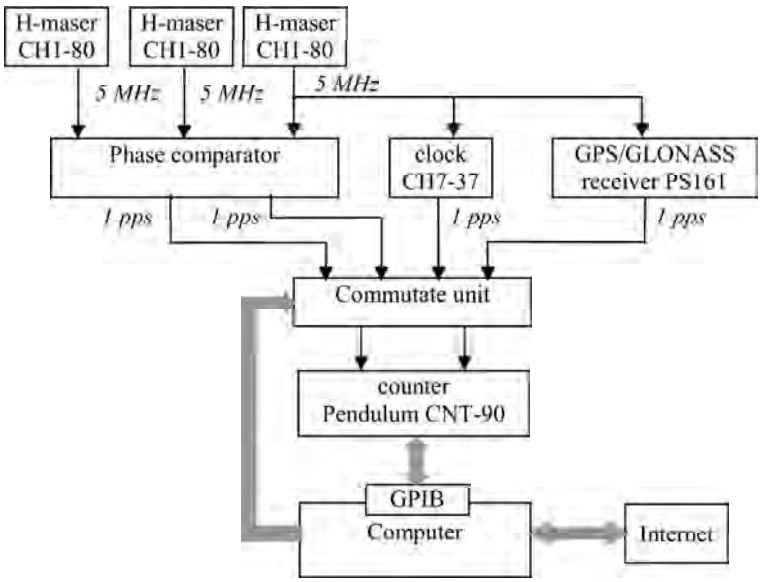

Figure 3. The block diagram of measuring equipment for internal and external comparisons

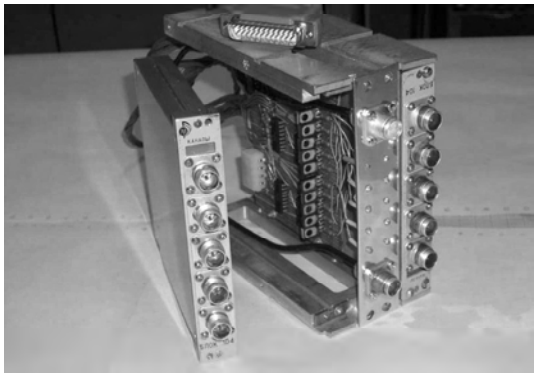

Figure 4. The commutation unit

internal and external comparisons of hydrogen standards of frequency. The key feature of the software, application of the components, allows to work with measuring devices in real time.

A synchronization of processes is carried out using an internal clock of a computer using protocol SNTP. Measuring installation carries out a full cycle of measurements under the schedule before data transmission. In a complex it is used two reports of an exchange: through a mail server and the link protocol "Data Socket" allowing to transmit data in real time.

The software has a user interface allowing the operator to control the measurement process.

3. Some Results

The results of internal comparison of three hydrogen masers at Badary observatory after carrying out of a complex of works as agreed target frequencies of masers are presented below. In Fig. 5 the relative differences of frequencies

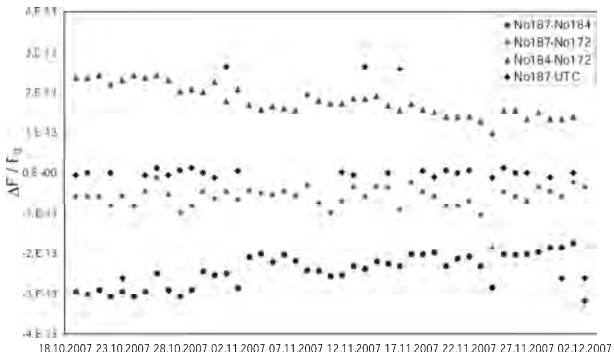

Figure 5. The relative differences of frequencies of pairs of hydrogen masers and UTC

of pairs of hydrogen masers with numbers 187, 184, and 172 are shown. The frequency of the maser N187 (basic maser) is coordinated with scale UTC. From the presented results it is visible that masers are coordinated on frequency at a level $10^{-13} - 10^{-14}$, that allows to keep value of frequency in case of the leading maser failure.

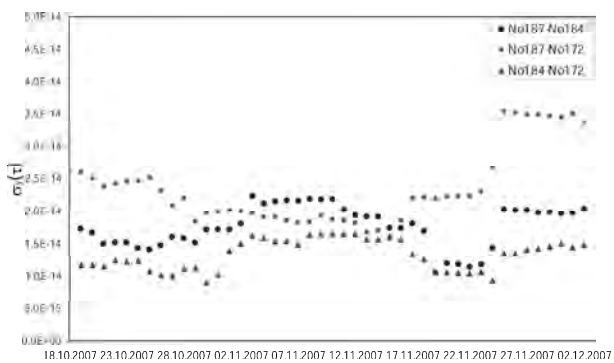

Figure 6. Alan dispersion of maser pairs ($\tau = 1$ day)

In Fig. 6 the results of Alan dispersion calculation of maser pairs on a daily interval of time are presented. As there are three pairs of masers independent comparison, it is possible to calculate Alan dispersion for each maser separately

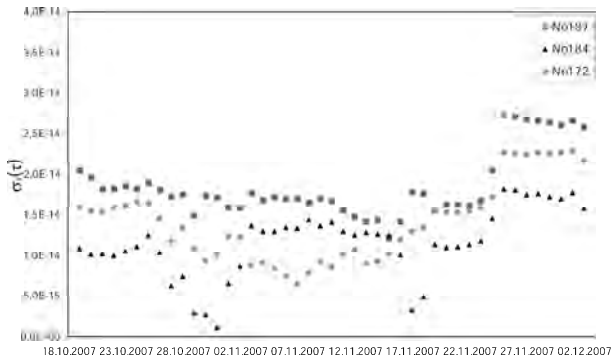

Figure 7. Alan dispersion of masers ($\tau = 1$ day)

(Fig. 7). From the presented data it is visible that stability of masers does not exceed 3×10^{-14}, that completely corresponds to passport data.

4. Conclusion

The developed automatic system provides internal comparisons between hydrogen masers with accuracy of 10^{-14} and transmits results in quasi-real time mode to IAA. It also allows external comparisons of the basic maser with GPS/GLONASS.

The automatic system also allows to supervise stability of the basic maser during a VLBI session. The stability data can be used while processing observations.

References

[1] Tompson, A.R., J.M. Moran, G.W. Swenson. Interferometry and Synthesis in Radio Astronomy. A Wiley-Intersciencience Publication John Wiley & Sons. Inc, 2001.

[2] Smolentsev, S., I. Rachimov. Svetloe Radio Astronomical Observatory. International VLBI Service for Geodesy and Astrometry 1999 Annual Report. N.R. Vandenberg and K.D. Baver (eds.), 2000.

[3] Dyakov, A., S. Smolentsev. Zelenchukskaya Radio Astronomical Observatory. International VLBI Service for Geodesy and Astrometry 2005 Annual Report. N.R. Vandenberg and K.D. Baver (eds.), NASA/TP–2007–214151, 2006.

[4] Smolentsev, S., R. Sergeev. Badary Radio Astronomical Observatory. International VLBI Service for Geodesy and Astrometry 2007 Annual Report. N.R. Vandenberg and K.D. Baver (eds.), 2008.

[5] Travis, J. LabVIEW for Everyone. Prentice Hall PTR, 2002.

The 5th IVS General Meeting Proceedings, 2008, p. 82–86

Local Ties between Co-located Space Geodetic Instruments at QUASAR Network Observatories

Iskander Gayazov, Elena Skurikhina

Institute of Applied Astronomy, Russian Academy of Sciences, Russia

Abstract. Local tie parameters between reference points of space geodetic instruments at the QUASAR VLBI network observatories have been derived from classical geodetic measurements. The results were compared with the eccentricity vectors obtained from VLBI and GPS observations.

1. Introduction

32-m radio telescopes (RT-32) and dual frequency GPS receivers with Choke Ring antennas are co-located space geodetic instruments at the QUASAR VLBI network observatories. At all observatories of the network GPS antennas are installed on concrete pillars constructed on the roofs of administrative buildings. The eccentricity vectors between reference points of co-located instruments were determined independently from different types of measurements: classical geodetic and space geodetic (VLBI and GPS). The obtained results are presented in this paper.

2. Local Tie Parameters from Geodetic Measurements

The local tie parameters between the RT-32 reference points and GPS markers at the observatories were derived from classical geodetic measurements carried out in 2005–2006. The geodetic measurements of different types within the local networks have been adjusted by using COLUMBUS software (3.6 DEMO version). Formal errors obtained in the course of these adjustments are in the range of 2–4 mm for horizontal components (N, E) and 5-8 mm for up-components (U). The main reason for this is the fact that the reference point of the radio telescope antenna is not accessible. It is supposed that the antenna reference point is located on the azimuthal axis of the telescope at the level of its elevation axis (the antenna offset is determined at this level). The horizontal coordinates of the reference point are presumed to coincide with a

point where the azimuthal axis intersects the horizontal platform of the telescope. Obviously, these coordinates could be determined more accurately than the up-component of the elevation axis.

Obtained local tie parameters are presented in Tabl. 1.

Table 1. Local ties between reference points from classical geodetic measurements

Observatory	Eccentricity vectors RT-32–GPS	
	Components	Values, m
Svetloe	N	−57.594
	E	58.483
	U	9.323
Zelenchukskaya	N	−64.746
	E	7.954
	U	8.755
Badary	N	61.882
	E	−73.496
	U	10.204

3. Geocentric Coordinates of Reference Points

The coordinates of reference points at all observatories have been determined in the ITRF2005 (epoch 2000.0) within the framework of IAA and EPN analysis centers activities. The results of these determinations are summarized in Tabl. 2–4.

Table 2. ITRF2005 coordinates of reference points at the Svetloe observatory

	RT-32	GPS
DOMES number	12350S001	12350M001
Observations used	VLBI (2003–2007)	GPS (1996–2006)
AC (software)	IAA (OCCAM/GROSS)	EPN (Bernese)
X, m	2730173.900 ± 0.004	2730155.439 ± 0.001
Y, m	1562442.612 ± 0.002	1562364.664 ± 0.001
Z, m	5529969.033 ± 0.007	5529989.227 ± 0.001

Table 3. ITRF2005 coordinates of reference points at the Zelenchukskaya observatory

	RT-32	GPS
DOMES number	12351S001	12351M001
Observations used	VLBI (2005–2007)	GPS (1996–2006)
AC (software)	IAA (OCCAM/GROSS)	EPN (Bernese)
X, m	3451207.790 ± 0.013	3451174.813 ± 0.001
Y, m	3060375.220 ± 0.010	3060335.365 ± 0.001
Z, m	4391914.907 ± 0.014	4391955.600 ± 0.001

Table 4. ITRF2005 coordinates of reference points at the Badary observatory

	RT-32	GPS
DOMES number	12338S003	12338M002
Observations used	VLBI (2006–2007)	GPS (2005–2007)
AC (software)	IAA (OCCAM/GROSS)	IAA (GRAPE)
X, m	-838200.729 ± 0.009	-838281.524 ± 0.002
Y, m	3865751.572 ± 0.021	3865777.318 ± 0.003
Z, m	4987670.962 ± 0.027	4987624.653 ± 0.002

The presented data show that the coordinates of GPS markers have significantly smaller formal errors when compared with the RT-32 coordinates. A greater number of GPS observations at much longer time intervals explains this effect. But the real accuracy of these coordinates may be at the same level. It is partly shown in the case of coordinate determinations at the Badary observatory.

The ITRF2005 coordinates at the Badary observatory have been obtained at the IAA Analysis Center by processing VLBI and GPS observations.

To derive the RT-32 coordinates, VLBI-observations of the QUASAR network under the Ru-E program have been processed with the OCCAM/GROSS software [1]. The series of coordinates obtained from 15 daily sessions of observations between Aug. 2006 and May 2007 are presented in Fig. 1. Weighted averages of coordinates are given in Tabl. 4.

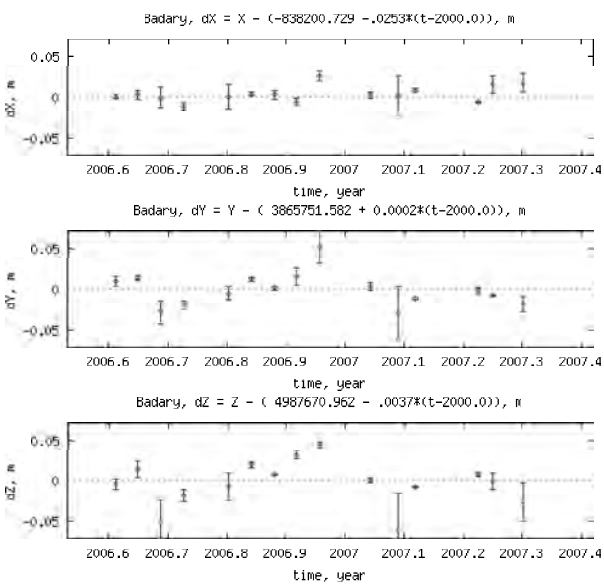

Figure 1. Coordinates of RT-32 at the Badary observatory

The coordinates of GPS-station BADG at the Badary observatory have been determined from GPS observations over a period from April 2005 to March 2007. Data processing was performed by using the software package GRAPE [2] in the mode of triple differences of phase observations. The daily series of observations from 30–40 IGS stations were processed under the condition that coordinates of all stations were fixed in the ITRF2005 except for BADG.

At the BADG station antenna LEIAT504 (Leica) with radome LEIS is used on a permanent basis. For experimental purposes, however, the radome was temporarily removed for the period between November 2005 and August 2006. While processing the observations, the displacements of the antenna phase centers according to IGS data were taken into account. The coordinates of the BADG station obtained from the daily series of GPS observations over a 2 year period are presented in Fig. 2. Some irregularities in coordinates

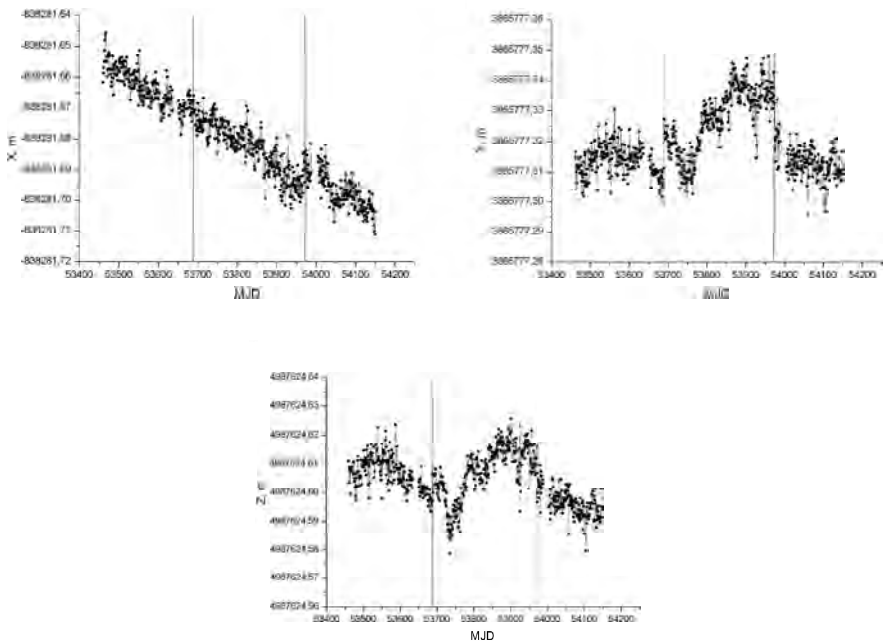

Figure 2. Coordinates of BADG station

are probably caused by seasonal effects. There is also an effect of inexact modelling of the phase center displacements. The vertical lines in the graphics show the days when the radome was removed and reinstalled. These days show noticeable jumps in coordinates and it is not possible to consider the series of obtained coordinates as homogeneous. Therefore, the series of coordinates were divided into three sections and data in the central section was extracted from the analysis in order to determine velocities and coordinates of the station for epoch 2000.0.

4. Consistency of VLBI, GPS and LGN Results

Consistency of the ITRF2005 coordinates with local tie results were also examined. The following differences

$$\Delta X = X_{RT-32} - X_{GPS}, \quad \Delta Y = Y_{RT-32} - Y_{GPS}, \quad \Delta Z = Z_{RT-32} - Z_{GPS}$$

have been formed using the ITRF2005 coordinates from Tabl. 2–4. When transformed to local NEU systems these eccentricity vectors can be compared with local tie parameters given in Tabl. 1. The results of such comparisons for each observatory of the QUASAR network are presented in Tabl. 5. They show that differences are at level of 1 cm except for the up-component of the Svetloe observatory and this should be investigated further.

Table 5. Differences between eccentricity vectors obtained by various methods

Components	Svetloe	Zelenchukskaya	Badary
N, mm	2.8	− 1.2	10.5
E, mm	0.9	−11.5	7.2
U, mm	23.4	− 9.1	−6.6

In general, the differences are comparable with error budget of the results obtained from VLBI, GPS and LGN data. The most likely reasons for these deviations are: a) the inconsistency of VLBI and GPS subsystems in ITRF2005 realization; b) using a limited subset of stations when determining the coordinates; c) errors in data processing algorithms; d) errors associated with local geodetic surveying. Seasonal variations can also be slightly different for VLBI and GPS antennas. For a detailed analysis of these effects the accumulation of observational data over more extended periods and regular monitoring of local geodetic networks are needed.

Acknowledgements

The authors are grateful to Igor Shakhnabiev for implementing the classical geodetic measurements at the QUASAR Network observatories.

References

[1] Malkin, Z.M., E.A. Skurikhina. OCCAM/GROSS software used at the IAA EOP Service for processing VLBI observations. IAA RAS Transactions, v. 12. “Nauka”, Saint Petersburg, 2005, 54–67 (in Russian).

[2] Gayazov, I.S., M.O. Keshin, A.M. Fominov. GRAPE software package and its use for experimental ERP determinations. IAA RAS Transactions, v. 6. Saint Petersburg, 2001, 291–299 (in Russian).

The 5th IVS General Meeting Proceedings, 2008, p. 87–92

Matera Site Survey and VLBI Invariant Point Determination

Roberto Lanotte [1], *Mauro Pirri* [1], *Giuseppe Bianco* [2]

[1)] *Telespazio, Centro di Geodesia Spaziale, Italy*

[2)] *Agenzia Spaziale Italiana, Centro di Geodesia Spaziale, Italy*

Abstract. The role played by CGS (Centro di Geodesia Spaziale), Matera, Italy as a fundamental geodetic station, hosting the main space geodetic technique systems SLR, VLBI, and GPS, makes the whole survey theme (measurements, related corrections and processing) of great importance for the CGS activities. The last geodetic survey at CGS was performed in Feb.–Mar. 2004 and involved measurements connecting 7 IERS geodetic reference points and 14 additional reference points in the local network. During July 2005, a measurement campaign was carried out to estimate the VLBI invariant point (IVP) from the geometrical surface described by four optical retro-reflectors mounted on the antenna structure.

1. Introduction

The purpose of this work is the determination of the tie vectors between the IERS geodetic reference points located at the CGS. To achieve the results, three steps have been performed. The first one was the determination of the local network that provided the ties between the GPS and the SLR instruments. The second one was the establishment of a small network around the VLBI antenna with several points in common with the previous network. Then the determination of the VLBI antenna invariant point (IVP) has been obtained recovering the geometrical figure described by four retro-reflectors on the antenna dish.

2. Analysis Software

An original software (GSMAT) for the analysis of a geodetic survey raw measurements has been developed at CGS. The main characteristics of this software are:

- atmospheric effects removed using continuously measured values of local temperature, pressure and humidity recorded by the local meteorological sensors;
- rigorous network adjustment (weighted least squares method) with minimal inner constraints (via SVD), using the whole covariance matrix at each step of the computation;
- outlier detection/rejection;
- the VLBI invariant point estimation by modeling the geometrical figure described by retro-reflectors located on the antenna;
- production of the SINEX file reporting the coordinates of the IERS reference points and VLBI IVP.

3. Matera Local Survey

3.1. Local Survey Description

The Matera local network is formed by 20 points, 6 of them being IERS reference points. The measurement instruments used were: a theodolite Tachymat Wild TC2002S, a laser distance meter Distomat Wild DI2002 and a corner cube reflector Wild GPH1P. Up to 967 measurements where carried out, each one composed by horizontal and vertical angles and slant distance between the theodolite and the corner cube mounted over the markers.

3.2. Local Survey Data Analysis

The procedure for the computation and analysis is the following.

1. Correction of distances for atmospheric refraction using the "Barrel and Sears" formula and meteo data.
2. Correction for the height differences between the instruments (tachometer and reflectors) and the markers.
3. For each setup of the theodolite, transformation of vectors from the topocentric polar reference system (azimuth, elevation, distance) in a topocentric rectangular reference system centered in the marker occupied by the theodolite with unknown orientation angle w.r.t. the astronomical azimuth.
4. Minimal inner constraints solution via Singular Value Decomposition to solve for unknown orientation angles and marker coordinates in an unique arbitrary topocentric rectangular reference system.
5. Use of the Polaris star to orientate the network w.r.t. the astronomical North direction.
6. Translation of the network to the ITRF2000 position of the GPS marker.

4. VLBI Invariant Point Determination

In order to determine the VLBI antenna IVP with respect to the local network, we placed 4 retro-reflectors on the antenna dish and measured their position while the antenna moved. This operation realizes a small network formed by several points belonging the the local network plus the IVP point. Adjusting this sub-network to fit the local network, the ties between the IVP and the other reference points has been obtained. The procedure can be summarized as follows:

- Analysis of the sub network around the antenna using the same procedure for the local network (see 3.2).
- Roto-translation of the sub-network to fit the whole local network.
- Estimation of the VLBI invariant point coordinates modeling the surface described by the corner cubes on the antenna as a tilted "spindle torus".
- Production of the SINEX with coordinates of the space geodetic instruments in the ITRF2000 reference frame.

4.1. IVP Mathematical Model

When the antenna moves, a point belonging to the dish structure describes a torus in the space. For the VLBI antenna at the CGS, in theory, such torus degenerates in a sphere since the azimuth and elevation axes do intersect each other at the IVP. However, in order to take into account possible construction errors, we treated it as a "spindle torus", with the internal radius shorter than the external one.

The weighted least square method implemented minimizes the following torus equation and determines the invariant point position (x_0, y_0, z_0), the radius of each torus being described by the corner cubes and the internal torus radius. The internal radius is the same for all corner cubes and it represents also the distance between the two rotational axes, that is the antenna axis offset.

$$f_i = \sqrt{\left(R \pm \sqrt{(y_i - y_0)^2 + (z_i - z_0)^2}\right)^2 + (x_i - x_0)^2} - R_k = 0\,. \qquad (1)$$

Where:
R = internal torus radius,
(x_0, y_0, z_0) = position of the invariant point of the antenna,
R_k = external radius of the torus described by the corner cube k,
(x_i, y_i, z_i) = position of the corner cube at observation i.

The $\pm$ sign is positive for the internal surface (called "lemon") and negative for the external one (called "apple"); our case is the "apple" type.

In order to take into account a possible non-verticality of azimuthal axis and non-perpendicularity between the two axes, we also introduced a tilt for

the torus and estimated two angles of rotation around the East and North directions

$$R = R_z(u)R_y(e) = \begin{pmatrix} \cos(u) & \sin(u) & 0 \\ -\sin(u) & \cos(u) & 0 \\ 0 & 0 & 1 \end{pmatrix} \begin{pmatrix} \cos(e) & 0 & -\sin(e) \\ 0 & 1 & 0 \\ \sin(e) & 0 & \cos(e) \end{pmatrix} . \quad (2)$$

Then the minimized function will be:

$$f_i = \sqrt{\left(R \pm \sqrt{y'^2 + z'^2}\right)^2 + x'^2} - R_k = 0 \,. \quad (3)$$

Where:

$$\begin{cases} x' &= \cos(e)\cos(u)(x - x_0) - \cos(e)\sin(u)(y - y_0) + \sin(e)(z - z_0) \\ y' &= \sin(u)(x - x_0) + \cos(u)(y - y_0) \\ z' &= -\sin(e)\cos(u)(x - x_0) + \sin(e)\sin(u)(y - y_0) + cos(e)(z - z_0) \,. \end{cases}$$

5. Results

The results of this work are the estimates of ties between the IERS reference points and the VLBI antenna axis offset. A comparison of our results for the local ties is given in Tabl. 1 in terms of cartesian coordinate differences. The differences for the GPS marker R are zero because the local network has been translated to its ITRF2000 position.

Table 1. Comparison of the local ties w.r.t. ITRF2000

Local marker name	CDP code	IERS dome number	DX, mm	DY, mm	DZ, mm	description
R	MATE	12734M008	0.000	0.000	0.000	GPS MATE
IVP	7243	12734S005	−2.634	−0.005	−2.918	VLBI IVP
M	7941	12734S008	0.072	3.991	−1.203	SLR MLRO
N	MAT1	12734M009	−10.403	0.529	13.103	GPS MAT1
B	7540	12734M005	−3.774	−0.666	6.914	SLR pad
C	7541	12734M004	−4.940	−2.366	8.776	SLR pad

Concerning the determination of the antenna axis offset, we estimated a value of −8.329 mm ±0.303 mm. A comparison of this value w.r.t. VLBI analysis results from different analysis center and different analysis software is given in Tabl. 2.

Table 2. Comparison of the antenna axis offset result with VLBI analysis results

VLBI solution	Axis offset value, mm	Agency	Software
gsf2007d	-3.4 ± 0.4	NASA/GSFC	CALC/SOLVE
iaa2007c	-5 ± 0.6	IAA	QUASAR
	-0.24 ± 0.16	MAO	SteelBreeze
usno2007a	-4.51 ± 0.44	USNO	CALC/SOLVE
gsi2007d	-4.07 ± 0.39	GSI	CALC/SOLVE
cgs2007a	-3.54 ± 0.66	CGS	CALC/SOLVE

6. Possible Improvements of the Results

Improvements of the results should be possible under the following refinements of the measurement and computation procedure.

- Using levelling measurements to decrease the errors on the vertical position of the markers.
- Increasing the coverage of the surface described by the antenna.
- Taking into account gravitational and thermal antenna deformations.

7. Conclusions

- A dedicated software (GSMAT) has been developed at CGS. It performs rigorous network adjustment, determines the antenna invariant point and antenna axis offset.
- The network adjustment has been obtained solving the weighted least squares problem with the minimal inner constraints to avoid network distortion and using the singular value decomposition.
- The whole variance-covariance matrix has been used at each step of the computation.
- The antenna invariant point and its axis offset have been successfully determinated using classical survey measurements and the mathematical model described in this work.
- The new geodetic survey results have been provided to IERS to be used in the inter-technique combination for the ITRF determination.

References

[1] Cenci, A., G. Vicomanni, G. Bianco. Determination of the invariant point and of the axes offset for the VLBI antenna at Medicina. Telespazio, Roma, 1988.

[2] Bianco, G., A. Caporali, A. Cenci, et al. Survey of a local network to check the stability of marker no.7545 situated in the Cagliari astronomical observatory for the WEGENER-MEDLAS project. Proceedings of the Fourth International Conference on the WEGENER/MEDLAS Project, TUDelft, 1990.

[3] Leick, A. GPS satellite surveying. John & Sons, Inc., ISBN 0-471-81990-5, 1990.

[4] Gilbert Strang and Kai Borre. Linear Algebra, Geodesy, and GPS. Wellesley-Cambridge Press, ISBN 0-9614088-6-3, 1997.

[5] Survey of the Matera site; http://geodaf.mt.asi.it/GEOD/INFO/matesr2004.pdf.

The 5th IVS General Meeting Proceedings, 2008, p. 93–97

Space Geodesy at Yebes: Station Motion from VLBI and GPS

Susana Garcia-Espada [1], *Rüdiger Haas* [2], *Francisco Colomer* [1]

[1] *National Geographic Institute (IGN), Spain*

[2] *Chalmers University of Technology & Onsala Space Observatory, Sweden*

Abstract. Analysis of VLBI sessions and GPS time series has been performed for the 14-m radiotelescope at Yebes site from 1995 to 2003. The best a priori geophysical models and auxiliary weather information from European Center for Medium-Range Weather Forecasts (ECMWF) have been used for the VLBI analysis. The results derived from VLBI measurements are consistent with the plate tectonic motion and no significant movements are detected. The GPS results might detect a deviation in the horizontal components, which is not supported by the VLBI results. We appear to detect a small relative motion between the VLBI and the GPS monuments.

1. Introduction

The National Geographical Institute (IGN) of Spain is active in space geodesy with VLBI and GPS observations using the instrumentation at the National Astronomical Observatory (OAN) at Yebes.

Between 1995 and 2003 the Yebes 14-m radiotelescope was used successfully in 32 geodetic VLBI experiments, including 19 European sessions. The 14-m telescope is not used anymore since 2005 and it will be replaced by the newly constructed 40-m radiotelescope in 2008. Additional to the geodetic VLBI data, there are GPS data from the Yebes site available since 1999.

Fig. 1 shows an aerial picture of the Yebes station. The GPS antenna is located on the roof of a building.

A local tie survey performed in 1999 [1] determined the distance between the 14-m radiotelescope and the GPS antenna to be 106.496 m $\pm$ 0.012 m. The approximate distance between the two radiotelescopes is 225 m.

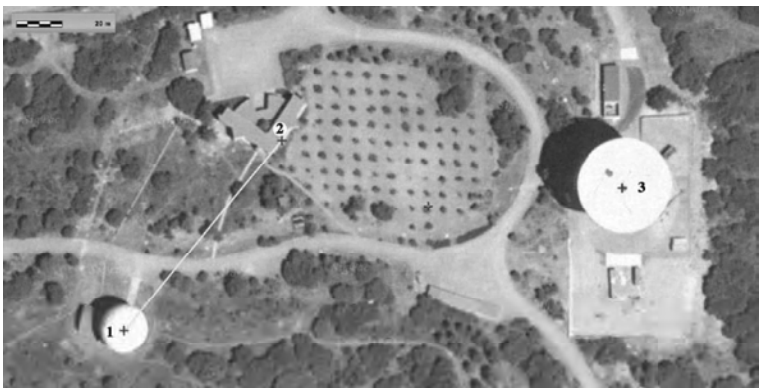

Figure 1. The IGN facilities at Yebes (Guadalajara, Spain). Displayed are (1) the 14-m radiotelescope used in VLBI observations, (2) the GPS antenna of the IGS station, and (3) the new 40-m radiotelescope

2. Analysis

The current project focuses on the analysis of Yebes station geodetic position using VLBI and GPS. The goal is the comparison, combination and interpretation of VLBI and GPS time series for Yebes. We focus on the European VLBI experiments from 1995 to 2003. In future work, we will include all the experiments in the analysis, not only European, in which the 14-m radiotelescope in Yebes participated in those years. For the GPS analysis we use all available data between the middle of 1999 and the end of 2007.

We use the Calc/Solve software package [2] for the analysis of the VLBI sessions and introduce the best a priori geophysical models. The FES2004 ocean model is used as the best a priori model for the ocean tide loading for all the European VLBI sites. The FES2004 tidal charts were computed using a variational assimilation strategy. The assimilated data are the tidal constants coming from the tide gauge and satellite sea level analysis [3].

We introduce auxiliary information from the European numerical weather model ECMWF (European Center for Medium-Range Weather Forecasts) [4] for experiments where we detected that weather data was missing or was obviously wrong. We make a comparison between solutions with original data and solutions in which we include ECMWF auxiliary data. We detected station position changes on the order of 2 mm in the vertical component in the worst case, and sub-millimeter changes for the horizontal positions.

For the estimation of the geodetic position for Yebes 14-m radiotelescope we treated all the other stations involved in the experiments so that their position and velocity were fixed in ITRF2005. Station coordinates for Yebes were estimated for every VLBI session, resulting in time series in a geocentric coordinate system. The station coordinates were transformed into a local geodetic coordinate system, and plate tectonic motion according to the Nuvel-1

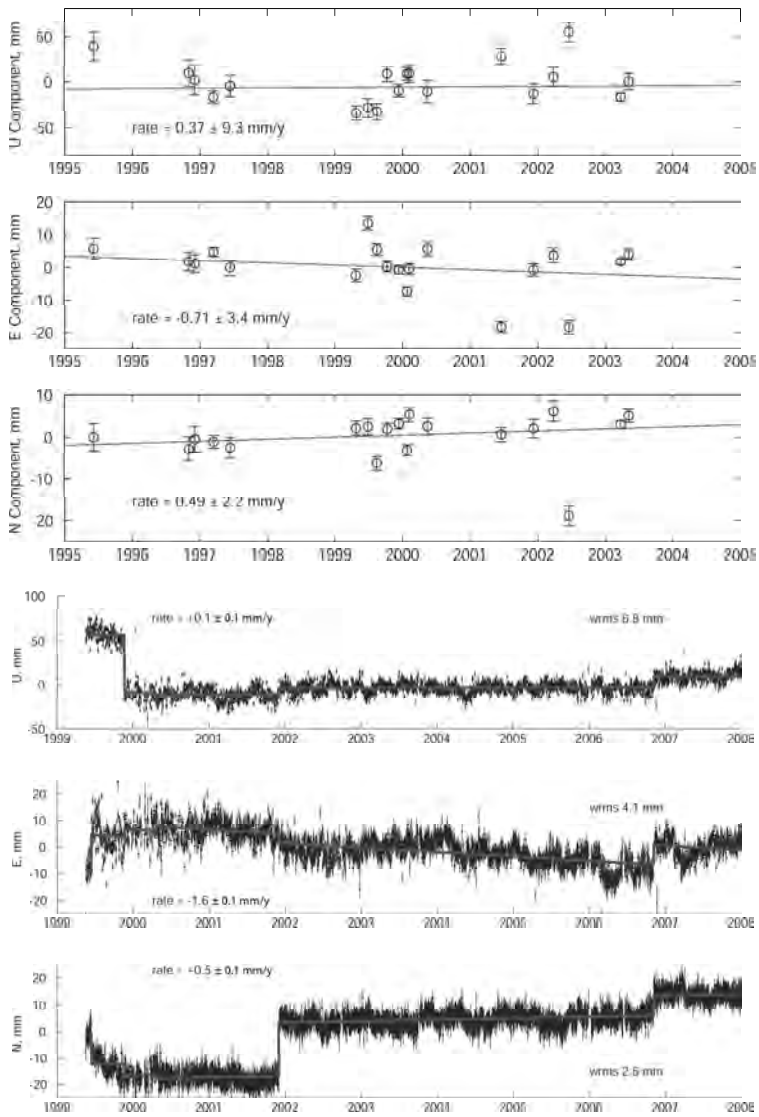

Figure 2. Time series of topocentric station position for the Yebes VLBI station (top) and GPS station (bottom). Plate motion according to Nuvel-1 has been subtracted

[5] was subtracted. The top graphs in Fig. 2 show time series of the resulting three-dimensional topocentric station position.

The GPS data analysis was performed with the Gipsy-Oasis-II software package [6] using the precise-point positioning (PPP) strategy. The resulting cartesian geocentric station positions were transformed into a local geodetic reference system, and the plate tectonic motion was removed according to

Nuvel-1 NNR [5]. The bottom graphs in Fig. 2 show the corresponding time series.

Based on the VLBI and GPS time series, we determined linear changes of topocentric station position. These station rates were estimated by a least-squares fit. For the GPS time series we took into account breaks in the time series, for example due to antenna replacements, according to the information given in the log-file on the IGS webpage [1]. Tabl. 1 shows the results.

Table 1. Topocentric rates from VLBI and GPS

Component	VLBI rate, mm/y	GPS rate, mm/y
Up	$+0.37 \pm 9.3$	$+0.1 \pm 0.1$
East	-0.71 ± 3.4	-1.6 ± 0.1
North	$+0.49 \pm 2.2$	$+0.5 \pm 0.1$

3. Discussion and Outlook

The determined topocentric station rates from VLBI are not significant. The statistical uncertainties are much larger than the determined rates. In the GPS case, the horizontal rates are significant in a statistical sense, while the vertical rate is not. Even though the standard deviations are probably too optimistic due to the large number of observations, we see in particular a significant westward motion by 1.6 mm/y relative to the plate motion model. The corresponding northward motion by 0.5 mm/y is less significant. The results indicate that we might detect a deviation from the plate tectonic model, which is not supported by the VLBI results.

We therefore also investigated the distance between the VLBI and GPS monument. Here we used the station positions in the cartesian geocentric system, i.e. ITRF05. We interpolated the GPS positions to the exact epochs of the few VLBI results and calculated the cartesian distance between the reference points. Unfortunately, there are only 12 common epochs between 1999 and 2003. The time series of distance between VLBI and GPS is shown in Fig. 3. We analyzed the time series and determined average values for the distance and its linear change with time. Again we used the epochs given on the IGS webpage [1] to introduce breaks in the time series. There are three sections in the time series and the average distances are 106.476 ± 0.001 m, 106.485 ± 0.001 and 106.495 ± 0.001, and the rate is -1.9 ± 0.1 mm/y. The distance corresponds reasonably well with the local tie results, however, the decrease in distance is surprising. The decrease in distance is consistent with the detected westward motion of the GPS station.

This result might indicate that there is some local motion at the Yebes station, possibly related to the building on where the GPS station is mounted.

Currently we work on a homogeneous reanalysis of all geodetic VLBI

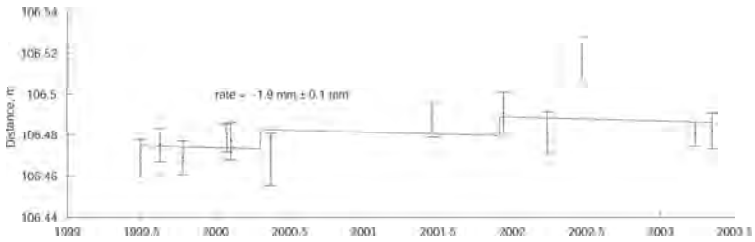

Figure 3. Time series of distance between VLBI and the GPS antenna at YEBES

sessions in which the Yebes 14-m radiotelescope participated, not only European experiments. We use auxiliary information from a numerical weather model as well as the best a priori geophysical models. In particular we are curious whether the results for local motions between the GPS and VLBI equipment at the station can be confirmed when we include more VLBI data. A complete reprocessing, together with planned local-tie measurements, is of major importance for the combination of the historic VLBI observations performed with the 14-m radiotelescope and the future observations with the new 40-m radiotelescope. Future geodetic VLBI sessions with the new 40-m radiotelescope will help to improve the results for the station position and velocity at Yebes.

References

[1] International GNSS Service (IGS); igscb.jpl.nasa.gov.

[2] Ma, C., J.M. Sauber, L.J. Bell, et al. Measurement of horizontal motions in Alaska using very long baseline interferometry. J. Geophys. Res., 95(2), 21991–22011, 1990.

[3] Letellier, T. Etude des ondes de marée sur les plateux continentaux. Thése doctorale, Université de Toulouse III, Ecole Doctorale des Sciences de l'Univers, de l'Environnement et de l'Espace, 2004.

[4] European Centre for Medium-Range Weather Forecasts; www.ecmwf.int.

[5] De Mets, C., R.G. Gordon, D.F. Argus, et al. Effect of recent revision to the geomagnetic reversal time scale on estimates of current plate motions. Geophys. Res. Lett., 21(20), 2191–2194, 1994.

[6] Webb, F.H., J.F. Zumberge. An introduction to the GIPSY/OASIS II. JPL Publ., D-1108 8, 1993.

The 5th IVS General Meeting Proceedings, 2008, p. 98–103

VLBI Activities of Tsukuba 32-m Station and Tsukuba Correlator

Shigeru Matsuzaka [1], *Kojin Wada* [1], *Etsuro Iwata* [1], *Hiromi Shigematsu* [1], *Shinobu Kurihara* [1], *Machida Morito* [1], *Kensuke Kokado* [1], *Daisuke Tanimoto* [2], *Kentaro Nozawa* [2]

[1)] *Geographical Survey Institute, Japan*

[2)] *Advanced Engineering Services Co., Ltd., Japan*

Abstract. We present an overview of the VLBI activities of Tsukuba 32-m station and Tsukuba Correlator by Geographical Survey Institute (GSI), Japan. During 2005 to 2007, we succeeded in introduction of K5/VSSP32 sampling/recording system, K-band (22 GHz) receiver and Parnassus (K5 correlation aiding software). On the other hand, we started observation with e–VLBI. In addition, with a prospect of becoming an IVS Analysis Center in the future, we are putting the global analysis into practices experimentally.

1. Tsukuba 32-m Station Observation Components

1.1. K5/VSSP32 SYSTEM

Tsukuba 32-m station introduced the K5/VSSP32 sampling/recording system (Fig. 1, Tabl. 1).

History:

Until May 2005

Mark 4 tape recording.

May 2005

K5/VSSP HDD recording started.

–At the beginning, we had some troubles.

March 2006

K5/VSSP32 was bought.

–About one year, we had made the testing and adjustment.

May 2007

K5/VSSP32 HDD recording started.

–No data missed!

(Fig. 2)

Table 1. Comparison of Specifications

	K5/VSSP	K5/VSSP32
Sampling frequency (MHz)	0.04, 0.1, 0.2, 0.5, 1, 2, 4, 8, 16	0.04, 0.1, 0.2, 0.5, 1, 2, 4, 8, 16, 32, 64
Built-in digital LPF (MHz)	N.A.	2, 4, 8, 16, through
Analog Input range	-1V to +1V	-1V to +1V
Analog Bandwidth	100 MHz	300 MHz
AD resolution (bit)	1, 2, 4, 8	1, 2, 4, 8
Number of channel per unit	1, 4	1, 4
Maximum Data Rate	16 Mbps/ch 64 Mbps/unit 256 Mbps/module	64 Mbps/ch 256 Mbps/unit 1024 Mbps/module
DC offset adjust	N.A.	available from host PC
Reference signals	1PPS, 10 MHz	1PPS, 10 MHz or 5 MHz
Interface to PC	PCI bus	USB 2.0

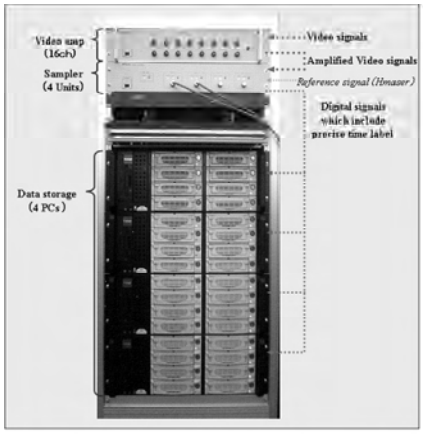

Figure 1. K5/VSSP32 system

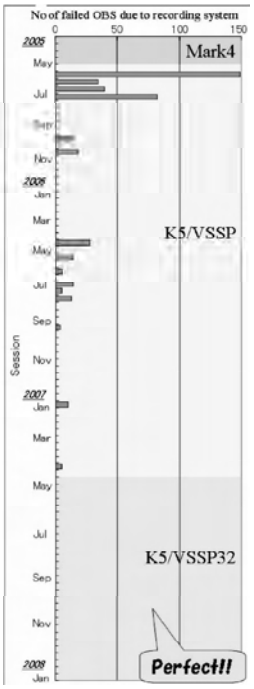

Figure 2. Number of failed OBS due to each recording system

1.2. K-band (22 GHz) Receiver

In a collaborative research with Tsukuba University, a K-band (22 GHz) receiver (Fig. 3) was introduced to the Tsukuba 32-m antenna.

History:
2006
–design and develop of 22 GHz receiver,
–set up and test of 22 GHz receiver,
–adjustment of observation system,
–test observations.
2007
–set up of related equipments,
–investigation to remove the standing wave,
–adjustment of 22 GHz receiver,
–pointing,
–single dish observation by Tsukuba University,

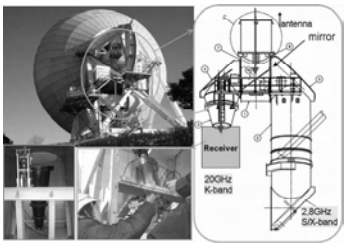

Figure 3. K-band (22 GHz) receiver

They succeeded in observing recombination lines, ammonia and water-vapor maser lines and continuum emission, in Dec. 15–16, 2007.
2008
–single dish observation.

1.3. The Special Maintenance and the Purchase of New Equipment

As the antenna and observation equipment show some signs of wearing out after 10 years of usage, we need special maintenance and the purchase of new equipments.

A panel of Tsukuba 32-m antenna fell down in strong wind in Jun. 2007 (Fig. 4).
We did "Total Check up" in Sep.–Oct. 2007.
–All bolts were tightened and problems were dug up.
–Worn-out antenna rail was pointed out in the check.

2. Observation with e–VLBI

Tsukuba 32-m station transfers the international VLBI observation data to correlator using high-speed network (Fig. 5). Since 2007, we have endeavored to observe with e–VLBI, and achieved rapid processing in UT1 measurement (Tabl. 2).

Figure 4. Tsukuba 32-m antenna repairing

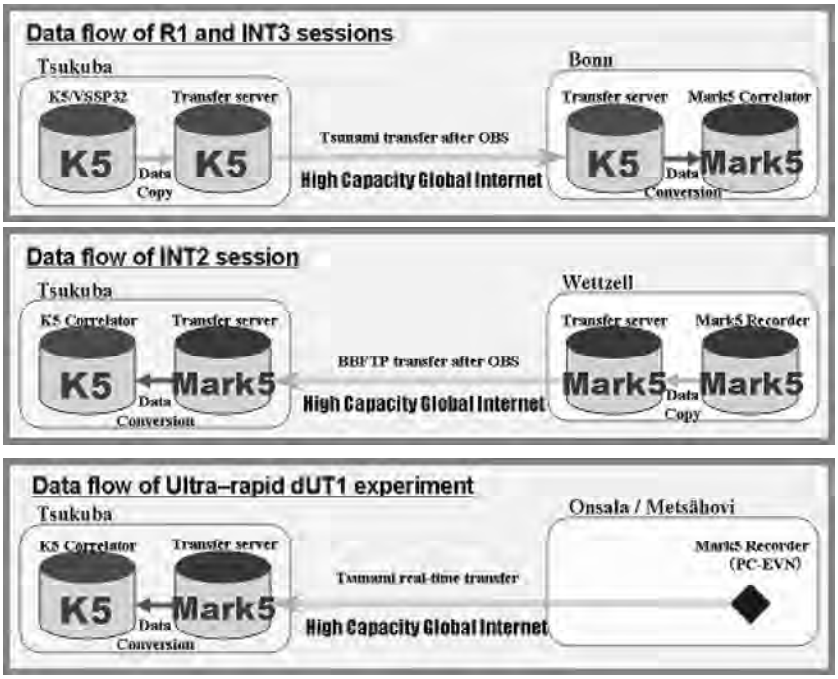

Figure 5. Data flow each session

3. Tsukuba VLBI Correlator: Development of Parnassus

We had developed Parnassus (Fig. 6), which is an intelligent application with graphical user interface to aid the operation of K5 kernel programs, during 2005 to 2007.

Table 2. Comparison of each UT1 measurement sessions

Session	Data Transfer Method (Transfer Time)	Latency Period of UT1 measurement	Stations	Correlator
INT1	Shipping (2–3 days)	3–5 days	Wz,Kk, (Sv)	Washington
INT2	BBFTP Transfer (about 3 hours)	1–3 days	Ts,Wz	Tsukuba
INT3	Tsunami Transfer (about 30 minutes)	a few hours	Ts,Wz, Ny	Bonn
Ultra-rapid dUT1	Tsunami Real-time Transfer (Direct)	a few minutes	Ts,Kb, On,Mh	Tsukuba Kashima

History of Parnassus development:
2005
–Ver1.0 Set up of correlation.
2006
–Ver1.2 Bandwidth synthesis covered.
2007
–Ver1.3 Corresponds to key program (by NICT) upgrade.
2008
–We would like to make all the processes automatic and faster.

Figure 6. First screen of Parnassus

Feature of Parnassus:
–Automatic fringe search with the coarse search function.
–Making of a priori file, automatic correlation, and the bandwidth synthesis in two or more obs and baselines.
–Various settings of processing can be done on the GUI screen.

4. Various VLBI Analysis Activities

We are putting various VLBI analysis into practice experimentally, with the prospect of becoming an IVS Analysis center in the future.
We have been doing various VLBI analysis:
– The analysis for 24-h sessions
(We have analyzed about 4 times/year latest result: gsi2008a),
– The analysis for 1-h sessions

(We have analyzed about 4 times/year latest result: int2008a),
- The analysis for CONT05 sessions
  (We have analyzed after CONT05 result: cont05).

References

[1] Fujisaku, J., K. Kokado, K. Takashima. Tsukuba 32m VLBI station. IVS 2005 Annual Report, 2005.

[2] Kokado, K., J. Fujisaku, K. Takashima. Tsukuba 32m VLBI station. IVS 2006 Annual Report, 2006.

The 5th IVS General Meeting Proceedings, 2008, p. 104–108

The Past Decade of Tsukuba 32-m VLBI Station

Shigeru Matsuzaka, Kozin Wada, Etsurou Iwata, Hiromi Shigematsu, Shinobu Kurihara, Morito Machida, Kensuke Kokado, Daisuke Tanimoto

Geographical Survey Institute, Japan

Abstract. Tsukuba 32-m VLBI station is operated by Geographical Survey Institute (GSI) VLBI group. The station was constructed in 1998, and GSI has been participating a lot of sessions and performing various experiments with the station. This report summarizes the past decade of the station.

1. 1998–2002

Before 2000, GSI had participated in domestic / international observations with Kashima 26-m antenna. In 2002, Kashima 26-m (Fig. 2) was dismantled because it became too old for work, and Tsukuba 32-m (Fig. 1) became a target of the azimuth from origin for horizontal coordinates in Japan (Fig. 3). Tsukuba 32-m has been participating in various geodetic VLBI observations as the key station of GSI VLBI network (Tabl. 1).

Figure 1. Tsukuba 32-m antenna

Figure 2. Kashima 26-m antenna

Table 1. Event Calender of Tsukuba 32-m VLBI Station

Year	Events
1998	– The Tsukuba 32-m VLBI station constructed with K4/Mark 4 equipments. – Opening ceremony.
1999	– The height of the antenna had changed +43.7 mm because of the AZ rail replacement.
2000	– Japan-Tie sessions (Kashima 26-m, 34-m and Tsukuba 32-m).
2001	– 1st co-location observation.
2002	– Dismantlement of Kashima 26-m antenna. – Revision of survey act (Tsukuba 32-m became a target of the azimuth origin).
2003	– Tsukuba 32-m installed high-speed optical fiber network "Super-SINET".
2004	– Contribution to Mars Exploration Rover Mission.
2005	– Installation of K5/VSSP system. – Start of the observations using the K5/VSSP system. – Discarded magnetic tapes and tape recorder. – Contribution to Deep Impact mission. – CONT05.
2006	– Installation of K-band receiver by Tsukuba University.
2007	– A insulator panel of Tsukuba 32-m was broken by strong wind. – Installation of K5/VSSP32 system with USB interface. – Success of ultra rapid dUT1 experiment (Onsala-Tsukuba).
2008	– 2nd co-location observation. – CONT08 (Plan).

GSI VLBI Group performed co-location observation to determine the relative position of GPS-based control station to Tsukuba 32-m antenna (Fig. 4).

2. 2003–2005

Tsukuba 32-m is engaging e–VLBI observations for IVS-INT2 and submits weekend observation database on Monday. This short latency had contributed to the success of Deep Impact mission by providing the newest UT1 parameter (Fig. 5).

Tsukuba 32-m has established a semi-unmanned observation system, utilizing K5/VSSP system to directly record the data on linux format and to check raw observation data (Fig. 6).

Figure 3. Target of Azimuth from Horizontal Origin Point

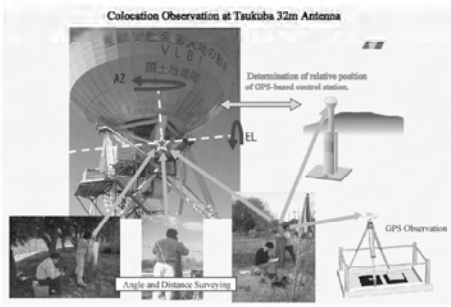

Figure 4. Colocation Observation

Figure 5. Deep Impact Mission

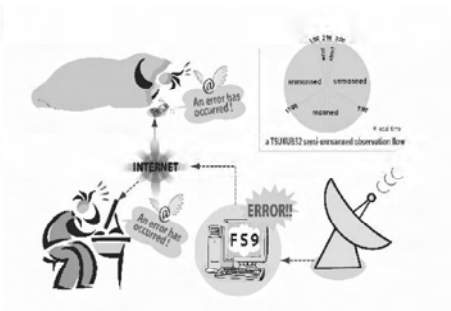

Figure 6. Observation System

3. 2006–2008

One of the insulator panels of the antenna was broken by strong wind and fell down to the ground on Jan. 3, 2007. After that, we implemented an overall check of the antenna.

Tsukuba 32-m has implemented experiments for Ultra Rapid UT1 measurement. The purpose of the experiment is to obtain the UT1 result within 30 minutes after the end of the last scan in the experiment. We succeeded in obtaining the UT1 result within 4 minutes after the experiment with ONSALA60 in Feb. 21, 2007.

4. Recorder Transition

So far, Tsukuba 32-m has changed the VLBI recorder 3 times (Fig. 7). The 1st recorder is K4/Mark 4 which recorded the observation data in magnetic tapes. The 2nd recorder is K5/VSSP which recorded the data as linux file, so we could check easily whether recording data was success. Now, we use K5/VSSP32 which enables us to record the data in 64 Mbps/ch (Total 1024 Mbps) with USB interface between the sampler and the hard disk.

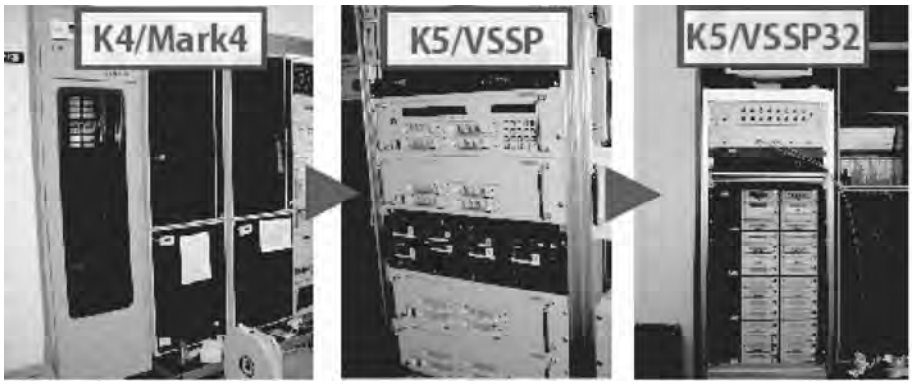

Figure 7. Recorder Transition of Tsukuba 32-m

5. Regular Sessions at Tsukuba 32-m

Tsukuba 32-m has participated in a lot of domestic and international sessions every year. The number of the sessions has steadily increased (Fig. 8). In 2007, the number reached 161 sessions. We plan to participate in about 190 sessions in 2008.

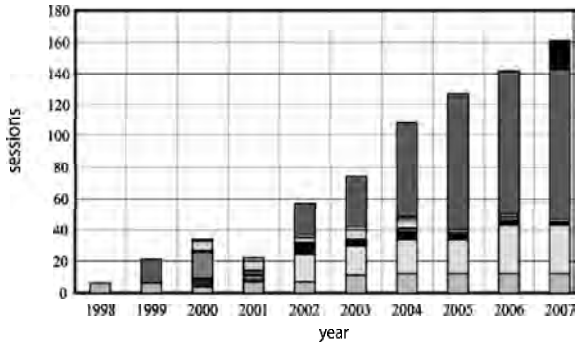

Figure 8. Regular Sessions at Tsukuba 32-m

References

[1] Fujisaku, J., K. Kokado, K. Takashima. Tsukuba 32 m VLBI station. IVS 2005 Annual Report, 2005.

[2] Kokado, K., J. Fujisaku, K. Takashima. Tsukuba 32 m VLBI station. IVS 2006 Annual Report, 2006.

The 5th IVS General Meeting Proceedings, 2008, p. 109–113

Twin Telescope Wettzell — a VLBI2010 Radio Telescope Project

Hayo Hase [1], *Reiner Dassing* [1], *Gerhard Kronschnabl* [1], *Wolfgang Schlüter* [1], *Walter Schwarz* [1], *Richard Kilger* [2], *Pierre Lauber* [2], *Alexander Neidhardt* [2], *Konrad Pausch* [3], *Willi Göldi* [4]

[1)] *Bundesamt für Kartographie und Geodäsie, Germany*

[2)] *Technische Universität München, Germany*

[3)] *Vertex Antennentechnik GmbH, Germany*

[4)] *MIRAD Microwave AG, Switzerland*

Abstract. With its Twin Telescope Wettzell (TTW) project BKG is realizing a radiotelescope system based on the specifications of the IVS VLBI2010 vision. It consists of a pair of identical fast moving radio telescopes of the 13.2 m class with innovative ring focus optics which are optimized for observations with a wide spectrum receiver up to at least 12 GHz (covering S/X band). The two radio telescopes will allow non-stop 24 h/d observations. The two antennas will also be used in an array mode for higher sensitivity. The project is scheduled to be carried out at the Geodetic Observatory Wettzell during 2008-2011.

1. Motivation

In the early 80s at the beginning of geodetic VLBI observations, a number of radio telescopes originally designed for astronomical or satellite tracking purposes, had been transformed into geodetic instruments. The Wettzell 20-m radio telescope was the first specifically designed for geodetic VLBI observations. It started operations in 1983. This instrument has been so far the most productive geodetic VLBI instrument worldwide. After more than 25 years of daily operations it is time to consider to meet future objectives and requirements with a modern replacement.

With the inception of the IVS in 1999 an official international organization for geodetic VLBI served as a platform to discuss common issues on the international level focusing on the improvement of the indispensible VLBI service. The IVS Working Group 2 "Product Specification and Observing Program" identified a number of IVS products which require a continuous 24 hours/7 days

VLBI operation [1]. The most important VLBI parameters are the Earth orientation parameters, station coordinates and some physical parameters related to the atmosphere.

For the realization of the updated product catalogue the "IVS VLBI2010 Vision" was developed by the Working Group 3 [2]. The task of this group was to analyze 1) the existing approach to geodetic VLBI observations with respect to newer technical components (wide band frontends, high speed sampler, digital backends), 2) the increasing problem of radio frequency interference at observing sites due to commercial exploitation of the S-band and X-band and 3) the need for more frequent observations to increase the global accuracy to 1 mm in the position and to 1 mm/y in the velocity level.

The VLBI2010 Vision concluded in a raw specification for the next generation VLBI instrument. The future instrument should:

- guarantee that the error in position and velocity of the reference point are less than 1 mm and 1 mm/y respectively. This must be achieved by the construction of the radio telescope.
- allow continuous observations of Earth orientation. Due to telescope maintenance cycles this is only possible with more than one radio telescope per site.
- observe much more sources per time unit. This requires a reduction of antenna idle and slewing time which calls for faster moving antennas.
- be less susceptible to external radio frequency interference. This implies the observation of a wider spectrum in a much larger range from $2 - 18$ GHz.

On the basis of these requirements the Wettzell VLBI group specified a new radio telescope project: The Twin Telescope Wettzell (TTW).

2. Twin Telescope Wettzell

The Twin Telescope Wettzell is a rigorous approach to comply with the demands of the VLBI2010 vision. It consists of two identical radio telescopes. The technical specification was written in Wettzell during 2006–2007 [3]. The bidding procedure followed afterwards and resulted in contracting the German company Vertex Antennentechnik GmbH as the main contractor. The project started in January 2008 and will finish by the end of 2011.

2.1. Technical Features

The challenges in the construction of radio telescopes for geodetic VLBI are 1) high stability of directivity and path length in the antenna optics to maintain phase coherence, 2) very low system noise temperature also at higher frequencies – contradicting with 3) a wide band feed system.

Based on these challenges the Vertex company proposed a rarely built ring focus design. Its radial symmetric concept combines the low noise advantage

of a dual-offset antenna with good mechanical stability, antenna control and weight of a common Cassegrain or Gregory design.

2.1.1. Ring Focus Optics

The ringfocus design is also known under the term axially-displaced ellipse reflector [4]. The radial symmetric reflector is achieved by a rotating parabel whose vertex is offset by a given radius vertical to the rotational axis. Hence the primary focus and the vertex itself transform into a focal ring instead of a point. In order to focus the ring beam of the primary reflector to a secondary focal point a rotating ellipse defines the shape of the subreflector. The parameters of the rotating ellipse must be chosen to ensure that the primary focus ring defines the first focal point of the ellipse and that the second focal point is located on the optical axis [5].

If the subreflector radius is not larger than the radius of the shifted vertex, there exists no obstruction by the subreflector in the main reflector. Only the support legs cause a small loss (Fig. 1).

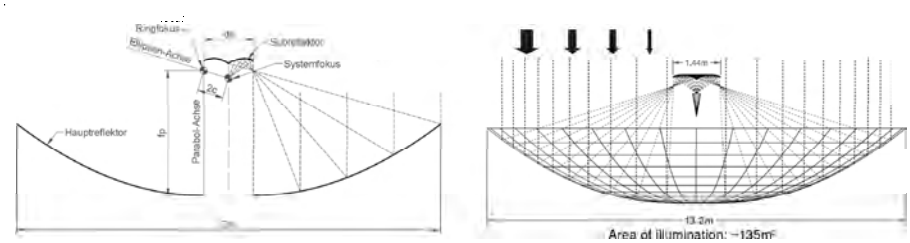

Geometric design elements. Illumination and path geometry.

Figure 1. Optics in an Axially-Displaced Ellipse Reflector (Ring Focus)

There are several advantages of the TTW ring focus design: 1) rays from the main reflector rim illuminate the pointed vertex of the subreflector and 2) rays from the main reflector central area illuminate the subreflector rim; 3) minimum reflection of energy towards the feed horn; 4) feed horn can be positioned close to the subreflector as it is needed for a cooled wide band feed.

The TTW radial symmetric main reflector will have a diameter of 13.2 m with an area of illumination of about 135 m^2. As Vertex is delivering 25 12-m radio telescopes to the Atacama Large Millimeter Array (ALMA) the TTW is benefitting from this thoroughly tested, slightly modified ALMA elevation over azimuth mount for the main reflector. The TTW reflector itself will be accurate for up to 40 GHz observations — although initially the observed band shall be in the $2 - 18$ GHz spectrum.

In order to keep path lengths constant and adjust the focus the subreflector is mounted on a hexapod positioner. This positioner provides 3 axial translations with a repeatability of 5 μm and a tilt of 5".

2.1.2. Feed System

According to the VLBI2010 vision the feed system has to accommodate a wide spectral range from $2 - 18$ GHz. The ideal wide band feed demonstrates a constant beam characteristic over the entire spectrum. It must further comply with the condition to have a fixed phase center for the spectrum range. Otherwise there will be no coincidence of the phase center with the focal point leading to a significant decrease of the aperture efficiency. Unfortunately currently known wide band feeds exhibit a fairly small gain in the range of $6-14$ dB and therefore will request permanent cooling. The cooling aspect is important for the definition of the lowest observable frequency which corresponds to the longest wavelength and which ultimately defines the outer dimensions of the feed: the smaller, the better.

Currently there are no satisfactory feeds available. They have to be developed and tested. A promising design is the so called Eleven Feed from Per-Simon Kildal [6]. Alternative designs with combinations of different feed architectures are under investigation. A final decision for the TTW feed system is anticipated by the end of 2008.

In any case, the ring focus design allows the mount of the feed to be close to the subreflector which will then serve as a sun heat shield.

2.1.3. Kinematic Parameters

The TTW radio telescopes will be fast moving. The kinematic parameters had been set to 12 deg/s and 6 deg/s for azimuth and elevation velocity respectively and to 3 deg/s^2 acceleration for both axes. These high velocities shall enable source observation and slewing to the next source in 30 s intervals.

A 27 bit encoder with 0.0003 deg resolution will provide the pointing accuracy.

2.2. VLBI2010 Operation

A 24h/7d operation will either require more staff at the stations or the introduction of a centralized network control which may travel with the daylight zones. This concept requires a corresponding operation control room, which contains e.g. one monitor per network station for remote controlled operation. The TTW operation control room will be designed with sufficient space to allow remote controlled network operation.

Remote control software has been developed in Wettzell and tested with O'Higgins. A PC-Field System remote control interface was also developed at the TIGO observatory and might serve for a future PC-Field System upgrade.

For the IVS Operation Centers the development of the scheduling modes for TTW is still an outstanding issue. If the two radiotelescopes operate simultaneously, they can either be used in the array mode to increase the sensitivity — or observe simultaneously in different directions. Both modes may even temporarily include the existing 20 m radio telescope in Wettzell as a third contributor to a VLBI2010 observing session.

3. Outlook

The major milestones of the TTW project are the following:

- end of 2008: Design review,
- end of 2009: Fundaments, operations building finished,
- in 2010: beginning of TTW assembly at Wettzell,
- end of 2011: final acceptance and start of operation.

4. Conclusion

The TTW-Project is the first rigorous approach to realize a suitable observing instrument according to the VLBI2010 vision of the IVS. It will guide the IVS to an improved service promising more accurate products. It is hoped that the transition time from current IVS operation to future 24h/7d operation can be made together with partners elsewhere in the world by sharing our upgrade experience.

References

[1] Schuh, H., et al. IVS Working Group 2 for Product Specification and Observing Programs. Final Report, 2002; http://ivscc.gsfc.nasa.gov/about/wg/wg2/IVS_WG2_report_130202.pdf.

[2] Niell, A., et al. VLBI2010: Current and Future Requirements for Geodetic VLBI Systems. International VLBI Service for Geodesy and Astrometry 2005 Annual Report. D. Behrend and K. D. Baver (eds.), NASA/TP–2006-214136, 2006, 13–40; http://ivscc.gsfc.nasa.gov/about/wg/wg3/IVS_WG3_report_050916.pdf.

[3] Dassing, R., et al. Technical Specification for the Design, Manufacturing and Construction of the Twin-Telescope Wettzell (TTW). BKG internal document, released version of 2007-07-11.

[4] Prata, A.Jr., et al. Displaced-Axis-Ellipse Reflector Antenna for Spacecraft Communications. Proceedings SBMO/IEEE MTT-S IMOC 2003, 391–395; http://ieeexplore.ieee.org/iel5/8799/27883/01244891.pdf.

[5] Granet, C. A Simple Procedure for the Design of Classical Displaced-Axis Dual-Reflector Antennas Using a Set of Geometric Parameters. IEEE Antennas and Propagation Magazine, v. 41, No 6, 64–71, 1999; http://ieeexplore.ieee.org/iel5/74/17654/00815319.pdf?arnumber=815319.

[6] Olsson, R., et al. Measurements of a 150 to 1700 MHz Low Loss Eleven Feed for the 42 m Radio Telescope at Green Bank; http://ieeexplore.ieee.org/iel5/11208/36089/01710528.pdf.

The 5th IVS General Meeting Proceedings, 2008, p. 114–118

Australian — New Zealand Geodetic VLBI Network Project

Oleg Titov [1], *Sergei Gulyaev* [2], *Jim Lovell* [3], *John Dickey* [3]

[1] *Geoscience Australia, Australia*

[2] *Auckland University of Technology, New Zealand*

[3] *University of Tasmania, Australia*

Abstract. Geodetic VLBI is a technique that maintains the International Celestial Reference Frame (ICRF) and contributes significantly to the International Terrestrial Reference Frame (ITRF) and Earth Orientation Parameter (EOP) service. Currently in Australia only the Hobart (Tasmania) radio telescope is involved in geodetic VLBI observations on a regular basis. A new VLBI network is planned which will consist of four new antennas (three Australian and one New Zealand), each comparatively small (12 meters in diameter) with fast slew rates (5 degrees per second in azimuth) equipped with Mark5B data recorders. All VLBI sites will be co-located with permanent GPS receivers, and some of them with SLR facilities to facilitate the frame-tie and verify the inter-technique performance. Computer simulation is presented which demonstrates that this network will have the potential to significantly improve the accuracy of the ICRF and hence of the ITRF in the Southern Hemisphere (to sub-mas and sub-cm levels, respectively). The first 12-m antenna of this series will be installed near Auckland, New Zealand in Aug. 2008.

1. Australian Network

National Collaborative Research Infrastructure Strategy (NCRIS) is a major initiative under the Government's Backing Australia's Ability — Building our Future through Science and Innovations. It aims to provide researchers with access to the infrastructure and networks necessary to undertake world-class research (http://www.ncris.dest.gov.au).

On Nov. 27, 2006 the Minister announced a funding allocation for twelve NCRIS priority areas. One of these twelve areas is "Structure and Evolution of the Australian Continent" which will help build an integrated national infrastructure system — AuScope. It has been awarded 42.8 million of Australian dollars, of which 15.4 million is committed to develop an enhanced national geospatial reference system.

The National Geospatial Reference System (NGRS) is a key element of the

AuScope providing a nationwide reference frame definition to support geodetic, seismic risk, neotectonic and geodynamics research, and also the basis for a wide range of spatial science applications.

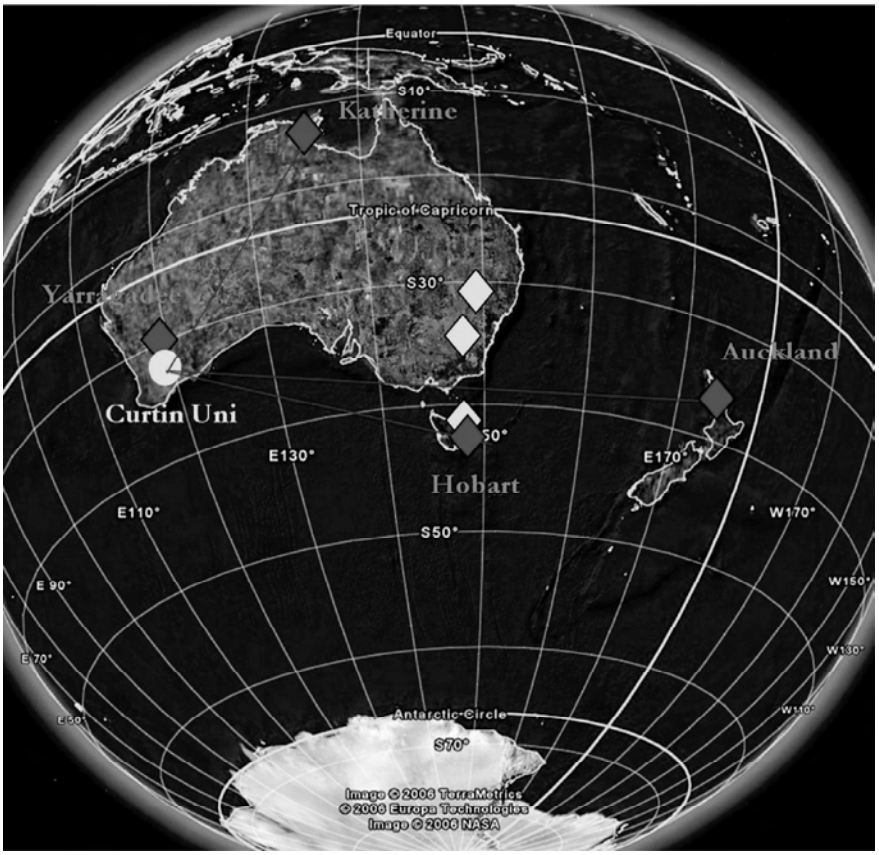

Figure 1. Location of the Australian and New Zealand radio telescopes

The AuScope proposal includes new VLBI sites at Yarragadee (Western Australia) and Katherine (Northern Territory) and a replacement of the Hobart (Tasmania) telescope. In addition, a software correlator system for correlation analysis of VLBI data will be developed at Curtin University within AuScope. In total 8.4 millions will be spent for VLBI infrastructure development in Australia including the correlator facility (6.7 within AuScope and 1.7 from other sources).

Fig. 1 shows the locations of the radio telescopes. They are separated by baselines of three–four thousand kilometers and produce a set of transcontinenal baselines ranging in length from three–eight thousand kilometers for Australian based radio telescopes.

Figure 2. 12-m dish "Patriot"

The 12-m fully steerable antenna (Fig. 2) was ordered from the "Patriot" manufacturers. Technical characteristics are in Tabl. 1.

Table 1. Technical specifications of the radio telescope

Diameter	12.1 m
Mount	Alt-Az
Surface accuracy	0.3 mm
F/D	0.375
Pointing accuracy	0.005 deg
Operation temperature	−15 to 55°C
Optics	Cassegrain with shaped primary and secondary reflectors
Frequency range	1.5–17 GHz
Slewing rate In azimuth In elevation	 5 deg/s 1.25 deg/s
Elevation limit	5 deg

We believe that the fast slew rate radio telescopes located in different parts of Australia and New Zealand will help to improve the geodetic positioning.

2. New Zealand Network

New Zealand, through the Institute for Radiophysics and Space Research (IRSR) at Auckland University of Technology (AUT), will operate a new geodetic VLBI 12-meter radio telescope near Warkworth (50 km north of Auckland), which is planned to be installed in Aug., 2008.

3. Simulations

Both Australia and New Zealand occupy a geographically strategic position for strengthening the global reference frame. Building new geodetic VLBI stations in Australia and New Zealand with fast slew rate antenna can provide a possibility for improving global reference frame accuracy.

Fig. 3 shows the improvement in vertical and horizontal components for Hobart site with respect to the existing Hobart 26-m radio telescope (slew rate 1 degree/second). The simulations have been done with a realistic schedule based on six existing telescopes in the Northern hemisphere, Hartrao (South Africa) plus a set of Australian and New Zealand sites. All components are expected to be improved by a factor of 3–4.

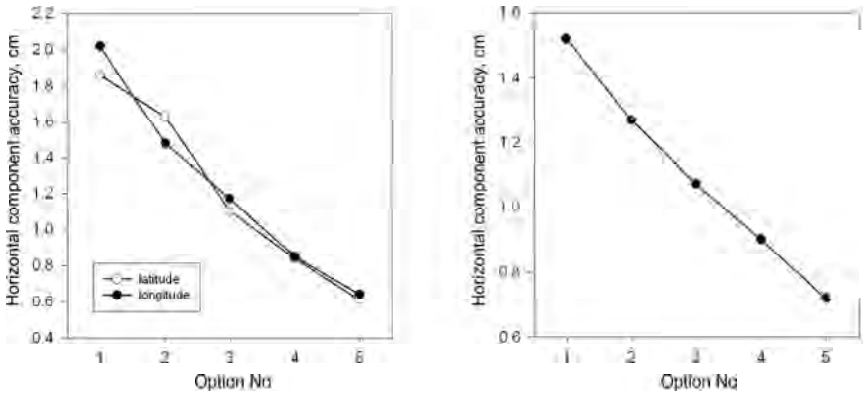

Figure 3. Improvement in horizontal and vertical accuracy for Hobart site with different options including six 'core' VLBI sites plus: 1 — the existing 26-meter Hobart dish; 2 — Hartrao and new Hobart dish; 3 — Hartrao, new Hobart and Yarragadee; 4 — Hartrao, new Hobart, Yarragadee and Katherine; 5 — Hartrao, new Hobart, Yarragadee, Katherine and Auckland

4. Data Correlation

A major requirement for VLBI data processing has been the correlation of interferometric signals received at the individual antennae. Until now this has been achieved by hardware correlators, and this has restricted the rates at which data can be collected. More recently, software correlators have been developed. This has led to a significant reduction in the cost of correlation. Coupled with the broadband network capabilities both in New Zealand (Kiwi Advanced Research and Education Network — KAREN) and Australia (AARNet), as well as with supercomputing capabilities both in Australia (Swinburne University of Technology, Curtin University of Technology and others) and in New Zealand (Blue Gene at University of Canterbury, New Zealand Supercomputing Centre in Wellington and others), it will permit Australia and New Zealand to perform near-real time analysis of the data collected under this programme.

Acknowledgements

We are thankful to Peter Shield for his kind permission to use the picture of the 12-m antenna and Dirk Behrend for producing the numerious simulated VLBI data files. The paper is published with the permission of the CEO, Geoscience Australia.

The 5th IVS General Meeting Proceedings, 2008, p. 119–123

The EVN Mark IV Data Processor at JIVE and e–VLBI Developments in the EVN

Robert Campbell, Arpad Szomoru

Joint Institute for VLBI in Europe, Netherlands

Abstract. We review the capabilities of the European VLBI Network (EVN) Mark IV Data Processor at JIVE, briefly touching on operations for EVN/global (astronomical) observations. The greatest strides in the past two years have come in establishing an operational real-time e–VLBI facility. The e–EVN has observed 17 proposal-driven real-time science experiments since 2006, using a 6-station array. We can now reliably sustain 512 Mbps data rates, and we anticipate more stations joining the e–EVN in 2008. Tests since the summer of 2007 have achieved real-time fringes at rates of 920–978 Mbps on 3–5 station arrays over a single Gbps connection via packet dropping, and also real-time fringes from Shanghai and Australian stations correlated at JIVE. The e–VLBI development has included work on a grid-based software correlator currently used for processing (non-real-time) the ftp fringe-tests in EVN sessions.

1. Current Capabilities

The EVN Mark IV Data Processor can correlate simultaneously up to 16 stations with 16 channels (8 dual-pol subbands (SB)) per station, each having a maximum sampling rate of 32 Msamples/s, for a maximum of 1 Gbps per station. We can currently correlate/provide: (*i*) Mark 5A or Mark 5B recordings (5B playback via 5A+) in either Mark4 or VLBA format with 1- or 2-bit sampling; (*ii*) full Stokes polarization output; (*iii*) up to 2048 frequency points per baseline/SB/pol; (*iv*) full-correlator integration times $t_{\rm int}$ down to 0.25 s; (*v*) oversampling at 2 or 4 times the Nyquist frequency, providing $BW_{\rm SB}$ down to 500 kHz; (*vi*) multi-pass correlation, (experiments requiring enhanced spectral-resolution per SB, or having $N_{\rm sta} > 16$); and (*vii*) real-time e–VLBI operation. Development of recirculation and Mark 5B playback is underway.

The total correlator capacity can be expressed as:

$$N_{\rm sta}^2 \cdot N_{\rm SB} \cdot N_{\rm pol} \cdot N_{\rm frq} \leq 131072\,. \tag{1}$$

Here, $N_{\rm frq}$ is the number of frequency points per baseline/SB/pol, $N_{\rm SB}$ is the number of subbands, and $N_{\rm pol}$ is the number of polarizations to correlate. The value of $N_{\rm sta}$ is "granular" in multiples of 4 (*e.g.,* for 5–8 stations, $N_{\rm sta}$=8).

Independent of equation 1, the maximum number of input channels ($N_{\rm SB} \cdot N_{\rm pol_{\parallel}}$) is 16, and the minimum and maximum $N_{\rm frq}$ are 16 and 2048. You can evaluate whether your experiment adheres to equation (1) interactively with the EVN calculator (via the Users' Guide on the EVN web site www.evlbi.org).

Recirculation time-shares the correlator chips for observations that don't use the maximum $BW_{\rm SB}$ (16 MHz). This effectively increases the correlator capacity for some types of experiments, by multiplying the right-hand side of equation (1) by a factor $\mathcal{R} = 16\,{\rm MHz}/BW_{\rm SB}$ up to a maximum $\mathcal{R}$ of 8. However, the maximum $N_{\rm frq}$ would remain 2048. The most significant benefit of recirculation would be increased spectral resolution for narrow-band global spectral-line observations.

The minimum $t_{\rm int}$ for a configuration using the whole correlator is now 1/4 s, and some configurations that use less than half the correlator can achieve $t_{\rm int}$ of 1/8 s. With recirculation, the minimum $t_{\rm int}$ would increase by a factor of $\mathcal{R}$ from its nominal value. Short integration times, coupled with the spectral resolution afforded by large $N_{\rm frq}$, allow mapping wider fields of view, via reduced bandwidth- and time-smearing in the u-v plane. The EVN calculator evaluates field-of-view limitations due to each of these smearing effects.

The standard distribution product is IDI FITS files (typically for further analysis in AIPS). One potential drawback to wide-field correlations (with the short $t_{\rm int}$ and large $N_{\rm frq}$ they require) is the rapid growth of the size of the output FITS files — reaching about 7–10 GB per correlator pass per hour of observation. The current record for the total size of output FITS files for a single experiment stands at 1028.7 GB.

2. Operations & Data Flow

The Science Operations & Support Group at JIVE provides assistance for all phases of a user's experiment — from proposing/scheduling, through correlation and review of the raw output, to analysis of the resulting FITS data. Refer to the contributions in the most recent EVN symposium [1] or EVGA Working Meeting [2] for further details related to the pre-observation/pre-correlation steps, the post-correlation data review process, the operation and content of the EVN pipeline, and the population and use of the EVN Data Archive.

3. Real-time e–VLBI in the EVN

One of the highlights at JIVE over the past two years has been the funding and commencement of EXPReS (Express Production Real-Time e–VLBI Service). This is a three-year I3 (Integrated Infrastructure Initiative) project funded by the EC (DG-INFSO), with the broad goals of (*i*) enabling an operational real-time e–EVN for astronomical applications and (*ii*) looking beyond the current 1 Gbps recording/correlation environment. The EXPReS web-site www.expres-eu.org provides the most up-to-date information.

By the time of the 4$^{\rm th}$ General Meeting, we had established a 5-station

e–EVN array (Westerbork, Jodrell Bank, Cambridge, Onsala, Torun) capable of reliable 128 Mbps operation. In Mar. 2006, Medicina became the sixth station, and in April 2006 we conducted our first successful real-time e–EVN user projects (two experiments spanning 16 h). Tests at the end of May 2006 achieved 256 Mbps from 6 stations. Further work on improving the reliability of the network connections and Mark 5 units at the stations and at JIVE led to the first user e–EVN experiments at 256 Mbps in Oct. 2006. We saw our first real-time e–VLBI fringes from Mh in Mar. 2007 (256 Mbps at K-band). In Jan. 2007, we achieved a sustained 512 Mbps for 1 h on a 5-station array (no Tr); 4 hours of 512 Mbps from all six stations came in Jun. 2007. Efforts in the winter of 2007/8 focused on approaching Gbps rates through packet dropping. In Dec., we maintained 920 Mbps for over an hour on a 5-station array (On did not then have an upgraded mother-board in their Mark 5 unit). By the end of Jan., we could sustain 978 Mbps for over 3 hours on a 3-station array (Mc, On, Tr) by dropping packets such that all track-frame headers remained intact. However, there was no synchronization among the stations in terms of the packet dropping. We are working towards a system in which we can target an entire VEX-channel exclusively for packet dropping.

During the late summer and autumn of 2007 we conducted various tests involving intercontinental data transmission. During the 24th APAN conference in Aug., we obtained real-time fringes on Sh–Mopra and Sh–Western-European baselines at 256 Mbps, with the data from Sh routed overland via Siberia. We also had about 10 minutes of fringes on the Mopra–Darnhall baseline — at 12304 km (NSW, Australia to Cheshire, UK) this may well be the longest real-time e-baseline to date. In Oct., we sustained real-time fringes at 512 Mbps for over 12 h from the Australian stations Parkes–Mopra–ATCA, with data streaming into the EVN correlator at JIVE along three dedicated light-paths across the Pacific. Fig. 1 shows the evolution of data rates and array sizes in e–VLBI science runs and tests through Feb. 2008.

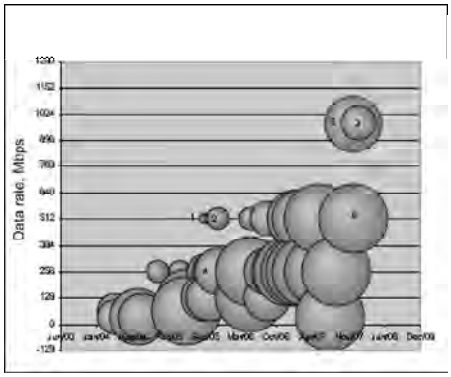

Figure 1. Evolution of e–VLBI data rates and array sizes. The size of the bubbles reflects the number of participating stations

In early Apr. 2008, the 100-m telescope at Effelsberg successfully participated in a real-time test for the first time, producing fringes at 512 Mbps. Inclusion of Ef along with the "original 6" more than doubles the sensitivity of the e–EVN array, clearly making it a much more attractive instrument for astronomers. Also in Apr., we conducted the first user experiments at 512 Mbps (two experiments spanning more than 20 h), including a $12^h48^m21^s$ stretch of continuous correlator output, which established a new record for our longest single job of any sort (e–, disk–, or tape–VLBI).

Connections to the currently participating e–EVN stations are at least 1 Gbps, and all but On and Ef now have dedicated dark fibre or a light-path. Besides the route over Siberia, Sh also has a light-path available across the Pacific at 622 Mbps. Arecibo (PR) has a 512 Mbps connection into Florida. See the EXPReS wiki (www.jive.nl/dokuwiki/doku.php?id=expres:expres) under NA4 for a network diagram showing how these and other stations route their data into the EVN correlator at JIVE.

Coming into the EVN correlator, we currently have a 5 Gbps IP-switched connection to SURFNET (the Dutch NREN), plus eight 1 Gbps light-paths, and 1 Gbps dark-fibre from Wb. To provide more control and independence, we also now have our own central switch and IP space. We have upgraded our Mark 5 units by replacing mother boards (dual 3.2 GHz Xeon CPUs, 2 GB of RAM), and boosting the power supply to 650 W. We are also migrating to DEBIAN linux for the OS. The increased processing capacity permits running modified Mark 5A code that incorporates use of UDP transfer protocols in conjunction with targeted packet dropping tactics, enabling real-time data rates above 512 Mbps.

3.1. Real-time e–VLBI Astronomy

The EVN has offered proposal-driven real-time e–VLBI observations since 2006. There have been 17 successful observations from 28 proposals. The key distinction of a real-time e–EVN experiment is the extremely reduced latency in receiving correlation results; final FITS files are available within a day of the end of observations. For sources that vary on short time-scales — flaring X-ray binaries, gamma-ray bursts, just-exploded supernovae — such short-latency high-resolution VLBI results are vital to adapting observing tactics based on the source's behavior.

e–EVN observing sessions are currently scheduled for 24 h on pre-arranged dates, about once per month. There have been paired dates only 2–3 days apart to permit following source changes on shorter time-scales. A new class of "triggered" proposal enables e–EVN observations of a pre-selected source when its behavior prior to an e–EVN session shows that it has entered an interesting state. The proposals themselves are due at the usual thrice-annual EVN deadlines, but the trigger request can be made up to 24 h before the start of an e–EVN session. The more frequent e–EVN sessions are also beneficial for astrometric monitoring. Work continues towards a more fully dynamic, on-demand observing capability at non-scheduled times.

4. Software Correlation at JIVE

We have been inserting ftp scans into the standard monitoring experiments during EVN sessions for some time. We originally processed those ftp scans using the NICT Software Correlator fx_cor [3], running on an 8-node dual-processor PC cluster, where independent baselines are assigned to different nodes/processors. An automatic-ftp feature added to the Field System has been exercised since the Nov. 2006 EVN sessions. This automatically copies a specified portion of a scan from the Mark 5 disk to a linux file and ftp's it directly to the cluster at JIVE, where the arrival of new data is detected, correlation performed, and results posted to a web page available to the stations. NICT has provided responsive support to enable correlation of new recording modes that they would not normally handle. The ftp fringe tests themselves have been very successful in identifying problems early enough to allow stations to repair them before user experiments would have been affected.

We now process the ftp fringe tests on the software correlator we are developing as part of the EXPReS. This addresses workflow management and correlation algorithms that can be applied to a real-time GRID-based correlator. A workflow manager application prototype, to route data to cluster computers such that the network keeps up with the incoming data, has been developed at Poznań Supercomputing and Networking Center. We are adapting the correlator algorithms developed for observing the descent of the Huygens probe onto Titan [4] to wide-field applications. The resulting XF software correlator has handled the EVN ftp fringe tests since June 2007. It currently runs on a single node, quad-processor CPU, and can correlate 1 second of data from an 8-station array with 8×8 MHz SBs, providing four polarizations per SB and 1024 frequency points per baseline/SB/pol, in ∼100 s.

References

[1] Campbell, R.M. Developments at the EVN Mk IV Data Processor at JIVE. Proceedings of the 8th EVN Symposium. A.R. Marecki (ed.), 2007, 396.

[2] Campbell, R.M., A. Szomoru. Recent Developments at the EVN Mk IV Data Processor at JIVE. Proceedings of the 18th European VLBI for Geodesy and Astrometry Working Meeting. J. Böhm, A. Pany, H. Schuh (eds.), 2007, 15.

[3] Kondo, T., Y. Koyama, H. Takeuchi, et al. Current Status of the K5 Software Correlator. IVS NICT-TDC News, v. 25, 23, 2004.

[4] Pogrebenko, S.V., L.I. Gurvits, R.M. Campbell, et al. VLBI Tracking of the Huygens Probe in the Atmosphere of Titan. Proc. of Planetary Probe Atmospheric Entry and Descent Trajectory Analysis & Science. D. Atkinson, A. Suleman (eds.), C-4.6, 2003.

The 5th IVS General Meeting Proceedings, 2008, p. 124–128

The IAA RAS 6-station VLBI Correlator

Igor Surkis, Vladimir Zimovsky, Alexey Melnikov, Violetta Shantyr, Artemiy Fateev, Andrey Bogdanov

Institute of Applied Astronomy, Russian Academy of Sciences, Russia

Abstract. The development of the 6-station hardware XF correlator at the IAA RAS has almost been completed. The correlator will be used for processing national geodetic VLBI observations. The correlator simultaneously processes VLBI signals from 6 stations (15 baselines) with 16 frequency channels per baseline. The correlator input signals are two-bit VLBI VSI-H signals with 32 MHz maximum clock frequency and maximum data rate of 1 Gbps. The correlator is going to be equipped with Mark 5B playback terminals. We plan to complete and test the correlator in 2009.

1. Introduction

At present the development of the new 6-station Astrometric Radiointerferometric Correlator (ARC) has finished and the production was started. The main goal of ARC is the processing of the national geodetic VLBI sessions. The ARC features are:

- simultaneous processing of VLBI signals from 6 stations (15 baselines);
- 16 frequency channels per each baseline;
- total processing 240 frequency channels;
- two-bit VLBI signals processing;
- 32 MHz maximum clock frequency;
- maximum data rate from each station — 1 Gbps;
- VSI-H input signals;
- Mark 5B playback terminals.

2. Basic Module of Correlator

The main part of ARC is called Basic Module of Correlator (BMC). This device carries out all the hardware data processing. BMC enables processing of

16 single-baseline frequency channels of a typical geodetic VLBI observation. BMC includes 16 correlation units which are a single-baseline single-channel XF correlators for calculating 64 complex delays and picking up phase-cal tones.

BMC is based on FPGA technology. Its schematic is shown in Fig. 1.

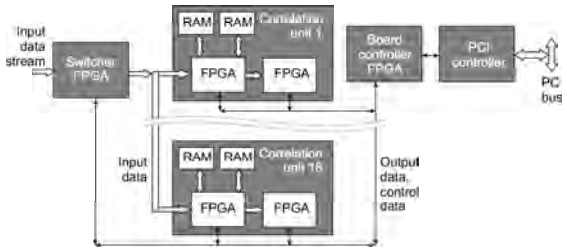

Figure 1. BMC schematic

BMC consists of correlation units, Switcher, BMC controller, and PCI controller. BMC's input data stream is separated and distributed to correlation units with the Switcher, which performs multiplexing of 64 input data bits and 2 valid bits to 16 correlation units. Each unit receives 6 bits – Sign, Mantissa and Valid for each station.

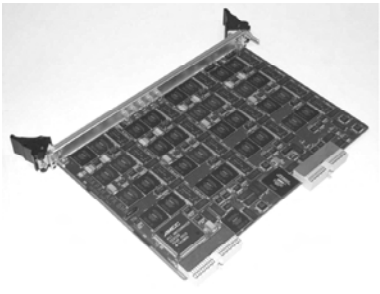

Figure 2. Single BMC board

Figure 3. 4 BMC boards in Compact PCI crate

BMC is a PCI board and controlled through PCI bus. Control commands and model parameters passes to correlation units and Switcher through PCI controller chip and BMC controller. Measured correlation data passes to the control computer through BMC controller, PCI controller and PCI bus. Each correlation unit consists of two FPGA chips and two RAM chips. The data processing algorithms are implemented as FPGA programs. BMC is a Compact PCI 6U front plug-in board. In Fig. 2 and 3 the BMC and 4 BMCs mounted in Compact PCI 6U crate are shown.

3. ARC Hardware Structure

The 6-station ARC includes 6 Mark 5B terminals and 15 BMC. BMCs are installed in four Compact PCI 6U crates. The Signal Distribution and Synchronization System (SDSS) distributes signals from Mark 5B to BMC, so as each BMC receives signals from two Mark 5B. Besides, the SDSS generates and sends synchronisation signals DPSCLOCK and DPS1PPS to Mark 5B terminals.

ARC contains one personal computer with the user interface. Crates with BMCs, Mark 5B terminals and a personal computer are joined into the local correlator network. ARC hardware block diagram is shown in Fig. 4.

SDSS has several types of Compact PCI boards in its constructions. SDSS block diagram is shown in Fig. 5.

The Generator of Synchronization Signals (GSS) produces DPSCLOCK and DPS1PPS signals.

The main part of data stream distribution was performed by Signal Distribution Modules (SDM). Boards receive synchronization signals from the GSS and passes to the Mark 5B terminals. The SDM produces five copies of Mark 5B output data stream from each one of the Mark 5B terminals and then distributes these streams to the BMCs. Each one of the 32-bit (and service bits) parallel LVDS-standard Mark 5B data streams is converted into 4-bit serial LVDS data stream enhancing data transfer characteristic.

The Interface Module of Correlator (IMC) receives 2 serial data streams coming from 2 SDMs, converts data streams into 2 parallel 32-bit TTL data streams and transfers them to the BMC.

SDM and GSS are Compact PCI 6U front plug-in boards. IMC is the Compact PCI 6U rear panel I/O board.

4. ARC Software

ARC software is a distributed system with parts in personal computer and in the four Compact PCI 6U crates. Crate coordination, Mark 5B control and data transfer are made via the local correlator network. The software includes a task-making program, ephemeris program, hardware control program and postprocessing program. At present the correlator results are available as NGS card files.

5. BMC Prototype

The prototype of BMC was developed at IAA RAS in 2004. This small device, named MicroParsec, is able to process two frequency channels simultaneously. It is connected to the S2-PT terminal working in VSI-H mode.

From 2004 to 2006 the 3-station correlator based on these devices has been developed. Now it is used for processing national VLBI experiments carried out with stations Badary, Svetloe and Zelenchykskaya and recorded with the

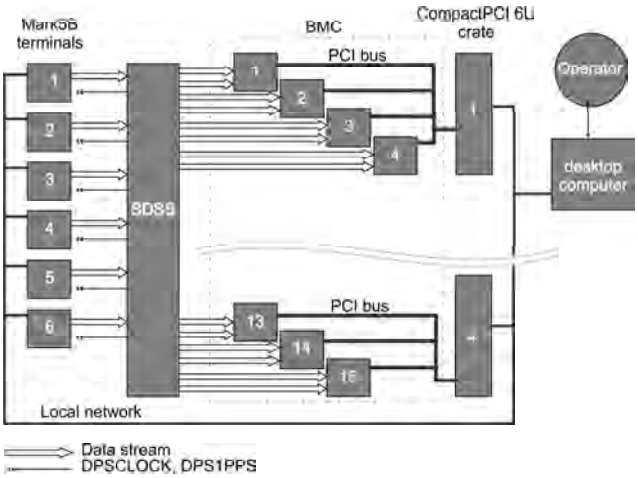

Figure 4. The ARC hardware block diagram

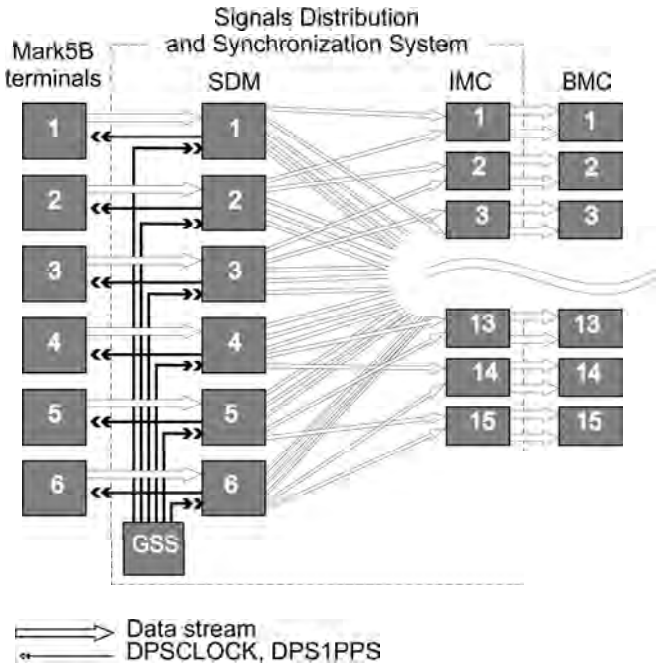

Figure 5. SDSS block diagram

S2-terminals. MicroParsec device and correlator are shown in Fig. 6, 7.

Figure 6. 24-channel correlator based on MicroParsec devices

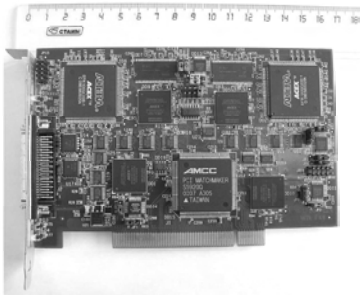

Figure 7. Single MicroParsec device

6. Conclusion

BMC development was started in 2004. To date number of experimental BMC devices have been produced. The production of the correlator prototype has been started. We plan to have a single-baseline ARC prototype in 2008. We plan to complete and to test the complete correlator in 2009.

References

[1] Surkis, I., V. Zimovsky, A. Melnikov, et al. IAA Correlator Center. International VLBI Service for Geodesy and Astrometry 2006 Annual Report. N.R. Vandenberg and K.D. Baver (eds.), NASA/TP–2007–214151, 2007, 143–146.

[2] Surkis, I., V. Zimovsky, A. Melnikov, et al. IAA Correlator Center. International VLBI Service for Geodesy and Astrometry 2007 Annual Report. N.R. Vandenberg and K.D. Baver (eds.), 2008.

[3] Surkis, I., V. Zimovsky, A. Melnikov, et al. The new generation correlators for Quasar VLBI network. IAA RAS Transactions, v. 16. “Nauka”, St.-Petersburg, 2006 (in Russian).

[4] Surkis, I., V. Zimovsky, A. Melnikov, et al. The The Correlator Center of The IAA RAS. IAA RAS Transactions, v. 17. “Nauka”, St.-Petersburg, 2007 (in Russian).

The 5th IVS General Meeting Proceedings, 2008, p. 129–133

CVN Software Correlator Development and Applications in Chinese Lunar Exploration Mission

Zheng Weimin, Luo Wuchao

Shanghai Astronomical Observatory, Chinese Academy of Sciences, China

Abstract. Being able to achieve very high angular resolution, the Chinese VLBI Network (CVN) was used as an auxiliary facility to track the Chinese lunar probe Chang'E-1 (CE-1) besides the traditional Unified S-Band (USB) command system. With great flexibility, the software correlator is well suited for VLBI deep-space tracking applications, so two software correlators (NRSC and WBSC), based on the commercial multiple processor servers were developed for the narrow band near real-time data processing and the wide band non-real-time data processing, respectively. NRSC has the abilities of fast satellite fringe search and multi-channel phase calibration abstraction, which are especially useful in spacecraft tracking. As the main correlation equipment, the software correlator played an important role in the one-month critical near real-time tracking mission, when CE-1 probe transferred from the phase orbit to the circumlunar orbit in 2007. Operation results indicate that the software correlator has the characteristics of flexible structure, reliability, scalability and it will be used in more CVN geodesy and astronomy observations, as well as deep-space exploration scientific activities in the near future.

1. Introduction

The Chinese VLBI Network (CVN) was used as an auxiliary facility to help the traditional Unified S-Band (USB) command system to fulfill the Tracking, Telemetry and Control (TT&C) task of the first Chinese lunar probe Chang'E-1 (CE-1). This mode is dubbed USB + VLBI.

CVN consists of four VLBI stations (in Shanghai, Beijing, Kunming and Urumqi) and a data processing center (in Shanghai Astronomical Observatory). The stations and the data center are connected by network.

In the tracking mission, the data center accomplished all the tasks such as VLBI observation schedule, data correlation, post processing, atmosphere delay correction, position determination and orbit determination and supplied the Beijing Aerospace Control Center (BACC) with the measurement results including delay, delay rate, and angle position. It also participated in the

orbit determination and prediction. To achieve high reliability, there are two independent data processing subsystems in the data center, while the software correlator and the hardware correlator is the kernel of them respectively.

CE-1 was successfully launched at 18:05 on Oct. 24, 2007. Three days later, CVN began to carry out a 2-stage tracking mission. The first stage was a near real-time critical flying mission, from Oct. 25 to Nov. 30, 2007. In this period the data was sent to the VLBI data center by network directly. The observation mode was 4-channel (2 S-band + 2 X-band) with the data rate of 16 Mbps/station. The tracking time was 15 hours/day. In this stage, all the data sent to the center must be processed in 10 minutes. The second stage was a non-real-time, long-term in-orbit operation mission, from Nov. 30, 2007 to the end of 2008. In this period, the data was first recorded on the Mark 5 hard disks and then sent to the data center by express mail. The data rate was up to 64-128 Mbps/station. The tracking time was 2 days/week. All the data sent to the center must be processed in 2 weeks.

To deal with the data correlation, we developed two software correlators. one is the Near Real-time Software Correlator (NRSC), another one is the Wide Band Software Correlator (WBSC).

2. Near Real-time Software Correlator

The fast development of the computer and network makes the VLBI software correlator based on the general-purpose computer becoming practical. Compared with the hardware correlator, software correlator is cheaper, more flexible and time saving, and so it is very suitable for the spacecraft tracking and navigation, besides geodesy and astronomy applications [1].

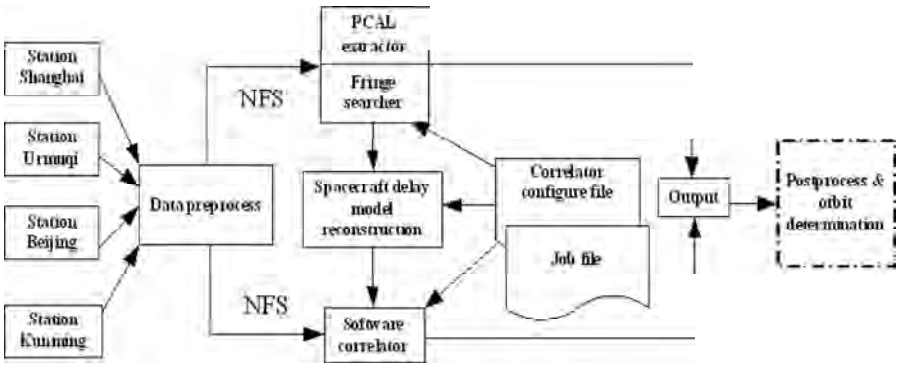

Figure 1. Block diagram of NRSC

We began the research of software correlator in 2003. The first prototype software correlator was a MATLAB program for fringe check through observing the satellite downlink telemetry signals. It was used in the first Chinese e–

VLBI experiment in 2003 [2]. At the beginning of the lunar project in 2004, a software correlator was needed as a debug tool and a slow speed backup of the hardware correlator. So it was designed as a 4-station correlator with speed of 8 Mbps/station. However, when NRSC was completed in 2007, it speed was up to 45 Mbps/station, when running on a 4-way, dual cores X86 PC server.

NRSC was a four station correlator (expanded to 10 stations later) with functions of near real-time correlation, fast satellite fringe search and PCAL (Phase Calibration) detection abilities (Tabl. 1). The data latency of NRSC is less than 3 minutes (Fig. 1).

In the near real-time mode, observation data are transferred to the center through network. To deal with the network congestion, we use a hard disk array as a data buffer. For this reason, a data preprocessing program was developed, which runs on a 4-way, dual core X86 architecture SMP PC server. This module receives the data from the station, and then performs data decoding, error correcting, synchronizing, and data dividing; then it stores the data into a batch of Linux files with one minute length on the disk array. Other modules can access them through the Network File System (NFS).

The software correlator module is the kernel. It adopts the FX structure and the parallel computation algorithm to fulfill the operations of decode, ISTC (Integral Sample Time Correction), Fringe stopping, FFT, FSTC (Fractional Sample Time Correction), MAC (Multiply And Accumulate). The hardware platform is a server identical to the preprocessing module platform.

Table 1. Specifications of the NRSC

Architecture	FX
Correlation station number	1∼10
IF number	1-16
Frequency channel	32∼4096/IF
Integration period	0.1∼60 second
Input data format	Mark 5
Output data format	CVN
Fringe search	2-4 stations
Correlation speed	45 Mbps/station (4 stations)
Data turnover	$<$ 3 minutes
PCAL detection	Yes

When doing correlation, a correlator needs accurate object delay models. For NRSC, such models are pre-calculated by the scheduler program and saved in the Job file. Usually the model of an extragalactic radio source is accurate enough. However, when tracking a spacecraft, if the prior orbit is inaccurate, there will be inevitable errors in the delay models. To solve this problem, a special program, the Fringe Searcher (FS), is integrated in the correlator system. This program is able to find out the onsite accurate delay and delay rate

of the spacecraft automatically without any orbit information. Once getting the delay (delay rate) value from FS, the Spacecraft Delay Model Reconstruction (SDMR) program will renew the prior model to an accurate reconstructed one.

The PCAL extractor module is able to extract the amplitude and phase of every PCAL signal. It has been applied to evaluate station performance.

FS, PCAL extractor and SDMR are running on one server. So there are 3 same SMP servers: one for the software correlator module itself, the other two for FS, PCAL extractor and SDMR of the NRSC and the hardware correlator separately. The Operation System (OS) is a Redhat Linux Enterprise version. Pthreads technology was used to realize the parallelization computation.

3. Wide Band Software Correlator

In the CVN wide band observation mode, the maximal data speed is up to 128 Mbps/station. To process this kind of data, we used the existing three identical SMP PC servers to construct a 3 computation nodes PC cluster, as the platform of a wide band software correlator. Each node contains 4 dual core AMD CPUs, this Beowulf cluster totally contains 24 CPU cores. All the nodes are connected by a high speed Gigabit Ethernet switch. A hybrid parallelism, which combined the intra-node shared-memory programming mode and the inter-node message-passing programming mode, has been used in this prototype software correlator [3].

The Message Passing Interface (MPI) is used to allocate the inter-node correlation job and to complete the reduction operations. Utilizing the data parallelism, the software correlator allots the total integration period operations to 3 computation nodes equally. Inside each computation node, the operations of different model periods in one integration period are allotted to the 8 CPUs using the similar multi-thread algorithm in NRSC.

Experiment results indicate that the inter-node MPI mode and the intra-node multi-thread mode can increase the computation speed of the software correlator remarkably; meanwhile, this correlator still keeps good scalability and flexibility. It is able to deal with 10 station data correlation at most. When doing the 4-station correlation, the speed is about 124 Mbps/station. When there are 10 stations, the speed is about 45 Mbps/station. Compared with NRSC, the speed-up ratio is about 3.

4. Applications

In the CE-1 mission, according to the BACC commands, the CVN observation data from the stations were sent to the VLBI data center in real-time. In most situations, the center performed data processing and sent BACC the satellite delay, delay rate and the angle position in 5 minutes. In this critical period, NRSC was the main data processing equipment. All the data sent to BACC were correlated by NRSC.

After Nov. 30, the CE-1 probe entered the lunar orbit successfully, CVN

changed the near real-time observatory mode into the long-term operation and post management mode. WBSC was also used in this period.

Actually, before the CE-1 mission, the software correlator has already been successfully used in many important experiments and observations: for example, the Chinese first VLBI joint track TC-1 experiment (Mar., 2005), the observation to determine the precise positions of the two new VLBI stations of Beijing and Kunming (May, 2006), the near real-time European SMART-1 and Chinese TC-1 satellite USB+VLBI joint tracking experiment (May 29 $\sim$ Jun. 1, 2006), the CVN tracking demonstration of Venus Express (Sep., 2006) and Mars Express (May, 2007). It was also a very important debug tool for the hardware correlator development and the station fringe check, as well as the station performance check.

In Dec. 20, 2006, we conducted a China-Japan 8-station joint VLBI tracking experiment. The object was the Japanese spacecraft GEOTAIL. We expanded NRSC to a 10-station correlator and completed the data processing.

5. Conclusions

The software correlator has validated its value in the CE-1 lunar probe tracking mission. It also indicates that the VLBI correlation algorithm is highly parallel and very suited to the multiprocessor computing environment. Based on the platform of high performance commercial SMP PC servers and the Linux operation system, the software correlator system is cost effective, reliable, flexible, portable, and scalable. We hope that the software correlator can be used for CVN astronomical and geodetic data correlation besides the deep space probe tracking in the future.

Acknowledgements

This research work is supported by the National Natural Science Foundation of China General Program under Grant No 10403009 and the CE-1 project. The author gratefully acknowledges the support of K.C. Wong Education Foundation, Hong Kong.

References

[1] Stephen T. Lowe. Softc: An Operational Software Correlator. IVS 2004 General Meeting Proceedings. Nancy R. Vandenberg and Karen D. Baver (eds.), NASA/CP-2004-212255, 2004, 191–194.

[2] Zheng, W.M., X.Z. Zhang, F.C. Shu. CVN harddisk system and software correlator in e–VLBI experiment. Progress in Astronomy, 23(3), 272–286, 2005.

[3] Zheng, W.M., D. Zhang. Parallel algorithm of VLBI software correlator under multiprocessor. SPIE, v. 6787, 678–722, 2007.

Measuring the Future

Part 3. VLBI Data Structure, Analysis Strategies and Software

The 5th IVS General Meeting Proceedings, 2008, p. 139–142

VLBI as a Tool to Connect Astrometry and Astrophysics

Yuri Gnedin

Central Astronomical Observatory at Pulkovo, Russian Academy of Sciences, Russia

Abstract. VLBI is the most powerful instrument for astronomical investigations and especially for determination of the scale of the Universe. Namely, the culmination of this millennium of astronomy is a tremendous growth in our understanding of the scale of the Universe and the range of astrophysical phenomena which underlies its apparent structure. Another important field of astronomical research is the observation of quasars. Evidence has been accumulating for several decades that quasars, the most luminous objects in the Universe are powered by accretion of matter onto massive black holes.

I review the following most important topics of VLBI in modern astrophysics: 1) determination of cosmological parameters; 2) probes of super massive black holes (SMBH); 3) high-resolution observations of spatial regions of relativistic jets of active galactic nuclei and trace their evolution and interaction with the nuclear environment; 4) VLBI as the instrument for research of effects of new physics and vacuum polarization; 5) new fields of VLBI: Space Polarization INterferometry (SPIN) and X-ray Interferometry – MAXIM Project.

1. VLBI and Determination of Cosmological Parameters

The angular size-redshift (θ_z) relation for cosmological objects (quasars, active galaxy nuclei, galaxy clusters) is a powerful probe of the large-scale geometry of the Universe. The final versions of the VLA FIRST survey and the optical Sloan Digital Sky Survey (SDSS) data release allow to find carefully selected criteria for defining largest populations of cosmological objects. As a result, it has become possible to place tighter constraints on cosmological parameters and distinguish among the different cosmological models, and determine the impact of the angular size-redshift studies in cosmology (Fig. 1-3) [2]. VLBI observations help our understanding of the behavior of the intergalactic medium (IGM) as a function of redshift and shed more light on the quasar-radio galaxy unification issue.

Another very important problem is connected with gravitational lensing. Typical angular distance images and typical time scales depend on gravitational lens mass. High resolution interferometry with radio waves gives excellent chance to investigate microlensing phenomena in astrophysics.

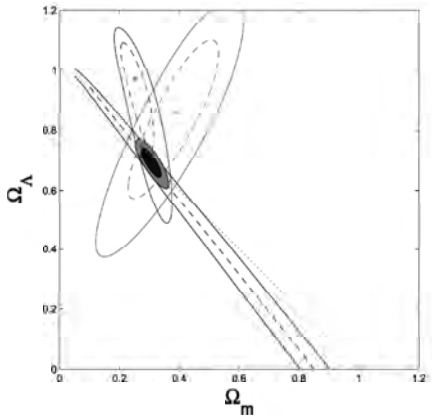

Figure 1. The constraints on the cosmological parameters: dimensional dark energy and dark matter densities

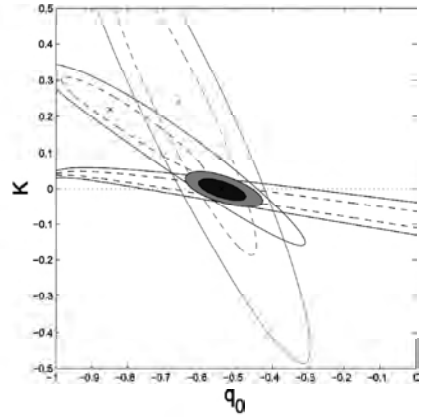

Figure 2. The constraints on the cosmological parameters from VLBI survey: the curvature vs deceleration constant

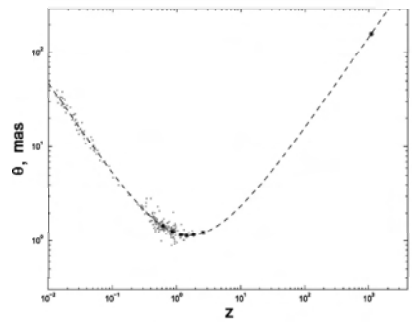

Figure 3. The angular-diameter redshift relation of the Legacy VLBI Survey data for ultra-compact radio sources at 2.29 GHz

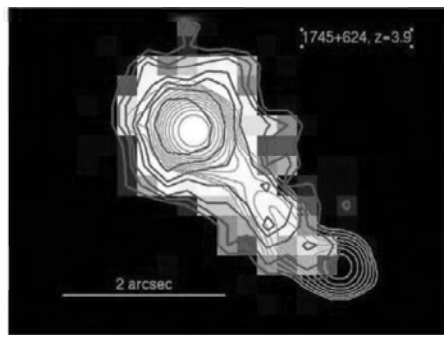

Figure 4. The image of high-z jet from QSO 1745+624: $z = 3.9$ [1]

2. VLBI Probes of Super Massive Black Holes (SMBH)

Nuclear activity in galaxies is closely connected to galactic mergers and SMBHs. Galactic mergers perturb substantially the dynamics of gas and the stellar population in the galaxies, and they are expected to lead to the formation of super massive binary black holes in the center of mass of the merged galaxies. VLBI is an excellent instrument for investigation of this phenomenon. It presents a unique opportunity to test the non-linear structure of general relativity.

SMBHs make ultra-relativistic jets (Fig. 4). Outflows (jets) are the main

mechanisms for transport of angular momentum. Long-term evolution of large-scale relativistic jets can be studied by VLBI observations.

Another example is connected with Legacy data [2]. VLBI survey of ultra-compact radio sources at 2.29 GHz was presented and fringe amplitudes for 917 such objects with total flux density > 0.5 Jy was given. A number of cosmological investigations based upon this survey are now developed.

3. Relativistic Jets and Their Basic Physical Properties

Substantial progress achieved during the past decade in studies of active galactic nuclei has brought an increasingly wider recognition of the presence of relativistic outflows (jets) in galactic nuclei presenting them as an effective probe of nuclear regions in galaxies. Emission properties, dynamics, and evolution of an extragalactic jet are closely connected to the physical characteristics of the super massive black hole, accretion disk and broad-line region in the nucleus of the host galaxy (Fig. 4). The jet continuum emission is dominated by non-thermal synchrotron and inverse Compton radiation. In radio waves the synchrotron mechanism is namely dominated, and the main physical properties of the emitting material can be extracted using the turnover point in the synchrotron spectrum, synchrotron self-absorption, and free-free absorption in emitting plasma. High-resolution radio observations access directly the regions where the jets are formed, and trace the evolution and interaction with nuclear environment. Evolution of compact radio emission and jet magnetic field determined from synchrotron radiation are now systematically studied with monitoring programs and large surveys using long baseline interferometry.

Jets are common features of radio-loud AGN at high redshift (up to $z = 4.7$). This conclusion is also based on VLBI measurements. The Chandra X-ray observations tell us about this result. Extending studies to these high redshifts should help us to distinguish between the competing synchrotron and inverse Compton models to determine if there is a redshift dependence and in X-ray jet emission.

These studies, combined with optical and X-ray studies, yield the most detailed picture of the galactic nuclei.

4. VLBI and New Physics

A number of physical effects of current interest manifest themselves as a birefringence appearing in response to the application of strong electromagnetic fields. The most known effect is the small degree of magnetically induced birefringence that arises in the Cotton-Mouton phenomenon. Such kind of effect is predicted to occur in vacuum arising under quantum electrodynamics (QED). A new technique capable of measuring birefringence with great precision has been recently suggested. The special device received name as a Resonant Polarization Interferometer. Angle size - redshift dependence allow us to shed light on what is the nature of Dark Energy (DE) and Dark Matter

(DM). One popular idea is the existence of the new states of matter at exceedingly high density and temperature. USA National Science and Technology Council and Committee on Science formulated eleven science questions for the New Century. Replies will give the explanation of origin of DE and DM.

5. New Aspects of Interferometry: X-Ray Interferometry — MAXIM Project

MAXIM means MicroArcsecond X-ray Imaging Mission. Recently an essential step in establishing the viability of X-ray interferometry has been made [3]. The interferometer must not only create fringes, but be of a design class that can be developed into an efficient system for astronomy. While there is no question that X-rays will exhibit the same wave properties than light rays in other bands, the extreme shortness of the X-ray waves make the development of real interferometry very difficult. Fortunately, the team from the Colorado University of USA has now built and successfully tested an X-ray interferometer of a class that can have practical application. It means that we can expect to get the angular resolution of astronomical objects in X-rays at the level $\sim 1\mu$sec.

Acknowledgements

This work was supported by the RFBR (project No 07-02-00535a), Program of Prezidium of RAS "Origin and Evolution of Stars and Galaxies", the Program of the Department of Physical Sciences of RAS "Extended Objects in the Universe".

This research was also supported by the Grant of President of Russian Federation "The Basic Scientific Schools" NS-6110.2008.2.

References

[1] Fan, X. Probing the End of Dark Ages with High-Redshift Quasars. The 22-nd Texas Symposium on Relativistic Astrophysics, 2004.

[2] Jackson, J.C., A.L. Jannetta. JCAP, v. 11, 2, 2006.

[3] Cash, W. Bulletin of the AAS, 35, 1416, 2003.

The 5th IVS General Meeting Proceedings, 2008, p. 143–152

IVS Working Group 4 on VLBI Data Structures

John Gipson

NVI, Inc./NASA Goddard Space Flight Center, USA

Abstract. In 2007 the IVS Directing Board established IVS Working Group IV on VLBI Data Structures. This note discusses the current VLBI data format, goals for a new format, the history and formation of the Working Group, and a timeline for the development of a new VLBI data format.

1. Introduction

At the Sep. 15, 2007 IVS Directing Board Meeting I proposed establishing a "Working Group on VLBI Data Structures". The thrust of the presentation was that, although the VLBI database system has served us very well these last 30 years, it is time for a new data structure that is more modern, flexible and extensible. This proposal was unanimously accepted, and the board established IVS WG4 (Working Group IV) with myself as chair.

One motivation for changing the data structure now is the advent of VLBI2010. The first VLBI2010 antennas are due to come on line in 2010, and the number is expected to increase rapidly. Because we want to tie these stations into our current geodetic network, these stations will have the capability of observing at S/X. However, 'native' VLBI2010 observing will be very different than our current observing in many ways. The receiving hardware will be broadband and observe over a much wider frequency range. It will likely record over many bands, as opposed to our current 2, and even the concept of "band" may no longer be meaningful. The system will record many more bits, which will result in greatly increased sensitivity. This will allow the use of small, fast antennas, which, combined with the increased sensitivity, will enable them to participate in on the order of 100 scans/hour instead of the current 10-15. Current operational sessions such as the R1s and R4s typically involve around 7 stations and make about produce $\simeq$ 3000 observations per session. We expect that the number of stations participating in a typical VLBI2010 session will increase to 16, 20, 32 or even more. Although the current RDV sessions may involve up to 20 stations, they are the exception rather than the rule. Simulation studies indicate that a 24-h VLBI2010 sessions with 16 stations may yield 100000–200000 observations, and larger networks would have

even more observations. In short, life will be much different when VLBI2010 is fully operational.

In this note I begin by reviewing the history of the VLBI database format. I then discuss some of the features and limitations of the current structure. This is used to motivate the desirable features of a new data structure. Following this I discuss the history, formation, composition and goals of WG4. I summarize the first meeting of WG4, and the next steps. Lastly I offer some concluding remarks.

2. Brief History of VLBI Database Format

The VLBI database format and associated software was developed in the mid-1970s, at the very beginning of geodetic VLBI. It was designed at NASA's Goddard Space Flight Center (GSFC) for use with the *calc/solve* analysis package, and is closely tied to this package. It is currently the IVS standard for archiving and distributing geodetic VLBI sessions. It is exceptional for anything in the software world to still be in use after 30 years. On the one hand, this is a testament to the design and robustness of the VLBI database format, which has been pushed to do things well beyond the original specifications. On the other hand, the VLBI database is a product of when it was designed, and suffers from this. The world has changed in the last 30 years: the VLBI technique has continued to evolve and mature; the speed and power of computer hardware has increased by almost 4 orders of magnitude; software has become more flexible and powerful. There is no doubt that if we were designing the database system today it would be much different.

3. Features of Current Database Format

In this section I review some of the features of the current VLBI database format. I want to emphasis that this is not done to disparage the current system, which has served us well. Rather, it is to see how it could be improved.

Provenance. A very positive feature of the database structure is that it encourages analysts to keep a history of what was done and by whom.

Redundancy due to baseline orientation. The VLBI database system was developed when VLBI sessions involved single baselines observing a single-band. Because of this the database is baseline observation oriented. In order to process and analyze an observation, a lot of information is needed, and most of this information is stored for each observation. However much of this information is the same for other observations within a scan. Since there are $(N-1) \times N/2$ observations in a scan, this leads to a tremendous amount of redundancy. Tabl. 1 gives examples of three kinds of data associated with an observation. **Baseline** dependent data varies from observation to observation within a scan. **Station & Scan** dependent data is common to all observations involving a given station within a scan. This only needs to be stored once per station per scan, instead of the current $(N-1)$ times. **Scan** dependent data is

the same for all observations within a scan, and needs to only be stored once, instead of the current $(N-1) \times N/2$ times. Tabl. 2 calculates the amount of redundancy for the different data types as a function of the number of stations in the scan. The effect is negligible for small networks but grows rapidly.

Table 1. Types of VLBI data associated with an observation

Baseline Dependent	Station & Scan Dependent	Scan Dependent
Delay	Met Data	Source
Rate	Elevation	Epoch
Ambiguity	Phase Calibration	EOP
Ionosphere Calibration	Cable Calibration	etc.
etc.	etc.	

Table 2. Data redundancy and storage efficiency for VLBI data types

Scan Size		Data Redundancy			Storage Efficiency		
Stations	Baselines	BL	Stat	Scan	BL	Stat	Scan
2	1	1	1	1	100%	100%	100%
3	3	1	2	3	100%	50%	33%
5	10	1	4	10	100%	25%	10%
10	45	1	9	45	100%	11%	2%
15	105	1	14	105	100%	7%	1%
20	190	1	19	190	100%	5%	1%
32	496	1	31	496	100%	3%	0%

Custom Format. Databases are written in a special format, and require special software—the database handler—to read and modify them. This was not an issue when everyone used the GSFC developed *calc/solve* analysis package, but became one with the development of alternative analysis packages. This software was written in FORTRAN in the 1970s and 1980s. It incorporates limitations of FORTRAN at that time. For example, the earlier code does not recognize character strings, and still uses Holleriths.

Speed of Retrieving Data. The database handler was written before the advent of modern database systems. It is slow in retrieving data, and can take many minutes to retrieve all of the data in a VLBI database. Because of this, institutions, including GSFC, have developed their own internal formats for processing and storing VLBI data.

Irrelevant/Obsolete Data. The VLBI database contains data which are no longer used. Some of this is due to computer hardware issues present at the time the database was designed, when numerical calculations were very costly. For example, the databases contain the numerical value for π.

Data used only by *calc/solve*. The database contains items, e.g., partial derivatives, which are computed by *calc* and stored for later use by *solve*. Other analysis packages do not use these or compute them "on-the-fly". Some of these items are not even used by *solve*. When *solve* was the only VLBI analysis package, this was not an issue. In principle, the IVS standard for archiving and transmitting data should not give preferential treatment to one analysis package.

Lack of Flexibility. The only people who can add new kinds of data to the database are those who have installed the database handler. In practice, this means individuals or institutions who have installed the *calc/solve* analysis system. This is an additional obstacle in improving the analysis of VLBI data.

Incomplete Data. When the database was originally designed, it was envisioned that it would contain all of the data necessary to process a VLBI session. However, there are currently many data items used in the analysis of VLBI sessions that are not contained in the database. These include EOP, pressure loading calibration, external mapping functions (e.g., VMF), etc.

Coupling of observables and models. In some sense, the database treats all data as equal. The observables, which never change, are on the same footing as geophysical models. They all live in the database together. One result of this is that as geophysical models change, the databases are updated. Although this is not required in principle, it is necessary at GSFC in order to test these models. This makes testing new models at GSFC cumbersome and time consuming, and results in changes in the version number of database when nothing fundamental has changed.

No Access to Primitive Data. The lowest level of data stored in the databases are the various kinds of delay output by the correlator program *fringe*. Although this is sufficient for most people most of the time, occasionally there are problems with the *fringe* output. The origin of these problems can sometimes be determined by looking at the raw-correlator output, which serves as input to *fringe* The database contains no natural "hooks" to this data. For experts it may be useful to have the ability to re-fringe the data using different assumptions, or, perhaps different algorithms.

4. Goals for the New Format

At a minimum, any new data format must be able to store the data currently required to process VLBI sessions. It should also handle the anticipated needs of VLBI2010 and beyond. Without these, there is no point at all in designing a new system. The current database system could be modified to handle the needs of VLBI2010 with considerable effort. This would still leave us with the current problems.

Based on the discussion of the previous section, following are some initial goals for a new VLBI data format.

1. Provenance. Analysts should be able to determine where the data came from and what happened to it.

2. Compact. The database structure should minimize redundancy.
3. Accessible. Users should be able to easily access the data without the need of custom software. Currently we do have such a format—NGS cards—but this suffers from other problems.
4. Cross platform/OS/language support. The same structure should be accessible by programs written in different languages running on different computers using different operating systems.
5. Speed. Users should be able to add, modify and retrieve data quickly.
6. Extensible. It should be possible to add new data types, e.g. source-maps, antenna temperatures, system gain information. Some of this information may not be currently useful, but may become so in the future.
7. Completeness. The data structure should include all data necessary for processing VLBI data. Analysts should be able to redo the entire analysis from start to finish.
8. Separable. Analysts should be able to retrieve just the data they are interested in.
9. Decoupling. There should be a clear distinction between fundamental observables (e.g., delay) and other data items.
10. Different levels of abstraction. There are many different kinds of users of VLBI data. The new structure should serve all of these equally. Most users may be interested only in the final delay. Experts may want access to data at a more primitive level.

5. History and Formation of the Working Group

At the 2007 IVS Analysis Workshop held in Vienna there was extended discussion about the need to revamp the VLBI data structure. In May I circulated a draft proposal to the IVS Directing Board proposing the formation of a Working Group for this purpose, and offered to chair it. At the request of the IVS Directing Board, I made a presentation at September 2007 Board meeting. The IVS Board unanimously approved the formation of IVS WG4.

Any change to the VLBI data format affects everyone in the VLBI community. Therefore, it is important that the working group have representatives from a broad cross-section of the IVS community. Tabl. 3 lists the current members of WG4 together with their affiliation. The initial membership was arrived at in consultation with the IVS Directing Board. On the one hand, we wanted to ensure that all points of view were represented. On the other hand, we wanted to make sure that the size did not make WG4 unwieldy. The current composition and size of WG4 is a reasonable compromise between these two goals. My initial request for participation in WG4 was enthusiastic: everyone I contacted agreed to participate with the exception of an individual who declined because of retirement.

Table 3. Membership in Working Group IV

Chair	John Gipson
Analysis Center Director	Axel Nothnagel
Haystack/ Correlator Representatives	Roger Cappalo Colin Lonsdale
GSFC/Calc/Solve	David Gordon
JPL/Modest	Chris Jacobs
Occam	Oleg Titov Volker Tesmer Johannes Boehm
Main Astronomical Observatory/ Steelbreeze Observatorie de Paris/PIVEX NICT	Sergei Bolotin Anne-Marie Gontier Thomas Hobiger Hiroshi Takiguchi

Communication is crucial to the success of WG4. This includes both communication between the members, and communication between WG4 and the broader IVS community. Following the lead of the VLBI2010 committee, I anticipate that much of our work will be done via email and teleconferences. Our email discussions are publicly available on the IVS web-site. In addition, we plan on having at least two face-to-face meetings each year. For the convenience of participants, these will occur as splinter meetings at the AGU, EGU and IVS General Meetings. These meetings are primarily for WG4 members, but other interested parties are encouraged and welcome to attend. We will also make regular presentations at the IVS General Meeting and other conferences as appropriate. Our goal is to make sure that everyone knows what we are doing, and that there will be no unpleasant surprises.

In addition, I or another member of WG4 will update the IVS Directing Board at each of their board meetings. This will keep the Board apprised of

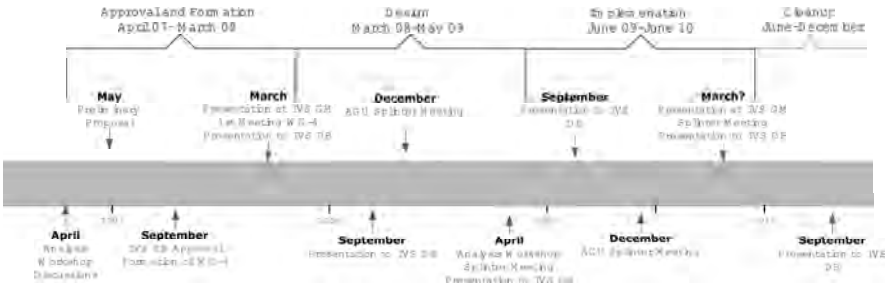

Figure 1. Past and future of working IVS WG4

what we are doing, and also serves as an opportunity for feedback. The current plan is that WG4 will be dissolved at the end of 2010.

Fig. 1 is a timeline of the past and future of IVS WG4 from its inception through 2010. Marked on the timeline are the proposed meetings of WG4, regular reports to the IVS Directing Board, and the various phases in the life of the WG4.

Table 4. Partial list of data to be included in new format

VLBI data	
Correlator output	
Original fringed data	Refringed data (if any)
Editing criteria	
Group delay ambiguity	Phase delay ambiguity
Fully calibrated and ambiguity resolved group delay	Fully calibrated and ambiguity resolved phase delay
VLBI calibrations	
Raw Phase calibration	Modified Phase calibration
Raw Cable calibration	Modified Cable calibration
Other raw calibrations	Other modified calibrations
Associated data	
Raw met data	Calibrated met data
Location of met sensors	
Physical antenna temperatures	Antenna height measurements
System temperatures	Gain measurements
Pointing measurements	Source maps
Geophysical models/effects	
Pressure loading	Ocean loading
Calculated mapping functions e.g., VMF	Slant path delay
Earth orientation parameters	
Miscellaneous files	
Schedule file	Experiment notes
Log files	Emails
Correlator summary	

6. Summary of Initial Meeting of Working Group

WG4 held its first meeting at the IVS General Meeting in St. Petersburg. This meeting was open to the general IVS community. Roughly 25 scientists attended: 10 WG4 members, and 15 others. This meeting was held after a long day of proceedings. The number of participants and the lively discussion that ensued is strong evidence of the interest in this subject. By the end of the

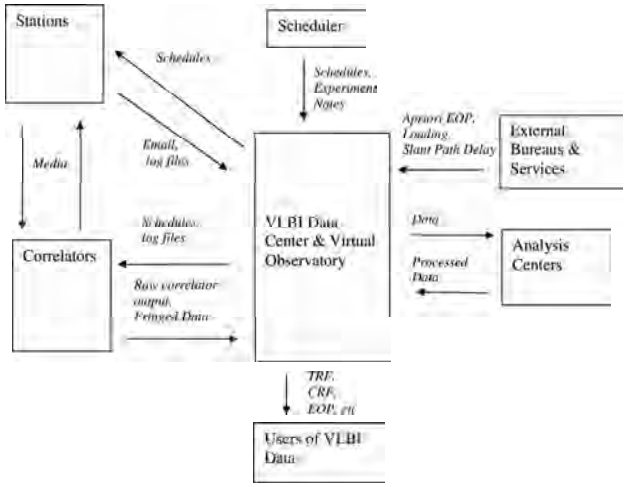

Figure 2. Under the proposed scheme a "virtual observatory" serves as the central depository of all VLBI related data

meeting we had arrived at the following consensus.

1. Users should be able to trace the origin and the history of all the data: where it came from; when it was processed; who processed it; what procedures they used, etc.
2. All VLBI data should be easily accessible from the web. This includes the whole data-flow of VLBI, from scheduling the session, through correlation and analysis. Tabl. 4 provides a rough draft of data that would be accessible.
3. VLBI data should be available at different levels of processing and abstraction. This ranges from raw correlator output, which rarely changes, to final edited and calibrated data. Experts should be able to access the data at a low level, but other users of VLBI data, who lack interest or expertise, should be able to access edited and calibrated data.
4. Other data used in processing and analysis of VLBI data should also be available at different stages of processing and calibration. For example, raw met data should be available, as well as smoothed and calibrated met data. This would allow research into alternative methods of calibration and smoothing.
5. The format should also include data which is externally derived, but used in VLBI analysis. Examples of this include pressure loading corrections, ocean loading corrections, antenna tilt corrections, etc.
6. Stations, Correlators, Analysis Centers and others would all contribute data, and all be viewed on an equal footing.

7. Analysis centers should be be encouraged to post the results of their processing. Examples include: editing criteria used; ambiguity resolution; calibration information; source maps or source corrections; etc. This would make it possible for others to use these results, and would also help ensure transparency in how data is analyzed.

Tabl. 4 is a first cut at the kind of information that would be accessible. As time goes on, other kinds of data will surely be added. In some sense, the above considerations imply a combination and extension of the current VLBI databases, the information contained on the IVS session web-pages, and lots more information. The idea of a "Virtual Observatory" for VLBI data arose as an outgrowth of these discussions. Fig. 2 is a schematic illustration showing how different institutions would interact with this.

The desires expressed in the first meeting were much more ambitious than I originally envisioned, and it is unlikely that all of these goals will be accomplished in the limited span of WG4.

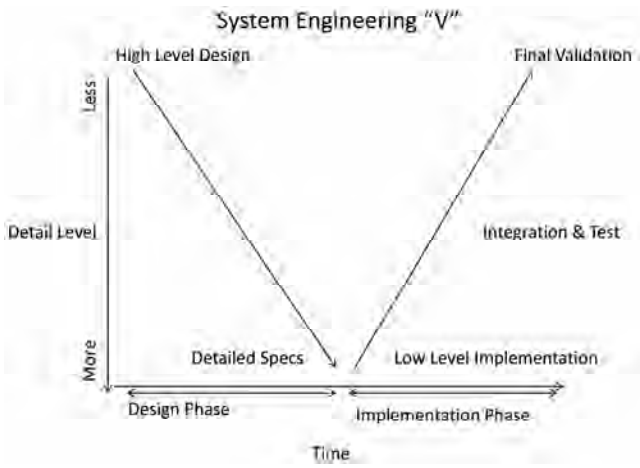

Figure 3. For optimal results, you should spend as much time on design as implementation

7. Next Steps

Fig. 3 is commonly used in system engineering to describe the steps involved in developing and implementing new systems. This is a useful paradigm for WG4. The system engineering process is divided into two parts: design and implementation. Design starts at a high level of abstraction and ends at a low level. Initially you define what your system is supposed to do, and then you start discussing how to do this in more and more detail. Implementation does just the opposite: you start at the bottom, building small parts of the system,

and work your way up, integrating the small parts together. Periodically you stop to test and validate what you are doing.

A natural tendency is to jump into implementation too soon. You think you know what you want, and start to build it. Experience has shown that the more time spent on specification and design, the less time you will spend fixing problems. Ideally, you should spend about as much time in the design part of the process as in the implementation part.

Based on the above, the first goal of WG4 will be to have a complete specification by mid-2009. Progress to date will be presented at the European VLBI meeting in April 2009. This will also provide an opportunity for IVS members to give feedback. Following this, we will begin the process of implementation. Our goal will be to have this completed by the end of 2010. We will give another status report at the IVS General Meeting, which will provide a chance to make last minute course corrections.

We are currently in the very early design stages. As part of this effort we will see what other groups with similar data handling issues have done. We anticipate that we will be able to borrow from and build on the work of others. For example, there are currently several excellent public domain structures to deal with various kinds of scientific data, such as NetCDF, FITS, HDF etc. There are interfaces to these data structures on a variety of platforms and from a variety of computer languages. Each of these has a large community of users, and each has and a large library of freely available utilities for extracting and handling data. We will study these formats in detail to see how well they would work for VLBI data and what the trade-offs are.

8. Conclusion

The goals of IVS Working Group IV are very ambitious. We can only achieve these goals if all of the members contribute to this effort. The Working Group will endeavor to operate in an open environment. We will make regular presentations to inform the community of our progress, and solicit input from all interested parties.

The 5th IVS General Meeting Proceedings, 2008, p. 153–156

MK3TOOLS — Seamless Interfaces for the Creation of VLBI Databases from Post-Correlation Output

Thomas Hobiger, Yasuhiro Koyama, Tetsuro Kondo

Kashima Space Research Center, National Institute of Information and Communications Technology (NICT), Japan

Abstract. MK3TOOLS have been developed in order to allow any user to create, read or modify geodetic VLBI databases without CALC/SOLVE being installed. It uses the NetCDF format to store the data and since interfaces exist for a variety of programming languages (FORTRAN, C/C++, JAVA, Perl, Python) it can be easily incorporated in existing and upcoming analysis software packages. A seamless and unattended processing chain from the correlator to the analyst could be realized for the Japanese K5 system. Applications like ultra-rapid UT1 measurements and automated ambiguity resolution benefit from MK3TOOLS as shown here.

1. Introduction

Driven by the need to replace the out-dated interfaces between the K5 correlator output and MK3 databases a set of utilities, named MK3TOOLS, written in C++ have been developed. Basically, MK3TOOLS are a collection of programs which allow to read/write MK3 databases without binding the CALC/SOLVE libraries and are written in a way which allows to obtain the same results, independent of the machines Endianess. The Network Common Data Format (NetCDF) has been chosen as an intermediate data format to which all information is written before MK3 databases are created. This enables easy editing and data manipulation without detailed knowledge about the MK3 database structure.

2. Description

Currently the MK3TOOLS include the following modules:

- READKOMB: reads K5 post-correlator output together with log-file information, applies known ambiguity shifts, computes ionosphere correc-

tions, outputs information to NetCDF files;

- WRITEMK3: translates the information stored in a NetCDF file into a consistent MK3 database, adds history information;
- READMK3: translates a MK3 database into a NetCDF file;
- WRITENGS: translates the content of a NetCDF file in a NGS card.

Interfaces to bandwidth synthesis output from the MK5 system as well as support for the VSI2000 correlator are planned for the near future. Additionally, MK3TOOLS contain a collection of SHELL (BASH), AWK and Python scripts which allow to manipulate NetCDF files and carry out small tasks like the extraction of relevant information from log-files. Fig. 1 summarizes how the different programs interact with each other.

3. Application Examples

3.1. Ambiguity Resolution with OCCAM

Until now OCCAM users have been relying on prior analysis from CALC/SOLVE which mainly included the resolution of ambiguities and the computation of ionosphere corrections. When MK3TOOLS are used together with OCCAM it is possible to resolve X- and S-band ambiguities, use this information to update the NetCDF files and compute the ionosphere corrections (Fig. 2).

3.2. Automated Processing of Ultra-Rapid UT1 Experiments

MK3TOOLS enable unattended analysis of ultra-rapid UT1 experiments, providing results within a few minutes after the last scan has been recorded. Using the ambiguity resolution strategy described above and running OCCAM, controlled by scripts, it is now possible to completely automate ultra-rapid e–VLBI experiments including observation, data-transfer, correlation and analysis without human interaction. First tests in Feb. 2008 in cooperation with the Geographical Survey Institute (GSI) and Onsala Space Observatory have shown that accurate automatized estimates of UT1 can be obtained when MK3TOOLS are utilized to within the processing chain [1].

4. Outlook

Since interfaces to NetCDF are existing for a variety of popular programming languages new analysis packages can be written without detailed knowledge about the database structure. Moreover it is possible to store additional information (e.g. source maps, antenna specs, troposphere corrections, ...) which are not considered in the MK3 database structure, but

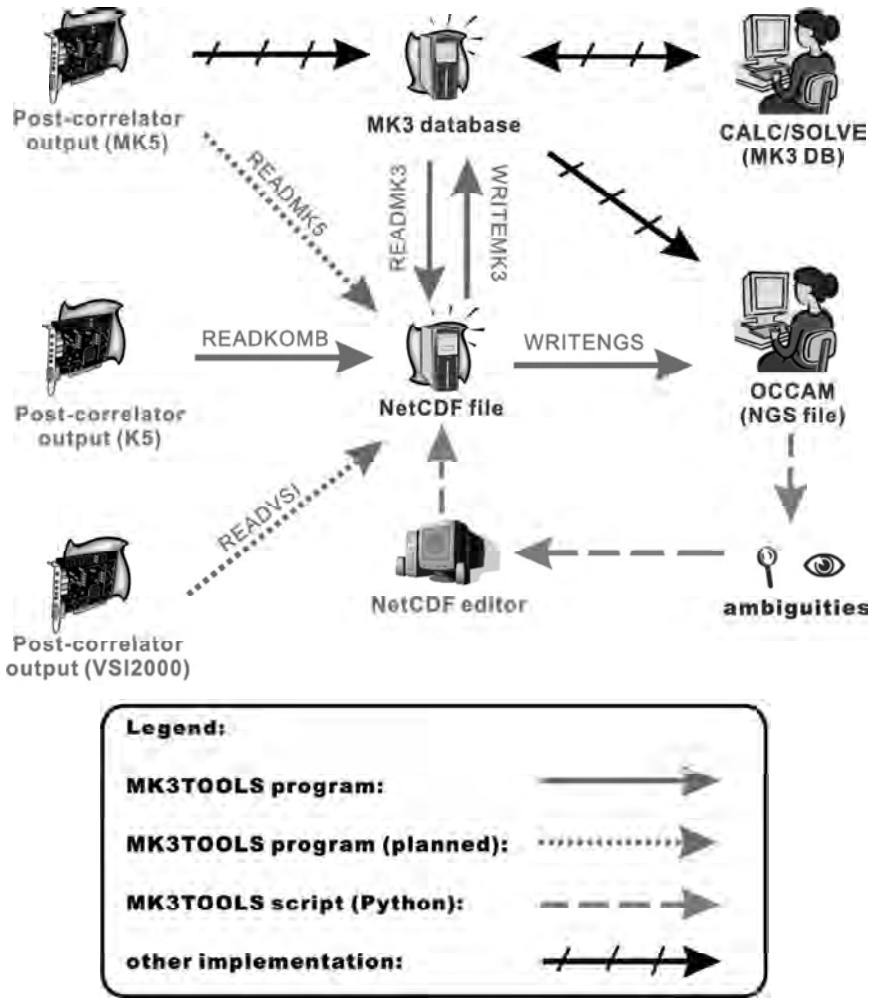

Figure 1. Interaction of MK3TOOLS with existing VLBI components

might be of interest for a newly designed analysis software. Additionally NetCDF editors and viewers enable experts from different scientific disciplines to add/extract relevant information to/from the databases and help to improve geodetic/astrometric results. New database structures are currently being discussed by a dedicated working group (WG4) within the IVS. Thus, the experiences gained from the development of MK3TOOLS might be useful for the design of the new format which handles observations of the VLB2010 systems. Moreover it is anticipated the MK3TOOLS can also be useful to ensure a smooth and consistent transition from the current databases to the new format.

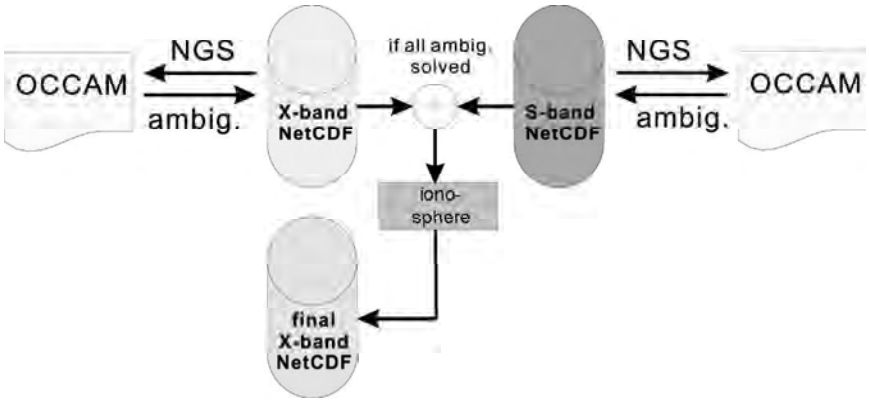

Figure 2. Ambiguity resolution with MK3TOOLS and OCCAM

Acknowledgements

We are very grateful to the Japanese Society for the Promotion (project P06603) for supporting our research. National Institute of Information and Communications Technology and the Kashima Space Research Center are acknowledged for providing the infrastructure.

References

[1] Koyama, Y., M. Sekido, T. Hobiger, et al. Developments of Automated Data Processing System for Ultra Rapid dUT1 e–VLBI Sessions. This volume.

The 5th IVS General Meeting Proceedings, 2008, p. 157–162

Improved Estimation in VLBI through Better Modeling and Analysis

John Gipson, Daniel MacMillan, Leonid Petrov

NVI, Inc./NASA Goddard Space Flight Center, USA

Abstract. We report on the effect of several modifications to the standard VLBI data analysis using the CONT05 dataset. These include: 1) varying re-weight constants; 2) introducing elevation dependent noise; 3) introducing correlation between observations; 4) use of VMF instead of NMF.

1. Introduction

The VLBI observable, colloquially called the "delay", is the difference in arrival time of a signal at two different antennas. Roughly speaking, the delay is measured by cross-correlating the signals received at the two stations and searching for a peak. This process has an uncertainty associated with it which, for clarity, we call measurement noise and denote by σ_{meas}. This noise is inherent to the correlation process and depends only on the signal strength, sensitivity of the antennas, frequency sequence, and number of bits recorded. One can show, assuming SNRs commonly used in VLBI, that the measurement noise on different baselines is uncorrelated. The normal assumption in VLBI is that the observational noise σ_{obs} equals the measurement noise: $\sigma_{meas} = \sigma_{obs}$.

There are several indications that this assumption is false. First, the reduced χ^2 from individual session solutions is much larger than it should be based on $\sigma_{meas} = \sigma_{obs}$. This implies that there are other noise sources, or that we are not correctly modeling the system. The standard approach is to re-weight the observations by adding additional noise until $\chi^2 \simeq 1$. We demonstrate below that this reduces baseline scatter. Second, even after re-weighting, baseline length scatter is larger than it should be based on the formal errors of individual sessions. Third, comparison of EOP measurements from simultaneous VLBI sessions are inconsistent with the formal errors. Fourth, comparison of EOP measurements from VLBI and GPS indicate that the formal errors from one or both techniques are two optimistic.

There are many other error sources besides measurement noise: 1) phase cal errors; 2) RF interference in the signals; 3) other correlator related errors;

4) source structure; 5) source position errors; 6) errors in geophysical models; 7) mis-modeling clocks and/or atmospheres; 8) underparametrizing the time variation of clocks and/or atmospheres; etc. All of these increase the noise of individual observations. Many also introduce correlation between observations.

In the following sections we present several modifications to the standard *solve* data-analysis, and study the effect on the CONT05 sessions observed during Sep. 12-26, 2005. This dataset has several advantages for this kind of work. The number of sessions (15) allows us to meaningfully compute statistics. The short time span reduces seasonal effects, and allows us to determine the intrinsic accuracy of the technique. Moreover, σ_{meas} is much smaller than for most VLBI sessions. Because of this, you may be able to see improvements in analysis which would not be apparent if σ_{meas} were larger.

In this note we use baseline scatter as a measure of goodness. A reduction in the scatter is strong internal evidence that the solution is better. In our studies we also looked at the agreement between VLBI and IGS estimates of EOP, which is an independent external test. Space constraints preclude us from describing these results in detail. In all cases where the baseline scatter was reduced, the agreement with IGS improved.

In Sec. 2 we examine the effect of re-weighting the data. Re-weighting has been standard practice at Goddard since at least the early 1990s.

In Sec. 3 we look at the effect of adding noise proportional to the mapping function. Such a term arises from some kinds of atmosphere mis-modeling. Including these terms reduces baseline scatter. Interestingly enough, we get better results if we turn-off re-weighting. This implies that much of the unmodeled noise is due to atmosphere-modeling error.

In Sec. 4 we look at the effect of introducing elevation dependent correlations between observations ("correlated noise"). This is a natural extension of the work of Sec. 3. In fact, elevation dependent noise is an approximation to elevation dependent correlation. We demonstrate that this further reduces the scatter.

At Goddard the standard mapping function is NMF (Niell Mapping Function) [4]. In Sec. 5 we study the effect of using the more recent mapping function VMF (Vienna Mapping Function) of J. Boehm and H. Schuh [1]. We show that this reduces scatter compared to NMF. We obtain the best results when we combine VMF with correlated noise and turn off re-weighting.

2. Re-weighting VLBI Data

If the VLBI observations were correctly modeled, and $\sigma_{obs} = \sigma_{meas}$, we should find $\chi^2 \simeq 1$ for individual sessions. Typically $\chi^2 \simeq 3-4$, indicating that: 1) we have underestimated σ_{obs}; 2) are mis-modeling the system; or 3) both. The standard fix is to add extra noise ϵ^2_{rewt} to the observations:

$$\sigma^2_{t,ij,obs} = \sigma^2_{t,ij,meas} + \epsilon^2_{t,ij,rewt}\,, \tag{1}$$

until $\chi^2 \simeq 1$. The subscripts t and ij label the time and the stations involved in the the observation. Although in principle the re-weight constants $\epsilon^2_{t,ij}$ can vary arbitrarily from observation to observation, in practice analysts usually make one of the following simplifying assumptions:

1. "global re-weights" are the same for all observations;
2. "station re-weights" depend only on the stations in an observation;
3. "baseline re-weights" depend only on the baselines in an observation.

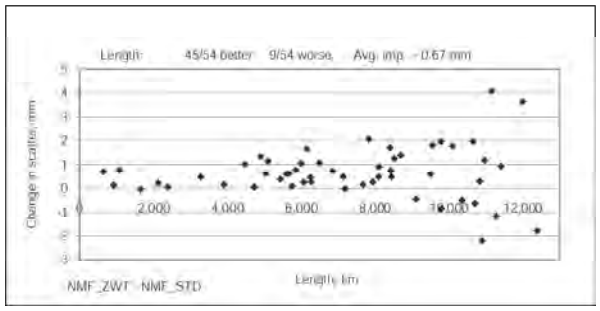

Figure 1. Reweighting reduces scatter

At Goddard we generally use either station or baseline re-weight constants. Fig. 1 plots the difference in baseline scatter between a solution with no re-weighting and one using standard baseline re-weighting. Each point represents a single baseline. If the point is above the X-axis, re-weighting reduces the scatter of 45/54 baselines, and the average reduction is 0.67 mm. Generally speaking, the longer the baseline, the greater the reduction in scatter. It is remarkable that re-weighting–which depends only on what is happening within a session–has such a large effect on intra-session scatter.

3. Elevation Dependent Noise

Delay residuals are larger at lower elevations, which is evidence of atmosphere mis-modeling. There are many plausible functional forms for this. We assume a noise term proportional to the mapping function $M_i(el_i)$. The particular mapping function is not important, and using a simple $1/sin(el)$ gives similar results. Analogous to (1) we assume that

$$\sigma^2_{ij,obs} = \sigma^2_{ij,meas} + \epsilon^2_{ij,rewt} + (\epsilon_i M_i(el_i))^2 + (\epsilon_j M_j(el_j))^2 \,.$$

The noise coefficients ϵ_i could be site and session dependent. For simplicity we assume the same values for all stations (we have investigated the more general case). We ran solutions varying ϵ_i from 0 to 15 ps. All of these values reduced the scatter, with the greatest reduction at $\epsilon_i \simeq 6\ ps$.

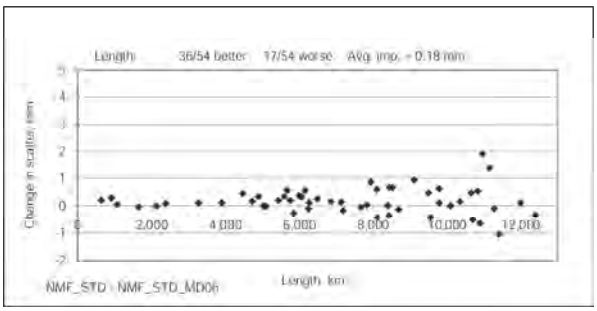

Figure 2. Elevation dependent noise

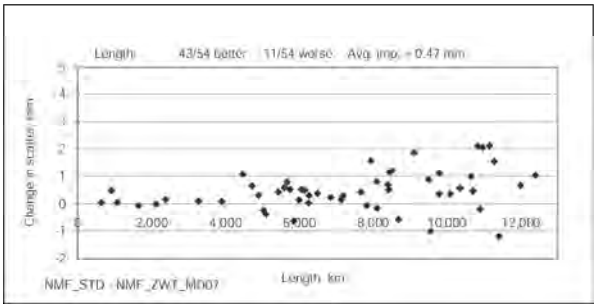

Figure 3. Elevation dependent noise with no re-weighting

Fig. 2 plots the difference in scatter between the standard solution and one with 6 ps of noise. Including this effect reduces scatter on 36/54 baselines, and the average improvement is 0.18 mm. Both solutions used our standard re-weights. Fig. 3 plots results of a similar solution where re-weighting is turned off. Surprisingly, this further improves the solution: 43/54 baselines are improved, and the average improvement is 0.47 mm.

4. Correlation Between Observations

Since atmosphere mis-modeling is station dependent, it effects all observations involving a given station in a given scan in the same way. In addition to adding noise to the observation, it introduces correlations between observations. The normal equations must be modified to correctly handle this. The details of this are beyond the scope of the present paper, but are given in [2, 3]. Other scientists [5–10] have also studied correlation between observations. Space constraints preclude us from adequately discussing their work, and we refer the reader to their papers. Fig. 4 plots the difference between the standard solution and one where we have introduced 6 ps of correlated elevation dependent noise.

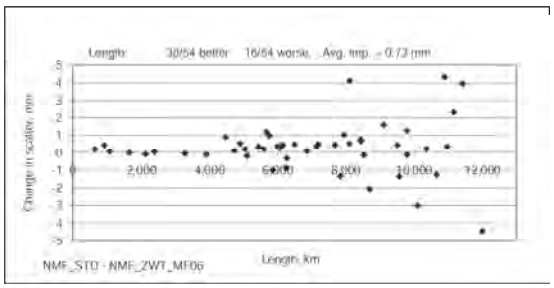

Figure 4. Incorporating correlated noise improves the solution

Average scatter is reduced by 0.73 mm. Most (38/54) baselines are improved. A few baselines involving HARTRAO are degraded.

5. Comparison of NMF and VMF Mapping Functions

The standard mapping function used at Goddard is NMF. This has the advantage that it is easily calculable. It has the disadvantage that it completely ignores the weather. In contrast, VMF uses ECMF data to derive station and session specific mapping functions. Fig. 5 plots the difference between

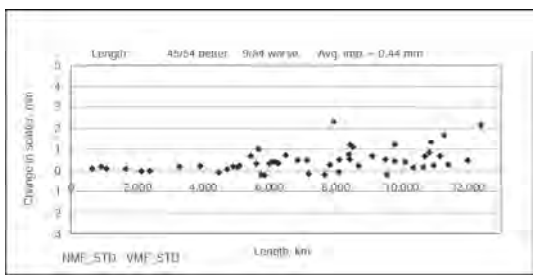

Figure 5. VMF

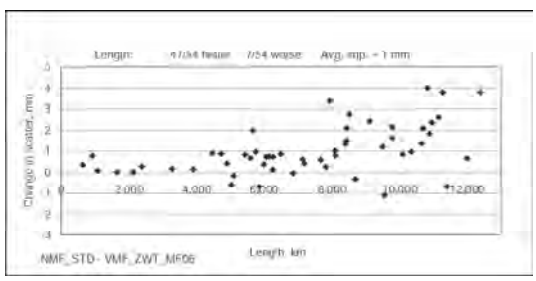

Figure 6. VMF with correlation and no re-weighting

a solution using NMF and one using VMF. On average baseline scatter is reduced by 0.44 mm, and 45/54 baselines improve. In Fig. 6 we have turned off re-weighting and included correlation effects. In this case, 47/54 baselines are better, and the average improvement is 1.0 mm.

6. Conclusions

In this note we presented several alternatives to the standard VLBI analysis. We demonstrated that re-weighting reduces scatter. Including elevation dependent noise further reduces scatter. Curiously enough, the results are better in this case if re-weighting is turned off. Including the effect of correlation between observations results in a significant reduction in scatter. We showed that using VMF reduces scatter compared to NMF. Our best results use VMF, correlated elevation dependent noise, and no re-weighting.

References

[1] Boehm, J., H. Schuh. Vienna mapping functions in VLBI analysis. Geophys. Res. Lett., 31(1), L01603, DOI 10.1029/2003GL018984, 2004.

[2] Gipson, J.M. Incorporating Correlated Station Dependent Noise Improves VLBI Estimates. European VLBI Meeting, 2007.

[3] Gipson, J.M. Correlation due to Station Dependent Noise. 2006 IVS General Meeting Proc. D. Behrend and K. Baver (eds), 2006, 286–290.

[4] Niell, A.E. Global mapping functions for the atmospheric delay at radio wavelengths. J. Geophys. Res., 101(B2), 3227–3246, 1996.

[5] Zhi-han, Q. The Correlation on VLBI Observables and Its Effects for the Determination of ERP. Shanghai Observatory, 1985.

[6] Schuh, H., A. Wilkin. Determination of Correlation Coefficients between VLBI-Observables. Proc. of the 7th Working Group Meeting on European VLBI. A. Rius (ed.), 1989, 79–91.

[7] Schuh, H., V. Tesmer. Considering A Priori Correlations in VLBI Data Analysis. IVS General Meeting Proceedings, 2000, 237.

[8] Tesmer, V. Refinement of the Stochastic VLBI Model: First Results. 16th Working Meeting on European VLBI for Geodesy and Astrometry, 2003, 207–218.

[9] Tesmer, V. Das stochastische Modell bei der VLBI-Anwertung. PhD thesis. University of Munich, Munich, Germany, 2003.

[10] Tesmer, V., H. Kutterer. An advanced Stochastic Model for VLBI Observations and its Applications to VLBI Data Analysis. 2004 IVS General Meeting Proceedings. N. Vandenberg and K. Baver (eds.), 2004, 296–300.

The 5th IVS General Meeting Proceedings, 2008, p. 163–167

Data Analysis at BKG in the Frame of IVS

Volkmar Thorandt, Gerald Engelhardt, Dieter Ullrich

Bundesamt für Kartographie und Geodäsie, Germany

Abstract. The VLBI group of the Federal Agency for Cartography and Geodesy (BKG) in Leipzig is part of the jointly operated IVS Analysis Center of BKG and the Institute for Geodesy and Geoinformation of the University of Bonn (IGGB). BKG is responsible for the computation of time series of Earth Orientation Parameters (EOP) and tropospheric parameters, the generation of SINEX (Solution INdependent EXchange format) files for 24-hours VLBI sessions and Intensive sessions, and quarterly updated global solutions for Terrestrial Reference Frame (TRF) and Celestial Reference Frame (CRF) realizations. The data processing steps are explained and also some problems in the procedure of data analysis are discussed. Additionally one of the three primary IVS Data Centers is managed at BKG.

1. General Information on Data Analysis

For purposes of data analysis at BKG the Mark 5 VLBI data analysis software Calc/Solve [1] including the Calc 10 implementation for complying with the IAU 2000 Resolutions and the IERS Conventions 2003 is running on a Linux operating system.

The Calc/Solve software was modified for using the Vienna Mapping Function (VMF1). Applying VMF1 in data analysis requires a daily update of the VMF1 data from the server of the Technical University of Vienna.

In addition, an independent technological software environment for the Calc/Solve software is available. The latter is used for linking up the Data Center management with the pre- and post-interactive part of the EOP series production and to monitor all Analysis and Data Center activities.

2. Processing of Correlator Output

A main task in data analysis at BKG is the generation of calibrated databases for the sessions correlated at the MPIfR/BKG Mark 5 Astro/Geo Correlator at Bonn (e.g. EURO, OHIG, T2) and submitting them to the IVS Data Centers.

3. Scheduling

BKG is responsible for scheduling the INT2 Intensive sessions on the baseline TSUKUBA-WETTZELL since Aug. 2005. The program system SKED developed by John Gipson (NVI, Inc/NASA Goddard Space Flight Center) is used for that.

4. Data Flow and Analysis at BKG

Fig. 1 gives an impression about the main work steps in VLBI data analysis at BKG.

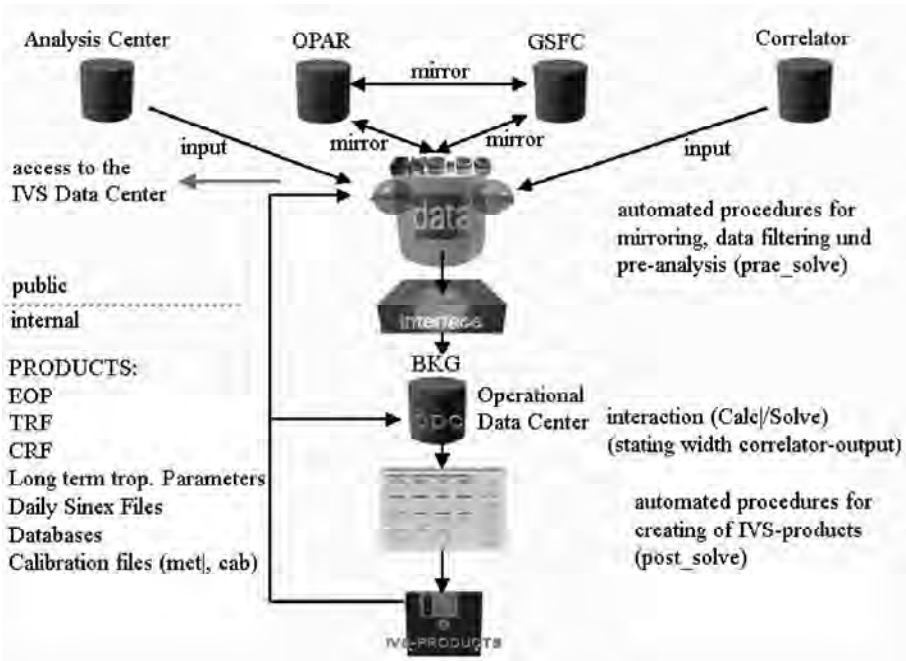

Figure 1. VLBI data flow and analysis activities at BKG

5. IVS EOP Time Series bkg00010

To create the EOP series the Vienna Mapping Function for modelling the tropospheric delay correction is used. The modelling for 3 stations was refined by non-linear site position variations estimation (GILCREEK, HRAS, PIETOWN). Furthermore the new official list of the VLBI antenna axis offsets, status May 17, 2007 and the a priori VTRF2005 are used in data processing.

After the preprocessing of any new VLBI session (correlator output data-

base version 1), a new global solution with 24-hours sessions since 1984 is computed and the EOP time series bkg00010 is extracted.

Some topics about statistics and solution description of bkg00010 are listed in the following:

- number of sessions more than 3500,
- main parameters: EOP, globally estimated station coordinates and velocities together with radio source positions, tropospheric parameters (zenith wet delays),
- local station parameters: BADARY (Russia), CTVASTJ (Canada), DSS65A (Spain), METSAHOV (Finland), ZELENCHK (Russia),
- minimal constraints for the datum definition are applied to achieve no-net-rotation and no-net-translation for 26 selected station positions and velocities with respect to VTRF2005 and no-net-rotation for 212 defining sources with respect to ICRF-Ext.1.

6. IVS UT1 Time Series bkgint07

VMF1 is used in the UT1 time series bkgint07 too. In addition to the observations of both baselines KOKEE-WETTZELL and TSUKUBA-WETTZELL, also the networks KOKEE-SVETLOE-WETTZELL and NYALESUND-TSUKUBA-WETTZELL, each with a duration of about 1 to 1.5 h, are processed regularly.

Series bkgint07 is generated with fixed TRF (VTRF2005) and fixed CRF derived from the global BKG solution for EOP determination. The estimated parameter types are only UT1, station clock, and zenith troposphere. The UT1 Intensive sessions are analyzed from 1999.01.01 on.

7. Quarterly Updated TRF and CRF Solutions for Submission to IVS

Every year quarterly updated solutions for the IVS products TRF and CRF are computed. There are no differences in the solution strategy compared to the continuously computed EOP time series bkg00010. The results of the radio source positions are submitted to IVS in IERS format. The TRF solution is available in SINEX format, version 2.1 and includes station coordinates, velocities, and radio source coordinates together with the covariance matrix, information about constraints, and the decomposed normal matrix and vector.

8. Tropospheric Parameters

The VLBI group of BKG continues regular submissions of long time series of tropospheric parameters to the IVS (wet and total zenith delays, horizontal gradients) for all available VLBI sessions since 1984. The tropospheric para-

meters are extracted from the standard global solution for the EOP time series bkg00010 and transformed to SINEX format.

9. Daily SINEX Files

In addition to the global solutions daily SINEX files for all available 24-hours sessions as base solutions for the IVS time series of baseline lengths and for combination techniques are submitted. Independent session solutions are computed for the parameter types station coordinates, EOP, and nutation parameters. The a priori datum for TRF is defined by the VTRF2005 and the fixed CRF derived from the global complete BKG solution for EOP determination is used for the a priori CRF information.

10. SINEX Files for Intensive Sessions

IVS SINEX files for Intensive sessions are created and submitted to IVS. The parameter types are station coordinates, pole coordinates and their rates, and UT1 with rate. Only the normal equations stored in the SINEX files are important for further combination with other space geodetic techniques.

11. Problems with Logfile Formats

To run the extracting program for calibration data (XLOG) in an automated mode normally different errors in the logfiles have to be fixed before. The program LOGFIX developed at BKG screens the logfiles in a pre-analysis step referring to a number of errors listed as follows:

- wrong filename of the logfile (i.e. euro87ro.log to euro876a.log),
- wrong station name in the header (i.e. NyAlesun to NYALES20),
- superfluous header records,
- records outside of observation time span,
- implausible meteorological data,
- empty records,
- wrong time fields,
- format error in meteorological data field,
- wrong cable sign.

An example for the program output of program LOGFIX is shown below:

```
LOGFIX: ———————— /disc2/data/log/euro85on.log ————————-
        Copy of logfile: /disc2/data/log/euro85on.log.ivs
        START OF SESSION 2007.008.12:00:00.00
```

```
        STOP OF SESSION 2007.009.12:00:00.00
        LOGFIX(format error): 2007.008.14:28:18.81;wxcom!@1h
        Number of records in original logfile: 43482
        Corrected station name in header:"Onsala" to "ONSALA60"
        Number of corrected wx-records: 2
        Outside of observation time span (records deleted): 379
        Empty records deleted: 1
        Format error in meteorological data (records deleted): 39
        Number of written records with meteorological data: 484
        Number of written records with cable data: 243
        Written records in /disc2/data/log/euro85on.log: 43063
LOGFIX: ———————— return ———————— .
```

12. Work on ICRF2

The VLBI group at BKG is part of the IVS working group for the second realization of the ICRF. An important step is the computation of time series for all radio sources. On the basis of former investigations [2] a new set of time series for all radio sources was computed with nearly no change in datum definition. Based on the globally estimated source coordinates from the standard global solution bkg00010 a new set of 183 radio sources was selected to define the datum with the no-net-rotation constraints. The identification of the 183 preliminary stable sources was the result of a former analysis [2]. The new time series of radio sources were derived with 24-hours VLBI sessions from Jan. 1984 to Jul. 2007 in a complete global solution. The overall solution statistics summary for data type delay (all) shows a slightly better weighted RMS residual of 28 ps for the new time series solution in contrast to the standard solution bkg00010 with 29 ps.

It is planned to investigate the long-term stability of radio sources based on the new time series of radio source positions by using a statistical test for normal distribution of residuals to the weighted mean of a radio source component.

References

[1] GSFC, NASA, Release of Mark 5 VLBI Analysis Software Calc/Solve Oct. 10, 2007.

[2] Engelhardt, G., V. Thorandt. First steps to Investigate Long-Term Stability of Radio Sources in VLBI Analysis. IVS General Meeting Proceedings 2006. D. Behrend and K.D. Baver (eds.), NASA/CP-2006-214140, 2006, 281–285.

The 5th IVS General Meeting Proceedings, 2008, p. 168–172

Real-Time Ray-Tracing through Numerical Weather Models for Space Geodesy

Ichikawa Ryuichi, Thomas Hobiger, Yasuhiro Koyama, Tetsuro Kondo

Kashima Space Research Center, National Institute of Information and Communications Technology (NICT), Japan

Abstract. Numerical weather models have undergone an improvement of spatial and temporal resolution in the recent years, which made their use for space geodetic applications feasible. Ray-tracing through such models permits the computation of total troposphere delays and ray-bending angles. At the National Institute of Information and Communications Technology (NICT) the so-called KAshima RAy-tracing Tools (KARAT) have been developed which allow to obtain troposphere delay corrections in real-time. Together with fine-mesh weather models from the Japanese Meteorological Agency (JMA) huge parts of the East Asian region, including Japan, Korea, Taiwan and East China, can be covered. Thus a short overview about the capabilities and functions of KARAT will be given and computation performance issues will be discussed. The ray-traced total troposphere slant delays can be used as a correction of space geodetic data on the observation level.

1. Introduction

The introduction of new mapping functions (e.g. [1, 5]) in recent years significantly improved space geodetic techniques. Although modern mapping functions are derived from numerical weather models the information from such meteorological data sets is reduced to a few time-dependent and location-dependent coefficients which relate slanted troposphere quantities to equivalent zenith measures. Moreover, the spatial variations of the troposphere above each station have to be estimated in the analysis process in the form of gradient parameters. As numerical weather models of regional size have undergone an improvement of accuracy and precision it became feasible to utilize ray-traced troposphere slant delays directly for the geodetic analysis of space geodetic techniques.

1.1. Mesoscale Analysis Models from the JMA

The Japanese Meteorological Agency (JMA) provides a variety of weather models ranging from global models to fine-mesh models which cover an area of only a few tens of kilometers. The meso-scale 4D-Var model (i.e. Meso-scale Analysis Data (MANAL)) from JMA [4] with its horizontal resolution of about 10 km was found to have the best trade-off between grid-spacing and area size. This model covers large parts of Eastern Asia, including Japan and its Southern islands, Korea, Taiwan, and Eastern China (Fig. 1). Moreover, the three hour time-resolution of the data sets makes the appliance of this model for positioning applications feasible.

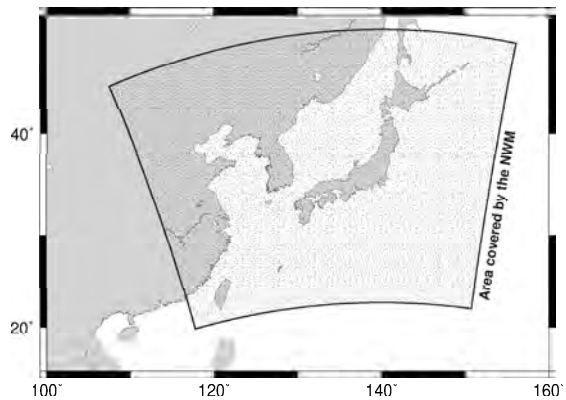

Figure 1. The spatial domain for which JMA meso-scale weather models are available

2. Kashima Ray-Tracing Tools (KARAT)

Based on the requirement to deliver ray-traced delays in real-time (assuming that numerical weather models are available as forecast data) a set of tools has been created in order to carry out the ray-tracing tasks. Coding in C++ does not only permit to design the modules close to machine language, but also allows to interface external classes which enable multi-core/multi-processor support. A detailed description about KARAT and its performance can be found in [2].

2.1. Preparing the Data

Since the grid points of the JMA mesoscale weather models are not equally spaced on a geographic coordinate system it is necessary to interpolate them onto a rectangular grid. Moreover, it is mandatory to transform the geopotential heights, which are used by the meteorologists, into geometric heights, which can be used for ray-tracing calculations. Thus, the first tool of KARAT handles all these tasks, using a sophisticated interpolation algorithm which allows

to compute refractivity values on a geographic grid with user-defined boundaries, resolution, and height steps. Each epoch of the numerical weather model is processed by this tool and binary files are created for follow-on processing. As described by [3], a dedicated height system helps to reduce the number of necessary height levels without accuracy degradation of the ray-traced slant delays.

2.2. The Ray-Tracer

The main module of KARAT is the ray-tracing engine which reads consecutive binary weather models, covering a 24-hour period and loads the refractivity fields into free memory. Once all the data is put to memory, ray-tracing cores can be launched independently. Each core is at idle status until station position and ray-geometry (i.e., time, azimuth, and elevation) are parsed to it. As KARAT uses OpenMP to take advantage of multi-core and multi-processor architectures, the number of available ray-tracing cores is only limited by the number of CPU cores which share the same memory. KARAT offers three different modes (Fig. 2) in which the ray-tracing can be carried out. The fastest,

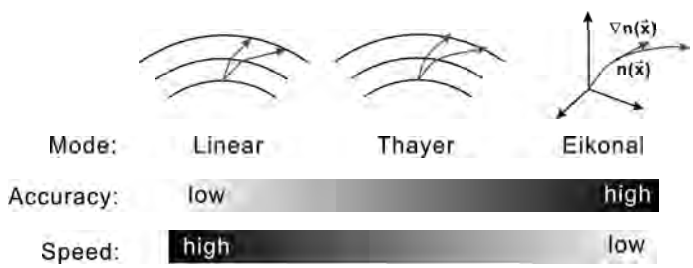

Figure 2. The three ray-tracing modes of KARAT together with their accuracy and speed performance

but least accurate one assumes linear ray-propagation between two height levels and computes the refraction when the ray-crosses a layer. The more advanced mode, considers that the ray is also bent when propagating between two levels. This mode is called Thayer, named after the corresponding paper [6]. Both modes fully consider the 3D refractivity field, but do not allow for out-of-plane propagation of the ray. The most sophisticated, but also slowest mode solves the Eikonal equation numerically and provides the 3D ray-path together with the total delay. As the differences between the Thayer and the Eikonal model hardly exceeds the mm-level at lowest elevations (3 deg) the Thayer mode is often selected as a compromise between speed and accuracy.
The ray-tracing module allows to handle geometry or reads RINEX files and computes the observing geometry using IGS orbit information. Moreover the reduction of troposphere delays is supported by correcting code and phase measurements directly in the RINEX files.

3. Ray-Traced Troposphere for Space Geodesy — First Results

In [2] the impact of ray-traced troposphere delays on precise point positioning with GPS was analyzed. As the numerical weather models currently do not allow to obtain mm-accurate slant troposphere delays, it was necessary to estimate a residual troposphere delay, when using ray-traced data sets. Station height repeatabilities of several GPS sites in East Asia could be improved when KARAT data was used. Moreover the RMS of the residuals were found to be at the same levels as those obtained from modern mapping functions and gradient estimation. Additionally, the authors could show that positioning solutions with cm-range accuracy could be achieved when the ray-traced data was analyzed without residual troposphere estimation.
In order to apply such corrections to VLBI measurements it is necessary that both stations are either within the same high-resolution weather model or that several regional numerical weather models are used to consider the weather conditions at each site. Although KARAT is currently only dealing with mesoscale data from JMA it is possible to handle numerical weather models from other weather agencies. Tests with ray-traced troposphere slant delays for East Asian VLBI networks are planned for the close future.

4. Kashima Ray-Tracing Service

In order to enable users of space geodetic techniques to take advantage of KARAT without the need to access numerical weather models by their own it was decided to provide ray-tracing as a service. Thus the ray-tracing tools will be embedded in an automatic processing chain, called Kashima Ray-Tracing Service (KARATS), which can be started via a Web interface. Fig. 3 shows how KARATS is expected to operate. Once a user (from the GPS or VLBI

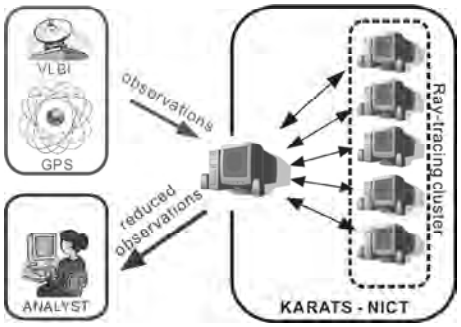

Figure 3. Flow chart of the KARATS processing chain. KARATS will subtract troposphere delays from the user's observation based on the geometry computed from precise orbits (GNSS) or source positions (VLBI)

community) has taken his observations, he can send the data in a common format (which will be RINEX for GPS and MK3/FITS for VLBI initially) via Internet to KARATS. Thereafter the Web server will do a rough data-check and compute the geometry from the observation file. As soon as a ray-tracing client becomes available it will send the geometry file to that machine. The client performs the ray-tracing through the weather model and sends the tropospheric delays back to the server. Thereafter the ray-traced delays are subtracted from the user's data and a "reduced" observation file is sent back to the user. Thus the analyst can estimate his target parameters without spending too much effort on estimating tropospheric delays. In the case that VLBI observations are submitted it is checked that both stations lie within the boundaries of the NWM and thereafter the tropospheric delays are computed at each station. In a final step the server will compute the differenced corrections and apply them to the VLBI observations.
Moreover it is planned to run KARATS for real-time applications. Since this mode needs weather prediction data from the JMA it will be limited to a selected user group. The KARATS post-processing mode will be free of charge and a turn-around time of one minute per (RINEX) file is anticipated.

Acknowledgements

The first author wants to thank the Japanese Society for the Promotion of Science (project P06603) for supporting his research.

References

[1] Boehm, J., B. Werl, H. Schuh. Troposphere mapping functions for GPS and very long baseline interferometry from European Centre for Medium-Range Weather Forecasts operational analysis data. J. Geophys. Res., v. 111, B02406, DOI 10.1029/2005JB003629, 2006.

[2] Hobiger, T., R. Ichikawa, T. Takasu, et al. Ray-traced troposphere slant delays for precise point positioning. Earth, Planets and Space, 2008 (in print).

[3] Hobiger, T., R. Ichikawa, Y. Koyama. Fast ray-tracing for real-time positioning applications using numerical weather models. To be submitted to Earth And Planetary Science Letters, 2008.

[4] JMA, Outline of the operational numerical weather prediction at the Japanese Meteorological Agency, 158, 2002.

[5] Niell, A.E. Global mapping functions for the atmosphere delay at radio wavelengths. J. Geophys. Res., v. 101(B2), 3227–3246, 1996.

[6] Thayer, G. A rapid and accurate ray tracing algorithm for a horizontally stratified atmosphere. Radio Science, v. 1, 249–252, 1967.

The 5th IVS General Meeting Proceedings, 2008, p. 173–177

VLBI Baseline Length Repeatability Tests of IVS-R1 and -R4 Session Types

Kamil Teke, Robert Heinkelmann, Johannes Boehm, Harald Schuh

Institute of Geodesy and Geophysics, Vienna University of Technology, Austria

Abstract. In this study, baseline length repeatabilities from analysis of geodetic VLBI data are investigated with the troposphere mapping functions NMF, GMF, and VMF1, and with different cut off elevation angles (between 3° and 30°) for IVS-R1 and IVS-R4 sessions. Each mapping function yields similar baseline repeatabilities for cut off angles 3°, 5°, 7° and 10°, but from 15° onwards the repeatabilities grow significantly. VMF1 gives the best repeatabilities in the interval 3° to 10° with the lowest value at 7°. Above 10° all three mapping functions more or less yield the same repeatabilities.

1. Introduction

The speed and the path of microwave radio signals that radiate from a quasar is altered when passing through the troposphere due to the particular atmospheric conditions. This effect is called tropospheric delay and is included in the mathematical model of VLBI measurements. VLBI has reached sub-centimeter precision for baseline lengths and station coordinates determined in a global terrestrial reference frame from 24 hour sessions [7]. However, future expectations are to improve the precision of these parameters to millimeter level. The baseline length and station coordinate repeatabilities depend on the amount of observables, the lengths of the baselines, but also on the accuracy of mathematical models, e.g. the tropospheric delay model including the mapping functions that are used to describe the relation between the tropospheric delay at zenith direction and at an arbitrary angle above the horizon. Due to the longer path through the atmosphere when decreasing the elevation angle, difficulties in tropospheric delay modeling increase. From this point of view observations should be made near the zenith zone. On the other hand, including observations that are widely separated over all elevation and azimuth angles allows us to decrease the observational correlations [3]. Thus, there is a trade-off between smaller correlations of zenith delays and station heights as well as larger mapping function errors when using low elevation observations. Baseline length repeatabilities can be considered as important accuracy crite-

ria for VLBI analysis, since baseline lengths are independent of rotations of the polyhedron formed by several VLBI stations [6]. For each baseline, the repeatability can be determined as the standard deviation of the n estimates Li with regard to the mean value L_0 on a regression polynomial of first order [1].

2. Baseline Length Repeatabilities of IVS-R1 and IVS-R4 Sessions

The major purpose of the IVS-R1 and IVS-R4 sessions is to provide twice-weekly Earth Orientation Parameters (EOP). The "1" and "4" indicate that in general the sessions are on Mondays and Thursdays, respectively. The "R" stands for rapid turnaround because the stations, correlators, and analysts have taken the commitment to make the time delay from the end of recording to results as short as possible. The time delay should not exceed 15 days. To determine the baseline length repeatabilities of the IVS-R1 and R4 sessions from 04/01/2002 (mjd:52278 begin with R4) to 29/06/2007 (mjd:54280 end with R4) a linear function was fitted as

$$B_i(t_j) = a_{i(1)} + a_{i(2)}(t_j - t_0), \tag{1}$$

where $B_i(t_j)$ is the baseline length of the baseline i for session j and t_j is the day of the session. $a_{i(1)}$ and $a_{i(2)}$ are the unknown parameters of the linear regression function for baseline i which are estimated by a least-squares adjustment. The RMS value of each fit is considered as the baseline length repeatability. The baseline length repeatabilities of the IVS-R1 and R4 sessions were determined using three mapping functions: Niell Mapping Functions [5], Global Mapping Functions [2], and Vienna Mapping Functions 1 [1]. The principle of Vienna Mapping Function (VMF1) is to use the best empirical coefficients b and c available, and to determine the coefficient a of the continued fraction form (2) from a ray-trace at $e_0 = 3.3°$ initial elevation angle through a Numerical Weather Model (NWM)

$$m(e) = (1 + a/(1 + b/(1 + c)))/(sin(e) + a/(sin(e) + b/(sin(e) + c))). \tag{2}$$

Two regression functions were formed before and after the Earthquake for the baselines with station Gilcreek, because of the Denali Earthquake (03/11/2002). For a more sophisticated model of the motion of Gilcreek we refer to [4]. The cut off elevation angle was set to 3°, 5°, 7°, 10°, 15°, 20°, or 30°. A quadratic polynomial was adjusted to the repeatabilities (without linear term) [6] as follows

$$r_n = k_{m(1)} + k_{m(2)}(B_n)^2, \tag{3}$$

where B_n is the baseline length, and r_n is the repeatability value of the baseline n, $k_{m(1)}$ and $k_{m(2)}$ are the unknown parameters of the regression function, m denotes the selected mapping function and the cut off elevation angle (e.g. $m = 1$ denotes VMF1, cut off angle 3°. The unknown parameters were estimated by a

least-squares adjustment. Fig. 1 and 2 show the repeatabilities of the baseline lengths for different mapping functions and cut off angles. The mapping functions yield similar baseline repeatabilities for cut off angles $3°, 5°, 7°$, and $10°$, but from $15°$ onwards, the repeatabilities grow significantly. VMF1 gives the best repeatabilities in the interval $3°$ to $10°$ with the lowest value at $7°$. Above $10°$ all three mapping functions more or less yield the same repeatabilities. Fig. 3 shows the sum of the repeatabilities for each mapping function and cut off elevation angle. The sum of the repeatabilities with VMF1 is smaller than

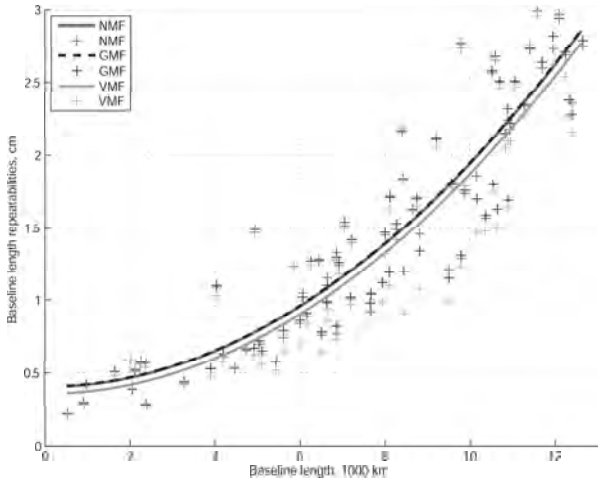

Figure 1. Baseline length repeatabilities with VMF1, GMF, and NMF for a cut off angle $3°$ for IVS-R1 and R4 sessions

with NMF or GMF, at least below ($10°$). Above ($10°$) all mapping functions produce approximately the same sum of repeatabilities. In Tabl. 1, the total number of observations of R1 and R4 sessions from 04/01/2002 to 29/06/2007 and the mean number of observations per session is given for each cut off elevation angle. In this time span, 277 sessions of R1 and 268 sessions of R4 were analysed.

3. Conclusions and Outlook

From the investigations of R1 and R4 sessions baseline repeatabilities for the mapping functions VMF1, GMF, and NMF and the cut off angles $3°, 5°, 7°, 10°, 15°, 20°$, and $30°$ the following conclusions can be drawn:

- VMF1 gives the best repeatabilities for low cut off angles $3°$ to $10°$,
- the repeatabilities are smallest with a cut off elevation angle of $7°$. For cut off elevation angles above $10°$, VMF1, NMF, and GMF yield approximately the same baseline length repeatabilities,

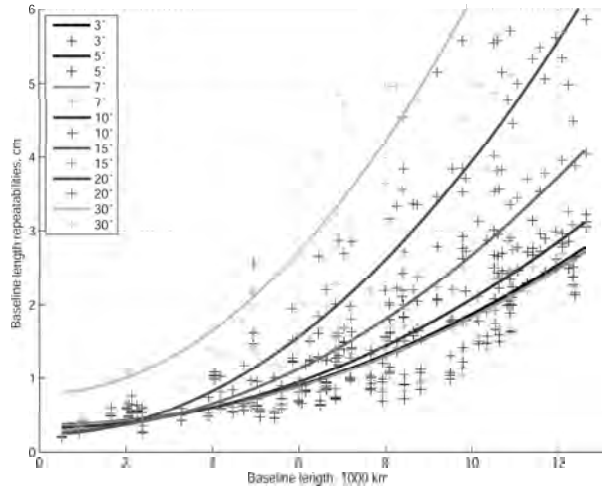

Figure 2. Baseline length repeatabilities with VMF1 for the cut off angles $3°, 5°, 7°, 10°, 15°, 20°$, and $30°$

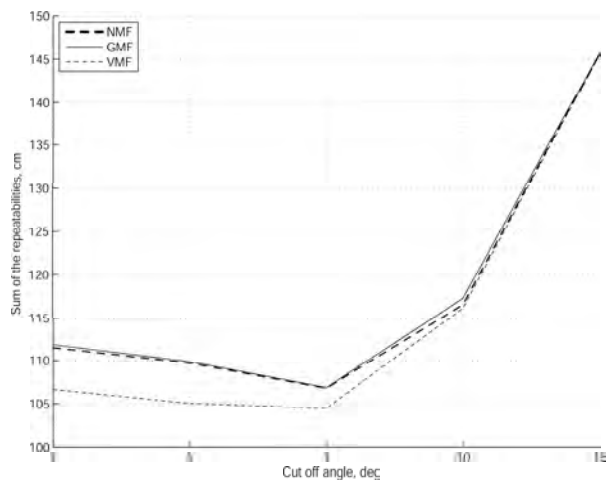

Figure 3. Sum of the baseline length repeatabilities with VMF1, GMF, and NMF for the cut off angles $3°, 5°, 7°, 10°$, and $15°$

- there is no significant difference in repeatabilities between NMF and GMF.

Using different cut off elevation angles means that not the same number of observations is used. Thus, these tests will be repeated removing observations randomly when a low cut off elevation angle is applied so that the number

Table 1. Number of observations for sessions from 04/01/2002 to 29/06/2007

Cut off	Total Obs.(R1)	Mean Obs.(R1)	Total Obs.(R4)	Mean Obs. (R4)
3^0	519259	1875	350536	1308
5^0	515212	1860	348347	1300
7^0	492457	1778	337583	1260
10^0	451846	1631	313850	1171
15^0	380012	1372	267530	998
20^0	312135	1127	220201	822
30^0	193116	697	139688	521

of observations is identical for all cut off angles. Investigations with down weighting of low elevation observations have to be carried out, too.

References

[1] Boehm, J., B. Werl, H. Schuh. Troposphere mapping functions for GPS and very long baseline interferometry from European Centre for Medium-Range Weather Forecasts operational analysis data. J. Geophys. Res., v. 111, B02406, DOI 10.1029/2005JB003629, 2006a.

[2] Boehm, J., A. Niell, P. Tregoning, et al. Global Mapping Function (GMF): A new empirical mapping function based on numerical weather model data. Geophys. Res. Lett., 33: L07304, DOI 10.1029/2005GL025546, 2006b.

[3] Malkin, Z. Influence of the Cut-off Elevation Angle and Elevation-Dependent Weighting on Parameter Estimates: A Case of CONT05. 5th IVS General Meeting, 2008. This volume.

[4] Heinkelmann, R., J. Freymueller, H. Schuh. A postseismic relaxation model for the 2002 Denali earthquake from GPS deformation analysis applied to VLBI data. 5th IVS General Meeting, 2008. This volume.

[5] Niell, A.E. Global mapping functions for the atmosphere delay at radio wavelengths. J. Geophys. Res., v. 101, B2, 3227-3246, 1996.

[6] Niell, A. Baseline Length Repeatability, Report. MIT Haystack Observ., 2006.

[7] Seeber, G. Satellite Geodesy. De Gruyter, 2nd edn. Berlin/Newyork, 2003.

The 5th IVS General Meeting Proceedings, 2008, p. 178–182

Influence of Elevation-Dependent Weighting on Parameter Estimates: A Case of CONT05

Zinovy Malkin

Central Astronomical Observatory at Pulkovo, Russian Academy of Sciences, Russia

Abstract. In this paper, results are presented on studies which have been performed to investigate the impact of the cut-off elevation angle and elevation-dependent weighting on the EOP estimates and baseline length repeatability.

1. Introduction

The precision and accuracy of observations made through the Earth's atmosphere grow with increasing elevation due to larger air mass and difficulties in modelling refraction effects at low elevation. From this point of view observations should be made in the near-zenith zone when possible. On the other hand, inclusion in processing of observations made at low elevations is important when highly correlated parameters are estimated simultaneously. In such a case using observations made in a widest range of elevation allows one to mitigate the correlations between unknowns. To meet these mutually exclusive requirements, elevation-dependent weighting (EDW) is used. In a special case of step-like weighting function, one rejects the observations made at the elevation less than the given limit, so-called cut-off elevation angle (CEA).

It is well known that EDW has a significant impact on the results of processing of the space geodesy observations. In particular, several studies on the subject were made in the framework of the IVS VLBI2010 Committee activity (http://ivscc.gsfc.nasa.gov/pipermail/ivs-v2c/). Those results were based on simulation. Gipson in [1] applied elevation dependent additive noise to the measurement error instead of using a weighting factor as it is usually being made. He tested his method with the actual CONT05 observations.

Results of both mentioned and other results are sometimes contradictory. This gave an impulse to the present work where some results are presented about an investigation of the impact of the CEA and EDW on the baseline length repeatability (BLR) and Earth orientation parameters (EOP) estimates.

2. Test Description and Results

For this test, CONT05 observations were processed with the OCCAM software with different EDW functions including CEA, keeping all other options as used during routine processing: Kalman filter mode (KF), random walk model for clocks (PSD=1.5 ps^2/s) and ZTD (PSD=0.25 ps^2/s), one NS and EW troposphere gradient estimate for each 24h session.

For the continuous EDW mode (continuous weighting function), the measurement error is multiplied by a factor

$$W_e = (\sin e_0 \,/\, \sin e)^p \,, \tag{1}$$

where e_0 and p are EDW parameters, e is the source elevation. Such a weighting function provides a smooth stepless change in weight for any e_0. One can see that a case of $e_0 = 90°$, $p = 1$ gives merely $W_e = 1/\sin e$, which is close to actual mapping function used in the last works by MacMillan and Gipson (private communications). EDW mode with $e_0 = 10$, $p = 2$ was implemented in the OCCAM/GROSS software [2] for routine data processing. It will be referred to hereafter as "normal mode". In a case of CEA we have

$$W_e = \begin{cases} 1, & \text{if } e >= e_0 \,, \\ 10^3 & \text{otherwise} \,. \end{cases} \tag{2}$$

The latter line corresponds to the KF realization used in OCCAM. For VLBI delay, the measurement error coming from the correlator is multiplied by two W_e values computed for both stations. In our test, $e_0 = 3(2)25°$ were used for CEA test, and $e_0 = 10, 25, 45, 90°$, $p = 1, 2$ were used for continuous EDW mode.

BLR obtained with different CEA are shown in Fig. 1. The case of $e_0 = 3°$ includes all the observations without weighting, since no CONT05 observations were made at the elevation less than 4°. Tabl. 1 shows EDW test results. Different EDW modes are denoted as 'e_0_p' corresponding to (1). Test results are given for quadratic approximation in percent with respect to the case of CEA with $e_0 = 3°$. One can see that several EDW modes show about the same improvement in the BLR.

Table 1. Baseline length repeatability for different EDW models

EDW	Baseline length, 10^3 km				EDW	Baseline length, 10^3 km			
mode	3	6	9	12	mode	3	6	9	12
10_1	98.0	97.2	97.3	97.6	45_1	101.7	90.0	84.6	81.9
10_2	95.3	95.0	95.5	96.1	45_2	104.0	97.2	101.8	107.6
25_1	102.6	92.8	87.2	83.8	90_1	101.3	90.5	85.4	82.8
25_2	95.7	91.8	91.4	91.9	90_2	109.6	127.3	161.1	191.1

To investigate the change in the baseline length obtained with different CEA and EDW models we compared them (mean of 15 daily estimates) to

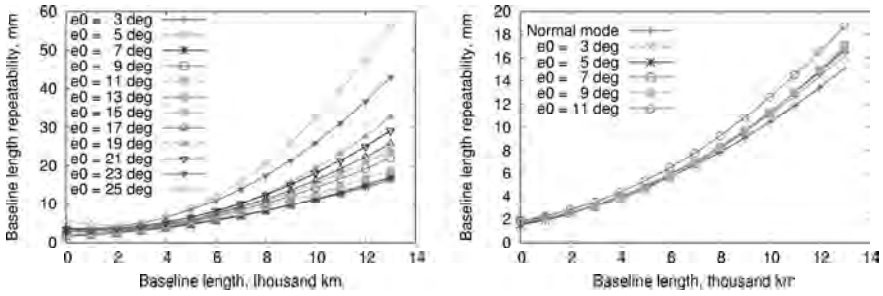

Figure 1. Baseline length repeatability for different CEA (quadratic regression)

the length value obtained with $e_0 = 3°$ (all the observations included). The comparison shows that change in the baseline length essentially depends on stations involved in the baseline under consideration. For stations located among others, for which observation sky coverage is close to uniform, change in baseline length may reach several millimeters with increasing of CEA. For outside stations, HARTRAO and especially TIGOCONC for CONT05, one can see very asymmetric sky coverage, and change in baseline length may reach 3 cm as CEA grows from 3° to 25°. EDW mode shows much less change in the baseline length, and in this case increasing e_0 leads to greater change in the baseline length too up to 1 cm for TIGOCONC and HARTRAO.

Fig. 2 shows EOP statistics for different CEA. Notation used is the following: Xp, Yp – terrestrial pole coordinates, Xc, Yc – celestial pole coordinates. Results of comparison of CONT05 EOP with the IGS time series are presented in Fig. 3. Xp and Yp wrms with respect to IGS EOP series are computed after removing the bias. Tabl. 2 shows the main EDW test results. Notation of the EDW modes is the same as used in Tabl. 1. The column labelled "All" corresponds to inclusion of all observations without weighting. One can see again that several EDW modes show about the same EOP precision and accuracy.

3. Conclusions

The preliminary conclusions from this test are the following.

The BLR steadily grows with the CEA increasing, remaining practically the same up to 9°. The same can be said for the bias in the baseline length. Maximal impact of the CEA on the baseline length bias is seen for the outside network stations with the most asymmetric observations sky coverage.

The Xp, Yp and UT1 uncertainties grow with the increasing CEA after about 10°. Most probably, this reflects the fact that only about 6% of the total number of CONT05 observations were made at the elevations below 10°. The Xc and Yc uncertainties and scatter depend on the CEA much less. Xp bias w.r.t. IGS slightly depends on the CEA, except the maximum tested CEA values, evidently unrealistic. In contrast, Yp bias substantially changes

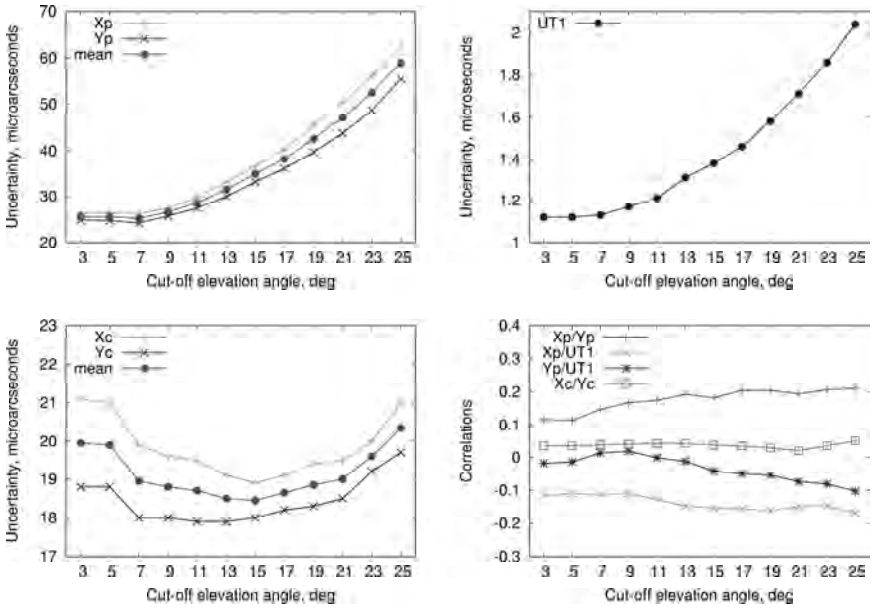

Figure 2. Statistics of EOP obtained from CONT05

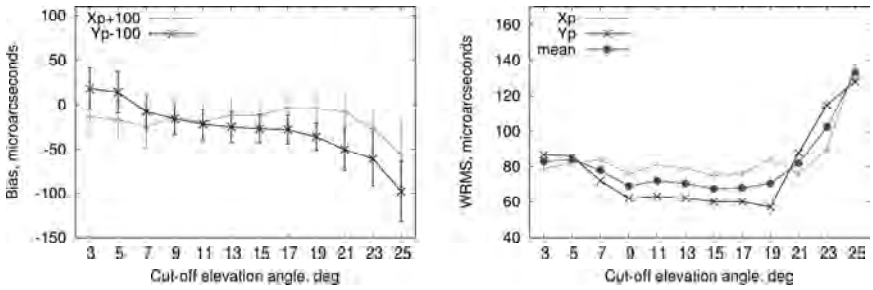

Figure 3. Comparison of EOP obtained from CONT05 with the IGS EOP series

with increasing CEA. Most probably, this can be explained by the CONT05 network orientation, for which the longitude of the central meridian $\lambda_0 = 265°$ just corresponds to the Yp direction. Some statistics, such as the uncertainty and the scatter of the Xc and Yc, as well as the WRMS of Xp and Yp w.r.t. IGS have the minimum at the CEA around 15°, which is interesting and deserves a supplement investigation. As one can expect, the correlations between EOP comprising Xp and Yp grow with increasing CEA, but remain small due to good CONT05 network geometry. The same can be expected for the IVS2010 network. The correlation between Xc and Yc remain practically the same for

Table 2. EOP statistics for different EDW models

Statistics	Unit	All	EDW mode							
			10_1	10_2	25_1	25_2	45_1	45_2	90_1	90_2
Xp uncertainty	μas	26	26	25	26	28	27	37	30	51
Yp uncertainty	μas	25	24	24	24	26	25	32	26	43
UT1 uncertainty	μs	1.1	1.1	1.1	1.1	1.1	1.0	1.3	1.1	1.6
Xc uncertainty	μas	21	21	20	20	19	20	22	22	27
Yc uncertainty	μas	19	18	18	18	18	18	21	20	27
Xp bias w.r.t. IGS	μas	–79	–75	–79	–77	–73	–80	–86	–81	–123
Yp bias w.r.t. IGS	μas	+135	+135	+128	+132	+129	+134	+127	+129	+92
Xp wrms w.r.t. IGS	μas	77	72	76	69	65	68	69	64	86
Yp wrms w.r.t. IGS	μas	73	74	72	69	61	68	63	71	83

all tested CEA, except the maximum tested CEA value, evidently unrealistic.

For most of the tests performed, the best result was obtained with EDW applied to the low-elevation observations. However, the test results are not always unambiguous. Further adjustment of the weighting method may be fruitful.

Finally, we can conclude that inclusion of the low-elevation observations, properly weighted, improves the baseline length and EOP estimates. On the contrary, filtering the observations using the CEA method may lead to degradation of geodetic results. However, it should be mentioned that the conclusions drawn from the result obtained in this paper has been proven with standard geodetic VLBI observations, where rather few observations were made at low elevations, as mentioned above. Perhaps, special R&D sessions with more uniform distribution of observations over the sky, including observations at very low elevations, may be useful for more detailed study on optimal scheduling and processing of the space geodesy observations.

It ought be mentioned that all the EDW modes considered in this paper in fact modify only diagonal elements of the corresponding covariance matrix. According to Gipson's work [1] best results can be achieved when correlations between observations are also accounted for. It seems to be interesting to investigate how this approach will work for the KF estimator.

References

[1] Gipson, J. Incorporating Correlated Station Dependent Noise Improves VLBI Estimates. Proc. 18th European VLBI for Geodesy and Astrometry Working Meeting. J. Boehm, A. Pany, H. Schuh (eds.), 2007, 129–134.

[2] Malkin, Z., E. Skurikhina. OCCAM/GROSS Software Used at the IAA EOP Service for processing of VLBI Observations. IAA RAS Transactions, v. 12. "Nauka", St. Petersburg, 2005, 54–67 (in Russian).

The 5th IVS General Meeting Proceedings, 2008, p. 183–187

Optical Characteristics of Astrometric Radio Sources

Zinovy Malkin [1], *Oleg Titov* [2]

[1)] *Central Astronomical Observatory at Pulkovo, Russian Academy of Sciences, Russia*

[2)] *Geoscience Australia, Australia*

Abstract. A new list of physical characteristics of 3914 astrometric radio sources, including all 717 ICRF-Ext.2 sources, observed during IVS and NRAO VCS sessions have been compiled. The source list was taken from the Goddard VLBI astrometric catalog astro_2007c with addition of two ICRF-Ext.2 sources. At this stage the source characteristics were mainly taken from the NASA/IPAC Extragalactic Database (NED). Our list includes source type, redshift, and visual magnitude (if available). In case of doubt detailed comment is provided. 667 sources from our list are included in the IERS list. A comparison of the two lists has shown a significant difference in characteristics for about half of the common sources. We compiled a list of frequently observed sources without known physical characteristics for urgent observation with large optical telescopes.

1. Introduction

Information on physical characteristics of the geodetic radio sources is important for planning VLBI experiments and analyzing VLBI data in order to do research in cosmology, etc. In particular, the primary driver for this work was to support the investigation of the systematic effects in apparent proper motion of geodetic radio sources [1, 2, 3, 4].

The official list of physical characteristics of the ICRF radio sources is supported by the IERS ICRS Product Center [5]. The latest version of the IERS list is available in the Internet[1]. However this list has some deficiencies:

- not all the sources observed in the framework of geodetic and astrometric experiments are included in the IERS list,
- the characteristics of some sources in the IERS list are outdated or doubtful.

[1] http://hpiers.obspm.fr/icrs-pc/info/car_physique_ext1

To overcome these problems, we performed a compilation of a new list with physical characteristics of all geodetic radio sources observed in the framework of the IVS and VCS programs using the latest information. In this paper we present the results of the first stage of this work.

The list of radio sources with their positions was taken from the Goddard VLBI astrometric catalog[2], version 2007c. We removed the duplicate source 1616+85A (L. Petrov, private communication) and added the two ICRF-Ext.2 [6] sources 1039-474 and 1329-665 that were not included in the Goddard catalog. This resulted in 3,914 geodetic radio sources in total.

At this stage we mainly searched the NASA/IPAC Extragalactic Database (NED)[3] for geodetic radio sources. Some of them were also checked with the CfA-Arizona Space Telescope LEns Survey (CASTLES)[4] and the HyperLeda[5] databases. We have included in our list only photometric and spectral optical characteristics, such as source type, redshift, and visual magnitude. The source flux parameters are not included in our list because they are available from other sources.

2. List Description

As mentioned above, our primary interest was to collect all available redshift z determinations for sources observed in the framework of the IVS and cooperative programs, such as the VLBA Calibrator Surveys (VCS), in support of previous studies of quasar apparent proper motions [1, 2, 3, 4]. In these studies, redshift values were taken from the ICRF list [5]. However, as rather tiny effects in the source motions are to be investigated, it is important to increase the number of sources involved in the processing. Searching the latest astrophysical databases, primarily the NED, we could considerably augment the list of geodetic radio sources with known redshift. Nevertheless, more than half of the geodetic radio sources have no measured redshift so far.

Evidently, the only direct way to get the redshift for other most frequently observed geodetic sources is to organize a dedicated observing program with large optical telescopes. The top list of the most frequently observed geodetic radio sources, for which measured redshift was not found, includes 0718+792, 1300+580, 1357+769, 1923+210, 0556+238, 0656+082, 0657+172, 1221+809. To help in preparing such a program, we also collected the source type and its visual magnitude for radio sources if this information is available. Also, it makes sense to include in this observational program sources with existing but inaccurately measured redshifts. The relevant comments are added to our list.

It should be noted that not all geodetic radio sources were reliably identified in the NED. We use the following identification procedure. In the first step, we search for sources by source name using 'ICRF' and 'IVS' prefixes. So,

[2] http://vlbi.gsfc.nasa.gov/solutions/astro
[3] http://nedwww.ipac.caltech.edu/
[4] http://cfa-www.harvard.edu/glensdata/
[5] http://leda.univ-lyon1.fr/

we rely on the source identification used in the literature and provided by the NED staff. Then about 500 sources, mostly from the VCS6 list, were searched by position. We took into account the angular distance between the VLBI and NED positions as well as the position uncertainty in the VLBI and NED catalogues. For some sources multiple NED objects were found within the error level. For 16 sources no appropriate objects were found in the NED, which is mentioned in the list comments. The problem of the source identification in the NED and other astrophysical databases hopefully will be solved once the VCS6 results are officially published and incorporated in the NED and other astronomical databases.

The list of optical characteristics of the geodetic radio sources is available at http://www.gao.spb.ru/english/as/ac_vlbi/sou_car.dat. Besides a common description, the following info for every source is given: IERS and IVS (if different from IERS) source name, position, redshift (if available), visual magnitude (if available), source type (if available, otherwise, 'R' type is quoted), and comments.

3. Statistics

The overall statistics of the new list is the following.

Number of sources:

total		3914 (100%)
ICRF	717 (18.3%)	
N	2376 (60.7%)	
S	1538 (39.3%)	
with known type		2369 (60.5%)
AGN	1581 (66.7%)	
galaxy	461 (19.5%)	
other	327 (13.8%)	
with known redshift		1790 (45.7%)
≤ 1	825 (46.1%)	
> 1	965 (53.9%)	
N	1185 (66.2%)	
S	605 (33.8%)	
with known visual magnitude		2300 (58.8%)
with known both z and magnitude		1739 (44.4%)
with known z or magnitude		2351 (60.1%)
with known magnitude and unknown z		561 (14.3%)
without characteristics		1563 (39.9%)

Fig. 1 shows the distribution of the sources with known redshift, and Fig. 2

shows the distribution of the visual magnitude. The right part of Fig. 2 gives an impression about the magnitude of the sources, for which the redshift is not yet determined.

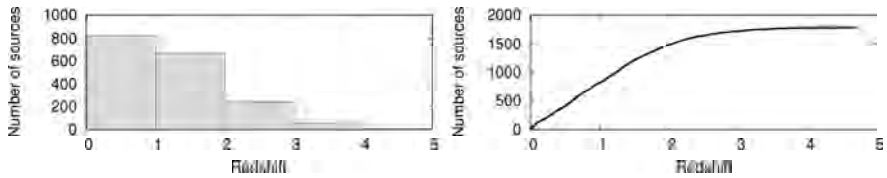

Figure 1. Distribution of the redshift (*left*) and cumulative number of sources (*right*)

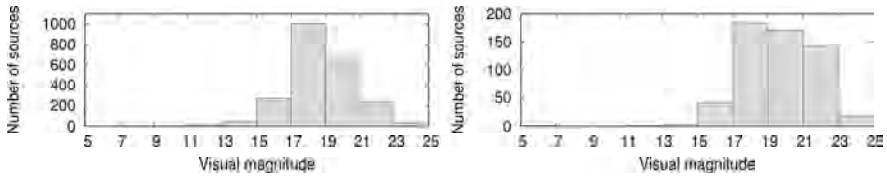

Figure 2. Distribution of the visual magnitude for all sources (*left*) and for sources without known redshift (*right*)

4. Comparison with the IERS List

We compared the new list with the IERS list of 667 sources. All 667 IERS sources are in our list. The comparison of these two lists resulted in rather large discrepancies:

- The first evident difference is in the number of sources: 3,914 vs. 667 objects in total, 2,351 vs. 555 objects with known redshift or visual magnitude. Our list contains 40 extra ICRF sources plus several hundreds of other sources.
- Unlike the authors of the IERS list, we did not try to trace all the details of the Active Galactic Nuclei (AGN) classification that is not always stable and unambiguous. So, all quasars and BL objects are designated as AGN.
- Redshifts for 55 more ICRF sources were found; redshifts for 4 sources presented in the IERS list were not included in our list for various reasons; for 30 sources the redshift differs by more than 0.01; the largest differences are 1.26 (1903-802), 1.20 (1600+431), and 0.70 (0646-306).
- Visual magnitudes for 70 more ICRF sources were found; for 2 sources magnitudes were not confirmed in our list; for 195 sources magnitudes differ by more than 0.5; the largest differences are 5.2 (1758-651), 5.0 (1156-094, 1322-427), and 3.9 (0241+622).

5. Conclusion

A new extended list of optical characteristics of the geodetic radio sources has been compiled. This is only the first stage of our work. We are planning the following steps:

- to continue the search for missing characteristics in the literature and astronomical databases,
- to continue the verification of the ambiguous characteristics through literature and astronomical databases,
- to organize photometric and spectroscopy observations of geodetic radio sources with missing redshift using large optical telescopes. In particular, such an observational program has been included in the plan of the Pulkovo Observatory for 2008. The application for observation time on the Russian 6-meter BTA telescope for the second half of 2008 was submitted in cooperation with Pulkovo astrophysicists Kirill Maslennikov and Alexandra Boldycheva.

The authors would be happy to know whether this new list is useful either as a database for VLBI data analysts or as a supplement material for the ICRF-2 compilation. We hope that this work will be continued in cooperation with other interested groups.

Acknowledgements

This research has made use of the NASA/IPAC Extragalactic Database which is operated by the Jet Propulsion Laboratory, California Institute of Technology, under contract with the National Aeronautics and Space Administration, the SIMBAD database, operated at CDS, Strasbourg, France, the HyperLeda database and the CASTLES survey.

References

[1] Gwinn, C.R., T.M. Eubanks, T. Pyne, et al. Quasar proper motions and low-frequency gravitational waves. Astroph. J., v. 485, 87–91, 1997.

[2] Macmillan, D.S. Quasar Apparent Proper Motion Observed by Geodetic VLBI Networks. ASP Conference Proceedings, v. 340, 477–481, 2005.

[3] Titov, O. Proper motions of reference radio sources. Journees 2007, Paris, France.

[4] Titov, O. Systematic Effects in Apparent Proper Motions of Radio Sources. This volume.

[5] Archinal, B.A., E.F. Arias, A.M. Gontier, et al. Physical characteristics of radio sources. IERS Technical Notes No 23, III-11–III-24, 1997.

[6] Fey, A.L., C. Ma, E.F. Arias, et al. The second extension of the International Celestial Reference Frame: ICRF-Ext.2. Astron. J., v. 127, No 6, 3587–3608, 2004.

The 5th IVS General Meeting Proceedings, 2008, p. 188–192

Effects of Surface Pressure and Temperature on the VLBI Reference Frames

Robert Heinkelmann, Johannes Böhm, Harald Schuh

Institute of Geodesy and Geophysics, Vienna University of Technology, Austria

Abstract. We quantify and compare effects on the VLBI reference frames and tropospheric parameters obtained by VLBI analysis applying meteorological input data from various sources: in situ measurements at the VLBI sites, interpolated values from analysis data of the European Centre for Medium-Range Weather Forecasts (ECMWF), empirical values obtained from the Global Pressure and Temperature model (GPT), and constant values for each site from the Berg model. While the surface pressure is necessary to separate hydrostatic and wet tropospheric delays, the thermal deformation models of the VLBI antennas depend on the temperature. While significant effects can be found on ZWD, vertical position time series, and sessionwise scale factors, the celestial reference frame and Earth orientation parameters show no significant variations applying meteorological data from the various sources.

1. Introduction

The analysis of space geodetic techniques at radio wavelengths (GNSS, VLBI, DORIS, etc.) is usually refined using meteorological quantities such as surface pressure and temperature at each site. In the case of VLBI, meteorological surface data can be used for three models to reduce the group delay, the primary observable of VLBI data analysis:

- hydrostatic (a priori) zenith delay,
- atmospheric (pressure) loading,
- antenna thermal deformations.

While the first two models require pressure values, the thermal deformations depend on the outside temperature, or the inside temperature in case the antenna is covered by a radome. In this study effects of atmospheric loading are not considered, i.e. atmospheric loading corrections [5] are applied but remain unchanged throughout the study. We investigate how pressure from various sources affects the determination of hydrostatic zenith delays and how temperature from various sources changes the antenna thermal deformation

corrections, both leading to variations in the primary geodetic parameters of interest: Terrestrial Reference Frame (TRF), Celestial Reference Frame (CRF), and Earth Orientation Parameters (EOP). Since the effects on the CRF and EOP are insignificant and of non-systematic nature, we focus on the TRF, vertical station position time series, and tropospheric zenith wet delays (ZWD). The reference temperature for the thermal deformation is realized as the mean temperature value from the in situ data over the whole observational history at the site (Malkin, pers. comm.).

2. Sources of Meteorological Data

Various sources of meteorological data maintain pressure and temperature and can be applied for VLBI analysis, e.g.:

- in situ data,
- numerical weather models,
- the Global Pressure and Temperature model (GPT),
- the Berg atmosphere model.

Since meteorological data (pressure and temperature) are continuously recorded during experiments at the VLBI sites and reported in standard VLBI data files (station log file or NGS file) the usual way for VLBI analysis is to simply use these records. However, with in situ data care has to be taken for two reasons: One reason is, that often some registrations are missing, and some other values are obviously outlying. It is necessary to replace both, missing values and outliers by an adequate substitute. For replacement, we suggest to interpolate from numerical weather models (NWM) such as the ERA-40 reanalysis model of the ECMWF. Such values can be accessed for all VLBI sites and throughout the VLBI observational history (1979.0 until today) from the URL http://mars.hg.tuwien.ac.at/~ecmwf1/VLBI/. The other reason is, that in some of the meteorological records significant shifts of the running mean value are present; the time series need to be homogenized. Shifts of the pressure records exceeding 2 hPa were already reported [3]. The temperature records show shifts of the running mean value, too. Due to missing meta data about the meteorological sensors, i.e. epochs and results of sensor calibration and reductions of pressure readings to the mean sea level (geoid), we cannot rely on the presently available mean value of the in situ data. Thus, we suggest to shift the mean value of sensor registrations to the mean value represented by the NWM. In doing so, we concatenate the global consistency of NWM and the higher temporal resolution of met sensors recording in situ.

If neither in situ data nor NWM data are available, we suggest to obtain meteorological data by the Global Pressure and Temperature model [2] which is a spherical harmonic expansion of degree and order nine of the mean values

and annual signals of pressure and temperature. In this respect, GPT should replace the simple Berg model [1].

Fig. 1 shows bias and RMS of temperature and pressure w.r.t. in situ values of twelve representative IVS network stations. The largest biases can be found between Berg and the in situ data. GPT shows still significant but much smaller biases. The biases between NWM and the in situ data are almost zero, since the mean values of the in situ data were shifted to match the NWM. They are not perfectly zero, because for the adjustment of the mean value inherent outliers were considered, though outliers were not considered for the determination of the biases shown in the plot. The RMS of GPT is slightly smaller than that one of Berg in the case of pressure and significantly smaller for the temperatures. This is due to the fact that pressure variations are more pronounced at weekly time scales, whereas the temperature clearly shows a seasonal pattern, which is well modelled by GPT's annual term. Variations at weekly time scales are not considered in both models, neither GPT nor Berg.

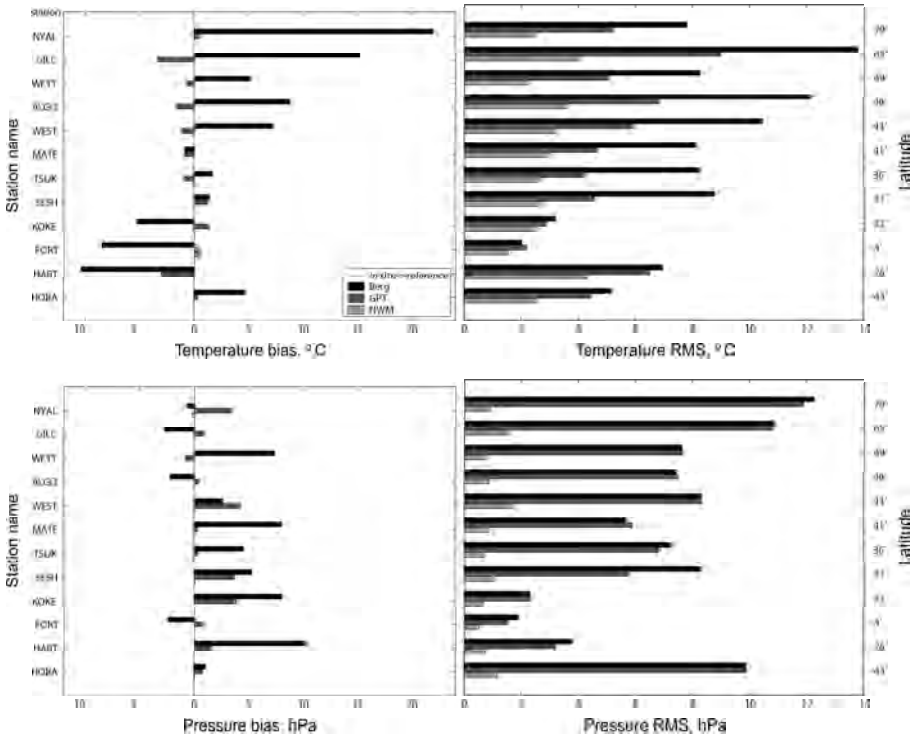

Figure 1. Bias and RMS of temperature and pressure w.r.t. in situ meteorological data of 12 IVS network stations ordered from northern latitudes (*top*) to southern latitudes (*bottom*)

3. Effects of Atmospheric Pressure and Temperature on Geodetic Parameters

Since pressure biases are not systematically positive or negative most of the impact on the TRF as a whole gets balanced out using one of the prior introduced pressure sources. The seven parameters of a similarity transformation between a TRF using in situ pressure data and a TRF applying one of the other sources are almost all insignificant. Nevertheless, the scale differs by 0.16 ppb, what equals 1.0 mm at one Earth radius, between TRFs derived using in situ or Berg pressure, respectively. Investigating time series the effects become more obvious: an assumed change of pressure of $\delta p = 1$ hPa corresponds to a change of zenith hydrostatic delay (ZHD) of $\delta ZHD = 2.3$ mm. A large fraction of δZHD can be absorbed by the zenith wet delay (ZWD), however, since hydrostatic and wet mapping functions do not exactly equal, a smaller fraction of δZHD affects the adjustments of other (geodetic) parameters. Due to correlations the station vertical position gets deformed in particular. The amount of deformation of geodetic parameters depends on how much the hydrostatic and wet mapping functions differ, and this difference depends on the latitude of the site and the elevation angle under which a specific observation is carried out. Stations at high latitudes more often observe at low elevations, therefore, the station latitude turns out to be the key factor for pressure dependent station height errors. In addition, pressure variations are more pronounced at higher latitudes. At station GILCREEK, Gilmore Creek, Alaska, USA, e.g. the vertical station position shows variations of up to 10 mm from peak to peak between Berg and in situ data, solely depending on the type of pressure data used. At some stations e.g. HARTRAO, Hartebeesthoek, South Africa, the pressure biases induce biases of the vertical station positions (Tabl. 1).
The temperature generally shows the well known diurnal and annual cycles. At high latitudes the annual cycle is more pronounced, whereas at low latitudes it can barely be found. GPT and Berg models do not consider diurnal cycles at all and thus, it is impossible to model diurnal antenna thermal deformations with temperatures of these models, whereas the NWM with its six-hourly resolution is capable to reproduce diurnal cycles. Significant differences in sessionwise scale factors can be found using Berg temperature where the annual amplitude

Table 1. Bias and RMS of pressure, ZWD and station height w.r.t. the solution using in-situ atmospheric pressures at station HARTRAO

	NWM		GPT		Berg	
	bias	RMS	bias	RMS	bias	RMS
Pressure, hPa	0.00	0.34	1.56	2.93	10.14	3.58
ZWD, mm	0.32	1.72	−2.08	7.18	−21.04	8.54
Station height, mm	−0.01	1.23	−0.46	1.54	−1.45	1.77

reaches 0.2 ppb (1.3 mm at one Earth radius), whereas in case of the GPT the amplitude stays well below the 1 mm level. A more detailed paper [4] is going to be published soon.

4. Conclusions

Since significant effects can be found on zenith delay and vertical position estimates the usage of precise and homogeneous pressure data is mandatory for the analysis of space geodetic techniques at radio wavelengths. To avoid seasonal deformations of the TRF determined by VLBI, thermal antenna deformations should be accounted for using precise and homogeneous temperature data. The most precise and accurate meteorological data for the analysis are in situ data after shifting the running mean value to match a global numerical weather model, e. g. ERA-40 of the ECMWF. For the replacement of missing values a numerical weather model should be used. For each VLBI site, such values are accessible from the URL http://mars.hg.tuwien.ac.at/∼ecmwf1/VLBI/ and can be linearly interpolated to the epoch of the observation.

Acknowledgements

This study could not have been prepared without the provision of excellent VLBI data by the IVS.

References

[1] Berg, H. Allgemeine Meteorologie. Dümmler Bonn, 1948, 337.

[2] Böhm, J., R. Heinkelmann, H. Schuh. Short Note: A global model of pressure and temperature for geodetic applications. J. Geod., v. 81(10), 679–683, 2007.

[3] Heinkelmann, R., J. Böhm, H. Schuh, et al. Combination of long time-series of troposphere zenith delays observed by VLBI. J. Geod., v. 81(6-8), 483–501, 2007.

[4] Heinkelmann, R., J. Böhm, H. Schuh, et al. The influence of meteorological input data on the VLBI reference frames. Proceedings of the FIG/IAG Meeting on Geodetic Reference Frames (GRF2006), IAG Symposium Series, 2008 (in print).

[5] Petrov, L., J.-P. Boy. Study of the atmospheric pressure loading signal in very long baseline interferometry observations. J. Geophys. Res., v. 109, B03405, DOI 10.1029/2003JB002500, 2004.

The 5th IVS General Meeting Proceedings, 2008, p. 193–198

The Contribution of CVN to the CE-1 Mission

Jinling Li

Shanghai Astronomical Observatory, Chinese Academy of Sciences, China

Abstract. In this report we present the current status of the Chinese VLBI network (CVN), the results of satellite tracking experiments in the past few years as related to the realtime processing of the CVN dataflow and the reliability and precision of the CVN measurements. In particular, we report on the realtime monitoring of the orbit evolution of the Chang'E-1 satellite by the CVN.

1. Current Status of the Chinese VLBI Network

The two 25 m radio telescopes at Sheshan of Shanghai and Nanshan of Urumqi began astrometric observations in 1987 and 1993, respectively. The Chinese mobile VLBI consists of a 3 m antenna and an S2 system. Observations could also be recorded on a hard disk system, which is compatible with the Mark 5. In May 2006, two new antennas with diameters of 50 m at Miyun near Beijing and 40 m at Fenghuangshan of Kunming participated in the tracking experiment of the Smart-1, a lunar satellite of the European Space Agency (ESA). The correlation center of the Shanghai Astronomical Observatory (SHAO) has successfully developed a five-station FX correlator and a system with PC-based hard disk recorder and playback. The dataflow rate per station is 256 Mbps. Up to now, in the background of the Chinese lunar exploration project Chang'E-1 (CE-1), the Chinese VLBI Network (CVN) has been developed into four permanent antennas, one mobile station and a correlation center. The CVN extends geographically by over 34° east-west and 18° south-north, with baselines ranging from 1115 km to 3249 km. Tabl. 1 lists some technical specifications of the four CVN permanent antennas, which are all equipped with the Mark 5 recording system.

Table 1. Technical specifications of CVN antennas

Specifications	Shanghai	Beijing	Urumqi	Kunming
Operation	1987	2006	1993	2006
Structure	BWGC[1]	Prime focus	BWGC	BWGC
Diameter, m	25	50	25	40
Pointing, $''$	20	19	15	30
Slewing, A/E, $^\circ/s$	1.0/0.6	1.0/0.5	1.0/0.5	1.0/0.5
Receiver	L, C, S/X, K	S/X	UHF, L, C, S/X, K	S/X
S/X efficiency, %	38/40	60/68	54/52	64/47
Terminal	Mark 5A, VLBA, S2	Mark 5A	Mark 5A	Mark 5A

[1]BWGC — Beam wave guide Cassegrain

2. The CVN Tracking Experiments of Satellites in the Past Few Years

Since the 1960s VLBI techniques have been demonstrating high precision in astrometry and geodesy studies, especially in establishing the celestial and terrestrial reference frames as well as in the determination of the Earth Orientation Parameters. In the Chinese lunar exploration project CE-1, VLBI is expected to contribute to realtime monitoring of the satellite orbit especially during the lunar capture stage. The CVN is mandated to fulfill a 10-minute task, that is, to provide the spherical coordinates of the satellite within a delay of 10 min, with a precision of 0.2 arcsec near perilune. This presents a great challenge to the ordinary processing of the VLBI dataflow, including the preparation of schedule, antenna tracking, data recording and transfer, correlation, extraction of VLBI observables, correction of systematic behavior and atmosphere delays, as well as deduction of the target spherical coordinates from observations.

2.1. The CVN Dataflow in the Realtime Running Mode

In the CVN realtime running mode, the schedule is sent via internet to the antennas. The tracking data are also transferred via internet to the data analysis center. The data are processed simultaneously by the hard and software correlators and then observables are extracted. As the antennas are tracking the satellite, observations from co-located GPS receivers are sent to the data analysis center too and atmospheric delay information is extracted. This information is combined with the VLBI observables and the systematic behavior corrections including the clock bias and the instrument delay deduced from observations of extragalactic radio sources in order to deduce the angular position of the satellite. All these steps are processed with a delay of less than ten minutes. At the end of the tracking pass the orbit is also determined.

2.2. The Tracking of the Smart-1

In the middle of 2006 ESA offered a great opportunity to the CVN people to test their hardware and software with a goal of completing the 10-minute task by tracking the Smart-1, a lunar satellite. Fig. 1 shows the difference between the angular positions of the Smart-1 deduced from the CVN realtime measurements and the ESA reconstructed orbit, which was post-stage determined with high precision. After removing some outliers, the standard deviation of the difference is about 0.1 arcsec, which demonstrates CVN measurements are reliable and with sufficient precision for the identification of the lunar capture of CE-1 satellite [2].

2.3. The Tracking of the TC-1

On Jan. 23, 2007, the CVN tracked a Chinese satellite TC-1. Fig. 2 shows the comparison of the angular positions with the orbit prediction. Before UTC 15.3 h the angular positions stem from four tracking antennas, while after that the antenna at Shanghai dropped out of the tracking. It is noticed that the data points before this epoch are more dispersed than afterwards. At first glance, this phenomenon shows some confliction with the common sense. Does this mean that the angular position determined from three antennas is better than from four? Or there is some problem in the tracking data of Shanghai? Or is it solely because there are some faults in the reduction algorithm and/or the software?

The angular coordinates (α, δ) at an epoch are deduced from the interpolated delays of data series according to baselines. When there are four tracking antennas, the independent delays are three and the two unknowns are deduced in a least squares adjustment (LS), which is unbiased estimation. While for the case of three tracking antennas, the two unknowns are deduced from only two independent delays and so the solution is unique. The unique solution is constrained to the adopted a priori geocentric distance of the satellite, which is smooth because it is the prediction of the initial orbit but could be in error by the magnitude of kilometers. So the unique solutions are less dispersed as demonstrated by Fig. 2 but could be seriously biased [1].

2.4. Realtime Monitoring of the CE-1 Orbit Evolution

CE-1, the first Chinese lunar satellite was launched on Oct. 24, 2007. It took about two weeks for the CE-1 to fly into the designed orbit to become a lunar satellite. The CVN began tracking of the CE-1 every day from Oct. 27 to Nov. 30, 2007, and timely provided the delay, rate and angular positions with a time lag of about five minutes. Since Dec. 18, 2007 the CE-1 entered into the long-term operation phase and the CVN changes the tracking mode as two-days per week.

The state vectors $(\vec{r}, \dot{\vec{r}})$ are deduced from the delay, rate, range and Doppler

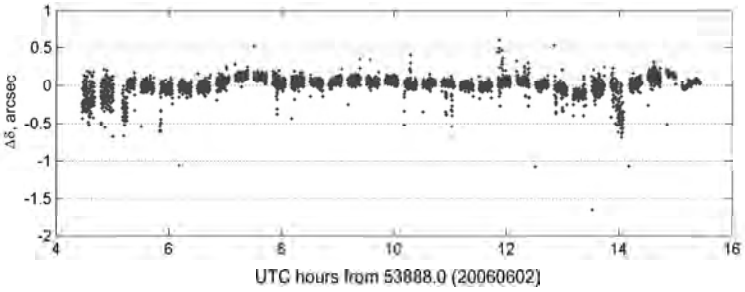

Figure 1. Comparison of the CVN realtime measurements and the ESA reconstructed orbit of Smart-1

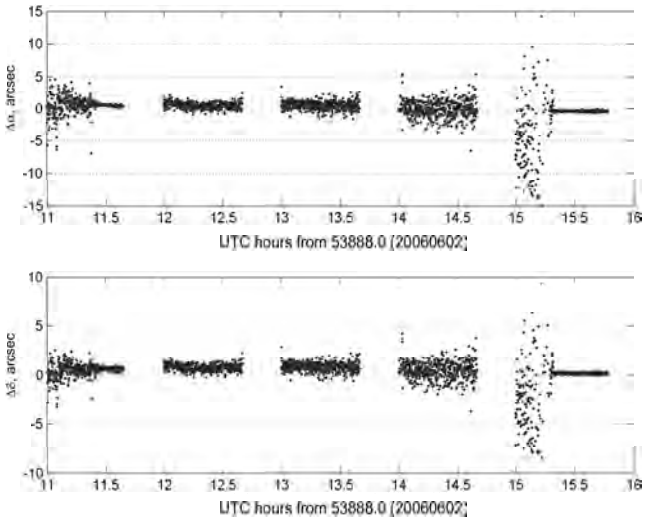

Figure 2. Comparison of the angular position determination with the TC-1 orbit prediction

observations and it is easy to transform them into the orbit elements. As demonstrated in Tabl. 2, by monitoring the evolution of the orbit eccentricity, we quickly declared the successful capture of the CE-1 by the Moon with a time lag of about five minutes because the eccentricity of a parabolic orbit is distinctively different from an ecliptic orbit. By the reduction of the state vectors we also successfully monitored the processes of the orbital manoeuvres, Tabl. 3 is an example.

Table 2. Monitoring the capture of CE-1 by the Moon

ymd	h:m:s	GC	a, km	e	Nb
hyperbolic orbit					
20071105	03:13:01	M	6618.708	1.29441	14
20071105	03:13:31	M	6641.511	1.29340	14
20071105	03:14:00	M	6664.319	1.29238	10
very near to a parabolic orbit					
20071105	03:17:07	M	3406.991	1.08194	08
captured					
20071105	03:20:53	M	2990.028	0.84911	06
20071105	03:20:58	M	3016.474	0.84918	06
elliptic orbit					
20071105	03:42:01	M	6205.055	0.68567	12
20071105	03:42:30	M	6154.900	0.68305	12
20071105	03:43:00	M	6155.691	0.68311	12

Table 3. Monitoring the orbit manoeuvre process (20071106)

h:m:s	a, km	e	$i,^\circ$	$\Omega,^\circ$	$\omega,^\circ$	$M,^\circ$
03:21:14	6015.141	0.67682	87.524	265.446	102.952	−3.881
03:22:43	4418.871	0.56143	87.503	265.290	105.717	−5.781
03:26:29	3360.283	0.42134	87.555	265.223	107.499	−4.906
03:28:46	3056.361	0.36189	87.581	265.279	105.912	−1.674
03:29:26	2971.901	0.34367	87.583	265.281	105.908	−0.747
03:33:46	2601.796	0.25105	87.578	265.396	100.429	10.520
03:36:43	2704.682	0.27867	87.531	265.484	101.783	14.158

3. Closing Remarks

Based on the methodology and software system of data reduction of the regular astrometric and geodetic VLBI, the reduction of the instantaneous state vectors of spacecraft by using VLBI tracking data is realized, which has contributed to the realtime orbit monitoring of the CE-1 with high precision. Compared to the precise and short-arc orbit determination, the reduction of the state vectors is characterized by the loose requirement on the length of tracking arc, no need on the precisely modelling of forces exerting on the satellite, geometrically monitoring the quality of the tracking data and the spacecraft orbit. Practice has shown it is a quick and practicable method.

The CVN has got tremendous development by contributing to Chinese national projects and it will definitely keep doing so. In the next stage of the Chinese lunar exploration, for example, VLBI will be applied to track the

orbiter and lander relative to radio sources. In the Chinese Martian exploration project Yinghuo-1, VLBI will be the maintenance technique for the determination of satellite position and orbit.

Acknowledgements

This work is supported by NSFC (No 10778635, No 10173019, No 10473019), Chinese lunar exploration project CE-1 and STC of Shanghai Municipality (06DZ22101).

References

[1] Guo, L., J.L. Li. A discussion on the angular positioning reduction of the experiment s7123a. Journal of Spacecraft TT&C Technology, v. 26(6), 30–35, 2007.

[2] Li, J.L., L. Guo, B. Zhang. The Chinese VLBI network and its astrometric role. Proceedings of the IAU Symposium 248, A Giant Step: from Milli- to Microarcsecond Astrometry. Wenjing Jin, et al. (eds.), 2008, 182–185.

The 5th IVS General Meeting Proceedings, 2008, p. 199–202

WEB Tools and WEB Service of the IERS Earth Orientation Centre

Christian Bizouard, Oliver Becker

Observatoire de Paris / SYRTE, France

Abstract. Since 2003 have been developed on the web site of the Earth Orientation Center (http://hpiers.obspm.fr/eop-pc) a panel of interactive tools devoted to the study of the Earth rotation : selection and plots of the Earth Orientation Parameters (EOP), numerical analysis of these parameters, Earth rotation matrix, comparison of EOP series, and analysis of the geophysical excitation responsible of the Earth rotation fluctuations. Those interactive tools are now completed by web service, that are downloadable executables of which input data on located on our web server.

1. Introduction

One task of the Earth Orientation Center located at the Paris Observatory is to archive various sets of Earth Orientation Parameters (EOP) obtained throughout the world, to validate them, and then to provide by combination a reference series (C04). Whereas pure numbers can satisfy engineer only interested in getting the matrix from the ground to the frame where the satellite orbits are computed, physicist or astronomer need graphical representation and numerical analysis for investigating the astronomical or physical process (sec. 4, 6) underlying the Earth rotation variability. For the user it is quite a waste of time to extract time series from the web, and then to process them by his own numerical and graphical means. Actually, such tools have been set up on the web site of the Earth Orientation Center [1], thank to the dynamical language PHP [2] and Apache Server. Following sections are devoted to the description and potentiality of those tools. For routine tasks, downloading of our data by the use of those tools or FTP may appears heavy. To escape to such a concern we started develop web service (sec. 7).

2. Drawing of the EOP

Our first endeavour has been focused on the selection and the graphical representation of the EOP, first of all. Presently it is possible to draw any time series: combined, operational, long term EOP time series, between two

selected dates, with choice of the format of the date (civil date/modified julian date/besselian year). The considered cases are the following:

- polar motion x time series,
- polar motion y time series,
- polhody $(x, -y)$,
- UT1–UTC, correspondent quantity free from zonal tides effect,
- UT1–TAI, correspondent quantity free from zonal tides effect,
- excess of the length of day (LOD), correspondent quantity free from zonal tides effect,
- earth rotation rate (only for reference combined series C04),
- nutation offset in longitude $d\psi$ time series, with respect to IAU 1980 nutation model,
- nutation offset in longitude $d\varepsilon$ time series, with respect to IAU 1980 nutation model,
- nutation offsets $(d\psi \sin \varepsilon_0, d\varepsilon)$ in the mean equatorial plane,
- nutation offset dX time series, with respect to IAU 2000 nutation model,
- nutation offset dY time series, with respect to IAU 2000 nutation model,
- nutation offsets (dX, dY) in the mean equatorial plane,
- time derivative of x pole coordinate,
- time derivative of y pole coordinate.

These EOP parameters can also be printed on the web browser rather than drawn.

3. Comparison of EOP Series

One important task of our service is to provide comparison of the operational EOP series with respect to the combined series C04 (standard deviation, bias). This comparison can be done for a selected set of the most representative EOP series: combined EOP series (long term C01, operational C04 and Bulletin A); operational series by techniques (9 GPS, 14 VLBI, 7 SLR, 2 DORIS, 1 optical series). After selection of two series and the period for comparison, both series can be compared graphically and their differences can be put into a ASCII file, plotted (with statistics), submitted to FFT or least square fit of any harmonic component and polynomial trend.

4. Numerical Analysis of the EOP

The here-above mentioned series can be drawn and treated by using various tools of numerical analysis: interpolation, spectral analysis, periodogram, least squares fit of any harmonic component and polynomial, Vondrak smoothing, Singular Spectral Analysis. The implementation of these tools is based upon an interface toward FORTRAN and C executables, especially the C library MIMOSA developed by S. Lambert (Observatoire de Paris).

5. Rotation Matrix

For practical purposes or tests we provide the rotation matrix from the terrestrial frame to the celestial frame including a prediction of 6 months. Such tool is of primary interest for geodesy or orbitography. We provide also derived parameters, especially the component of the instantaneous rotation vector within the crust or the celestial reference frame. It is possible possible to set independently polar motion, UT1-UTC and nutation offsets to zero, as well to include diurnal and semi-diurnal effect associated the oceanic tides.

6. Excitation of the Earth Rotation

Among all the users, geophysicist will have particular interest in the interactive comparison of the atmospheric and oceanic angular momentum to the total excitation found in polar motion, length-of-day and nutation. The time interval can be selected, but also the Chandler frequency, the Free Core Nutation frequency, and their respective quality factors, which are critical parameters for computing the equatorial excitation functions. Until now the choice of atmospheric and oceanic data is restricted to NCEP reanalysis model and ECCO model respectively, but we project to extend that choice in the future.

7. Web Service

Since 2008, a user can obtain download on his computer executables, of which the run calls EOP or related data on the Paris Server hpiers.obspm.fr during the execution. That avoids to open web page or FTP connection for downloading the basic data, and that simplification is precisely the essence of web service. Executables are designed for Windows (work in the command line mode with the MSDOS windows) and Linux. Until now we proposed two downloadable executables.

- First one permits to obtain the EOP (combined series C04) from the civil date.
- Second one permits to obtain the Earth Orientation Matrix from the international terrestrial reference system to the international celestial

reference frame at a given instant. It can be helpful for tracking celestial body from ground station with a high precision.

Once downloaded such executables can be integrated in any kind of program: FORTRAN, C, C++, Perl, PHP and do not require the knowledge of the location of the underlying data, which are automatically downloaded from our server.

8. Conclusion

Interactive tools on web for studying the Earth rotation have been developed at the Earth Orientation Center of the IERS since 2003. By a few "clicks" they provide a clear and flexible representation of the phenomena involved in the Earth rotation, as well as fast numerical analysis and inter-comparison of the involved time series. This is also an easy way to watch at the last fluctuations of the Earth rotation, and to detect possible episodic effects. We have started to develop web service which allow the user to get the most recent real time data without any programming. Design of more sophisticated tools according to the needs of the VLBI community and more specifically specialist of the Earth rotation will continue in the future.

References

[1] http://hpiers.obspm.fr/eop-pc.

[2] http://php.net.

The 5th IVS General Meeting Proceedings, 2008, p. 203–206

The Astronomical Virtual Observatory and Application to Earth's Sciences

Sébastien Lambert [1], *Florent Deleflie* [2], *Anne-Marie Gontier* [1], *Philippe Berio* [2], *Christopher Barache* [1]

[1)] *Observatoire de Paris, Département SYRTE, France*

[2)] *Observatoire de la Côte d'Azur, Département GEMINI, France*

Abstract. This paper presents the astronomical Virtual Observatory (VO), an international proposal that provides uniform, convenient access to disparate, geographically dispersed archives of astronomical data from software which runs on the computer on the astronomer's desktop. Though we did not participate in the birth of the VO, we have been helping for a few years in the developments of standards which permit the inclusion of astrometry and geodesy products in the VO. After an overview of the existing VO, we discuss some of our efforts.

1. The Virtual Observatory

The astronomical International Virtual Observatory Alliance (IVOA) was born in June 2002. It aims to "facilitate the coordination and collaboration necessary for the development and deployment of the tools, systems and organizational structures necessary to enable the international utilization of astronomical archives as an integrated and interoperating Virtual Observatory." The IVOA now comprises 16 VO projects from Armenia, Australia, Canada, China, Europe, France, Germany, Hungary, India, Italy, Japan, Korea, Russia, Spain, the United Kingdom, and the United States. The work of the IVOA focuses on the development of standards using a process modeled after the World Wide Web Consortium. Recommendations proposed by the working groups are ultimately endorsed by the Virtual Observatory Working Group of Commission 5 (Astronomical Data) of the International Astronomical Union.

Several OS independent Java-based tools have been developed in the VO framework. These tools can either be downloaded and set up in personal computers as Java standalone applications, or used through a web browser as Java applets and a simple previewer. Among these applications, VOPlot and TopCat are devoted to astronomical data plotting and cross-identifications. The Aladin software package, created in 1999, is an interactive software sky atlas

allowing the user to visualize and manipulate digitized astronomical images in multi-wavelength, superimpose entries from astronomical catalogues or databases, and interactively access related data and information from the Simbad database, the VizieR service and other archives for all known sources in the field. All the VO softwares are interfaced with the VizieR database, developed by the Centre de Donnes astronomiques de Strasbourg (CDS), and that provides access to the most complete library of published astronomical catalogues and data tables available on line, organized in a self-documented database.

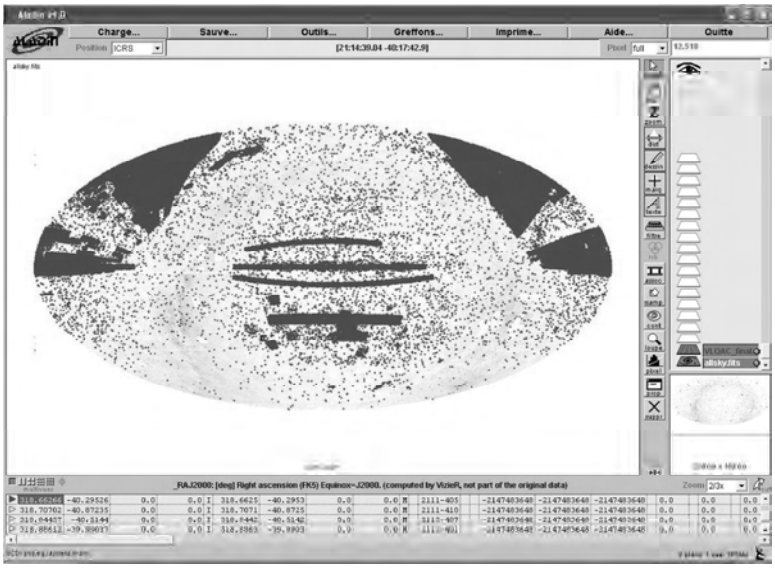

Figure 1. Example of the Large Quasar Astrometric Catalogue as plotted with Aladin

As an example of the use of VO tools within our community, it is worth noting that the construction of the Large Quasar Astrometric Catalogue [2, 3] made an extensive use of cross-identifications between a dozen of quasar catalogues (Fig. 1). Most of them were already entered in the VizieR database. The cross-identifications were led using both (i) homemade Fortran programs, and (ii) scripts using command line VO tools like Stilts or Vizquery, that allow one to easily manipulate catalogues (concatenations, cross-matchings, plots) and to make queries to the database.

2. The VOTable Data Exchange Format

VOTable is a XML-based format for representing astronomical catalogues. Catalogues, i.e., tables gathering celestial objects properties (celestial coordinates, fluxes, brightness, redshifts, etc.), are very important in astronomy and constitute a significant component of the VO. The VOTable has been defined in

terms of XML in order to take advantage of computer-industry standards and to use standard software and tools. Astronomical tables are rich in metadata (content descriptors), which in this context means annotation, interpretable by either computers or humans, both of the tables and the individual columns that they contain. It is important that these metadata should be preserved with the table and the VOTable has features to permit this.

3. Using the VO for Geodesy

VO standards have been developed for Earth-centered or body-centered reference frames in order to extend the VO to Earth and planetary sciences. Nevertheless, some improvements have to be made to adapt the existing VO to geodesy. The Observatoire Virtuel pour la Géodésie et l'Astronomie Fondamentale, France (OV-GAFF), a VO-France working group led by the authors, has recently proposed to the IVOA the adoption of new standards relevant to the Earth orientation data (polar motion, UT1–UTC, nutation, etc.) and to space geodesy.

At the same time, the Observatoire de la Côte d'Azur/GEMINI and the Observatoire de Paris/SYRTE have been developing tools that are interoperable with the existing VO tools and especially with the existing VOTable format. The first step on this development was to provide our data and products in VOTable format with correct metadata. For instance, the Observatoire de Paris offers all the IVS OPAR products and the IERS/ICRS-PC products in VOTable format, including radio source and station coordinates and Earth orientation parameter time series. It means that all catalogues can be read using VO tools and can be directly compared to any other catalogue contained in the astronomical VizieR database.

The Observatoire de la Côte d'Azur/GEMINI is developing the Reference System Database, that contains time series of station positions and EOP from IVS, ILRS, IDS and IGS. All solutions are processed with CATREF (Combined Analysis of Terrestrial Reference Frames, a software developed and maintained at IGN/LAREG [1]), to get (i) a combined TRF consistent over the whole period of the solutions, (ii) transformation parameters between individual TRFs and the combined one, and (iii) EOP series consistent with the combine TRF. The Java applet permits the visualization and the comparison of the consistent EOP and site coordinate time series. Output files are either in ASCII or in VOTable format.

4. Other Resources

Here are some VO and OV-GAFF resources:
The International Virtual Observatory Alliance web site: http://www.ivoa.net.
The IVS OPAR Analysis Center: http://ivsopar.obspm.fr.
The IERS/ICRS Product Center: http://hpiers.obspm.fr/icrs-pc.

The Reference System Database:
http://maestro.obs-azur.fr/gemini/donnees/sys_ref.

References

[1] Altamimi, Z., P. Sillard, C. Boucher. CATREF Software: Combination and Analysis of Terrestrial Reference Frames. Publication LAREG SP08, 2004.

[2] Souchay, J., A.H. Andrei, C. Barache, et al. The Large Quasar Astrometric Catalogue and the radio-optical link. This volume.

[3] Souchay, J., A.H. Andrei, C. Barache, et al. The construction of the Large Quasar Astrometric Catalogue (LQAC). Submitted to Astron. Astrophys., 2008.

Part 4. Interpretation of VLBI Results in Geodesy, Astrometry and Geophysics

The 5th IVS General Meeting Proceedings, 2008, p. 211–220

Secular Decrease of the Earth's Ellipticity from the Analysis of VLBI Data of 1984–2006, and the Long-term Systematic Errors of the Precession-Nutation Models IAU 2000 and IAU 2006

George Krasinsky

Institute of Applied Astronomy, Russian Academy of Sciences, Russia

Abstract. At present, the series of the Celestial Pole offsets, provided by VLBI geodetic programs, become sensitive to the secular decrease $\dot{e}$ of the Earth's ellipticity e (the effect of the so-called post-glacial rebound). Indeed, the SLR-based value $\dot{e} = -7.9 \times 10^{-9}$/cy should manifest itself in the VLBI residuals of the precession angle ϕ as a quadratic trend -8 mas/cy^2 (the trend is negative for the adopted left-hand coordinate frame). For the 25-year time-span of the VLBI data, the effect reaches 0.5 mas, a value which is quite detectable. Unfortunately, this effect can not be studied making use of any of two standard IAU 2000/2006 models of the precession-nutation motion, as the present analysis has revealed significant positive quadratic trends of unknown origin in the residuals of the angle ϕ of 23 ± 4 mas/cy^2 for IAU 2000 and an even bigger 30 ± 4 mas/cy^2 for IAU 2006. As a result, processing the VLBI data with these theories leads to the large positive rate $\dot{e} = (27 \pm 4) \times 10^{-9}$/cy which is incompatible with the SLR value and physically meaningless. The IAU 2006 estimate is corrected for $\dot{e}$ value that has been already embedded into this model to account for the SLR results. On the other hand, applying the numerical theory ERA of the Earth's rotation [3, 4], the estimate $\dot{e} = -(14 \pm 4) \times 10^{-9}$/cy has been obtained, statistically in accordance with the SLR-based value of $\dot{e}$. For the increasing time-span T of observations, the error of the VLBI-derived rate $\dot{e}$ falls as $1/T^2$ while that of the SLR-based rate diminishes only as $1/T$; thus, the VLBI technology in the near future will provide the most accurate estimates for this important geodynamical parameter. For that, however, usage of an Earth's rotation theory more adequate than the adopted IAU 2006 is indispensable.

1. Introduction

In our papers [3] and [4], the experience of constructing the numerical theory ERA of the Earth's rotation, adequate in accuracy to the best VLBI-based series of the Earth's rotation parameters, is described. The version ERA-2005

was shown to provide a better fit to the VLBI data than the analytical theory IAU 2000 adopted as the international standard up to the year 2006, when it was replaced by the new IAU 2006 standard of the same level of accuracy. In [4], by comparing ERA-2005 with IAU 2000, it was predicted that since the year 2007 the IAU 2000 residuals of the precessional angle ϕ will not oscillate around zero level but will keep their sign, increasing the absolute values with T^2 for the time interval T. The sign of this trend is negative, but one should bear in mind that these results have been given for the right-hand reference frame, in accordance with the standard mathematical practice, while in astronomical work, a left-hand reference frame is commonly used to make the precession motion positive. That is the reason why the residuals $d\phi$ in [4], as well as in the present paper, are of the opposite sign to those calculated in most other astronomical studies. In the Abstract of the present paper, the numerical results are reformulated for the left-hand reference frame to avoid possible confusion.

The detected significant positive quadratic trend in the precession angle of IAU 2000 is rather surprising, because the adopted value of the secular decrease $\dot{e}$ of the ellipticity (given in IERS standard in the form of the secular rate of the coefficient of C_{20} of the geopotential) should manifest itself as a negative trend of about -8 mas/cy^2. As the model of the new IAU 2006 standard includes this correction, one should expect that the discrepancies of IAU 2006 with VLBI data will become even bigger.

In the present paper, the long-term systematic errors of the IAU 2000/2006 theories are studied by direct analysis of their residuals against VLBI data and making use of the numerical model ERA as a reference only as an additional control. The main difficulty of this approach is the unmodelled Free Core Nutation (FCN) oscillations of the period $\mathrm{T_{FCN}} \approx 435$ days which conceal the systematic errors of the forced precession-nutation motion. As the 22-year time-span of the available VLBI data is long enough, the FCN oscillations may be filtered out by various methods making it possible to study the long-term behavior of the residuals. The striking feature of the filtered IAU 2000 and IAU 2006 residuals proves to be large quadratic trends in the precession angle ϕ. In the right-hand coordinate system used, they are -23 mas/cy^2 and -30 mas/cy^2 for IAU 2000 and IAU 2006, respectively.

For the larger time interval 1984–2019, a similar analysis of the differences between the current version ERA-2006 of the numerical theory ERA and IAU 2000/2006 has been carried out. Note that for constructing the version ERA-2005, the effect of the secular decrease of the ellipticity e was ignored. Taking into account this effect, the estimates of the quadratic trends in the precessional angle of IAU 2000/2006 theories derived directly from the VLBI data in the interval 1985–2006 and those derived from the differences between ERA-2006 and IAU 2000/2006 in the interval 1985–2019 became to be in a good accordance, while for the analogous differences of ERA-2005 with IAU 2000/2006 the deviations were two times bigger than the observed ones.

Table 1. Statistics of residuals $\sigma_{d\theta}$, $\sigma_{d\phi}$, mas

series	σ_θ	N_{used}	N_{del}	$\sin\theta\sigma_{d\phi}$	N_{used}	N_{del}
GSFC	0.130	3775	140	0.122	3790	125
USNO	0.130	3474	108	0.125	3470	112
BKG	0.135	3091	162	0.125	3086	167
IAA	0.136	3183	172	0.126	3189	166

2. Numerical Theory ERA-2006 of the Earth Rotation and Estimation of the Secular Decrease of the Earth's Ellipticity

Slightly improving the dynamical model of [3] and correcting minor programming deficiencies, somewhat better fitting to the VLBI data in comparison with ERA-2005 and significant improvement in comparing with the IAU 2000/2006 theories have been reached. In the ERA-2006 model, only three empiric parameters have been introduced: two corrections to the amplitudes of annual harmonics (formally, they are seasonal variations of the ellipticity e) and the parameter E_2 which has the meaning of a scale-factor for the harmonics brought about by dissipation in the fluid core (Sec. 3.4 of [4]). In contrast to ERA-2006, six empirical parameters have been estimated for ERA-2005, including four coefficients of the annual harmonics. The coefficients of four annual harmonics of ERA-2005 were strongly correlated, and reducing their total number only to two coefficients made the analysis of the VLBI data more robust, practically without any degradation of accuracy. Unfortunately, the estimated amplitudes of the seasonal oscillations of the ellipticity e exceed by an order of magnitude the analogous amplitudes reliably derived from LAGEOS data. Thus, they still should be related to as some empiric parameters of unclear physical meaning.

We have analyzed to what degree the choice of the series for the Celestial Pole offsets may affect the resulting numerical theory. For that, in addition to the series GSFC of the Goddard Space Flight Center, the following three alternative series were used: USNO (US Naval Observatory), BKG (Bundesamt für Kartographie und Geodäsie) and IAA (Institute of Applied Astronomy). For each constructed numerical theory, Tabl. 1 gives the total number of observations being used, the number of observations deleted (the standard 3σ criterion for outliers being used), and the weighted root mean square (wrms) errors for the interval January 1984 – March 2007. Tabl. 1 shows that the GSFC series, firstly, is most complete and, secondly, demonstrates the best accuracy. The wrms errors of the residuals in Tabl. 1 should be compared with those for IAU 2000: $\sigma_{d\theta} = 0.203$ mas and $\sin\theta\sigma_{d\phi} = 0.158$ mas (the same outliers being deleted).

For each of these series, the value $\dot{e}$ was estimated and compared (after

Table 2. Estimates of the Love number k_2 and the secular trend $\dot{c}_{20}$

Series	k_2	$\dot{c}_{20} \times 10^{-10}$
GSFC	0.27204(28)	21(6)
USNO	0.27197(30)	27(6)
BKG	0.27215(32)	27(7)
IAA	0.27288(32)	40(7)

conversion) with the adopted satellite-based secular rate $\dot{c}_{20} = 12 \times 10^{-10}$/cy of the normalized coefficient c_{20} of the geopotential [6]. The actually estimated parameter $\dot{e}/e$ was transformed into the corresponding value $\dot{c}_{20}$ making use of the relation $\dot{c}_{20}/c_{20} = -\dot{e}/e$. The derived estimates of $\dot{c}_{20}$ are given in the last column of Tabl. 2. All the values $\dot{c}_{20}$ in Tabl. 2 agree at the 3σ level with the adopted value $\dot{c}_{20}$ (for the IAA series, on the 4σ level).

Among other findings obtained with ERA-2006, it seems to be noteworthy that the new estimate of the Love number $k_2 = 0.27204(28)$ is compatible with the estimate $k_2 = 0.27272(36)$ of [4] based on the VLBI observations of 1984–2005. Shirai and Fukushima [7] obtained the estimate $k_2 = 0.2788(11)$ from earlier VLBI data of 1980–2000 making use of the original analytical theory of the precession-nutation motion. All the VLBI-based estimates of k_2 given above are in reasonably good agreement. Shirai and Fukushima [7] also presented a brief review of k_2 values obtained by other (not VLBI) methods since 1968. They are quite inaccurate, varying in the range from 0.252 to 0.343. Note that the value $k_2 = 0.29525$, adopted in the last version of the IERS standards, was obtained from purely theoretical considerations. It seems improbable that such calculations could ensure the correct five digits given by the IERS standards. Thus, one can see that the available VLBI-based Celestial Pole offsets provide an excellent opportunity of estimating k_2 with an accuracy unattainable by other methods. In [5] which presents the theoretical basis of the IAU 2000 nutation, VLBI data also have been analyzed but no explicit estimate of k_2 is given. However, if one derives k_2 from the published value of the so-called compliance κ making use of the standard relation $\kappa = ek_2/k_s$ ($k_s = 0.93831$ is the secular Love number), the derived value $k_2 = 0.2953(22)$ strongly disagrees with other VLBI-based results. It practically coincides with the a priori value $k_2 = 0.29525$ confirming the guess of [3] that the IAU 2000 model is of semi-empirical nature being based on the Fourier analysis of the residuals.

In the next section, four methods of studying the long-term systematic errors of the IAU 2000/2006 and ERA-2006 theories from the analysis of the VLBI data are described. In good accordance, the results demonstrate significant quadratic trends in the VLBI residuals ($d\phi \approx -23$ mas/cy^2 for IAU 2000 and $d\phi \approx -30$ mas/cy^2 for IAU 2006) and the absence of such a trend in ERA-2006.

3. Long-Term Systematic Errors of IAU 2000 and IAU 2006 from the Analysis of VLBI Data

3.1. Determination of the Rate $\dot{e}$ Making Use of the IAU 2000 and IAU 2006 Theories

Firstly, the rate $\dot{e}$ was estimated for the IAU 2000/2006 theories using the partials that had been calculated for ERA-2006 in the process of the numerical integration by varying the parameters under estimation. The physical meaning of these parameters is explained in [4]. It is important that they include the initial values of the angular velocity of the fluid core as a whole and those of its inner part. As it is shown in [4], these parameters make it possible to model satisfactorily the complex two-modal structure of the FCN oscillations in the time interval of the available VLBI data. Such approach proved to be workable also for the analytical theories IAU 2000/2006 significantly reducing the amplitudes of the FCN oscillations in the post-fit residuals. As a result, the wrms errors of the post-fit residuals are drastically improved: $\sigma_{d\theta} = 0.136$ mas and $\sin\theta\sigma_{d\phi} = 0.134$ mas while for the original pre-fit residuals of IAU 2006 they were: $\sigma_{d\theta} = 0.203$ mas and $\sin\theta\sigma_{d\phi} = 0.158$ mas. (The estimated correction $\dot{e}$ for IAU 2006 has been added to the theoretical value $\dot{e} = -7.9 \times 10^{-9}$/cy used in this model; however, when deriving the apparent secular trend in IAU 2006, this reduction should not be applied). The corresponding quadratic trends $d\phi$ in IAU 2000/2006 are as follows:

$$d\phi = \begin{cases} -23 \pm 3 \text{ mas/cy}^2 \text{ for IAU 2000,} \\ -30 \pm 3 \text{ mas/cy}^2 \text{ for IAU 2006.} \end{cases} \tag{1}$$

3.2. Analysis of the Averaged VLBI Residuals of IAU 2000 and IAU 2006 Theories

In a second approach, the averaged values of the IAU 2000/2006 and ERA-2006 residuals were obtained by filtering out the FCN oscillations, as well as the oscillations of higher frequencies, by linearly fitting the raw residuals for each of the adjoining 435-day intervals of the FCN oscillations. In this fit, the weights for the residuals were assigned in accordance with their a priori errors. For more reliability, this procedure was repeated twice shifting the initial date of the averaging by half a period of the FCN oscillations. For a better filtering of these oscillations, we restricted the time interval by the maximally possible number of the complete FCN periods. As a result, 38 points were obtained for each of the two Euler angles of the three theories under consideration (IAU 2000, IAU 2006 and ERA-2006; see Fig. 1 where the top and bottom plots present the residuals $d\phi$ and $d\theta$, respectively). The most salient feature of the $d\phi$ plot is the pronounced parabolic trend in both the IAU 2000 and IAU 2006 theories, and the absence of a similar trend in the ERA-2006 residuals. To fit these data, we use the model

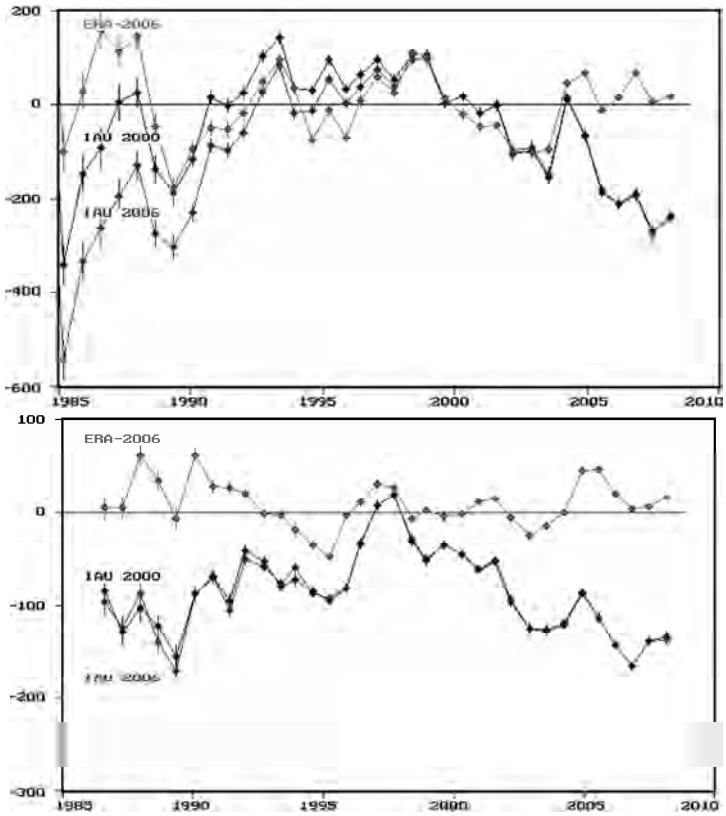

Figure 1. Averaged residuals of IAU 2000/2006 and ERA-2006 (in μas) $d\phi$ (top) and $d\theta$ (bottom)

$$d\phi = A_0 + A_1 T + A_2 T^2 + A_{\cos} \cos f + A_{\sin} \sin f, \quad (2)$$

$$d\theta = B_0 + B_1 T + B_2 T^2 + B_{\cos} \cos f + B_{\sin} \sin f, \quad (3)$$

where T is counted from the epoch JD2000 in centuries, f is the fundamental argument of the main 18.6 year harmonics of the nutational theory.

As the coefficients $A_{\sin}$ and $A_{\cos}$ appeared to be within their statistical errors, they were excluded from the final solution for which the quadratic errors of IAU 2000/2006 models have been obtained as follows:

$$d\phi = \begin{cases} -25 \pm 3 \text{ mas/cy}^2 \text{ for IAU 2000,} \\ -33 \pm 3 \text{ mas/cy}^2 \text{ for IAU 2006.} \end{cases} \quad (4)$$

For ERA-2006, the coefficient A_2 is within its statistical error and thus

negligible. Note that estimates (1) and (4) are in a good agreement notwithstanding that they have been obtained in quite different ways.

Viewing the averaged residuals of $d\theta$ of IAU 2000/2006 in Fig. 1 (the bottom plot), one might suggest that they also demonstrate significant quadratic trends. And indeed, if the terms $B_{\cos}$, $B_{\sin}$ are ignored, the coefficient B_2 of the quadratic approximation becomes rather large. However, the general five-parametric solution gives a negligible quadratic trend B_2 but rather large values for the shift B_0 and the cosine amplitudes $B_{\cos}$. The most reliable estimates correspond to the solution in which the quadratic term B_2 is set equal to zero. The coefficients B_0 and $B_{\cos}$ for this solution are consistent with those for the five-parametric solution 2 and have twofold lesser error (due to the absence of any strong correlations).

For a control, we also tried the version in which the constant shift and the amplitudes of the sine and cosine harmonics of the FCN oscillations were estimated for each of the adjoining 435-day intervals (repeating the process by shifting these intervals on the half of the FCN period). After that, the obtained estimates of the shifts were fitted by the models (2), (3). The results appeared to be in accordance with the estimates given above. In particular, for the quadratic term in precession angle, the following estimates were obtained:

$$d\phi = \begin{cases} -22 \pm 3 \text{ mas/cy}^2 \text{ for IAU 2000,} \\ -30 \pm 3 \text{ mas/cy}^2 \text{ for IAU 2006,} \end{cases} \tag{5}$$

which are practically coincide with estimates (1).

3.3. Analysis of the Differences Between ERA-2006 and the Theories IAU 2000 and IAU 2006 in the Interval 1985–2020

In this method, the differences of the theories ERA-2006 and IAU 2000/2006 were calculated in the larger time interval 1985–2019 and studied after averaging them in the same way as described in Section 3.2. For this interval, we have obtained 60 averaged points for each of two Euler's angles. In Fig. 2, the top plot presents the differences of the angles ϕ, the bottom one those for the angle θ (note the different scales in the plots). One can see that the main peculiarity of the ϕ-differences is again the quadratic trend. After fitting the model (2) to the ϕ-differences, the following estimates were obtained for the quadratic terms:

$$d\phi = \begin{cases} -25.5 \pm 0.7 \text{ mas/cy}^2 \text{ for IAU 2000,} \\ -31.9 \pm 0.7 \text{ mas/cy}^2 \text{ for IAU 2006.} \end{cases} \tag{6}$$

These quadratic trends should be attributed to the errors of IAU 2000/2006 but not of ERA-2006.

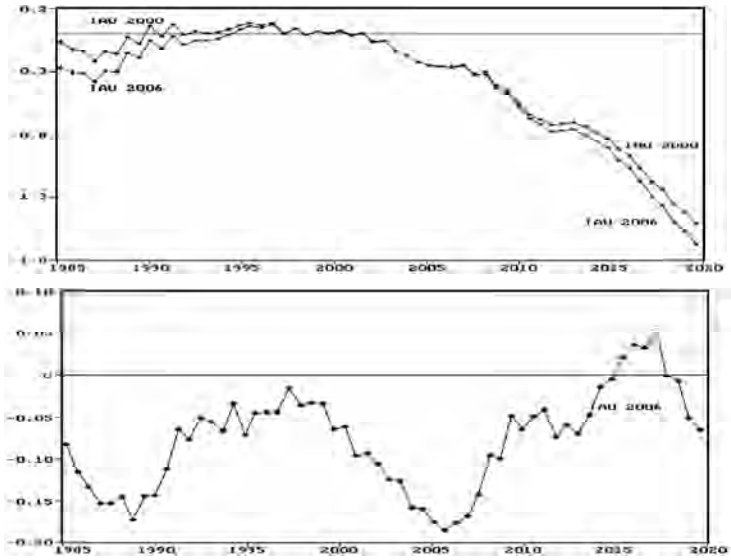

Figure 2. Averaged differences ERA-2006 minus IAU 2000, and ERA-2006 minus IAU 2006 (in mas) $d\phi$ (top) and $d\theta$ (bottom)

The main feature of the θ-differences between ERA-2006 and IAU 2000/2006 is the constant shift $B_0 = -0.096(4)$ mas and the cosine amplitude $B_{\cos} = -0.066(5)$ of the main nutation term of the period 18.6 years. These values are consistent with the estimates $B_0 = -0.090(5)$ mas, $B_{\cos} = -0.048(7)$ derived directly from the analysis of the VLBI residuals and thus it is clear that they are the errors of the IAU 2000/2006 theories.

In Fig. 3, the original (non-averaged) differences in the Euler's angles $d\theta$, $d\phi$ (in the sense ERA-2006 minus IAU 2000) are presented for the time span 1985–2019 (the solid lines). The FCN oscillations seen in Fig. 3 have arisen because the model of these oscillations is embedded automatically into the numerical theory ERA-2006 while no such model is available in this time interval for the IAU 2000/2006 theories. On these plots, the residuals of IAU 2000 against the VLBI data (supplied with the bars of the a priori errors) are also presented. The black solid line should be considered as a prognosis of the deviations of the IAU 2000 model from the future VLBI data up to the year 2020. It is predicted that the deviation of the precession angle of IAU 2000/2006 in 2020 will exceed 2 mas.

4. Concluding Notes

From the above considerations, the following conclusions may be derived:

1. The available VLBI data are accurate enough for detecting the secular decrease $\dot{e}$ of the ellipticity e. Applying the numerical theory ERA-2006, the

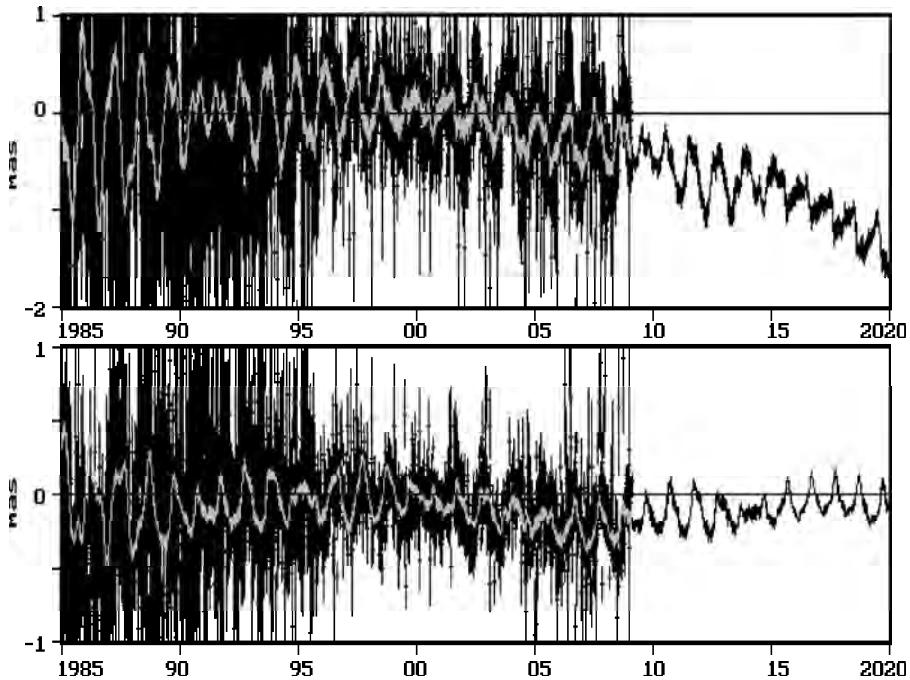

Figure 3. Prognosis of IAU 2000 residuals (in mas): $d\phi$ (top) and $d\theta$ (bottom)

estimated $\dot{e}$ proves to be in accordance with the results of satellite tracking. As the error of the VLBI-based $\dot{e}$ decreases with T^{-2} with increasing time interval T, while the error of the SLR estimates diminishes only with T^{-1}, the VLBI technology will provide the most accurate estimates for this important geodynamic characteristic in the near future.

2. The conclusion of [4] about the fast increasing systematic error of the IAU 2000 precession angle is confirmed by the direct analysis of the VLBI residuals of IAU 2000, independently of the validity of the ERA numerical theories. It is clear now why the larger value $d\phi \approx -40$ mas/cy^2 (instead of $d\phi \approx -22$ mas/cy^2 of the present work) has been obtained for the quadratic trend $d\phi$ from the analysis of the differences ERA-2005 minus IAU 2000 in [4]. The reason is the disregard of $\dot{e}$ in the ERA-2005 model.

3. The large and steadily increasing systematic error $d\phi = -22 \pm 3$ mas/cy^2 of IAU 2000 and the even bigger $d\phi = -30 \pm 3$ mas/cy^2 of IAU 2006 may be easily corrected introducing these quadratic terms into the precession formalism of IAU 2000 or IAU 2006. That is an acceptable approach for practical applications but not for the scientific study of geophysical effects in the Earth's rotation. Unfortunately, this empiric term would not be unique in the IAU 2000/2006 theories; see Introduction to [3] for more details. In particular, these

theories ignore the torques caused by the tidal friction, as well as by the tides in the fluid core, instead making use of the semi-empiric approach and including the large empirical secular trend -25.24 mas/cy into the obliquity motion. In [8] it is shown that this trend has arisen mainly (but not completely) due to ignoring some indirect lunar perturbations in the rigid body part of nutation. An introduction of this empirical trend makes IAU 2006 unsuitable for the study of the geophysical nature of dissipation which brings about the secular obliquity rate.

The IAU 2000/2006 errors in precession motion are too small to be detected by the classic optical observations of the previous two centuries. Because the errors increase with T^2, the earlier VLBI observations also were insensitive to this effect, and only at present, after a 25-year time-span for the geodetic VLBI observations, the effect became quite noticeable.

4. Our analysis of the systematic errors of IAU 2006 has demonstrated that the adoption of the P03 precession as the international standard IAU 2006 at the IAU General Assembly (Prague, 2006) was a false step, because the detected P03 errors substantially exceed those of the previous standard IAU 2000.

References

[1] Capitaine, N., P.T. Wallace, J. Chapront. Improvement of the IAU 2000 precessional model. Astron. Astrophis., v. 432, 355, 2005.

[2] Hilton, J.L., N. Capitaine, J. Chapront, et al. Report of the International Astronomical Union Division 1 Working Group on Precession and Ecliptic. Celest. Mech. and Dyn. Astron., v. 94, 351–367, 2006.

[3] Krasinsky, G.A. Numerical theory of rotation of the deformable Earth with the two-layer fluid core. 1. Mathematical model. Celest. Mech. and Dyn. Astron., v. 96, 169–217, 2006.

[4] Krasinsky, G.A., M.V. Vasilyev. Numerical theory of rotation of the deformable Earth with the two-layer fluid core. 2. Fitting to VLBI data. Celest. Mech. and Dyn. Astron., v. 96, 267–288, 2006.

[5] Mathews, P.M., T.A. Herring, B.A. Buffet. Modeling of nutation and precession: New nutation series for non-rigid Earth and insights into the Earth's interior. J. Geophys. Res., v. 107, No B4, DOI 10.1029/2001JB000390, 2002.

[6] McCarthy, D.D., G. Petit. IERS Conventions 2003. IERS Technical Note, No 32. Verlag d. Bund. f. Kartographie u. Geodäsie, Frankfurt am Main, 2004.

[7] Shirai, T., T. Fukushima. Construction of a new forced nutation theory of the nonrigid Earth. A.J., v. 121, No 1746, 3270–3283, 2001.

[8] Williams, J.G. Contribution to the Earth's obliquity rate, precession, and nutation. Astron. J., v. 108, No 2, 711–724, 1994.

The 5th IVS General Meeting Proceedings, 2008, p. 221–230

Comparisons of Precession-Nutation Models

Nicole Capitaine [1], *P.M. Mathews* [2], *Véronique Dehant* [3],
Patrick T. Wallace [4], *Sébastien Lambert* [1]

[1)] *SYRTE Department, Observatoire de Paris, France*

[2)] *Department of Theoretical Physics, University of Madras, India*

[3)] *Royal Observatory of Belgium, Belgium*

[4)] *Space Science & Technology Department, STFC/RAL, UK*

Abstract. We first summarize the key characteristics of the IAU 2000 and IAU 2006 precession-nutation models, (i.e., the IAU 2000 nutation and the P03 precession). Then we discuss some aspects of the numerical ERA-2005 model for Earth-rotation variations in comparison with the semi-analytical IAU models. We point out severe flaws in the ERA model (that have already been noted in a recent comments paper) regarding various aspects of this model, such as the expression for the centrifugal perturbation, Love number formalism, the modeling of the dissipative phenomena, the Earth model, and the estimation of parameters. We finally report on comparisons of those precession-nutation models with VLBI observations and with the INPOP06 numerical integration.

1. Introduction

This paper has been prompted by recent discussions about a comments paper by Mathews, Capitaine and Dehant [1] on the ERA-2005 model [2, 3] that pointed out a number of severe deficiencies in the theory and its fit to data.

The aim of this paper is to make clear the fundamental differences in the main features of the IAU 2000/2006 and the ERA-2005 precession-nutation models and to report on the differences of the models with respect to VLBI observations.

2. Key Characteristics of the IAU Precession-Nutation

2.1. The IAU 2000/2006 Resolutions on Precession-Nutation

The IAU has adopted a high precision model for precession and nutation in two successive steps.

The first step (IAU 2000 Resolution B1.6) was the adoption of the IAU 2000 precession-nutation [4], which has been implemented in the IERS Conventions 2003. This model is composed of a nutation part and a precession part. In addition there are frame bias values between the J2000 mean pole and equinox and the Geocentric Celestial Reference System (GCRS). The IAU 2000A nutation is expected to have an accuracy of about 10 μas for most of its terms. In contrast, the so-called free core nutation (FCN), which is due to geophysical effects and is largely unpredictable, is not part of the model. The precession part, which consists only of corrections to the precession rates of the IAU 1976 precession, was known not to correspond to a dynamical theory; this is why IAU 2000 Resolution B1.6 recommended the development of new expressions for precession consistent with dynamical theories and with IAU 2000A nutation.

The second step (IAU 2006 Resolution B1) was the adoption of the P03 Precession [5, 6] as a replacement to the precession part of the IAU 2000A precession-nutation. The P03 model has provided improved expressions for both the precession of the ecliptic and the precession of the equator, the latter being consistent with dynamical theory, while matching the IAU 2000A precession rate for continuity reasons.

2.2. The Characteristics of the IAU Model

The IAU 2000 nutation is based on the REN2000 solution [7] for the nutation of a rigid Earth model transformed to nutation of a non-rigid Earth model with the MHB2000 "transfer function" [4]. This was derived from the solution of equations obtained by generalization of the SOS equations [8] with Basic Earth Parameters fitted to VLBI data. The semi-analytical series (see IERS Conventions 2003 Tabl. 5.3a and 5.3b) is composed of 1365 luni-solar and planetary terms with "in-phase" and "out-of-phase" components with amplitudes from 17.2 arcsec to 0.1 μas and periods between 3 d and 101 cy.

The IAU 2006 precession [5] was derived from the dynamical equation expressing the motion of the mean pole about the ecliptic pole. The solution is based on values at J2000.0 for the mean obliquity of the ecliptic, ϵ_0, and for the precession rate in longitude and obliquity. The first order contributions to the precession rates have been derived from the MHB values [4] and the P03 value for ϵ_0 (i.e., 84381.406 arcsec). The other contributions to the P03 precession rates are from [9] and [4] and the geodesic precession is from [10]. It takes into account the effect of the Earth's J_2 rate (mostly due to the post-glacial rebound), with a value [9] for dJ_2/dt of -3.0×10^{-11}/y (i.e. $de/dt = -9.1 \times 10^{-11}$/y); this is responsible for an additional contribution of about -7 mas/cy^2 to the t^2 term in the precession in longitude.

The P03 value for the Earth's dynamical flattening, $H_d = 3.27379448 \times 10^{-3}$ is quite consistent with the MHB value of $(3.27379492 \pm 0.00000120) \times 10^{-3}$. The largest differences between the P03 semi-analytical expressions for the precession quantities and expressions corresponding to other recent precession

models [11, 12] are of the order of a few mas/cy for the precession rates and 7 mas/cy^2 for the t^2 term in longitude due to the J_2 rate contribution which is taken into account in P03 while it is not in other models (e.g. [11]).

The largest uncertainty in the IAU precession is due to the current uncertainty (of the order of 1 mas/cy) in the observed precession rate. Additionally, the complexity of the J_2 variations causes a large uncertainty in the J_2 rate value and consequently in the quadratic term of the precession in longitude [14]. While the secular decrease in J_2 has to be taken into account to provide a precession model valid over the long term, it cannot be predicted over periods of 10 years with a good accuracy. A recent study [13] of the observed variations of J_2 over the past 28 years based on a large set of satellite laser ranging data showed that in addition to the secular decrease (of about -2.8×10^{-11}/y, i.e. $de/dt \approx -8.5 \times 10^{-11}$/y), there are seasonal annual variations (with a mean amplitude of 2.9 $\times 10^{-10}$), significant inter-annual variations with timescales of 4-6 years (related to strong El Niño-SO events) and a variation with a period of 21 years and an amplitude of about 1.4 $\times 10^{-10}$ (with a minimum in Dec. 1988). This latter variation is large enough to mask the secular change in J_2 during certain time spans of VLBI observations.

3. Comparison Between the IAU and ERA Models

3.1. Centrifugal Perturbation and Love Number Formalism

MHB 2000 is based on the SOS equations of Sasao-Okubo-Saito [8] for the variations in rotation of the Earth's mantle and fluid core. The following concepts are fundamental to the SOS/MHB theories:

1) The tidal contribution to the centrifugal potential is only the incremental part arising from the time dependent part dΩ of the angular velocity vector Ω, generated by the action of the perturbing potential; the deformational response to it is characterized by the Love number k_2.

2) The response to forcing by the constant centrifugal potential due to $\Omega_0 = \Omega - d\Omega$ is very far from that of an elastic solid; it is characterized by the fluid/secular Love number $k_f = k_s \approx 0.9 \approx 3k_2$, appropriate to a fluid-like behavior, and is responsible for the Earth's dynamical ellipticity e.

3) It follows from the SOS/MHB equations that the scale factor for the precession rate is $S_{MHB} = H_d = e/(1+e)$.

ERA-2005, in contrast, starts with the "revised SOS equations" based on the following concepts:

1) the centrifugal potential due to the full angular velocity vector $\Omega = \Omega_0 +$ dΩ is treated as a "tidal" perturbation (though Ω_0 is quite unrelated to tidal potentials),

2) the Earth's deformational response to constant forcing is just like its elastic response to periodic forcing at tidal frequencies; the Love number k representing the response has the same value $k_2 \approx 0.3$ in both cases,

3) it follows from the revised SOS equations that the scale factor for the precession rate is $S_{ERA} = e/(1 + e - e\sigma/3)$, with $\sigma = k_2/k_s \approx 0.3$.

The dependence of the scale factor on the deformability (through k_2/k_s) is a radical change, which modifies significantly the value of the precession rate and nutation amplitudes. Using the ERA value S_{ERA} would give a difference with respect to IAU 2000 of -0.14 arcsec/cy in the precession rate and 0.4 mas in the 18.6 y nutation. Note that this is at odds with the difference of (-0.82 ± 0.22) mas/cy between the linear trend in the residuals between the ERA and IAU time series that is reported in the ERA-2005 paper [3] (i.e. ≈ 170 times lower), which raises serious doubts about the physical trustworthiness of the ERA nutation-precession time series.

3.2. Modeling of the Dissipative Phenomena

MHB 2000 spells out the mechanisms which produce the out-of-phase parts of nutation amplitudes and models them on the basis of actual observational data on the various phenomena involved:

1) mantle anelasticity is based on the Wahr and Bergen model, deduced from seismological observations; this model is incorporated into the expressions for the increments of inertia of the whole Earth and the fluid core,

2) ocean tide heights are those from CSR4 tables based on space-geodetic observations,

3) core-mantle and outer core to inner core couplings due to the magnetic fields at the boundaries is modeled from theory and the complex coupling constants K^{CMB} and K^{ICB}.

ERA-2005 in contrast invokes no specific physical mechanisms for the dissipation:

1) it models dissipation in the Earth in terms of three phase delay parameters $\delta, \delta_c, \delta_i$ for the deformational responses in the mantle and the outer and inner fluid cores to tidal perturbations, plus the dissipative part κ_{dis} of a CMB coupling,

2) the ocean tide effects in nutations are introduced through an increment dk_2 to the Love number k_2, which is not constrained by any ocean-tides observations. The expression for that increment is $dk_2 = k_2^{(1)} \cos\theta_B + k_2^{(2)} \cos^2\theta_B$, which depends only on the co-latitude θ_B of the tide producing body in the sky at that instant and has identical values at all points of the globe at any instant. This is very unphysical because the ocean tide is well-known to be highly non-uniform over the Earth's surface.

Note that a similar-looking formula of Kaula [15] has no dependence on the co-latitude of the tide producing body as in ERA-2005; it depends instead on the co-latitude of the observation site, which makes sense physically.

None of the information available from seismological studies and from the detailed observations of ocean tides has been used in the modeling of dissipation. In fact the ERA ocean tide model has no dissipation at all, since $dk_2^{(1)}, dk_2^{(2)}$ are real.

As realistic models for dissipation are essential for computing the out-of-phase nutations, an unphysical model cannot represent these terms correctly.

3.3. Earth Model

MHB 2000 uses spherically symmetric classical models of the radial variation of the properties of a non-rotating Earth, based on seismological data (e.g. PREM). Models of the ellipsoidal structure of the interior of the steadily rotating Earth are derived from such models using hydrostatic equilibrium theory (Clairaut's theory).

In contrast ERA-2005 rejects the "classical" Earth models. The ERA theory is such that even the non-rotating Earth has to have ellipticity of about $(2/3)e$, as the centrifugal potential of the steadily rotating Earth can account for only $\approx (1/3)e$ with k taken as k_2 (instead of k_s) even under constant forcing. No mechanism is proposed to determine the detailed interior structure.

There are large deviations of the ERA estimates for some of the Earth parameters from values computed on the basis of seismological Earth models (e.g. the ERA estimate for e_f being higher than e instead of being significantly lower).

The ERA model postulates a fluid inner core region which has the same physical properties as the fluid outer core, and yet is considered dynamically distinct from the latter.

As a model for the dynamics of the Earth's interior is essential for computing the non-rigid Earth nutations, the use of a non-realistic Earth model prevents us from computing correct nutations.

3.4. Estimation of Parameters

In the MHB 2000 solution, seven parameters were treated as adjustable and employed for fitting the theoretical outputs to the VLBI. The chosen parameters were the four Earth parameters e, e_f, k, γ, and three of the four real and imaginary parts of the the complex coupling constants K^{CMB} and K^{ICB} coefficients. The nutation amplitudes are influenced independently by these parameters, and are expected to be sensitive enough to permit estimation of their values. Minor empirical adjustment of the input values of one of the two parameters in the anelasticity model and one parameter in the ocean tide model was done at the end; and the real and imaginary parts of the prograde annual amplitude were taken as adjustable; the obliquity rate was also fitted to VLBI.

In the ERA-2005 solution, the estimated parameters are:

(i) e and k_2, (ii) e_c, k_2^c, k_2^v and α, which have high mutual correlations, (iii) ν_v, k_{el} and k_{dis} which do not appear in any of the resonance frequencies, (iv) four other "geophysical" parameters together with six "empirical" parameters, such as E_1 in order to adjust the ratio of the retrograde and prograde 18.6 y nutation amplitudes and E_2 to adjust the out-of-phase nutations.

The FCN frequency as obtained by earlier authors from their own fits is used as an input constraint while estimating the ERA parameters.

It should be noted that a low RMS of residuals may be produced by using a large number of adjustable parameters for estimation, but the presence of high correlations among, and lack of clear physical meaning of, many parameters makes the solution unreliable.

4. Comparisons of the Models with VLBI Observations

Residuals have been computed by subtracting time-series of VLBI observed celestial offsets from IAU precession-nutation predictions.

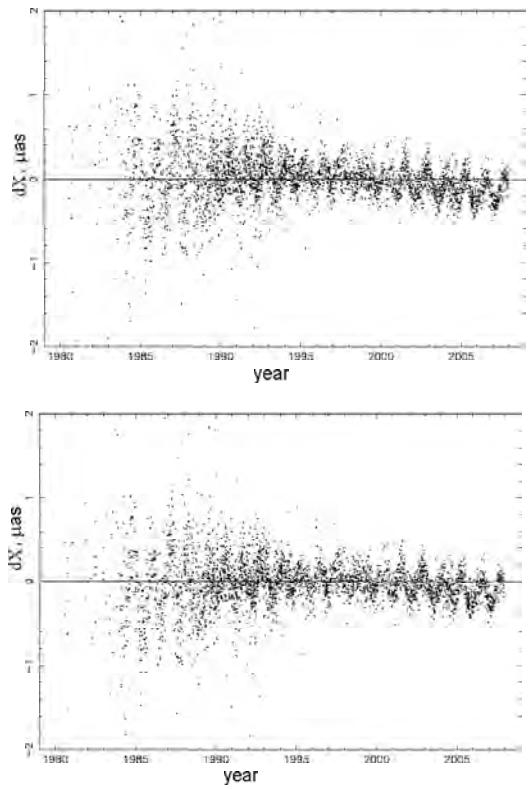

Figure 1. dX residuals of the IAU 2000 precession-nutation (top) and P03 precession plus IAU 2000A nutation (bottom) w.r.t. the IAA VLBI time series

We used either the IAU 2000A precession-nutation, or the P03 precession plus the (P03-adjusted) IAU 2000A nutation. Several data centers have been used as well as combined IVS series based on different procedures. Different empirical models were used for removing the free core nutation, one of them be-

ing a nutation of time-varying amplitude but constant period of −430.23 days. In all cases, after removal of the FCN, a "curvature" is visible in the two CIP coordinates X and Y in the GCRS, with approximately the same amplitude and the same phase (modulo π); the mean RMS is of the order of 125 μas in X and 170 μas in Y.

Fig. 1 provides two plots for residuals from the IAA time series (IAU 2000 and P03) that are almost indistinguishable by eye. Fig. 2 provides the VLBI residuals (with respect to GSFC time series) for the X and Y components, respectively, after the free core nutation has been removed.

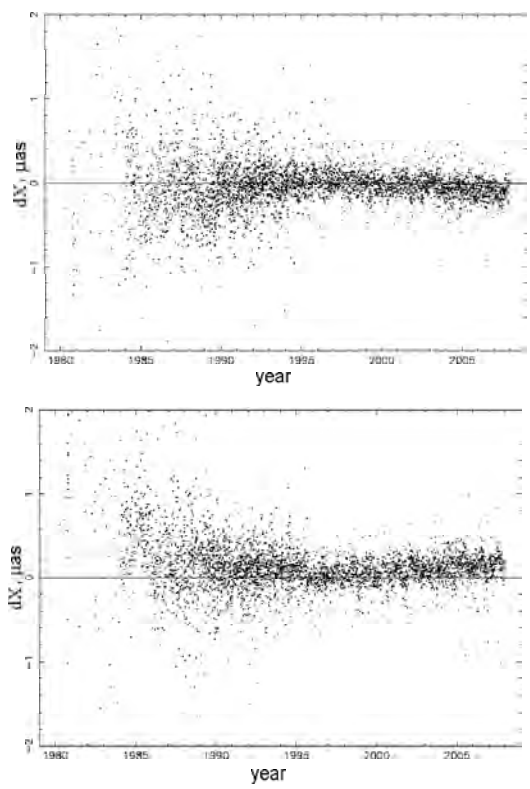

Figure 2. The residuals dX (top) and dY (bottom) of the IAU 2000/2006 precession-nutation w.r.t. GSFC VLBI time series after removing the FCN

We have looked at different possibilities to explain the observed form of the residuals. The effects due to celestial frame instability or due to the inaccuracy in the quadratic terms of the model were shown to be much too small.

One way to reduce the "curvature" was to remove a parabola fitted to the residuals. Tabl. 1, which provides results for different data centres, models and IVS combined series, shows that the coefficients of the fitted parabola are very sensitive to the VLBI time-series. It should be noted that interpreting the

residuals in terms of a parabola was only for simplification and that the fit of a linear term plus a correction to a 18.6 y periodic term with an amplitude of a few tens of microarcseconds was shown to be as efficient as a parabola. In both cases, the post-fit RMS are reduced by about 10% in X and 30% in Y w.r.t. the pre-fit RMS. More reliable interpretation will only be possible with a longer interval of observations.

A recent study [17] also indicates that the curvature may be partly absorbed by a combination of long-period nutations with very small changes in their amplitudes and/or phases.

Table 1. Weighted fits of a parabola in the residuals corresponding to the IAU 2000 model and the P03/IAU 2000 models for different data centres (from 1980 to 2008) or various IVS combined series; unit: μas

		t^0	t	t^2
IAU2000−IAA	dX	-4 ± 3	-1172 ± 43	-6533 ± 787
IAU2000−OPA	dX	-43 ± 2	-862 ± 35	-2686 ± 679
P03−IAA	dX	-2 ± 3	-1004 ± 43	-9465 ± 787
P03−GSFC	dX	3 ± 3	-579 ± 38	-11217 ± 671
IAU2000−IAA	dY	26 ± 3	1287 ± 45	17428 ± 799
IAU2000−OPA	dY	16 ± 2	1422 ± 35	18984 ± 663
P03−IAA	dY	26 ± 3	774 ± 43	17401 ± 799
P03−GSFC	dY	58 ± 3	448 ± 40	14940 ± 690
IAU2000−`ivs07q4e`	converted to dX	-12 ± 3	-1113 ± 43	-11181 ± 718
IAU2000−`ivs07q4e`(*)	dX	-11 ± 3	-1261 ± 60	-13113 ± 873
IAU2000−`ivsM6q4e`(*)(**)	dX	-19 ± 3	-1086 ± 77	-8944 ± 893
IAU2000−`ivs07q4e`	converted to dY	51 ± 3	1529 ± 44	15970 ± 708
IAU2000−`ivs07q4e`(*)	dY	51 ± 3	1548 ± 60	16169 ± 873
IAU2000−`ivsM6q4e`(*)(**)	dY	33 ± 3	1639 ± 74	21729 ± 824

(*) truncated at 24/Oct/05; (**) originally referred to IAU 1976/1980 precession-nutation.

5. Comparisons Between the P03 Precession and INPOP06

The numerical planetary ephemeris INPOP06 [16] provides a solution for the precession-nutation of the axis of angular momentum, which takes into account the external torque acting on a non-rigid Earth model. A comparison over 5000 years of the P03 precession with INPOP06 showed a good agreement up to 1000 years. The large discrepancies appearing after that limit are due to the polynomial representation of the P03 semi-analytical precession.

A comparison over 400 years of the P03 precession/IAU 2000A nutation with the INPOP06 numerical precession-nutation shows no quadratic differences. This can be considered as a valuable check of the P03 quadratic terms as the two solutions are totally different and are based on totally independent models (except for the linear term in X which was fitted to P03).

6. Comparison Plots in the Time Domain

The effectiveness of the ERA-2005 theory as a predictive tool can be tested by comparing the projections made in 2006 [3, 18] with the subsequent VLBI observations.

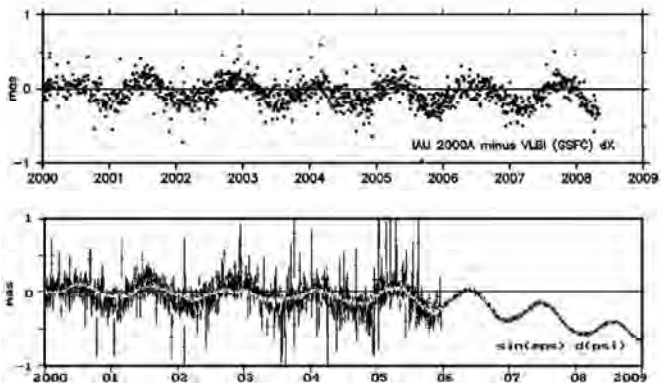

Figure 3. Comparison between the models and VLBI. Top: differences between the IAU 2000 predictions (which do not include FCN) and VLBI observations. Bottom (from [18]): differences between the IAU 2000 predictions and VLBI observations (points and error bars) and between IAU 2000 and ERA-2005 (line)

Fig. 3 provides comparison plots of the IAU 2000A and ERA-2005 models with the VLBI GSFC time series. The solid line in the lower plot (reproduced from [18]) represents the $d\Delta\psi \sin\epsilon$ differences of IAU 2000 with respect to ERA-2005 for the period 2000-2009. The runaway increase in these predicted differences beyond 2006 were attributed by this author to increasing errors in the IAU 2000 predictions. However, the actual differences dX $(= d\Delta\psi \sin\epsilon)$ of IAU 2000 with respect to VLBI observations, represented by the dots in the upper plot, do not show any significant increase in the deviation between IAU 2000 and VLBI measurements. So the large slope appearing in the solid line after 2006 in the lower plot is a measure of the failure of the predictions from the ERA-2005 theory. Moreover, we note that although the ERA-2005 model for the free core nutation model matches throughout the observed period (i.e. up to the end of 2006), though with insufficient amplitude, the extrapolations to the present go badly wrong. In the opinion of the authors, this comparison casts doubt on the physical reality of ERA-2005 and, by implication, subsequent models constructed in the same manner.

7. Summary

In this study devoted to comparisons of precession-nutation models:

- we have reviewed the key characteristics of the IAU 2000/2006 precession-nutation model and shown that no significant discrepancies appear be-

tween the IAU models and other semi-analytical solutions. We have also reported on the very good agreement between the P03 precession and the completely independent INPOP06 numerical integration [16];

- comparison between the IAU and ERA-2005 models has confirmed the severe deficiencies in the ERA-2005 theory [2] and its fit to data [3], which were pointed out in a recent comments paper [1];
- comparison of the IAU models with VLBI observations has shown an unexplained "curvature". As quadratic discrepancies do not seem physically possible, we can suspect an unmodeled long-periodic effect, or a spurious effect of the analyses; this shows that the IERS celestial offsets are still necessary to predict precession-nutation with microarcsecond accuracy.

References

[1] Mathews, P.M., N. Capitaine, V. Dehant. arXiv:0710.0166, 2007.

[2] Krasinsky, G. Celes. Mech. Dyn. Astr., 96, 3–4, 169, 2006.

[3] Krasinsky, G., M.V. Vasilyev. Celes. Mech. Dyn. Astr., 96, 3–4, 219, 2006.

[4] Mathews, P.M., T.A. Herring, B.A. Buffett. JGR, 107, B4, DOI 10.1029/2001JB000390, 2002.

[5] Capitaine, N., P.T. Wallace, J. Chapront. Astron. Astrophys., 412, 567, 2003a.

[6] Hilton, J., N. Capitaine, J. Chapront, et al. Celes. Mech. Dyn. Astr., 94, 351, 2006.

[7] Souchay, J., B. Loysel, H. Kinoshita, et al. Astron. Astrophys. Suppl. Series, 135, 111, 1999.

[8] Sasao, T., S. Okubo, M. Saito. Proceedings of the IAU Symposium 78. E.P. Federov, M.L. Smith, P.L. Bender (eds.), 165, Hingham, Mass., D. Reidel, 1980.

[9] Williams, J.G. A.J., 108, 711, 1994.

[10] Brumberg, V. Essential Relativistic Celestial Mechanics. Adam Hilger Publ., 1991.

[11] Bretagnon, P., A. Fienga, J.-L. Simon. Astron. Astrophys., 400, 785, 2003.

[12] Fukushima, T. A.J., 126, 494, 2003.

[13] Cheng, M., B.D. Tapley. JGR, 109, B09402, DOI 10.1029/2004JB003028, 2004.

[14] Bourda, G., N. Capitaine. Astron. Astrophys., 428, 691, 2004.

[15] Kaula, W.M. A.J., 74, 1108, 1969.

[16] Fienga, A., H. Manche, J. Laskar, et al. Astron. Astrophys., 477, 315, 2008.

[17] Koot, L., A. Rivoldini, O. de Viron, et al. JGR, 2008 (in print).

[18] Krasinsky, G. Abstract for Joint Discussion 16. 26th IAU General Assembly, 2006; http://www.astronomy2006.com/Astro2006_0157.html.

The 5th IVS General Meeting Proceedings, 2008, p. 231–235

The Phase Variations of Retrograde Free Core Nutation

Vadim Gubanov

Institute of Applied Astronomy, Russian Academy of Sciences, Russia

Abstract. The application of an envelope method to the analysis of celestial pole offsets in the interval 1984-2007, published by IERS and NEOS services, has shown that the mean value of the RFCN period is close to −444 solar days. However there are three consecutive intervals of time when this period sharply changed and had values -421.4 ± 0.1, -614.7 ± 1.1, and -447.1 ± 0.2 days.

1. Introduction

The basic feature of the Earth's interior is the presence of a hot fluid outer core capable to free near-daily spin in a cavity limited by lower mantle. In a Celestial Reference System (CRS) this spin causes circular offsets of the Celestial Intermediate Pole (CIP) with a period of about −430.2 solar days which refers to the Free Core Nutation (FCN). The modern theory of the Earth's rotation [1] asserts that the FCN period is induced by the ellipticity of the fluid outer core and should be constant over a long time.

However, because of active physical processes in the Earth's core, its dynamics hardly can be named "free". It is considered that the outer fluid core consists basically of iron and its central part named the inner core consists of iron and nickel in a rigid crystal condition. Both parts of the core can contain impurities of silicates and other light elements. Being hot but cooling down, the fluid core has convective and gravitational movements, which due to high electric conductivity of iron and nickel create a magnetic field penetrating all of Earth's body and going out into space. This phenomenon is referred to as an electromagnetic dynamo.

It is established also that the external layer of the outer core rotates more slowly than the mantle of the Earth, which cannot be explained by the viscosity of the core but by its electromagnetic connection with the mantle [2, 3]. It results in the western drift, no-dipole part of the magnetic field.

There are numerous publications devoted to the influence of the electromag-

netic connections of the core and mantle on angular velocity and polar motion of the Earth. The problem related to CIP offsets was discussed only in one work [4], where it is shown that in 1992 and 1998 changes of the FCN phase coincided with geomagnetic jerks. Below it will be shown that modern VLBI observations give new important information for studying the fluid core of the Earth and its influences on geodynamics.

2. Stochastic Model of RFCN

After 1984 the accuracy of VLBI observations has increased so that it is practically possible to study FCN as variation of CIP offsets with the amplitude limited by 0.5 ms. It appears that this near-harmonic variation has a negative frequency; therefore it started to be named Retrograde Free Core Nutation (RFCN). To the naked eye, the amplitude of RFCN varies over a wide range. Therefore, in the numerical models constructed by T. Herring in 1998 [5] and S. Lambert in 2007 [6], it is represented as piecewise linear functions under the condition that the RFCN period is constant and equal to -430.21 solar days. Simultaneously an analysis of amplitude and phase variations was undertaken by Z. Malkin and D. Terentev in 2003 [7].

In addition to S. Lambert's most exact model (LAM), we constructed another numerical model of RFCN by means of the least squares collocation technique (LSC) [8]. The basic difference of this method to all other linear procedures is that it uses the covariance function of the desired signal as a priori information. Generally, for the construction of such a model it is necessary to remove a low-frequency trend and then a white noise from the observational series [9, 10]. The last procedure is defined by the formula $\boldsymbol{t} = \boldsymbol{Q}_{tt}(\boldsymbol{Q}_{tt}+\sigma^2\boldsymbol{I})^{-1}\boldsymbol{l}$ where $\boldsymbol{l}$ is the vector of one component of the observed CIP offsets (dX or dY), $\boldsymbol{t}$ is a vector of corresponding model, σ^2 is a variance of white noise of observation errors, $\boldsymbol{Q}_{tt}$ is a Toeplitz covariance matrix. This matrix is constructed from the positive definite function $q_{tt}(\tau)$ as model of empirical auto-covariance $q_{ll}(\tau)$. The variance σ^2 is defined as the difference between these functions at the zero point.

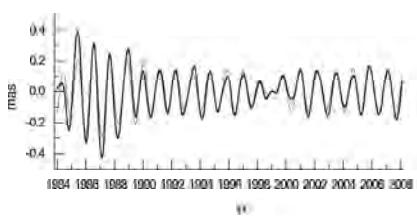

Figure 1. X-component of RFCN as follows from LSC and LAM models (thick and thin lines, respectively)

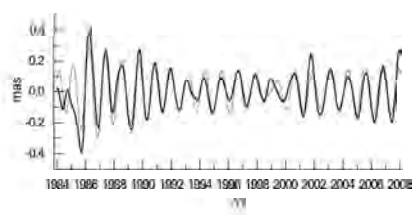

Figure 2. Y-component of RFCN as follows from LSC and LAM models (thick and thin lines, respectively)

The comparison of the LAM and LSC models are shown in Fig. 1-2. The RMS of IERS(dX) and IERS(dY) offsets and their residuals with respect to LAM and LSC models are given in Tabl. 1. The values in columns 3 and 4 correspond to a filtering of the series, whereas columns 2 and 5 show the accuracy of the predictions. For all available IERS and NEOS series the LSC model appreciably better corresponds to observations than the LAM model.

Table 1. RMS of CIP offsets and residuals with LAM and LSC models in mas

Span of observations in MJD	45700-46274	46275-50370	50371-54446	54467-54518
Offsets number	575	4096	4096	52
IERS(dX)	.534	.353	.198	.143
IERS(dX)-LAM	.506	.322	.179	.135
IERS(dX)-LSC	.485	.315	.176	.130
IERS(dY)	.430	.366	.222	.296
IERS(dY)-LAM	.453	.338	.202	.191
IERS(dY)-LSC	.400	.329	.193	.142

3. Phase Analysis

The theory outlined below is referred to as an envelope method [11]. This method allows to evaluate the amplitude and phase of stochastic processes for each moment of observation. We shall consider CIP offsets as near-harmonic oscillations on a plane (X, Y), which is tangent to the celestial sphere in a point set by the IAU 2000 precession-nutation theory:

$$x(t) = E(t)\cos F(t), \quad y(t) = E(t)\sin F(t),$$

$$E(t) = \sqrt{x(t)^2 + y(t)^2}, \quad F(t) = \arctan(y(t)/x(t)).$$

Let $F(t) = qt + p(t)$, where q is a negative frequency and $p(t)$ is a phase variation not containing a linear trend. Designating $u =\mid q \mid> 0$ we obtain $F(t) = -ut + p(t)$ and the following relations:

$$x(t) = A(t)\cos ut + B(t)\sin ut, \quad y(t) = -A(t)\sin ut + B(t)\cos ut,$$

$$A(t) = x(t)\cos ut - y(t)\sin ut, \quad B(t) = x(t)\sin ut + y(t)\sin ut,$$

$$E(t) = \sqrt{A(t)^2 + B(t)^2}, \quad p(t) = \arctan(B(t)/A(t)).$$

LSC models of the same name CIP offsets for IERS and NEOS series appeared very close, therefore they have been averaged. The amplitudes and phases of RFCN for both models were calculated with an accepted period of $P_0 = -1/u = -444$ day. This period was chosen because the global phase trend

over the entire span of used observations was found to be equal to zero. The functions $E(t)$ and $p(t)$ obtained after removing phase jumps equal to $\pm\pi$ are shown in Fig. 3-4. As seen from Fig. 4 the phase linear trend was calculated for three sequential intervals of time bounded by MJD dates 46275, 51080, 51520, 54518 for the LSC model and 46275, 50844, 51402, 54518 for LAM. Two inner dates were obtained by the least squares method assuming that the total trend was uninterrupted.

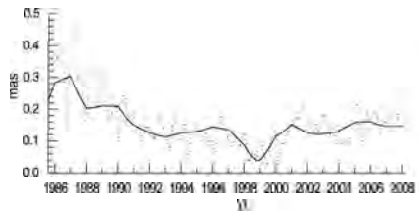

Figure 3. RFCN amplitudes derived from the LAM (solid line) and LSC (dotted line) models

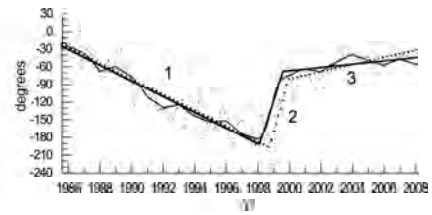

Figure 4. RFCN phase variations and their trends derived from the LAM (solid line) and LSC (dotted line) models

Let the observed phase be $p(t) = (du)t + dp(t)$ in degrees, where du is the factor for a linear trend [degree/year], and $dp(t)$ is a residual variation not containing a linear trend. Because the frequency of the envelope function is equal to $F(t) = -ut + p(t) = -ut + (du)t + dp(t) = -(u - du)t + dp(t)$, the new absolute value of the RFCN frequency will be $w = u - du$. The coefficients of the linear phase trend for the three mentioned above intervals of observation du_1, du_2, du_3 are obtained by the least squares method. Taking into account the relations $P = -1/w$, $\sigma_P = \sigma_w/w^2$, we receive the corresponding periods (Tabl. 2).

Table 2. Linear phase trend and periods of RFCN

Model	Par.	1	2	3	Dim.
LAM	du	-14.2 ± 0.1	$+80.5 \pm 0.2$	$+2.0 \pm 0.1$	degree
LSC		-14.2 ± 0.1	$+96.9 \pm 0.7$	$+5.2 \pm 0.1$	per year
LAM	P	-423.7 ± 0.1	-609.8 ± 0.3	-447.0 ± 0.1	solar
LSC		-421.4 ± 0.1	-614.7 ± 1.1	-447.1 ± 0.2	days

4. Conclusions

- The mean value of the RFCN period in the time span 1985.6–2008.2 is approximately equal to -444 solar days and is not constant.
- In the initial interval from 1985.6 until 1998.0, the period amounted to

about −422.5 days. Then, during 1998, it suddenly changed up to near −612 days, and after another year it again changed to −447 days.

- As is apparent from Fig. 1-3, the continuous process of RFCN practically ceased in 1999 and a sharp change in phase and period occurred subsequently.
- The first numerical RFCN model was constructed by T. Herring based on observational data up to 1998. Therefore the period that he derived (−430.2 days) is close to the one mentioned above for the same interval. S. Lambert did not reconsider T. Herring's RFCN period. period.
- If changes of the RFCN frequency are real, the resonance effects in terrestrial tides and lunar-solar nutation must be unstable, which has great significance for geodynamics. To check this effect it is necessary to construct a new transfer function for resonances, obtain a new decomposition for the lunar-solar nutation for the three mentioned above intervals of time and reprocess all VLBI observations. The new series of CIP coordinates should be more precise than the previous.

References

[1] Mathews, P., T. Herring, B. Buffett. Modeling of nutation and precession: New nutation series for nonrigid Earth and insights into the Earth's interior. Journal of Geophysical Research, v. 107, No B4, ETG 3–1, 3–26, 2002.

[2] Zharkov, V., V. Trubizyn, L. Samsonenko. Physics of the Earth and Planets. Science, Moscow, 1971, 89–99 (in Russian).

[3] F. Stacey. Physics of the Earth. J. Wiley & Sons, Inc., New York, London, Sydney, Toronto, 1968 (Russian translation: Moscow, 1972, 141–176).

[4] Shirai, T., T. Fukushima, Z. Malkin. Detection of Phase Jumps of Free Core Nutation of the Earth and their Concurrence with Geomagnetic Jerks. arXiv: physics/0408026.

[5] ftp://tai.bipm.org/iers/conv2003/chapter5/IAU2000A.f

[6] ftp://tai.bipm.org/iers/convupdt/chapter5/fcnnut.f

[7] Malkin, Z., D. Terentev. Investigation of the Parameters of the Free Core Nutation from VLBI data. IAA Communications, v. 149. St. Petersburg, 2003.

[8] Gubanov, V. Generalized Least-Squares Method. Theory and application in astrometry. Science, St. Petersburg, 1997, 136–138 (in Russian).

[9] Gubanov, V., S. Petrov. Filtering and forecasting of EOP series by least-squares collocation technique. Proc. of 5th Russian Symp. "Metrology of Time and Space". Mendeleevo, 1994, 208–211.

[10] Petrov, S., A. Brzezinski, V. Gubanov. A stochastic model for polar motion with application to smoothing, prediction and combining. Artificial Satellites, Planetary Geodesy, v. 31, No 26, 51–70, 1996.

[11] Levin, B. Theoretical foundation of statistical radio technique. Soviet Radio, Moscow, 1969, 353–356 (in Russian).

The 5th IVS General Meeting Proceedings, 2008, p. 236–239

Comparison of the Prediction Force of the Nutation Theories IAU 2000 and ERA-2005

Sergey Pasynok [1,2]

[1)] *VNIIFTRI, All-Russian research institute of physical-technical and radiotechnical measurements, Russia*

[2)] *SAI MSU, Sternberg State Astronomical Institute, Moscow State University, Russia*

Abstract. A comparison of the nutation theories IAU 2000 and ERA-2005 has been carried out on the efficiency of their use in a nutation angles prediction program. As a result, the used prediction procedure yielded similar results for ERA-2005 and IAU 2000 to within the uncertainties of the measurements.

1. Introduction

According to the IAU Resolution B1.6 (2000), beginning on Jan. 1, 2003, the IAU 1976 Precession Model and IAU 1980 Theory of Nutation were replaced by the precession-nutation model IAU 2000 (MHB 2000, based on the transfer functions of Mathews, Herring and Buffett [1]). Besides this, the IAU recommends to continue the theoretical developments of non-rigid Earth nutation series for a more accurate account of some processes which are difficult to model.

Observations over the last five years have evidently shown that the best agreement of the theoretical and observable nutation angles is provided by the theory IAU 2000.

However, according to the carried out works [2, 3], higher accuracy is provided with the numerical theory ERA-2005 developed by George Krasinsky. Nevertheless, this direct comparison of the IAU 2000 and ERA-2005 nutation theories with VLBI observations does not allow to compare these theories properly for the following reasons:

– the rms of the discrepancies with VLBI observations for IAU 2000 theory is differs from the same value for ERA-2005 theory less than on about 10% rms of the discrepancies with VLBI measurements for IAU 2000 theory;

– the nutation theory ERA-2005 in particular describes retrograde nutation component which is treat as retrograde free core nutation (RFCN) in IAU 2000 theory. But according to IERS Technical Note No 29, the RFCN, being a free motion that cannot be predicted rigorously, is not a part of the IAU 2000 model.

Therefore the prediction power method is offered for the comparison of the nutation theories.

2. The Method

In this section the method of comparison is discussed and results of applying this method to some nutation theories are shown.

2.1. Explanation of the Method

The following idea underlies the offered comparison method. It is known that the disagreement of the predicted and the measured values grows with distance from the last point of the history (the observable data which were used for the construction of the prediction). Therefore, though disagreements of theories from the measured values are comparable, the disagreements of the prediction with use of these theories from the measured values grow with distance from last point of history. Therefore, there is such earliness of the prediction (in this paper the earliness of the prediction is understood as time distance of a prediction point up to the last history point) that disagreement of the prediction under one theory and the prediction under another theory will become large enough.

Fig. 1 explains the comparison method graphically.

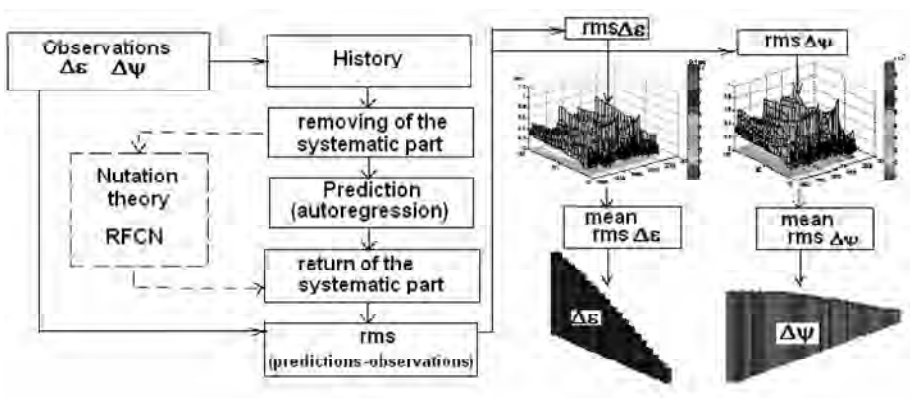

Figure 1. Explaining of the basis of the method

The prediction of each theory was calculated by the following algorithm:

1) The systematic part, which consisted of theoretical nutation angles, linear part, and RFCN mode, was subtracted from the history. Therefore RFCN was taken into account in a similar way for all compared theories.

2) The differences were predicted for 100 days forward with the help of autoregression.

3) After that the systematic part was added to the predicted values of the differences.

4) The measured values were subtracted from the obtained prediction for the same dates resulting in discrepancies between predicted values and observations.

5) The mean rms of the discrepancies between prediction and observation over the period from 1988 to 2008 were calculated for each value of earliness (from 10 to 100 days).

6) Further received mean rms for theories were compared among themselves. The limits of rms differences were estimated considering that 2σ for the observable nutation angle $d\varepsilon$ is 200 μs. Therefore, after dividing these values by the square root of the number of points one obtains that 2σ for mean rms values of $d\psi$ and $d\varepsilon$ nutation angles are 11 and 4 μs. These values were accepted as significant.

2.2. The Method Approbation

For approbation of the method two nutation theories were examined: IAU 2000 [1] and GF 1999 [4]. As a results the IAU 2000 nutation theory showed the best agreement between prediction and observations. The differences of rms were greater than 2σ.

3. Comparison of IAU 2000 and ERA-2005 Theories

After that the method described above was used to compare the theories IAU 2000 and ERA-2005. The mean rms values for the period from 1988 to 2008 are shown in Tabl. 1.

4. Conclusions

1. For the procedure of the prediction given, the results of the prediction for ERA-2005 and IAU 2000 yield similar results to within errors of measurements.

2. A smoothing average estimation was also provided in order to check the very exciting prediction of ERA-2005 of a super precession in the dpsi nutation angle. But super precession was not detected within the measurement errors.

Table 1. Comparison of IAU 2000 and ERA-2005 theories results: mean rms, differences mean rms and significant levels

Earliness days	$d\varepsilon$, μas				$d\psi$, μas			
	ERA-2005	IAU 2000	Δ	2σ	ERA-2005	IAU 2000	Δ	2σ
10	248.5	248.9	0.4		581.6	584.0	2.4	
15	251.8	252.1	0.3		597.4	598.8	1.4	
20	252.9	253.1	0.2		608.2	608.6	0.4	
5	254.1	253.8	−0.3		606.3	605.9	−0.4	
30	254.0	253.6	−0.4		608.2	607.3	−0.9	
35	254.2	253.7	−0.5		612.9	611.2	−1.7	
40	255.5	254.6	−0.9		611.1	608.7	−2.4	
45	254.7	253.9	−0.8		611.7	608.5	−3.2	
50	255.0	253.9	−1.1		614.8	610.9	−3.9	
55	256.2	254.8	−1.4	4	613.2	608.5	−4.7	11
60	255.9	254.5	−1.4		613.7	608.8	−4.9	
65	256.0	254.5	−1.5		616.1	610.5	−5.6	
70	257.1	255.3	−1.8		615.1	608.6	−6.5	
75	257.1	255.3	−1.8		616.0	609.1	−6.9	
80	257.4	255.4	−2		619.1	611.6	−7.5	
85	258.4	256.3	−2.1		618.9	610.8	−8.1	
90	258.8	256.6	−2.2		620.3	612.0	−8.3	
95	259.1	256.8	−2.3		622.7	613.5	−9.2	
100	259.7	257.4	−2.3		622.5	612.3	−10.2	

Acknowledgements

The author thanks professor G.A. Krasinsky for ERA-2005 nutation angles series. This work has been supported by the Russian Foundation for Basic Researches (No 08-02-00971 and No 08-05-00256).

References

[1] Mathews, P., T. Herring, B. Buffet. J. Geophys. Res., 107(B4), DOI 10.1029/2000JB000390, 2002.

[2] Krasinsky, G. Numerical theory of rotation of the deformable Earth with the two-layer fluid core. Part 1: Mathematical model. CMDA, v. 96, 169–217, 2006.

[3] Krasinsky, G., M. Vasilyev. Numerical theory of rotation of the deformable Earthwith the two-layer fluid core. Part 2: Fitting to VLBI data. CMDA, v. 96, 219–237, 2006.

[4] Getino, J., J. Ferrandiz. Proceedings of IAU Colloquium 180, 2004, 236–241.

The 5th IVS General Meeting Proceedings, 2008, p. 240–245

Combination of Nutation Time Series Derived from VLBI and GNSS

Maria Kudryashova, Kristýna Šnajdrová, Robert Weber, Robert Heinkelmann, Harald Schuh

Institute of Geodesy and Geophysics, Vienna University of Technology, Austria

Abstract. In this work we concentrate on the combination of 2-years (2005-2006) series of nutation offsets from VLBI and nutation rates from GNSS obtained w.r.t. the IAU 2000 nutation model. In order to take advantage of both series the combined smoothing method introduced by Vondrák and Čepek has been used. From combined series amplitude corrections to the IAU 2000 model at selected frequencies have been estimated.

1. Introduction

VLBI is the unique space geodetic technique which provide a direct access to the high-stable celestial reference frame, based on extragalactic objects (ICRF). Therefore, only VLBI allows to estimate nutation offsets with a long-term stabilit straightforwardly. In case of GNSS (Global Navigation Satellite System) technics measurments of the Earth orientation are carried out w.r.t. the satellite orbits. Due to the high correlations between some EOP (nutation angles and UT1-UTC values) and orbital parameters [1], the satellite methods can provide only the first time derivatives of those EOP (i.e. nutation rates $\Delta\dot{\psi}\sin\varepsilon_0$, $\Delta\dot{\varepsilon}$ and LOD). And even in this case, nutation rates can be estimated only over the time interval where satellite orbits can be modeled accurately enough, i.e. 1-3 days. Nevertheless, it is expected that GNSS observations can contribute essentially to the determination of nutation parameters in the high frequency domain (periods from 5 to 28 days).

2. Strategy of Nutation Offsets/Rates Estimation from VLBI and GPS Observations

The VLBI solution has been obtained by the OCCAM v.6.1 software using the least squares method (LSM). In order to produce this solution the celestial

as well as the terrestrial reference frames have been fixed to ICRF-Ext.2 catalog and ITRF 2005, respectively. Nutation offsets have been estimated w.r.t. the IAU 2000A nutation model. Diurnal and semidiurnal EOP variations according to the IERS Conventions 2003 [2] have been taken into account.

Nutation offsets ($\Delta\psi$, $\Delta\varepsilon$) as well as other EOP have been modeled as linear functions. The parameters offset and rate (both fully unconstrained) have been estimated once per session. Troposphere parameters and station clocks have also been estimated in this solution. We used all 24-hours VLBI sessions within the interval from Jan. 1, 2005 to Dec. 31, 2006 for obtaining of this solution.

In order to obtain nutation rates from GPS observations we used the Bernese v.5.0 software [3]. As a priori information IGS precise orbits and the radiation pressure model developed by the Center for Orbit Determination in Europe (CODE) were taken. All calculations have been made for a network of 116 globally distributed stations which are a part of IGS realization of the ITRF 2005. Nutation rates have been estimated w.r.t. the IAU 2000 nutation model. For diurnal and semidiurnal EOP variations IERS Conv. 2003 model have been applied.

To calculate nutation rates series we have to establish very stable satellite orbits. Therefore the orbits have been characterized by one set of Keplerian elements and corresponding radiation pressure parameters once per three days arc. We estimated corrections to the tracing station positions under NNR condition. Pole coordinates and LOD have been estimated once per 24-hours session and nutation rates – once per 3-days solution (related to the middle day of this 3-days interval). Initial phase ambiguities as well as site-specific troposphere parameters have been pre-eliminated before the LSM adjustment.

As a result we come up with a homogeneous (from the point of view of processing strategy) time series of nutation rates covering the period from Jan. 1, 2005 to Jul. 29, 2006.

3. Analysis of Uncertainties

The uncertainties of nutation rates clearly show some systematic effects (Fig. 1a). Spectral analysis of the uncertainties revealed three main periodical terms with periods of about 60, 90, and 180 days. It seems that the 180 days period stems from the correlations of satellite orbits at long time scales with pressure radiation parameters. The terms with periods of about 60 and 90 days could be explained by the precession of GPS orbits (see Rothacher et. al., this volume).

The uncertainties of VLBI solution do not show any systematic effects, but there are some sessions in 2006 with larger errors (Fig. 1b). The quality of nutation offsets could be affected by the geometry of the VLBI network which changes from one session to another according to the stations participating in a particular experiment.

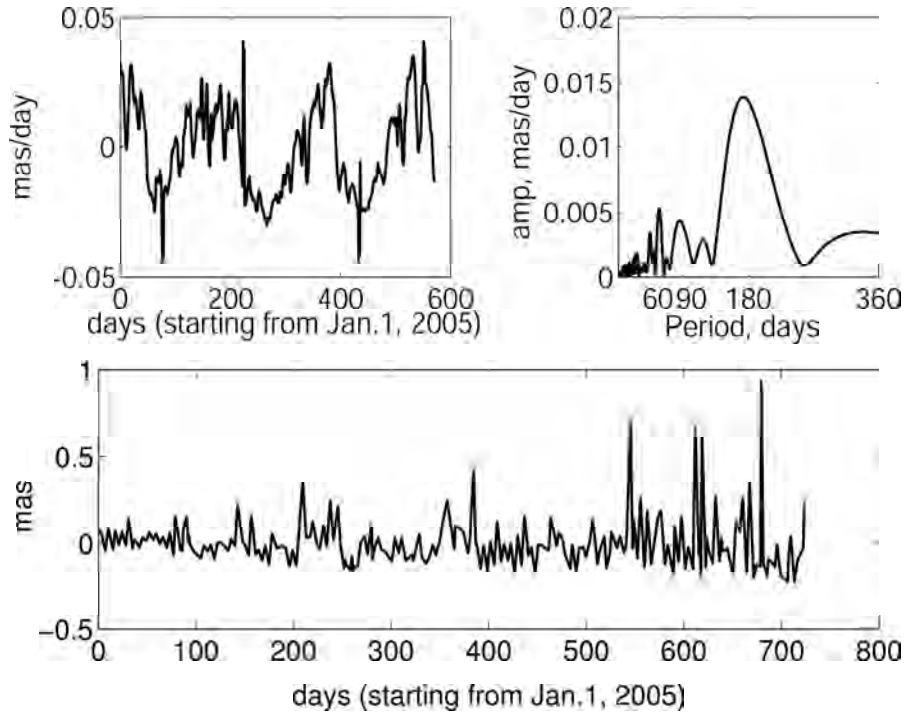

Figure 1. Upper, left: uncertainties of GPS based nutation rates in longitude; right: amplitude spectrum of uncertainties reveal peaks with the periods of about 60, 90, and 180 days. Lower: uncertainties of VLBI based nutation offsets in longitude

4. Combination Method

In order to combine the two series described above we applied the Vondrák combined smoothing method [4]. The method has been developed for combining the function values F and their first time derivatives $\tilde{F}$. A solution is looked for in a form of smooth curve (with smoothness S) which fits both observed series. For this purpose the following weighted sum has to be minimized:

$$Q = S + \varepsilon F + \tilde{\varepsilon}\tilde{F} = min, \tag{1}$$

where $\varepsilon, \tilde{\varepsilon} \geq 0$ are the smoothing coefficients expressing the relative importance of each item: the larger the value of the coefficients the closer is the smoothed curve to the observations. The choice of numerical values of these coefficients $\varepsilon = \left(\frac{12.6}{P_{min}}\right)^6 \approx 34, \quad \tilde{\varepsilon} = \left(\frac{16.9}{P_{min}}\right)^4 \approx 34$, is based on the conclusions given in [4, 5].

Such a choice of numerical values of smoothing coefficients assures that the

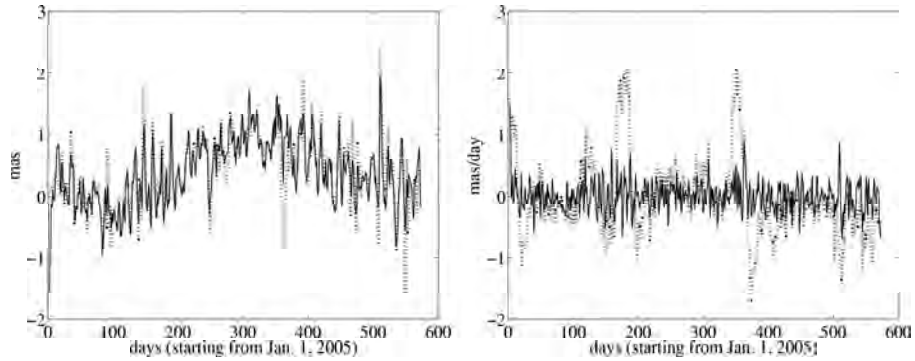

Figure 2. Combined (solid line) and original (dotted line) time series of nutation in longitude

smoothness is weak enough in order to keep the signals with periods longer than 7 days unchanged and at the same time is sufficiently strong in order to suppress all periods shorter than 2 days (i.e. high frequency noise of the observations). The combined series are presented in Fig. 2.

In Tabl. 1 the a posteriori uncertainties, computed from residuals (between observed and smoothed values), are compared with the a priori values. The table clearly shows that the a posteriori values of uncertainties for nutation rates ($\Delta\dot{\psi}\sin\varepsilon_0, \Delta\dot{\varepsilon}$) are about five times larger than the a priori values. Rates uncertainties are underestimated due to the fact that we take into account only the random part of the errors but not the systematic part which is caused by difficulties in orbit modeling.

5. Estimation of Amplitude Corrections w.r.t. the IAU 2000 Nutation Model from Combined Series

Since the main impact from the combination of GPS and VLBI series in comparison with VLBI series has been expected only in high frequencies, we estimated corrections to 10 nutation terms with periods from 4.684 days to 27.555 days. From the combined nutation offset series amplitude corrections to the IAU 2000 nutation model have been estimated in according to:

Table 1. A priori and a posteriori uncertainties

uncertainties	$\Delta\psi\sin\varepsilon_0$, mas	$\Delta\dot{\psi}\sin\varepsilon_0$, mas	$\Delta\varepsilon$, mas	$\Delta\dot{\varepsilon}$, mas
a priori	0.231	0.066	0.096	0.029
a posteriori	0.140	0.455	0.054	0.149

$$\Delta\psi \sin\varepsilon_0 = a + bt + \sum_{i=1}^{10} A_i^{in} \sin(arg) + A_i^{out} \cos(arg), \quad (2)$$

$$\Delta\varepsilon = c + dt + \sum_{i=1}^{10} B_i^{in} \cos(arg) + B_i^{out} \sin(arg), \quad (3)$$

where a, b, c, d – parameters of linear trends, A_i^{in}, B_i^{in} – in-phase components, A_i^{out}, B_i^{out} – out-of-phase components, $arg = \sum_{j=1}^{5} N_j F_j$ with the Delaunay variables F_j. The results are presented in Tabl. 2.

Table 2. Estimated amplitude corrections w.r.t the IAU 2000 nutation model from the combined series

Periods, day	comp.	Ampl., μas	σ, μas	Periods, day	comp.	Ampl., μas	σ, μas
4.684	A^{in}	1	34	10.085	A^{in}	−1	34
	A^{out}	10	34		A^{out}	−12	34
	B^{in}	0	15		B^{in}	6	14
	B^{out}	27	14		B^{out}	−21	14
5.492	A^{in}	−37	34	13.661	A^{in}	11	34
	A^{out}	−3	34		A^{out}	−128	34
	B^{in}	−2	14		B^{in}	42	14
	B^{out}	−9	14		B^{out}	15	14
5.802	A^{in}	−15	34	14.765	A^{in}	−20	34
	A^{out}	22	34		A^{out}	132	34
	B^{in}	−10	14		B^{in}	−25	14
	B^{out}	−16	14		B^{out}	−33	14
7.096	A^{in}	31	34	23.942	A^{in}	−35	34
	A^{out}	57	34		A^{out}	−41	34
	B^{in}	−2	14		B^{in}	−3	14
	B^{out}	29	14		B^{out}	−15	14
9.133	A^{in}	27	34	27.555	A^{in}	112	34
	A^{out}	−62	34		A^{out}	139	34
	B^{in}	−7	14		B^{in}	−13	14
	B^{out}	−24	14		B^{out}	19	14

6. Conclusions

It has been shown that GPS based nutation rates suffer from large long periodic systematic effects with amplitudes of about 0.02 mas/day. Spectral analysis of the uncertainties reveals three main periods of about 60, 90 and 180 days. All these periods can be explained by correlations between the estimated parameters (radiation pressure parameters and orbital elements) and by a mis-

modeling of GPS satellite orbits at long time periods. Due to the fact that we do not take into account this systematic part of the errors, the values of nutation rate uncertainties seem to be highly underestimated.

Since we did not perform a calibration of GPS based nutation parameters to VLBI based values, systematic errors mentioned above could propagate into the combined series. Consequently, these effects could distort estimated amplitude corrections, even of high-frequency terms.

Acknowledgements

M. Kudryashova is very grateful to Descartes/Nutation Advisory Board for financial support of this work (in frame of project GALILEO/nutation).

References

[1] Rothacher, M., G. Beutler, T. A. Herring, et al. Estimation of Nutation Using the Global Positioning System. J. Geophys. Res., 104(B3), 4835–4859, 1999.

[2] IERS Conventions 2003. IERS Technical Note, No 32. D.D. McCarthy and G. Petit (eds.), 2004.

[3] Bernese GPS Software v. 5.0. U. Hugentobler, R. Dach, P. Fridez (eds.), 2007.

[4] Vondrák, J., A. Čepek. Combined smoothing method and its use in combining Earth orientation parameters measured by space techniques. Astron. Astrophys. Suppl. Ser., v. 147, 347–359, 2000.

[5] Vondrák, J., C. Ron, R. Weber. Combined VLBI/GPS series of precesion-nutation and comparison with IAU 2000 model. Astron. Astrophys., v. 397, 771–776, 2003.

The 5th IVS General Meeting Proceedings, 2008, p. 246–250

Earth's Interior from VLBI and Superconducting Gravimeter Data

Séverine Rosat [1], *Sébastien Lambert* [2]

[1] *Ecole et Observatoire des Sciences de la Terre, France*

[2] *Observatoire de Paris, Département SYRTE, France*

Abstract. We analyze VLBI delays back to 1984 from the permanent geodetic network, and ten superconducting gravimeter records from the Global Geodynamic Project spanning more than 7 years. From the former data, we deduce nutation offsets, and from the latter we get gravimetric factors. Comparison of these observed quantities against theoretical expressions of the core and mantle admittance to the tidal potential allows us to estimate Love numbers and resonant frequencies and quality factors of the core. We point out strengths and deficiencies of each technique in their ability to retrieve the Earth's interior parameters.

1. Surface Gravity Changes and Earth's Rotation Variations

The Earth's structure leads to resonance effects that enhance the response of the planet to tidal excitation. The enhancement follows a frequency-dependent resonance law, which resonance frequencies and strength functions are expressed in terms of Earth's structural and rheological parameters. Within the diurnal band, the main resonance is associated with the free wobbling of the core, or retrograde free core nutation (RFCN) which theoretical expression of the frequency in the space-fixed frame of reference $\sigma'_{\mathrm{f}} = -\Omega(A/A_{\mathrm{m}})(e_{\mathrm{f}} - \beta)$. Here, e_{f} is the core flattening, A and A_{m} the equatorial moments of inertia of the Earth and of the mantle, respectively, and β stands for a compliance expressing the deformability of the core-mantle boundary (CMB) under the centrifugal potential due to the core wobble [1].

One phenomenon that undergoes the resonance effects is the surface gravity change given by [2, 3, 4]

$$\Delta g = \left[\delta_2 \left(1 - \frac{Ae - A_{\mathrm{f}}\gamma}{A_{\mathrm{m}}} + \frac{A_{\mathrm{f}}}{A_{\mathrm{m}}} \frac{(e-\gamma)\sigma'_{\mathrm{f}}}{\sigma - \sigma_{\mathrm{f}}}\right) + \delta_1 \frac{A}{A_{\mathrm{m}}} \frac{(e-\gamma)\Omega}{\sigma - \sigma_{\mathrm{f}}}\right] \frac{-2W}{a}, \quad (1)$$

where a is the Earth's radius, W the degree two external gravitational potential, σ the excitating frequency, e the Earth's dynamical flattening, A_{f} the equatorial moment of inertia of the core. The compliance γ expresses the deformability of the CMB under the influence of an external potential. The gravimetric factor δ_2 represents the static response of the Earth to the tidal potential, and δ_1 is the Love number that characterizes the elastic response of the Earth to the inner pressure at the CMB.

Another phenomenon is the celestial motion of the Earth's figure axis, defined by the nutation angles $dY - idX = -\omega(\sigma)/\sigma'$ where the wobble ω of the whole Earth can be expressed in a resonant form as

$$\omega = \left[\frac{Ae - A_{\mathrm{f}}\gamma}{A_{\mathrm{m}}} + \frac{A_{\mathrm{f}}}{A_{\mathrm{m}}}(e-\gamma)\frac{\sigma'_{\mathrm{f}}}{\sigma - \sigma_{\mathrm{f}}}\right]\frac{3W}{\Omega a^2}. \tag{2}$$

The surface gravity changes are measured locally by superconducting gravimeters (SG). These devices can detect variations at the level of 1 nanogal and have been recording data roughly for 10 years. Nutation variations have been densely measured VLBI for more than 20 years. The accuracy now reaches ~0.2 mas. Though VLBI-only data have recenlty led to precise determinations of Earth's structural parameters including the dissipative part of σ_{f} ([5], hereafter referred to as MHB), we address the possibility of using SG measurements as well, since both VLBI and SG observables involve the same geophysical quantities.

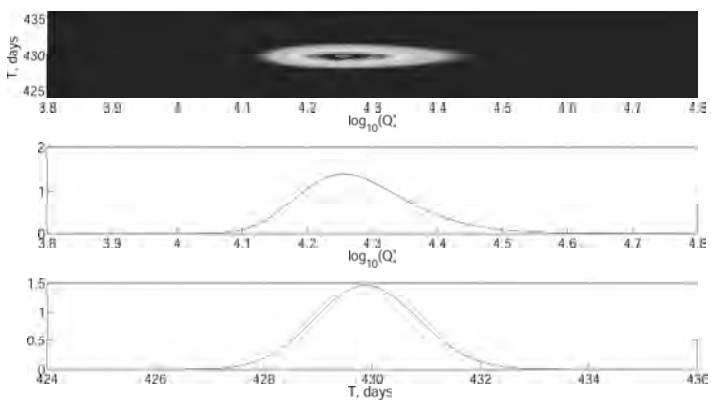

Figure 1. Probability density functions from the analysis of VLBI nutation offsets against the MHB model

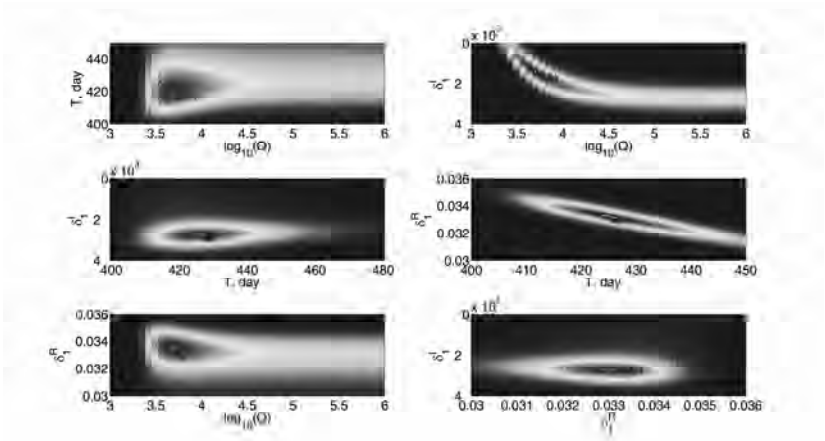

Figure 2. Probability density functions from the analysis of the combination of 7 SG data

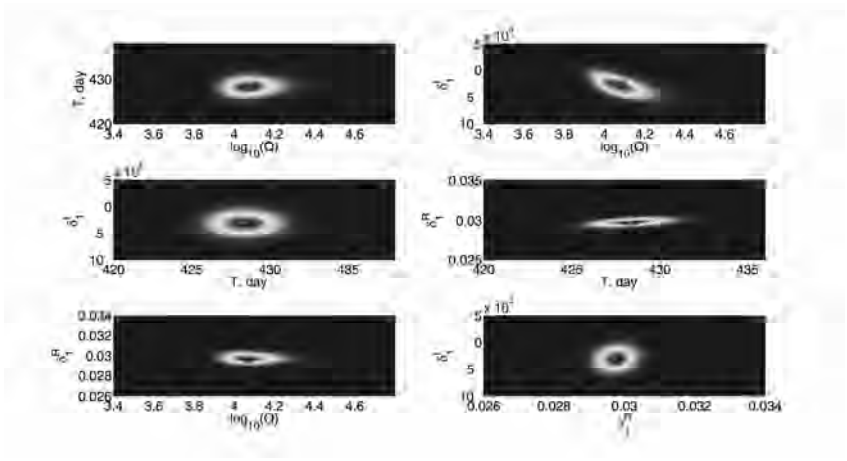

Figure 3. Probability density functions from the analysis of the combination of 16 SG data with the weighting method of Ducarme [12]

2. Data and Results

Nutation offsets since 1984 are obtained by a global inversion of delays accumulated in 3762 diurnal sessions. To maintain the celestial reference frame, a no-net rotation condition has been applied to the coordinates of 247 stable radio sources selected by Feissel-Vernier et al. [6].

The resonance effects on the amplitudes at tidal frequencies are estimated

by least-square fits. For SG data, we fit the amplitudes for the following diurnal tidal frequencies: $Q_1, O_1, M_1, P_1, K_1, \Psi_1, \Phi_1, J_1$ and OO_1. It has to be noticed that the error on Ψ_1 and Φ_1 is much larger than for other frequencies. Since these waves are near the resonance, this will have some negative consequences on the ability to determine the resonant frequency with gravity measurements. For VLBI, we fit at the same frequencies in addition to the 18.6-year and 9.3-year terms.

All SG amplitudes have been corrected from local oceanic tidal loading effects using the FES 2004 model [7]. An extra error of 0.3 nm/s^2 has been added in order to account from the error on the oceanic model. VLBI amplitudes have been freed from the effect of non-linear terms [8, 9] so that all effects not directly linked to non-rigidity are removed.

A Bayesian inversion approach [10, 11] has been developped, starting from (1) and (2), to estimate σ_{f} and δ_1 as complex parameters. The latter parameter is estimated from SG only.

First, the algorithm has been tested on VLBI nutation amplitudes in order to get an estimate of the RFCN frequency. Our nutation data set being offsets with respect to the MHB model, we expect the RFCN frequency estimate to be very close to the MHB value. Expressing the RFCN frequency as $\sigma_{\mathrm{f}} = \frac{2\pi}{T}(1 + i/2Q)$, where the quality factor Q expresses the damping with time, we find $T = 429.9 \pm 0.9$ days, and $Q = 19093 \pm 3968$, which is in good agreement with [9] and with MHB within the error bars (Fig. 1).

Fig. 2 shows the probability density functions of the estimated parameters for the combination of 7 European SG records: Bad-Homburg, Moxa and Wettzell (Germany), Membach (Belgium), Medicina (Italy), Strasbourg (France), and Vienna (Austria). One readily remarks the large uncertainties, a low value for Q, and a significant correlation between T and δ_1^{R}, and between Q and δ_1^{I} for lower Q. These results find their origin first in the above-mentioned large error for the amplitude at Ψ_1. Indeed, the diurnal wave most affected by the resonance is Ψ_1. However, Ψ_1 has a weak amplitude and its measurement within SG data is therefore difficult. It results in a poor constraint on the resonance parameters. Incidentally, the dissipation of Ψ_1 should provide a strong constraint on the quality factor. Another factor is the deficient ocean loading correction: gravity measurements are widely affected by oceans, atmosphere and hydrological effects at small wavelengths. It results in noisier time series at high frequencies. For comparison purpose, in VLBI nutation series, the annual retrograde nutation Ψ_1 is well-determined (large amplitude). Moreover, the oceanic, atmospheric and hydrological effects are much lower in nutation than in surface gravity.

Ducarme et al. [12] provided mean values of 16 gravity records as well as a presumably improved ocean loading correction that led to smaller uncertainties on the fitted diurnal amplitudes (especially for Ψ_1). Using this data set, it turns out that we obtain much better constrained parameters and a better agreement with the results from nutations for the RFCN frequency (Fig. 3). Both T and Q now appear to be in agreement with the VLBI within the error

bars. Nevertheless, correlations already pointed out in Fig. 2 still show up between δ_1^{I} and Q, but to a smaller extent.

To conclude, it comes out from these preliminary studies that it becomes worth using simultaneously VLBI and SG data, especially since the parameter δ_1 exclusively plays through gravity data. It encourages the use of VLBI for constraining other parameters and strengthening the SG determination of the core potential Love number k_1^{f}. However, some problems do remain, that are linked to local loading corrections at SG locations, although recent attempts to free data from these effects using wise combination methods, look promising.

References

[1] Sasao, T., S. Okubo, M. Saito. A simple theory on dynamical effects of stratified fluid core upon nutational motion of the earth. Proc. International Astronomical Union Symposium 78. R.L. Duncombe (ed.), D. Reidel Publ. Co., Dordrecht, Holland, Boston, 1980, 165.

[2] Hinderer, J. Resonance effects of the Earth's fluid core. Earth Rotation: Solved and Unsolved Problems. A. Cazenave (ed.), Reidel, Dordrecht, 1986, 277.

[3] Hinderer, J., W. Zürn, H. Legros. Interpretation of the strength of the nearly diurnal free wobble resonance from stacked gravity tide observations. Proc. 11th Int. Symp. Earth Tides. J. Kakkuri (ed.), Schweitzerbart Verlag, Stuttgart, 1991, 549.

[4] Dehant, V., J. Hinderer, H. Legros, et al. Analytical approach to the computation of the Earth, the outer core and the inner core rotational motions. Phys. Earth Planet. Int., v. 76, 259, 1993.

[5] Mathews, P.M., T.A. Herring, B.A. Buffett. Modeling of nutation and precession: New nutation series for nonrigid Earth and insights into the Earth's interior. JGR, 107(B4), DOI 10.1029/2001JB000390, 2002.

[6] Feissel-Vernier, M., C. Ma, A.-M. Gontier, et al. Analysis strategy issues for the maintenance of the ICRF axes. Astron. Astrophys., v. 452, 1107, 2006.

[7] Lyard, F., F. Lefevre, T. Letellier, et al. Modeling the global ocean tides: modern insights from FES2004. Ocean Dynamics, v. 56, 394, 2006.

[8] Lambert, S.B., P.M. Mathews. Second-order torque on the tidal redistribution and the Earth's rotation. Astron. Astrophys., v. 453, 363, 2006.

[9] Lambert, S.B., V. Dehant, A.-M. Gontier. Celestial frame instability in VLBI analysis and its impact on geophysics. Astron. Astrophys., v. 481, 535, 2008.

[10] Tarantola, A., B. Valette. Generalized nonlinear inverse problems solved using the least squares criterion. Rev. Geophys. Space Phys., v. 20, 219, 1982.

[11] Florsch, N., J. Hinderer. Bayesian estimation of the free core nutation parameters from the analysis of precise tidal gravity data. Phys. Earth Planet. Int., v. 117, 21, 2000.

[12] Ducarme, B., H.P. Sun, J.Q. Xu. Determination of the free core nutation period from tidal gravity observations of the GGP superconducting gravimeter network. J. Geodesy, v. 81, 179, 2007.

The 5th IVS General Meeting Proceedings, 2008, p. 251–255

Some Challenges in Developing the Second ICRF

Chopo Ma, David Gordon, Daniel MacMillan, Leonid Petrov

NASA Goddard Space Flight Center, USA

Abstract. The generation of the second realization of the ICRF catalog is scheduled for the beginning of 2009. VLBI data and analysis have both improved significantly since the first ICRF, which was completed in mid 1995. The observed data distribution is still inhomogeneos spatially and temporally, although the IVS monitoring source monitoring program has led to a larger, better observed set of candidate defining sources. The vast majority of observations have been made by northern hemisphere networks observing ∼100 geodetic sources. Analysis of radio source position time series will provide measures of source stability, which will be supplemented with source structure information from an extensive set of radio source images. Since there will be many catalogs generated by different analysis groups using different strategies, methods for selecting the best solution will be required to generate the final ICRF-2.

1. Introduction

The ICRS is the idealized barycentric coordinate system to which celestial positions are referred. It is kinematically nonrotating with respect to the ensemble of distant extragalactic objects. It has no intrinsic orientation but was aligned close to the mean equator and dynamical equinox of J2000.0 for continuity with previous fundamental reference systems. Its orientation is independent of epoch, ecliptic or equator and is realized by a list of adopted coordinates of extragalactic sources.

The ICRF is a set of extragalactic objects whose adopted positions and uncertainties realize the ICRS axes and give the uncertainties of the axes. It is also the name of the radio catalog whose 212 defining sources are currently the most accurate realization of the ICRS. The IAU adopted the ICRF effective Jan. 1, 1998. The orientation of the ICRF catalog was carried over from earlier IERS radio catalogs and was within the errors of the standard stellar and dynamical frames at the time of adoption. The original ICRF was based on the analysis of S-Band and X-band data collected through from 1979 to 1995 [3].

Analysis of the statistics of these astrometric solutions yielded a source position uncertainty floor of 250 μas and an accuracy of the reference frame axes of about 30 μas. Successive revisions of the ICRF, ICRF-Ext.1 and ICRF-Ext.2 [1] were intended to minimize rotation from its original orientation. Fig. 1 shows the the latest revision, ICRF-Ext.2, which keeps unchanged the positions of the original 212 defining sources, improves positions of the remaining sources and adds ~15% more sources.

VLBI data and analysis have both improved significantly since the first ICRF, which was completed in mid 1995. However, difficulties remain because of the inhomogeneity of the data distribution spatially and temporally, in particular the relative dearth of observations in the southern hemisphere and the two-order range in the number of observation epochs by source. The data set is still dominated by the ~100 sources observed regularly in EOP and TRF sessions, some of which are not ideal in terms of astrometric stability.

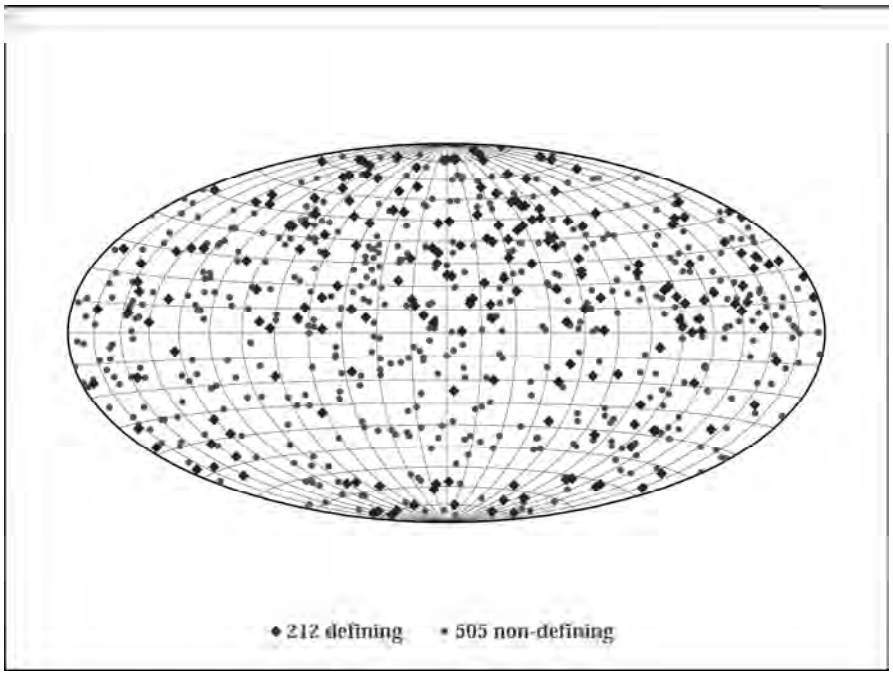

Figure 1. ICRF-Ext.2 sources: 212 defining, 505 non-defining

2. Current Data Set

The original set of ICRF defining sources is dominated by sources in the northern hemisphere, because most observing has been done with northern hemisphere geodetic networks. Since the time histories of many non-geodetic

sources were sparse, the IVS started the CRF monitoring program in 2004 to monitor stable, potentially stable, and ICRF defining sources. This should remedy gaps in the astrometric observing profile and allow a somewhat larger, better observed set of defining sources for the second ICRF.

To assess the statistics of current available source position data, we generated time-series files for 626 sources observed during the period 1979–2007. More details about the analysis of these time series and the determination of a new set of "defining" sources is given in [2]. Fig. 2 shows the statistics of these 626 sources. Clearly, sources at declinations less than $-30°$ were observed much less frequently, almost by an order of magnitude than the bulk of northern hemisphere sources.

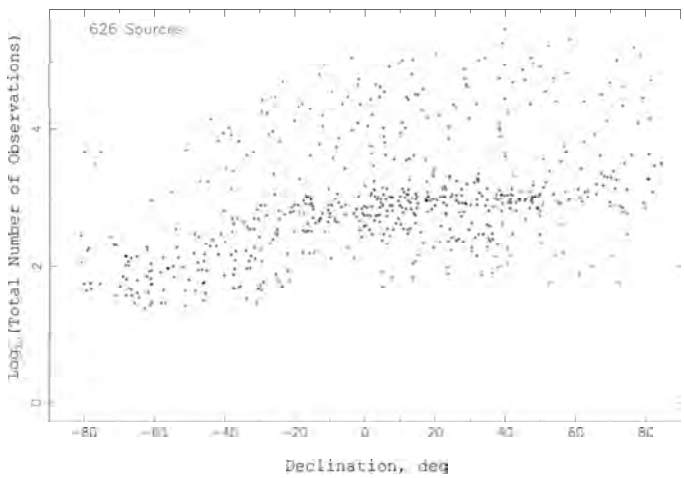

Figure 2. Total number of observations of each source

3. Criteria for the ICRF-2 Defining Sources

To construct ICRF-2, we need to determine the criteria that must be met by the new set of "defining" sources. Two possible criteria are: 1) stability of the source position time series and 2) source structure information from radio images. We now have available extensive source structure information to supplement the identification of stable and unstable sources from position time series. It still may be necessary for the criteria for defining sources to have some flexibility in order to have more uniform spatial distribution since the frequency of source observation as such a strong declination dependence.

When a source has been observed frequently, it is possible to identify clear systematic variations in the estimated source position. For instance, of the 107 geodetic sources, there are a number of sources that have unstable source positions. Fig. 3 shows time-series for 2145+067, which has clear non-linear

variation. However, one of the difficulties in determining the stability from position time-series is that many sources have a very sparse observing history. The number of observing sessions per source varies from 5 to more than a thousand sessions.

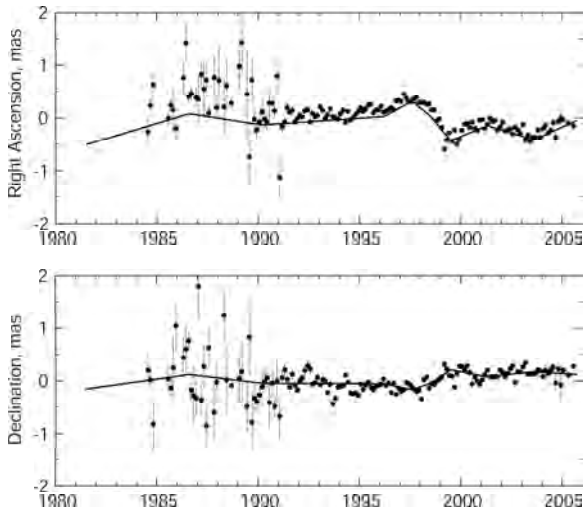

Figure 3. Radio source position time-series in right ascension and declination for 2145+067. Positions shown are 45-day averages

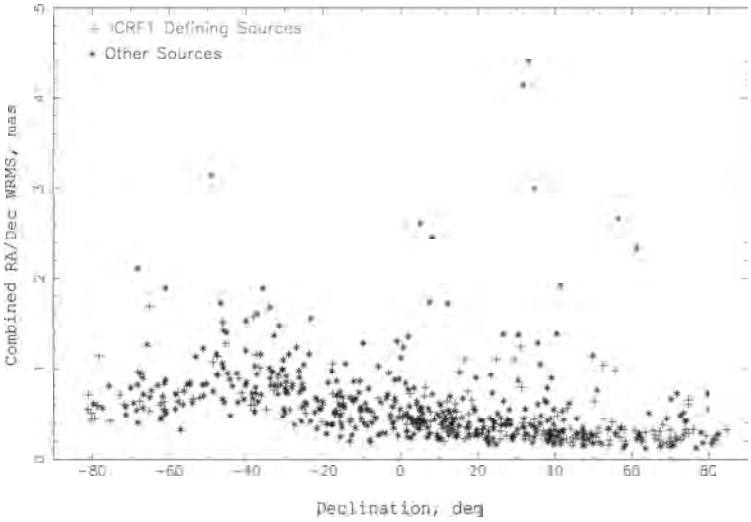

Figure 4. Combined RA/Dec Position WRMS's of GSFC Time Series

One possible criteria for source stability is the WRMS of the RA and DEC position time series for each source. The combined (added in quadrature) WRMS of the RA and DEC series is plotted as a function of declination in Fig. 3. The WRMS is clearly worse for sources south of $-20°$, because the vast majority of observations are made with northern hemisphere stations.

4. ICRF-2 Analysis Plan

The development of ICRF-2 will involve the following issues:

- selection of defining sources;
- treatment of source position variations;
- improvement of geophysical and astronomic modeling;
- data weighting;
- selection of data;
- integration of ICRF, ITRF, and EOP;
- generation of the final catalog.

In the analysis for the second ICRF it will be necessary to improve the estimation of gradients, correlated noise, source position variations and observation weighting. As there will be many catalogues generated by the various analysis groups, methods for selecting the best solution among several or for combining solutions will be needed. The provisional milestone timeline for the analysis leading to the final ICRF-2 is:

spring 2007	Working Group Meeting, Vienna;
fall 2007	Generation, comparison of time series (Working Group Meeting, Paris);
spring 2008	Analysis of time series (Working Group Meeting, St. Petersburg);
mid 2008	Defining source criteria;
fall 2008	Selection of defining sources, analysis configuration;
spring 2009	Generation of ICRF-2 catalogue.

References

[1] Fey, A., C. Ma, F. Arias, et al. The second extension of the ICRF. Astron. J., 127, 3587, 2004.

[2] Gordon, D., C. Ma, J. Gipson, et al. On Selection of "Defining" Sources for ICRF-2. This volume.

[3] Ma, C., F. Arias, T. Eubanks, et al. The International Celestial Reference Frame as realized by very long baseline interferometry. Astron. J., 116, 516, 1998.

The 5th IVS General Meeting Proceedings, 2008, p. 256–260

On Construction of ICRF-2

Zinovy Malkin

Central Astronomical Observatory at Pulkovo, Russian Academy of Sciences, Russia

Abstract. In this paper, several issues are considered, related to the construction of the next ICRF generation, ICRF-2. Between them, the following points are touched: ICRF-2 structure, ICRF Core sources selection, and some expected user's requirements.

1. Introduction

By now, more than 6 million geodetic and astrometric VLBI observations were made, much more than were available for the construction of ICRF, and methods of data analysis were substantially advanced. This opens up new opportunities for ICRF improvement. For this purpose, two ad hoc Working Groups were organized by IAU, and jointly IERS and IVS[1], and preparation to ICRF-2 creation was started [1]. In particular, one of the main tasks of the preparation campaign is to investigate possible strategies that are or may be used for ICRF-2, the second ICRF realization. In this paper several issues related to construction of ICRF-2 are touched.

2. ICRF-2 Structure

It is suggested that ICRF-2 comprises two source lists. The first list may be called ICRF Core. The main features of the ICRF Core are:

- realizes ICRS definitions;
- consists of about 400 sources evenly distributed over the sky, i.e. 1 source per 100-deg^2;
- provides the long-time system stability.

The second list may be called ICRF Extension or ICRF Supplement. The main features of the ICRF Extension are:

[1] http://rorf.usno.navy.mil/ICRF2/

- consists of about 3600 sources;
- keeps ICRF system;
- provides ICRF densification for extended user's needs;
- serves as a set of calibrators for the phase reference VLBI;
- may have more dense source distribution in the ecliptic belt to be used in the space navigation.

These two lists give 4000 sources in total, i.e. 1 source per 10 deg^2. Suggested total number of sources is close to the number of sources already observed in the IVS and VCS sessions, and for most of them reliable positions are derived, mostly for declination > -40 deg.

It seems to be reasonable to schedule in 2008 several dedicated IVS sessions to obtain positions for 300–500 sources with reasonable precision in the southern hemisphere zone with declination < -40 deg to complete ICRF Supplement list in the sky regions poorly filled with astrometric radio sources.

In principle, it is advisable to have as many Core sources as possible in order to minimize the impact on the individual source instability. At the moment, 400 sources may be a good compromise between this requirement and the real number of the well observed sources. As the VLBI system becomes more sensitive, which allows us to observe more weak compact sources, and number of well observed and investigated sources grows new sources should be included in the ICRF Core catalog to provide better system stability. However, it is important to add new sources to the ICRF Core in such a way to keep uniform distribution of the Core sources over the sky.

3. Core Source Selection

A key issue is how to select ICRF-2 Core sources. Different criteria for source selection have been proposed by many authors, based on:

1. time series analysis: velocity of the apparent source motion, scatter parameters (indices) such as (w)rms, χ^2 and Allan deviation; other statistics;
2. observation history: time span of observations, number of sessions or observations (correlation between them is at a level of 0.9), observation density, etc.;
3. physical characteristics: structure index, redshift;
4. other criteria, e.g. position uncertainty from global analysis.

In this paper only criteria of the first two groups are considered. These criteria were applied to the time series submitted by IVS Analysis Centers to the ICRF-2 data pool. For all the computations, original source positions derived from analysis of single session and reported by the analysis centers were used. Reported uncertainties in the source positions were used for weighting.

For the criteria of the first group, when possible, 2D estimates were used, e.g. source velocity was computed as $V = \sqrt{(V_\alpha \cos\delta)^2 + V_\delta^2}$, WRMS of source position computed analogously, Allan deviation computed using the

2D weighted estimate WMADEV as developed in [2]. The uncertainty in the velocity estimate was also used as a new scatter index.

The first conclusion made from this analysis is that source behavior and consequently source position variation (scatter) indices may differ significantly between the analysis centers, as can be seen from Fig. 1, 2.

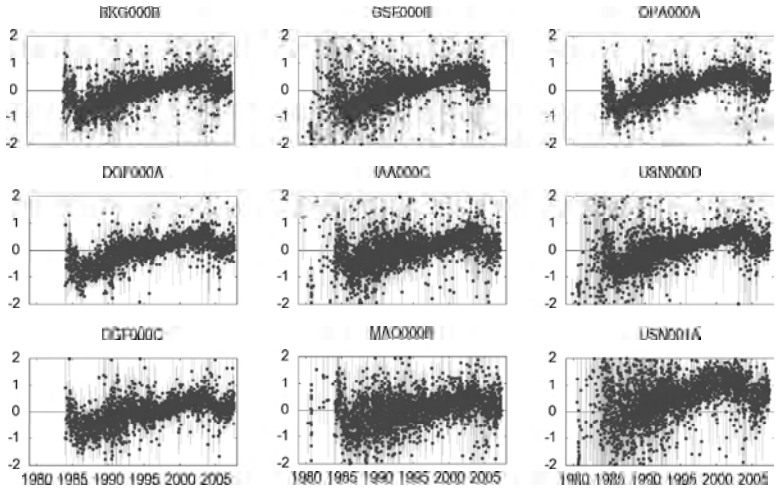

Figure 1. Several time series for 0923+392 (3C39.25) RA. In this example, several solutions show similar behavior of the source coordinate but different scatter

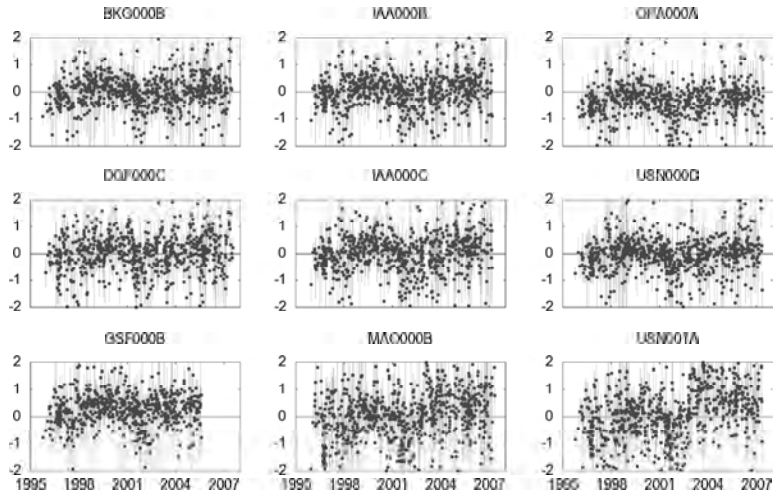

Figure 2. Several time series for 0003-066 DE. In this example, several solutions show both different behavior of the source coordinate and scatter

In Tabl. 1 an example is given for velocity estimate using several time series.

Table 1. 2D velocity of the source 0656+082 computed from different source position time series

Series	Nepochs	V, μas/yr
mao000b	197	45 ± 38
usn000d	189	53 ± 28
dgf000a-g	188	80 ± 30
opa001a	186	101 ± 29
iaa000c	168	107 ± 24
usn001a	189	124 ± 43
iaa000b	168	163 ± 24
aus001a	179	165 ± 42
gsf000b	131	235 ± 50

As can be seen from Tabl. 1, despite large number of epochs and considerable time span about 7.5 y, velocity estimates for source 0656+082 differ by several times, which shows that analysis strategy has large impact even on the estimated radio source velocity, a parameter, which is often attributed to physical processes such as jet motion, and which should seem most robust with respect to the analysis strategy. Large difference between available time series can be observed also for other scatter indices, cf. also Fig. 1, 2.

So, results of source position time series analysis heavily depend on method used for time series computation and should be used with care. Under this circumstance, maybe the number of sessions, network diversity and time span should be a first criteria to select ICRF Core candidates. Only sufficient time span and number of sessions can provide reliable conclusion on the source position variations. This inference can also be drawn from the position time series for some sources where one can see quite different velocity and scatter at different part of the interval of observations.

At the first glance we can find sufficient number of sources with large observations history, see e.g. Fig. 3, but only at the first glance. The well known problem is that distribution of the well observed sources are far from uniform, with clear deficiency in the southern hemisphere.

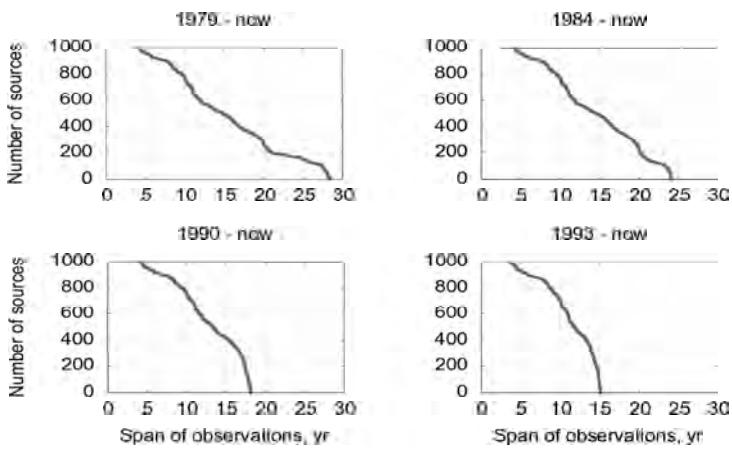

Figure 3. Number of sources for given start epoch and data span. Four plots are shown for different criteria for the data selection discussed in literature

Evidently, at the moment we have not enough sources of the highest quality (compactness and position error) to fill in all the evenly distributed 100-deg^2 sky cells. The following strategy for the nearest years can be considered:

- for the first ICRF-2 version, one, the best of available, source in each 100-deg^2 cell should be taken; at this stage a list of sources of insufficient quality (time span, number of sessions, position error) is identified;
- at the next stage, the sources of insufficient quality should be observed in 2009-2010 to be able to issue the second version of ICRF-2 by the end of 2010–beginning of 2011.

This should be mentioned that if two or more good sources fell to the same cell, they will not be lost for users since they will be included in the ICRF Extension. The general logic of this approach is to give priority to even source distribution, which presumably has advantage in maintenance of the ICRF orientation and further comparison with GAIA CRF realization.

4. ICRF for Users

From user's point of view, a source position catalog is a tool to predict the source coordinates at given epoch with known error. Currently, a user can use the source position error given in the catalog. These errors are usually obtained from least square adjustment, and can be considered as the precision only. To assess the accuracy of the source coordinates, one can analyze the source coordinates time series. For example, the uncertainty in the position of the source 0923+392 (3C39.25) given in the ICRF-Ext.2 catalog is 0.035 mas. However, one can see from Fig. 1 that this value is well underestimated, and actual position error for certain epochs may be as large as 1 mas. The error in source position based on time series analysis may be computed by the method proposed in [3], which allows us to account for both precision and scatter of the session position estimates.

Based on this considerations we can conclude that the End User Error (EUE) concept, based on the realistic estimate of the source position accuracy, may be more adequate for ICRF instead of or in addition to the *defining* or *stable* concepts, since it show just what a user gets using the catalog. Also, we can consider the Index of Position Variability (IPV) based on existing and/or new methods of analysis and computed as a continuous function, instead of the stepwise index 1-2-3-... widely used now, which should be given in a ICRF catalog to give a user a quantitative measure, or at least an impression, of the real error in the source position.

References

[1] Ma, C. Some Challenges in Developing the Second ICRF. This volume.

[2] Malkin, Z. J. Geod., v. 82, 325, 2008.

[3] Malkin, Z. Proc. 15th Working Meeting on EVGA. Barcelona, 2001, 55.

The 5th IVS General Meeting Proceedings, 2008, p. 261–264

On Selection of "Defining" Sources for ICRF-2

David Gordon [1], *Chopo Ma* [2], *John Gipson* [1], *Leonid Petrov* [1], *Daniel MacMillan* [1]

[1)] *NVI, Inc./NASA Goddard Space Flight Center, USA*

[2)] *NASA Goddard Space Flight Center, USA*

Abstract. Generation of the second realization of the ICRF catalog is scheduled for the end of this year. Selection of a subset of so-called "defining" sources with very stable measured positions is necessary in the next few months. Towards this goal, 8 institutions generated source position time series files using thousands of VLBI databases. Using these time series files, we investigated whether there are enough stable sources distributed evenly about the sky to adequately define the frame of the ICRF-2. Using data from the GSFC time series file, we were able to select 300 stable sources distributed evenly in declination, and fairly evenly in right ascension. It is necessary to use the one-baseline southern hemisphere CRF sessions conducted over the past few years by USNO in order to accomplish this.

1. Introduction

The second realization of the International Celestial Reference Frame, ICRF-2, is scheduled to be generated at the end of 2008 and presented to the IAU for approval in 2009. Therefore, selection of a set of "defining" sources must be made soon. The first ICRF used 212 "defining" sources. These were sources whose positions were initially solved for, and then held fixed to these "defined" positions. They provided a rigid framework which essentially defined the ICRF-1 reference frame. However, some problems became apparent in the realization of this rigid framework. The southern hemisphere was very under-represented in the list of 212 defining sources, and many of the far-south defining sources were only sparsely observed. Also, quite a few of the original defining sources have turned out to be unstable; their effective positions have varied by tenths of milli-arc-seconds or more due to structure brightness variations. A goal for the second realization of the ICRF should be to avoid these two deficiencies. What is needed is a set of defining sources distributed more evenly around the sky, and with long histories of stable positions.

2. Time Series Solutions

In order to study the positional stability of the VLBI geodetic sources, the analysis centers participating in ICRF-2 development were asked to generate time series files. These were to be large files of each source's position in each session. Eight analysis centers generated such files and submitted them to a designated FTP site. The 8 analysis centers and the software systems were:

gsf	NASA/GSFC	Calc/Solve,
usn	USNO	Calc/Solve,
bkg	BKG	Calc/Solve,
opa	Paris Observatory	Calc/Solve,
dgf	DGFI	Occam,
aus	Geoscience Australia	Occam,
iaa	Inst. Applied Astronomy	Quasar,
mao	Main Astronomical Obs.	Steel Breeze.

At GSFC, we produced a time series file called gsf001a.ts. A preliminary list of 300 sources was selected based on sky coverage, observing history, and stability in the usn001a.ts time series. A first Solve/Globl solution was run in which the positions of these 300 sources were solved for globally, and all others source positions were solved as arc parameters (a separate position for each session). Four other solutions were run in which a different 75 of the 300 stable sources were solved as arcs. All of the arc solutions were then combined and sorted to give a large time series file of source positions. For the GSFC solution, we included all of the one-baseline southern hemisphere CRF sessions that USNO has been performing over the past few years to improve the source statistics in the south. Only the GSFC, DGFI, and USNO groups included these sessions in their solutions, and it turns out that their use is crucial towards obtaining an evenly distributed set of defining sources.

At GSFC, we studied our own and the other time series files. We computed the WRMS of each source's RA and Dec positions, and made various plots. The position WRMS's represent a combination of observing noise and source structure position variations. A plot for the gsf001a.ts file is shown in Fig. 1. Plotted is the combined RA and Dec WRMS's (added in quadruture) versus declination. A clear declination effect is seen. Data for sources south of approximately $-20\,^{\circ}$ is clearly noisier, with a peak at around $-40\,^{\circ}$. Much of the data for sources in the far-south comes from one-baseline CRF sessions, and without them, this area would be very sparsely represented. Presumably, southern sources are not inherently less stable than northern sources, they are just less well observed.

3. Results

An initial goal of this study was to determine if a set of prospective "defining" sources could be picked that filled the sky fairly evenly with "stable"

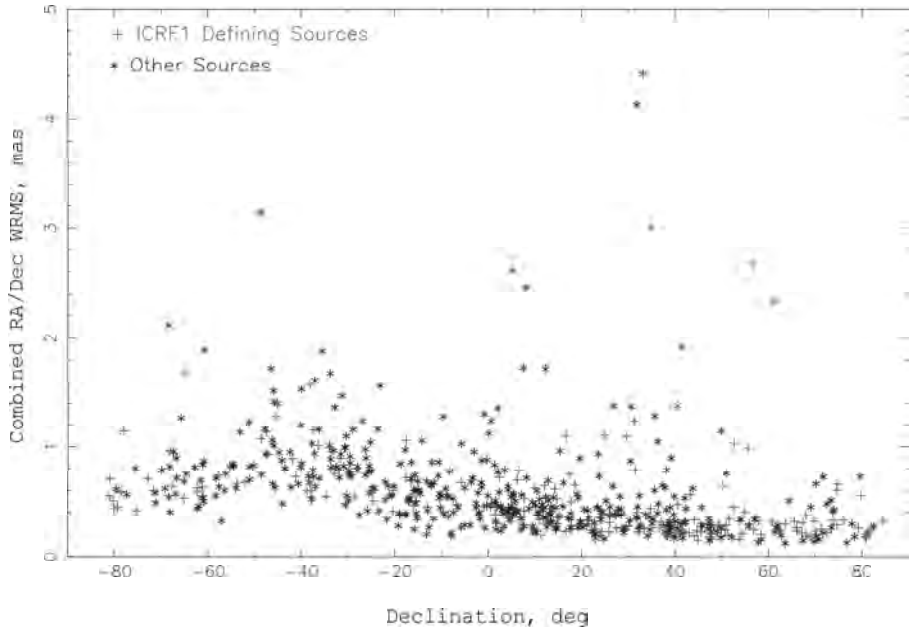

Figure 1. Combined RA/Dec position WRMS's for GSFC time series

sources. We chose arbitrarily 300 as the number of prospective defining sources. As a start, we sorted the sources from gsf001a.ts by increasing combined RA and Dec WRMS's. The sky distribution of the 300 sources with the smallest combined WRMS's is shown in Fig. 2. Clearly the southern sky is under-represented and this would not be an adequate way to select defining sources.

Next we split the sky into 17 declination zones - two 15-degree polar caps and fifteen 10-degree wide zones in between. Sources were sorted by increasing combined RA and Dec WRMS's in each zone, and we picked the best sources in each zone. The number of sources per zone was set proportional to the cosine of the average declination of the zone. There were 26 in the equatorial zone, decreasing to 5 in the polar zones, and adding up to 300 sources. There was no attempt to get even RA distribution. We further looked through time series plots of each source picked, and identified 4 that showed clear systematic position variations, even though their WRMS's were small. These 4 were replaced by other stable sources in their zones. A plot of these 300 prospective defining sources is shown in Fig. 3. This list contains 111 of the original ICRF-1 defining sources. The sky distribution is clearly a large improvement over ICRF-1, and demonstrates that there should be enough stable southern sources to adequately anchor the ICRF-2 reference frame without the deficiencies seen in ICRF-1, provided the one-baseline southern hemisphere CRF sessions are used.

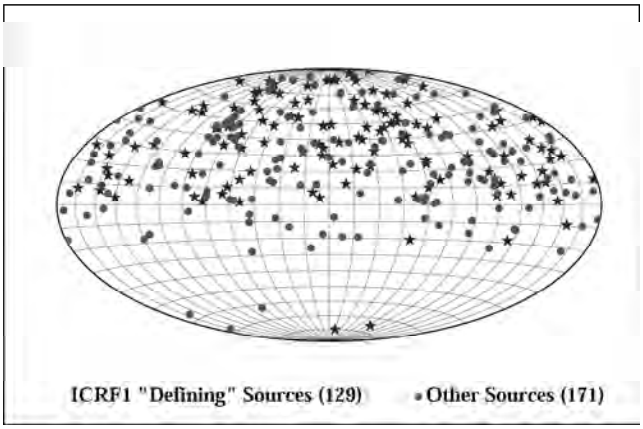

Figure 2. 300 best sources

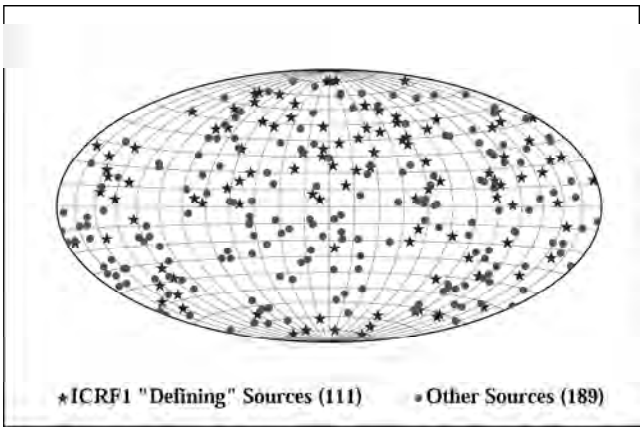

Figure 3. 300 best sources by declination zones

The 5th IVS General Meeting Proceedings, 2008, p. 265–269

Systematic Effects in Apparent Proper Motion of Radio Sources

Oleg Titov

Geoscience Australia, Australia

Abstract. The galactocentric rotation of the Solar system generates a systematic effect in proper motions known as 'secular aberration drift'. This tiny effect (about five microseconds per year) in the quasar proper motion can be measured by VLBI. However, the motions of relativistic jets from the active extragalactic nuclei can reach several hundred microseconds per year and mimic the proper motions of the observed radio sources. These apparent motions exceed the secular aberration drift by a factor of 10–100. In this paper we search for ways to overcome the difficulties and discuss our estimates of the secular aberration drift using OCCAM software.

1. Introduction

Multifrequency VLBI techniques measure accurate positions of the reference extragalactic radio sources. From the analysis of a global set of VLBI data the positions are estimated with an accuracy of up to 0.1 mas for frequently observed radio sources (more than 10,000 observations per source). However, the effect of the intrinsic source structure causes linear and non-linear variations in the sources' astrometric positions [1]. The apparent proper motion can reach several hundred microarcsec/year for some radio sources. The positional variations are supposed to be uncorrelated over the sky, and do not produce any systematic pattern. Nonetheless, some systematic effects in the apparent radio sources proper motions has been predicted. The galactocentric acceleration of the Solar system barycenter should cause the first order electric type vector spherical harmonic of the magnitude 4–5 microarcsec/year [2, 3, 4, 5, 6]. Primordial gravitational waves in the early Universe would produce second order vector spherical harmonics of electric and magnetic types [2, 7]. A more generalized expression for proper motion in the frame of general relativity has been published [8]. The authors found that in the expanding Universe the proper motion of distant objects could increase with distance.

Some attempts to detect systematic effects have been done by different authors [2, 9, 10]. Gwinn el al. [2] did not find any systematics in the proper

motions using data from 1979 until 1996. MacMillan [9] used VLBI data from 1979 until 2002 and detected some systematics but did not give any details. Titov [10] found some statistically significant amplitudes of first and second degree electric-type harmonics using data from 1980 until 2007.

This paper presents more rigorous results than [10] on the systematic effects in radio source proper motion. This includes a separate consideration of the vector spherical harmonics of the first and second order. The second degree 'magnetic' spherical harmonics were added to the list of estimated parameters. More red shifts of the reference radio sources are available from the database recently developed by Malkin and Titov [11].

2. Vector Spherical Functions

Let us consider $\vec{F}(\alpha,\delta)$ as a vector field of a sphere decribed by the components of the proper motion vector ($\mu_\alpha \cos\delta$, μ_δ)

$$\vec{F}(\alpha,\delta) = \mu_\alpha \cos\delta \vec{e}_\alpha + \mu_\delta \vec{e}_\delta,$$

where $\vec{e}_\alpha$, $\vec{e}_\delta$ — unit vectors. A vector field of spherical functions $\vec{F}(\alpha,\delta)$ can be approximated by vector spherical functions as follows

$$\vec{F}(\alpha,\delta) = \sum_{l=1}^{\infty} \sum_{m=-l}^{l} (a^E_{l,m} \vec{Y}^E_{l,m} + a^M_{l,m} \vec{Y}^M_{l,m}),$$

where $\vec{Y}^E_{l,m}$, $\vec{Y}^M_{l,m}$ — the 'electric' and 'magnetic' transverse vector spherical functions, respectively

$$\vec{Y}^E_{l,m} = \frac{1}{\sqrt{l(l+1)}} (\frac{\partial V_{lm}(\alpha,\delta)}{\partial \alpha \cos\delta} \vec{e}_\alpha + \frac{\partial V_{lm}(\alpha,\delta)}{\partial \delta} \vec{e}_\delta),$$

$$\vec{Y}^M_{l,m} = \frac{1}{\sqrt{l(l+1)}} (\frac{\partial V_{lm}(\alpha,\delta)}{\partial \delta} \vec{e}_\alpha - \frac{\partial V_{lm}(\alpha,\delta)}{\partial \alpha \cos\delta} \vec{e}_\delta).$$

The function $V_{lm}(\alpha,\delta)$ is given by

$$V_{l,m}(\alpha,\delta) = (-1)^m \sqrt{\frac{(2l+1)(l-m)!}{4\pi(l+m)!}} P^m_l(sin\delta) \exp(im\alpha),$$

where $P^m_l(sin\delta)$ — the associated Legendre functions.

The coefficients of expansion $a^E_{l,m}$, $a^M_{l,m}$ to be estimated are

$$a^E_{l,m} = \int_0^{2\pi} \int_{-\frac{\pi}{2}}^{\frac{\pi}{2}} \vec{F}(\alpha,\delta) \vec{Y}^{E*}_{l,m}(\alpha,\delta) \cos\delta d\alpha d\delta,$$

$$a^M_{l,m} = \int_0^{2\pi} \int_{-\frac{\pi}{2}}^{\frac{\pi}{2}} \vec{F}(\alpha,\delta) \vec{Y}^{M*}_{l,m}(\alpha,\delta) \cos\delta d\alpha d\delta,$$

where $*$ means a complex conjugation. This system of equations can be solved by the least squares method. In this investigation the coefficients are estimated as global parameters from a large set of VLBI data.

3. Observations and Discussion of Results

The first and second degree spherical harmonics were estimated by the least squares collocation method [12]. The database comprises about 3.9 million observations of group delay with different baselines and sources made in 3,554 24-hour sessions between April 1980 and April 2007. The equatorial coordinates of more than 2,000 radio sources were observed as global or 'arc' parameters (see solution description below). The Earth orientation parameters, corrections to IAU 2000 nutation offsets, and station coordinates were estimated as 'arc' parameters. NNR and NNT constraints were imposed on the station positions for each 24-hour session. Clock offsets, troposphere wet delays, and north-south and east-west gradients were estimated as stochastic parameters for each observational epoch. The vector spherical harmonics were treated as global parameters, similar to the approach used by MacMillan [9].

The first solution was based on all radio sources observed in geodetic and astrometric VLBI programs without separation into 'stable' and 'unstable'. In the second and third solutions no 'unstable' radio sources were used for the reference frame according to the Feissel-Vernier classification [13]. The number of radio sources with measured red shift has increased significantly since the previous publication [10]. The second solution was based on 486 non-'unstable' radio sources with z≤1 and the third solution based on 582 non-'unstable' radio sources with z≥1. Thus, the first solution includes more sources and observations. On the other hand, some of the sources are not astrometrically stable; therefore, the harmonic estimates for the first solution may be corrupted.

Table 1. Estimates of the vector spherical harmonics $l = 1$ for different sets of the reference radio sources

Solution	All radio sources	$z \leq 1$ no 'unstable'	$z \geq 1$ no 'unstable'
Secular aberraton drift, μas/year	25.1 ± 1.1	25.0 ± 2.1	24.3 ± 3.2
Right Ascension	263 ± 3	269 ± 5	278 ± 6
Declination	20 ± 5	45 ± 7	40 ± 8

Tabl. 1 presents estimates of the first degree spherical harmonics for three solutions. The estimates of the first degree electric spherical harmonics are stable with respect to changes in reference radio sources. The magnitudes of the differential secular aberration vector lie within their standard deviation errors. The first solution in Tabl. 1 provides better formal statistics. However,

the direction of the vector in the first solution is different from the two other solutions, presumably due to the effect of the radio source structure instability.

Table 2. Estimates for the vector spherical harmonics for different combinations of parameters: $l = 1$ only; $l = 1$ and $l = 2$; and $l = 2$ only. All radio sources were used as reference ones

Parameter	(l, m)	$l = 1$ only	$l = 1$ and $l = 2$	$l = 2$ only
Secular aberration drift, μas/year		25.1 ± 1.1	15.6 ± 2.1	
Right ascension, deg		263 ± 3	279 ± 6	
Declination, deg		20 ± 5	26 ± 15	
Electric harmonics, μas/year	(2,0)		0.5 ± 1.8	3.5 ± 1.0
	(2,1)		-5.4 ± 0.9	-11.3 ± 0.6
	(2,−1)		-3.7 ± 0.8	-3.2 ± 0.6
	(2,2)		4.5 ± 0.6	4.6 ± 0.6
	(2,−2)		0.5 ± 0.5	0.7 ± 0.5
Magnetic harmonics, μas/year	(2,0)		-5.9 ± 0.8	-5.6 ± 0.8
	(2,1)		3.2 ± 0.7	2.7 ± 0.6
	(2,−1)		-9.7 ± 0.7	-13.1 ± 0.6
	(2,2)		2.4 ± 0.5	2.3 ± 0.6
	(2,−2)		1.4 ± 0.5	1.4 ± 0.5

Tabl. 2 shows the estimates of $l = 1$ and $l = 2$ spherical harmonics. The first solution was based on all radio sources observed in VLBI programs. The magnitude of the differential secular aberration vector reduces by 40 per cent if the second degree harmonics are added. However, this vector direction does not change significantly. The estimates for the second degree spherical harmonics are statistically significant. Some of them increase if the first degree spherical harmonics are not estimated. Uneven distribution of the reference radio sources results in high correlation among the $l = 1$ and $l = 2$ harmonics (up to 0.8). Until more radio sources in the southern hemisphere are observed, it is necessary to explore whether higher degree harmonics are significant or not.

4. Conclusion

The systematic effects in the reference radio source proper motions have been investigated through a global analysis of geodetic VLBI data. The first and second degree harmonic estimates were statistically significant. A disproportionate reference radio source distribution over the sky causes a high correlation between these parameters and can result in a bias of the harmonic

estimates. More astrometric VLBI observations in the southern hemisphere should be done in order to reduce the mutual correlation.

Acknowledgements

I am thankful to S. Klioner, M. Eubanks, M. McClure, V. Vityazev, D. Jauncey, V. Zharov, D. MacMillan, and N. Brown for the fruitful discussions in the preparation of the manuscript.

This paper is published with the permission of the CEO, Geoscience Australia.

References

[1] Ma, C., E.F. Arias, T.M. Eubanks, et al. The international celestial reference frame as realised by very long baseline interferometry. A.J., v. 116, 516–546, 1998.

[2] Gwinn, C.R., T.M. Eubanks, T. Pyne, et al. Quasar proper motions and low-frequency gravitational waves. Astrophys. J., v. 485, 87–91, 1997.

[3] Sovers, O.J., J.L. Fanselow, C.S. Jacobs. Astrometry and geodesy with radio interferometry: experiments, models, results. Rev. Mod. Phys., v. 70, 1393–1454, 1998.

[4] Kovalevsky, J. Aberration in proper motions. Astron. Astrophys., v. 404, 743–747, 2003.

[5] Klioner, S. A practical relativistic model of microarcsecond astrometry in space. A.J., v. 125, 1580–1597, 2003.

[6] Kopeikin, S.M., V.V. Makarov. Astrometric effects of secular aberration. A.J., v. 131, 1471–1478, 2005.

[7] Pyne, T., C.R. Gwinn, M. Birkinshaw, et al. Gravitational Radiation and Very Long Baseline Interferometry. Astrophys. J., v. 465, 566–577, 1996.

[8] Kristian, J., R.K. Sachs. Observations in cosmology. Astrophys. J., v. 143, 379–399, 1966.

[9] MacMillan, D.S. Quasar apparent proper motions observed by geodetic VLBI networks. Future Directions in High Resolution Astronomy, The 10th Anniversary of the VLBA. Romney, J.D. and M.J. Reid (eds.), astro-ph/0309826v1, 2003.

[10] Titov, O. Proper motion of reference radio sources. astro-ph/0804.1403, 2008.

[11] Malkin, Z., O. Titov. Optical characteristics of astrometric radio sources. This volume.

[12] Titov, O. Construction of a celestial coordinate reference frame from VLBI data. Astron. Rep., v. 48, 941–948, 2004.

[13] Feissel-Vernier, M. Selecting stable extragalactic compact radio sources from the permanent astrogeodetic VLBI program. Astron. Astrophys., v. 403, 105–110, 2003.

The 5th IVS General Meeting Proceedings, 2008, p. 270–274

Comparison of Radio Source Positions from Individual Solutions

Sergei Bolotin, Svitlana Lytvyn

Main Astronomical Observatory, National Academy of Sciences of Ukraine, Ukraine

Abstract. Various VLBI analysis centers that participate in the IVS/IERS Working Group on ICRF-2 provided their results of source coordinate estimations as well as time series of source position variations. In this presentation results of a comparison of these catalogs are discussed.

1. Introduction

The International Celestial Reference Frame (ICRF) is realized by positions of extragalactic radio sources which are obtained from data analysis of geodetic and astrometric VLBI observations. Efforts of many VLBI analysis centers are focused on producing new solutions of source coordinates in the frame of the international project ICRF-2, the second realization of the ICRF (e.g., [3]).

In order to study systematic errors in the construction of celestial reference frames, two types of solutions were obtained by various analysis centers: "catalog" and "time series". A purpose of the first type of solutions is to investigate systematic effects in realizations of celestial reference frame (CRF) by different analysis centers. The second type of solutions is aimed at studies of stability of sources positions and selection of so-called DEFINING radio sources for the ICRF-2 implementation.

In this article the results of catalog comparisons are presented. Also, preliminary results of time series analysis are shown.

2. Comparisons of Catalogs

Four VLBI analysis centers submitted solutions for the celestial reference frame. The general characteristics of the obtained catalogs and the reference catalog ICRF-Ext.2 [1] are presented in Tabl. 1. The σ_α and σ_δ columns of the table correspond to mean formal uncertainties of the solutions in right

ascension and declination. The solutions are based on almost the same set of VLBI observations, collected since 1979 until mid-2007. The exception is the inclusion of the VCS sessions in two of the solutions (aus000a and mao000a) and their omission in the other two solutions.

Table 1. General characteristics of CRF solutions

Solution ID	Number of Sources	σ_α, μas	σ_δ, μas	Software	Analysis Center
ICRF-Ext.2	717	1224	1243		
aus000a	1515	1433	1752	OCCAM6.2	Geoscience Australia
gsf000a	923	473	521	CALC/SOLVE	NASA GSFC
mao000a	2541	529	888	SteelBreeze	MAO NASU
usn000a	923	523	521	CALC/SOLVE	US Naval Observatory

A comparison of the catalogs was performed in the following way: first, the parameters of a model of transformation between two catalogs were estimated with the least squares method. Then, the model was applied to coordinates of one of the catalogs and weighted root mean square residuals were calculated for the right ascension and declination.

We applied a transformation model similar to the one was used in the IERS Annual Reports (e.g, [2]), with added harmonic terms. The differences in right ascension, $\Delta\alpha$, and declination, $\Delta\delta$, are presented as:

$$\begin{aligned}\Delta\alpha &= A_1 \tan\delta \cos\alpha + A_2 \tan\delta \sin\alpha - A_3 + D_\alpha(\delta - \delta_0) + C_\alpha \sin(\alpha + \varphi_\alpha),\\ \Delta\delta &= -A_1 \sin\alpha + A_2 \cos\alpha + D_\delta(\delta - \delta_0) + B_\delta + C_\delta \sin(\alpha + \varphi_\delta),\end{aligned}$$

where A_1, A_2, and A_3 are small angles of global rotations about three axes; D_α and D_δ are slopes in right ascension and declination as functions of declination; B_δ is a bias in the declination; C_α, φ_α and C_δ, φ_δ are amplitudes and phases of harmonic oscillations in right ascension and declination.

Table 2. Number of common sources in the catalogs (all, defining)

ID	aus000a		gsf000a		mao000a		usn000a	
ICRF-Ext.2	572	210	708	212	665	211	717	212
aus000a			678	210	1231	210	671	210
gsf000a					800	211	905	212
mao000a							798	211

To calculate the parameters of the model, the coordinates of common (between twoh catalogs) DEFINING radio sources were used. Then, after the model was applied, the WRMS were evaluated for the whole set of common radio sources. The numbers of common DEFINING and all sources for each pair of catalogs are presented in the Tabl. 2.

Table 3. Comparison of catalogs: ICRF.Ext-2 vs individual solutions

A_1, μas	A_2, μas	A_3, μas	D_α, μas/rad	D_δ, μas/rad	B_δ, μas	S_α, μas	φ_α, deg	S_δ, μas	φ_δ, deg
ICRF-Ext.2 – aus000a									
−16.7	6.4	−51.4	−79.1	−193.3	173.9	65.0	62.0	91.7	148.5
118.1	106.4	76.7	139.6	70.2	60.1	98.5	87.0	137.2	80.7
ICRF-Ext.2 – gsf000a									
58.7	−7.7	−19.7	−25.0	0.8	−3.1	33.2	55.8	78.6	349.3
36.5	32.3	23.5	42.8	21.5	18.4	30.1	52.6	42.5	28.5
ICRF-Ext.2 – mao000a									
61.7	76.0	−37.2	−27.7	−28.1	6.7	50.8	75.0	58.4	350.2
40.0	35.7	25.9	47.1	23.8	20.4	33.6	37.2	46.7	42.4
ICRF-Ext.2 – usn000a									
90.2	−48.4	−35.7	−43.7	0.4	−10.4	48.5	141.2	100.5	17.3
39.4	35.0	25.6	46.4	23.1	19.9	33.3	38.5	45.2	24.7

The results of the least squares estimation of model parameters are given in Tabl. 3 and 4. Tabl. 3 shows the comparison of the reference catalog, ICRF-Ext.2, with the individual solutions. Mutual comparisons between the individual solutions are presented in Tabl. 4. In the tables the first lines for each pair

Table 4. Comparison of catalogs: mutual comparison of individual solutions

A_1, μas	A_2, μas	A_3, μas	D_α, μas/rad	D_δ, μas/rad	B_δ, μas	S_α, μas	φ_α, deg	S_δ, μas	φ_δ, deg
aus000a – gsf000a									
19.8	−69.4	31.4	32.8	17.7	−21.0	32.7	70.3	26.6	36.6
26.7	25.8	19.3	33.3	19.4	16.8	23.1	40.4	28.3	69.0
aus000a – mao000a									
27.8	1.0	18.2	45.6	7.6	−37.0	50.9	77.5	24.3	79.4
25.0	25.6	19.9	33.0	19.7	17.6	22.3	27.0	28.9	69.8
aus000a – usn000a									
51.8	−112.6	22.0	33.0	36.2	−47.8	51.4	132.3	64.1	49.8
42.2	40.6	29.8	52.4	31.2	27.1	34.1	42.0	45.0	45.4
gsf000a – mao000a									
15.8	78.6	−13.0	13.8	−6.2	−19.0	15.1	100.7	6.4	162.1
6.5	6.6	5.1	8.6	5.4	5.0	5.4	23.9	7.8	66.7
gsf000a – usn000a									
30.8	−51.9	−11.6	−3.2	−2.5	−7.8	39.4	169.2	39.6	72.1
5.2	5.1	3.8	6.7	4.2	3.8	4.6	6.4	5.9	9.0
mao000a – usn000a									
16.3	−131.1	0.6	−16.8	4.2	9.0	34.6	192.1	40.0	60.1
7.6	7.7	5.9	10.1	6.4	5.9	7.3	10.4	8.7	13.3

of catalogs give the estimated values, on the second lines standard deviations are shown. Here, the parameters A_1, A_3, A_3, B_δ, S_α, and S_δ are measured in μas; units for D_α and D_δ are μas/rad, and the phases φ_α and φ_δ are in degrees.

In Tabl. 5 weighted post-fit residuals are shown. The residuals were evaluated for each pair of the catalogs after the estimated models of transformation were removed.

Table 5. Weighted post-fit residuals ($\Delta\alpha\cos\delta$, $\Delta\delta$), μas

ID	aus000a		gsf000a		mao000a		usn000a	
ICRF-Ext.2	206	659	263	228	279	257	280	254
aus000a			128	178	106	180	133	319
gsf000a					34	44	31	34
mao000a							42	52

The comparisons between the individual solutions and the current realization of the ICRF, ICRF-Ext.2, reveals shortcomings of the latter. The fact that the standard deviations of the parameters of the transformation model between recent solutions are about five–six times smaller than those obtained from comparisons with ICRF-Ext.2 indicates that the coordinates of most of the DEFINING radio sources should be improved.

Also, the results show that the solution aus000a differs significantly from the other three solutions. The solutions gsf000a, mao000a, and usn000a are close; however, there are systematic effects between them. It is interesting to note that the solutions gsf000a and usn000a are obtained with the same software and for the same set of data; nonetheless, there are systematic differences between them.

To study the systematic effects in catalogs of radio sources more solutions are necessary, especially those obtained with OCCAM and QUASAR software.

3. Comparisons of Time Series

Time series of source positions usually are estimated simultaneously with the Earth orientation parameters for each session. Therefore they are presented in its own CRF, unique for each session. Before starting an investigation of source variability, one has to transform the CRF solutions of each session onto some reference celestial frame. On the other hand, the length of arc connecting two radio sources is invariant to the chosen CRF. Therefore, studying the variability of the arc lengths, it is possible to infer the stability of the radio sources.

Time series of three arcs, which form a closed triangle with radio sources 0955+476, 2145+067 and 2234+282, are shown in Fig. 1. These arc lengths are evaluated using gsf001a. From the plots it is obvious to conclude that the radio sources 0955+476 and 2145+067 are stable, while the position of the source 2234+282 is varying with time.

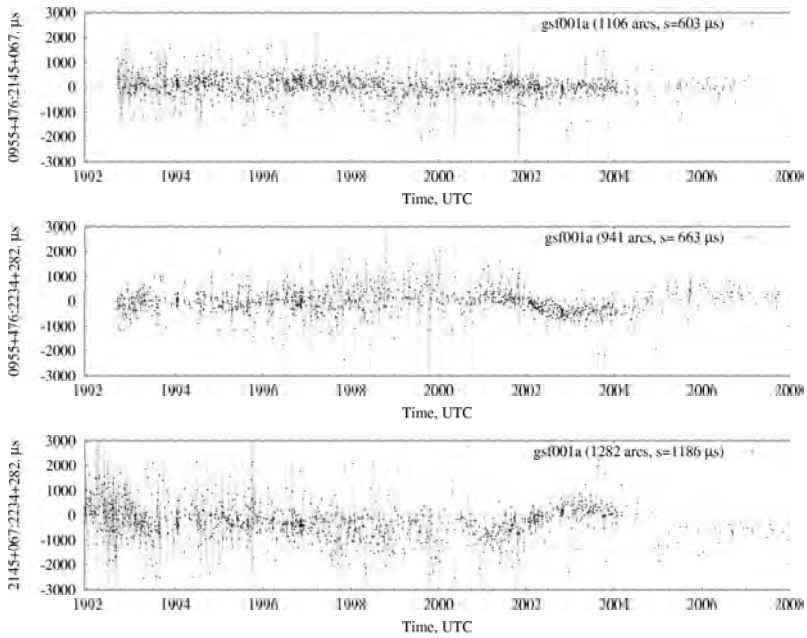

Figure 1. Time variability of the arc lengths between three radio sources

Acknowledgements

The authors are grateful to the VLBI analysis centers that provided the results of estimation radio source positions. Our solution is based on the VLBI observations provided by the International VLBI Service for Geodesy and Astrometry [4].

References

[1] Fey, A.L., C. Ma, E.F. Arias, et al. The second extension of the International Celestial Reference Frame: ICRF-Ext.2. A.J., v. 127, 3587–3608, 2004.

[2] IERS Annual Report 1993. Observatoire de Paris, Paris, France, 1994.

[3] Ma, C. Progress in the 2nd Realization of the ICRF. Proc. Journées 2007, The Celestial Reference Frame for the Future. Paris, France (in print).

[4] Schlueter, W., E. Himwich, A. Nothnagel, et al. IVS and Its Important Role in the Maintenance of the Global Reference Systems. Advances in Space Research, v. 30, No 2, 145–150, 2002.

The 5th IVS General Meeting Proceedings, 2008, p. 275–278

Comparison and Combination of CRF Catalogs

Julia Sokolova, Zinovy Malkin

Central Astronomical Observatory at Pulkovo, Russian Academy of Sciences, Russia

Abstract. In 2007, a joint IERS/IVS Working Group has been established to consider practical issues of creating the next generation ICRF, ICRF-2. The goal of the WG is to seek after ways to improve the existing ICRF. In this study we investigate a possibility of ICRF improvement by means of using a combined ICRF catalog instead of a catalog computed at a single analysis center, even though using most advanced models and software. In this work, we present a new version of the Pulkovo combined catalog of radio source positions computed using the method proposed in [5]. Radio source catalogs that were submitted in 2007 in the framework of the WG activity were used as input for mutual comparison and combination. Four combined catalogs have been calculated: the first two provide a stochastic improvement of the ICRF, and the other two allow us to account also for systematic errors in the current ICRF version.

1. Introduction

The celestial reference frame (CRF), as realized by a set of coordinates for selected celestial objects, is widely used for numerous astronomy, navigation, time and other measurements. The CRF accuracy and stability are all-important for successful solutions of all these tasks. After publishing the first VLBI radio source catalog (RSCs), attempts were made to improve the accuracy of radio-band CRF by means of constructing combined catalogs, as it was customary in optical astronomy, where fundamental catalogs served as an international standard for astrometry and other measurements on the sky. Different methods were used to obtain a combined RSC, e.g. [1, 2, 3, 4] Also, up to 1995, the IERS (International Earth Rotation Service, now International Earth Rotation and Reference Systems Service) used derived combined RSC for the maintenance of the IERS Celestial Reference Frame. In 2007, a joint IERS/IVS Working Group has been established to consider practical issues of creating the next generation ICRF, dubbed ICRF-2. The goal of the WG is to seek after ways to improve the existing ICRF. Large experience accrued by optical astrometry over centuries shows that combining catalogs of star positions

leads to better random and systematic accuracy than individual catalogs. In this work, we present a new version of the Pulkovo combined catalog of radio source positions computed using the method proposed in [5]. Radio source catalogs that were submitted in 2007 in the framework of the WG activity were used as input for mutual comparison and combination. Four combined catalogs have been calculated.

1. The first two catalogs (the first has been calculated using all input catalogs, while the second one used only catalogs obtained with the CALC/SOLVE software) provide a stochastic improvement of the ICRF.
2. The other two catalogs allow us to account also for systematic errors in the current ICRF version.

All computations have been done for the set of 194 ICRF defining sources included in all input catalogs.

2. Input Catalogs and Comparisons

Table 1. Information about input catalogs

IVS Centre	Soft	Time span (mon/yr)	# of delays	# of sources
AUS, Australia	OCCAM	11/1979 - 04/2007	2647809	1515 (212 def)
BKG, Germany	Calc/Solve	01/1984 - 10/2007	5156489	1076 (212 def)
DGFI, Germany	OCCAM	01/1980 - 01/2005	3650771	686 (199 def)
CGS, Italy	Calc/Solve	08/1979 - 07/2006	4640972	625 (161 def)
USNO, USA	Calc/Solve	08/1979 - 05/2007	5238056	923 (212 def)
GSFC, USA	Calc/Solve	08/1979 - 03/2007	5510462	923 (212 def)
MAO, Ukraine	SteelBreeze	04/1980 - 05/2007	5194922	2541 (26 def)
IAA, Russia	QUASAR	08/1979 - 05/2007	5116010	907 (212 def)

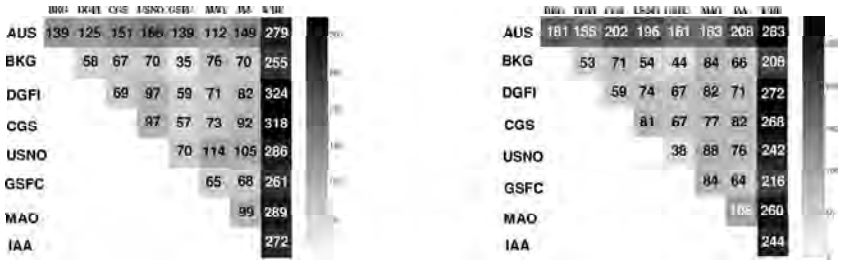

Figure 1. WRMS of the intercomparison of the source coordinates by $\Delta\alpha$ (left) and by $\Delta\delta$ (right) for 194 common sources. Unit: microarcseconds

Weighted root-mean-square (WRMS) differences of the radio source coordinates between the input catalogs and ICRF are shown in Fig. 1. One can see

from Fig. 1 that WRMS differences have the smallest values for catalogs computed with the Calc/Solve software, both in intercomparisons of these catalogs and in comparison with the ICRF. The latter is most probably caused by the fact that the ICRF was constructed using the Calc/Solve software. Moreover, it can be clearly seen that all the input catalogs demonstrate rather large differences with the ICRF, which may indicate significant systematic errors in the latter.

3. Combined Catalogs

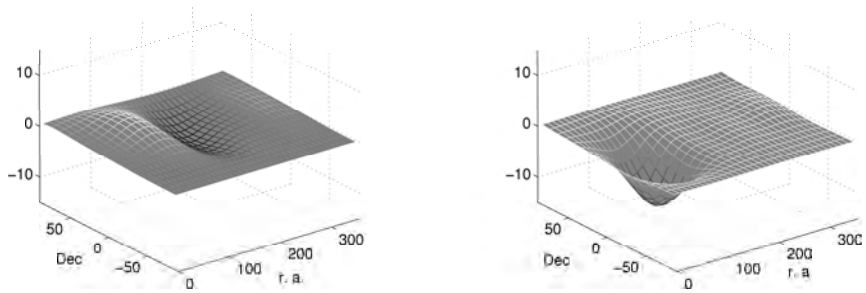

Figure 2. PUL08C01a – ICRF, by $\Delta\alpha$ (left) and by $\Delta\delta$ (right), Unit: mas

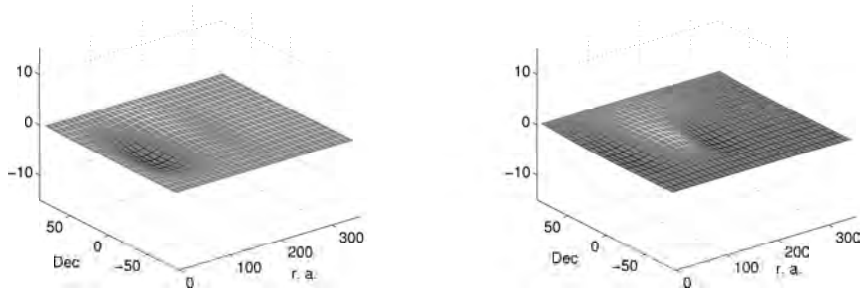

Figure 3. PUL08C01b – ICRF, by $\Delta\alpha$ (left) and by $\Delta\delta$ (right), Unit: mas

The systematic differences between the input catalogs and the ICRF found by LF method were applied to all the input catalogs in order to transform them into the ICRF system. After that, the coordinates of all sources in the transformed catalogs were averaged with weights depending on the formal errors of the coordinates. As a result, the combined catalog PUL08C01a and PUL08C01b (only input catalogs constructed using CALC/SOLVE were used) were constructed.

Fig. 2 shows the systematic differences between the combined catalog PUL08C01a and the ICRF. One can see that the catalog PUL08C01a rep-

resents the ICRF system at a level of about 10 μas.

Fig. 3 shows the systematic differences between the combined catalog PUL08C01b and the ICRF. The catalog PUL08C01b represents the ICRF system at a level of about 5 μas.

4. Short Summary

Four combined radio source catalogs have been constructed. The first two of them, PUL08C01a and PUL08C01b, can be considered as stochastic improvement of the current realization of ICRF. The final combined catalogs PUL08C02a and PUL08C02b provide both stochastic and systematic improvements of the ICRF.

References

[1] Walter, H.G. Astron. Astrophys., 210, 455, 1989.

[2] Walter, H.G. Astron. Astrophys. Suppl. Series, 79, 283, 1989.

[3] Yatskiv, Ya.S., A.N. Kur'yanova. Inertial Coordinate System on the Sky. Proc. 141th IAU Symp. J.H. Lieske, V.K. Abalakin (eds.), 1990, 295.

[4] Kur'yanova, A.N., Ya.S. Yatskiv. Kinemat. Fiz. Nebesnyh Tel, 9, 15, 1993.

[5] Sokolova, Ju., Z. Malkin. Astron. Astrophys., v. 474, 2007, 665–670.

The 5th IVS General Meeting Proceedings, 2008, p. 279–283

Source Selection for NNR Constraints from Source Position Time Series

Sergey Kurdubov, Elena Skurikhina

Institute of Applied Astronomy, Russian Academy of Sciences, Russia

Abstract. Time series for more than 600 sources were calculated using the QUASAR software for VLBI data processing. Source positions for every source were obtained from single series analysis by fixing the coordinates of all other sources. A priori source positions were used from the ICRF-Ext.2 radio source position catalog. Time series analysis is performed with covariation analysis technique. The global solutions with different sets of sources for NNR constraints were obtained. Transformation parameters between obtained source catalogs were calculated and compared.

1. Introduction

The main goal of this study is to propose the parameter which can be used for selecting stable and unstable sources from the analysis of source position time series. We calculate the covariance function for the time series and try to use its second point as the characteristic parameter. Its value shows how much the time series was correlated independent of the way it was correlated (random walk, piece-wise linear, or any other technique).

The source position time series iaa000b, iaa000c were calculated using the QUASAR software [1, 4]. Most available VLBI observations (excluding DSN and VCS sessions) between Aug. 1979 and May 2007 were used. The time series were generated from a single session solution for each source: one source for the session with the coordinates of all other sources fixed. The station positions were not estimated for both series. The TRF was fixed to ITRF2005, the CRF was fixed to ICRF-Ext.2. The following parameters were estimated in these solutions: position of one source, EOP (X_p, Y_p, $UT1 - UTC$, X_c, Y_c) (only for iaa000b solution), WZD (linear trend and stochastic), troposphere gradient east and north, station clock offset (quadratic trend and stochastic).

We use the covariance functions from the time series analysis. Because there are no standard algorithms for obtaining covariance functions of non-equidistant time series, we use the following two methods.

First method.

For non-equidistant time series:

$$\{x_i\}_{i=1}^{N},\ x_i = x(t_i),\ t_1 < t_2 < ... < t_N,\ i = 1, ..., N. \tag{1}$$

Estimation of the covariance function for equidistant time shifts:

$$\tau_k = \Delta\tau \cdot k,\ \Delta\tau = \frac{t_N - t_1}{M}, k = 0, ..., M-1,\ M < N,$$

was calculated by formula

$$q(\tau_k) = \frac{M-k}{M}\left(\sum_{i,j:\tau_k<|\gamma_{ij}|<\tau_{k+1}} x_i x_j\right)/m_k, k = 0, 1, ..., M-1.$$

Here $\gamma_{ij} = t_i - t_j$ and m_k — the number of γ_{ij} in the range from τ_k to τ_{k+1}. The $\Delta\tau$ was chosen to 14 days.

Second method.

Estimation of the covariance function q_k for non-equidistant averaged time shifts τ_k:

$$q_k = \frac{\sum_{j=k+1}^{N-k} x_{k+j} x_j}{N},\ \ \tau_k = \frac{\sum_{j=k+1}^{N-k}(t_{k+j} - t_j)}{N-k},\ k = 0, 1, 2, ..., N-1. \tag{2}$$

Using these methods we obtained covariance functions for all time series of all analysis centers (the data are available on the ftp server of the WG on ICRF-2). The covariance functions for long time series are similar and in further computations we use the first one.

In the further analysis, we use the values of q_1 — the second point of the covariance function. The first point q_0 is the variance of the time series. But the second point characterizes the variance of the correlated part in the time series.

The second point of the covariance function shows how much the time series are correlated independent of the origin of the correlation (random walk, piece-wise linear, or any other technique).

We calculated the coefficient $k = Max(q_1^{RA*cos(DE)}, q_1^{DE})$ for each time series with more than 75 sessions and used it to estimate how stable the sources are. The list of 140 sources was obtained and sorted by our stability criteria. In Tabl. 1 the most stable sources are shown ($k < 0.1$) and in Tabl. 2 most unstable sources are shown ($k > 0.5$). 15 sources from Tabl. 1 are contained in M. Feissel's list of stable sources and four sources from Tabl. 2 are in the unstable list.

2. Global solutions

In order to test our stability criteria described above, we calculated 15 VLBI global solutions using various sets of sources from our list of NNR constraints the origin of the Celestial Reference Frame.

A short description of these solutions is as follows:

Table 1. First 20 most stable sources ($k < 0.1$)

Source	N_{sess}	k	Source	N_{sess}	k	Source	N_{sess}	k
1351-018	489	0.040	1255-316	121	0.078	1908-201	386	0.096
0111+021	109	0.048	1606+106	1854	0.082	0743+259	400	0.096
1128+385	955	0.049	1652+398	218	0.087	0642+449	937	0.096
2318+049	426	0.060	0556+238	385	0.089	0804+499	1115	0.096
0201+113	378	0.065	1417+385	173	0.091	0602+673	328	0.097
2209+236	139	0.068	1144+402	93	0.093	0749+540	630	0.098
0133+476	1027	0.076	0657+172	112	0.095			

Table 2. Last 11 most unstable sources ($k > 0.5$)

Source	N_{sess}	k	Source	N_{sess}	k	Source	N_{sess}	k
0355+508	269	0.556	1354+195	78	0.688	1642+690	96	0.852
2128-123	558	0.573	1053+815	351	0.725	1253-055	140	1.212
1641+399	813	0.575	2007+777	224	0.777	0316+413	96	1.305
1226+023	709	0.581	1313-333	99	0.835			

- celestial reference frame: ICRF-Ext.2,
- terrestrial reference frame: VTRF2005,
- IAU2000A precession-nutation model,
- definition of the origin TRF by NNR/NNT constraints for 11 stations,
- estimated parameters: celestial frame: right ascension, declination (global), terrestrial frame: X, Y, Z, rates (global), Earth orientation: X_p, Y_p, $UT1 - TAI$, X_c, Y_c (local), zenith troposphere delay: linear+stochastic signal (local), troposphere gradient: east and north (local), station clocks: quadratic+stochastic signal (local).

Definition of the origin CRF.

- In the solutions $q55_1$ through $q55_5$ for NNR constraints, 55 sources were used from the first 65 most stable sources excluding the first 10 for $q55_1$, excluding the second 10 sources for $q55_2$, etc.
- In the solutions q65 through q140 for NNR constraints between 65 and 140 sources were used from our list correspondingly.
- Solution q212 used 212 ICRF defining sources for NNR constraints.

3. Comparison of Obtained CRF Catalogues

The 15 catalogs obtained were compared with the ICRF original catalog. Transformation parameters for M. Feissel's list of 199 stable sources were calculated using the standard IERS transformation model with 6 parameters:

$$\Delta\alpha = A_1 \tan\delta \cos\alpha + A_2 \tan\delta \sin\alpha - A_3 + D_\alpha(\delta - \delta_0),$$

$$\Delta\delta = -A_1 \sin\alpha + A_2 \cos\alpha + D_\delta(\delta - \delta_0) + B_\delta,$$

here parameters A_1, A_2, A_3 represent the rotation angles between two catalogs and $D_\alpha, D_\delta, B_\delta$ the deformations. Transformation parameters are shown in Tabl. 3 and 4.

Table 3. Transformation parameters (rotation angles) between obtained solutions and ICRF-Ext.2

Sol. ID	$A_1, \mu as$	$A_2, \mu as$	$A_3, \mu as$
$q55_1$	-7.1 ± 10.4	19.1 ± 9.7	-1.6 ± 11.6
$q55_2$	-7.1 ± 10.4	30.8 ± 9.8	-7.5 ± 11.7
$q55_3$	-16.2 ± 10.3	17.3 ± 9.7	-6.0 ± 11.5
$q55_4$	-9.6 ± 10.4	18.3 ± 9.7	-6.0 ± 11.6
$q55_5$	3.5 ± 10.3	16.1 ± 9.7	-14.1 ± 11.5
q65	-7.8 ± 10.4	20.6 ± 9.7	-8.4 ± 11.6
q75	-1.5 ± 10.3	22.9 ± 9.7	-12.6 ± 11.5
q85	-4.0 ± 10.4	26.4 ± 9.7	-14.5 ± 11.6
q95	-6.4 ± 10.4	28.1 ± 9.7	-15.7 ± 11.6
q105	-9.7 ± 10.4	25.7 ± 9.7	-20.4 ± 11.6
q115	-9.0 ± 10.4	25.0 ± 9.7	-21.3 ± 11.6
q125	-8.2 ± 10.4	29.1 ± 9.7	-26.4 ± 11.6
q135	-5.5 ± 10.4	25.9 ± 9.7	-27.3 ± 11.6
q140	-2.9 ± 10.4	23.7 ± 9.7	-25.6 ± 11.6
q212	-4.1 ± 10.4	-41.4 ± 9.7	23.2 ± 11.6

4. Discusson

We try to use our stability criteria based on covariation analysis for forming the best set of sources for NNR constraints for global solutions. When we used the sets of most stable sources (first part of Tabl. 3) for the constraints, the obtained catalogs had different rotation angles (A2 from 16 μas to 30 μas with formal errors of 10 μas). However, the analysis shows the difference between the rotation angles of q212 catalog and all others. We can surmise that this is due to the presence of sources with short observation history in the list of defining sources, because even most unstable sources in our list have more than 75 sessions of observations. This conclusion needs to be tested.

Table 4. Transformation parameters (deformations) between obtained solutions and ICRF-Ext.2

Sol. ID	$D_\alpha, \mu as$	$D_\delta, \mu as$	$B_\delta, \mu as$
$q55_1$	0.0±0.4	-0.2 ± 0.3	-1.7 ± 11.3
$q55_2$	0.2±0.4	-0.3 ± 0.3	2.0 ± 11.4
$q55_3$	0.1±0.4	-0.3 ± 0.3	1.9 ± 11.3
$q55_4$	0.0±0.4	-0.1 ± 0.3	-9.4 ± 11.3
$q55_5$	0.0±0.4	-0.1 ± 0.3	-10.6 ± 11.3
q65	-0.1 ± 0.4	-0.2 ± 0.3	-4.9 ± 11.3
q75	0.4±0.4	-0.2 ± 0.3	-0.5 ± 11.3
q85	0.6±0.4	-0.2 ± 0.3	-7.1 ± 11.3
q95	0.6±0.4	-0.1 ± 0.3	-13.0 ± 11.3
q105	0.6±0.4	-0.2 ± 0.3	-8.9 ± 11.3
q115	0.6±0.4	-0.2 ± 0.3	-6.2 ± 11.3
q125	0.6±0.4	-0.2 ± 0.3	-4.6 ± 11.3
q135	0.6±0.4	-0.2 ± 0.3	-3.4 ± 11.3
q140	0.6±0.4	-0.2 ± 0.3	-0.7 ± 11.3
q212	0.6±0.4	-0.5 ± 0.3	22.3 ± 11.3

References

[1] Gubanov, V., Yu. Rusinov, I. Surkis, et al. Project: Global Analysis of 1979-2004 VLBI Data. Proc. IVS 2004 General Meeting. N. Vandenberg and K. Baver (eds.), NASA, 2004, 315–319.

[2] Ma, C., et al. The International Celestial reference Frame as Realized by Very Long Baseline Interferometry. A.J., v. 116, 516–546, 1998.

[3] Fey, A., et al. The Second Extension of the International Celestial reference Frame: ICRF-Ext.2. A.J., v. 127, 3587–3608, 2004.

[4] Kurdubov, S. QUASAR software in IAA EOP service: Global Solution and Daily SINEX. EVGA Proceedings. J. Boem, A. Pany, H. Schuh (eds.), ISSN 1811-8380, 2007, 79–81.

[5] Feissel-Vernier, M. Selecting stable extragalactic compact radio sources from the permanent astrogeodetic VLBI program. Astronomy and Astrophysics Manuscript No MS3523, 2003.

The 5th IVS General Meeting Proceedings, 2008, p. 284–288

Extending the ICRF above S/X-band: X/Ka-band Global Astrometric Results

Christopher Jacobs [1], *Ojars Sovers* [2]

[1] *Jet Propulsion Laboratory, California Institute of Technology, USA*

[2] *Remote Sensing Analysis Systems Inc., USA*

Abstract. In order to extend the International Celestial Reference Frame from its S/X-band (2.3/8.4 GHz) basis to a complementary frame at X/Ka-band (8.4/32 GHz), we began an ongoing series of X/Ka observations starting in mid-2005 using NASA's Deep Space Network (DSN) radio telescopes. This paper will report global astrometric results from the first 33 sessions. These sessions covered the full 24 hours of right ascension and declination down to −45 degrees. Our analysis produced a radio frame of 318 sources with median formal position uncertainties of ≈ 0.25 mas. A comparison of our X/Ka-band frame against S/X-band shows WRMS differences of ≈0.25 mas. These differences include zonal errors the largest of which is a trend vs. declination. We will discuss our error budget including systematic errors from limited sensitivity, mis-modelling of the troposphere, and uncalibrated instrumental effects. We will discuss our plan for addressing the current limiting errors and the resulting prospects for improved accuracy over the next few years.

1. Introduction

For almost three decades now, radio frequency work in global astrometry, geodesy, and deep space navigation has been done at S/X-band (2.3/8.4 GHz). While this work has been tremendously successful in producing 100 μas level global astrometry [3] and sub-cm geodesy, developments made over the last decade have made it possible to consider the merits of moving to a new set of dual-band frequencies. In this paper we present global astrometric results from X/Ka-band (8.4/32 GHz) observations. Complementary single-band results at 24 and 43 GHz are presented by Lanyi (this volume).

Moving the observing frequencies up by approximately a factor of four has several advantages. For our work in the Deep Space Network, the driver is the potential for higher telemetry data rates to and from probes in deep space. Other advantages include: 1) the spatial distribution of flux becomes significantly more compact lending hope that the positions will be more stable

over time, 2) Radio Frequency Interference (RFI) at S-band would be avoided, 3) ionosphere and solar plasma effects on group delay and signal coherence are reduced by a factor of 15!

While these are very significant advantages, there are also disadvantages. The change from 2.3/8.4 GHz to 8.4/32 GHz moves one closer to the water vapor line at 22 GHz and thus increases the system temperature from a few Kelvins per atmospheric thickness up to 10-15 Kelvins per atmosphere or more. Thus one becomes much more sensitive to weather. Furthermore, the sources themselves are in general weaker and many sources are resolved. Also, with the observing wavelengths shortened by a factor of 4, the coherence times are shortened so that practical integration times are a few minutes or less-even in relatively dry climates. The shorter wavelengths also imply that the antenna pointing accuracy requirements must be tightened by the same factor of 4. The combined effect of these disadvantages is to lower the system sensitivity. Fortunately, recent advances in recording technology (cf. Whitney, this volume) make it feasible and affordable to offset these losses in sensitivity by recording more bits. Thus while the X/Ka results presented in this paper used the same overall bit rate as previous S/X work, efforts are now underway to increase our bit rate by a factor of 4 to 8 within the next few years.

This paper is organized as follows: We will describe the observations, modelling, and present the results. Next, we will estimate the accuracy by comparing to a recent S/X celestial reference frame. This will be complemented by a discussion of the error budget. Finally, we will provide conclusions and anticipated directions for further research.

2. Observations and Modelling

The results presented here are from 33 VLBI observing sessions of 24 hour duration done from July 2005 until Jan. 2008 using NASA's Deep Space Stations (DSS) 25 or 26 in Goldstone, California to either DSS 34 in Tidbinbilla, Australia or DSS 55 outside Madrid, Spain to form interferometric baselines of 10,500 and 8,400 km length, respectively.

We recorded VLBI data simultaneously at X (8.4 GHz) and Ka-band (32 GHz) sampling each band at a rate of 56 Mbps. Each band's 7 channels (each ± 2 MHz) spanned a bandwidth of $\approx$360 MHz. The data were filtered, sampled, and recorded to tape using the MKIV VLBI system. The data were then correlated with the JPL BlockII correlator [5]. Fringe fitting was done with the FIT fringe fitting software [2]. This procedure resulted in 6363 pairs of group delay and phase rate measurements covering the full 24 hours of right ascension and declinations down to -45 deg. Each observation was approximately 2 minutes in duration.

The above described set of observations were then modelled using the MODEST software [6]. A priori Earth orientation was fixed to the MHB nutation model [4] and empirically determined UT1-UTC and Polar Motion from the Space 2006 series [1]. The celestial frame was aligned to the ICRF [3] by fixing

the RA and Dec of OJ 287 and the declination of CTD 20. Station locations were estimated, but velocities were fixed to a decades-long S/X-band VLBI estimates.

3. Results

In all, we detected 318 extragalactic radio sources which covered the full 24 hours of RA and declinations down to $-45°$. In Fig. 1 below, these sources are plotted using an Aitoff projection to show their locations on the sky. RA=0 is at the center. The ecliptic plane is shown by a dashed line and the Galactic plane is indicated as a black line shaped approximately like an Ω. The sources are coded according to their 1-σ formal declination uncertainties with the value ranges indicated in the figure's legend. Note that the declination precision decreases as one moves toward the south. This is a result of having significantly less data on the California to Australia baseline combined with the need to observe sources closer to the horizon as declination moves south thus incurring greater error from higher system temperatures and tropospheric mismodelling.

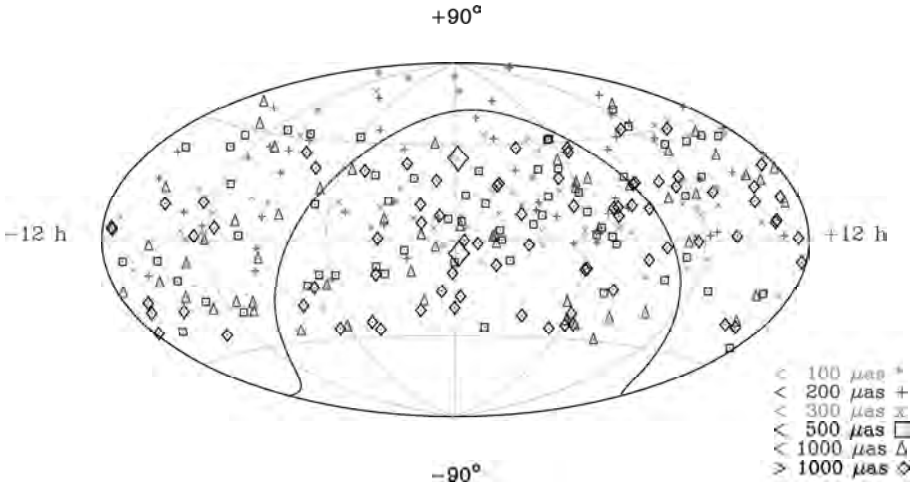

Figure 1. Distribution of 318 X/Ka-band sources detected to date. Symbols indicate 1-σ formal declination uncertainties with size bins defined in the legend at lower right. $(\alpha, \delta) = (0, 0)$ is at the center.

4. Accuracy and Zonal Errors

Experience shows that formal uncertainties tend to underestimate true errors. External estimates of errors were obtained by comparing our X/Ka-band RA and declinations to estimates from our analysis of S/X data covering the

period 1978–2007. For 255 common sources, the weighted RMS (WRMS) differences are 241 μas in RA cos(dec) and 290 μas in declination. These differences reveal decreasing accuracy RA and declination as one moves south.

In astrometry, it is usually much easier to measure the relative positions of nearby sources than to accurately measure sources that are separated by long arcs. In order to investigate this tendency, we calculated for both X/Ka and S/X the arclengths between all pairs of sources, binned them in 5 deg bins and then differenced the arcs. We then took the mean arclength difference for each bin. As expected, arclengths agree better for short arcs and gradually worsen as arcs grow longer out to a mean difference of 70 μas at arcs of 90 deg. This is one measure of the level of zonal errors in our comparison.

5. Error Budget and Conclusions

Having assessed the size of errors in our positions using the much larger S/X data set as a standard of accuracy, we now discuss the major contributions to the errors of the X/Ka measurements: SNR, instrumentation, and troposphere. Fig. 2 shows the weighted RMS group delay vs. log10 of the Ka-band SNR. We conclude that for SNR < 30, the thermal error dominates the error budget. For higher SNRs, troposphere and instrumentation errors become important. Binning of WRMS delay vs. airmass thickness shows that troposphere is not the dominant error due to the generally low SNRs just mentioned. However, the phase rates (which carry much less weight in the fit) are dominated by errors from tropospheric mismodelling, thus hinting that troposphere will become more important as our SNR improves. The last major category of errors comes from un-calibrated instrumentation. A proto-type phase calibrator has been developed for calibrating from the feed to the digitizer. Test data indicate an approximately diurnal instrumental effect with $\approx$180 ps RMS. Although the data themselves can be used to partially parametrize this effect, we believe that phase calibrators will be needed in order to achieve accuracy of better than 200 μas in a timely manner.

Conclusions: The S/X-band ICRF has now been extended to the four times higher frequency of X/Ka-band (8.4/32 GHz). A total of 318 sources have been successfully detected. For the 255 sources with sufficient overlap to warrant comparison to S/X results, we find positional agreement of 241 μas in RA cos(declination) and 290 μas in declination with zonal errors of 70 μas.

As positive as these results are, we note that our X/Ka work still relies on ongoing S/X work for various geophysical models (nutation, precession, UT1−UTC). Thus it will be premature to speak of ending S/X observations for many years to come. Our current limiting errors are SNR and lack of instrumental phase calibration. We plan to address the SNR issue by increasing the recorded bit rate by a factor of 4–8. A proto-type phase calibrator has been built and we are seeking funding for operational units. If these goals are achieved, we believe that we can achieve 200 μas or better by 2010.

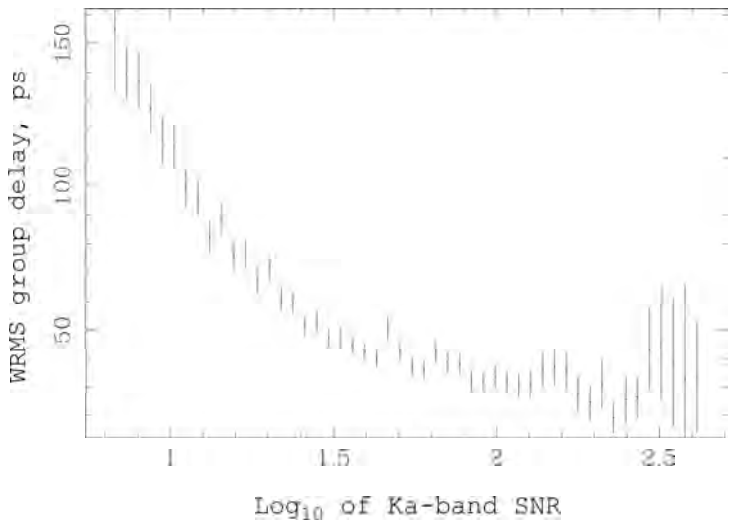

Figure 2. The WRMS residual group delay vs. the log10 of the Ka-band SNR. Note the noise floor of ≈30 ps as other error sources such as troposphere and instrumentation begin to dominate once the SNR becomes > 30

Acknowledgements

The research described in this paper was performed at the Jet Propulsion Laboratory of the California Institute of Technology, under a contract with the National Aeronautics and Space Administration.

References

[1] Gross, R.S. SPACE2006, JPL Publ., 07-5, Pasadena CA, 2007.

[2] Lowe, S.T. JPL Publ., 92-7, Pasadena, CA, 1992.

[3] Ma, et al. The ICRF as Realized by VLBI. A.J., 116, 516, 1998.

[4] Mathews, Herring, Buffet. JGR, 107, B4, 2002.

[5] O'Connor, T. BlockII Correlator. JPL internal publication. Pasadena CA, 1987.

[6] Sovers, Fanselow, Jacobs. Rev. Mod. Phys., 70, 4, 1998.

The 5th IVS General Meeting Proceedings, 2008, p. 289–292

Astrometry from VLBA Observations at 24 and 43 GHz

Gabor Lanyi [1], *David Boboltz* [2], *Patrick Charlot* [3], *Alan Fey* [2], *Ed Fomalont* [4], *Barry Geldzahler* [5], *David Gordon* [6], *Christopher Jacobs* [1], *Chopo Ma* [6], *Charles Naudet* [1], *Jonathan Romney* [4], *Ojars Sovers* [7], *Liwei Zhang* [1]

[1)] *Jet Propulsion Laboratory, California Institute of Technology, USA*

[2)] *U. S. Naval Observatory, USA*

[3)] *Laboratoire d'Astrophysique de Bordeaux, France*

[4)] *National Radio Astronomical Observatory, USA*

[5)] *National Aeronautics and Space Administration, USA*

[6)] *Goddard Space Flight Center, USA*

[7)] *Remote Sensing Analysis Systems Inc., USA*

Abstract. Astrometric results are obtained from a collaboration formed to study extragalactic objects at radio frequencies between 20 and 50 GHz: The K-Q VLBI Survey Collaboration. We analyzed ten 24-hour observing sessions at the VLBA interferometer over a 5-year period, including nearly three hundred radio sources. Our analysis indicates reduction in source structure effects on source positions relative to X-band observations. The median formal uncertainties of right ascension and declination are 0.08 and 0.15 milliarcseconds, and the average absolute difference between the K-band (24 GHz) and the S-X estimated source positions are 0.17 and 0.23 milliarseconds, respectively. These differences are partly due to absent or inadequate modeling of physical effects.

1. Goals

Early in this decade, we formed the K-Q VLBI Survey Collaboration in order to extend radio-based celestial reference frames above 8 GHz (X-band). Our goals were:

- Enabling Deep Space Navigation at 32 GHz (Ka band).
  - This requires radio source positions above X band.
  - This requires source structure information.

- Improving reference source positions above X-band.

The VLBA had the imaging capability and it allowed us efficiently to

- observe at enveloping frequencies of 24 and 43 GHz.
- obtain radio source catalogs at these enveloping frequencies.

It was important to obtain source structure information from imaging in order to assess the compactness of the sources and thus their suitability for high accuracy work.

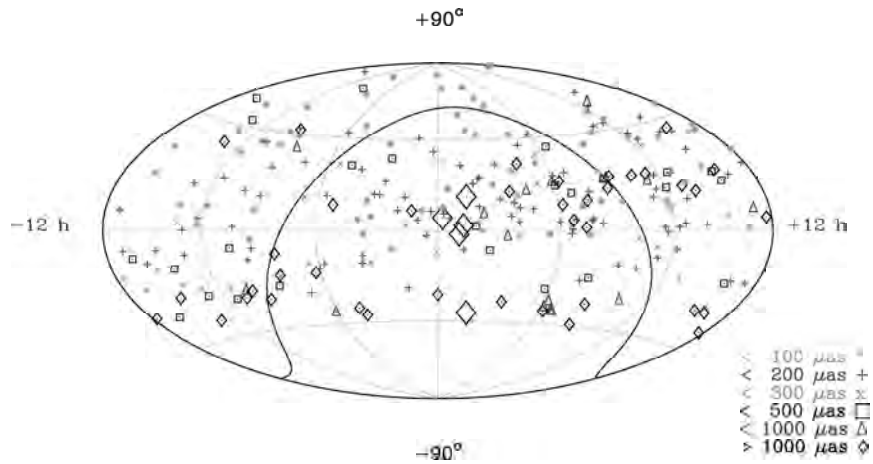

Figure 1. Distribution of 275 K-band sources. Symbols indicate 1-σ formal declination uncertainties with size bins according to legend at lower right. $(\alpha, \delta) = (0, 0)$ is at the center. The ecliptic plane is indicated by a dashed line. The galactic plane is indicated as a black line approximating the shape of Ω

2. Results

We observed by the VLBA on 10 different dates starting in May 2002 and most recently in Mar. 2007. Each session was approximately 24 hours in duration and contained multiple snapshots per source in order to allow imaging. We obtained:

- 275 source positions and images at 24 GHz (K band).
- 132 source positions and images at 43 GHz (Q band).
- Reduced source structure K vs. X.
- Reduced position error due to source structure.
- Formal position uncertainty at the 0.17 mas level at K-band.

Fig. 1 shows the distribution of K-band sources. Q-band's reduced sensitivity relative to K-band coupled with the smaller number of sessions resulted in a smaller catalog of 132 sources.

3. Source Structure Effects

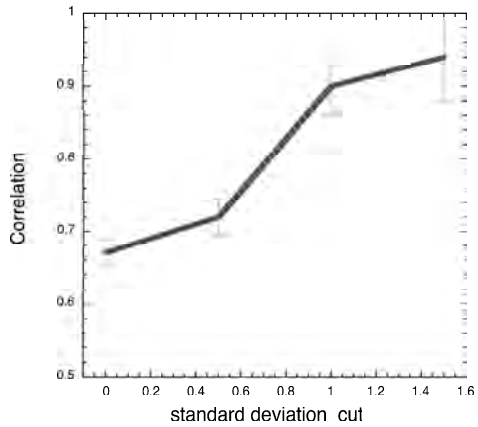

Figure 2. Astrometry vs. Image based source structure magnitude correlation. Correlation between differential R.A. and structure delay. Structure effect becomes significant above noise level. Left to Right: Sources are removed below specified error level

Our analysis shows that source structure was reduced at K vs. X-band thus reducing position error due to structure (see Charlot, this volume for further details). To exhibit the connection between the image based structure contribution to source positions and the astrometric position measurement, we performed:

- imaging: Estimation of structure induced position displacements,
- astrometry: Calculation of absolute differences between K and X-band coordinates,
- correlation coefficients between the above two quantities including all overlapping sources,
- coefficients are grouped according to lower bounds on positional error.

Fig. 2 shows this average correlation coefficient starting with all data and then for data sets that required the position shifts to be greater than thresholds of 0.5, 1.0, and 1.5 standard deviation. The plot shows that the structure induced shifts become more significant above the noise level, as expected. This trend gives us confidence that imaging considerations and astrometry are in agreement.

4. Conclusions

The K-Q VLBI Survey Collaboration has completed 10 survey experiments using the VLBA resulting in astrometric catalogs and imaging for 275 objects at K-band and 132 objects at Q-band. Both astrometry and imaging data are in agreement that sources become more compact at K-band than at X-band. The obtained catalogs and imaging data will be useful for high accuracy navigation and phase reference astrometry.

Acknowledgements

The research described in this paper was partly supported by NASA grants, including a contract between NASA and California Institute of Technology, and has also made use of the United States Naval Observatory Radio Reference Frame Image Database. VLBA instrumental allocation is supported by NSF.

References

[1] Charlot, P., et al. The Celestial Reference Frame at Higher Radio Frequencies: LBA Imaging Observations at 24 and 43 GHz. 2008 (in preparation).

[2] Lanyi, G., et al. The Celestial Reference Frame at Higher Radio Frequencies: Astrometry from VLBA Observations at 24 and 43 GHz. A.J., 2008 (in preparation).

The 5th IVS General Meeting Proceedings, 2008, p. 293–296

Results from K-band Geodetic VLBI Using VERA

Takaaki Jike, Seiji Manabe, Yoshiaki Tamura

Mizusawa VERA Observatory, National Astronomical Observatory of Japan, Japan

Abstract. Monitoring the positions and movements of VERA stations is one of the purposes of the VERA internal 1 Gbps geodetic VLBI observations. Regular geodetic VLBI has been carried out for three years to supply coordinates of VERA stations with several millimeters accuracy to support VERA astrometry observations and analysis. The VERA observation system demonstrates best performance at K-band. We started experimental geodetic VLBI observations using K-band in January 2006, aiming at obtaining more precise geodetic solutions and confirming the feasibility of geodetic VLBI using a new frequency band which is capable of replacing S/X bands. From the analysis of these observations, we obtained geodetic solutions with higher precision than S/X band observations.

1. Introduction

VERA (VLBI Exploration of Radio Astrometry) [1] is a project to clarify the three dimensional structure and dynamical motion of our Galaxy. This project aims at the measurement of annual parallax with 10 μas orders accuracy. Four observation sites (Mizusawa, Iriki, Ogasawara, and Ishigakijima) form the VERA network on the Japanese islands operating a 20 m parabolic antenna at each site. Geodetic VLBI observations are crucial to maintain the highly accurate astrometry of VERA. Monitoring the station positions and their time variations within the VERA network is one of the main purposes of the VERA geodetic observations.

VERA-internal geodetic VLBI observations at S/X bands started in Nov. 2004 [2]. These observations regularly use the 1 Gbps recording system DIR2000. Site coordinates and their time variations are obtained with a few mm and 0.1 mm/yr precisions and are used in observation scheduling and analysis of VERA astrometry.

In Jan. 2006, experimental K-band (23 GHz) geodetic VLBI observations were started in the framework of the VERA operations, aiming at obtaining

more precise and more stable geodetic solutions and confirming the feasibility of geodetic VLBI at a new frequency band replacing S/X bands. After an examination period of one year, K-band geodetic VLBI observations were included in a series of the VERA-internal geodetic VLBI observations.

2. Specifications of the K-band Geodetic VLBI System of VERA

Background factors for moving from S/X-band to K-band are as follows. First, the VERA observation system has demonstrated best performance at K-band. Tabl. 1 summarizes the specifications of the VERA observation system at S-, X-, and K-band, respectively. What is evident from this table is that the performance of the K-band observation system is better than that of the S/X-bands most of the times. Next, we expect that simpler source structure at K-band will stabilize the geodetic solutions in the time series. Also, the fringe detection sensitivity improves thanks to 1 Gbps recording.

Table 1. Performance of observation in VERA geodetic VLBI

Specification of observation	S-band	X-band	K-band
Trx, K	300	100	60
Receiver Type	HEMT	HEMT	Cooled HEMT
Polarization	RHCP	RHCP	LHCP
Tau0	0.05	0.05	0.1-0.3
Aperture Efficiency	0.3	0.4	0.6
Receivable Frequency, GHz	2.21-2.37	8.18-8.60	21.5-23.8
Recorded I/F Bandwidth, MHz	128	368	498
Bandwidth, MHz - bit - Stream	16-2-4	16-2-12	16-2-16

The specifications of the observation system at each band are applied in the observation scheduling. The number of scans shown in Tabl. 2 are scheduling results. The number of scans at S/X-bands is typically 500/station/24 hours, while that at K-band is about 800 thanks to the high sensitivity in this band. By the way, the number of scans changes depending on meteorological conditions in the season. The receivable bandwidth of S-band is narrow. And, the interference of cell phones have degraded the sensitivity of the S-band receiving system recently. The fringe detection sensitivity of the VERA-internal geodetic VLBI using S/X-bands is limited by the sensitivity of S-band.

3. Geodetic Solutions at K-band

There is no special item in the analysis of K-band VLBI. We use the Mitaka FX Correlator for correlation processing and the CALC3/MSOLV package

Table 2. Setting of scans in VERA geodetic VLBI scheduling

Parameter Setting	S/X-band	K-band
Integration Time, s	20-240	20-120
Minimum Level of S/N	20-30	35-40
Number of Scans/Site/Session	400-600	600-800

for geodetic analysis, both being VLBI analysis systems developed at NAOJ [3]. ICRF and ITRF catalogs are used for star and site coordinates. Site coordinates, zenith atmosphere delay, and clock offset/rate are solved for simultaneously.

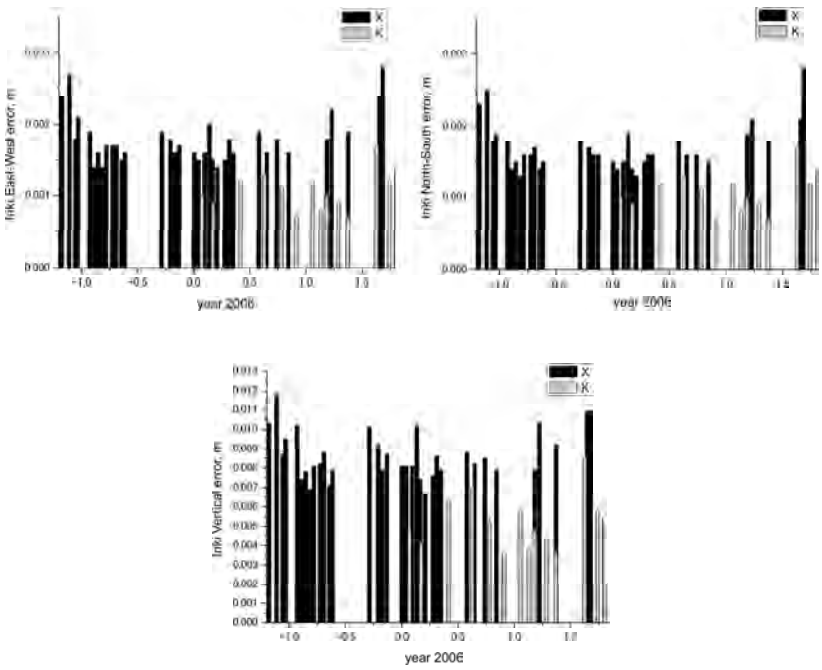

Figure 1. Error size of coordinate solutions. The period is from Nov. 2004 to Oct. 2007

The precision of the site topocentric coordinates in S/X-bands are 1–2 mm and 7–8 mm for the horizontal and vertical components, respectively. Those of K-band observations are better than 1 mm and 4–5 mm in most observations. The errors of K-band are 1.5–2 times smaller as compared with those of S/X-bands, as is evident from Fig. 1. In time series of the coordinates solutions, no significant systematic difference is found in the estimated coordinates between

S/X- and K-band, and K-band solutions look more stable than those for X-band.

4. Summary and Outlook

Experimental K-band geodetic VLBI observations aim at obtaining more precise geodetic solutions and confirming the effectiveness of a new frequency band that can replace S/X-bands. Experimental K-band geodetic VLBI observations started in Jan. 2006 and continues in the framework of the VERA internal geodetic VLBI sessions. High precise geodetic solutions were obtained from these observations. From these results, we recognized that K-band geodetic VLBI will become the main frame of VERA geodetic VLBI observations in the near future.

We try to enhance the K-band geodetic VLBI network for connecting the VERA network to other VLBI networks. VERA has the fifth 1 Gbps recording system for recording at Mitaka Correlation Center. This system in used to record VLBI raw data sent from other antennas linked to Mitaka via optical fiber networks. In Oct. 2007, Gifu University's 11 m antenna joined temporarily in VERA internal K-band geodetic VLBI session. VLBI raw data of Gifu station was transferred to Mitaka via 10 Gbps optical fiber network and recorded in Mitaka. The observation and analysis were both successful.

References

[1] Sasao, T., H. Kobayashi, N. Kawaguchi, et al. VERA: A Tool for Drawing a Stereo Map of the Galaxy. Journal of the Physical Society of Japan, v. 57, No 5, 313–320, 2002.

[2] Jike, T., Y. Tamura, S. Manabe, et al. The first year of VERA geodetic Experiments. International VLBI Service for Geodesy and Astrometry 2006 General Meeting Proceedings. D. Behrend and K. D. Baver (eds.), NASA/CP-2006-214140, 2006, 56–57.

[3] Jike, T., Y. Fukuzaki, K. Shibuya, et al. The first year of Antarctic VLBI observations. Polar Geoscience, v. 18, 26–40, 2005.

The 5th IVS General Meeting Proceedings, 2008, p. 297–301

The Large Quasar Astrometric Catalog and the Radio-Optical Link

Jean Souchay [1], *Alexandre Andrei* [2], *Christophe Barache* [1], *Sébastien Bouquillon* [1], *Anne-Marie Gontier* [1], *Sébastien Lambert* [1], *Christophe Le Poncin-Lafitte* [3], *François Taris* [1], *Elisa Felicitas Arias* [4], *Daniel Suchet* [1], *Mathieu Baudin* [1]

[1)] *SYRTE, Observatoire de Paris, France*

[2)] *Osservatorio de Valongo, UFRJ, Rio de Janeiro, Brasil*

[3)] *Lohrmann Observatory, Dresden Tech. Univ., Germany*

[4)] *BIPM, Pavillon de Breteuil, Sevres, France*

Abstract. Face to the huge and always increasing number of quasars recorded in various surveys and catalogues, we made a general compilation of all these objects, by including their best astrometric estimates and a large quantity of informations concerning their photometry, radio fluxes, and redshift. Moreover we evaluated the absolute magnitude of all the objects with up-to-date cosmological parameters and galactic extinction maps. A flag was adopted for the main catalogues of our compilation which enables a direct information of the cross- identifications. Our catalog is quoted as LQAC (Large Quasar Astrometric Catalog) and contains 113653 quasars at all.

1. Strategy for the LQAC Compilation of Quasars

The first guiding principle of our compilation is to insist on the astrometric quality. For this purpose we retain for each quasar the a priori most accurate value of its celestial coordiantes with respect to the ICRF (International Celestial Reference Frame). This leads to a hierarchy in the catalogues taken into account with a flag represented by a letter corresponding to its place in the hierarchy. For instance the ICRF-Ext.2 will be considered as the most accurate one and consequently will be attributed the flag "A", followed by the VCS catalogue with flag "B" etc... When an object is found in common to two or more catalogues, through an appropriate procedure of cross-identifications, then it will be characterized by its best equatorial coordinates according to

our hierarchy. Notice that roughly 90% of our quasars sample are included in only 11 catalogues, whereas the remaining ones are found in more than 200 small ones. Consequently we use the flags "A" to "L" to symbolize each of the 11 leading catalogues (concerning the VLA catalogue two flags will be used as will be explained in the following), and flag "M" to characterize the remaining ones. In this last case a number designates the catalogue of origin in which the object has been detected for the first time. In the following we recall the characteristics of the catalogues participating in our compilation.

• The ICRF-Ext.2 catalogue (Flag "A")

The up-coming of the ICRF-Ext.1 and of the ICRF-Ext.2 [7] brought 109 new sources in the catalogue, thus leading to a total number of 717 radio-sources. Notice that among the ICRF-Ext.2 catalogue, a very small sample of objects are not quasars : 10 of them are ranged in the category of AGN (Active Galactic Nuclei) and 10 of them in the category of BL LAC (BL Lacertae). Although we are a priori exclusively considering quasars in our compilation, we keep these particular objects thanks to their remarkable astrometric accuracy.

• The VLBA Calibrator Survey (VCS) catalogue (flag "B")

In the original VCS1 campaign [3] 1811 sources were observed but the final VCS1 catalogue contained 1289 sources from dual frequency solutions, with 43 sources from the 8.4 GHz only solution. Our catalogue used in our compilation contains finally 3357 objects. As given the very high acccuracy in the equatorial coordinates of the quasars, we put this catalogue in second position, with flag "B", just after the ICRF-Ext.2. The only additional information that we pick up from the original catalogue are the radio fluxes in the two bandwidths above.

• The VLA catalogue (flags "C" and "H")

The VLA catalogue of quasars contains information concerning the accuracy of source positions. Therefore we decided to separate the original catalogue in two parts, one with accuracy better (less) than $0.15''$ and another containing all the sources with accuracy worse than this value. The first sub catalogue, with flag "C", contains 1701 quasars with an astrometric precision around 10 mas whereas the second one, with flag "H" is much smaller with only 157 quasars with an accuracy around $0.2''$. For all objects, fluxes are given at 6 frequencies: 0.3 GHz, 4 GHz, 5 GHz, 8.4 GHz, 15 GHz, and 23 GHz. Nevertheless, only a few of these flux determinations are given for the objects.

• The radio JVAS catalogue (flag "D")

Our JVAS (Jodrell Bank-VLA Astrometric Survey) catalogue contains 2118 sources with 8.4 GHz flux information [11, 4, 17]. The associated technological device is MERLIN (Multi-Element Radio Linked Interferometer Network) which represents the UK's national radio imaging facility. It is operated by the University of Manchester and consists in an array of radio telescopes distributed around Great Britain, with separations up to 217 km. It operates at frequencies ranging from 151 MHz to 24 GHz, with a resolution better than 50 mas at 5 GHz.

• The optical SDSS catalogue (flag "E")

The SDSS (Sloan Digital Sky Survey) is covering about one quarter of the

sky, observed from a dedicated 2.5-m telescope located at Apache Point, New Mexico. Images are obtained in five broad optical bands (designated by u, g, r, i, z) covering the wavelength range of the CCD response from atmospheric ultraviolet cutoff to the near infrared [8]. The astrometric calibration [13] yields an accuracy per coordinate of 45 mas when reduced against the USNO CCD Astrograph catalogue (UCAC) and 75 mas when reduced against Tycho-2.

Our SDSS quasars input catalogue is by far the largest one, thanks to the DR5 release. It contains 74 868 objects [14]. and gives extensive photometric information for the quasars with magnitudes estimations in the u, b, v, g, r, i, z colors and a presise redshift evaluation.

• The 2QZ catalogue (flag "F")

The 2-degree Field (2dF) QSO Redshift Survey, quoted as 2QZ [5] is based on a pre-selection of quasars candidates from well defined criteria from a broad-band u, b_j, r colors obtained starting from automated plate measurements (APM) of UKST photographic plates. Then a spectroscopic follow-up of the QSO's candidates already selectioned was completed by a χ^2 minimization technique. The survey area comprises 30 fields arranged in two $75° \times 5°$ declination strips, one passing across the South Galactic Cap, centered on $\delta = -30°$ and the other passing across the North Galactic Cap, centered on $\delta = 0°$.

At total the sample contains 22 971 quasars in the 2QZ for our compilation. Notice that a little more than 2000 quasars are found in common in the 2QZ and SDSS catalogues. Recently, [15] analyzed the global rotations between the two catalogues thanks to these common objects.

• The FIRST catalogue (flag "G")

The FIRST radio survey [9] has provided a new resource for constructing a large quasar sample, with positions accurate to better than $1''$, and with high radio sensitivity. One of the main tasks consisted in matching the radio catalogue from the NRAO VLA survey [1] with an optical catalogue provided by the Automated Plate Machine (APM) digitization of Palomar Sky Survey Plates. Optical selection was accompanied by several spectroscopic campaigns in order to refine the selection criteria. The first release concerned $300 deg^2$ and contained about 200 objects. It was completed by a second release (White et al.,2000) containing 636 quasars distributed over $2682 deg^2$ and a third one [2] in the South Galactic Cap, containing 321 quasars for $589 deg^2$. For our compilation we use 972 quasars of the most recent catalogue. In addition to their position supposed to be accurate at the level of $1''$, we kept the r and b magnitudes together with the radio flux at 1.4 GHz (20 cm) and the redshift.

• The Hewitt and Burbridge catalogue (flag "I")

About fifteen years ago [10] have published a catalogue containing all known quasars with measured emission redshifts, that is to say 7245 objects, nearly all QSO's. From this catalogue we extract for each object, when available and when they have not been already recorded by the "A" to "H" catalogue compilation, the informations which are useful for our compilation, i.e. the u, b, v, g, r, i magnitudes together with the redshift. An important problem presented by this catalogue is the poor accuracy of the equatorial coordinates

for a significant proportion of the quasars in the list.

• Additioning informations with the 2MASS (flag "J"), GSC2.3 (flag "K") and B1.0 (flag "L") catalogues

The USNO-B1.0 catalogue [12] presents magnitude photometric accuracy in up to three colors (Johnston B, R and I), for 1 042 618 261 objects on all-sky basis . The photometry results from scans of 7 435 Schmidt plates taken for the various sky surveys and calibrated using Tycho-2 stars. The resulting photometric accuracy is 0.3 mag., reaching up to $V = 20$.

The GSC2.3 catalogue established from the Space Telescope Science Institute (Stsci) and the Osservatorio Astronomico di Torino, 2006 is an all-sky catalogue of 945 592 683 objects, resulting from photographic Sky Survey plates, at two epochs and three bandpasses, from the Palomar and UK Schmidt telescopes (DSS). The magnitudes are consistent with B, R, and I Johnston, and an estimation of the V magnitude is also given. The GSC2.3 has no formal magnitude limit. The parameters of the bright objects, overexposed on the Schmidt plates, are taken from the Tycho-2 catalogue.

The 2MASS (Two Micron All-Sky Survey) catalogue [6] results from a uniform scanning of the entire sky in three near-infrared bands to detect and characterize point sources brighter than about 1 mJy in each band, with signal-to-noise ratio (SNR) greater than 10. The detectors worked at J (1.25 μm), H (1.65 μm), and Ks (2.17 μm) bands s, to a 3σ limiting sensitivity of 17.1, 16.4 and 15.3 mag. respectively. The 2MASS Point Source Catalogue has a total of 470 992 970 sources.

These three catalogues do not bring a new set of quasars, but enable to complete the data lacking up to this point, especially concerning the photometry. For instance cross-identifications with the 2MASS catalogue adds the infrared magnitudes in J and K bands for 13 647 quasars of our total sample, whereas the GSC2.3 catalogue brings b magnitudes for 69 355 quasars and v magnitude for 41 517 quasars.

2. The LQAC and Future Prospects

Our LQAC catalogue contains a large majority of the recorded quasars at the present time, with 113 666 entries, that is to say 25% more than the 85 182 quasars in the last release of the Véron-Cetty and Véron catalogue [18], which constituted the largest compiled catalogue available until now. Moreover we have included in the LQAC additional informations, when available : they are ranged in 20 columns corresponding to 9 photometric bands (u, b, v, g, r, i, z, J, K), one redshift determination, five radio-fluxes at 1.4 GHz (20 cm), 2.3 GHz (13 cm), 5.0 GHz (6 cm), 8.4 GHz (3.6 cm) and 24 GHz (1.2 cm) and 6 columns related on the estimation of the absolute magnitudes at two bands, i and b. Notice that a large fraction of quasars of the LQAC, i.e. 104 944 objects that is to say 92.33% of the total sample, are coming from only 11 catalogues, the largest one being the last release DR5 of the Sloan Digital Sky Survey. One of the characteristics of the LQAC is to give a flag for each of

these leading catalogues above, which enables to know immediately for which of these catalogues a given quasar has been identified.

In the LQAC related paper [16] we have also studied the homogenity of the data, both in the astrometric and photometric fields, by comparing the parameters as equatorial coordinates , magnitudes and redshifts, as given by two or more different catalogues. We have also presented some statistics concerning the spatial distribution of the objects. At last we think that we have carried out a precise and very careful method to determine with the best accuracy the absolute magnitudes of the quasars at two bandwidths M_i and M_b, by taking into account the most recent models of galactic extinction, of K correction and of luminosity distance.

At last we schedule to up date the LQAC in an annual basis, by adding new discovered quasars, by completing the data and improving its quality, and carrying out statistical studies. We think that this work should be very useful for the VLBI community as well as in the frame of the preparation of future astrometric surveys and space missions as GAIA.

References

[1] Becker, R.H., R.L. White, D.J. Helfand. Astrophys. J. Suppl. Series, 135, 277, 1995.

[2] Becker, R.H., R.L. White, D.J. Helfand. Astrophys. J., 450, 559, 1995.

[3] Beasley, A.J., A.B. Peck, L. Petrov. Astrophys. J. Suppl. Series, 141, 13, 2002.

[4] Browne, I.W.A., A.R. Patnaik, P.N. Wilkinson, et al. MNRAS, 293, 257, 1998.

[5] CRoom, S.M., R.J. Smith, B.J. Boyle, et al. MNRAS, 349, 1397, 2004.

[6] Cutri, R.M., M.F. Skrutskie, S. Van Dyk, et al. NASA/IPAC Infrared Science Archive, 2003.

[7] Fey, A.L., C. Ma,, E.F. Arias, et al. A.J., 127, 3587, 1998.

[8] Fukugita, M., T. Ichikawa, J.E. Gunn, et al. A.J., 111, 1748, 1996.

[9] Gregg, M.D., R.H. Becker, R.L. White, et al. A.J., 112, 407, 1996.

[10] Hewitt, A., G. Burbridge. Astrophys. J. Suppl. Series, 87, 451, 1993.

[11] Patnaik, A.R., I.W.A. Browne, P.N. Wilkinson, et al. MNRAS, 254, 655, 1992.

[12] Monet, D.G., S.B. Levine, B. Canzian, et al. A.J., 125, 1559, 2003.

[13] Pier, J.R., J.A. Munn, R.B. Hindsley, et al. A.J., 125, 984.

[14] Schneider, D.P., P.B. Hall, G.T. Richards, et al. A.J., 130, 367, 2005.

[15] Souchay, J., S. Lambert, A.H. Andrei, et al. Astron. Astrophys., 2007 (in print).

[16] Souchay, J., A. Andrei, C. Barache, et al. Astron. Astrophys., 2008 (in print).

[17] Wilkinson, P.N., I.W.A. Browne, A.R. Patnaik, et al. MNRAS, 300, 790, 1998.

[18] Véron-Cetty, M.P., P. Véron. Astron. Astrophys., 455, 773, 2006.

The 5th IVS General Meeting Proceedings, 2008, p. 302–306

Using Singular Spectrum Analysis for the Investigation of Troposphere Parameters

Natalia Miller, Zinovy Malkin

Central Astronomical Observatory at Pulkovo, Russian Academy of Sciences, Russia

Abstract. In this paper, the method of Singular Spectrum Analysis (SSA) is applied to the investigation of the zenith troposphere delay time-series derived from VLBI observations. With the help of this method we can analyze the structure of time-series and separate the harmonic and irregular (trend) components. Combined IVS time-series of zenith wet and total troposphere delays obtained at IGG were used for the analysis. For this study, several VLBI stations with the longest time series of troposphere zenith delays were selected, also taking into consideration the geographic region where the station is located. The investigations were carried out using SSA mode. As a result, trends and seasonal components (with annual and semiannual periods) were obtained for all the stations. Using of SSA enabled us to determine nonlinear trends in zenith delay, and also to study variations in the amplitude and the phase of the seasonal components with time.

1. SSA Method

In this research, we have investigated the combined IVS troposphere zenith delay (TZD) series and focused on behavior trends and seasonal components with the help of Singular Spectrum Analysis (SSA) [1]. Additional information on SSA method, its abilities and the corresponding software can be found on the site http://www.gistatgroup.com/cat/. With the help of this method we can:

– Recognize certain components in the equally spaced time series, which have been obtained from observations. The result of this procedure is a decomposition of the time series into components that usually can be identified as trends, periodical or oscillatory, and noise components.

– Extract components with well-known periods and estimate values of phase shift and variation of amplitude of pseudo-harmonic signals.

– Find periodicities that are not known in advance.

– Extract trends of different resolutions. Natural decomposition of the time

series is constructed on the base of the unique parameter (the window length). Grouping different subsets of the decomposition components one can obtain both the tendency and accurate trend.

– On the basis of the chosen components smooth out the initial data.

In contrast to the standard spectral analysis, where the basic functions are given a priori as the sines and cosines of the Fourier method, in SSA they are determined from the very data to form orthogonal bases.

2. Analysis of Zenith Delay Time Series

The zenith total delay (ZTD) is the sum of the zenith hydrostatic (ZHD) and zenith wet delays (ZWD). The SSA method gives the opportunity to detect features of main ZTD and ZWD (ZD) trends and to compare them with the main trends of other time series, such as hydrostatic zenith delay, wet zenith delay, pressure at the site, temperature at the site, water vapor pressure at site, which were taken from the VMF1 files provided by the IGG. The combined IVS time series of ZD, obtained at IGG, were used in the analysis [2]. Six VLBI stations (Gilcreek, Kashima, Kokee, Onsala, Westford, Wettzell) with the longest time series of troposphere zenith delays were selected for the study. Linear interpolation of data was carried out to get equally spaced series with a step of 0.01 year which was used for SSA. For all time series we used the same time interval 1984.88 – 2004.87, series length N=2000 points (20 years), and the maximum window length M=N/2=1000. After decomposing with the SSA method in all series the trends, hereafter referred to as trend SSA, annual and semiannual components were found. Fig. 1–2 show ZD trends as obtained by SSA from the combined IVS series and their linear approximation. The fact that the stations located in the same geographic region (Onsala and Wettzell) reveal similar trend features is of special interest. Moreover, all trends have the same small curving about the year 1995. Original series obtained by analysis centers BKG, GSFC, IAA, MAO show the same properties, which are shown in Fig. 3 for Wettzell as an example.

It is interesting to compare non-linear trends found in the ZD with those in the meteorological parameters. For this purpose, the decomposition of the meteorological parameters for Wettzell and Gilcreek has been made using SSA. Fig. 4 shows the trends for the hydrostatic zenith delay, pressure at the site from the VMF1, and ZTD-ZWD computed from the IVS combined series. The coincidence of all these curves is obvious for Wettzell. For Gilcreek one can see a difference in shape of the curves. Fig. 5 shows the trends for wet zenith delay, temperature at the site, and water vapor pressure at the site from the VMF1 and ZWD. The ZWD trend is very close to the trend of water vapor pressure for the Wettzell. But for Gilcreek similar curves do not show such an agreement. Gilcreek is the only station where we failed to extract the trend of the site temperature series.

Fig. 6–7 show the annual and semi-annual components ZWD for the researched stations. The components have a steady phase but variations in

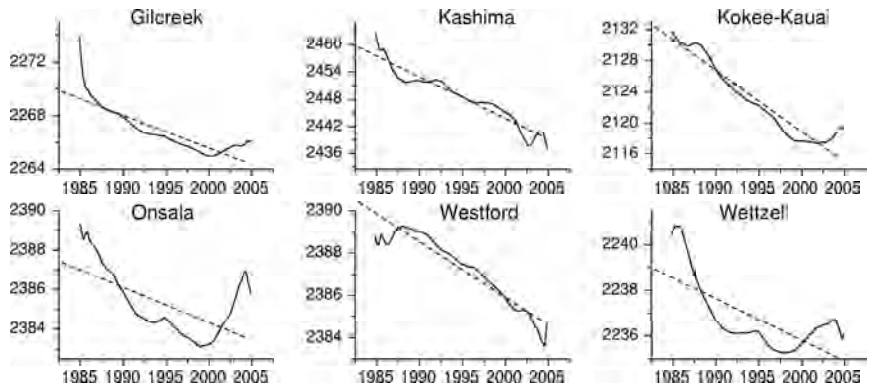

Figure 1. SSA trends of ZTD (solid line) and their linear approximation (dashed line). Unit: mm

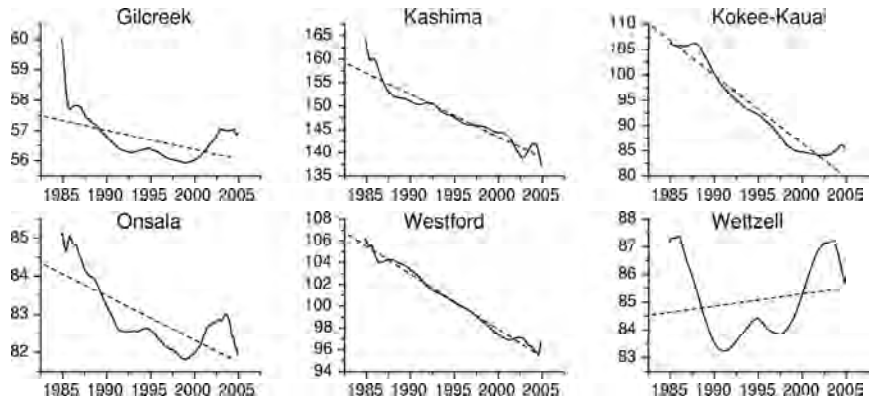

Figure 2. SSA trends of ZWD (solid line) and their linear approximation (dashed line). Unit: mm

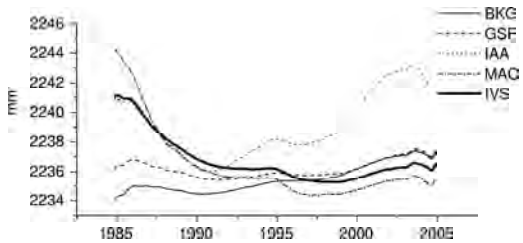

Figure 3. SSA trends in ZTD for individual series for Wettzell

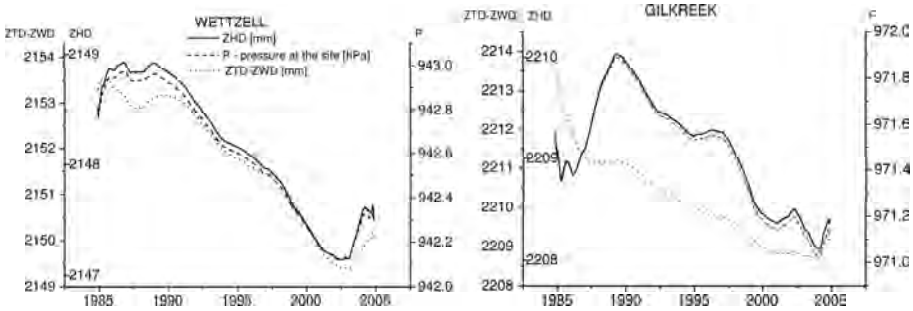

Figure 4. SSA trends of hydrostatic zenith delay, pressure at the site and ZTD–ZWD

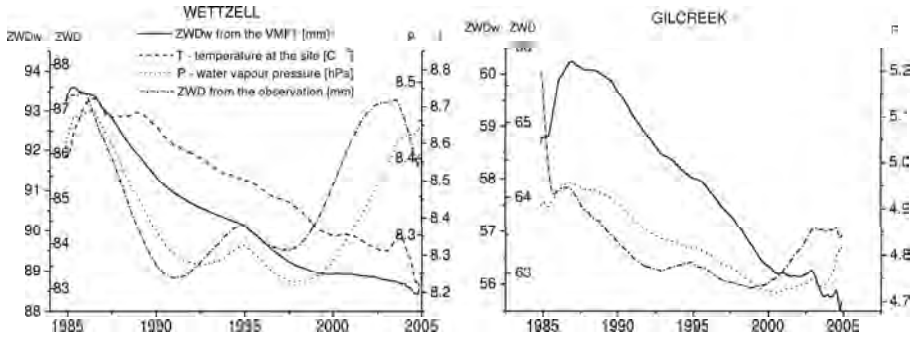

Figure 5. SSA trends of wet zenith delay, temperature at the site, water vapor pressure and ZWD

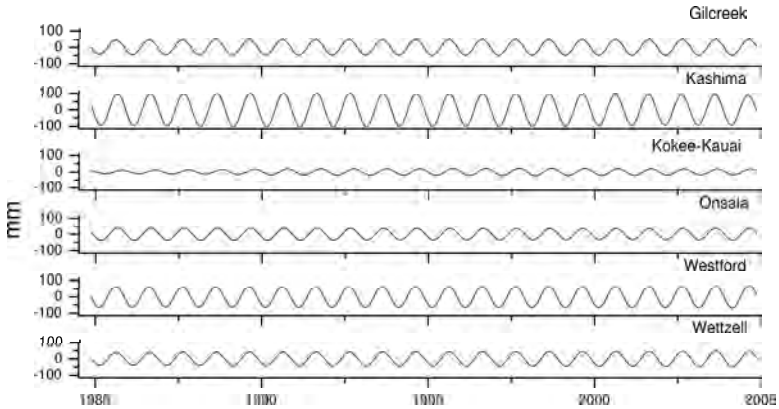

Figure 6. The annual components in reconstructed ZWD series

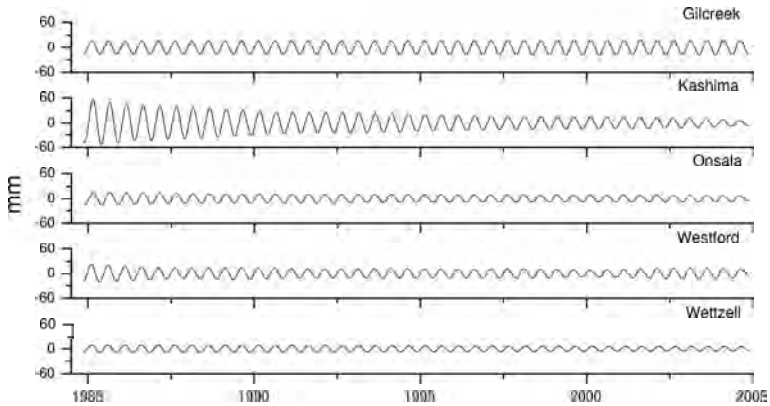

Figure 7. The semiannual components in reconstructed ZWD series

amplitude. It should be mentioned that the contribution of the semiannual component is comparatively small, near noise level, and therefore this component needs more careful study. For Kokee a semiannual component was not found, and so for ZTD at Onsala. For Kashima, the amplitude of the semiannual component is larger in the beginning of the time interval than at the rest of interval.

3. Conclusions

In this paper, we have examined the ability of the SSA method in the analysis of the zenith troposphere delay. Non-linear trends and variations of the amplitude of seasonal components have been detected. Some interesting peculiarities in their behavior have individual character for every site. A comparison of the trends with meteorological parameters also is presented to show possible similarities that deserve further investigations.

References

[1] Golyandina, N., V. Nekrutkin, A. Zhigljavsky. Analysis of Time Series Structure: SSA and Related Techniques. Chapman and Hall/CRC, New York, 2001.

[2] Heinkelmann, R., J. Böhm, H. Schuh. Combination of Long-term Time Series of Tropospheric Parameters Observed by VLBI. IVS 2006 General Meeting Proceedings. D. Behrend, K.D. Baver (eds.), NASA/CP-2006-214140, 2006, 341–343.

The 5th IVS General Meeting Proceedings, 2008, p. 307–313

Atmospheric Loading Coefficients Determined from Homogeneously Reprocessed GPS and VLBI Height Time Series

Volker Tesmer [1], *Johannes Boehm* [2], *Barbara Meisel* [1], *Markus Rothacher* [3], *Peter Steigenberger* [4]

[1)] *Deutsches Geodätisches Forschungsinstitut (DGFI), Germany*

[2)] *Institute of Geodesy and Geophysics, TU Vienna, Germany*

[3)] *GeoForschungsZentrum Potsdam (GFZ), Germany*

[4)] *Institute for Astronomical and Physical Geodesy, TU Munich, Austria*

Abstract. This investigation compares homogeneously reprocessed VLBI (OCCAM6.1e at DGFI) and GPS (Bernese5.1 at GFZ and TUM) long-term height series. Furthermore, atmospheric loading coefficients are estimated from these series using local ECMWF pressure and simple linear regression. The VLBI and GPS data analysis used fully homogenized models in both software packages and the solutions were run twice, once with simple tropospheric modeling (NMF and constant a priori zenith delay) and once with state-of-the-art models (VMF1 and a priori zenith delay from ECMWF). The results indicate that the similarity between both techniques is better using the state-of-the-art models. However, a comparison of the loading signals derived from the VLBI- and GPS-estimated coefficients with time series of modeled atmospheric loading crustal displacements shows good agreement only for a few sites.

1. Introduction

This paper investigates two issues.

- "Can position time series be improved using state-of-the-art models?"

  by applying several criteria to the similarity of homogeneously reprocessed VLBI and GPS height series at colocations (e.g. estimated harmonic annual signals and atmospheric loading regression coefficients).

- "Can a simple regression approach describe the atmospheric loading signal compared to corrections computed from global approaches?"

  where regression-derived height corrections are compared to corrections described by [5].

2. Data

The VLBI and GPS height time series used in this investigation were completely reprocessed with data 1994 – 2005 (VLBI at DGFI with OCCAM 6.1, LSM [6], GPS at GFZ and TUM with Bernese 5.1 [3], for details on the reprocessing see [8]). They were computed twice with all models carefully adapted:

- **iteration 1:** using "old" models, e.g. NMF (Niell Mapping Function), constant a priori zenith delay (ZD),
- **iteration 2:** using "state-of-the-art" models, e.g. VMF1 (Vienna Mapping Function 1 [1]), a priori ZD computed from ECMWF [7] and thermal deformation correction for VLBI [6].

ECMWF pressure was used to estimate the atmospheric loading regression coefficients ($\Delta h = coef \cdot \Delta p$) from the height time series. The atmospheric loading crustal deformations to evaluate the regression approach are by [5].

3. Results I: Homogeneously Reprocessed VLBI and GPS Height Time Series

It is quite difficult to assess the similarity of daily VLBI and GPS height time series with objective criteria, as:

- if the a priori modeling is state-of-the-art, the expected signals usually are quite small compared to the noise floor of daily height estimates,
- there are not many VLBI- and GPS-colocation sites with a high number of overlapping observation days (we use 17 sites),
- the "daily" estimates for VLBI and GPS do usually not represent the same 24 h interval,
- the approach to compare time series must account for inhomogeneous formal errors of the estimated heights (especially for the VLBI data),
- some approaches to evaluate similarity of time series only account for linear dependency, like correlation coefficients, which will e.g. ignore differences in amplitudes of harmonic signals.

A discussion of this problem is given in [2], where a Kalman filter is applied.

3.1. Height Time Series

In a first step, the height time series of both iterations were compared after smoothing them by a weighted mean (±35 day windows each 7 days). Many of these VLBI- and GPS-series show a large number of episodic and annually recurrent common patterns, like the sites Wettzell (Germany, Fig. 1, left) and Ny-Ålesund (Spitsbergen, Norway, Fig. 1, right). [2] reveals comparable results using the ITRF2005 data. Nevertheless, not all sites show such a good similarity of VLBI and GPS, and for some of them, the VLBI sites do not have dense enough data to compare the data adequately.

Without sophisticated analysis, it is difficult to judge for which iteration the VLBI and GPS series are more similar (with exceptions like Ny-Ålesund). However, at some sites, one can see several patterns change from iteration 1 to 2, with the tendency to smoother behaviour for iteration 2 (see Fig. 1).

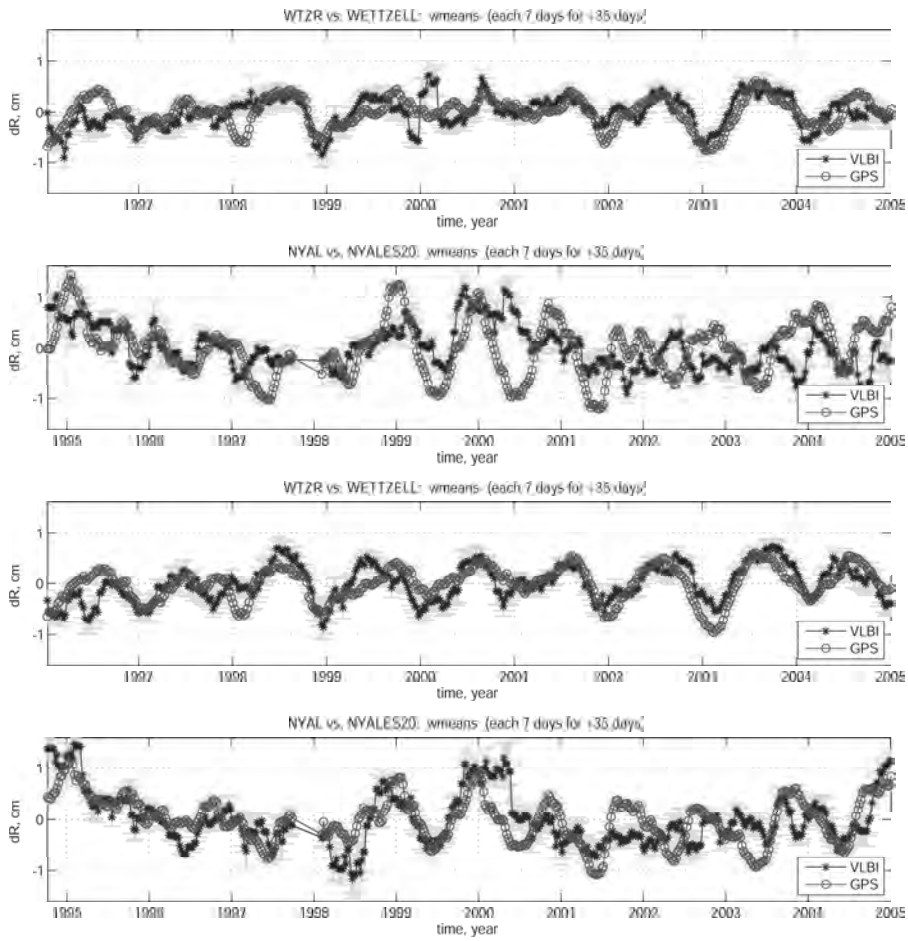

Figure 1. VLBI and GPS height series of the sites Wettzell (Germany, left) and Ny-Ålesund (Spitsbergen, Norway, right). The upper row illustrates the smoothed (70 day weighted mean) series of iteration 1, the lower row the ones of iteration 2

3.2. Annual Signals in Height Time Series

In order to get an impression of the improvement of the similarity between homogeneous VLBI and GPS height time series, it seems to be appropriate

to have a closer look at the annual behaviour of the series. One possiblilty is to simply estimate harmonic annual signals from the VLBI and GPS series of both iterations and compute WRMS values for the VLBI-GPS differences of the amplitudes and phases (comparable studies have also been made by [2]).

If one of the compared series is not very dense or unevenly distributed, such a criterion should generally be more robust than comparing the time series directly, as the information extracted from the data is more compact than the time series themselves (although it might not be very robust in all cases).

For the 17 colocated sites, the VLBI-GPS differences of the amplitudes and phases of iteration 1 have a WRMS of 2.2 mm and 44° and 1.8 mm and 43° for iteration 2. As the series of iteration 2 is available beyond the year 2005 into 2007, this can additionally stabilize the similarity of the annual signals (the WRMS for all the data 1994 – 2007 of iteration 2 is 1.7 mm and 38°).

4. Results II: VLBI and GPS Estimated Atmospheric Loading Coefficients

In this section, we estimate atmospheric loading regression coefficients ($\Delta h = coef \cdot \Delta p$) from the VLBI and GPS time series, using "local" pressure interpolated from ECMWF. This approach has been applied several times, [4] gives an overview and compares the estimated coefficients of related publications. Theoretically, iteration 2 can better display the atmospheric loading deformation, as shortcomings of both, the mapping function and the constant a priori ZD of iteration 1 unintendedly absorb parts of this signal.

4.1. Atmospheric Loading Coefficients

Although computing atmospheric loading corrections by a linear regression coefficient multiplied with local pressure is a very basic approach to model crustal deformation, such coefficients have much more direct physical meaning than a harmonic annual signal. Like this, we hope to conclude that the iteration with smaller VLBI-GPS differences of the regression coefficients produces the more "physical" height series, as they represent more clearly "real" height motion rather than apparent motion, e.g. from tropospheric mismodeling.

Fig. 2 indicates that iteration 2 yields better results: firstly, the similarity of VLBI and GPS coefficients is much better for iteration 2 than 1 (the WRMS of the differences is 0.134/0.083 for iterations 1 and 2 in mm/mbar). This is quite robust, as using the full time series of station positions of iteration 2 up to 2007 only improves the WRMS slightly to 0.080 mm/mbar. Secondly, the similarity of these coefficients to those of the GGFC (Global Geophysical Fluids Center [11]) also improves much: the WRMS of the VLBI-GGFC differences is 0.301/0.154, of the GPS-GGFC differences 0.232/0.161 mm/mbar (iteration 1/2). The GGFC regression coefficients were fitted to NCEP pressure data 1980 – 1997 vs. modeled crustal displacements (by convolving Green's functions with inverse barometric ocean, see [10]).

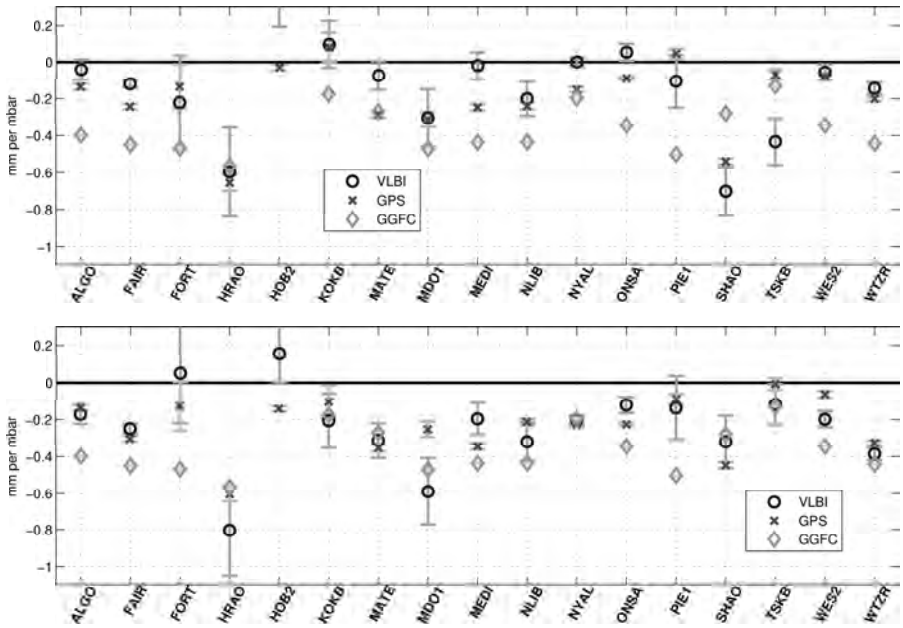

Figure 2. Atmospheric loading regression coefficients and their formal errors, determined from VLBI- (circles) and GPS- (crosses) height series (left/right: iteration 1/2), and coefficients provided by the GGFC (diamonds)

4.2. Comparing Pressure-Times-Coefficient Series to Modeled Crustal Displacements

To assess the "physical interpretability" of the estimated coefficients, we compared the correction series computed with the VLBI-derived coefficients and the local pressure to the modeled crustal displacements according to [5].

Fig. 3 is an example for good agreement. But zooming into the series (only 2005, on the right), it is very obvious that the corrections computed from the raw pressure (in black) have much more energy in the high frequency domain than the modeled crustal displacements (in grey).

This is why efforts were made to smooth the pressure-times-coefficient series with moving medians, computed for each data point (each 6 hours). Finally, a smoothing interval of 92 days was chosen, as the minima and maxima of the pressure-times-coefficient series for most of the stations then have the same order of magnitude as the modeled crustal displacements.

Gilmore Creek, Alaska (USA) and Hartebeesthoek (South Africa) in the upper row of Fig. 4 (with the smoothed pressure series), are examples for good accordance in the annual domain. However, for some stations variations on shorter time scales do not agree as indicated in the right graph of Fig. 3.

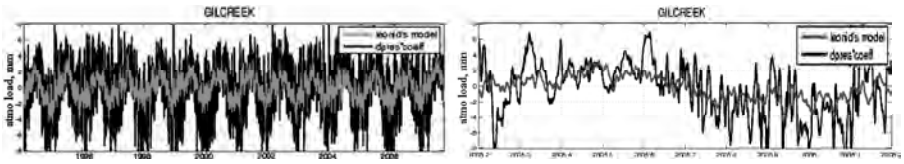

Figure 3. Comparison of corrections "raw-pressure-times-coefficient" (black) and modeled crustal displacements (grey) for Gilcreek. The right graph is the year 2005 zoomed

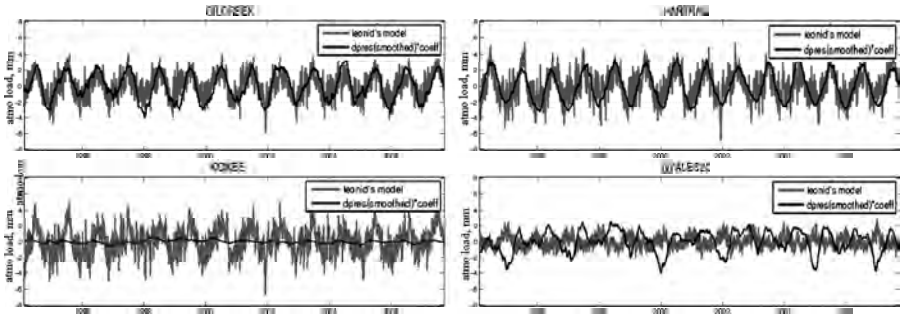

Figure 4. Comparison of "92-days-smoothed-pressure-times-coefficient" (black) and modeled crustal displacement series (grey) for the stations Gilcreek, Hartrao, Kokee and Nyales20

The lower row shows Kokee, Hawaii (USA) and Ny-Ålesund, examples for a bad agreement. Kokee has only 2 mbar RMS of pressure variations during 1994 – 2008 (the 17 sites have between 2 and 12 mbar RMS), and very small VLBI-, GPS- and GGFC-estimated coefficients (Fig. 2, right graph). Thus, almost no signal in the pressure-times-coefficient series are found. In contrary, the modeled crustal displacements clearly vary annually with ±3 mm, which is unexpected, as the deformations for the island Hawaii should be "damped" by the inverse barometric handling of the ocean. The two series for Ny-Ålesund even seem to show a different sign for many of the bump-like features. As for Kokee, the VLBI-, GPS- and GGFC-estimated coefficients for Ny-Ålesund agree well (Fig. 2, right graph). Possible reasons for the disagreements are:

- a linear regression model with local pressure is physically too simple,
- VLBI- and GPS-estimated coefficients are "polluted" by mismodeling,
- the modeled crustal displacements are not good enough in some areas.

5. Summary

- "Can position time series be improved using state-of-the-art models?"

  Using the iteration 2 data, the similarity of harmonic annual signals of homogeneous VLBI and GPS height series improves. This is particularly significant for the estimated atmospheric loading coefficients.

- "Can a simple regression approach describe the atmospheric loading signal compared to corrections computed from global approaches?"

This needs further research: Comparing corrections computed by multiplying the VLBI-derived coefficients with local pressure with the modeled crustal displacements according to [5] makes clear, that sub-annual patterns in both series do not agree. The annual signal is in good accordance for some sites, for others not at all.

Next steps will be to investigate which approach improves geodetic results more (such as station position repeatability, similarity of EOP of the simultaneous CORE-A and NEOS-A VLBI sessions, etc).

Acknowledgements

This study made extensive use of VLBI- and GPS-observations by the Int. VLBI Service for Geodesy & Astrometry (IVS) and the Int. GNSS Service (IGS). Thanks to all IVS and IGS components.

References

[1] Boehm, J., B. Werl, H. Schuh. Troposphere mapping functions for GPS and very long baseline interferometry from European Centre for Medium-Range Weather Forecasts operational analysis data. J. Geophys. Res., v. 111, B02406, DOI 10.1029/2005JB003629, 2006.

[2] Collilieux, X., Z. Altamimi, D. Coulot, et al. Comparison of very long baseline interferometry, GPS, and satellite laser ranging height residuals from ITRF2005 using spectral and correlation methods. J. Geophys. Res., v. 112, B12403, DOI 10.1029/2007JB004933, 2007.

[3] Dach, R., U. Hugentobler, P. Fridez, et al. Bernese GPS Software Version 5.0. Astronomical Institute, University of Bern, 2007.

[4] Haas, R., H.-G. Scherneck, H. Schuh. Atmospheric Loading Corrections in Geodetic VLBI and Determination of Atmospheric Loading Coefficients. Proc. of the 12th Working Meeting on European VLBI. Petersen, B. (eds.), 1997, 122–132.

[5] Petrov, L., J.P. Boy. Study of the atmospheric pressure loading signals in very long baseline interferometry observations. J. Geophys. Res., v. 109, B03405, DOI 10.1029/2003JB002500, 2004.

[6] Nothnagel, A., M. Pilhatsch, R. Haas. Investigations of Thermal Height Changes of Geodetic VLBI Telescopes. Proc. of the 10th Working Meeting on Eur. VLBI. Lanotte, R., G. Nianco (eds.), 1995, 121–133.

[7] The ERA-40 Project Plan. ERA-40 Project Report Series No 1. Simmons, A.J., J.K. Gibson (eds.), 2000; http://www.ecmwf.int.

[8] Steigenberger, P., M. Rothacher, R. Dietrich, et al. Reprocessing of a global GPS network. J. Geophys. Res., v. 111, B05402, DOI 10.1029/2005JB003747, 2006.

[9] Titov, O., V. Tesmer, J. Boehm. OCCAM v.6.0 software for VLBI data analysis. IVS 2004 GM Proc. Vandenberg, N., K. Baver (eds.), NASA/CP-2004-212255, 2004, 267–271.

[10] http://www.iers.org/MainDisp.csl?pid=43-1100132.

[11] http://www.ecgs.lu/ggfc.

The 5th IVS General Meeting Proceedings, 2008, p. 314–318

Re-assessment of Ocean Tidal Terms in High-Frequency Earth Rotation Variations Observed by VLBI

Sigrid Englich, Robert Heinkelmann, Harald Schuh

Institute of Geodesy and Geophysics (IGG), Vienna University of Technology, Austria

Abstract. Periodic changes in the ocean heights and currents, driven by the tidal acceleration due to the Moon and Sun, are the main cause for diurnal and semidiurnal variations in polar motion (PM) and Universal Time (UT1). It has been shown, e.g. by Gipson [1], that VLBI observations can be used for the derivation of high-frequency Earth rotation variations and hence for the determination of ocean tidal terms. In this study we present a re-processing of 23 years of VLBI observational data with the purpose of obtaining high-resolution Earth Rotation Parameters (ERP). The time series allows for the separation of tidal terms, which differ by only one cycle in 18.6 years. We solved for 77 tidal terms, to gather a VLBI-based estimation of ERP variations occuring in the diurnal and subdiurnal frequency band. The rms differences of the estimated tidal coefficients w.r.t. the conventional model [12] are on the level of 5 μas for PM and 0.5 μs for UT1 variations, respectively.

1. Introduction

The effects of diurnal and semidiurnal ocean tides on the Earth rotation parameters have been subject to many different studies in the past. First predictions of the effects were based on theoretical ocean tide models, derived from Laplace's tidal equations [2]. In [3] derived the effect of the oceanic M2 tide on UT1, using a hydrodynamical model. Brosche et al. published a follow-up study, incorporating effects of more partial tides [4]. Ocean tidal variations were then detected in UT1 data from VLBI observations [5]. They were followed amongst others by Gipson [1] and more recently by Haas and Wünsch [6]. Ultra-short period ERP variations were also seen in measurements of Satellite Laser Ranging (SLR) [7] and Global Positioning System (GPS) e.g. [8, 9]. Ray et al. [10] predicted variations in the Earth's rotation rate induced by ocean tides on the basis of empirical tide models deduced from TOPEX/Poseidon altimetry measurements. A complete compilation of publications on the topic

is provided in [11].

The model for diurnal and subdiurnal variations in UT1 and PM, that is recommended in the current IERS (International Earth Rotation and Reference Systems Service) Conventions [12] contains the amplitudes of 71 tidal constituents and was provided by Eanes. This model is an extension of the IERS Conventions model from 1996 calculated by Ray, which consisted of the eight major tidal terms: Q1, O1, P1, K1 in the diurnal band and N2, M2, S2, K2 in the semidiurnal band. The aim of our work was to re-assess the amplitudes and phases of the tidal constituents included in the model, from high-frequency PM and UT1 observed by VLBI. A number of the considered terms are very close in frequency and differ by only one or two cycles in 18.6 years (period of the lunar ascending node). In previous studies it was therefore necessary to introduce constraints on the amplitudes in order to separate these adjacent terms, because the observations only covered shorter time spans. At present we have more than 23 years of VLBI observation data available, permitting us to estimate major tidal terms and sideband terms in an unconstrained solution.

2. ERP Solutions

We generated two VLBI solutions with the VLBI software OCCAM applying the Gauss-Markov model with two different Terrestrial Reference Frames (TRF). In solution "IGG07" the coordinates of the stations were fixed to a recent IGG VLBI-TRF solution. For the second solution called "ITRF05" the current ITRF2005 was employed. The used observations cover the period 1984.0-2007.5. For reasons of consistency we processed the same sessions for the derivation of the ERP as were carefully selected for the IGG TRF solution. PM and UT1 parameters were estimated with hourly resolution without any constraints. Nutation was fixed to the IAU2000 model [12].

3. Analysis of High-Frequency ERP Variations

All low-frequency signals inherent in the ERP series (excited by atmosphere, oceans, solid Earth tides, Chandler Wobble) were removed by subtracting interpolated values of the IERS C04 05 ERP series. The remaining diurnal and semidiurnal variations in PM and UT1 were introduced in a least squares adjustment as pseudo-observations. The formal errors of the observations were introduced as weights for the ERP variations. We estimated the same set of tidal terms that are present in the IERS2003 model, except one sideband of the S1 tide, since the two terms differ by only 2 cycles in 20942 years (period of the solar perigee). Additionally we implemented six "zero" terms at periods where actually no significant tidal signal is expected. The magnitude of this zero terms should give an estimate of the noise level of the observed variations and serve as a kind of validation for the formal errors of the adjustment. Furthermore the terdiurnal term M3 was also included in the estimation. The same

series expansion as in the IERS Conventions was used as observation equation (1) for the observed variations in the pole coordinates (ΔX, ΔY) and UT1 ($\Delta UT1$). We use ΔERP representative for each of the parameters:

$$\Delta ERP(t) = \sum_{i=1}^{n} [A_i sin\xi_i(t) + B_i cos\xi_i(t)] \quad with \quad \xi_i(t) = \sum_{j=1}^{5} N_{ij} F_j(t). \quad (1)$$

A_i and B_i denote the cosine and sine coefficients belonging to the tidal wave i, while n specifies the number of tides considered. The time-dependent angle argument $\xi_i(t)$ is built as a linear combination of the five fundamental arguments $F_j(t)$. Each period is specified by a sequence of integer multipliers N_{ij}, with i labeling again the tide [12]. In our study the number of tidal waves n was 77 (70 ocean tidal waves, 6 zero periods and the M3 tide). For better physical understanding the resulting sine and cosine coefficients for ΔX and ΔY were then represented as prograde and retrograde ΔPM amplitudes. This sums up to 111 (43 diurnal prograde, 34 semidiurnal prograde, 34 semidiurnal retrograde) ΔPM terms and 77 (43 diurnal, 34 semidiurnal) $\Delta UT1$ terms. We derived two empirical models from the two ERP solutions, a model called "IGG07" and a second called "ITRF05". Additionally we obtained a third model in order to test the impact of the previously mentioned amplitude constraining, which is in fact not necessary from the mathematical point of view. For this model we used the approach of Gipson [1], where the amplitudes of the terms with very close periods are constrained with the ratio of the corresponding amplitudes in the tidal potential. The constrained adjustment was applied on the IGG07 ERP series only, the resulting empirical model is therefore referred to as "IGG07c".

4. Results and Comparison to IERS2003 Model

The rms difference of coefficients is taken as a measure for the difference between two models. The formalism for the rms difference can be found, e.g., in [8]. Tabl. 1 gives the resulting values for the three empirical models w.r.t. the conventional model IERS2003.

Table 1. Mean rms differences w.r.t. IERS2003

IERS2003	ITRF05	IGG07	IGG07c
ΔPM, μas	5.04	5.06	4.49
$\Delta UT1$, μs	0.52	0.50	0.43

Fig. 1 shows "phasor plots" of the differences w.r.t. IERS2003 for the eight major terms and for S1. The three-fold uncertainty of the adjustment is indicated by the circles. The previously mentioned zero terms were also included in the plot in order to give a visual validation of the formal errors (ΔPM: 2.1 μas, $\Delta UT1$: 0.2 μs). The amplitude of the largest zero term in the diurnal band is 11 μas for ΔPM and 0.8 μs for $\Delta UT1$, in the semidiurnal band

the values are 4 μas and 0.3 μs. The estimated amplitudes for the M3 tide are even smaller than the formal errors and cannot be considered as significant. Although S1 is not one of the major ocean tidal terms, the difference for S1 is displayed here, because we expect significant signal in the observations coming from the diurnal atmospheric tide also labeled S1, which is not part of the IERS model.

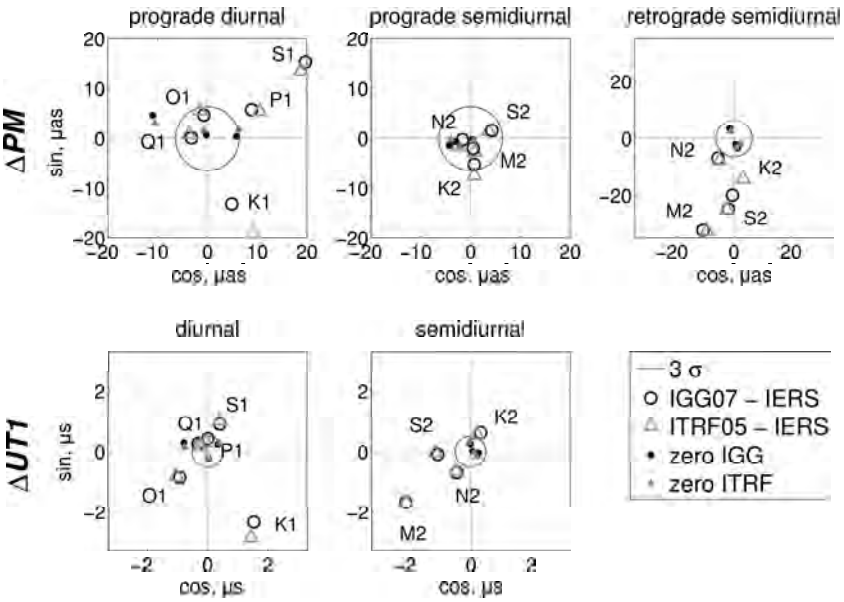

Figure 1. "Phasor plots" of amplitude differences of the eight major tidal terms and S1 to IERS2003 and absolute amplitudes of the zero terms

5. Discussion and Conclusions

The rms differences of the empirical model w.r.t. IERS2003 show differences < 0.03 μas/μs when comparing the solutions, for which different reference frames were used. In terms of unconstrained estimation versus constrained estimation a clear reduction of the rms difference and hence a better alignment to the IERS model is noted for the constrained approach. This reduction of the amplitude differences mainly occurs for the sideband terms. The separation of the sideband terms from the main band terms is possible without any additional information, but the constraints obviously force the preservation of the tidal signature of the variations and restrain other (non-tidal) signals. For each solution notable deviations occur w.r.t. the model in most of the major tidal terms. The largest differences, in terms of ΔPM as well as $\Delta UT1$ arise for the K1 term in the diurnal band and for the M2 term in the (retrograde)

semidiurnal band and are in the range of 20–34 μas and 2–3 μs, respectively. In case of prograde semidiurnal ΔPM almost all estimated differences are within the three-fold formal errors. The amplitudes of the zero terms agree with the magnitude of the 3σ uncertainty, except for one diurnal term with a period of 26.56 h, where significant signal seems to be present in both ERP variations. In summary we conclude that important future tasks are further comparisons and also combined estimates with observations from other space geodetic techniques. In addition thorough investigations of the contribution of the atmospheric tides S1 and S2 and of the effect of the triaxial shape of the Earth on the ERP, as well as corresponding updates of the conventional model are needed.

References

[1] Gipson, J.M. Very long baseline interferometry determination of neglected tidal terms in high-frequency Earth orientation variation. J. Geophys. Res., v. 101, No B12, 28051–28064, 1996.

[2] Yoder, C.F., J.G. Williams, M.E. Parke. Tidal variations of Earth rotation. J. Geophys. Res., v. 86, 881–891, 1981.

[3] Baader, H.R., P. Brosche, W. Hövel. Ocean tides and periodic variations of the Earth's rotation. J. Geophys., v. 52, 140–142, 1983.

[4] Brosche, P., U. Seiler, J. Sündermann, et al. Periodic changes in Earth's rotation due to oceanic tides. Astron. Astrophys., v. 220, 318–320, 1989.

[5] Brosche, P., J. Wünsch, J. Campbell, et al. Ocean tide effects in Universal Time detected by VLBI. Astron. Astrophys., v. 245, 676–682, 1991.

[6] Haas, R., J. Wünsch: Sub-diurnal earth rotation variations from the VLBI CONT02 campaign. J. Geodyn., v. 41, 91–99, 2006.

[7] Watkins, M.M., R.J. Eanes. Diurnal and semidiurnal variations in Earth orientation determined from LAGEOS laser ranging. J. Geophys. Res., v. 99, No B9, 18073–18079, 1994.

[8] Rothacher, M., G. Beutler, R. Weber, et al. High-frequency variations in Earth rotation from Global Positioning System data. J. Geophys. Res., v. 106, No B7, 13711–13738, 2001.

[9] Steigenberger, P., M. Rothacher, R. Dietrich, et al. Reprocessing of a global GPS network. J. Geophys. Res., v. 111, B05402, DOI 10.1029/2005JB003747, 2006.

[10] Ray, R.D., D.J. Steinberg, B.F. Chao, et al. Diurnal and Semidiurnal Variations in the Earth's Rotation Rate Induced by Oceanic Tides. Science, 264, 1994.

[11] Gross, R.S. Earth Rotation Variations — Long Period. Treatise on Geophysics, v. 3. G. Schubert (ed.), Elsevier, Amsterdam, 2007, 239–294.

[12] IERS Conventions 2003. IERS Technical Note, No 32. D.D. McCarthy and G. Petit (eds.), Frankfurt am Main: Verlag des Bundesamts für Kartographie und Geodäsie, 2004.

The 5th IVS General Meeting Proceedings, 2008, p. 319–323

QUASAR National Programs of EOP Determination

Andrey Finkelstein, Elena Skurikhina, Igor Surkis, Alexander Ipatov, Ismail Rahimov, Sergey Smolentsev

Institute of Applied Astronomy, Russian Academy of Sciences, Russia

Abstract. In Aug. 2006 regular determinations of Earth orientation parameters from VLBI observations using the Russian "Quasar" Network have been put into practice. The observations are carried out in the framework of two domestic programs: 24-hour sessions for the determination of all five EOP using all three network observatories (Ru-E program) and 8-hour sessions for the determination of Universal Time using the baselines "Svetloe"–"Zelenchukskaya" or "Svetloe"–"Badary" (Ru-U program). Both session types are observed twice per month. The analysis of Ru-E observations shows that the RMS deviations of the Earth orientation parameters from the IERS EOP 05 C04 series are 0.83 mas for X_p and 1.04 mas for Y_p, 36 μs for $UT1 - UTC$, and 0.55 mas and 0.62 mas for X_c and Y_c, respectively. The RMS deviations of the Universal Time values from the IERS EOP 05 C04 series for the Ru-U program are 127 μs. In the near future it is anticipated to improve the Earth orientation parameters' accuracy for the 24-hour sessions and to determine Universal Time using e–VLBI mode.

1. Introduction

The VLBI observations with the "Quasar" Network for determining the Earth orientation parameters in the frame of IVS observing programs take about 50% of the total observational time. The "Quasar" Network consists of three radio astronomical observatories: "Svetloe" observatory (Leningradsky region), "Zelenchukskaya" (Republic Karachaevo-Cherkessia), and "Badary" (Republic Buryatia). The stations are connected via digital communication channels to the Processing Center, which is located at the Institute of Applied Astronomy in St. Petersburg. Regular domestic determinations of Earth orientation parameters have been performed since Aug. 2006. In the following we present current results of the analysis of these observations.

2. The Domestic Observational Programs

Fig. 1 shows the geometry of the "Quasar" Network [1]. Having put into operation the "Badary" observatory [7], IAA started an absolutely new type of activity—the determination of the Earth orientation parameters solely using domestic VLBI observations. The observations are carried out in the framework of two programs: Ru-E and Ru-U. The main purpose of the first program is to determine all five EOP using 24-hour observations on all three network observatories, whereas the main aim of the second program is to obtain the Universal Time using measurements collected within the 8-hours session on the "Svetloe"–"Zelenchukskaya" or "Svetloe"–"Badary" baselines. All stages of the VLBI process from preparing an observation schedule up to the analysis of the measurements are being done at IAA. The correlation processing of the observations is done with the MicroParsec correlator [2]. At present, both Ru-E and Ru-U observations are carried out biweekly in S/X range recording data on magnetic tapes in S2 format using data acquisition systems DAS Mark IV, DAS VLBA, and DAS P1000 [3]. The observational session technology is similar to the one of the IVS. The Program Committee establishes an observational schedule for a period of a month [4]. The Operational Center prepares a control file with the session time-table. After finishing the observational session the magnetic tapes are shipped to the IAA Correlator for processing. After that the files written in NGS-format are available for the Analysis Center for further EOP calculation. In a typical Ru-E session each station observes about 28 sources with fluxes of about 0.86-10.83 Jy. The total number of scans for each station is about 250–265 for the session. A typical Ru-U session consists of 80 scans of about 16 sources with the same fluxes. Examples of sources distribution for Ru-E and Ru-U sessions are presented in the Fig. 2. The number of the domestic programs carried out in 2006 and 2007 and planned for 2008 is shown in Tabl. 1.

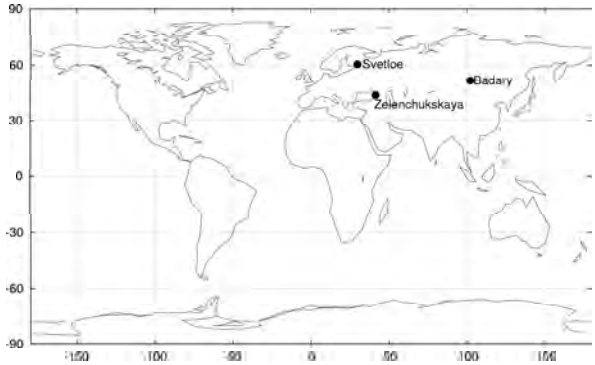

Figure 1. Stations configuration for Ru-E and Ru-U sessions

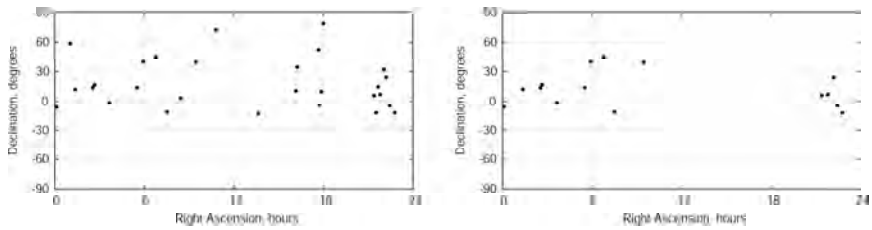

Figure 2. Sources configuration for Ru-E and Ru-U sessions

Table 1. Observational activities of the QUASAR network stations Svetloe (Sv), Zelenchukskaya (Zc), and Badary (Bd) in the domestic VLBI observation programs

year	2006			2007			2008		
Experiment Stations	Sv	Zc	Bd	Sv	Zc	Bd	Sv	Zc	Bd
Ru-E	9	9	9	9	9	9	24	24	24
Ru-U		5	5	7	8	16		24	24

3. First Results of EOP Determination

For obtaining a more accurate EOP solution, it is necessary to calculate the "Badary" and "Zelenchukskaya" station coordinates in the ITRF 2005 system. The estimation of the "Badary" coordinates was made in the first domestic VLBI sessions [5]. In this paper we used "Badary" and "Zelenchukskaya" positions obtained from both IVS and domestic VLBI sessions (28 sessions for "Badary" observatory and 77 for "Zelenchukskaya"), using velocity components obtained from GPS data in both cases. The results of this determination are presented in the Tabl. 2. Having improved the positions of the observatories, the EOP were obtained. Differences of EOPs obtained within the domestic programs and standard IERS EOP 05 C04 series are shown in Fig. 3 and 4. Root mean square residuals (EOP IAA minus IERS EOP 05 C04) after removing systematic trends are presented in Tabl. 3.

Table 2. Station positions and velocities for Zc and Bd, epoch 2000.0, in ITRF2005

Station	Station position, m			Velocity, m/year		
	X	Y	Z	V_x	V_y	V_z
Bd	−838200.729 ± 0.008	3865751.573 ± 0.008	4987670.956 ± 0.009	−0.0253	−0.0002	−0.0037
Zc	3451207.821 ± 0.012	3060375.231 ± 0.008	4391914.941 ± 0.015	−0.0220	0.0156	0.0082

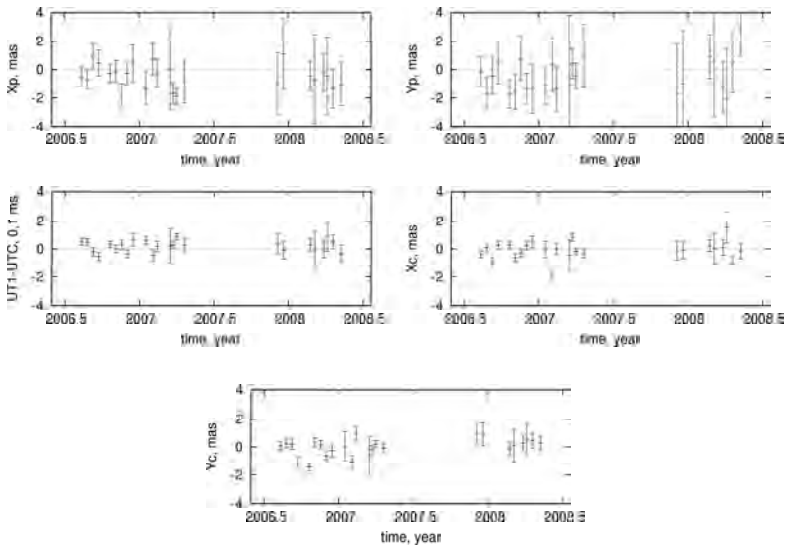

Figure 3. Differences between EOP estimations of IAA and EOP 05 C04 for Ru-E

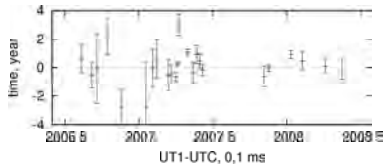

Figure 4. Differences between UT estimations of IAA and EOP 05 C04 for Ru-U

Table 3. Rms differences with EOP IERS 05C04

program N_{sess}	Ru-E 20					Ru-U 22
EOP	X_p, mas	Y_p, mas	UT, μs	X_c, mas	Y_c, mas	UT, μs
rms	0.83	1.04	36	0.55	0.62	127

4. Outlook

To further improve the EOP accuracy from the "QUASAR" network observations we plan first to use the Mark 5B registration and reproduction system, secondly to perform raw data processing at the new correlator ARC [8], and thirdly to use e–VLBI mode for determining UT.

The current results of the domestic VLBI programs show that the "Quasar" VLBI Network can be used as a basis for precise EOP determination within

national projects. The use of the new generation Mark 5B data acquisition system in the near future, processing raw data with the new ARC correlator, and using e–VLBI mode [6] to transfer data within the Ru-U sessions will permit to improve the accuracy of the EOPs obtained in the framework of the domestic programs.

Acknowledgements

We would like to thank Alexey Melnikov for producing observational schedules. We also wish to thank Andrey Dyakov and Roman Sergeev for providing observation support at the "Zelenchukskaya" and "Badary" observatories, respectively.

References

[1] Finkelstein, A., A. Ipatov, S. Smolentsev. Radio Astronomy Observatories Svetloe, Zelenchukskaya and Badary of VLBI Network QUASAR. IVS 2004 General Meeting Proc. N.R. Vandenberg, K.D. Baver (eds.), NASA/CP-2004-212255, 2004, 161–165.

[2] Surkis, I., V. Zimovsky, A. Melnikov, et al. IAA Correlator Center. International VLBI Service for Geodesy and Astrometry 2006 Annual Report. N.R. Vandenberg and K.D. Baver (eds.), NASA/TP–2007–214151, 2006, 143–146.

[3] Fedotov, L. VLBI Terminal in Badary Observatory. Proceedings of the 18th European VLBI for Geodesy and Astrometry Working Meeting. J. Bohm, A. Pany, H. Schuh (eds.), ISSN 1811-8380, TU Wien, 2007, 222–224.

[4] http://quasar.ipa.nw.ru/vlbi/

[5] Skurikhina, E., S. Kurdubov, V. Gubanov. IAA VLBI Analysis Center Report 2006. International VLBI Service for Geodesy and Astrometry 2006 Annual Report. D. Behrend and K. Baver (eds.), NASA/TP-2007-214151, 2007, 204–207.

[6] Finkelstein, A., E. Skurikhina, I. Surkis, et al. Using the Quasar VLBI Network for the Fundamental Time-Positioning Service of GLONASS. Astronomy Letters, v. 34, No 1, 59–69, 2008.

[7] Smolentsev, S., R. Sergeev. Badary Radio Astronomical Observatory. International VLBI Service for Geodesy and Astrometry 2007 Annual Report.

[8] Surkis, I., V. Zimovsky, A. Melnikov, et al. The IAA RAS 6-stations VLBI Correlator. This volume.

The 5th IVS General Meeting Proceedings, 2008, p. 324–328

Comparison and Validation of VLBI Derived Polar Motion Estimates

Thomas Artz [1], *Sarah Böckmann* [1], *Axel Nothnagel* [1], *Volker Tesmer* [2]

[1)] *Institut für Geodäsie und Geoinformation der Universität Bonn, Germany*

[2)] *Deutsches Geodätisches Forschungsinstitut, Germany*

Abstract. For a rigorous combination of VLBI and GPS data, they should not be subject to systematic differences. However, at some periods of time such systematic differences of up to 0.2 mas are present when comparing the official polar motion time series of the International VLBI Service for Geodesy & Astrometry and the International GNSS Service.

In a careful analysis of VLBI sessions we try to relate these systematic differences in polar motion to various possible causes. As the GPS terrestrial reference frame is much more stable than the one from VLBI the discrepancies are expected to be caused by VLBI. Therefore, we examine the VLBI solution setup and the data itself regarding network changes, analysis options and observation schedules.

1. Introduction

The International VLBI Service for Geodesy & Astrometry (IVS) provides an official combined VLBI solution. This combined product is calculated from the contributions of several IVS Analysis Centers (ACs). The ACs provide datum-free normal equations in the Solution Independent Exchange (SINEX) format which is used as input for the IVS combination. This combination is computed at the IVS Analysis Coordinator's office (e.g. [1, 5]).

As a rough quality assessment, the derived combined time series of the EOP is compared to those of the International GNSS Service (IGS). The differences of the y-pole component show a systematic behaviour around 2006-2007 (Fig. 1). These systematics are present between the IGS time series and the IVS combined solution as well as between the IGS and the individual solutions of the ACs calculated from the SINEX files. Furthermore, these systematics can also be seen in EOP-series computed by the ACs themselves. Since the IVS and the IGS solutions differ in terms of modelling and parametrization, such differences are not astonishing. But even between completely homogenized so-

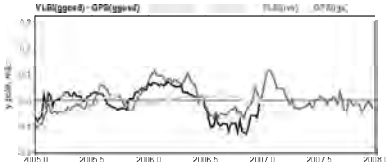

Figure 1. Y-pole differences (smoothed by a 70-day median filter; offsets removed) of IVS and IGS solution (dark gray), homogenized VLBI and GPS solutions (black) as well as the GPS differences (light gray)

lutions, produced in the German research project GGOS-D [3], such effects are present. Therefore, the systematics can not simply be explained by different solution setups.

In this study, a detailed analysis is performed on the basis of the IVS R1 and R4 sessions from the years 2005 to 2007. The VLBI analysis was done with the software package CALC/SOLVE [4]. Here, a state of the art modelling with VMF1, thermal deformation and atmospheric pressure loading was used. However, the change of these options as well as changes in the parametrization setup do not change the studied systematics significantly. In order to estimate the EOP, the station positions are fixed to their a priori values (ITRF2005[1]). As these a priori values are not totally consistent to our data, this might possibly lead to systematic effects. Nevertheless, this approach has been chosen since the use of a consistent TRF did not revise the situation.

The aim of this investigations is to validate whether the VLBI observables are responsible for the systematics. Changes in network geometry, the sensitivity of the solution on presence or absence of stations and analysis options are considered. Furthermore, the sensitivity of each individual session in view of the estimation of the y-pole component will be addressed.

2. Network Differences

In the time span considered, the R1 and R4 networks are subject to some changes. These are, on the one hand, the stop of operation at Fairbanks (end of 2005) and Algonquin Park (middle of 2006). On the other hand new stations started observing. The global distribution of stations is mainly changed by the absence of Fairbanks due to it's unique location in Alaska. But the overall volume of the observing network has not varied a lot.

The situation turns out to be slightly different if R1 and R4 networks are examined independently. This is shown in Fig. 2. The station distribution of the R1 network is fairly global. The station participation differs from session to session. Thus, the volume of the observing polyhedron varies but is comparably big on average. In contrast, the R4 network is concentrated on the western part of the world and is dominated by the stations Kokee Park and Wettzell. The volume of the R4 networks does not change a lot but it is significantly smaller than the volume of the R1 network. These differences in the network volume

[1] Except those of Zelenchukskaya and Svetloe which have been estimated from all VLBI observations up to the end of 2007.

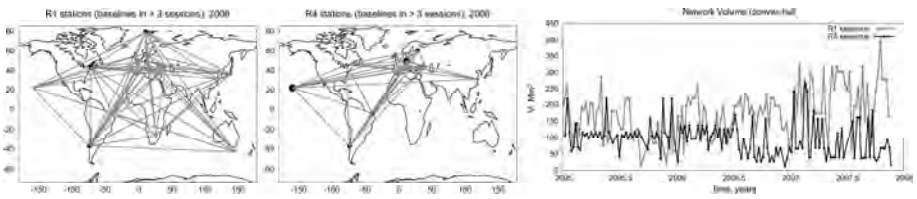

Figure 2. Station distribution of the R1 (left) and R4 (right) networks in 2006 as well as the volume of the session-wise observing polyhedron in 2005-2007 (right: R1 (gray) and R4 (black))

correspond to the quality deviations of the y-pole time series that are derived from the two individual sub-nets separately (Fig. 3). It can be seen that the systematics shown in Fig. 1 are mainly produced by the observations of the R4 network. The y-pole estimated from R1 sessions only shows systematics at the end of 2005 where the network volume is small, too.

Obviously, there is a relation between the y-pole systematics and the volume of the observing network. That corresponds to the fact that the network volume is somehow proportional to the formal errors [2]. The connection of the formal errors and the systematics under investigation will be discussed in more detail in section 4.

3. Impact of Single Stations

To verify the impact of single stations on the y-pole estimation two tests have been carried out. In the first test, the datum definition has been modified with respect to the standard solution to see whether one single station is responsible for the systematics. Step by step, one single station has been excluded from the datum definition. This means that all but one of the station's positions are fixed to their a priori values to estimate the EOP. As shown exemplarily for Fairbanks in Fig. 4, the estimates are affected systematically during specific time spans depending on the stations that are used to define the datum. Thus, for each independent session it should be decided which stations must not be fixed to their a priori values to take part in the datum definition. However, there are only a few observing stations and the fewer stations are used to define the datum, the weaker the EOP estimation is due to the correlation of EOP and the estimated station positions. Furthermore, it is not possible to choose the defining sub-nets doubtlessly until now: no connection between the variations in polar motion and the non-fixed stations can be seen. Neither is there a connection with the values of the estimated station positions nor do the correlation coefficients of the y-pole and the estimated coordinates exhibit any relations.

In the second test, a network change was simulated by removing all observations of a single station. Thereby, the scatter of the polar motion estimates is increased. And depending on the excluded station almost arbitrary new systematic variations can be created. These results have to be judged very carefully and critically since the original schedule of the session is disturbed and the remaining observations are not chosen to be optimal for the remaining network. Nevertheless, they document the delicateness of the equation system and the sensitivity on single station variations.

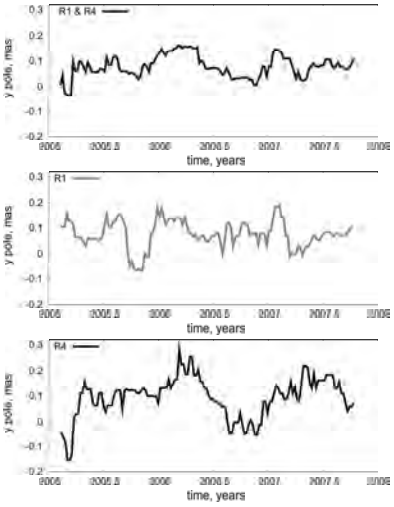

Figure 3. Y-pole differences to IGS (smoothed by a 70-day median filter) for estimates from R1 and R4 sessions (top), R1 sessions (middle) and R4 sessions (bottom) only

4. Sensitivity Due to Y-Pole Estimation

This section gives a deeper insight into the observation equation system itself and therefore into the effective observing geometry. This leads to a better understanding of how good the y-pole is defined by the observations in different sessions.

In general, the stochastic properties (formal error and correlations with other parameters) of a parameter describe how stable this parameter can be estimated from the given observations equations. In Fig. 5, the formal errors are displayed. The most obvious fact is that the formal errors are high during time spans where the systematic differences are high as well (Fig. 3).

Another possibility to judge the quality of the parameter estimation are the correlation coefficients. However, they are small and no significant difference between R1 and R4 sessions could be detected.

5. Conclusions

The IVS R1 and R4 sessions from 2005 onwards were analyzed regarding the estimation of the y-pole. Several aspects have been considered to explain systematic differences of VLBI and GPS derived estimates.

No coherence between the systematic differences and station position variations has been found. However, the systematics can be assigned to a weak network geometry. It was revealed that the R1 and R4 networks result in different y-pole estimates. Above all, the time series from R1 sessions is more stable and does not show such distinct systematics in comparison to GPS as the one derived from R4 sessions does.

To improve the stability of polar motion estimates, large networks, i.e. more stations with even distribution, should be scheduled. This would lead to a bet-

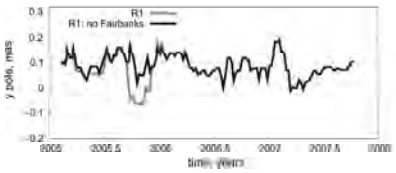

Figure 4. R1 y-pole differences to IGS from the standard approach (gray) and without Fairbanks in the datum definition (dark gray)

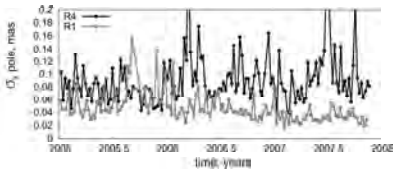

Figure 5. Formal errors of y-pole estimates in R1 (gray) and R4 (black) sessions

ter definition of the hemisphere over each telescope, particularly for those on the southern hemisphere and, thereby, to a better separation of estimated parameters. Furthermore, it should be noted that the participation of stations may differ from session to session as long as the volume of the observing polyhedron remains big. There are less systematics in the R1 y-pole estimates and the scatter of the individual estimates is less than the one from R4 sessions where the station participation is more unique.

Acknowledgements

This research has been funded by the project "GEOTECHNOLOGIEN" of the German ministry of education and research under reference FKZ 03F0425D and by the Deutsche Forschungsgemeinschaft under the reference DFG Gz: No 318/2-1.

References

[1] Böckmann, S., T. Artz, A. Nothnagel, et al. Comparison and combination of consistent VLBI solutions. Proceedings of the 18th European VLBI for Geodesy and Astrometry Working Meeting. Geowissenschaftliche Mitteilungen der TU Wien 79, 2007, 82–87.

[2] Malkin, Z. On dependence of EOP precision and accuracy on VLBI network. Proceedings of the 18th European VLBI for Geodesy and Astrometry Working Meeting. Geowissenschaftliche Mitteilungen der TU Wien 79, 2007, 75–81.

[3] Nothnagel, A., M. Rothacher, D. Angermann, et al. GGOS-D: A German Project on the Integration of Space Geodetic Techniques. Submitted to Proceedings of Journees 2007 Systemes de Reference Spatio-temporels, 2007.

[4] Petrov L. Mark-5 VLBI Analysis Software Calc/Solve; http://gemini.gsfc.nasa.gov/solve/.

[5] Vennebusch M., S. Böckmann, A. Nothnagel. The contribution of Very Long Baseline Interferometry to ITRF2005. J. Geodesy, DOI 10.1007/s00190-006-0117-x, 2006.

The 5th IVS General Meeting Proceedings, 2008, p. 329–334

The Variance Component Approach in the IVS Combination

Sarah Böckmann, Axel Nothnagel

Institute of Geodesy and Geoinformation, University of Bonn, Germany

Abstract. Within the International VLBI Service for Geodesy and Astrometry (IVS) several analysis centers contribute their solutions as input to the official combined products. In order to account for the different levels of variance of the individual solutions, relative weighting factors are determined by means of the variance component estimation method. In this paper, the variance component approach within the IVS combination is explained and the computed variance factors of each contribution are discussed. Furthermore, comparisons are presented showing the benefit of the variance component approach.

1. Introduction

Several IVS Analysis Centers (ACs) analyze geodetic VLBI observations with different software packages and provide their solutions to the official IVS combined VLBI solution as datum-free normal equations in SINEX format containing EOP and station positions. At the moment six ACs contribute to the combination using three different software packages (Tabl. 1).

Table 1. IVS ACs contributing to the combination with the software packages used

AC	Name	Software
BKG	Federal Agency for Cartography and Geodesy	CALC/SOLVE
DGFI	German Geodetic Research Institute	OCCAM
GSFC	Goddard Space Flight Center	CALC/SOLVE
IAA	Institute of Applied Astronomy	QUASAR
OPA	Paris Observatory	CALC/SOLVE
USNO	US Naval Observatory	CALC/SOLVE

From this input, time series of EOP are calculated as the official IVS combined product. Additionally, station position time series are computed for quality assessment. In this study, the variance component estimation is used to determine weighting factors for each contribution. Comparisons are carried out to investigate whether this approach leads to an improvement of the combined time series.

2. Variance Component Estimation

The variance component estimation (VCE), e.g. [1, 3], is used as a tool to determine relative weighting factors for individual solutions. Fig. 1 shows a flowchart of the combination process as performed here for each daily session.

1. All input data are converted from SINEX format into a binary format for the combination software DOGS-CS [2].
2. Every solution is transformed to the same epoch and an identical set of a priori parameters.
3. Station positions of each individual solution are calculated after adding an NNR/NNT datum.

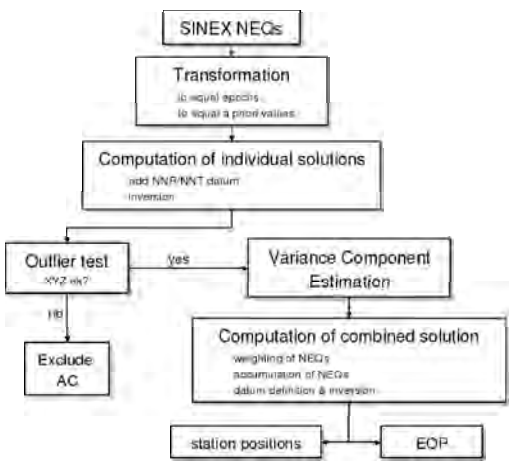

Figure 1. Data flow of the combination

4. As outlier test, the median of each station component over all individual solutions is computed. A contribution is rejected if the individual solution differ from the median by 3σ with a general threshold of 5 cm.
5. Relative weighting factors are determined by VCE.
6. The combined solution is calculated by accumulating the weighted datum-free normal equations and adding a datum definition.

Further details about the combination process can be found in [5].

The basic idea of the VCE is to compute one variance factor for each individual solution instead of one common a posteriori variance factor. The estimated variance factors can thus be used to weigh each solution before the combination. The VCE is performed in an iterative way until convergence is reached, i.e. until the update of the variance components is less than 1%.

In general terms, this should be done for each session independently. However, the redundancy of one single session is too small to estimate stable variance factors. To overcome this problem a sliding window over all sessions of

one month (generally 8 sessions) has been used. There are two disadvantages of this approach: the estimated variance factors can only be considered as an approximation and the VCE itself cannot be used as outlier test. Fig. 2 shows the estimated variance components for all R1 and R4 sessions between 2002 and 2008.

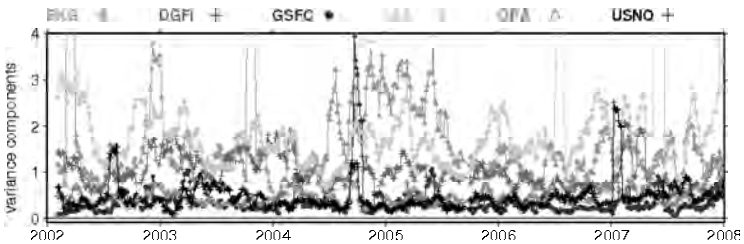

Figure 2. Estimated variance components of all R1 and R4 sessions

3. Validation

The individual and combined station positions of each single observing session are used as input for the VCE. Therefore, to validate the estimated variance components the station position time series of each input series are analyzed. Fig. 3 shows the height component of the station NyAlesund w.r.t ITRF2005 of each single solution. To better visualize the differences only sliding medians are displayed. Especially between 2004 and 2006, the estimated corrections of the BKG solution are bigger than of any other solution. This can directly be connected to the higher variance component estimates of the BKG solution during this time span (Fig. 2).

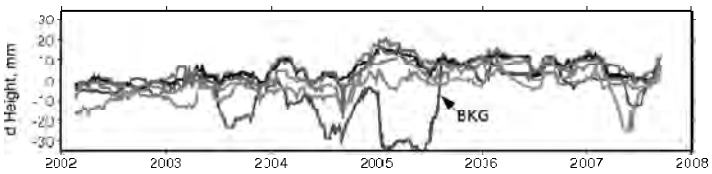

Figure 3. Median smoothed station positions of NyAlesund height component

Another example is displayed in Fig. 4. Here, the median smoothed time series of the height components of the station Algonquin Park is shown. The phase of the yearly signal of the IAA solution is shifted with respect to the yearly signal of all other single solutions. The same effect is visible in the height component of Westford (not shown here). Most probably, this is the reason for the higher variance component values for IAA over the whole time span.

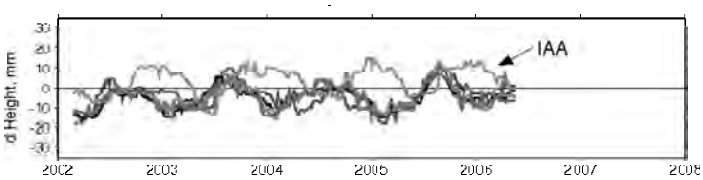

Figure 4. Median smoothed station positions of Algonquin Park height component

Although the station position time series of the DGFI solution does not show any bigger variations than the GSFC, OPA and USNO solutions, the variance factors estimated for the DGFI solutions are considerably higher than for the GSFC, OPA and USNO solutions. Due to the fact that the DGFI solution is the only solution computed with OCCAM, this leads to the assumption that the combined solution could be dominated by the GSFC, OPA and USNO solutions which are all analyzed with the same software (CALC/SOLVE) together with a similar modelling and parametrization.

To verify this assumption, variance components are estimated only for the contributions of 4 ACs. All of them are using either a different software package or a different parametrization and modelling. The results of this test are visualized in Fig. 5. While the estimated variance components of the BKG and IAA solutions remain nearly the same as for the estimation with all six ACs, the levels of variance of the USNO and DGFI solutions are nearly equal. This reflects the general problem of the IVS combination that four of six ACs use the same software package.

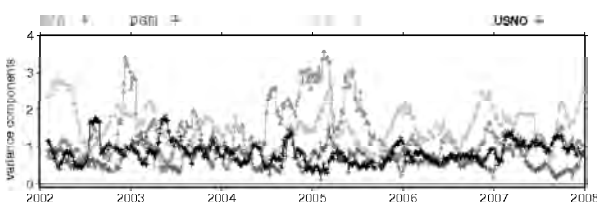

Figure 5. Estimated variance components for the contributions

4. Comparisons

To assess the benefit of the variance component approach, comparisons of station positions and EOP are carried out. For these comparisons three different combined solutions are computed to distinguish between the influence of the outlier test and the VCE. The first combined solution is calculated as described in Sec. 2, but without applying the outlier test and the VCE. The second combined solution is calculated with outlier test but without the VCE while for the third solution both the outlier test and the VCE are applied. In

addition, station positions and EOP are estimated from the individual normal equations in a single estimation process applying NNR/NNT conditions on the site coordinates.

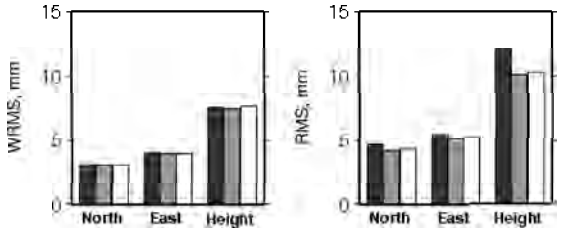

Figure 6. Station position repeatabilities w.r.t ITRF2005 of the three combined solutions, (black: without outlier test and VCE, gray: with outlier test, without VCE, white: with outlier test and VCE)

As a main result of these tests, station position repeatabilities w.r.t. ITRF2005 are computed from single session position estimates of all R1 and R4 sessions between 2002 and 2008. WRMS and RMS are calculated after offsets, rates and annual signals are removed with a least squares fit.

The common WRMS and RMS of all 17 stations of the three combined solutions are shown in Fig. 6. While no significant changes are visible neither for the WRMS of the horizontal components nor for the height, the unweighted RMS values show an improvement of 2.5 mm in the height component due to the outlier test. This simply indicates, that the detected outliers exhibit big formal errors.

Although no significant improvement of the station position repeatabilities is reached due to the outlier test and the VCE, the combined solution (outlier test and VCE applied) shows smaller WRMS values than any individual input series. For the horizontal components the WRMS is about 1 mm smaller than the smallest WRMS of all single solutions, the height WRMS about 2 mm.

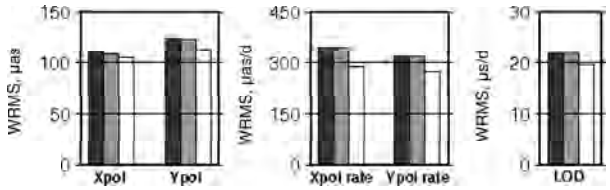

Figure 7. WRMS of the differences between the three VLBI combined EOP time series and the IGS EOP series (black: without outlier test and VCE, gray: with outlier test, without VCE, white: with outlier test and VCE)

In the same way as for the station coordinates, EOP series from 2002 till 2008 have been computed and compared to the IGS EOP series (igs00p03.erp, ftp://cddis.gsfc.nasa.gov/pub/gps/products). Offsets and rates are removed before computing the WRMS of these differences. Fig. 7 summarizes the results of the three combined solutions. The achieved improvement due to applying the outlier test only is rather small, but the VCE leads to improvements of about 10 % for the polar motion offsets, of 20 % and 15 % for the polar motion

rates and more than 10 % for LOD.

Comparing the VLBI EOP series of the six individual solutions and the combined solution (outlier test and VCE applied) with the IGS EOP series, the combined solution fits better to IGS than any individual solution in all components.

5. Summary and Outlook

The comparisons of the station positions have shown that a small improvement of the combined solution due to the outlier test was reached but no additional improvement due to the VCE. Nevertheless, in the comparison with the all input solutions, the combined solution shows smaller station position repeatabilities w.r.t. ITRF2005 than any single solution.

Concerning the EOP, improvements of up to 20 % were obtained by applying the outlier test and the VCE in the combination process. Furthermore, the combined series agrees better with the IGS EOP in all components than any individual solution.

At the moment these investigations were only carried out for the R1 and R4 session. In the future this promising approach will be applied to the quarterly solution including all daily VLBI sessions from 1984 till now. Moreover, we are working on stabilizing the estimation of the variance components, so that these components can be estimated for one session individually. We expect that this leads to more realistic variance factors for individual observing session and not only to an approximate level of variance over 8 sessions.

Acknowledgements

This research has been funded by the project "GEOTECHNOLOGIEN" of the German Ministry of Education and Research under reference FKZ 03F0425D.

References

[1] Grafarend, E.W., A. Kleusberg, B. Schaffrin. An introduction to the variance-covariance component estimation of Helmert type. Zeitschrift für Vermessungswesen, v. 105, 161–180, 1980.

[2] Gerstl, M., R. Kelm, H. Müller, et al. DOGSCS Kombination und Lösung grosser Gleichungssysteme. DGFI Interner Bericht Nr. MG/01/1995/DGFI, 2001.

[3] Koch, K.R. Schätzung von Varianzkomponenten. AVN 85, 264–269.

[4] Kusche J. Noise variance estimation and optimal weight determination for GOCE gravity recovery. Adv. Geosci., 1:81–85, 2003.

[5] Vennebusch, M., S. Böckmann, A. Nothnagel. The contribution of Very Long Baseline Interferometry to ITRF2005. J. Geodesy, DOI 10.1007/s00190-006-0117-x, 2006.

The 5th IVS General Meeting Proceedings, 2008, p. 335–340

A Postseismic Relaxation Model for the 2002 Denali Earthquake from GPS Deformation Analysis Applied to VLBI Data

Robert Heinkelmann [1], *Jeffrey Freymueller* [2], *Harald Schuh* [1]

[1)] *Institute of Geodesy and Geophysics (IGG), Vienna University of Technology, Austria*

[2)] *Geophysical Institute (GI), University of Alaska Fairbanks, USA*

Abstract. Five years after the 2002 Denali, Alaska, earthquake a postseismic deformation model based on GPS time series analysis is available and implemented into the new solution IGG08R01. The non-linear deformation model includes a logarithmic and an exponential term with decay factors derived from the GPS solution and reduces the 3D RMS fit w.r.t. VLBI estimates by 2.5 mm in comparison to the 'classical' approach using a coseismic displacement and a constant velocity (IGG07R04). By our comparisons we find good agreement between postseismic GPS and VLBI coordinate time series, i.e. the latter for station Gilmore Creek, which leads us to the conclusion that GPS and VLBI measure the same co- and postseismic surface deformations induced by the earthquake.

1. Introduction

Driven by the continuous lithospheric processes the Pacific Plate is steadily shifted northwards subducting beneath the North American Plate (Fig. 1). The collision of the Yakutat Block (YAK), a block of thickened and buoyant crust, has caused the Wrangell Subplate, a piece of the North American Plate, to break loose and rotate counter-clockwise. The Denali and Totschunda Faults form the northeastern margin of the Wrangell Subplate [7].
The M7.9 Denali earthquake on Nov. 3, 2002 22:12:42 UT, was the largest strike-slip earthquake in North America since 1857. Surface rupture occurred along 340 km of the Susitna Glacier, Denali, and Totschunda Faults [3]. The earthquake triggered significant postseismic deformation, and [4] showed that a multiple mechanism model is well suited to describe postseismic deformation observed at both near-field (< 50 km) and far-field (< 300 km) GPS sites. The primary mechanisms of postseismic stress relaxation are summarized in Fig. 2.

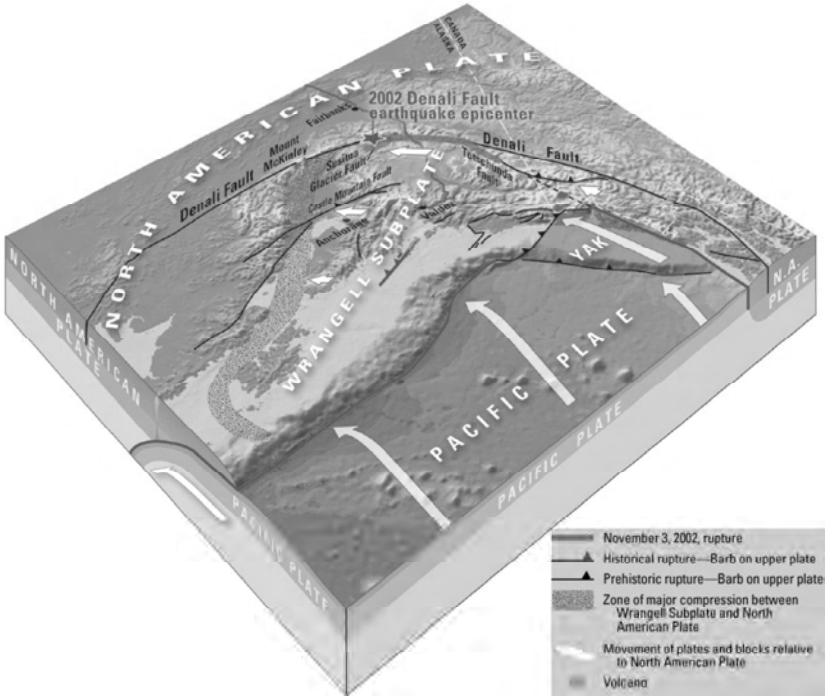

Figure 1. Regional tectonics [7]

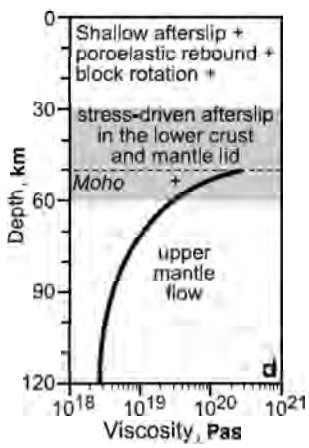

Figure 2. Multiple mechanism model [4]

- **afterslip:** coseismic stress causes aseismic slip after the earthquake.
- **poroelastic rebound:** excess fluid pressure in the near-field region (here 10 to 30 km) causes fluid flow resulting in postseismic deformations and stress change.
- **viscoelastic relaxation:** weaker lower crust and upper mantle do not sustain coseismic stress changes, but relax viscously within years to decades.

2. Time Series Modelling and Analysis of Surface Deformations

Postseismic surface deformations can be modelled by fitting analytical functions to the topocentric position time series using the following equations:

$$y(t) = a + b \cdot \lg\left(1 + \frac{t - t_0}{l_\tau}\right) + c \cdot \left(1 - \exp\left(-\frac{t - t_0}{e_\tau}\right)\right), \qquad (1)$$

where y denotes a specific station position component (e.g. φ, λ, or h), coefficient a describes the instantaneous coseismic displacement at the epoch of event $t = t_0$, and b and c are coefficients of the logarithmic term with $l_\tau = 0.05$, and the exponential term with $e_\tau = 3.0$, respectively, based on the fit to several GPS time series. Before the coefficients a, b, and c are estimated by least-squares adjustment the positions y are corrected with

$$y(t) = y(t) - \left[d + e \cdot t + \sum_{i=1,2} f_{i,1} \cdot \sin(2i\pi t) + f_{i,2} \cdot \cos(2i\pi t)\right], \qquad (2)$$

where the variables d, e represent preseismic tectonics (offset and slope), and the coefficients $f_{i,j}$ ($j \in \{1, 2\}$) consider seasonal positional variations. Equations (1) and (2) may be fit separately or combined into a single equation, depending on the time span of the data. The seasonal variations might be different for VLBI and GPS, if they are due in part to systematic errors, but the other terms in the model should be identical for all geodetic techniques.

3. New VLBI Solution IGG08R01

Unlike prior Institute of Geodesy and Geophysics (IGG) TRF solutions such as IGG07R04, the new global solution IGG08R01 includes a non-linear deformation model (1) for GILCREEK (Gilmore Creek, Alaska, USA) VLBI site after the Denali earthquake. Other earthquakes such as the Loma Prieta, California, earthquake [2] on Oct. 1, 1989 are still modelled by a single coordinate jump. Compared to previous analysis results, i.e. [5, 6], the time series model was extended by a logarithmic term and the decay factor of the exponential term was enlarged to 3.0 years. The new model is determined including VLBI data until 2006.0, i.e. until the termination of geodetic VLBI activities at Gilmore Creek Observatory. The GPS solution is provided by the Geophysical Institute (GI), University of Alaska Fairbanks, and represents daily solutions. Tabl. 1 and Fig. 3 clearly indicate that IGG08R01 provides the best fit to postseismic deformations at Gilmore Creek after the Nov. 3, 2002 Denali earthquake.

The piecewise linear function (PWLF), which models the postseismic deformations in the ITRF2005 (Fig. 3) partly deviates from VLBI estimates, in

Table 1. Unweighted RMS w.r.t. VLBI data obtained with (3)

RMS	ITRF2005	IGG07R04	IGG08R01	GPS data
Latitude, mm	3.8	6.1	3.1	13.8
Longitude, mm	3.8	5.1	3.1	17.6
Height, mm	8.3	7.8	7.5	10.5
3D, mm	9.8	11.2	8.7	24.7

particular the first two postseismic pieces of the height component.
The unweighted RMS given in Tabl. 1 were computed with:

$$RMS = \left\{ \frac{1}{N} \sum_{1}^{N} \left[(obs_j - model_j)^2 \right] \right\}^{1/2}, \tag{3}$$

where obs_j denotes the VLBI estimate at epoch j and $model_j$ the corresponding model value at the same epoch j or the GPS estimate at the nearest epoch. Since VLBI and GPS sessions are not performed at the same time the RMS of model fit cannot be directly compared to the RMS between VLBI and GPS

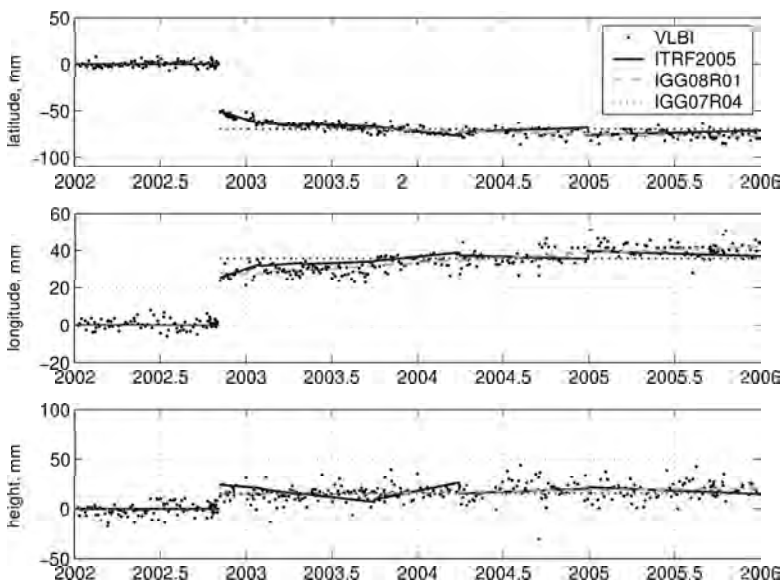

Figure 3. Topocentric position of GILCREEK observed by VLBI and modelled in the ITRF2005 [1] and in the two TRF solutions of the IGG, Vienna, described in the text

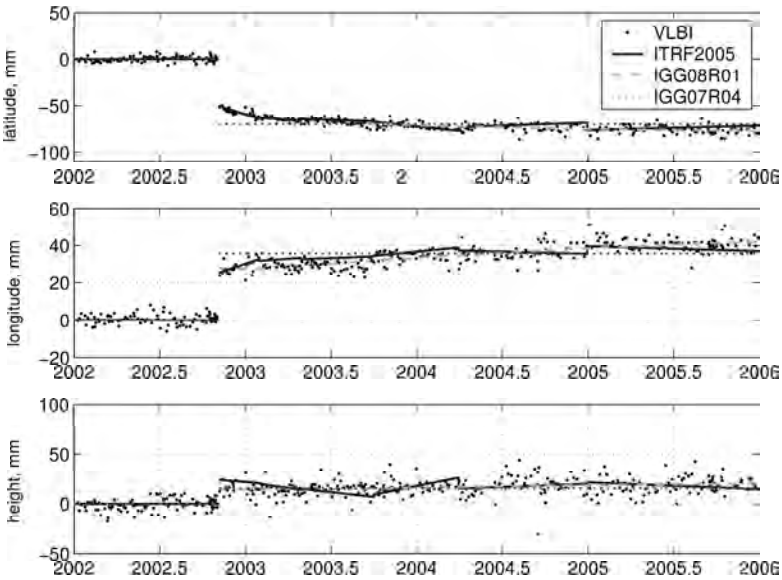

Figure 4. Comparison of topocentric positions at FAIR/GILCREEK co-located site obtained by GPS and VLBI solutions. The GPS solution was provided by the Geophysical Institute, Fairbanks, and the VLBI solution was computed at the Institute of Geodesy and Geophysics, Vienna

estimates. A divergence between GPS and VLBI (Fig. 4) from about 2003.8 to 2004.16 can be found, which shows up mainly in the longitudinal component. This effect is present in other GPS time series as well, e.g. SOPAC (Scripps Orbit and Permanent Array Center, http://sopac.ucsd.edu/) and remains unexplained at the moment. It does not appear at an independent GPS site located 25 km away (CLGO), therefore, it appears to represent some kind of station-specific error.

4. Conclusions

For modelling the postseismic surface deformations of the Denali earthquake, the non-linear (1) is well-suited for both, GPS and VLBI analysis, since both space geodetic techniques were subject to the same coseismic and postseismic displacements. Adjusted a posteriori station positions do not differ significantly using a single coordinate jump and a constant station velocity model (IGG07R04), or a non-linear model (IGG08R01). Therefore, the application of such a refined model for a priori coordinates is only mandatory, if station positions are fixed, i.e. not estimated during the parameter estimation, or in the development of a time-dependent model such as ITRF.

Some of the linear pieces of the ITRF2005 solution of station GILCREEK follow the seasonal variations of GPS positions and deviate significantly from the VLBI estimates. This effect is most obvious in the height component (Tabl. 1, Fig. 3–4).

Acknowledgements

This study could not have been prepared without the provision of excellent VLBI data by the IVS.

References

[1] Altamimi, Z., X. Collilieux, J. Legrand, et al. ITRF2005: a new release of the International Terrestrial Reference Frame based on time series of station positions and Earth orientation parameters. J. Geophys. Res., v. 112, B09401, DOI 10.1029/2007JB004949, 2007.

[2] Clark, T.A., C. Ma, J. M. Sauber, et al. Geodetic measurement of deformation in the Loma Prieta, California earthquake with very long baseline interferometry. Geophys. Res. L., v. 17, 1215–1218, 1990.

[3] Eberhart-Phillips, D., P.J. Haeussler, J.T. Freymueller, et al. The 2002 Denali Fault Earthquake, Alaska: A Large Magnitude, Slip-Partitioned Event. Science, v. 300, 113–119, 2003.

[4] Freed, A.M., R. Bürgmann, E. Calais, et al. Implications of deformation following the 2002 Denali, Alaska, earthquake for postseismic relaxation processes and lithospheric rheology. J. Geophys. Res., v. 111, B01401, DOI 10.1029/2005JB003894, 2006.

[5] MacMillan, D.S., S. Cohen. Postseismic transient after the 2002 Denali Fault Earthquake from VLBI measurements at Fairbanks. International VLBI Service for Geodesy and Astrometry 2004 General Meeting Proceedings. N.R. Vandenberg and K.D. Baver (eds.), NASA/CP–2004-212255, 2004, 491–495.

[6] Titov, O., P. Tregoning. Post-seismic motion of Gilcreek geodetic sites following the November, 2002 Denali Earthquake. International VLBI Service for Geodesy and Astrometry 2004 General Meeting Proceedings. N.R. Vandenberg and K.D. Baver (eds.), NASA/CP–2004-212255, 2004, 496–500.

[7] U.S. Geological Survey, Rupture in South-Central Alaska – The Denali Fault Earthquake of 2002. U.S. Department of the Interior, U.S. Geological Survey, Fact Sheet 014–03;
http://pubs.usgs.gov/fs/2003/fs014-03/fs014-03.pdf.

The 5th IVS General Meeting Proceedings, 2008, p. 341-344

Measuring the Relativistic Parameter γ Using the Current Geodetic VLBI Data Set

Sébastien Lambert [1], *Christophe Le Poncin-Lafitte* [2]

[1] *Observatoire de Paris, Département SYRTE, France*

[2] *Lohrmann Observatory, Dresden Technical University, Germany*

Abstract. We used VLBI to measure the gravitational light deflection by Solar System bodies of radio waves emanating from distant compact radio sources. It is well known that this bending is characterized only by the post-Newtonian parameter γ within the standard parametrized post-Newtonian formalism, which is unity in General Relativity. Using a larger geodetic VLBI data set than in previous work, we studied the stability of the analysis and obtained $\gamma = 0.99995 \pm 0.00020$. We discussed also possible issues concerning systematic biases through an analysis of subgroups of data.

1. Light Deflection in General Relativity

Nowadays, relativity belongs to the toolbox of astronomers. As the gravitational field of the Solar System is not intense, it is however common to use the relativistic theories of gravitation in their asymptotic limit, namely the weak field approximation, to describe gravitational effects taking place in the Solar System. This can be done by the use of the parameterized post-Newtonian formalism enabling us to test all possible effects such as light deflection, time delay of light, or perihelion precession. This formalism has a dozen parameters, among them the very well-known β and γ. Experiments of light deflection are particularly sensitive to γ and VLBI is an important technique to study this effect when the light ray coming from quasars are grazing the Sun. This enables us to determine a value of the parameter γ, which is equal to unity in General Relativity (GR), and thus to constrain possible signatures of the scalar field in the Solar System.

If ϕ is the angle between the Sun and the source seen from the Earth, and b the impact parameter, the deflection angle is

$$\theta \approx (\gamma + 1)\frac{GM}{c^2 b}(1 + \cos\phi). \tag{1}$$

A grazing ray at the Sun's limb is deflected by $1.7''$.

2. Close Approaches to the Sun

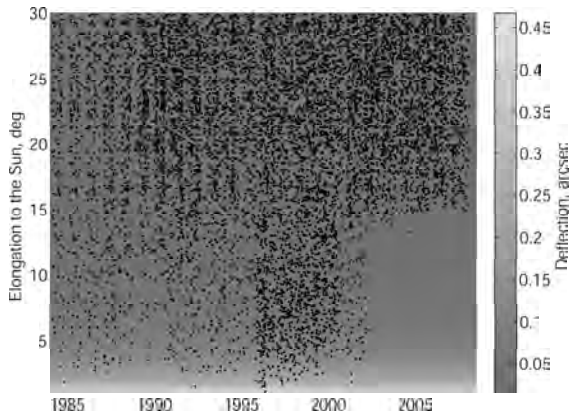

Figure 1. Observational history of the sources at less than 30° elongation to the Sun. The scale gives the deflection angle

Fig. 1 displays the observational history of the sources at less than 30° to the Sun in the 3762 24-hour geodetic sessions fully or partly processed in the upcoming analyses. The VLBI observing schedule included a number of radio sources that were observed at less than 15° to the Sun. As it is shown on Fig. 1, this number was quite uniform during 1984–1996, and then substantially increased during 1996–2002. Later, sources at less than 15° have no longer been observed, at least not in the permanent geodetic VLBI program whose data is released by the IVS. Fig. 1 naturally yields three time spans on which we propose to run the analyses: 1984–2007 (maximum number of data), 1996–2002 (higher density of close approaches), and 1984–2002 (compromise between density and number of data).

3. Analysis Strategies

Our analysis scheme is as follows.

1. Generate a base solution by a global inversion of all the data over 1984–2008. The radio source coordinates are estimated as global parameters and constrained by a no-net rotation (NNR) on the 247 stable sources [2] w.r.t. ICRF-Ext.2. The obtained celestial reference frame will be taken as a priori for all the other solutions. The station coordinates are estimated as global parameters with a NNR and no-net translation on 35 sites. Stations having non-linear motions are modeled by splines. EOP, rates, and nutation offsets are estimated as arc parameters.
2. Run two global solutions over 1984–2008, both with EOP and station coordinates as session parameters, γ as global parameter, and with (i)

source coordinates estimated as global parameters and constrained to stay within 10^{-8} rad around the a priori without any non rotation condition, (ii) source coordinates not estimated.

3. Run another two solutions over 1984–2008 in independent mode (i.e., no global parameter) where γ is obtained as time series and (i) source coordinates are estimated (same constraint as above), (ii) source coordinates are not estimated.

4. Repeat 2 for 1996–2002 and for 1984–2002.

In solutions 2–4, EOP, rates, nutation offsets, and station coordinates are estimated as session parameters. Troposphere zenith delay is estimated as a continuous piece-wise linear function at 20-min interval. Troposphere gradients are estimated as 8-hour East and North piece-wise functions at all stations except for a set of 110 stations. Elevation cut-off for radio sources is set to 5°. We used the Calc/Solve software package. Solution characteristics and γ estimates are gathered in the Table below.

Table 1. Characteristics of the solutions and estimated value of γ

	Number of sessions	Postfit rms delay, ps	γ		
			Sources estimated	Sources not estimated	Per session
1984–2008 (S1)	3762	34.3	1.00039 ±0.00016	1.00041 ±0.00015	1.00038 rms 0.0125
1996–2002 (S2)	753	32.6	0.99961 ±0.00022	0.99969 ±0.00021	0.99969 rms 0.0077
1984–2002 (S3)	2883	23.2	1.00015 ±0.00018	0.99995 ±0.00018	0.99990 rms 0.0125

4. Results and Discussion

All solutions are consistent with GR within $\sim 5\times 10^{-4}$. From the solutions in independent mode, we estimate weighted averages of γ over the above three time spans (last column of the Table). They are in good agreement with the global estimates. Solution (S1) shows the highest departure to the unity and is discussed later. Global solution (S2) appears to have the lowest postfit rms delay. The estimates of γ (with or without estimating the radio source positions) are consistent with GR at 0.0002, which is the difference between the two estimates of γ. This value is slightly higher than the formal standard error and we will substitute it to the standard error. Moreover, the estimate of γ in the solution where the source coordinates are not estimated is expected to be more reliable since correlations between γ and source coordinates are cut. Our final reference value is $\gamma = 0.99995 \pm 0.00025$.

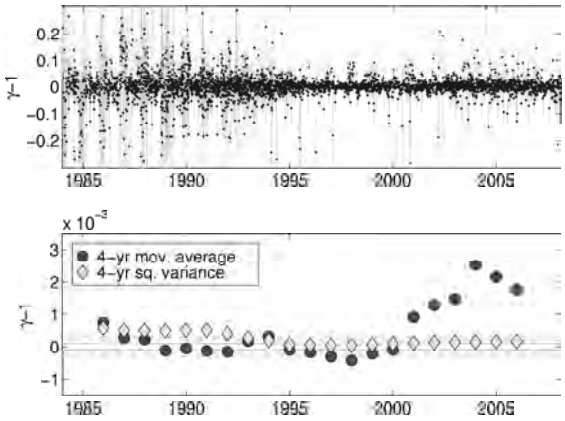

Figure 2. Solution per session for γ. Top: session estimates. Bottom: yearly values. Grey lines are spaced by 10^{-4} apart from zero

This value has to be compared to other recent estimates: Shapiro et al.[2] found 0.9998±0.0004 by the analysis of VLBI delays over 1979–1999. Our study constitutes an independent check of their work and adds moreover the 1999–2002 observational period which is rich in close approaches below 10° to the sun. Bertotti et al. [1] derived from a spacecraft tracking time-delay experiment a value that is consistent with GR with an error of 0.00002. Although we are slightly better than [1, 2] have an error smaller than ours by a factor of ten.

Solution (S1) exhibits a significant systematic effect of $\sim 4\times 10^{-4}$. It corresponds to a degradation of the estimates after 2002 showing up in Fig. 2, whose cause is not cleared up yet. Whether it is an effect of the lack of close approaches after 2002 or of the network, remains unclear at this stage of our research. Such a feature can be correlated with several changes appearing in the VLBI network organization after 2002. The year 2002 is also a key date: the entrance of the IVS R1/R4 parallel network leads to a smaller postfit rms for these sessions. Also, an examination of the baseline lengths shows that 12,000-km long baselines are extensively used after 2002 whereas they were only seldomly solicited before, resulting in a different relative geometry between the array and the sources.

References

[1] Bertotti, B., L. Iess, P. Tortora. Nature, 425, 374, 2003.

[2] Feissel-Vernier, M., C. Ma, A.-M. Gontier, et al. Astron. Astrophys., v. 452, 1107, 2006.

[3] Shapiro, S.S., J.L. Davis, D.E. Lebach, et al. Physical Review Letters, 92, 121101, 2004.

The 5th IVS General Meeting Proceedings, 2008, p. 345-354

Astrophysical Stability of Radio Sources and Implication for the Realization of the Next ICRF

Patrick Charlot

Laboratoire d'Astrophysique de Bordeaux, Université de Bordeaux, France

Abstract. The intrinsic radio structure of the extragalactic sources is one of the limiting errors in the definition of the International Celestial Reference Frame (ICRF). This paper reports about the ongoing work to monitor the structural evolution of the ICRF sources by using the Very Long Baseline Array and other VLBI telescopes around the world. Based on more than 6000 VLBI images produced from such observations, we assess the astrometric suitability and compactness of the ICRF sources at 2 GHz, 8 GHz, 24 GHz and 43 GHz. The number of VLBI images available for a given source varies from 1 for the least-observed sources to 28 for the most intensively-observed sources at the standard 8 GHz geodetic frequency. Overall, about one-third of the ICRF sources are found to be astrometrically suitable at 8 GHz, while the corresponding fraction at the higher frequencies (24 and 43 GHz) is above 80%. Conversely, only marginal differences in source compactness is found between the four frequencies. The astrometric suitability and compactness of the sources vary with time because of evolution in the astrophysical source morphology.

1. Introduction

The International Celestial Reference Frame (ICRF), which has been the official IAU reference frame in use since 1 January 1998, is currently based on the VLBI positions of 717 extragalactic radio sources. Of these, 608 sources are from the original ICRF built in 1995, with a categorization that comprised 212 well-observed *defining* sources (which served to orient the axes of the frame), 294 less-observed *candidate* sources, and 102 *other* sources showing coordinate instabilities [1]. The accuracy in the individual ICRF source positions has a floor of 250 μas, while the axes of the frame are stable to about 20 μas in orientation. Since then the positions have been improved for the non-defining sources and the frame has been extended by 109 *new* sources in ICRF-Ext.1 and ICRF-Ext.2 using additional data acquired in the period 1995–2002 [2].

At the IAU XXVIth General Assembly in Prague (August 2006), the com-

munity decided to engage in the realization of the successor of the ICRF, to be presented at the next IAU General Assembly in 2009. The motivation for generating this new celestial frame is to benefit from recent improvements in VLBI modeling (e.g. for the troposphere) and to take advantage of the wealth of VLBI data that have been acquired since the time the ICRF was built. A major issue to be addressed in this new realization is the revision of the source categorization, in particular the choice of the defining sources. Such a revision is necessary because some of the original ICRF defining sources were found to have extended structures [3] or position instabilities (e.g. [4]), and are therefore improper for defining the celestial frame with the highest accuracy.

The selection criteria that are considered by the working group in charge of the realization of the next ICRF for the identification of proper defining sources are based either on structure information (VLBI images), to evaluate the astrometric suitability of the sources, or on time series of source coordinates, to assess their position stability. In this paper, we discuss only the former. There are now more than 6000 VLBI images available at multiple epochs and several frequency bands (2 GHz, 8 GHz, 24 GHz and 43 GHz) to evaluate the source quality, whereas these were less than a hundred at the time the ICRF was built, thereby permitting considerable progress. In Sect. 2, we present the observational data used in this work, while our results are discussed in Sects. 3 and 4. These are presented in terms of astrometric suitability and source compactness, with specific emphasis on the time variability of such indicators.

2. Observational data

The VLBI maps used in our analysis were produced from a total of 46 VLBI sessions conducted between 1994 and 2007, which were imaged either at USNO or at Bordeaux Observatory. These comprise:

- 8 dedicated dual-frequency (8 GHz/2 GHz) imaging sessions conducted with the Very Long Baseline Array (VLBA) between July 1994 and January 1997 [3, 5, 6];
- 23 dual-frequency (8 GHz/2 GHz) Research & Development VLBA (RDV) sessions conducted between January 1997 and June 2007; these sessions were carried out with the 10 VLBA stations and up to 10 additional geodetic telescopes;
- 5 dedicated southern-hemisphere 8 GHz imaging sessions conducted between July 2002 and April 2004 with the Australian Long baseline Array, augmented by radio telescopes in South-Africa, Hawaii, and Japan [7, 8];
- 10 VLBA sessions conducted at either 24 GHz or 24/43 GHz between May 2002 and March 2007 for the purpose of extending the ICRF to higher frequencies [9]; data at 8 GHz/2 GHz were also obtained during one of these sessions while another session acquired data at 8 GHz.

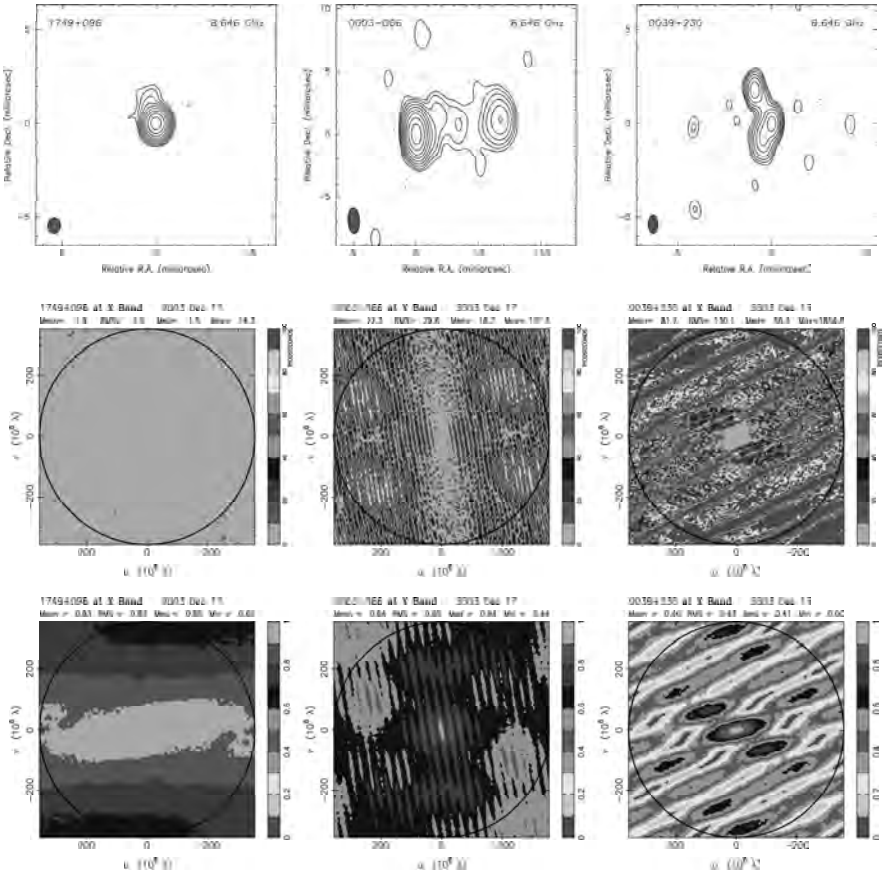

Figure 1. VLBI images at X band (8 GHz) for three ICRF sources (1749+096, 0003−066, 0039+230) as derived from the data of a RDV session conducted on 2003 December 17 (upper sub-panels). The middle sub-panels show the corresponding structure correction maps (used to calculate the structure index), while the lower sub-panels show the corresponding visibility maps (used to calculate the source compactness). The circle drawn in these panels corresponds to baselines that have a length equal to one Earth diameter. The color scale for the structure correction maps goes from 0 to 100 ps, while that for the visibility maps is between 0 and 1 (since visibility amplitudes are normalized by the total source flux density

Altogether, this represents a total of 2697 maps at X band (8 GHz) from 577 ICRF sources, 2388 maps at S band (2 GHz) from 492 ICRF sources, 1072 maps at K band (24 GHz) from 202 sources, and 267 maps at Q band (43 GHz) from 112 sources. There are up to 28 VLBI epochs available at X band for the most intensively-observed source, whereas only one epoch is available for 216 less-observed sources; 81 sources have X-band images available for 10 epochs or more. Less sources have been imaged at S band (compared

Table 1. Structure index series at X band (8 GHz) for a sample of 20 ICRF sources

Source name	Structure index values															
0003−066	3	2	2	2	2	2	2	2	2	2	2	2	3	3	3	...
0014+813	1	2	2	2	2	2	2	2	2	2	3	2	3	2	2	...
0048−097	1	1	1	1	1	1	1	1	1	1	1	1	1	2	2	...
0059+581	2	1	1	1	1	1	1	1	1	1	1	1	2	1	1	...
0111+021	3	3	3	3	3	3	3	3	3	3						
0119+041	2	2	2	2	2	2	2	2	2	2	2	1	2	3	3	...
0119+115	2	1	1	1	2	2	3	3	2	2	2	2	2	2	3	...
0133+476	2	2	1	1	1	2	1	1	1	1	1	1	2	1	1	...
0201+113	2	2	2	3	3	2	3	3	3	3	3	3	3	2	2	...
0202+149	2	2	2	2	2	2	2	3	3	3	2	2	3	3	2	...
0229+131	2	3	2	2	2	2	2	2	1	2	1	2	2	2	2	...
0234+285	3	2	2	2	2	2	2	2	2	2	2	2	2	2	1	...
0235+164	1	1	2	2	1	1	2	1	2	1	2					
0238−084	4	4	4	4	4	4	4	4	4	4	4	4	4	4	3	
0336−019	2	2	3	2	2	2	2	2	2	2	1	2	3	2	2	...
0402−362	1	2	2	1	2	2	2	3	2	2	2	3	2	3	2	...
0430+052	4	4	3	4	4	4	4	4	4	4	4	4	4	4	4	...
0454−234	2	1	1	2	1	1	1	1	1	1	1	1	2	2	1	...
0458−020	2	2	2	2	2	2	2	2	2	2	2	2	2	2	2	...
0528+134	1	1	2	2	2	2	2	2	3	2	2	2	2	2	2	...

to X band) because the southern-hemisphere sessions were carried out only at the single 8 GHz band. 18 sources were observed in all ten K band sessions.

A sample of X-band VLBI images for three ICRF sources, as derived from the data of a RDV session conducted in December 2003, is shown in Fig. 1 (upper sub-panels), along with the corresponding structure corrections maps (middle sub-panels) and visibility maps (lower sub-panels). These maps are the basis for calculation of the source structure index and compactness (see Sec. 3 and 4). Based on this calculation, it is found that only one of the three sources in Fig. 1 (1749+096) has a good astrometric suitability (structure index value of 1); the two other sources (0003−066 and 0039+230), with structure index values of 3 and 4, have a poorer astrometric quality, as also reflected by the extended morphology that their VLBI images reveal. This fraction of suitable sources is consistent with that found in the entire ICRF, as discussed below.

3. Astrometric suitability

Based on the VLBI image database described above, we derived the expected effects of intrinsic source structure on the VLBI delay astrometric quan-

Table 2. Structure index series at K band (24 GHz) for a sample of 18 ICRF sources

Source name	Structure index values									
0149+218	1	1	1	1	1	1	1	1	2	2
0300+470	1	1	1	2	2	1	1	2	2	1
0454−234	1	1	2	2	2	2	2	2	1	1
0458−020	1	1	1	1	1	1	1	1	1	1
0648−165	2	1	2	1	1	1	2	1	2	2
0749+540	1	1	2	2	2	1	1	1	1	1
0754+100	2	2	2	2	2	2	2	1	3	2
0804+499	1	1	1	1	1	1	1	1	1	2
0808+019	1	1	1	1	1	1	1	1	1	1
0953+254	2	2	1	2	2	2	2	2	1	2
1045−188	2	1	2	2	2	2	2	1	1	2
1124−186	1	1	1	1	1	1	1	1	1	1
1308+326	1	1	1	1	1	2	2	2	2	2
1502+106	1	2	1	2	2	2	2	2	2	1
1726+455	1	1	1	1	1	1	1	1	1	1
2008−159	2	1	1	2	1	2	1	2	2	2
2136+141	2	2	2	2	2	2	2	3	2	2
2255−282	1	1	1	1	1	1	1	1	2	1

tities over the entire u-v plane (see Fig. 1, middle sub-panels), following the algorithm of [10]. We then used the "structure index" indicator to define the astrometric source quality, as devised by [6]. Structure index values of 1 and 2 point to excellent and good astrometric suitability, respectively, while values of 3 and 4 point to poor suitability. A given source may have differing structure indices at different frequency bands, depending on properties of the brightness distribution. The structure index may also vary with time because of possible temporal evolution of the brightness distribution.

For each source, we obtained a series of structure index at each band according to the number of VLBI images available. Table 1 shows a sample of the structure index series available at X band for 20 intensively-observed ICRF sources, while Table 2 shows the results obtained at K band for the 18 sources that have been observed in all ten K band sessions. Overall, it is found that the variability of the structure index is generally not random but follows regular trends, probably reflecting the astrophysical evolution of the sources. Adopting a conservative approach, we chose the maximum value of the structure index as the source quality indicator when multi-epoch structure indices are available. In other words, if a source shows a structure index value of 3 or 4 at one or more epochs, it should be regarded as unsuitable for highly-accurate astrometry even though it has structure index values of 1 or 2 at some other epochs.

By using this multi-epoch indicator, we compared the structure index dis-

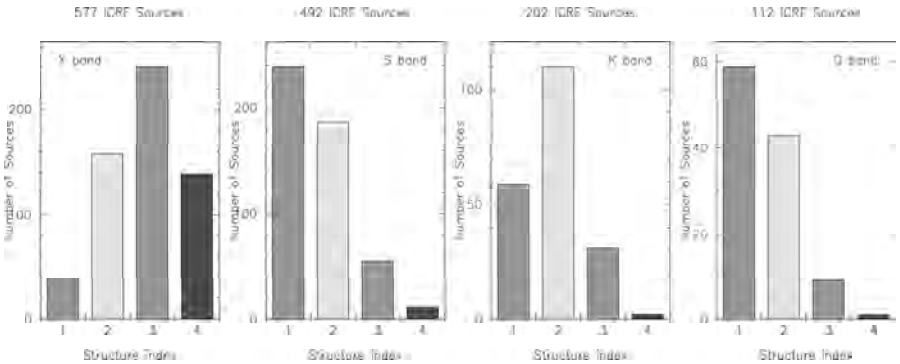

Figure 2. Structure index distribution at X band (8 GHz), S band (2 GHz), K band (24 GHz), and Q band (43 GHz), for all ICRF sources that have been imaged at these frequencies. The fraction of ICRF sources for which the structure index has been derived is 80% at X band, 69% at S band, 28% at K band, and 16% at Q band

tribution for each frequency band (8 GHz, 2 GHz, 24 GHz, and 43 GHz), as shown in Fig. 2. At X band, it is found that roughly one-third of the sources (197 sources out of a total of 577 sources) are astrometrically-suitable according to our criterion (maximum structure index value of either 1 or 2) while at S band, 86% of the sources (424 sources out of a total of 492 sources) fulfil this condition. As noted in [6], the contribution of the S-band structure to the dual-frequency (S/X) calibrated delay is usually smaller compared to the X-band contribution because S band structure delays are downweighted by a factor of 13 in this combination. Although less sources have been imaged at the higher frequencies (K band and Q band), it is striking that the astrometric suitability of the sources appears to be much better compared to that at X band, with about 90% of the sources that have a structure index value of either 1 or 2.

In addition, we have also studied the temporal variability of the structure index by determining the upper and lower values of the structure index for each source and by calculating the scatter about the mean structure index value. This study is most easily carried out at X band because of the many VLBI sessions that have been imaged at this frequency band. For the 81 sources that have X band structure indices available for at least 10 epochs, it is found that the largest shift (difference between the upper and lower structure index values) is 1 or 2 for 90% of these sources, while the scatter about the mean peaks at about 0.5 (Fig 3, left panels). This indicates that a variability of the X-band structure index of one unit is likely for most of the sources. When carrying out a similar calculation for the 18 sources that have been observed in all ten K band sessions, one finds that the largest structure index shift is 0 or 1 for all sources except one (Fig 3, right panels). Therefore, the variability appears to be smaller at K band compared to X band, which is not surprising considering the higher astrometric quality of the sources at K band. However, one has to be cautious in this interpretation because of the poorer statistics.

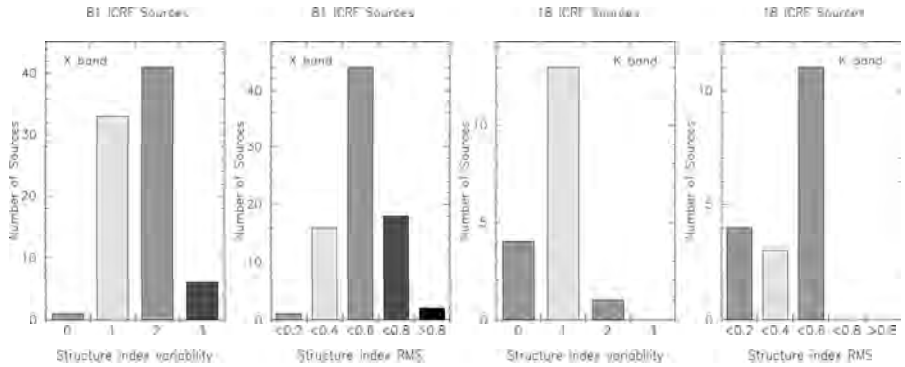

Figure 3. Variability of the structure index at X band (8 GHz) and K band (24 GHz) for all the ICRF sources that have data available in at least ten different epochs (81 sources at X band and 18 sources at K band). The variability is defined as the difference between the higher and lower values of the structure index over these epochs, while the RMS is calculated against the mean structure index value

4. Source compactness

The source compactness may be defined in a similar way as the structure index [6] from statistics of the visibility amplitude (correlated flux density) over all the u-v plane. This calculation is carried out for all projected VLBI baselines that could be possibly observed with Earth-bound VLBI based on the spatial brightness distribution of the source. The compactness is then defined according to the median of such values, after normalization of the visibility amplitudes by the total source flux density. With this normalization, the compactness has a value of 1 for a point-like source while it has a value of 0 for a source that is totally resolved out. It should be stressed that the compactness defined in this way does not provide a measure of the "true" source compactness but rather a measure of the source compactness relative to the interferometer resolution. A sample of the visibility maps that have been used for this evaluatation is shown in Fig. 1 (lower sub-panels) for three ICRF sources with different VLBI morphologies. As previously, we adopted a conservative approach when multi-epoch values are available for the compactness with the minimum of all values used as the compactness indicator for each source.

Based on the above definition, we compared the source compactness at each frequency band (2 GHz, 8 GHz, 24 GHz and 43 GHz) for all ICRF sources that have been imaged so far (Fig. 4). Unlike in the case of the structure index, there is no such a striking difference when going to the higher frequencies. There is a possible trend indicating that the sources become slightly more compact at higher frequencies (about 30%, 31% and 35% of sources with compactness higher than 0.6 at X band, K band and Q band, respectively) but this may not be significant. On the other hand, the sources appear to be more compact at S band (about 45% of sources with compactness higher than 0.6). We have also

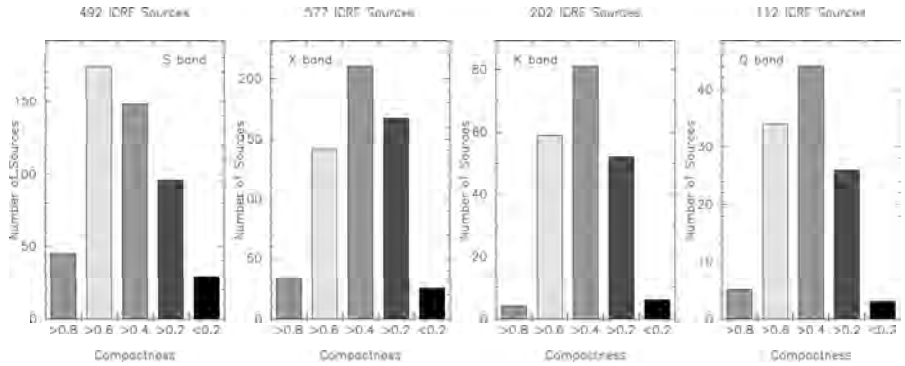

Figure 4. Distribution of compactness at S band (2 GHz), X band (8 GHz), K band (24 GHz), and Q band (43 GHz), for all ICRF sources that have been imaged at these frequencies. The smallest value of the compactness found for each source has been used in this study when multi-epoch values are available

studied the compactness variability in a similar way to that carried out for the structure index, and the corresponding histograms are shown in Fig. 5 for the sources that have been observed in at least 10 different epochs (81 sources at X band and 18 sources at K band). About 62% of the sources show a variability lower than 0.4 at X band, while the corresponding fraction is 82% at K band. This may reflect a lower structure variability at higher frequency but since the statistics at K band are poor, it is again difficult to make a firm statement.

5. Conclusion

We have evaluated the astrometric suitability at the standard 8 GHz geodetic frequency for 80% of the ICRF sources, based on multi-epoch VLBI images of their brightness distributions. It is anticipated that the remaining 20% of ICRF sources for which the astrometric suitability has not been assessed (mostly in the southern sky) will be imaged in the near future through further VLBI observing programs in the southern hemisphere. In addition, the astrometric suitability for roughly one-third of the ICRF sources has been estimated at 24 GHz, taking advantage of a new VLBI observing program that was set up 5 years ago to extend the ICRF towards higher frequencies.

The comparison between statistics on astrometric suitability at 8 GHz and those at 24 and 43 GHz strongly indicates that the sources are much more astrometrically suitable at the higher frequencies. On the other hand, no significant difference in source compactness is found between the 8 GHz, 24 GHz, and 43 GHz bands. Both the astrometric suitability and source compactness are subject to variability, although generally in a smooth way, because of the astrophysical evolution of the sources. The astrometric suitability of the sources already imaged, which has been discussed in this paper, will continue to be refined as new VLBI sessions are processed and new structure maps become

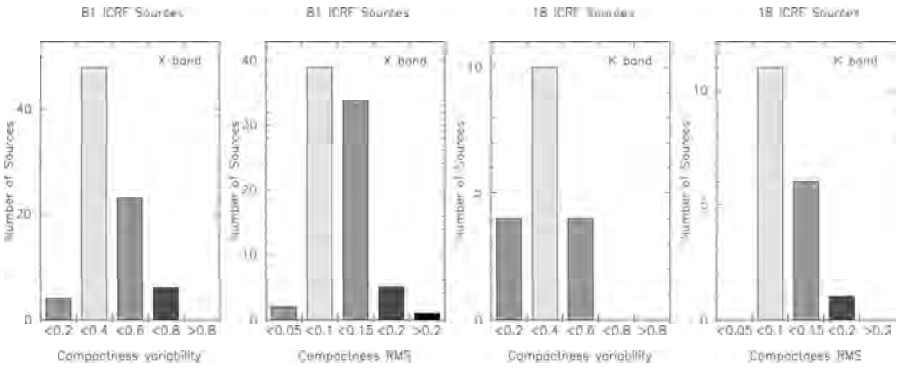

Figure 5. Variability of source compactness at X band (8 GHz) and K band (24 GHz) for all the ICRF sources that have data available in at least ten different epochs (81 sources at X band and 18 sources at K band). The variability is defined as the difference between the higher and lower values of the source compactness over these epochs, while the RMS is calculated against the mean compactness value

available. This information will be essential for selecting the proper defining sources and generating the next ICRF by 2009.

6. Acknowledgements

This work would not have been possible without the contribution of many collaborators. Among them are Alan Fey, Dave Boboltz, Roopesh Ojha, Arnaud Collioud and Julio Camargo, who produced the VLBI maps used in this study. The Very Long Baseline Array (VLBA) is a facility of the National Radio Astronomy Observatory (NRAO), which is operated by Associated Universities, Inc., under cooperative agreement with the National Science Foundation.

References

[1] Ma, C., E.F. Arias, T.M. Eubanks, et al. The International Celestial Reference Frame as Realized by Very Long Baseline Interferometry. A.J., v. 116, 516–546, 1998.

[2] Fey, A.L., C. Ma, E.F. Arias, et al. The Second Extension of the International Celestial Reference Frame. ICRF-Ext.2. A.J., v. 127, 3587–3608, 2004.

[3] Fey, A.L., P. Charlot. VLBA Observations of Radio Reference Frame Sources. III. Astrometric Suitability of an Additional 225 Sources 2000. Astrophys. J. Suppl.Series, v. 128, 17–83, 2000.

[4] MacMillan, D.S.. Radio Source Instability in the Analysis of VLBI Data. International VLBI Service for Geodesy and Astrometry 2006 General Meeting Proceedings, D. Behrend,K. D. Baver (Eds.). NASA/CP-2006-214140, 274–278, 2006.

[5] Fey, A.L., A.W. Clegg, E.B. Fomalont, et al. VLBA Observations of Radio Reference Frame Sources. I. Astrophys. J. Suppl.Series, v. 105, 299–330, 1996.

[6] Fey, A.L., P. Charlot. VLBA Observations of Radio Reference Frame Sources. II. Astrometric Suitability Based on Observed Structure. Astrophys. J. Suppl.Series, v. 111, 95–142, 1997.

[7] Ojha, R., A.L. Fey, K.J. Johnston, et al. VLBI Observations of Southern Hemisphere ICRF Sources. I. A.J., v. 127, 3609–3621, 2004.

[8] Ojha, R., A.L. Fey, P. Charlot, et al. VLBI Observations of Southern Hemisphere ICRF Sources. II. Astrometric Suitability Based on Intrinsic Structure. A.J., v. 130, 2529–2540, 2005.

[9] Lanyi, G.E., C.S. Jacobs, C.J. Naudet, et al. The Celestial Reference Frame at Higher Radio Frequencies: Astrometry from VLBA Observations at 24 and 43 GHz. A.J. (in preparation).

[10] Charlot P. Radio-Source Structure in Astrometric and Geodetic Very Long Baseline Interferometry. A.J., v. 99, 1309–1326, 1990.

Part 5. Progress in Technology Development and the Next Generation VLBI System

The 5th IVS General Meeting Proceedings, 2008, p. 361–370

Modeling Tropospheric Delays with Atmospheric Turbulence Models

Tobias Nilsson, Rüdiger Haas

Department of Radio and Space Science, Chalmers University of Technology, Onsala Space Observatory, Sweden

Abstract. In this work we show how atmospheric propagation delays for radio signals can be simulated based on the theory of atmospheric turbulence. We also discuss how to obtain station specific parameters, e.g. the refractive index structure constant C_n, from analysis of high resolution radiosonde data. As an example, atmospheric delays for the station Gilmore Creek and the CONT05 campaign are simulated.

1. Introduction

Atmospheric turbulence causes small scale fluctuations in the refractive index of air. These fluctuations cause variations in the atmospheric propagation delay of radio signals. Such variations are an important error source for space geodetic techniques, such as VLBI.

One way to assess how much the atmospheric turbulence degrades the accuracy of the parameters estimated in VLBI data analysis is to use simulations. The propagation delay of the VLBI signals in the neutral atmosphere can be simulated using the method presented in [1]. This approach requires knowledge of the magnitude of the turbulent variations in the refractive index. This magnitude can be described using the refractive index structure constant C_n. This parameter varies both in time and as function of location. The C_n parameters can be measured using a number of different techniques, for example using high resolution radiosonde data [2–5].

In this work we first describe in Sec. 2 how to simulate atmospheric delays, as well as how to obtain C_n using high resolution radiosonde data. In Sec. 3 we present C_n profiles obtained from radiosonde data from a number of high resolution radiosonde stations in order to investigate the variability of C_n between different climate regions as well as with season. In Sec. 4 we simulate atmospheric delays for the VLBI station Gilmore Creek, Alaska, using C_n profiles estimated using radiosonde data obtained from a nearby radiosonde

launch site. We also investigate how much the turbulence limits the accuracy of the station position estimates using a simple PPP (Precise Point Positioning) approach. Finally, we present the conclusions in Sec. 5.

2. Theory

2.1. Simulating Tropospheric Delays

The turbulence induced fluctuations in the refractive index of air can be characterized using the Kolmogorov turbulence theory [6]. According to this theory, the spatial variations in refractive index, n, between two points, $\mathbf{r}_i$ and $\mathbf{r}_j$, can be described using a structure function D_n [7–9]:

$$D_n(\mathbf{r}_i, \mathbf{r}_j) = \left\langle [n(\mathbf{r}_i) - n(\mathbf{r}_j)]^2 \right\rangle = C_n^2 \left(\frac{z_i + z_j}{2} \right) \frac{\|\mathbf{r}_i - \mathbf{r}_j\|^{2/3}}{1 + \left(\frac{\|\mathbf{r}_i - \mathbf{r}_j\|}{L} \right)^{2/3}}, \quad (1)$$

where $\langle \cdot \rangle$ denotes expectation value, C_n is the refractive index structure constant, L is the saturation length scale, and z_i the vertical component of $\mathbf{r}_i$. Temporal variations in the refractive index can be described similarly by assuming Taylor's frozen flow hypothesis [10]. This hypothesis assumes that the turbulent structure of the atmosphere is frozen and moves with the air, i.e. $n(\mathbf{r}, t) = n(\mathbf{r} - \mathbf{v}\, t)$ where $\mathbf{v}$ is the wind vector and t the time. The variations in refractive index between location $\mathbf{r}_i$ at time t_i and location $\mathbf{r}_j$ at time t_j can then be described by:

$$\left\langle [n(\mathbf{r}_i, t_i) - n(\mathbf{r}_j, t_j)]^2 \right\rangle = D_n(\mathbf{r}_i - \mathbf{v}\, t_i, \mathbf{r}_j - \mathbf{v}\, t_j). \quad (2)$$

In this work Equivalent Zenith Wet Delays (EZWDs) are simulated, i.e. slant wet delays divided by their corresponding mapping functions. An EZWD l_i^z of a radio signal observed after propagated along the path S_i, is given by:

$$l_i^z = \frac{1}{m_i} \int_{S_i} [n(\mathbf{r}_i(s)) - 1]\, ds = \int_0^\infty [n(\mathbf{r}_i(z)) - 1]\, dz, \quad (3)$$

where m_i is the mapping function between zenith and the elevation angle of the slant path S_i. Given a known initial EZWD l_0^z in some direction and at some time instant, (like the zenith wet delay at time zero), we can calculate the covariance between two EZWDs, l_i and l_j, given by:

$$[C]_{ij} = \left\langle (l_i^z - l_0^z)\, (l_j^z - l_0^z) \right\rangle = \int_0^\infty \int_0^\infty [D_n(\mathbf{r}_i(z), \mathbf{r}_0(z')) + D_n(\mathbf{r}_j(z), \mathbf{r}_0(z')) - D_n(\mathbf{r}_i(z), \mathbf{r}_j(z')) - D_n(\mathbf{r}_0(z), \mathbf{r}_0(z'))]\, dz dz'. \quad (4)$$

Calculating this for every pair of EZWDs we want to simulate, we obtain a covariance matrix C. Since C is symmetric we can perform a Cholesky decomposition [11]:

$$C = DD^T. \quad (5)$$

A vector of simulated EZWDs, $\mathbf{l}^z$, can then be obtained by [1]:

$$\mathbf{l}^z = l_0^z + D\,\mathbf{n}, \tag{6}$$

where $\mathbf{n}$ is a vector of zero-mean Gaussian distributed random numbers with variance 1.

For the simulations we need the profile of C_n, the wind velocity, and the initial EZWD l_0^z. For the structure constant, an often used approximation is to assume that C_n is constant up to an effective tropospheric height H and zero above [9]. This approximation was for example used in the simulations in [1]. In this work we simulate EZWDs using both this approximate model and using vertical C_n profiles estimated from high resolution radiosonde data.

2.2. Estimating the Structure Constant from Radiosonde Data

The structure constant C_n can be estimated from radiosonde data. The method used in this work is described in, for example, [2–5]. It is briefly summarized below.

The mixing of the air inside a turbulent eddy will cause any large scale gradient in the refractive index to be mixed into creating small scale refractive index fluctuations. By knowing the size of the large scale gradient and the typical mixing distance the magnitude of the fluctuations, i.e. C_n^2, can be estimated. The typical mixing distance is related to the so called *outer scale of atmospheric turbulence*, L_0. C_n^2 can be estimated by:

$$C_n^2 = a^2 \left\langle L_0^{4/3} \right\rangle F\,M^2, \tag{7}$$

where $a^2 \approx 2.8$, F is the fraction of the air that is turbulent, and M the vertical potential refractive index gradient. The outer scale is normally not known exactly, but its expectation value can be calculated by assuming that L_0 is uniformly distributed between some minimum and some maximum values, for example between 3 m and 100 m [4]. The potential refractive index gradient M is not the full vertical gradient of the refractive index; it only contains the part caused by the gradients in quantities conserved under adiabatic motion in the atmosphere, i.e. the potential temperature θ and the specific humidity q (these are only conserved when there are no clouds, hence the method can only be used under cloud free conditions). Thus, M is calculated by:

$$M = \frac{\partial n}{\partial \theta}\frac{\partial \theta}{\partial z} + \frac{\partial n}{\partial q}\frac{\partial q}{\partial z}. \tag{8}$$

When estimating the derivatives using radiosonde data it is important to remember that only the large scale gradients in θ and q should by considered, not the small scale fluctuations due to turbulence. Hence the gradients should be calculated using data obtained at a vertical sampling larger than L_0 where

the gradient can be assumed larger than the turbulent fluctuations. However, the sampling needs to be small enough that the large scale variations in θ and q can be described by a first order Taylor expansion. In this work we use a sampling distance of 150 m.

The intermittency factor F is required to take into account that only some layers of the atmosphere may be turbulent, while other layers may be non-turbulent or in a state where they fluctuates between a turbulent an a non-turbulent state. Typically $F \approx 0.1$ [2], however it can vary in time and with height. It is possible to estimate F using statistical methods:

$$F = \int_{S_c}^{\infty} p_S(S) dS, \tag{9}$$

where $S = \left\| \frac{\partial \mathbf{v}}{\partial z} \right\|$ is the wind shear, p_s the probability density function of S, and S_c the wind shear required to make the Richardson number equal to the critical Richardson number [3]. Typically the following expression for p_S is used [3, 4]:

$$p_S(S) = \frac{S}{\sigma_S^2(z)} exp\left(-\frac{S^2 + \langle S(z) \rangle^2}{2\sigma_S^2(z)}\right) I_0\left(\frac{S \langle S(z) \rangle}{\sigma_S^2(z)}\right), \tag{10}$$

where $\langle S(z) \rangle$ is the wind shear estimated using the wind measurements in the radiosonde data, and I_0 is the modified Bessel function of the first order. The parameter $\sigma_S = 0.18\, L_0^{-0.3} \left| \frac{g}{\theta} \frac{\partial \theta}{\partial z} \right|^{0.25} \rho^{-0.15}$, where g is the acceleration due to gravity and ρ the density of the air [4].

3. Examples of C_n^2 Profiles

Fig. 1 shows mean and median C_n^2 profiles estimated from high resolution radiosonde data, for six different locations. As seen, the mean values are typically larger than the median ones, meaning that the distribution for C_n^2 is not symmetrical (probably it is log-normal [4]). We can also note that the average C_n^2 profiles decay almost exponentially with height, and that C_n^2 usually is larger for the stations closer to the equator.

In Fig. 2 the seasonal variation of C_n^2 is shown. As seen C_n^2 is clearly larger in summer compared to winter, especially at lower altitudes. The likely reason is that there is more water vapor in the atmosphere in the summer. The result with higher C_n in summer is in agreement with the results in [12], where slant wet delays inferred from microwave radiometer data were used to estimate C_n. We can also see that there are large variations also over short time scales, of the order of days or shorter.

4. Simulations

We made simulations for the VLBI station Gilmore Creek, Alaska, for the continuous VLBI campaign CONT05. The structure constant profiles used in

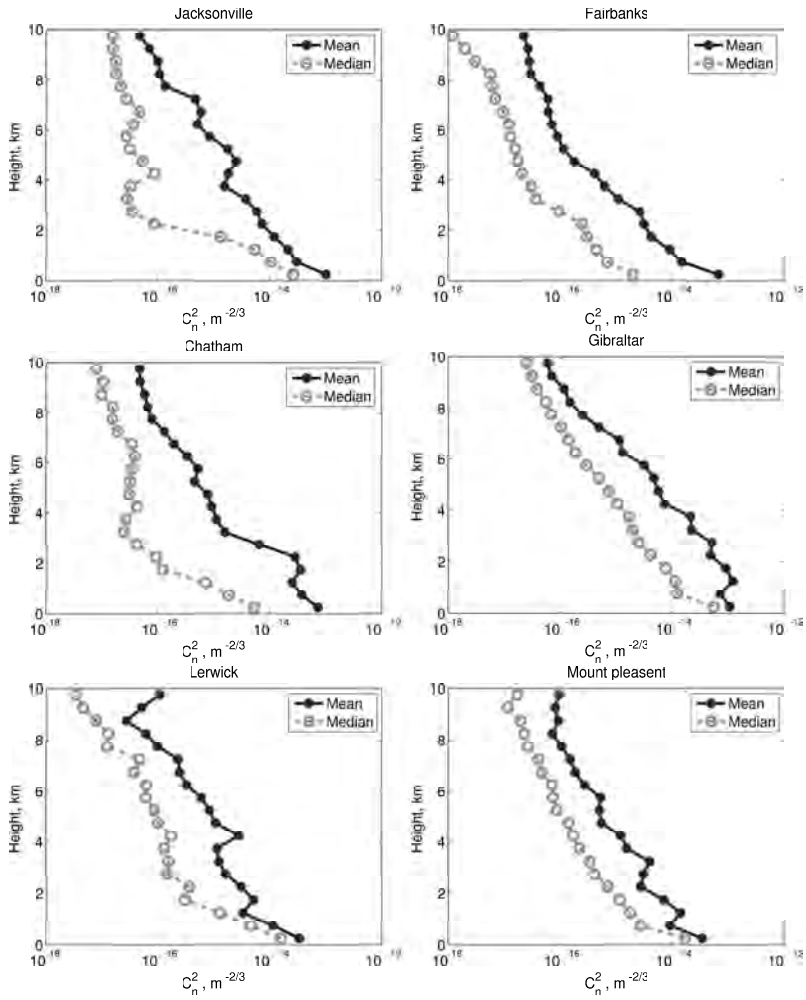

Figure 1. Mean and median C_n^2 profiles for 2005 estimated from radiosonde data

the simulations were those estimated from the nearby radiosonde launch site in Fairbanks, located 30 km away from the VLBI station. From the radiosonde data, there were five different C_n^2 profiles that could be used during the period Sep. 12–28, 2005. The C_n^2 profiles at times in between two radiosonde launches were estimated by linear interpolation of the C_n^2 profiles estimated from the radiosonde data. The wind speed data were obtained from ECMWF data [13]. We made the approximation that the wind speed and direction were constant with height (equal to the ECMWF wind data at the 850 hPa level), but varying with time.

We also made simulations using the simplifying assumption of a constant C_n up to an effective tropospheric height H and zero above. The effective

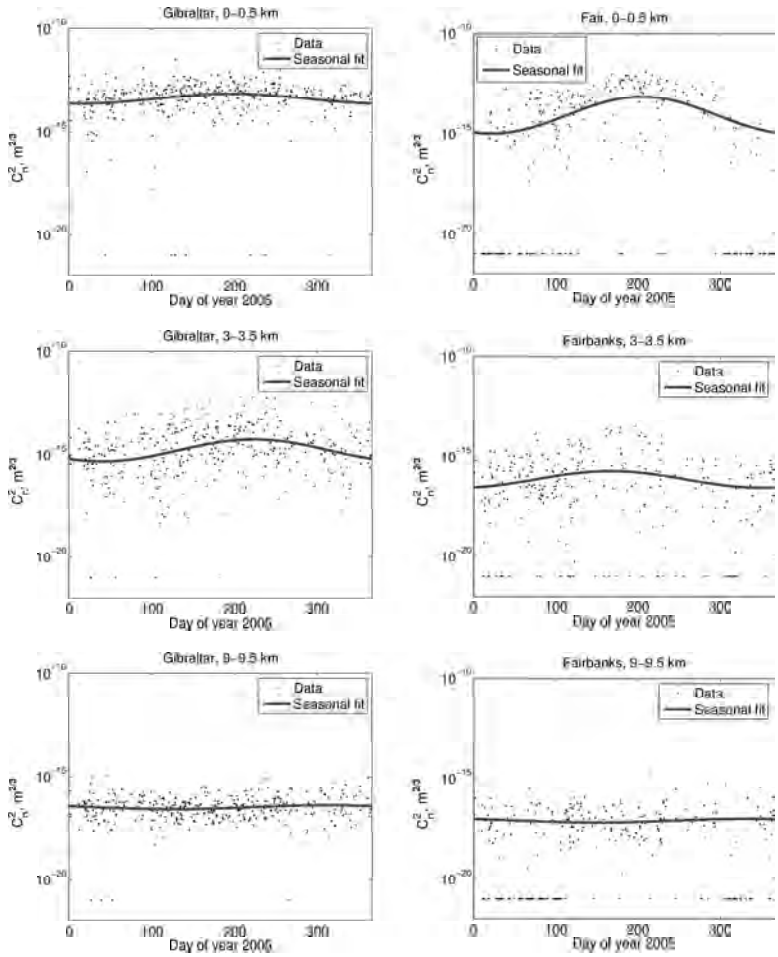

Figure 2. Seasonal variations in C_n^2 observed at Gibraltar and Fairbanks

tropospheric height were estimated as the scale height of the C_n profile, i.e. it was obtained by fitting $\log(C_n(z))$ to the model $\log(C_n(z)) = A - z/H$. The constant C_n value was then estimated so that $C_n \cdot H$ would be equal to the the integral of the mean C_n profile for the CONT05 period. The obtained parameters were H =3170 m and C_n=0.9·10^{-7} m$^{-1/3}$. The wind speed and direction used in these simulations were constant both in time and with height (equal to the mean speed and direction for the period as given by ECMWF for the 850 hPa level).

To investigate the effect the seasonal variations of C_n^2 have on the results, we also made simulations using the C_n^2 profiles obtained in the period Mar. 12–28, 2005 (i.e. six months before CONT05).

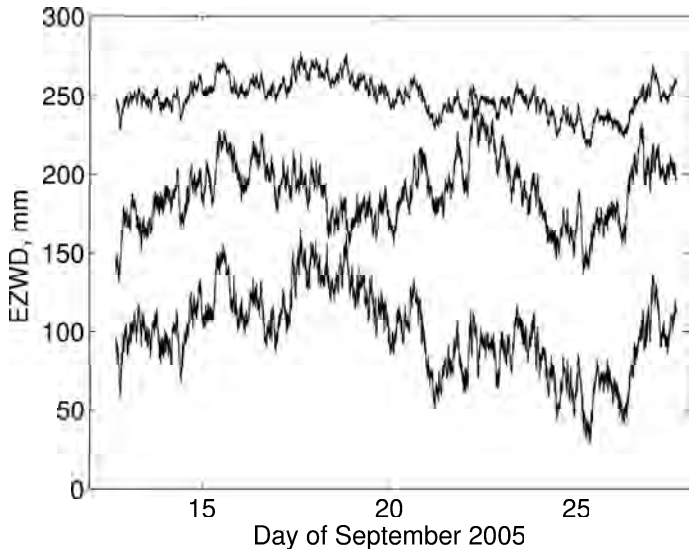

Figure 3. Simulated EZWD for Gilmore Creek during the CONT05 campaign. Shown are delays simulated using C_n profiles estimated using radiosonde data (lower line), as well as delays simulated using constant C_n up to an effective tropospheric height and zero above (middle line, offset by 50 mm), and delays simulated using C_n profiles from March 2005 (upper line, offset by 150 mm)

The time-series of the simulated EZWDs are shown in Fig. 3. The azimuth and the elevation angles of the simulated EZWDs are those observed by the Gilmore Creek VLBI telescope during CONT05. The same random numbers were used in the simulation using the C_n profiles from the radiosonde data and for the simulation using the simplification with constant C_n up to the height H. We can observe that the variations in these time-series look rather similar. However, for the simulations using the data from March 2005, the variations are smaller, a result of smaller C_n in March compared to Sep.

To test how the turbulence affects the accuracy of the position estimates, we used the simulated delays in a simple Precise Point Positioning (PPP) processing. In the PPP processing we made one solution for each one day period. For each day the station position, station clock error (modeled as a second degree polynomial), zenith wet delay (modeled as piecewise linear function in one hour intervals), and tropospheric gradients (modeled as piecewise linear functions in two hour intervals) were estimated. No other error source than the tropospheric delay were simulated.

The obtained repeatabilities for the coordinates are shown in Fig. 4. We can see that the coordinate errors for the simulations using the advanced approach (i.e. using the C_n profiles) and using the simpler approach are similar. When using the advance approach the RMS repeatabilities for the whole period were 1.3 mm, 1.3 mm, and 4.1 mm for the north, east, and vertical component

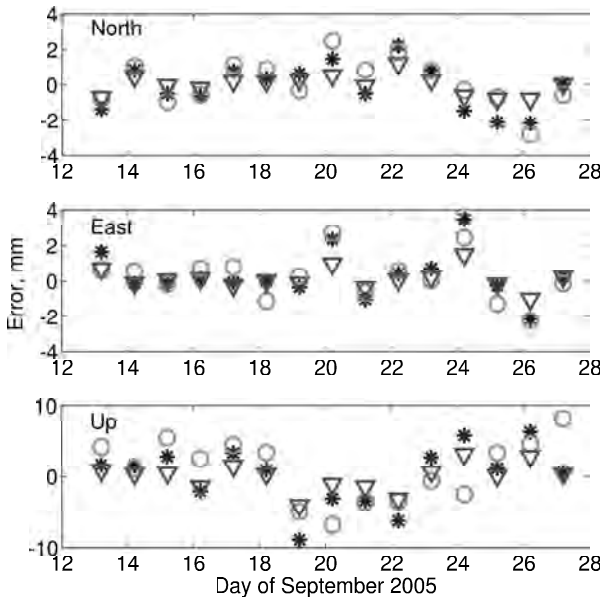

Figure 4. Station position repeatabilities. Shown are the results from the simulations using the advanced approach (∗), the simplified approach (∘), and the advance approach but using C_n from March 2005 (▽)

respectively. The same values when using the simpler approach were 1.3 mm, 1.3 mm, and 4.4 mm, i.e. hardly any differences at all. For the simulation using C_n profiles from March 2005 the repeatabilities are significantly better: the RMS values for these simulations were 0.5 mm, 0.6 mm, and 1.9 mm respectively.

5. Conclusions

Atmospheric turbulence causes fluctuations in the atmospheric delay of the VLBI signals, both as function of time and as function of direction. Since the models used in the processing of VLBI data cannot describe these fluctuations properly, it will cause errors in the parameters estimated in the VLBI analysis. For example, as seen for the simulations presented in this work the error in the estimated vertical coordinates can be several millimeters. The error is season dependent since the structure constant C_n has a seasonal variation.

The C_n profile can be estimated using high resolution radiosonde data. It should however be noted that there is some uncertainty in the C_n profiles estimated using this method. For example, the L_0 value is normally not known very well. In this work we assumed L_0 to be uniformly distributed between

3 m and 100 m, however the maximum and minimum values can be different for different location. In [3] the range 30 m to 100 m is given for the maximum L_0 value. If we would use 30 m instead of 100 m as the maximum value of L_0 the estimated C_n values would be smaller by about a factor 2. More research is needed in order to improve the knowledge about L_0. Another way would be to estimate the C_n profile from the radiosonde data using the alternative approach presented by [5]. That approach however, requires a vertical sampling rate of around 10 m or less (some radiosonde data used in this work only have 50 m sampling), and the method is probably more sensitive to measurement noise in the radiosonde data.

Simplifying the simulations by assuming a C_n constant up to an effective height H and zero above will not affect the simulated delays significantly as long as appropriate C_n and H values are used. Some differences between the simulated time-series using the advanced and simplified approach can be seen. These are likely caused by the fact that there is variations in time in the C_n used in the advanced approach but not in the simplified approach. The repeatabilities obtained from the PPP analysis are similar. It is however important to take into account the seasonal variations of C_n.

The method of simulating atmospheric delays can be used to determine the accuracy that can be reached with space geodetic techniques such as VLBI. For example, the method is presently being used in simulations performed in order to evaluate the performance of the future VLBI system, VLBI2010 [14]. Simulated atmospheric delays can also be used in order to improve the modeling of the atmospheric delays in the VLBI analysis.

Acknowledgements

The radiosonde data used in this work were obtained from the British Atmospheric Data Centre [15] and from the Stratospheric Processes and Their Role in Climate [16] data center. Tobias Nilsson is supported by a grant from the Swedish National Space Board.

References

[1] Nilsson, T., R. Haas, G. Elgered. Simulations of atmospheric path delays using turbulence models. Proc. of the 18th EVGA Working Meeting. J. Böhm, A. Pany, H. Schuh (eds.), 2007, 175–180; http://mars.hg.tuwien.ac.at/evga/proceedings/S64_Nilsson.pdf.

[2] VanZandt, T.E., J.L. Green, K.S. Gage, et al. Vertical profiles of refractivity turbulence structure constant: Comparison of observations by the Sunset Radar with a new theoretical model. Radio Sci., v. 13, No 5, 819–829, 1978.

[3] d'Auria, G., F.S. Marzano, U. Merlo. Model for estimating the refractive-index stucture constant in clear-air intermittent turbulence. Applied Optics, v. 32, 2674–2680, 1993.

[4] Vasseur, H. Prediction of tropospheric scintillation on satellite links from radiosonde data. IEEE Trans. Antennas Propag., v. 47, No 2, 293–301, 1999.

[5] Nilsson, T. Measuring and modelling variations in the distribution of atmospheric water vapour using GPS. Ph.D. dissertation. Chalmers University of Technology, 2008;
ftp://gere.oso.chalmers.se/pub/tobias/.

[6] Kolmogorov, A.N. The local structure of turbulence in incompressible viscous fluid for very large Reynolds numbers. Dokl. Akad. Nauk SSSR, v. 30, No 4, 299–303, 1941 (English translation: Proc. R. Soc. Lond. A, 434:9-13).

[7] Tatarskii, V.I. The Effects of the Turbulent Atmosphere on Wave Propagation. Israel Program for Scientific Translations, Jerusalem, 1971.

[8] Ishimaru, A. Wave Propagation and Scattering in Random Media. Academic Press, New York, 1978.

[9] Treuhaft, R.N., G.E. Lanyi. The effect of the dynamic wet troposphere on radio interferometric measurements. Radio Sci., v. 22, No 2, 251–265, 1987.

[10] Taylor, G.I. The spectrum of turbulence. Proc. Roy. Soc. Lond. A, v. 164, No 919, 476–490, 1938.

[11] Press, W.H., S.A. Teukolsky, W.T. Vetterling, et al. Numerical Recipies in C: The Art of Scientific Computing, 2nd ed. Cambridge University Press, Cambridge, 1992.

[12] Nilsson, T., L. Gradinarsky, G. Elgered. Correlations between slant wet delays measured by microwave radiometry. IEEE Trans. Geosci. Remote Sensing, v. 43, No 5, 1028–1035, 2005.

[13] European Centre for Medium Range Weather Forecasts, 2008;
http://data.ecmwf.int/.

[14] Niell, A., A. Whitney, B. Petrachenko, et al. VLBI2010: Current and future requirements for geodetic VLBI systems. International VLBI Service for Geodesy and Astrometry 2005 Annual Report. D. Behrend and K. Baver (eds.), NASA/TP-2006-214136, 2006.

[15] UK Meteorological Office, UK High Resolution Radiosonde Data, British Atmospheric Data Centre, 2008;
http://badc.nerc.ac.uk/data/rad-highres/.

[16] Stratospheric Processes and Their Role in Climate (SPARC) Project, US High Resolution Radiosonde Data, 2008;
http://www.sparc.sunysb.edu/html/hres.html.

The 5th IVS General Meeting Proceedings, 2008, p. 371–375

Composite Applications for Radio Telescopes

Dean Chalmers [1], *Gordon Lacy* [1], *Peter Dewdney* [1],
William Petrachenko [2], *Gary Hovey* [1]

[1)] *National Research Council Canada, Herzberg Institute of Astrophysics, Canada*
[2)] *Natural Resources Canada, Canada*

Abstract. Development of construction techniques for composite reflectors is an active R&D focus at the National Research Council's Dominion Radio Astronomical Observatory (DRAO), near Penticton, Canada. The team at DRAO constructed and tested its first 10-m diameter prototype reflector in 2007 and is currently incorporating improvements in performance and manufacturability for the next prototype to be built in the spring of 2008. Composite materials offer a range of benefits over traditional metal structures in the construction of large (> 10 m diameter) reflectors. The high specific modulus of composite materials results in the construction of lighter and stiffer reflectors and the low CTE of these materials yields thermally stable structures. A lighter stiffer reflector allows higher accelerations with a given power input and the thermal stability allows for high performance over wide operating temperature ranges. New developments in composite manufacturing processes have the potential to make composites a cost effective alternative for reflector antennas.

1. Introduction

The Composite Applications for Radio Telescopes (CART) project at the Herzberg Institute of Astrophysics' (HIA) Dominion Radio Astrophysical Observatory (DRAO) in Penticton, Canada is an ongoing effort to investigate the potential application of composite materials to radio telescope structures. The primary motivation is to provide cost-effective collecting area for the Square Kilometre Array (SKA) telescope, but several other potential radio astronomy projects could benefit from the unique properties of composite materials including VLBI 2010.

1.1. Composite Material Properties

Composite materials have a wide variety of properties, allowing them to be tailored very precisely to a given application. Of particular interest to radio telescopes are high specific stiffness, high specific strength, and low coefficient

of thermal expansion. While composite materials do have a high specific cost ($/kg), the mass of structures is low, so the overall cost can be competitive.

Composite structures have been in use for over 30 years in high UV, marine environments, and advances in material coatings and processes in recent years have improved the quality and longevity of composite structures.

1.2. Composite Fabrication Processes

Until recently none of the available composite fabrication processes were appropriate to the manufacture of large radio reflectors. The vacuum infusion process (VIP) now offers a viable alternative: fabric and core materials are laid dry in a mold, and sealed under a vacuum tight bag. Resin is then drawn into the part under vacuum. The size of the part is limited only by the height to which the resin can be drawn, ~ 6 m, allowing diameters up to ~ 100 m.

VIP requires very little capital investment, typically a couple of large vacuum pumps, various common shop tools, and a facility with a moderate degree of climate control. For large structures, the mold and equipment to handle the completed structure are the major expenses, but with moderate production quantities these are quickly amortized. The simple infrastructure requirements allow the fabrication to take place at or near the site.

2. The CART Project

The CART project aims to demonstrate the cost-effective fabrication of high-performance, one-piece composite radio reflector. A 10 m diameter was selected as it is typical of reflectors under consideration for upcoming projects.

2.1. Prototype Design

The following prototype specifications were chosen:

Reflector Diameter: 10 m	Design Wind Speeds
Optics: Centre-fed parabolic reflector	Operating: 35 km/h (10 m/s)
f/D Ratio: 0.45	Slew to stow: 50 km/h (14 m/s)
Max operating frequency: ~ 10 GHz	Survival: 160 km/h (44 m/s).

To select a reflective surface material, the reflectivity of various materials was tested using a closed cavity method developed by JPL [1]. Several alternatives were identified that offered noise temperatures only a factor of 2 higher than aluminum (~ 0.13 K).

The reflector structure was designed using finite-element methods to meet the specifications for deflection and strength. The design chosen used a reflective surface with a rim and integral structural beams on the backside.

Infusion flow modelling was performed in order to ensure that the structure would fill evenly and within a reasonable time. This involved a mix of measurement of flow properties of the particular materials and laminate schedules to be used in the structure, and computer modelling.

The surface accuracy that can be realized in the final part is dependent on the surface accuracy of the mold. The mold used was measured to have 0.015 mm RMS and a maximum deviation of 1.8 mm.

2.2. Results

The first 10 m CART prototype was constructed in mid-2007. Fig. 1 shows the completed reflector on the mount. The final mass of the reflector was measured to be 1 tonne, which includes all of the back structure.

Figure 1. The completed reflector on the mount

The reflector was measured using both laser-tracking and holography. The laser tracking was performed at an elevation of 90° with the tracker mounted at the center of the reflector. The holography (at 12 GHz) employed a geostationary satellite signal at elevation 34°. Both results are shown in Fig. 2. The strong similarity despite the large elevation difference attests to the stiffness of the structure.

The RMS deviation of the surface compared to the best-fit parabola is 1 mm, and the maximum deviation is ~ 4 mm, with the best-fit parabola having a focal length 22 mm shorter than the design because of shrinkage.

Note that there are some high regions between 2 and 4 o'clock and 8 and 10 o'clock. These are believed to arise because of differential cure in the large structural beams, which were infused subsequent to the surface, rim, and smaller beams. Fig. 3 shows the layout of the beams superimposed on the measurement results. The heavy black lines indicate the beams added in the second infusion.

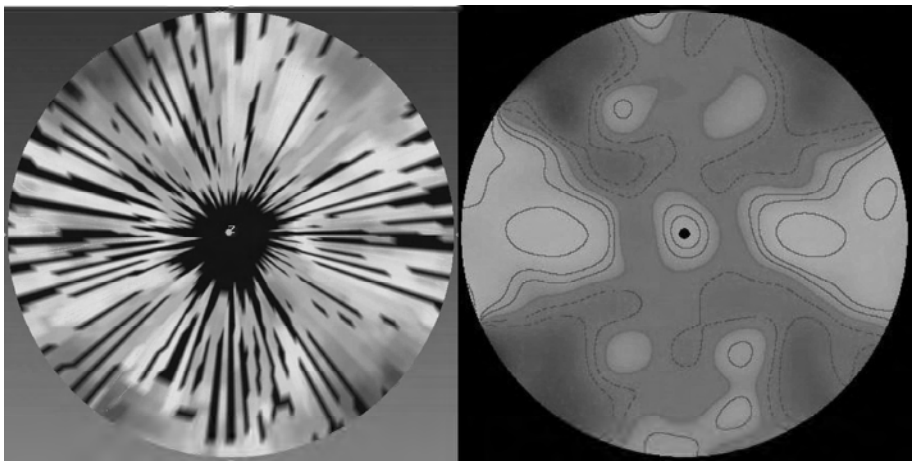

Figure 2. Laser tracker (left) and holography (right) results

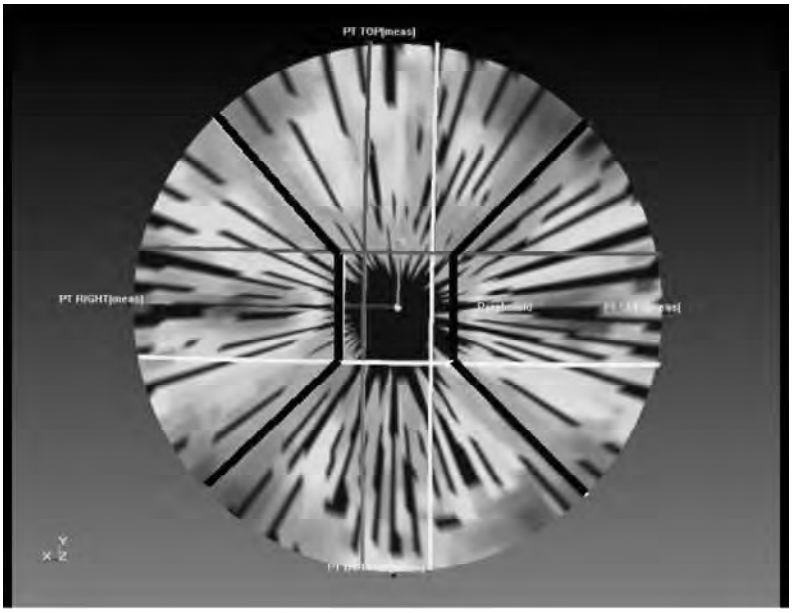

Figure 3. The layout of the beams superimposed on the measurement results

3. Future Plans

The CART Mk2 program is underway at DRAO to design and build a second prototype. The goals of the Mk2 program are to improve the structural design, design for production, and improve process design and control.

The Mk2 design is shown in Fig. 4. The surface and rim will be infused on

the mold in one piece, eight beams and a hub will be fabricated separately and bonded on while it is still on the mold. The symmetry of the surface and rim will maintain symmetrical shrinkage during cure and the beams and hub will hold the surface in shape. The predicted mass is slightly less than that of the first prototype.

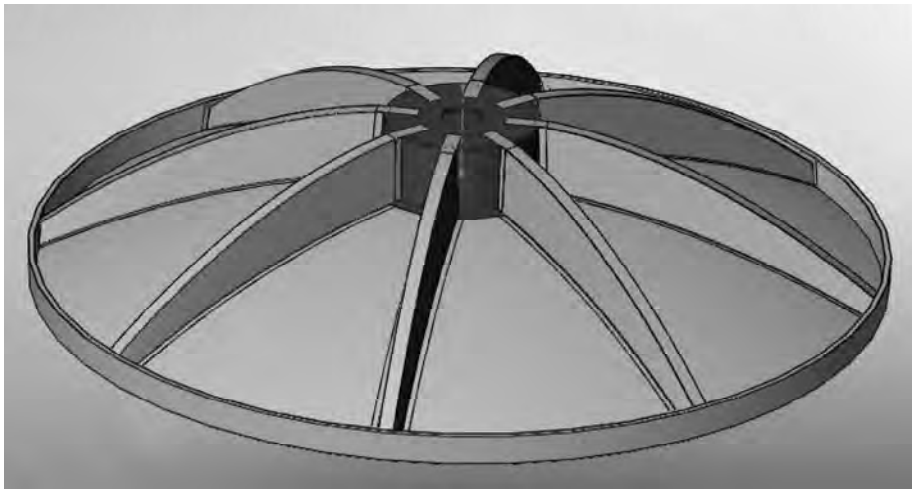

Figure 4. The Mk2 design

4. Conclusions

Composite materials have properties that make them very attractive for use in radio telescopes; lightweight, stiffness, and low coefficient of thermal expansion. New processes show promise for cost effective production of large accurate structures using composites. The Composite Applications for Radio Telescopes project has successfully produced its first 10 m prototype reflector. The mass of this reflector is 1 tonne including backing structure. The RMS deviation of the surface with respect to the best-fit parabola is 1 mm, but the deviations are not random. The cause of the major components of the deviations has been identified and development of a second prototype is underway to address these issues.

References

[1] Clauss, R., P.D. Potter. Jet Propulsion Labs Communications Elements Research Section, Improved RF Calibration Techniques: A Practical Technique for Accurate Determination of Microwave Surface Resistivity. JPL Technical Report 32-1526, v. XII.

The 5th IVS General Meeting Proceedings, 2008, p. 376–380

DBBC Development Status

Gino Tuccari [1], *Walter Alef* [2], *Alessandra Bertarini* [3], *Salvatore Buttaccio* [1], *Dave Graham* [2], *Gaetano Nicotra* [1], *Alan Roy* [2], *Michael Wunderlich* [2]

[1)] *Istituto di Radioastronomia — INAF, Italy*

[2)] *Max Planck Institute fuer Radioastronomie, Germany*

[3)] *IGG Bonn, Germany*

Abstract. More DBBC units of version 1 have been built. DBBC version 2 has reached an advanced stage of development and realization. The detailed status of the project is presented including: the existing hardware versions and their layout, the main differences between DBBC.1 and DBBC.2, the new elements which are under development, the implementation timing for DBBC version 2, and observational tests. Moreover possible uses of the DBBC hardware as a general purpose backend for VLBI and radio astronomy are presented.

1. Hardware

A new class of boards has been developed for the DBBC in the version 2. This new implementation greatly improves performance and reduces the number of elements to realize the entire functionality of a Mark4 equivalent rack. A description of the main element is reported below.

The first ADB2 board prototype has been completed and initial testing has commenced. The board offers several operation modes with demultiplexing in two or four buses. Maximum sampling clock is 2.2 GHz, maximum signal frequency to be sampled is 3.5 GHz, 10-bit representation. A board ADB2 can feed as piggy-back element a FiLa10G, giving the possibility to place the sampling element at the receiver site, connecting the DBBC through optical fibers.

The new processing unit Core2 board, in the V5 version, was delivered and now is under test. The board is compatible with ADB1 and ADB2 and supports a minimal equivalent of four Core1 functionality. The PCB has a number of 40 equivalent layers and all the connections for signal transfer are differential, twisted, and matched in delay and impedance between the pads of the dice

and the pins of the bus connectors. A piggy-back element can be adopted for additional functionality, like memory bank for pulsar de-dispersion, memory corner or other needs where a significant memory addition is to be adopted. The memory piggy-back is under the final stage of development.

The CaT boards (Clock and Timing) are ready and under test: the Clock board is able to generate a highly flexible number of synthesized sampling clock values (e.g., 2048 MHz, 1024 MHz), phase locked with an external 10 MHz. Low phase-noise and very small sensitivity to temperature are the main performance. The Timing board is producing 1PPS synchronization signals for all the ADB boards and the entire digital chain. Frequency selection with the use of different VCOs for large range selection is programmed by using the DBBC internal PC Set.

The FiLa10G boards realization is under way and the first prototype of the board is expected in summer 2008. It can be used as piggy-back board for any ADB2 sampler, giving the possibility to transmit and receive at the same time a high data rate of 20 Gbps + 20 Gbps. The bidirectional functionality could be required for instance when an RFI mitigation is needed to be realised in a remote location with respect to the sampling and processing site. With the typical sampling frequency of 2.048 MHz and the full 10-bit data representation, a double optical fibre set meets the full data handling requirements. Moreover the board is equipped with two additional transceivers able to operate at 1-2-4 Gbps for slower connections. The full number of transceivers is four and all or a subset can be used, with the possibility to populate the board with any number of them, depending on the needed functionality. The board indeed can even support the data tx-rx of 2×2 VSI connections and in such a case can still be used as p-b element of an ADB2 or as stand-alone element. The configuration files can be also loaded by the on board stand alone flash memory. The entire triangle connectivity HSI/HSIR–VSI-in/VSI-out–Optical-Fibers is supported. The board can support the connection with the Mark 5C recorder and its ancillary in a DBBC system as long as MK5C is not in the field. The FiLa10G is at an excellent level of development, and a test bench is progressing in MPI in parallel with the final board preparation. On the test bench it is possible to hardware-verify the entire data flow from the data input (as coming from samplers or from a down-converted data stream) up to the optical physical layer. The final board, after verification with the test bench will be finalized for a complete prototype. The first complete FiLa10G prototype is expected in June, final delivery time is September. FiLa10G is necessary only for MK5C connection through 10G, while DBBC.2 will in any case be usable with 2 VSI connection even at 4 Gbps.

2. Firmware

Some elements of the already developed configurations still need to be improved, mainly the xxx.99 MHz tuning setting, now achievable with a fractional difference of about 9 mHz, and a high sensitivity in the correlation amplitudes

with the IF levels. Several approaches are taken into consideration and an iterative process of observations-correlation-configuration modification is followed. The same method is going to be realized for testing other features. In order to accelerate this process, EVN members, that will be willing to contribute to the development, could dispose of a small DBBC kit to verify their implementation. The same kit can be used for developing different functionalities of the backend system. Several groups are already working on different kinds of functionalities with the DBBC programmable kit; the products are expected to be shared among the system users. Related to the VLBI functionality it can be cited, for instance, a multiband fixed tuning configuration that is in development and shortly expected, to be used as an alternative to the standard base band converter configurations. This configuration is what the IVS2010 is suggesting as back-end method for the wide band observations.

3. Observation

The Europe89 was observed for 12 hours in September using 8 BBC equivalent in X band and 3 BBC equivalent in S band: fringes have been detected in all the sub-bands. Euro90 observed 24 hours at Wettzell with all the standard number of sub-channels (8 BBC equivalent in X band and 6 in S band).

A technique to compensate for fractional frequency offset is under evaluation. Indeed a frequency correction is needed at the internal DDS frequency resolution, as geo observation needs to detect cal at 10 kHz from the integer MHz. More options are possible and observational tests are underway to determine the best solution. An ad-hoc DDS based on binary-decimal phase counters can be adopted. It could be applied a firmware millisecond phase adjustment using the available frequency setting in a dedicated sequence to achieve the avarage exact frequency. The method has been demonstrated at the Bonn correlator with 24+1 sequence in a 25 seconds long scan correlation with the Europe90 experiment.

The digital system use requires to optimize or to equalize the IF flatness in band: a new version of Conditioning Module is under development to optimize this aspect, but a good equalized band is expected from the receiver. Additional observational tests will be realized with the Wz unit. Testing will be accelerated with the introduction of a DBBC.2 system even in Effelsberg for a fast evaluation time with the correlator.

A further improvement is also expected by the introduction of better in/out band filter rejection, achievable with the additional resources available in the Core2 boards.

Dedicated Web pages have been added to the Noto Internet server with information about the DBBC system. A document series is in preparation and it started to be available in these pages, so as a page with News.

The integration with the FS is now almost ready. It is realised in a first time as a collection of station commands, as the software structure the DBBC is able to recognize. The system gain information in the different part of the

instrument are recorded in a log that can be available under a specific FS command request for calibration purposes.

4. Production

INAF is going to support a spin-off company creation for the DBBC production. This process started about one year ago and will be completed in the first semester 2008, as soon as all the bureaucracy will be completed. A final documentation will be ready in the end of Apr. and the final approval is expected in summer.

The company will have an agreement with IRA-Noto Section, where laboratories will be placed for a part of the production. Its under evaluation the possibility to take an other part of the production in MPI, for an initial setting phase.

The production phases have been carefully defined and a certain number of operations will be realised by external companies. The full process time for a complete system, tested in laboratory, will be three months, and in parallel more systems (1–6) could be built, with the initial manpower and logistic capability.

5. System Deployment

On Nov. 5, 2007 a geodetic version of DBBC arrived in Wettzell. The Wettzell DBBC system comprises 4 IFs and 14 equivalent base band converters. In the same month it was installed and integrated with the other VLBI equipment. Recording of its output is realized with a Mark 5B+ system. Europe90 observation has been done for testing the equipment. Fringes have been found on all channels and data analysis in underway. Some elements require to be revised, mainly related to the calibration tones exact tuning and the sensitivity of the correlation amplitude to the IF amplitude. The second and third system for Wettzell are ready in all the other parts and waiting for completion of the final delivery of the new Core2 boards. Indeed even if the three units have been ordered in the 256 MHz IF version, without synthesizer, equipped with Core1 boards, the new version will be delivered, and also the first unit will be upgraded as DBBC.2.

The DBBC system for Irbene (Latvia) has been completed and in the first days of February it was transferred by Latvian colleagues to their station. The Irbene DBBC is a reduced version having two IFs and 2 Core1 boards. As soon as Irbene will be able to upgrade the system, few Core boards will be added to achieve a complete architecture. At present the system will allow to perform the first observations and tests of the antenna and the 6 cm receiver.

A system similar to the Irbene one has been delivered to the Arcetri Observatory. The main purpose is to use it as a development system for FPGA configurations devoted to the realization of spectrometer, pulsar, total power, polarimetry back-end. The Arcetri team is part of an FPGA team established

to support firmware development on the DBBC platform.

Other complete DBBC.2 systems are under construction for Yebes, Effelsberg, Noto, Medicina; and in particular the Medicina unit is expected to support the multibeam 22 GHz receiver (7 feeds $\times$ 2 polarization $\times$ 2 GHz bwd/ea) for VLBI and single dish applications.

6. Linear to Circular and Stokes Conversion

Different projects are under development within the DBBC hardware. One is described in this section. The main goals are the conversion from linear polarization to circular polarization and the formation of Stokes parameters in the DBBC for single-dish broad-band polarimeter. The reason for requiring this is that Effelsberg and geodetic antennas are moving to broad-band feeds and extremely-broad bands are possible only with linear polarization.

It looks as VLBI is simplest with circular polarization, and existing analog polarizers are narrow band due to imperfect 90 phase shift. A possible solution is envisaged by making perfect 90 phase shift across broad bandwidth digitally (e.g., Hilbert transform).

Processing Steps in this process:
1) receive time series from ADC at 1 Gbps,
2) measure gain and phase difference between X and Y polarizations,
3) fourier transform time series to frequency domain,
4) equalize the gain using result from 1),
5) shift phase of one polarization by 90 in each frequency channel,
6) D-term correction (idea by Koyel Das):
   6.1)correct for leakage between X and Y,
   6.2)form X Dxy Y and Y Dyx X outputs using an adaptive filter,
   6.3)filter to adjust D to minimize the output power.
7) fourier transform back to time domain.
8) form circular polarization by summing X and phase-shifted Y.
9) send result from 8) on to existing DBBC processing stages.
10) take result from 6) and form Stokes parameters and integrate in time.

The expected result would be excellent circular polarization over wide bandwidth, zero D-terms, Stokes parameters in many channels over wide bandwidth.

The 5th IVS General Meeting Proceedings, 2008, p. 381–385

Progress of Wideband VLBI Digital System Development at SHAO

Xiuzhong Zhang [1], *Wenren Wei* [1], *Ying Xiang* [1], *Bin Li* [1], *Fengchun Shu* [1], *Renjie Zhu* [1], *Zhijun Xu* [1], *Zhong Chen* [1], *Weihua Wang* [1], *Weimin Zheng* [1], *Zhuhe Xue* [1], *Q. Ling* [1], *R. Zhao* [1], *Jingling Wang* [1], *Qingyuan Fan* [1], *Yusufu Aili* [3], *Huihua Li* [1], *Y. Wu* [2], *L. Chen* [2], *J. Luo* [2]

[1)] *Shanghai astronomical Observatory, Chinese Academy of Sciences, China*

[2)] *Graduate University of the Chinese Academy of Sciences, China*

[3)] *Urumqi Station, National Astronomical Observatory, Chinese Academy of Sciences, China*

Abstract. Several wideband VLBI devices, such as wideband DBBC, and a 5-station correlator have been developed at Shanghai Astronomical Observatory. The design concept and the applications of these devices are reported in this paper.

1. Project Overview

In support of the Chinese Lunar Project, in the past two years two new VLBI stations were built in China. One of them is a 50 m telescope, which is located in Mijun near Beijing. The other is a 40 m telescope, which is located in Kunming in southern China. As VLBI station, the VLBI equipment such as the data acquisition system, are needed for these two VLBI stations. Also the correlator is required for data reduction. As a project requirement, we started to develop a 5-station correlator and a data acquisition system in the past several years. The 5-station correlator was completed in 2006. The Data Acquisition System (DAS) with digital base band converter is under development now.

2. The Data Acquisition System

The DAS is the key equipment at a VLBI station. The traditional DAS with analog Base Band Converter (BBC) are used in most VLBI stations in the world now. Unfortunately, this type of DAS is not manufactured anymore. The new type DAS with digital BBC comes slowly onto the market. After long time discussion, the SHAO started the development of a DAS with digital BBC in the beginning of 2007. The system will be operated at 4 Chinese VLBI stations by the end of 2008. The new type DAS is called NDAQ. It is fully compatible with the traditional DAS, which currently runs at the VLBI stations. But the total bandwidth of NDAQ is 4GHz. NDAQ has two data output interfaces. One is Mark IV interface and the other is VSI interface. With different IP core, the NDAQ could be compatible with DBBC and DBE, which are being developed by EVN and Haystack Observatory, respectively. NDAQ has the following characteristics:
- use 5 MHz as standard frequency signal input,
- use 1 pps as a time signal input,
- 4 IFs, the bandwidth of each IF may be 512 MHz or 1024 MHz selectable,
- two MK4 interfaces to MK4 Formatters or two VSI to MK5B/C Disk Arrays,
- fully compatible FS interface of traditional DAS (hardware and software),
- PCAL and auto-spectrum output,
- two channel DAC for channel output signal monitor,
- PCI interface for control.

Fig. 1 shows the diagram of NDAQ. There are three parts in NDAQ. They are RF AGC, Digital Part, and Output Module.

2.1. RF AGC

The Automatic Gain Controller (AGC) amplifies the IF signals from the standard astronomical receiver to the optimum power level for the subsequent high-speed digital A/D converter. One AGC unit contains four separate channels which share one digital interface board and could be synchronously processed. Each channel can accept either lower IF (DC 512 MHz) input or higher IF (512 MHz, 1024 MHz) input by setting the internal switches. Each channel has maximal 50 dB gain and above 60 dB dynamic range. The 0.25 dB finest attenuation step and less than 50 ms close-circle adjusting time allow the AGC unit to provide stable output signals. The AGC unit and the 1024 MHz synthesizer are integrated in a 3U EMC shielding metal box. The AGC unit can be remote monitored and controlled through a simple RS-232 interface.

2.2. Digital Module

The main part of the digital module's hardware consists of four FPGA-based processing boards, each one containing one Atmel AT84AD001B Analog-

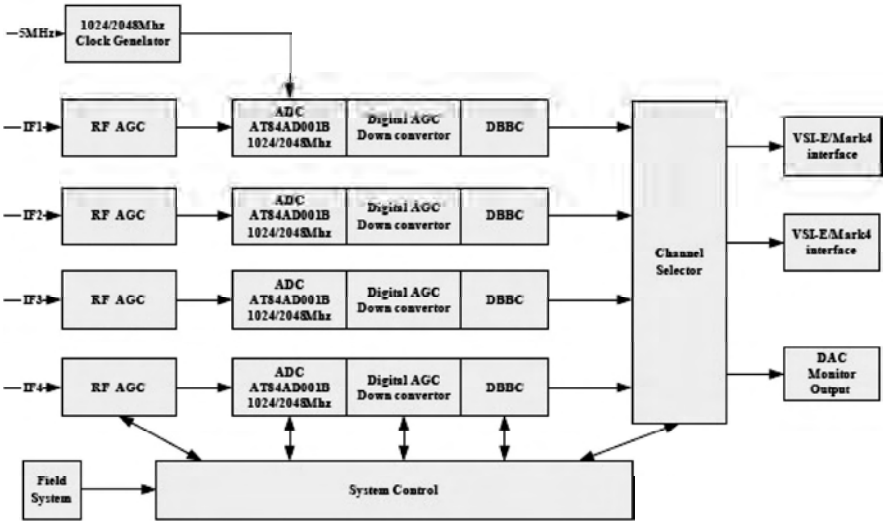

Figure 1. Diagram of NDAQ

to-Digital Converter (ADC), four Xilinx XC4VLX160 Virtex-4 FPGAs with 152k configurable logic cells, and one Xilinx XC4VFX60 integrated with two PowerPC CPU cores. The board's size is 6U that could be installed in the corresponding commercial chassis with cPCI interface backplane. The Atmel ADC on the board could work on 1024 Msamples/sec or 2048 Msamples/sec (interleave mode). With the different firmware in the four XC4VLX160, the NDAQ could implement different functions. The Xilinx PCI IP core (OPB-PCI) and communication program are in the XC4VFX60 that could configure the 4 XC4VLX160 and monitor the board state.

2.3. Output Module

The output module selects a usable data channel to the output interface. The PCAL fetch function and two DAC channels in the output module. After zero baseline tests at Seshan station, two NDAQ test models were integrated at the Seshan and Nanshan stations to start with regular test observations followed by VLBI observations of CE-1. Some results are shown in Fig. 2 and Fig. 3.

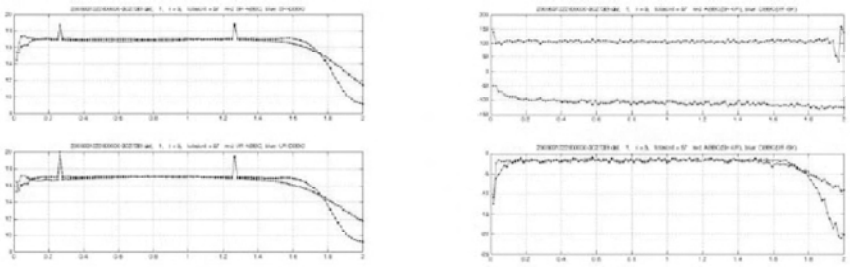

Figure 2. Comparison of the results of ABBC and NDAQ, source: 3C273B, one minute integration time; light line for ABBC and dark line for NDAQ. Left: auto spectrum of Seshan (top), Nanshan (bottom). Right: phase of cross spectrum (top), amplitude of cross spectrum (bottom)

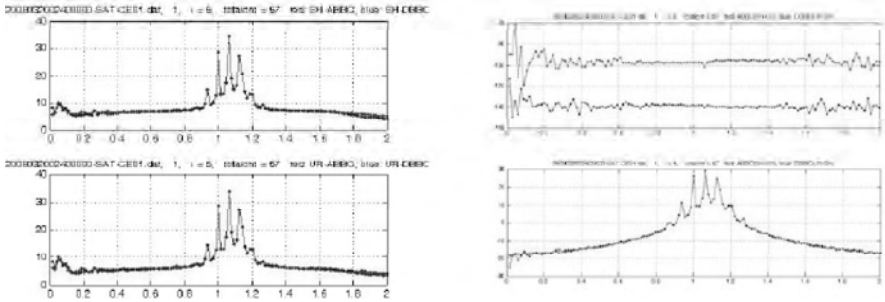

Figure 3. Comparison of the results of ABBC and NDAQ, source: CE-1 satellite one minute integration time; light line for ABBC and dark line for NDAQ. Left: auto spectrum of Seshan (top), Nanshan (bottom). Right: phase of cross spectrum (top), amplitude of cross spectrum (bottom)

3. The Correlator

The diagram of the 5-station correlator is shown in Fig. 4. It is based on XILINX Virtex-4 chips (XC4VSX35).

4. The Future Plan

By the end of 2008 we will develop four NDAQ to install at four VLBI stations in China. The 5-station correlator will be extended to 10 stations with VSI.

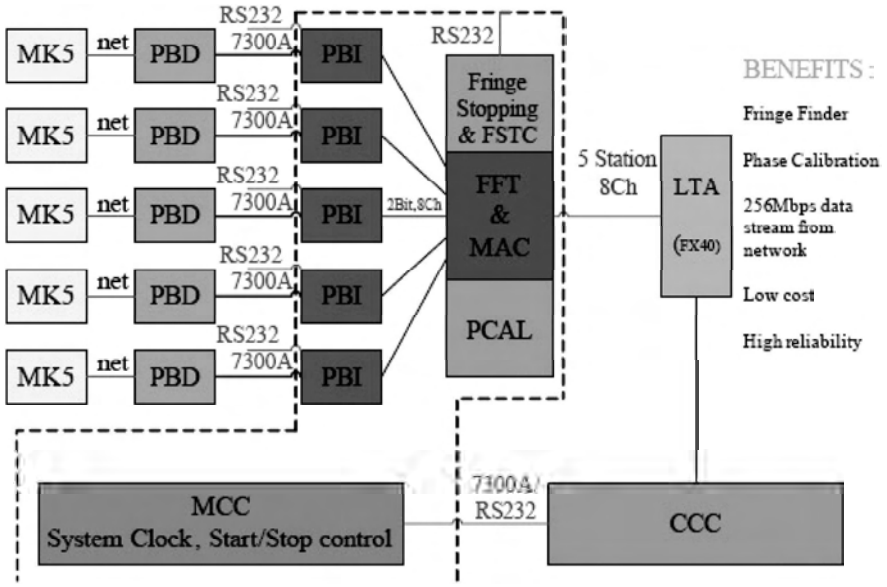

Figure 4. Diagram of 5-station correlator

Acknowledgements

Thanks to the colleagues at the Seshan and Nanshan VLBI stations to support NDAQ test observations and to all staff members of the CVN data processing center to help us to do the data correlation.

References

[1] Zhang, X.Z., et al. CVN Correlator and its Future, New Technologies in VLBI. Astronomical Society of the Pacific, Conference Series Volumes, v. 306, 287–300, 2003.

[2] Xu, Z., et al. Real Time Correlator in FPGA. IVS 2006 General Meeting Proceedings, 89–92.

[3] Tuccari, G., et al. DBBC — A Flexible Platform for VLBI Data Processing. IVS 2006 General Meeting Proceedings, 185–189.

[4] Whitney, A.R., et al. A Wide-Band VLBI Digital Backend System. IVS 2006 General Meeting Proceedings, 72–76.

The 5th IVS General Meeting Proceedings, 2008, p. 386–389

Mark 5 Disk Drive Performance and Reliability

Dan Smythe

MIT Haystack Observatory, USA

Abstract. This paper shows how the write and read speed of a Mark 5 disk pack can be limited by the disk drive itself, the ATA data bus, or the StreamStor board. It also presents some data on disk drive reliability.

1. Disk Drive Performance

The performance of the Mark 5 VLBI data recording system is limited by three factors: 1) the disk drive, 2) the data bus, and 3) the StreamStor disk controller. This paper examines each of these limits and demonstrates each of them with measurements showing how the write and read data rates depend on the position of the write and read pointers. In all of the data presented here, the data rates (Mb/s) are 1-minute averages for the slowest bus in the pack, multiplied by the number of buses in the pack.

Fig. 1 shows how the write rate is limited by the disk itself. It shows that for this modern disk, the speed drops from more than 500 Mb/s at the beginning to less than 256 Mb/s at the end.

Fig. 2 shows how the data rate can be limited by the 66 MB/s (528 Mb/s) data rate of the PATA bus used by the XF2 StreamStor board used in the Mark 5A and Mark 5B. Because of some overhead in reading and writing the disk drives, the data rate does not quite reach the bus speed of 528 Mb/s. And it can be seen that the speed of the disk drives slows down near the end. The Amazon StreamStor board used in the Mark 5B+ clocks the PATA bus at 100 MB/s and increases this bus speed limit from 528 Mb/s to 800 Mb/s.

The data rate of an 8-pack in a Mark 5A or Mark 5B recorder is limited by the XF2 StreamStor board to 1775 Mb/s read and 1715 Mb/s write. The data rate goes up slightly to 1845 Mb/s for reading and writing, when using two 8-packs in non-bank mode.

With the Amazon board in the Mark 5B+ recorder, the maximum data rate increases to 3090 Mb/s read and 2980 Mb/s write, until limited by the speed of the disk drives, as shown in Fig. 3. This data rate is near the maximum data rate for four 100 MB/s PATA buses or 3200 Mb/s. Note that the rate stays

above 2 Gb/s until the module is almost full. Note also that the rate shown in the figure is for the slowest of the 4 buses. In our testing and operations, an 8-pack module populated with modern disk drives 250-GB or larger can record reliably at 2048 Mb/s to the end.

When using two 8-packs in a Mark 5B+ in non-bank mode, the data rate almost doubles, to 5800 Mb/s for reading and 6070 Mb/s writing, until limited by the speed of the disk drives, as shown in Fig. 4. Note that this pair of modules stays above 4096 Mb/s until full, based on the slowest bus.

To summarize, the data rate of a Mark 5A or Mark 5B recorder with 8 or more disk drives is limited to about 1700 Mb/s by the XF2 StreamStor board. With the Amazon board in the Mark 5B+, most modern 8-packs can record reliably at 2048 Mb/s, and a pair of 8-packs can record at 4096 Mb/s in non-bank mode.

2. Reliability

For the last 5 years we have been keeping a record of every Mark 5 disk drive replaced at Haystack. About half of these disks were replaced under warranty by the disk drive manufacturer. Fig. 5 shows the age distrbution of the failed disks. A few of these "failures" were disk drives that were too slow to support Mark 5 recording at 128 Mb/s/drive, but still passed the manufacturer's drive fitness test. Not counted in this analysis are disk drives that failed during initial testing or the first "conditioning" of the Mark 5 disk pack. This initial screening probably accounts for the low number of failures during the first 6 months.

Figure 1. Single Hitachi 500 GB disk drive

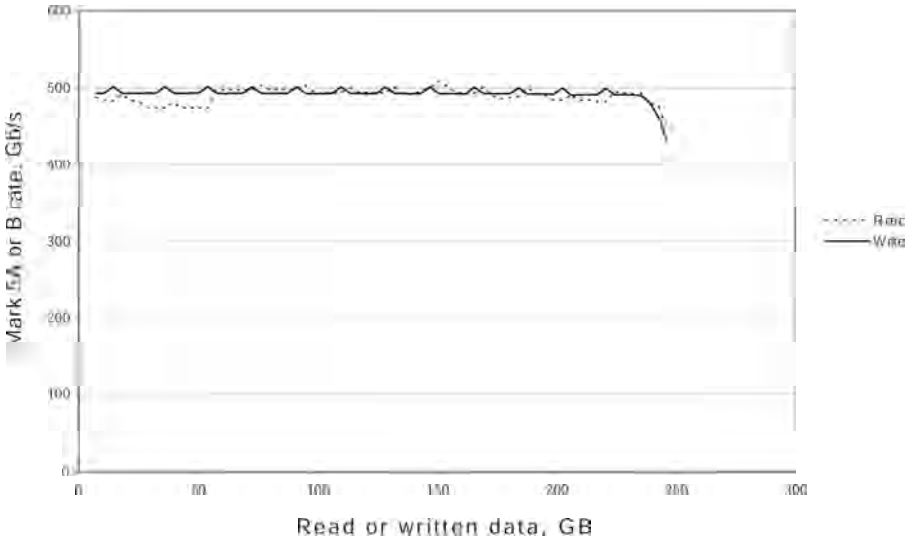

Figure 2. Master-slave pair with Mark 5A or Mark 5B

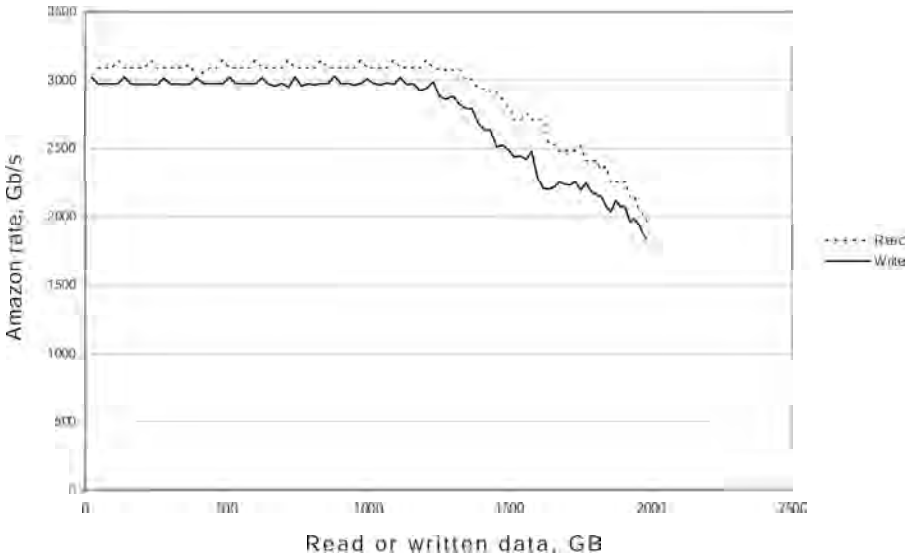

Figure 3. Mark 5B+ performance with an 8-pack of 250-GB disk drives

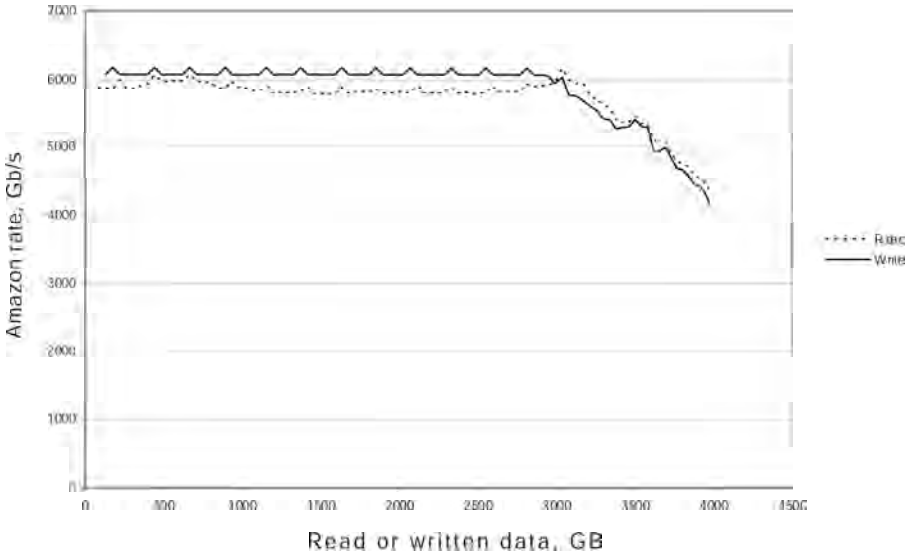

Figure 4. Mark 5B+ performance with two 8-packs in non-bank mode

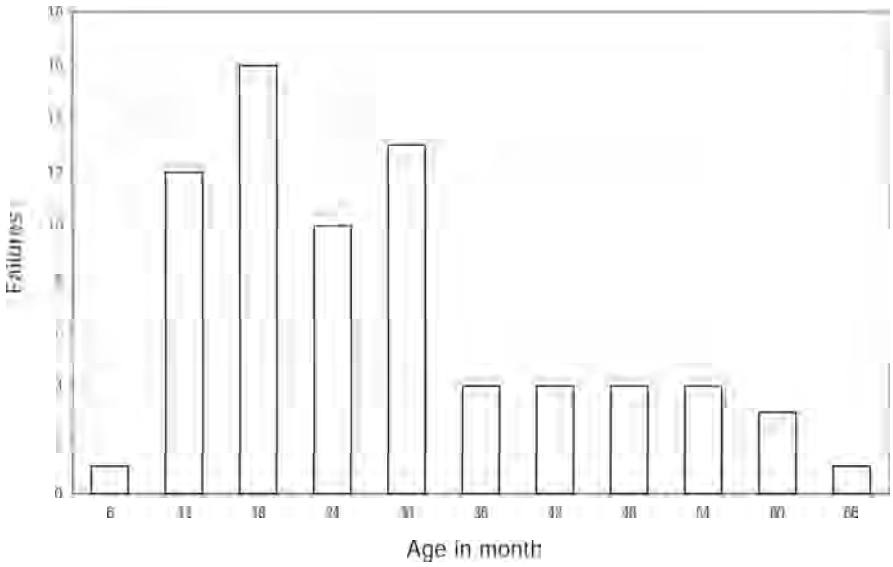

Figure 5. Disk drive failures as a function of age

The 5th IVS General Meeting Proceedings, 2008, p. 390–394

The Mark 5C VLBI Data System

Alan Whitney

MIT Haystack Observatory, USA

Abstract. The Mark 5C VLBI data system is being developed as the next-generation Mark 5 system built on the same basic platform as the Mark 5A, Mark 5B and Mark 5B+. The Mark 5C will have the following characteristics:

- dedicated 10 Gigabit Ethernet data-input port,
- recording rates to 4096 Mbps using two Mark 5 modules (16 disks),
- full compatibility with existing Mark 5 modules,
- playback will be through a high-performance motherboard and 10 GigE NIC,
- targeted for use on software-correlator systems.

Data sources for the Mark 5C system will be based on new digital backends now being developed, specifically the DBE2/VDBE in the U.S. and the dBBC in Europe. Mark 5C data formatting is organized as one-frequency-channel per Ethernet packet, which supports an arbitrary number of frequency channels and allows fine increments in tuning aggregate data rates for better matching with available e–VLBI network bandwidths. A data mode which writes a disk module in a format compatible with playback on a Mark 5B system is planned. The Mark 5C system specification and development is being supported by Haystack Observatory, NRAO and Conduant Corporation. Prototype Mark 5C systems are expected in mid-2008.

1. Introduction

The Mark 5C is being designed as the next-generation Mark 5 system, with a capability of recording sustained data rates to 4096 Mbps. It will use the same disk modules as the Mark 5A and Mark 5B, thus preserving existing investments in disk modules.

The data interface for both recording and playback will be 10 Gigabit Ethernet, which is rapidly becoming a widely supported standard. The use of 10 GigE interfaces comes with some significant implications, however. Firstly, data sources must be designed to provide data streams in a format compatible with the Mark 5C requirements. And secondly, data playback through

a 10 GigE interface is a good match for a rising generation of software correlators. In the interests of backwards compatibility, the Mark 5C will also support a mode which writes disk modules in Mark 5B data format which can be correlated on existing Mark 4 correlators that support Mark 5B.

The Mark 5C will be implemented using the existing Amazon StreamStor disk-interface card (used in the Mark 5B+) from Conduant Corp along with a new 10 GigE-specific interface daughterboard being designed by Conduant. Unlike the Mark 5A and Mark 5B, no separate specialized I/O card will be necessary in the Mark 5C.

2. Data Sources

One major implication of the Mark 5C model is that the data source is responsible for all data time-tagging, formatting and creation of Ethernet packets. This is a departure from the VSI-H model used by the Mark 5B, which has basically only 32 parallel sample bit-streams, a clock, and 1pps tick flowing between the data source and the Mark 5B, with the Mark 5B being responsible for creating data frames with higher level time-tagging and formatting. Fortunately, VLBI data sources capable of creating such formatted Ethernet packets are now being developed in both the U.S. and Europe as part of the development of digital downconverters and backends. Suitable 10 GigE data sources to drive the Mark 5C are expected to be available sometime in the first half of 2008. Normally, each Ethernet packet from the data source will contain sample data from only a single frequency channel, although a Mark 5B-compatible data mode is specified which will write disk modules in a format that can be re-played on a Mark 5B playback unit; this will provide the ability to process the recorded data on existing Mark 4 hardware correlators.

3. Correlation

A major shift is currently developing to move from hardware-based correlators to software-based correlators, some of which already exist. Unlike the Mark 5A and Mark 5B, the Mark 5C will have no streaming hardware playback interface. Instead, the data files will appear to the user as standard Linux files and will be read as such. We expect that the standard interface for playback to a correlator will be through a standard 10 GigE interface implemented on a commercial NIC. Unlike existing hardware correlators, software correlators do not demand constant-rate streaming inputs. As such, the Mark 5C playback is well suited for interfacing to software correlators, but not well suited or intended to interface to hardware correlators.

4. General Mark 5C Characteristics

The Mark 5C will have the following characteristics:

- Mark 5C will be fully compatible with all existing Mark 5 disk modules, however some modules with older disks may limit record/playback data rates;
- at data rates above about 2 Gbps, it will be necessary to record to two 8-disk modules simultaneously, in so-called non-bank mode, which is not normally used by Mark 5A or Mark 5B/5B+;
- a 10 GigE interface for receive only will be implemented on the Amazon StreamStor disk-interface card (currently used in the Mark 5B+) by replacing the FPDP I/O daughterboard on the Amazon card with a newly designed 10 GigE daughterboard. This 10 GigE interface will be receive-only, optimized for sustained real-time recording of at least 4096 Mbps from a data source. Received Ethernet packets can be OSI Layer 2 or higher, but will only be processed by the Mark 5C at the Layer 2 level. Jumbo Ethernet packets up to 9000 bytes will be supported. The data source is required only to transmit Ethernet packets, and is not required to process any received packets;
- the entire data payload from each arriving Ethernet packet, sans a specified length of payload header (which may contain higher OSI Layer parameters or other information), will be recorded to disk. In this sense, the Mark 5C is entirely 'formatless'; i.e. all data formatting must be done by the data source. This allows each user to format the recorded data according to his/her needs;
- the Ethernet data payload may contain a user-generated 32-bit "Packet Sequence Number" (PSN), whose position within the data payload can be specified to the Mark 5C. The Mark 5C can be commanded to a "PSN monitor mode" that will parse this serial number from every packet to identify missing or out-of-order packets. Out-of-order packets, within some reasonable limits, will be restored to proper order, while the user data from each missing packet will be replaced by user-specified "fill-pattern" data. The MSB of the PSN may also be used as an 'invalid' marker to prevent recording data from a packet. If "PSN monitor mode" is disabled, data are recorded to disk in the order that packets are received; no checks are made for out-or-order or missing packets;
- similar to the Mark 5A/B, the Mark 5C will record data as "scans", where a scan is defined as the period between starting and ending the recording of a particular observation. The duration of a scan may be from several seconds to many minutes. The host application software will maintain a directory of scans for easy identification and access. No duplicate-named scans are allowed;

- scans will appear as normal Linux files to the host PC. Data playback on the Mark 5C will be through a 10 GigE NIC interface on the host PC . A planned upgrade by Conduant of the Amazon card, which interfaces to the PCI-X bus, will support the PCI e bus to allow substantially higher playback rates from Mark 5 disk modules.

5. Physical Connections

Because the interconnection between the data source and the Mark 5C is a standard 10 Gigabit Ethernet connection, there is considerable flexibility in connection topology between data-source units and Mark 5C units. Fig. 1 illustrates the general case where multiple data-source units provide data to multiple Mark 5C units through a standard Ethernet switch. The Ethernet switch allows Ethernet packets from either of the two DBE2 units to be arbitrarily routed to any of four Mark 5C units, providing an easy way to manage route data packets in an arbitrary manner, but is particularly useful to manage data-rate mismatches between individual data sources and individual Mark 5Cs. For example, an 8 Gbps packet stream from a single DBE2 could be separated into two 4 Gbps packet streams to two Mark 5C units.

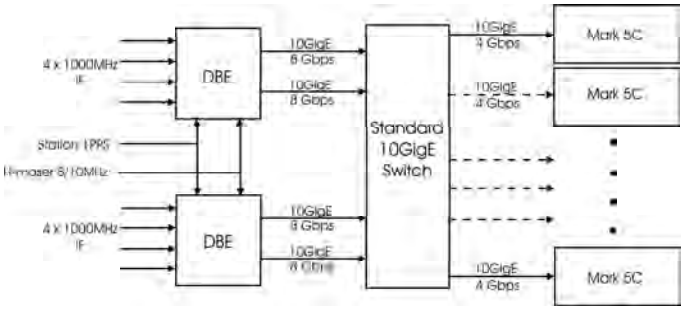

Figure 1. Generic signal-connection diagram for Mark 5C

6. Data-Organization Philosophy

Previous generations of VLBI data recorders, such as Mark 3/3A/4/5A/5B have generally formatted multiple observing frequency channels as multiple-parallel bit-streams representing simultaneous samples from all channels. Also, typically, the per-channel data rate is constrained to 2^n Mbps and the number of channels is also usually constrained to be integer powers of 2, thereby also constraining total data rates to be 2^n Mbps. This type of data organization has been satisfactory for the type of hardware correlators that have been predominant over the past 30 years, but is not well matched to todays needs. Modern VLBI data management relies increasingly heavily on the use of standardized

local and global computer networks whose capacities are not well matched to the 2^n Mbps paradigm of established VLBI data systems. Furthermore, VLBI correlation processing is moving rapidly towards fully software solutions operating on clustered computer networks. Both of these trends argue for improved flexibility in aggregate VLBI data rates and repackaging of data into more convenient forms for processing by standard computer hardware.

7. Slow-Disk Management

Considerable experience has shown a low, but significant, occurrences of "slow" disks, that is disks that still function to read and write, but at a reduced data rate due presumably to marginal or bad sectors on the disk. Normal RAID systems will simply slow down to accommodate such disks in a RAID array since they are not designed for real-time operation. The StreamStor disk-interface cards in the Mark 5 units are designed to re-distribute the load to normal-performing disks in the face of one or more "slow" disks in the recording array so as not to lose critical real-time data. Playback through a software correlator is generally non-critical as to playback rate, though the correlation speed may be slower than normal. If correlation speed is important, a playback mode may be invoked whereby data not received in time from slow disks will be replaced with a specified "fill pattern".

8. Upgrade Path from Mark 5A, Mark 5B or Mark 5B+

The Mark 5C requires an Amazon StreamStor card ($\sim$ \$9500) plus a 10 Gbps Ethernet daughter board ($\sim$ \$3000–4000); no VLBI-specific I/O board is required. Upgrade from Mark 5A or Mark 5B requires an Amazon board and 10 GigE daughterboard. Upgrade from a Mark 5B+ requires only a 10 GigE daughterboard.

9. Summary

The Mark 5C development is being support by Haystack Observatory, NRAO and Conduant Corporation. Prototype Mark 5C systems are expected in mid-2008.

Detailed Mark 5C and Mark 5C data-format specifications and the corresponding data-format specifications are avaiable at http://www.haystack.edu/tech/vlbi/mark5/mark5/memo.html (particularly memos 57 and 58). Other information related to Mark 5C is also available at this site.

The 5th IVS General Meeting Proceedings, 2008, p. 395–399

Mark 5C Software Development Program

Chester Ruszczyk

MIT Haystack Observatory, USA

Abstract. The product road map for Mark 5C software development program that will support 4 Gbps recording over a 10 GigE data connection is presented.

The Mark 5C software development effort is being staged as a three phase project. The first phase of the project will accept data via a standard network interface card and store data to a COTS storage device. The second phase of the project, dubbed 'Mark 5C-', will accept data from a standard network interface card and will have the capability to store the data in Mark 5B format to either a standard Mark 5 disk modules or to a standard filesystem (at a reduced data rate). This second phase will allow other software applications to communicate with the Mark 5C application, with the aim to reduce the time to deliver/debug the software, and to help facilitate the burst-mode development effort. The final phase of the project will release the fully functional Mark 5C application that will configure, control and manage the actual Mark 5C hardware.

The Mark 5C software development effort is being supported by MIT Haystack Observatory and NRAO.

1. Introduction

The Mark 5C software development programs objective is to create an application that can support a 4 Gbps recording capability on a Mark 5C hardware platform by the end of 2008. The paper in this proceeding [1] provides an overview of the ongoing Mark 5C VLBI data program at Haystack Observatory from a hardware and system point of view.

The software development effort of Mark 5C application, referred to in this article as the VLBI transfer application, will focus on record functionality required to minimize the software development time after a functional Mark 5C hardware system is available. Playback of the data is expected to be supported through the use of 3rd party applications with all storage devices appearing as a standard filesystem or transfer of the recorded data in Mark 5B compatibility mode to an existing hardware correlator.

2. VLBI Transfer Application

The development of the VLBI transfer application will use a phased approach. The goal of this approach is twofold: 1) develop an application without the availability of fully functional hardware, and 2) allow third party developers the opportunity to begin integration of the application into their own software development time-line, at a reduced feature set. The result will be two preliminary software releases followed by the first official release.

Each release will support a target goal and a specific set of features. The goals will focus on a specific record and playback path, or the path the incoming data takes from the network interface to the storage device, and vice verse, and the features will focus on the command and control functions necessary and the method used to communicate this information to the application. The goals and features of each individual release, referred to by their version numbers, are introduced in Sec. 2.1–2.3.

It should be noted that once a feature is introduced to the application that it is not removed from the application but carried forward to the next release along with bug fixes.

Key characteristics of the VLBI transfer application are:

- developed in "C" to maximize the development team strengths;
- targeted to execute on the latest Linux distribution, e.g. Debian lenny, with the latest kernel, 2.6.24;
- provide an initialization option, via a configuration file loaded up at start-up;
- the periodic update of status information;
- support for Ethernet "Layer 2" data communications as specified in the Mark 5C V1.0 Specification [2];
- command and control of the application through a:
  - TCP port,
  - VSI-S [3] standard protocol syntax.

To aid in the software development cycle of the application, we will utilize the following standard software practices:

- software version control, e.g. CVS;
- linux software version numbering;
- major feature releases;
- standard Linux packaging;
- bug reporting system.

Fig. 1 shows the featured record and playback data paths that each version will support.

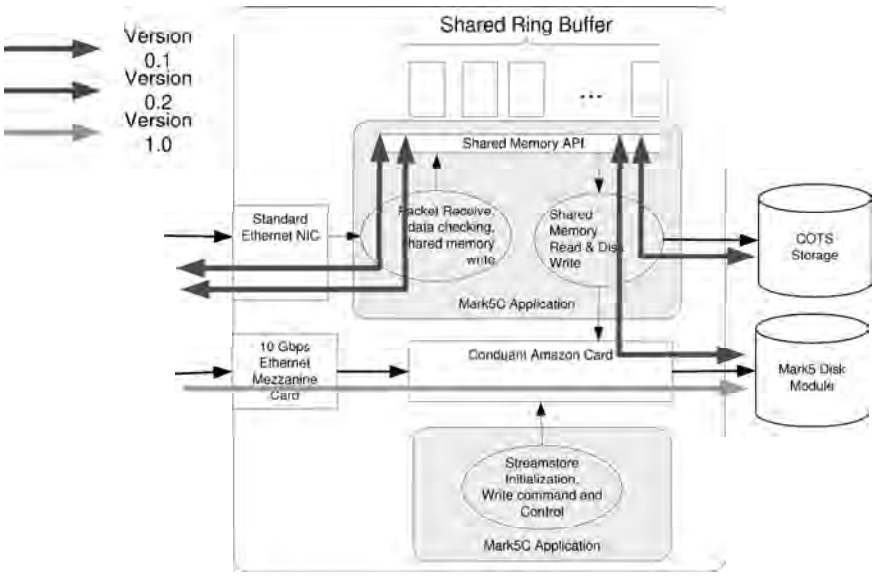

Figure 1. The VLBI Transfer Application Record and Playback Paths

2.1. Version 0.1

The goal of version 0.1 of the VLBI transfer application is to provide the initial framework for the application with support for a maximum record and playback capability of 512 Mbps. Version 0.1 will accept data from a standard 1 or 10 Gbps Ethernet Network Interface Card (NIC) at layer 2 and store it on a COTS storage device, e.g. system disk, RAID array. The recommended playback capability is to use a 3rd party application to read data from the standard COTS storage device and output it over the standard NIC.

To control the VLBI transfer application a separate control application will provide a command line interface for basic configuration, record and status commands. This application will support a subset of the Mark 5C commands [4] and focus on commands associated with non-Streamstor command and control. This application will use a standard TCP socket to communicate with the VLBI transfer application using the VSI-S syntax.

2.2. Version 0.2

The goal of version 0.2 of the VLBI transfer application is to add support to record data to Conduant disk module via the Conduant's Streamstor Amazon controller card using their Software Development Kit (SDK) version 8.X at a maximum rate of 512 Mbps. Version 0.2 will receive data from the standard 1 or 10 Gbps Ethernet NIC at layer 2 and store it to Conduant's storage device in a Mark 5B compatibility format [5].

To read, or playback, the data from the Conduant disk modules it is recommended that a Linux kernel module known as File in UserSpacE (FUSE) [6] and a separate application, e.g. Fuse Mk 5A [7], be used to allow the Conduant disk module to appear as a standard filesystem. As in version 0.1, then any 3rd party application can access and transfer the data as if it was a standard COTS storage device, via the standard NIC interface.

Support for additional commands of the Mark 5C Software Interface Specification [4] will be available via the control application that targets traditional transfer of data from the motherboard to the disk modules. In addition an initial version of a Graphical User Interface (GUI) application will be made available supporting a limited command set.

2.3. Version 1.0

The goal of version 1.0, the official release, of the VLBI transfer application is to add support to record data at a rate of 4 Gbps. This capability requires a fully functional Mark 5C hardware system that includes Conduant's 10 Gbps Ethernet daughter card attached to the Amazon card and the corresponding version of their SDK. Therefore, the applications primary function is the initialization, monitoring, command and control of the hardware supporting all of the features specified in [2].

To playback data, the functionality is identical to that of Version 0.2 and will require that the appropriate application, e.g. fuseMk5A, can support the latest version of the SDK and it associated features.

A fully functional command and control set for the VLBI transfer application will be available via command line interface or a GUI.

Corresponding to the release of the software a users manual and design documentation will be made available.

3. Summary

The Mark 5C software development road map, being supported by both MIT Haystack Observatory and NRAO, with the goal to support 4 Gbps recording capability was presented. Preliminary versions of the software are expected in August 2008 and the official release date of the application of December 2008.

References

[1] Whitney, A. The Mark 5C VLBI Data System. IVS 2008 General Meeting Proceedings. This volume.

[2] MIT Haystack Observatory, NRAO, Mark 5C Specification. NRAO VLBA Sensitivity Upgrade Memo 12 or Mark 5 Memo 57, Version 1.0 Feb. 19, 2008; http://www.haystack.edu/tech/vlbi/mark5/mark5_memos/057.pdf.

[3] Whitney, A. VLBI Standard Interface — Software. 2003;

http://www.haystack.edu/tech/vlbi/vsi/docs/2003_02_13_vsi-s_final_rev_1.pdf.

[4] MIT Haystack Observatory, NRAO, Mark 5C Software Interface Specification. NRAO VLBA Sensitivity Upgrade Memo 18 or Mark 5 Memo 61, Jan. 7, 2008; http://www.haystack.edu/tech/vlbi/mark5/mark5_memos/061.pdf.

[5] MIT Haystack Observatory, NRAO, Mark 5C Data Frame Specification. NRAO VLBA Sensitivity Upgrade Memo 13 or Mark 5 Memo 58, Version 1.0 Feb. 19, 2008;
http://www.haystack.edu/tech/vlbi/mark5/mark5_memos/058.pdf.

[6] Filesystem in UserSpace, FUSE, Open Source Software;
http://fuse. sourceforge.net/fuse.

[7] Wagner, J. fuseMk5A Software Application;
http://sourceforge.net/projects /fusemk5a/.

The 5th IVS General Meeting Proceedings, 2008, p. 400–404

Development of a Compact VLBI System for Providing over 10-km Baseline Calibration

Ichikawa Ryuichi [1], *Ishii Atsutoshi* [1], *Takiguchi Hiroshi* [1], *Kuboki Hiromitsu* [1], *Kimura Moritaka* [1], *Nakajima Junichi* [2], *Koyama Yasuhiro* [1], *Kondo Tetsuro* [1], *Machida Morito* [3], *Kurihara Shinobu* [3], *Kokado Kensuke* [3], *Matsuzaka Shigeru* [3]

[1)] *Kashima Space Research Center, NICT, Japan*

[2)] *NICT, Japan*

[3)] *Geographical Survey Institute, Japan*

Abstract. We are developing a compact VLBI system with 1.6 m diameter aperture antenna in order to provide reference baseline lengths for calibration. The reference baselines are used to validate surveying instruments such as GPS and EDM and maintained by the Geographical Survey Institute (GSI). The VLBI system is designed to be assembled with muscle power simply in order to perform short-term (about one week) measurements at several reference baselines in Japan islands. We have evaluated a front-end system with a wide-band quad-ridged horn antenna by installing it on the 2.4 m diameter antenna at Kashima. On Dec. 5, 2007 we have successfully detected fringes of the 3C84 signal for S/X band. In addition, a geodetic VLBI experiment using a LD-pumped cesium gas-cell atomic frequency standard was successful.

1. Introduction

National Institute of Information and Communication Technology (NICT) are developing a compact VLBI system with 1.6 m diameter aperture antenna in collaboration with GSI. GSI has the responsibility to calibrate and validate survey instruments such as GPS receivers and Electro-Optical Distance Meters (EDM). The validation work is operationally carried out at a 10 km reference baseline maintained by GSI, which is located about 5 km east of GSI headquarters, Tsukuba, Japan (Fig. 1).

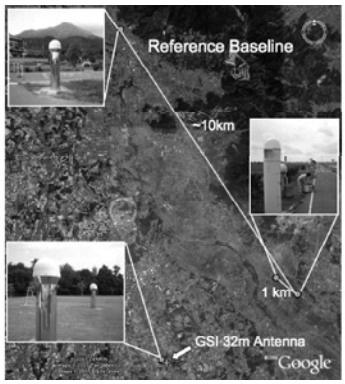

Figure 1. GSI reference baseline

Along the baseline, pillar monuments made of stainless steel are installed. To guarantee the quality of validation, the baseline length has to be evaluated routinely. In addition, GSI compares an operational EDM equipment and a iodine-stabilized He-Ne laser wavelength standard in order to keep its traceability for length to a national standard maintained by the National Institute of Advanced Industrial Science and Technology (AIST).

However, since it is too long to get a line of sight from the end to the other end by EDM at the actual reference baseline, calibration works at present are only performed at the shorter baseline in stead of a measurement of the entire 10 km length.

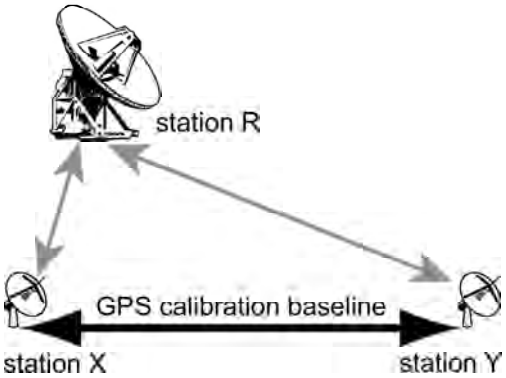

Figure 2. MARBLE concept

On the other hand, the geodetic VLBI technique can give an independent measurement to examine the baseline with a few millimeter accuracy using the hydrogen-maser. Moreover, the hydrogen-maser frequency standard can be considered as the traceable technique to the national standard. Thus, we started to develop a compact VLBI system with 1.6 m diameter aperture antenna in order to measure the accurate length of the reference baseline.

In this short article, we describe the technical requirements, system concept, and feasibility study of the VLBI system dedicated to 10 km measurement.

2. Development

2.1. MARBLE System

The compact VLBI system will be installed at both ends of the reference baseline in order to perform baseline calibration. However, it is too insensitive to detect fringes between both stations using such compact antenna. Thus,

we have designed a new observation concept which includes one large antenna station into the baseline observation. The schematic image of the new concept is shown in Fig. 2.

We can detect two group delays between each compact antenna and the large one based on conventional VLBI measurements. A group delay between the two compact antennas, ΔXY, can be indirectly calculated using the simple equation

$$\Delta XY = \Delta RY - \Delta RX, \tag{1}$$

where ΔRX and ΔRY are two group delays obtained conventionally (Fig. 2). We named the idea Multiple Antenna Radio-interferometry of Baseline Length Evaluation (MARBLE).

2.2. Compact VLBI System

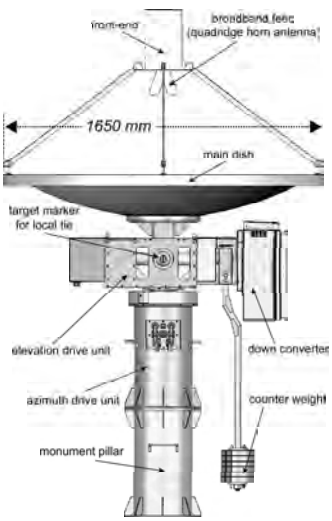

Figure 3. Schematic image of the MARBLE compact VLBI system

The core equipment of the MARBLE system is the compact VLBI system as described so far. To perform short-term (about one week) measurements at several reference baselines in Japan islands, the most important idea in developing the VLBI system is transportability.

The VLBI system consists of a 1.6 m diameter aperture antenna with a broadband feed, an azimuth drive unit, an elevation drive unit, an IF downconverter unit, an antenna control unit (ACU), a counterweight, and a monument pillar (Fig. 3). Each drive unit is equipped with a zero-backlash harmonic drive gearing component. These are designed to be assembled with muscle power simply.

3. Experiments

3.1. Geodetic VLBI Experiment using LD-pumped Cesium Gas-cell Atomic Frequency Standard

A portable and stable frequency standard is desirable to carry out the field VLBI measurements using the MARBLE compact VLBI system. In addition,

it is also important that such frequency standard is easy to handle under a rough temperature control. To prepare a hydrogen-maser frequency standard and a thermostatic chamber at both ends of the reference baseline is not practical. One of the possibilities to resolve this problem is to use an LD-pumped cesium gas-cell atomic frequency standard (hereafter, we call this "CS gas-cell standard") made by Anritsu [1].

Figure 4. LD-pumped cesium gas-cell atomic frequency standard

We carried out a VLBI experiment between Kashima 34 m and Koganei 11 m on Jul. 19, 2007 in order to evaluate the CS gas-cell standard in the geodetic VLBI measurements. At Koganei we used a hydrogen-maser frequency standard. On the other hand, at Kashima we installed the CS gas-cell standard in place of the hydrogen-maser one. The analyzed baseline length is well consistent with those obtained by previous VLBI measurements using the conventional way (Tabl. 1).

Table 1. Results of experiments. In the first column of the table, 'H' and 'Cs' denote the use of a hydrogen-maser frequency standard and a CS gas-cell standard, respectively

date	WRMS residual, ps	baseline vector, mm	sigma, mm		
			length	horizontal	vertical
2007.06.15 (H)	32	109337424.10 ± 1.17	1.17	0.76	4.82
2007.06.17 (H)	29	109337422.26 ± 1.00	1.00	0.67	4.09
2007.06.20 (H)	37	109337421.45 ± 0.76	0.76	0.51	3.12
2007.07.19 (Cs)	39	109337422.58 ± 1.26	1.26	0.92	5.14

3.2. First Fringe Test using Broadband Feed

We developed a new front-end system for the MARBLE compact VLBI system. For geodetic purposes, the S/X dual-band frequency receiver is indispensable in order to calibrate ionospheric path delay error. We use a broadband dual-polarized quad-ridge horn antenna (type 3164-05 ranging 2 GHz–18 GHz [2]) made by ETS-Lindgren within the present front-end system. We installed the new front-end system on the 2.4 m diameter antenna at Kashima and we have successfully detected fringes of the 3C84 signal for both S and X bands on Dec. 5, 2007 (Fig. 5).

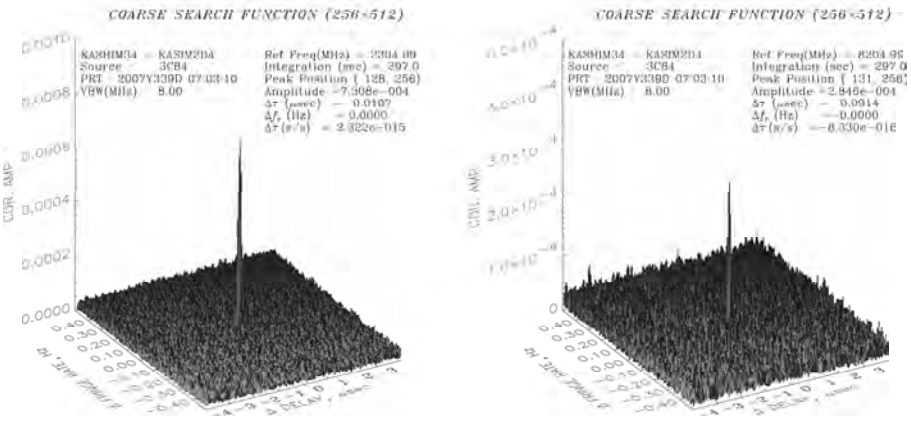

S-band X-band

Figure 5. Detected first fringes using broadband feed

4. Concluding Remarks

We are developing a compact VLBI system with 1.6 m diameter aperture antenna in order to provide reference baseline lengths for GPS and EDM calibration maintained by GSI. We successfully detected fringes of the 3C84 signal for both S and X bands using the new front-end system with a wide-band quad-ridged horn antenna by installing it on the 2.4 m diameter antenna at Kashima. In addition, a geodetic VLBI experiment using an LD-pumped cesium gas-cell atomic frequency standard provided a consistent baseline length with the previous results obtained using a hydrogen maser frequency standard.

References

[1] Suga, H., Y. Ohuchi, T. Ueno, et al. LD-pumped cesium gas-cell atomic frequency standard. Proceedings of the The Institute of Electronics, Information and Communication Engineers General Conference, No 1(19990308), 349, 1999 (in Japanese).

[2] Lindgren, ETS-Lindgren, The Model 3164-05 Open Boundary Quadridge Horn, Data Sheet, 2005.

The 5th IVS General Meeting Proceedings, 2008, p. 405–409

Developments of Automated Data Processing System for Ultra Rapid dUT1 e–VLBI Sessions

Yasuhiro Koyama, Mamoru Sekido, Thomas Hobiger, Hiroshi Takiguchi, Tetsuro Kondo

Kashima Space Research Center, National Institute of Information and Communications Technology, Japan

Abstract. Timeliness of the data processing of the international VLBI observations has been continuously improved in the past decades. In particular, e–VLBI technique has proved that it has the capability to shorten the latency by transferring the observed data to the correlator by using high speed communication networks. The method has been introduced to routine intensive VLBI sessions to monitor dUT1. To improve the timeliness even further, we started an initiative to develop automated data transfer and data processing systems using Europe-Japan baselines. On Feb. 21, 2008, we succeeded to demonstrate the effectiveness of the developed systems and estimated the dUT1 parameter 3 minutes 45 seconds after the last scan of the one hour intensive style e–VLBI session. This achievement was realized by the developments of the K5/VSSP32 data acquisition terminal, automated data processing and analysis software.

1. Introduction

Improving the timeliness of the analyzed results from global VLBI sessions is one of the important and challenging themes for IVS. Since UT1-UTC, or dUT1, randomly varies reflecting dynamic phenomena on the surface and the interior of the Earth, the accuracy of the predicted dUT1 values deteriorates with time. Therefore, it is expected that the accuracy of the predicted dUT1 can be improved by shortening the delay time from the observations to the data processing for global geodetic VLBI sessions. The report of the IVS Working Group 2 for Product Specification and Observing Program pointed out that it is very important to shorten this processing time delay to improve the accuracy of the Earth Orientation Parameters (EOP) including dUT1. The report also sets the goal of the IVS observing program to make the time delay from observation to product less than one day by the year 2005. This goal was partially realized by introducing e–VLBI scheme to the routine intensive VLBI sessions.

Currently, both INT-2 and INT-3 regular intensive sessions are performed

in a similar way. The observed data are transferred to the correlator site after the session. After all the data are transferred, file format conversion, correlation, and data analysis processing are performed manually by an operator at the correlator site. We considered that it is possible to further improve the latency to obtain the results if we can transfer data in parallel with the observations and process the data automatically without manual interactions. By developing necessary hardware and software, we successfully demonstrated the concept. In the following sections, details of these developments will be explained.

2. Developments of K5/VSSP32 System

The developments of the K5 recording terminal began with the developments of a specialized A/D sampling board called K5/VSSP board. The board was designed to be installed in a PCI expansion bus slot of a commodity PC running FreeBSD or Linux operating system. Each board is capable to sample 4 channels of analog inputs from VLBI base band converters by referring to the external 10 MHz standard signal from a Hydrogen Maser system. One K5/VSSP recording terminal is composed of four rack-mounted PC systems with one K5/VSSP board for each PC system, and it can record 16 channels of baseband signals for usual geodetic VLBI sessions. The K5/VSSP terminals were introduced at Kashima (34 m and 11 m), Koganei, Tsukuba, and Syowa IVS stations from 2002 and were used for regular IVS sessions since then. Each PC systems of the K5/VSSP terminal is equipped with an on-board commodity network interface, so that it became possible to transfer the observed data over the high speed networks right after the VLBI sessions for e–VLBI operations. However, it was not possible to transfer the data files while the recording is on-going at very high speed data rate. To improve this situation, we started to develop new data acquisition terminal K5/VSSP32. The pictures of the new K5/VSSP32 terminal are shown in the Fig. 1.

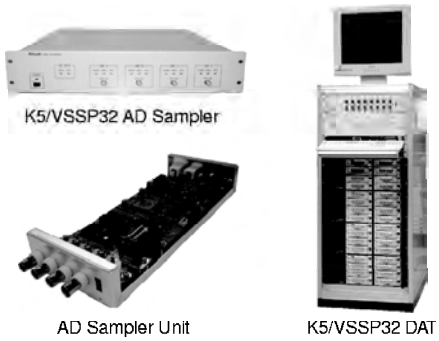

Figure 1. Pictures of the K5/VSSP32 data acquisition terminal (right) and K5/VSSP32 USB 2.0 external AD sampler unit (left)

In the K5/VSSP32 data acquisition terminal, the A/D sampling unit was designed as an independent external unit which is interfaced with a commodity PC system using USB 2.0. Each unit can sample 4 baseband channels. 4 units are configured in one rack mountable chassis to support 16 input channels. Since each unit is designed as an external device from the PC system, it became very simple to install the unit under the Linux PC systems. The K5/VSSP32 terminal is composed of 4 Linux PC systems with one K5/VSSP32 unit connected to each PC. Comparing the previous K5/VSSP terminal, the new K5/VSSP32 terminal can support observing data rate up to 1024 Mbps (256 Mbps per unit) whereas the old K5/VSSP system can only support up to 512 Mbps. It also became possible to read and transfer recorded data files even while another scan is being recorded. The K5/VSSP terminals at five IVS stations have been replaced with the new K5/VSSP32 terminal system gradually since 2007. By using this terminal, it now became possible to process the observed data for file format conversion and correlation processing even if the recording of the other scan is happening as illustrated in the Fig. 2.

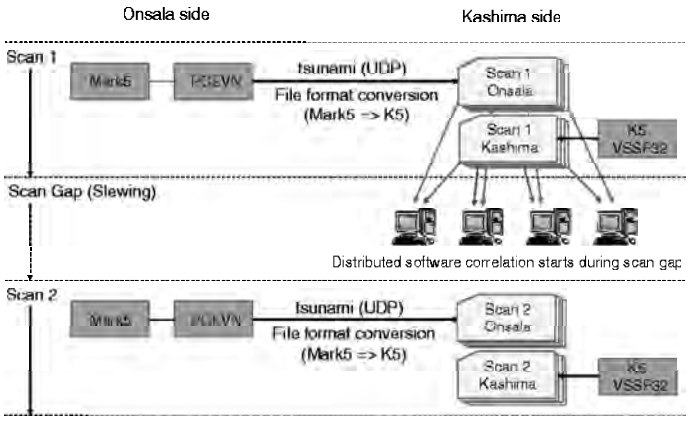

Figure 2. The processing flow of the ultra rapid e–VLBI intensive sessions

3. Automated Data Processing and Analysis

As shown in Fig. 2, a set of programs have been developed to perform the distributed data correlation processing. PC-EVN system is installed at Onsala station to transfer the observed data in real-time to the correlation site at Kashima using Tsunami data transfer protocol. The same configuration is set up at Metsähovi and Tsukuba stations, respectively. The Tsunami protocol is a UDP-based protocol designed to transfer high speed digital data effectively over the long distance high speed networks. A format conversion program from Mark 5 file format to K5 file format has been implemented to the Tsunami receiver client program, so the K5 format data files are created on the Tsunami receiver client at Kashima after each scan is completed. At the same time,

K5/VSSP32 terminal at Kashima generates the K5 format data files. As soon as the scan has been completed, the K5 data files, one from the Onsala station and the other from the Kashima station, are accessed by the K5 software correlation program for correlation processing. Since four K5 data files are usually generated from one geodetic VLBI scan, it is easy to distribute the correlation processing tasks to four independent CPUs. Usually, the correlation processing finishes before the next scan starts. But even if the next scan starts before the correlation processing of the previous scan, it does not cause any problem. In the next scan, the data from Onsala station is transferred to Kashima no matter whether the correlation processing of the previous scan is finished or not, and the correlation processing of the next scan starts as soon as the data transfer completed.

Typically, 20 to 30 scans are observed within one ultra-rapid dUT1 intensive VLBI session, and the last correlation processing finishes after a few minutes from the last scan. By applying this method alone, the required time to process the data is tremendously reduced from about an hour to a few minutes by transferring the data in parallel with the observation session. As soon as the correlation processing of all scans finishes, the Mark 3 format database files will be generated and the data are analyzed automatically (Fig. 3).

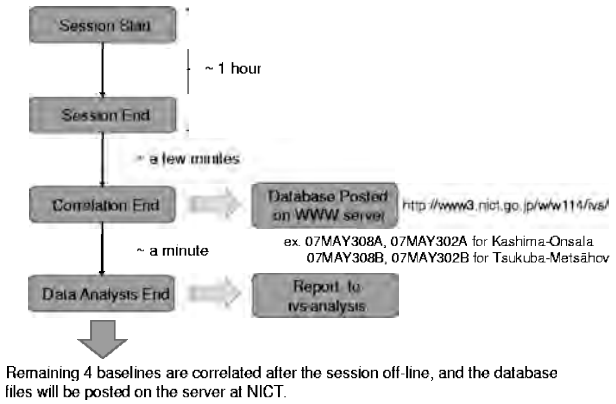

Figure 3. Typical data flow for the ultra rapid dUT1 e–VLBI intensive sessions

To realize this data flow, we have developed a set of programs to interface between bandwidth synthesis output files and database files in various formats as illustrated in Fig. 4. To support both CALC/SOLVE and OCCAM data analysis software, a new database based on the NetCDF architecture has been designed. From the NetCDF database, it is possible to generate the Mark 3 database files for CALC/SOLVE software and NGS-card data files for OCCAM software. It is also possible to produce NetCDF database files from Mark 3 database files. To obtain the estimated value of the dUT1, it is necessary to resolve group delay ambiguities caused by the bandwidth synthesis processing. The procedure to resolve ambiguities is also automated by integrating the

OCCAM data analysis software and scripts to perform iterative processes to resolve ambiguities. Once the ambiguities are resolved, the estimated results of dUT1 will be posted on a Web server to make it available to the wide user community, and the NetCDF database and Mark 3 database files are updated with the correct group delay information to make them free from group delay ambiguities.

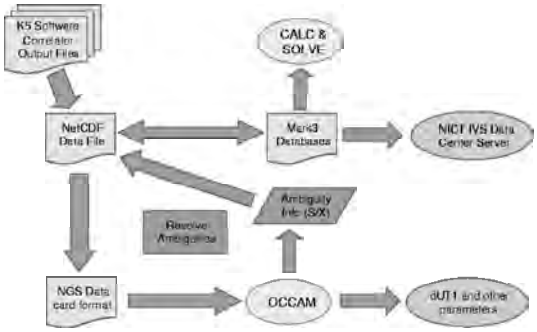

Figure 4. Relationship between the newly designed NetCDF database file and other format database files, analysis software, and output files from bandwidth synthesis processing

4. Conclusions and Future Plan

By using the newly developed hardware and software systems described in the previous sections, we succeeded in estimating dUT1 only 3 minutes 45 seconds after the intensive style e–VLBI session between Onsala and Tsukuba stations performed on Feb. 21, 2008. Although this results from a special R&D setup, it will be a straight forward process to introduce the same method to the routine intensive dUT1 VLBI sessions like INT-2 in the near future. To make this transition from R&D stage to the routine operation stage, we are planning to continue similar e–VLBI sessions until this procedure of the ultra rapid e–VLBI intensive sessions become reliable and robust. In the future, it will also become possible to process the large scale global VLBI sessions if all of the network stations are connected each other by high speed research networks.

Acknowledgements

The authors would like to acknowledge many members of the Geographical Survey Institute of Japan, Onsala Space Observatory of Chalmers University of Technology, Sweden, Metsähovi Radio Observatory of Helsinki University of Technology, Finland for the close cooperations for the ultra rapid dUT1 e–VLBI initiative. We also appreciate precious help from many organizations including high speed research network operators and many IVS components.

The 5th IVS General Meeting Proceedings, 2008, p. 410–415

VLBI2010 Antenna Slew Rate Study

Bill Petrachenko [1], *Johannes Boehm* [2], *Daniel MacMillan* [3], *Arthur Niell* [4], *Andrea Pany* [2], *Anthony Searle* [1], *Joerg Wresnik* [2]

[1)] *Geodetic Survey Division, Natural Resources Canada, Canada*

[2)] *Institute of Geodesy and Geophysics/University of Technology, Vienna, Austria*

[3)] *NVI, Inc./NASA Goddard Space Flight Center, USA*

[4)] *MIT Haystack Observatory, USA*

Abstract. A relationship is developed between VLBI antenna slew parameters (rate and acceleration) and station position accuracy. The relationship supports the specification of antenna slew parameters for the next generation VLBI2010 system.

1. Introduction

The following three sections describe respectively the method used in the study, results, and conclusions.

Note: source-switching interval refers to the time between the start of one scan and the start of the next (including both on-source time and slew time between sources), and, the term scan refers to the effect of a group of antennas simultaneously observing the same source.

2. Method

The analysis is carried out in three steps: 1) VLBI schedules are generated, each with a different uniform source-switching interval; 2) a relationship is developed between source-switching interval and position accuracy using schedules from step 1 and Monte Carlo simulators; 3) a relationship is developed between slew parameters and position accuracy using the results of step 2 and software that was developed to relate slew parameters to source-switching interval.

2.1. Schedule Generation

Four 24 h schedules were generated, each with a different uniform source-switching interval, e.g. 15, 30, 45 and 60 s, using a well-distributed global network of 16 stations and a list of 230 compact sources suggested for geodetic use by Leonid Petrov. In the scheduling software, scans are scheduled in pairs with sources as close to 180 degrees apart as possible; an attempt is made to approach uniform spatial coverage over the celestial sphere by selecting the next source to be the one that is furthest from its nearest neighbor (of the eleven most recently observed source pairs), i.e. filling the largest hole in the current source distribution; and, an attempt is made to observe each source roughly an equal number of times over the course of each 24 h session. In practice, schedules are generated scan-by-scan with each candidate source being assigned a score and the highest scoring source being selected for the next scan.

Since the uniform sky algorithm typically generates long inter-scan slews, scans were reordered in groups of five to minimize slew time. Also, since it was hypothesized that one antenna often has a disproportionately long slew time to undo the azimuth cable wrap, the last antenna to arrive on source for each scan pair was always dropped.

2.2. Monte Carlo Simulators

Monte Carlo simulators were developed [1] previously for other VLBI2010 studies. Simulated input data include the effects of reference clock drift (modelled as a random walk plus integrated random walk with ASD 10^{-14} at 50 m), atmosphere instability (modelled as a moving turbulent screen with latitude dependent parameters from high resolution radiosonde data) and delay measurement error (modelled as a Gaussian random variable with sigma 4 ps). Output statistics are based on a sample of 25. The figure of merit for a run is the median 3D rms position error, which is taken as a proxy for station position accuracy.

Three simulators have been developed, one at GSFC based on Solve (least squares), one at TU Wien based on OCCAM (Kalman filter), and one at TU Wien based on precise point positioning (PPP) (Kalman filter). Although the last is not entirely realistic for VLBI, it is useful for assessing new analysis strategies.

2.3. Slew Parameters

A second simulator was developed to relate input slew parameters to source-switching interval. In it, source-switching interval is broken down into two components, on-source time and slew time.

On-source time is based on SEFD's of 2450 (assuming D = 12 m, eff = 0.5 and Tsys = 50 K), a data rate of 8 Gbps per band (assuming BW = 1 GHz, dual polarizations, and 2-bit Nyquist sampling), a correlated flux for the scheduled source based on the weaker of the S and X tabulated fluxes at 13000 Km, and

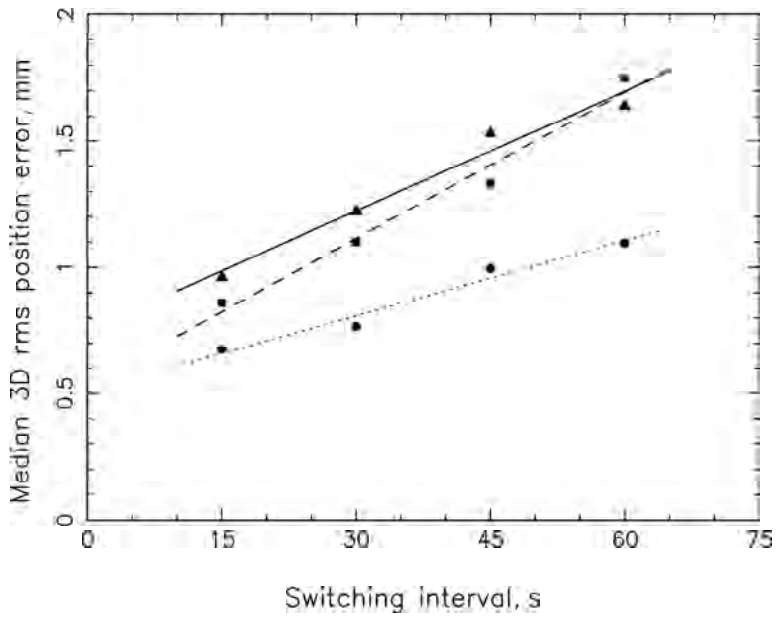

Figure 1. Median 3D rms position error vs Switching interval. The solid line and triangles are for the Solve Monte Carlo simulation; the dashed line and squares are for the OCCAM simulation; and the dotted line and circles are for the PPP simulation

a minimum SNR of 10, which is the minimum required to ensure successful application of the broadband delay technique.

Slew time is based on antenna mount type, number of antennas at a site, and slew parameters. Two mount types were considered. Both were of the azimuth/elevation (az/el) type with azimuth range -270 to +270 degrees. The elevation range of one mount was 5 to 90 degrees. (standard) and the other was 5 to 175 degrees (over-the-top). Both the case of a single antenna at a site and a pair of antennas at a site were handled.

Using this software and input slew parameters, an average source-switching interval was calculated for a schedule and then, through trial and error, families of slew parameters were determined that achieve a specified source-switching interval (and hence a specified position accuracy).

3. Results

The Monte Carlo simulators were each run using schedules with 15, 30, 45 and 60 s source-switching interval. The results are summarized in Fig. 4. Although, as expected, the PPP solution is somewhat optimistic since it doesn't require separation of atmospheres between stations, some of its better performance is also due to the use of elevation dependent weighting and spherical

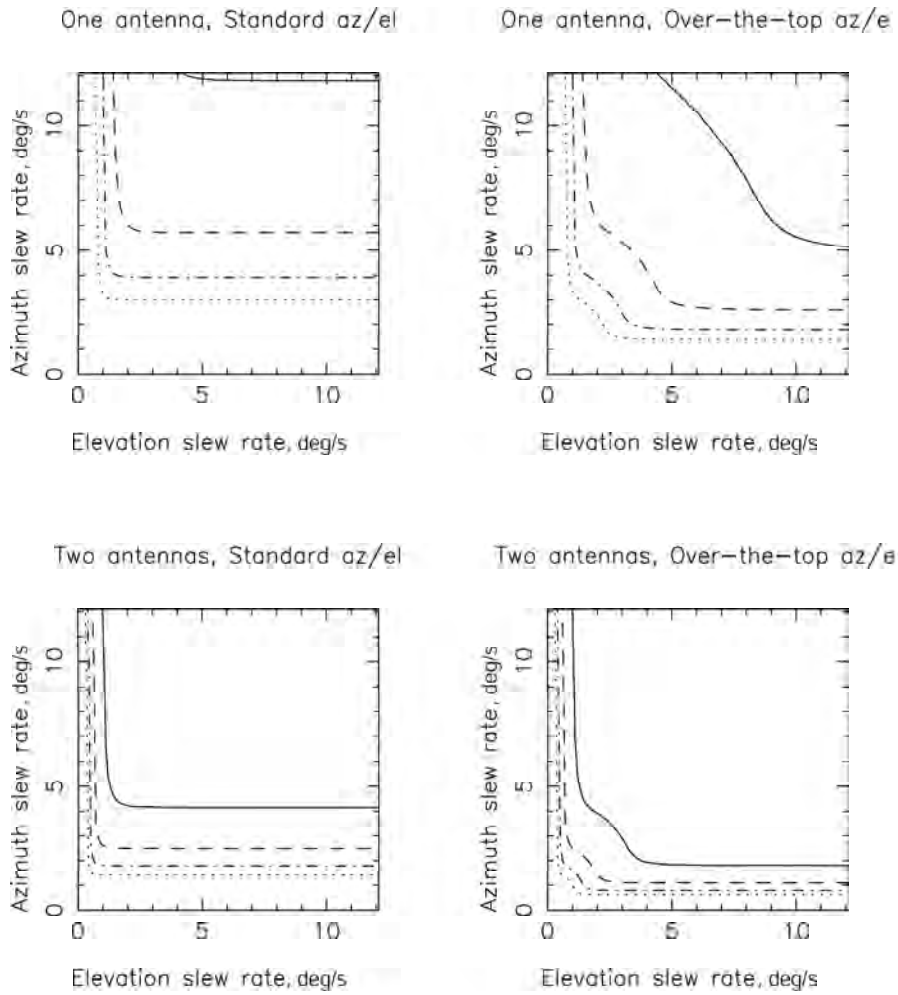

Figure 2. Azimuth vs elevation slew rate to achieve 3D rms position errors (as predicted by the OCCAM Monte Carlo simulator using an optimized uniform sky schedule). The solid line is for 1 mm position error; the dashed line 1.25 mm; the dashed-dotted line 1.50 mm; and the dotted line 1.75 mm. In all cases, 3 deg/s^2 slew acceleration is assumed for both axes. All slew rate combinations above and to the right of a line achieve the level of performance of that line

harmonics in the analysis. As expected, the Solve and OCCAM results are fairly close. Based on the OCCAM result, rms position errors of 1, 1.25, 1.5 and 1.75 mm were associated with switching intervals of 24, 37, 50 and 63 s respectively in the remainder of the study.

Using the OCCAM switching results, the slew parameter simulator, and a

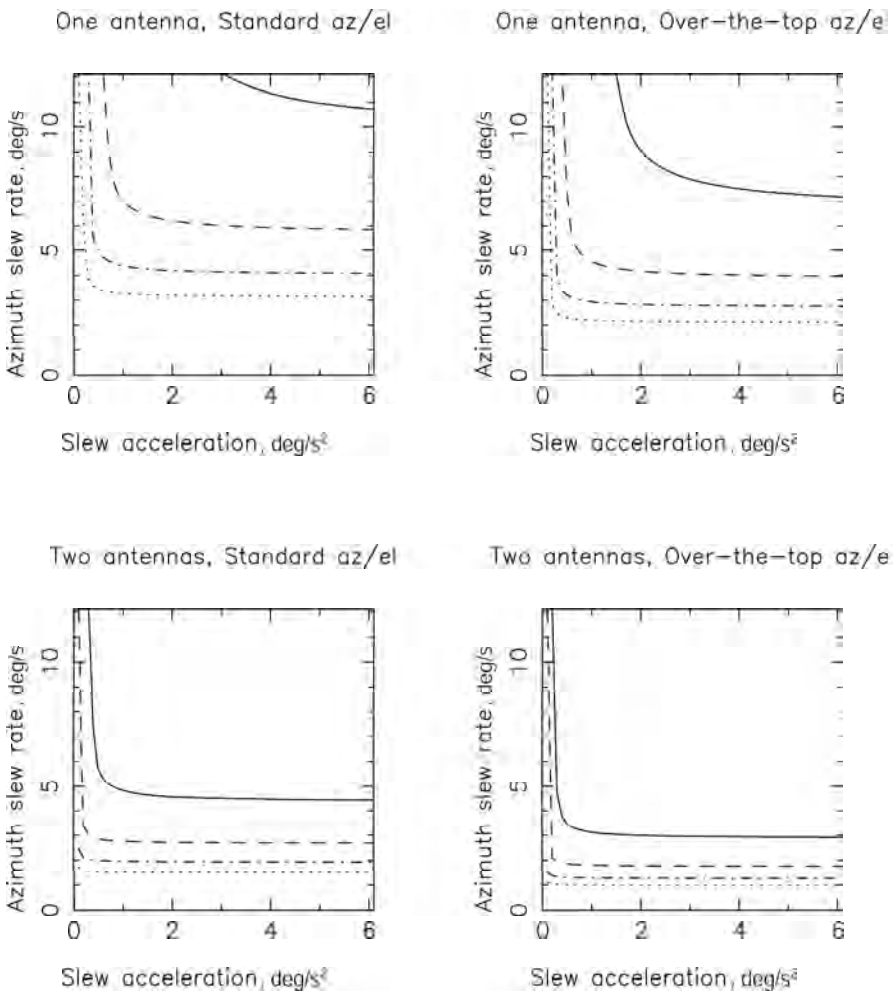

Figure 3. Azimuth slew rate vs acceleration to achieve 3D rms position errors (as predicted by the OCCAM Monte Carlo simulator using an optimized uniform sky schedule). The solid line is for 1 mm position error; the dashed line 1.25 mm; the dashed-dotted line 1.50 mm; and the dotted line 1.75 mm. Elevation slew rates are set to 0.33 of the azimuth slew rate for the standard mount and equal to the azimuth slew rate for the over-the-top mount. All azimuth slew rate and acceleration combinations above and to the right of a line achieve the level of performance of the line

fixed slew acceleration in both axes of 3 deg/s^2, it was possible to find families of azimuth and elevation slew rates that achieve the switching rates of 24, 37, 50 and 63 s corresponding to position errors of 1.00, 1.25, 1.50 and 1.75 mm respectively (Fig. 2).

In a similar way, families of azimuth slew rate and acceleration were developed corresponding to the position errors of 1.00, 1.25, 1.50 and 1.75 mm repectively. Acceleration was assumed to be the same in both axes (Fig. 3).

4. Conclusions

Within the limitations of the Monte Carlo simulators, the following antenna configurations and slew parameters (e.g. azimuth slew rate (deg/s), elevation slew rate (deg/s), and acceleration for both axes (deg/s^2)) can be expected to achieve the VLBI2010 station position accuracy goal of 1 mm:

- a single antenna with standard mount and slew parameters of 12, 4, and 3 (or for 1.25 mm accuracy, slew parameters of 6, 2, and 2);
- a single antenna with over-the-top mount and slew parameters of 9, 9, and 2 (or for 1.25 mm accuracy, slew parameters of 4.5, 4.5, and 1);
- a pair of antennas with standard mounts and slew parameters of 5, 1.7, and 1;
- a pair of antennas with over-the-top mounts and slew parameters of 3.5, 3.5 and 0.4.

5. Acknowledgements

Andrea Pany is a recipient of a DOC-fFORTE fellowship of the Austrian Academy of Sciences.

References

[1] Behrend, D., et al. Recent Progress in the VLBI2010 Development. Accepted for publication in Proceedings of the XXIV IUGG General Assembly, 2007.

The 5th IVS General Meeting Proceedings, 2008, p. 416–420

Simulation Analysis of the Geodetic Performance of Networks of VLBI2010 Stations

Daniel MacMillan

NVI, Inc./NASA Goddard Space Flight Center, USA

Abstract. The IVS is performing simulations of networks of new-generation VLBI2010 stations to find optimal antenna specifications and network site locations for the VLBI2010 observing system. To determine the precision (repeatability) of estimated geodetic parameters, I performed Monte Carlo simulations with input simulated tropospheric, clock, and observation noise, where the troposphere noise is based on a realistic model of atmospheric turbulence. I investigated the dependence of station position precision on antenna slew rate. I determined the improvement in reference frame scale and EOP precision resulting from an increase in the number of network sites.

1. Introduction

The IVS (International VLBI Service for Geodesy and Astrometry) is designing a new observing system called VLBI2010 [1], which will consist of a global network of small (at least 12-m diameter) fast-slewing antennas. One of the VLBI2010 goals is to choose antennas that are both mechanically reliable and cost effective enough to be reproduced economically so that more international groups can afford to install antennas. The global network of new VLBI stations will provide much better global coverage compared to the current network of antennas that is dominated by Northern Hemisphere sites. A critical specification for VLBI2010 is the antenna slew rate which will determine the observation rate at each station. I used a Monte Carlo procedure for simulating the performance of antennas with different slew rates and global observing networks of increasing size. The results of the simulations are estimates of the geodetic precision of the system.

2. Models and Simulation Procedure

To determine the WRMS precision (repeatability) of estimated geodetic parameters for a given scenario, I performed a Monte Carlo simulation by

making repeated (typically 25 times) VLBI analysis solutions with the same 24-hour observation file but with different input simulated noise. The simulated noise consists of tropospheric, clock, and observation noise delay contributions. The current model used for the input simulated noise of an observation on the baseline between station 1 and station 2 is

$$O - C = [m_w(elev_2)\tau_{wz2} + clk_2] - [m_w(elev_1)\tau_{wz1} + clk_1] + \sigma_{obs} \qquad (1)$$

Here, m_w is the wet troposphere mapping function and $elev_1$ and $elev_2$ are the observation elevation angles at station 1 and 2. The τ_{wz} and clk terms are the wet zenith and clock delays at the two sites. The observation uncertainty is given by the white noise contribution σ_{obs}. The wet zenith delays are either a random walk series or the equivalent zenith delays derived from a turbulent troposphere model. Clock delays are the sum of a random walk and an integrated random walk to match the performance level (Allan Standard Deviation) of the maser that is modeled. The turbulence model is based on the analysis of Treuhaft and Lanyi [3], which assumes that the refractivity of wet tropospheric refractivity spatial fluctuations is described by Kolmogorov turbulence theory. It is assumed that temporal fluctuations are caused by the "frozen flow" of spatial fluctuations that are carried horizontally past a site by the wind. Nilsson [2] describes the procedure used here for generating turbulent delays for a 24-hour schedule that are correlated according to Kolmogorov turbulence. The parameters of the turbulence model are the strength C (refractive index structure constant), the wind velocity, and the effective troposphere height.

3. Comparisons Between Simulation and Observed Scatter

To see how simulations compare with observed results, I performed tests by running simulated noise through observing schedules that were used for actual VLBI experiments. The first comparison is for the CONT05 series of 15 continuous days of VLBI observing. These R&D experiments represent the best level of VLBI precision. Clocks were modeled as a random walk plus integrated random walk corresponding to an Allan standard derivation of $2{\cdot}10^{-14}$ at 50 minutes. I used turbulent delays derived using a latitude-dependent structure constant model and wind velocities and effective atmosphere height derived from ECMWF data for the CONT05 period [2]. On average, the simulated CONT05 Weighted Root Mean Square (WRMS) baseline length repeatabilities in Fig. 1 are 72% of the observed repeatabilities.

In a second comparison, I looked at the RDV (Research and Development VLBA) network experiments. These are run approximately every two months with an 18-20 site network consisting of the 10 VLBA (Very Long Baseline Array) antennas (operated by the National Radio Astronomy Observatory) plus 8 to 10 of the IVS geodetic antennas. Fig. 2 shows the observed length WRMS from a several year series of RDV experiments compared with a simulation (25 repetitions) for a recent RDV experiment (January 2007) using turbulent delays generated with the parameters given in [3].

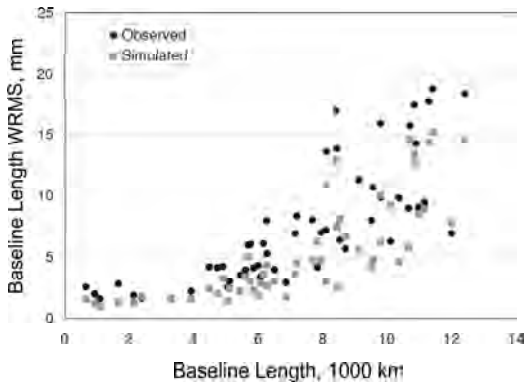

Figure 1. Comparison of observed (solid circles) and simulated (gray squares) WRMS length repeatabilities from the CONT05 series

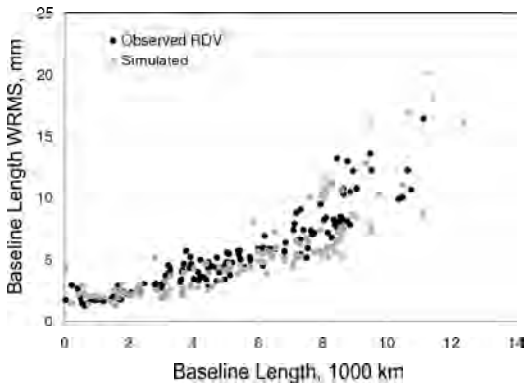

Figure 2. Comparison of observed RDV length repeatabilities over several years (solid circles) with a single RDV session (January 2007) simulation (gray squares)

4. VLBI2020 Antenna Slew Rate Specification

A critical antenna design choice for the VLBI2010 antennas is the antenna slew rate. Higher slew rates allow an antenna to move across the sky faster and make more observations. As part of the work of the IVS VLBI2010 committee, I investigated the effect of antenna slew rate on geodetic precision using observing schedules for a 16-site globally-distributed subset of the network shown in Fig. 3. Turbulent delays were generated with a site-dependent turbulence model where the C_n were based on a latitude-dependent model derived from high-resolution radiosonde data [2] and winds and troposphere heights were from ECMWF data. Two types of schedules were analyzed: 1) schedules made with the operational VLBI scheduling program SKED and 2) uniform

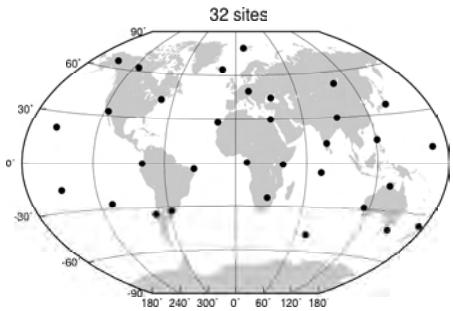

Figure 3. Global 32-site simulation network

sky schedules designed by B. Petrachenko [4] to have uniform site sky coverage every consecutive 12 observations. Fig. 4 for the uniform sky schedules shows that the 3D position WRMS repeatability improves significantly when the azimuth slew rate for an azimuth/elevation antenna is increased from 2 deg/s to 5 deg/s, but not signficantly for larger rates. Analysis using the observing schedules generated with SKED yielded a similar conclusion.

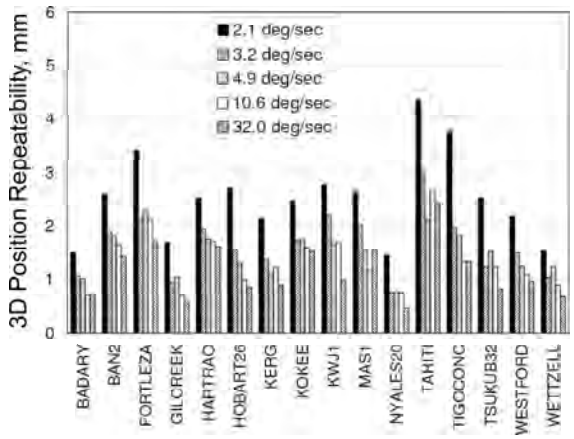

Figure 4. Improvement of 3D position repeatability versus antenna azimuth slew rate for uniform sky schedules. The median 3D repeatabilities were: 2.53 mm (2.1 deg/s), 1.64 mm (3.2 deg/s), 1.53 mm (4.9 deg/s), 1.21 mm (10.6 deg/s), 0.96 mm (32 deg/s)

5. Network Simulations

I investigated the dependence of scale and Earth Orientation Parameters (EOP) precision (repeatability) for the network in Fig. 3 and for subset networks of 24, 16, and 8 sites. Troposphere delay contributions were generated

from a turbulence model with Treuhaft-Lanyi parameters [3]. Fig. 5, 6 show the improvement in precision (repeatability) of the reference frame scale and EOP estimates as network size increases. The observing schedules were uniform sky schedules [4]. Stations observed about 70 scans/hour compared to current operational schedules, where stations typically observe 10 scans/hour.

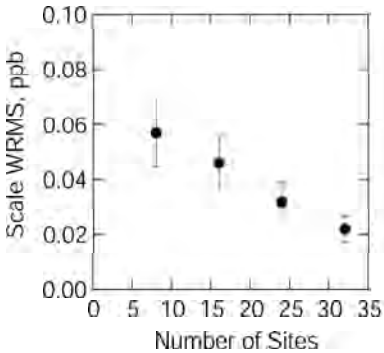

Figure 5. Scale precision

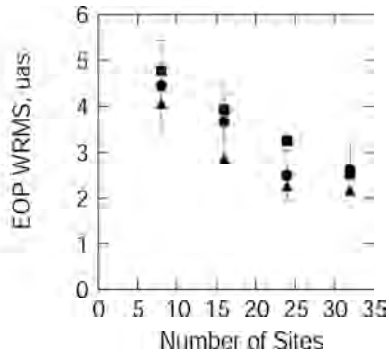

Figure 6. EOP precision: x-pole (circle), y-pole (square), UT1 (triangle)

6. Conclusions

Monte Carlo simulations show that increasing the antenna azimuth slew rate beyond 5-6 deg/s does not significantly improve site position 3D precision. Reference frame scale and EOP precision (repeatability) are improved by about a factor of 2 as VLBI2010 network size increases from 8 to 32 sites.

References

[1] Niell, A.E., A. Whitney, B. Petrachenko, et al. VLBI2010: Current and Future Requirements for Geodetic VLBI Systems. Report of IVS Working Group 3, 2005.

[2] Nilsson, T., R. Haas, G. Elgered. Simulations of Atmospheric Path Delays Using Turbulence Models. Proc. 18th European VLBI for Geodesy and Astrometry Working Meeting. J. Boehm, A. Pany, H. Schuh (eds.), 2007, 175–180.

[3] Treuhaft, R.E., G.E. Lanyi. The Effect of the Dynamic Wet Troposphere on Radio Interferometric Measurements. Radio Science, v. 22, 251–265, 1987.

[4] Petrachenko, B., J. Boehm, D. MacMillan, et al. VLBI2010 Antenna Slew Rate Study. This volume.

The 5th IVS General Meeting Proceedings, 2008, p. 421–426

VLBI2010 Simulations at IGG Vienna

Joerg Wresnik, Johannes Boehm, Andrea Pany, Harald Schuh

Institute of Geodesy and Geophysics, Vienna University of Technology, Austria

Abstract. VLBI2010, simulations are carried out at the Institute of Geodesy and Geophysics (IGG), Vienna to support the design of a new geodetic VLBI system. The main part of these simulations is a Monte Carlo simulator which produces artificial group delays by modeling the stochastic processes caused by the station clocks, the wet zenith delays, and additional system errors. The clocks are simulated with a random walk plus integrated random walk, the wet zenith delays are derived from a turbulence model, and the system errors are represented by white noise. For the analysis of the simulated data, the Monte Carlo simulator is implemented in a modified version of the software package OCCAM. Because of limitations due to the huge number of observations in the OCCAM Gauss-Markov algorithm, the Kalman Filter approach of OCCAM was applied. Different variance rates for the stochastic parameters in the Kalman Filter solutions are tested and the best values are used for antenna slew speed tests. Various schedules with antennas of different slew speeds (from 1.5°/s to 12°/s in azimuth and 0.7°/s to 3.1°/s in elevation) are compared w.r.t. baseline length repeatabilities and rms values of station position residuals. The investigation shows that there is hardly any improvement with antennas faster than 6°/s in azimuth and 2.1°/s in elevation. Alternative scheduling strategies, such as achieving uniform sky coverage, are also tested.

1. Introduction

At the Institute of Geodesy and Geophysics (IGG), Vienna University of Technology, different simulations are performed to evaluate new observing strategies and schedules, to improve the modeling of troposphere refraction and clocks, to find the best antenna design and to optimize the network geometry. A sequence of software programs is used for the simulations. After scheduling the observations with SKED [4], they are transformed to NGS format and then used as input to the VLBI analysis software package OCCAM [3], which was adapted for our simulations. The main part of the simulation studies is a so-called Monte Carlo simulator which creates the artificial observations based on realistic properties of the wet zenith delays and clocks. The observed group

delay minus computed group delay $o - c$ can be described as follows:

$$o - c = (wzd_2 \cdot mfw_2(e_2) + cl_2) - (wzd_1 \cdot mfw_1(e_1) + cl_1) + wn_{bsl}\,. \quad (1)$$

In (1), $wzd_{1,2}$ are simulated wet zenith delays based on the turbulence model [2], $cl_{1,2}$ are simulated clock values modeled as a random walk plus integrated random walk [1] at station 1 and 2, and $mfw_{1,2}(e_{1,2})$ are the wet mapping functions for the elevation angle $e_{1,2}$ which are assumed to be error-free in our studies. For each baseline observation an additional white noise wn_{bsl} is added to model the instrumental errors of station 1 and 2. The Monte Carlo simulator, implemented in OCCAM, imports wet zenith delay values from the turbulence model, creates clock values for each station and epoch, and adds white noise for each observation. Performance and evaluation of the Monte Carlo simulator are presented by Wresnik et al. [5]. The following criteria can be used to evaluate the potential of the VLBI system: baseline length repeatabilities, the root mean square (rms) of the 3D station position residuals, formal errors and standard deviations of the EOP, and the standard deviation between the simulated stochastic processes (troposphere delays, clocks) and their estimates. In this paper, we are focusing on the baseline length repeatabilities and the rms of the 3D station positions to evaluate and compare different observing strategies and scenarios.

2. Slew Speed Tests

One of the main goals of the simulations is to obtain information about antenna specifications for the new VLBI2010 system by testing different slew speeds. The test values used here range from 1.5°/s to 12°/s in azimuth and from 0.7°/s to 3.1°/s in elevation. The schedules for the analysis were produced by J. Gipson (NASA/GSFC, Greenbelt, USA). To get a sufficiently dense schedule, about 100 of 230 radio sources were taken from a recently compiled list of geodetic sources, and the on-source time was reduced to a maximum of 5 to 10 s. Statistics for the schedules are summarized in Tabl. 1. As can be seen, the schedule performance improves steadily from the 1.5/0.7°/s to the 6.0/2.1°/s case, but improvement is rather small from the 6.0/2.1°/s to the 12.0/3.5°/s case. This is because on-source time and accelerate/decelerate phases begin to dominate over the maximum slew speed phase of the observing cycle. More investigations on optimizing scheduling strategies have to be carried out.

For the Monte Carlo simulations, the wet zenith delays are simulated using the turbulence model, the clocks are simulated with an Allan Standard Deviation (ASD) of $2{\cdot}10^{-15}$ at 15 min, and the white measurement noise is simulated using a 4 ps 1-sigma Gaussian random variable. The very small white noise corresponds to that one predicted for the new VLBI2010 antenna systems. Regarding the baseline length repeatabilities (Fig. 1) a very clear improvement from slow antennas to antennas with a slew speed of 4.5°/s in azimuth and 2.1°/s in elevation can be seen.

Table 1. Number of observations/hour/station (obs/h/st) and number of observations in total for different antenna slew speeds in azimuth and elevation for a 16 station network. The right column shows the median values of 3D station positions for the various schedules

slew speed		avg	min	max	N obs.	median 3D
az, °/s	el, °/s	obs/h/st	obs/h/st	obs/h/st		stat. pos., mm
1.5	0.7	47	39	55	59392	2.15
3.0	0.7	61	46	76	83149	1.71
4.5	2.1	101	76	121	134134	1.14
6.0	2.1	120	89	144	159088	1.20
12.0	3.5	131	96	155	173831	1.05

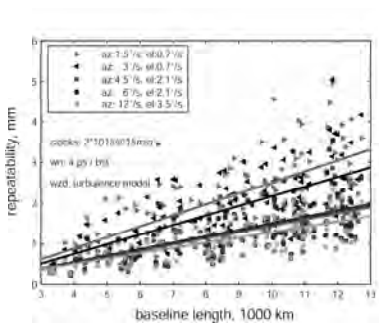

Figure 1. Baseline length repeatabilities for different slew speeds.

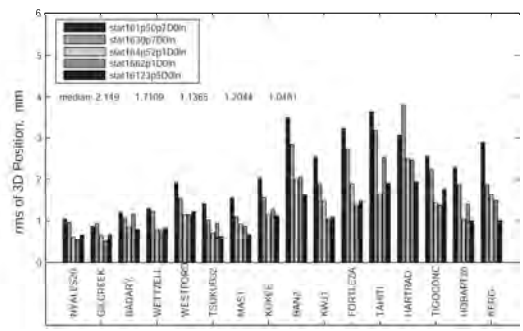

Figure 2. Simulated rms values of the 3D station positions for all 16 stations (station order: North-South)

The biggest improvement is gained when using antennas with the highest slew speed of 12°/s in azimuth and 3.5°/s in elevation, but the enhancement compared to slower antennas with a slew speed of 4.5°/s or 6°/s in azimuth and 2.1°/s in elevation is relatively small. Fig. 2 shows the simulated rms values of the 3D station positions. The median values for the different slew speeds are summarized in Tabl. 1.

3. Uniform Sky

Another scheduling strategy is to achieve uniform sky coverage at each station, which is essential to de-correlate wet zenith delays, clock parameters, and station heights. This was realized by a source-based scheduling, which means that the scheduler selects e.g. a pair of radio sources, which are located on opposite parts of the sky, from the catalogue without regarding their direct impact

on individual stations. This strategy requires different sub-nets throughout the session in order to optimize geometry and number of observations. Thus, all possible baselines of the network are observed. In the following, the switching interval between the observed sources was set to a minimum of 15 and a maximum of 120 s and the uniform sky coverage was achieved for time intervals of 3 to 24 min. Tabl. 2 shows the settings for switching interval, time interval for uniform sky coverage, number of observations of the schedule and the slew speeds that are needed to realize the schedule. The uniform sky schedules were produced by Tony Searle (Natural Resources Canada). In Fig. 3, examples for the different sky coverages of the schedules used for the slew speed test and the uniform sky schedules can be seen clearly.

Table 2. Switching interval for the uniform sky coverage schedules. The right column shows the median values of 3D station positions for the various schedules

st.	switching interval, s	uniform coverage, min	slew speed		N obs.	median 3D stat. pos., mm
			az, °/s	el, °/s		
16	120	12	2.1	0.6	34 806	3.29
16	60	12	4.8	1.1	69 708	1.52
16	45	9	7.3	1.8	93 231	1.29
16	30	6	12	3.2	139 564	1.01
16	15	3	32	8	278 830	0.88

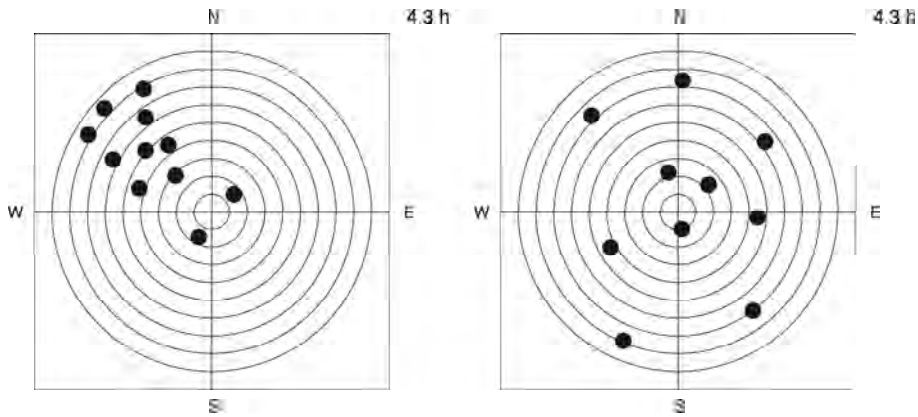

Figure 3. Sky coverage of 6 min at station FORTALEZA for different scheduling strategies. Left plot: a D0ln schedule created with the automatic scheduling software SKED, where the observation is often clustered. Right plot: a uniform sky schedule created with a source dependent scheduling strategy, where the observations are well destributed

Using the same approach for the simulations as for the slew speed tests, but a worse ASD for the clocks (10^{-14} at 50 min), the baseline length repeatabilities and the rms of the 3D station positions have been estimated. Fig. 4 shows that the schedule with the shortest switching interval and most observations yields the best results, but that there is hardly any difference between the schedules with the 15 and 30 s switching interval.

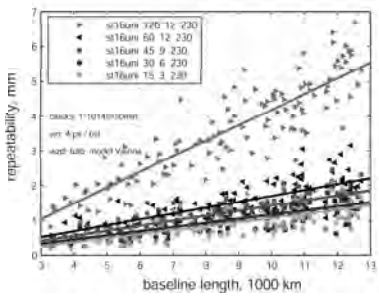

Figure 4. Baseline length repeatabilities for different uniform sky schedules with different switching times

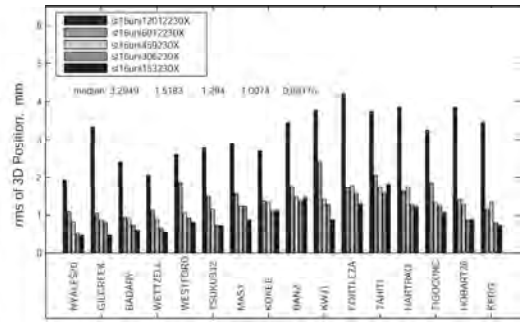

Figure 5. Simulated rms values of the 3D station positions for all 16 stations (station order: North-South)

The simulated rms of the 3D station positions can be seen in Fig. 5. It shows the improvement for the schedule with the shortest switching interval. Tabl. 2 summarizes the median values for the different schedules, e.g., the scheduling with the minimum of 15 s switching interval achieves a median value for the 3D station positions of 0.88 mm.

4. Conclusions

For the VLBI2010 Committee, simulation studies are of very high interest because decisions about the next generation VLBI system will be mainly based on these results. Therefore, the Monte Carlo simulator has to be able to reproduce real observations [5]. Since wet zenith delays have the largest influence on the simulation results, they have to be simulated as realistically as possible. Thus, applying a turbulence model, which is assumed to yield the most realistic description of the stochastic properties of troposphere up to date, is an important part of these Monte Carlo simulations. The determination of optimal slew speeds for the VLBI2010 antennas was a very critical issue for the VLBI2010 committee. The estimated baseline length repeatabilities are improved considerably for antennas with slew speeds up to 4.5°/s in azimuth and 2.1°/s in elevation, but for faster antennas the enhancement is hardly significant. To profit from very fast moving antennas, more investigations on scheduling (e.g. reducing the idle time of the antennas) have to be carried out.

The baseline length repeatabilities of the schedules with uniform sky coverage yield a significant improvement for the schedules with 15 s and 30 s switching intervals and 3 and 6 min intervals of uniform sky coverage. The median value of the rms of 3D station position for these schedules is at the 1 mm level, which is the defined goal of the VLBI2010 Committee. Considerable improvements can be expected with the use of twin telescopes, i.e. two identical antennas at each site. Tests for the use of twin antennas will be carried out with the Monte Carlo simulator in the near future.

Acknowledgements

The authors would like to thank the Austrian Science Fund (FWF) for supporting this work (P18404-N10).

References

[1] Boehm, J., J. Wresnik, A. Pany. Simulation of wet zenith delays and clocks. IVS Memorandum 2006-013v03, 2007; http://ivscc.gsfc.nasa.gov/publications/memos/index.html.

[2] Nilsson, T., R. Haas, G. Elgered. Simulations of atmospheric path delays using turbulence models. Proceedings of the 18th European VLBI for Geodesy and Astrometry Working Meeting. Boehm, J., A. Pany, H. Schuh (eds.), 2007, 175.

[3] Titov, O., V. Tesmer, J. Boehm. OCCAM v. 6.0 software for VLBI data analysis. Proceedings of the third IVS General Meeting. Vandenberg, N.R., Baver K.D. (eds.), 2004, 267.

[4] Vandenberg, N. Interactive/Automatic Scheduling Program, Program Reference Manual. NASA/Goddard Space Flight Center, NVI, Inc., 1999.

[5] Wresnik, J., J. Boehm, A. Pany, et al. Towards a new VLBI system for geodesy and astrometry. Adv. Geosci., AOGS 2007, 2008 (accepted by the editor).

The 5th IVS General Meeting Proceedings, 2008, p. 427–432

Vienna VLBI2010 PPP Simulations

Andrea Pany [1,2], *Jörg Wresnik* [1], *Johannes Böhm* [1],
Harald Schuh [1]

[1)] *Institute of Geodesy and Geophysics, Vienna University of Technology, Austria*

[2)] *Recipient of a DOC-fFORTE fellowship of the Austrian Academy of Sciences, Austria*

Abstract. Within the frame of Vienna's contribution to VLBI2010, a precise point positioning (PPP) simulation software has been developed. Similar to the simulation studies carried out with OCCAM and Calc/Solve, an artificial group delay time series is generated, consisting of wet slant delays provided by a turbulence model, stochastic variations of station clock and thermal noise of the receiving system. In contrast to the simulations that are based on VLBI analysis software packages, the delay time series are generated for single stations. The group delays are used as observations to perform a PPP - with the classical Gauss-Markov approach as well as with Kalman filtering. Different parameterizations of zenith wet delay, i.e. gradients and spherical harmonics, are tested using different time intervals and constraints. Performing a PPP for all stations of a VLBI schedule allows comparisons to the results of OCCAM and Calc/Solve simulations in order to validate how close the results of PPP are to what can be expected from real VLBI data.

1. Introduction

With the establishment of the Global Geodetic Observation System (GGOS) in 2006, it has become clear that VLBI, being the only space geodetic technique that is linking terrestrial and celestial reference frame, should be able to provide sub mm accuracy on global baselines in near future. Based on the recommendations and suggestions of Working Group 3 (WG3) [5], which was entrusted with the development of strategies to reach this high level of accuracy, Monte Carlo simulations are carried out within the IVS. Main goal of these simulation studies is to investigate different scheduling strategies, antenna slew speeds and the impact of network size, as well as to improve analysis strategies. Currently, the results of three Monte Carlo simulators are contributing to VLBI2010. In addition to Monte Carlo simulators based on the VLBI analysis software packages Calc/Solve and OCCAM [8], a VLBI2010 Precise Point Positioning (PPP) Simulator has been developed. Heart of the Monte Carlo PPP Simulator is a

fake delay generator that produces artificial group delay observables

$$delay_{group} = mf_w(el) \cdot zwd + clk + wn. \quad (1)$$

In (1), zwd denotes tropospheric zenith wet delay, mf_w wet mapping function, el elevation, clk clock, and wn white noise. The elevation angles are taken from artificial VLBI2010 schedules which were generated either by John Gipson (NVI/Inc., NASA GSFC, USA) or by Anthony Searle (Natural Research Council, NRC, Canada). The generation of artificial zenith wet delays is based on turbulence theory [7], following the approach proposed by Nilsson et al. [6]. The parameters driving the turbulence, i.e. wind velocity and wind direction, the refractive index structure constant C_n, and the effective height H of wet troposphere, are derived from numerical weather models or from empirical fits to radiosonde data, respectively, and are provided by Tobias Nilsson from Onsala Space Observatory, Sweden. Variations of station clock are simulated as sum of random walk and integrated random walk stochastic processes [8], typically with power spectral densities corresponding to Allan standard deviations (ASD) of 10^{-14} at 50 min, 10^{-14} at 15 min, or $2 \cdot 10^{-15}$ at 15 min. The white noise accounts for the thermal noise of the receiving system. For the PPP simulations, a white noise of $4/\sqrt{2}$ ps per station is added. The artificial group delay observables are used as observations to perform a PPP, either with the classical Gauss-Markov approach or a Kalman filter. The parameters to be estimated are troposphere parameters, clock parameters and station coordinate residuals. Goal of the PPP simulations is to re-gain the single contributions of troposphere and clock to the cumulative group delay. Troposphere, clock and the vertical component of station position are highly correlated. The separation of these parameters is possible because of their distinct dependencies on elevation angle or zenith distance, respectively. The whole procedure (simulation of group delay observables, estimation of parameters) is repeated 25 times to obtain a sample of output parameters that can be analyzed statistically.

2. The PPP Simulator

2.1. PPP with Kalman Filtering

The PPP Simulator is based on a covariance propagating Kalman filter, as described thoroughly by e.g. Gelb [2]. Tropospheric wet delays are modeled as zenith wet delay (mapped with a mapping function) with superimposed gradients, all of which are treated as random walk stochastic processes, using variance rates of 0.7 ps^2/s for zenith wet delays and 0.5 ps^2/s for gradients. This corresponds to the parametrization that is used in the OCCAM Kalman Filter for VLBI2010 simulation studies [8]. Clocks are modeled with a rate (deterministic parameter), and a random walk offset (variance rate 1 ps^2/s). Station coordinates are estimated as deterministic parameters.

When using a Kalman filter, only those observations between the first time epoch and a specific time epoch t_k are included in the filter estimate at t_k.

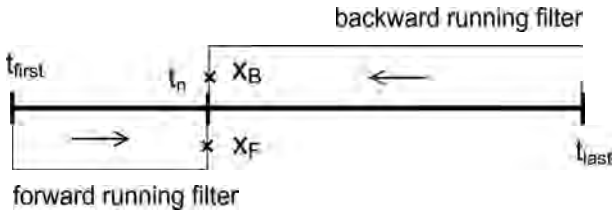

Figure 1. Principle of smoothing [2]

For the estimation of stochastic parameters, all available information should be included. Herring et al. [3] thus proposed to use a smoothing algorithm. A smoother is a combination of two Kalman filters that run in opposite direction (Fig. 1). The forward running filter (FRF) starts at the first time epoch, the backward running filter (BRF) at the last time epoch. At time epoch t_k, both filters together include all available observations. The smoothed estimate x_S is computed as weighted average of the FRF and BRF estimates (x_F and x_B) at each time epoch:

$$x_S = x_F + P_F(P_F + P_B)^{-1}(x_B - x_F)^{-1}, \tag{2}$$

where P_F and P_B are the covariance estimates of FRF and BRF, respectively. The final solution for deterministic parameters, i.e. clock rate and station position, is taken from the final FRF estimate, whereas stochastic parameters, i.e. zenith wet delays, gradients, and clock offset are taken from the smoothed solution.

2.2. PPP with the Classical Gauss-Markov Model

The stochastic model of the classical Gauss-Markov method is widely known and shall not be discussed in detail here. As for the Kalman filter solution, tropospheric wet delays are modeled as zenith wet delay (mapped with a mapping function) with superimposed gradients, which are all parameterized as piecewise linear functions with rather short estimation intervals (e.g. 6 min). The rates of the piecewise linear functions are constrained to zero by introducing pseudo-observations with standard deviations of 15 mm/h for zenith wet delays and 48 mm/h for gradients. Clocks are modeled as quadratic polynomial, estimated once per 24 hours, with superimposed piecewise linear functions (1 hour intervals, constrained with 54 mm/h). Station coordinates are estimated once per 24 hour session.

2.3. Validation of the PPP Simulator

For validation, a comparison to OCCAM Kalman Filter results was carried out. Since OCCAM is evaluating baselines, it has not only to separate the contributions of troposphere and clock, but also the contributions of the two stations forming the baseline. The PPP results might thus be too optimistic.

Another difference is that the stochastic model of the OCCAM Kalman Filter is more sophisticated than the stochastic model of the PPP Simulator. E.g., the OCCAM Kalman Filter performs a reweighting of observations when the difference between prediction and observation is too large. This is not the case for the PPP software, since it is only used for simulation studies, where no outliers will occur unless simulated. In order to carry out a valid comparison, the simulations of group delay observables were performed with the same turbulent zenith wet delay and clock time series. For each 24 hour session and station, the 3D position error was computed. The rms of 3D position errors over 25 sessions were computed for each station and are plotted in Fig. 2, which shows OCCAM results in black and PPP results in grey. As expected, the PPP solution is a little too optimistic, but, regardless of that, the same conclusions can be drawn from the results.

3. Investigations and Results

The PPP is, in case of VLBI, a purely theoretical approach. Nevertheless, due to the simplicity and compactness of the simulator, it is a very powerful tool that helps understanding the highly correlated main stochastic error sources — troposphere and clock. Since the input to the PPP is exactly known, a direct comparison of input and output is possible as well as investigations on how errors in troposphere and clock parameter estimation impact on the determination of geodetic parameters such as station position. The PPP Simulator was used to carry out studies on the length of estimation intervals for the piecewise linear functions, constraints and variance rates, different troposphere models (i.e. gradients and spherical harmonics), the impact of different clocks and white noises, elevation dependent downweighting and the influence of the parameters driving the turbulence on position repeatabilities. As an example, the investigation on modeling tropospheric wet delay with spherical harmonics will be discussed in more detail below.

The functional form used for modeling tropospheric wet delays is based on the approach by Böhm and Schuh [1]:

$$\Delta L(el, az) = mf(el) \cdot L^z + mf(el) \cdot \mathrm{ctg}(el) \cdot SH_{nm}(zd, az). \tag{3}$$

In (3), ΔL denotes tropospheric wet delay, el elevation angle, az azimuth, mf mapping function, L^z zenith wet delay, SH_{nm} spherical harmonics of degree n and order m and zd zenith distance. The spherical harmonics are scaled with $ctg(el)$ to account for the increasing horizontal change in refractive index along the ray path when the zenith distance increases [1]. Several spherical harmonics expansions of different degrees and orders were tested on their ability to model the fast variations of turbulent zenith wet delay on short time scales. For the PPP Kalman Filter, spherical harmonics of degree and order 1 have been found to yield best results. In this case,

$$SH_{nm}(zd, az) = (-\sin(zd)) \cdot [a_{11} \cdot \cos(az) + b_{11} \cdot \sin(az)], \tag{4}$$

where a_{11} and b_{11} are the coefficients of SH_{11}. The classical gradient model as recommended by the IERS Conventions [4] is given as

$$\Delta L(el, az) = mf(el) \cdot L^z + mf(el) \cdot \mathrm{ctg}(el) \cdot [G_N \cdot \cos(az) + G_E \cdot \sin(az)], \qquad (5)$$

where G_N and G_E denote north and east gradient, respectively. The troposphere parameters to be estimated are L^z, a_{11} and b_{11} for the spherical harmonic model and L^z, G_N and G_E for the classical gradient model, the number of troposphere parameters thus being the same in both cases. Substituting (4) in (3) and comparing with (5) it can be seen that the only difference between these two approaches is their different dependence on zenith distance.

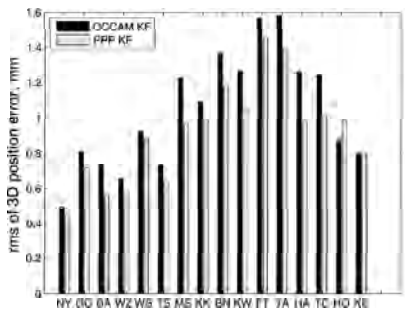

Figure 2. Comparison of rms of 3D position error of OCCAM (black) and PPP (grey) Kalman Filter for the VLBI2010 schedule st16uni_30_6_230. The clock was simulated with an ASD of 10^{-14} at 50 min. Variance rates: 0.7 ps^2/s for zenith wet delay, 0.5 ps^2/s for gradients, 1 ps^2/s for clock offset

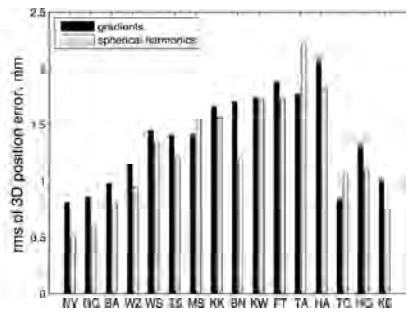

Figure 3. Comparison of rms of 3D position error for the PPP Kalman Filter for the VLBI2010 schedule st16uni_60_12_230. The clock was simulated with an ASD of 10^{-14} at 50 min. Variance rates: 0.7 ps^2/s for zenith wet delay, 0.5 ps^2/s for gradients, 0.01 ps^2/s for spherical harmonics and 1 ps^2/s for clock offset

Fig. 3 presents rms of 3D position error for a VLBI2010 16 station test schedule and shows a clear improvement for almost all stations if using spherical harmonics instead of the gradient model. The significant degradation for station Tahiti (TA) was shown to be due to the specific sequence of random noise used for the generation of the turbulent zenith wet delay time series.

4. Summary and Conclusions

Though a theoretical approach, the PPP Simulator was found to be very helpful for VLBI2010 simulation studies. Of course one has to bear in mind that results obtained with PPP might be too optimistic and have thus to be interpreted with care. Findings concerning improvement of analysis strategies

have to be confirmed with VLBI analysis software packages. Nevertheless, the PPP Simulator has numerous advantages that make it a powerful tool: Based on MATLAB script files, it is compact and clear, making it easy to implement modifications. Analyzing data for a couple of single stations instead of station networks, makes it possible to test many different strategies in very short time. Promising strategies can then be applied to the analysis of all stations in a VLBI2010 network. Furthermore, since the contributions of zenith wet delay and station clock to the artificial group delay observables are known, Monte Carlo simulations of this kind, and — due to their simplicity — especially the PPP simulations, enable a basic understanding of how troposphere and clock parameters are correlated and how errors in their determination affect the estimation of geodetic parameters.

References

[1] Böhm, J., H. Schuh. Spherical Harmonics as a Supplement to Global Tropospheric Mapping Functions and Horizontal Gradients. Proceedings of the 15-th European VLBI for Geodesy and Astrometry Working Meeting. D. Behrend and A. Rius (eds.), 2001; http://www.ieec.fcr.es/hosted/15wmevga/proceedings/boehm/boehm.html.

[2] Gelb, A. Applied Optimal Estimation. MIT Press, Cambridge Mass., 1974.

[3] Herring, T., I. Shapiro. Geodesy by Radio Interferometry: The Application of Kalman Filtering to the Analysis of Very Long Baseline Interferometry Data. J. Geophys. Res., v. 95, No B8, 12561–12581, 1990.

[4] McCarthy, D., G. Petit. IERS Conventions 2003. Verlag des Bundesamtes für Kartographie und Geodäsie, Frankfurt am Main, 2004.

[5] Niell, A., A. Whitney, B. Petrachenko, et al. VLBI2010: Current and Future Requirements for Geodetic VLBI Systems. IVS Memorandum 2006-008v01, 2004.

[6] Nilsson, T., R. Haas, G. Elgered. Simulations of atmospheric path delays using turbulence models. Proceedings of the 18-th European VLBI for Geodesy and Astrometry Working Meeting. J. Böhm, A. Pany, H. Schuh (eds.), 2007; http://mars.hg.tuwien.ac.at/evga/proceedings/S64_Nilsson.pdf.

[7] Treuhaft, R., G. Lanyi. The effect of the dynamic wet troposphere on radio interferometric measurements. Radio Science, v. 22, No 2, 251–265, 1987.

[8] Wresnik, J., J. Böhm, A. Pany, et al. Towards a new VLBI system for geodesy and astrometry. Adv. Geosci., AOGS 2007, 2007 (accepted by the editor).

The 5th IVS General Meeting Proceedings, 2008, p. 433–438

Imaging Capabilities of the Next Generation VLBI System

Arnaud Collioud, Patrick Charlot

Laboratoire d'Astrophysique de Bordeaux, Université Bordeaux 1, France

Abstract. We study the capabilities of the VLBI2010 system to produce images of reference sources, which are the basis of the International Celestial Reference Frame (ICRF). To this end, we have developed a procedure to simulate VLBI data, based on VLBI2010 technical recommendations, and to automatically image the sources from such simulated data. Our results confirm that the VLBI2010 system will be able to produce high-quality VLBI images. By comparing results of simulations, we also investigate the effect of network configuration, depending on the source declination, the impact of the number of observations and observing strategy.

1. Introduction

In Sep. 2005, the IVS Working Group 3 VLBI2010 gave recommendations for the next generation VLBI2010 system [1]. This system is based on 12m-class fast-moving antennas associated with broadband recording system, and is being designed to improve the IVS products: the Earth Orientation Parameters, the International Terrestrial Reference Frame, and the International Celestial Reference Frame (ICRF).

An important issue concerning ICRF is the correction of the effect of source structure since most of ICRF sources are not point-like on VLBI scales [2]. In practice, source structure modeling requires imaging the sources on a regular basis, which is currently conducted through dedicated bimonthly RDV (Research and Development VLBA) sessions. In the future, it is anticipated that this may be done on a daily basis with VLBI2010 system, providing a significant contribution to astrophysics, in addition to its primary geodetic and astrometric goals.

In this study, we evaluate VLBI2010 system capabilities for producing high-quality images, based on VLBI2010 technical recommendations in terms of networks and schedules. To this end, we have designed a two-step procedure presented in Sec. 2 to simulate VLBI images, considering a realistic source model. The results of the simulations are then used to explore the imaging

capabilities of 16- and 32-station VLBI2010 networks and for different types of schedules as discussed in Sec. 3.

2. Simulation of VLBI2010 Images

The procedure we have designed to produce simulated VLBI images comprises two successive steps: the simulation of VLBI2010 data using a specific pipeline, and the automatic source imaging from these simulated data.

2.1. Generating VLBI2010 Data

A dedicated pipeline was built for generating VLBI2010 data. This pipeline includes home-made Perl and python scripts, which integrate several programs from the Caltech VLBI Package (fake, merge,...)[1]. The major selection criteria for such simulations are as follows.

1. A VLBI2010 schedule. The simulations presented in this paper are based on 16- and 32-station networks [3]. Actual VLBI2010 schedules[2] depend on antenna slew rates and observing strategies. Details about these are provided in Sec. 3 together with the results of our simulations.

2. A structure model of the source. A structure model of the source is required to simulate VLBI amplitude and phase data. In our calculations, we used a simple model comprising one point-like core component plus five Gaussian components, with separations from the core up to 7 mas. Components were approximately aligned along a straight line to reproduce a typical core-jet structure as shown in Fig. 1.

3. A frequency setup. A 4-frequency setup (8406, 8476, 8791 and 8896 MHz), corresponding to the setup used at X band in the RDV sessions, was used in all simulations.

4. Realistic noise. An additive noise of 30 mJy (corresponding roughly to the first contour level in the images) along with a multiplicative noise of 5% of the expected visibility amplitudes was added to simulated amplitude data. In a similar way, a random noise of 10° was added to the phase data. Finally, random station-dependent calibration errors of up to 6% were incorporated to account for the imperfect knowledge of the gain of the antennas.

2.2. Producing Images

The simulated data generated in the previous step are stored in uvfits file. These data are then processed to image the source by using the DIFMAP soft-

[1]For help on Caltech VLBI programs, see http://www.astro.caltech.edu/~tjp/citvlb/
[2]VLBI2010 schedules are available at http://mars.hg.tuwien.ac.at/~vlbi2010/

Flux, Jy	Separation, mas	P.A., °	Major axis, mas	Axis ratio	Phase, °
3.0	0.0	-	-	-	-
3.0	3.0	135	1.0	0.5	20
2.0	4.0	135	2.0	0.5	−45
2.0	4.5	135	1.0	0.3	−45
1.0	6.0	130	1.5	0.8	110
1.0	7.0	135	1.5	0.8	110

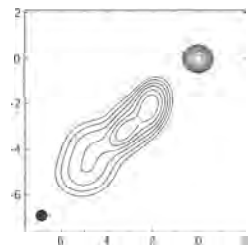

Figure 1. (Left) Components of the source structure model. (Right) Image derived by convolving the model components with a typical VLBI2010 beam (0.5×0.5 mas^2), plotted in the lower left-hand corner of the image. The first contour level is 15 mJy/beam (0.5% of the peak brightness), with successive contours increasing by a factor of two. Units: mas

ware in automatic mode [4]. The procedure is based on the hybrid-mapping technique [5] with a point-source model at start. Visibilities are self-calibrated, Fourier inverted, and CLEANed. Uniform weighting and, after several iterations, natural weighting, are successively applied to derive the final image.

3. Results of Simulations

In this section, we present the results of our simulations with emphasis on specific parameters: the network configuration (16- or 32-station network), the number of observations, and the selected observing strategy.

3.1. Effect of Network Configuration

Simulations were carried out for sources at three different declinations (−40°, 0°, +40°), based on schedules derived from 16- and 32-station networks. Such schedules were produced by maximizing the number of sources observed with slew rates of 6°/sec in azimuth and 2.1°/sec in elevation.

The resulting images (Fig. 2) indicate that the overall source structure is generally well reconstructed, down to the level of 0.5% of the peak brightness. However, it is found that the weak extended feature at 6–7 mas from the core is not correctly reconstructed with the 16-station network, especially at low declination (Fig. 2, upper panels). This is most probably due to a lack of short baselines, which is clearly visible when comparing the u-v planes for the two networks. On the other hand, the 32-station network reconstructs extended structures more reliably, whatever the source declination (Fig. 2, lower panels).

3.2. Impact of the Number of Observations

VLBI2010 schedules include several thousands of 5 to 22-second long scans (i.e. the number of times each source is observed) per 24 hours, observed by

at least 8 stations simultaneously. The average number of scans per source is typically 60 for a 16-station network and 50 for a 32-station network, with 90% of the sources within a ±10-scan range. However, some sources happen sometimes to have a number of scans quite distinct from the average.

In order to study the impact of the number of scans on the image quality, we have compared the simulated images for two sources at similar declination (+20°) but with 22 and 66 scans, respectively. From this comparison, it is found that the extended structure of our source is reasonably well reconstructed when the source is observed 66 times, whereas that is not the case when it is observed only 22 times. This means that the number of scans is a major parameter on image quality. Based on our tests, we suggest a minimum of 40–50 scans per day on each source with a uniform number of scans on every source for a proper image reconstruction.

3.3. Influence of Observing Strategies

In the framework of VLBI2010 project, two main observing strategies are being studied:

• *Observing as many sources as possible per day*, to maximize the number of observations. In this case, the number of scans per day is roughly 6000 for a 16-station schedule and 5000 for a 32-station schedule. Schedules previously used in Sec. 3.1 and 3.2 above were obtained with this strategy.

• *Observing sources distributed all over the sky (uniform sky schedule)*, with the goal of accurately estimating the troposphere above the VLBI stations on short times scales. Such schedules require more slewing time, which implies less observing time spent on the sources. Consequently, the number of scans per day drops by 20–30% to about 4000. As the number of sources observed is still the same (about 100 sources), there are less scans scheduled on each of them compared to the previous strategy.

In order to compare the two strategies, we repeated the 16-station analysis described in Sec. 3.1 with a uniform sky schedule; in this strategy, the sky is covered in 9 minutes with 45-second switching time between sources. As previously, we faced the same problem in reconstructing extended structures for low-declination sources, while replacing the 16-station network with a 32-station network, considering a schedule with similar characteristics, does improve significantly the recovery of extended structures. From this test and other additional ones, we conclude that the selected observing strategy (obtaining a uniform sky coverage or maximizing the number of observations) appears to have no significant impact on the image quality.

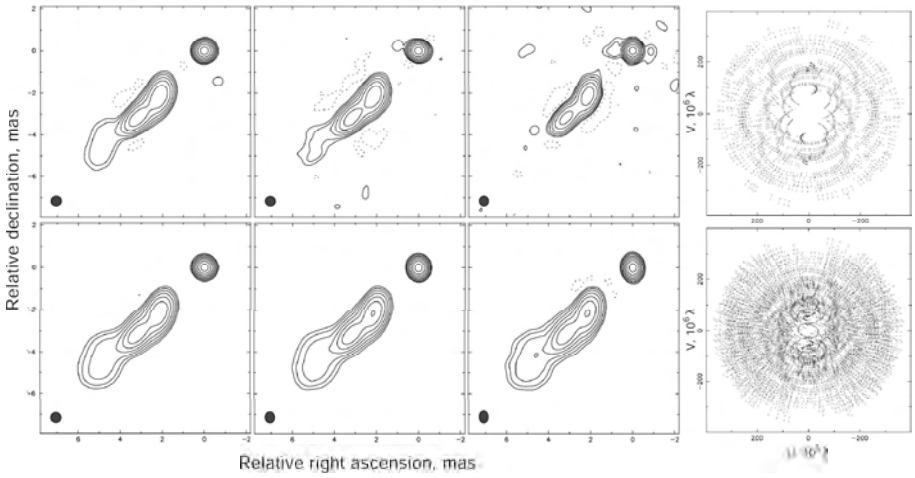

Figure 2. Reconstructed VLBI images at three declinations ($-40°$, $0°$, $40°$) and u-v coverage (decl. $-40°$) for typical VLBI2010 schedules with 16 stations (upper panels) and 32 stations (lower panels). Contour levels are the same as in Fig. 1.

4. Conclusion

In this study, we evaluated VLBI2010 system capabilities for producing high-quality images, based on VLBI2010 technical recommendations in terms of networks and schedules. To this end, we developed a two-step procedure to simulate VLBI2010 data and automatically image the sources.

Overall, the results of our simulations showed that VLBI2010 system is well adapted to produce high-quality images, with roughly the same dynamic range as that currently obtained from RDV sessions. In addition, they highlight that 32-station networks should be preferred over 16-station networks since the latter fails to reconstruct extended structures for sources at low declination. We also found that the number of observations scheduled on each source has a significantly impact on the image quality; based on our tests, we suggest a minimum of 40–50 scans per day on every source to properly reconstruct images. On the other hand, the choice of the observing strategy (optimizing the sky coverage or maximizing the number of sources observed) appears to have no significant impact on the reconstructed images.

In the future, further simulations will be targeted to study the impact of the noise added to the data, and to repeat the analysis presented here for weaker sources.

References

[1] IVS Working Group 3 'VLBI2010', Final Report, 2005.

[2] Fey, A., P. Charlot. Astophys. J. Suppl. Series, 128, 17, 2000.

[3] Niell, A. IVS Memorandum, 'Simulation Networks-1', 2007-001v01, 2007.

[4] Shepherd, M.C., T.J. Pearson, G.B. Taylor. Bulletin Amer. Astron. Society, v. 27, No 2, 903, 1995.

[5] Readhead, A.C.S., P.N. Wilkinson. Astophys. J., 223, 25, 1978.

The 5th IVS General Meeting Proceedings, 2008, p. 439–444

First Considerations on the Feasibility of GNSS Observations by the VLBI Technique

Vincenza Tornatore [1], *Gino Tuccari* [2], *Erhu Wei* [3]

[1] *DIIAR Politecnico di Milano, Italy*

[2] *INAF-IRA, National Astrophysical Institute — Radio Astronomy Institute, Italy*

[3] *School of Geodesy and Geomatics, The Key Laboratory of Geospace Environment and Geodesy , Ministry of Education, Wuhan University, China*

Abstract. GNSS (Global Navigation Satellite System) is a global navigation satellite system consisting of different satellite constellations that transmit ranging signals used for positioning and navigation anywhere around the globe. In this work we present first investigations on the possibility to observe GNSS signals using the VLBI technique with the main goal to obtain satellite orbits by VLBI. The achievement of this goal could represent the opportunity to obtain a direct link between VLBI and the different GNSS reference systems; moreover, it could be also useful internally to the GNSS system itself to establish an external link among the different GNSS reference systems of each constellation.

The different characteristics of the GNSS system will be presented to evaluate if it is possible to observe any of these different constellations with present VLBI antennas. Then the contribute that the new VLBI2010 antennas and data acquisition system could bring to the observation of GNSS signals will also be examined.

1. Introduction

The most important and complicated mission of modern geodesy and geodynamics is the definition, realization and interconnection of different reference systems, which include the Conventional Inertial System (CIS) fixed in space and defined by radio sources, the Conventional Terrestrial System (CTS) fixed to the earth and defined by a series of observation stations on the ground, and the dynamic reference system defined by the movement of the satellite.

Since 2003 with the establishment of the IVS working group 3, the VLBI community is devoting several efforts to designing the next generation of geodetic VLBI system called VLBI2010 that would provide enhanced perfor-

mances. In the meantime a demand of higher positioning accuracy for the global earth parameter estimation is growing too. A combination/integration of different spatial geodetic techniques is the key to ensure the consistency and to improve the accuracy of the resulting geodetic products.

At present VLBI solutions, and solutions from other positioning techniques (such as GPS, SLR, LLR, etc.,) are jointly used for indirect interconnection between CIS and CTS [1]. The local geodetic ties between GPS and VLBI antennas play an essential role within the inter-technique combination. However several studies already revealed non-negligible discrepancies between the terrestrial measurements and the space-geodetic solutions. Causes of these inconsistencies can be different, among them local tie uncertainties that have a significant influence on estimated geodetic parameters [4]. An indipendent link (a sky link) could help to discriminate between different possible error sources. Then with the development/advent of different Navigation satellite systems, each one referred to its own reference system, it will become necessary for high level accuracy applications to know with precision the transformation from one reference system to another one.

In this work we make first steps to investigate on the possibility to determine GNSS orbits by the VLBI technique. The knowledge of GNSS orbits in the VLBI system would allow to obtain terrestrial GNSS coordinates in a unique reference system, the VLBI one, without the need of making local ties, besides this method could also be the key to link the different GNSS reference systems among them. After a short overview on GNSS characteristics, the possibility to receive the GNSS signals using the present VLBI antennas and also the future VLBI2010 antennas will be examined. In particular the signal frequencies and strength has been considered, since they will be on the wings of the filters and feed response.

2. GNSS Characteristics

GNSS has shown a rapid growth in the last few years: the U.S. Global Positioning System (GPS/Navstar GPS), and the Russian GLObal NAvigation Satellite System (GLONASS) have started an extensive modernization, moreover there are plans to develop a European GALILEO system and China is planning to have its own version called Compass. The main features of GNSS constellations are presented in Tabl. 1. IGS, the International GNSS Service, formerly the International GPS Service, is a voluntary federation of more than 200 worldwide agencies that pool resources and permanent GPS and GLONASS station data to generate precise GPS and GLONASS products. The conventional GPS data processing techniques are also being modified to incorporate the new satellite system of GNSS which poses major challenges of different satellite signals, different reference frames and different time scales to be incorporated for combined processing. In this paper we have not considered the two regional systems: the Japanese QZSS (Quasi –Zenith Satellite system) that will be used to enhance GPS in Japan and the IRNSS (Indian RadioNavigation

	GPS	GLONASS	GALILEO	COMPASS
Planned satellites Number	21+3 active spares MEO	24 MEO	27+3 non active spare MEO	30 non GEO, 5 GEO
Orbital height	20200 km	19100 km	23200 km	21500 km
Orbital planes inclination	55°	64.8°	56°	
Orbital planes	6, spaced by 60°	3, spaced by 120°	3, non uniformly spaced	
Satellites per orbital plane	6, unequally spaced	8, unequally spaced	10, unequally spaced	
Revolution period and ground track repeatability	11h 58min; every sidereal day	11h 16min; every eight sidereal day	14 h	
Reference frame	WGS84	PZ 90	GTRF	
UTC correction	UTC (USNO)	UTC(SU)	UTC(GST)	
Satellite separation technique	CDMA (Code Division Multiple Access)	FDMA (Frequency division Multiple Access)	CDMA	
Carrier Frequencies MHz	Constant L1(E1): 1575.42 L2 : 1227.60 L5 : 1176.45	Variable L1: 1602...1615.5 L2: 1246...1256.5 L3: 1201.5 for channel number 0-24	Constant L1(E1) E6 (L5) E5a E5b	Constant B1-2 B1 B3 B2
Code Number	One for service (and satellite)	One for service and frequency (band)	One for service (and satellite)	One for service (and satellite)
Commercial Services	No	No	Yes	Yes
Integrity	No (yes with GPS III)	No (Yes con GL-K)	Yes	

Figure 1. GPS, GLONASS, GALILEO, Compass Constellation Characteristics

Satellite System). IRNSS will seek to maintain compatibility with other GNSS systems of the region and to provide services for critical national application.

The panorama of existing and planned navigation systems is very wide and diversified. In the GNSS community there are efforts to harmonize all the GNSS system.

3. GNSS Signals Compatibility with Present VLBI Antennas and Data Acquisition System

Several experiments have been performed in the last years using VLBI for spacecraft tracking [5]. VLBI is the technique with highest angular resolution and e-VLBI showed rapid progress in recent years: with the improvement of these characteristics the VLBI technique can be more and more used for spacecraft tracking.

Emission from GNSS satellites are in a range between 1100 and 1600 MHz, well below the 2 GHz limit that the VLBI2010 receiver would have to cover

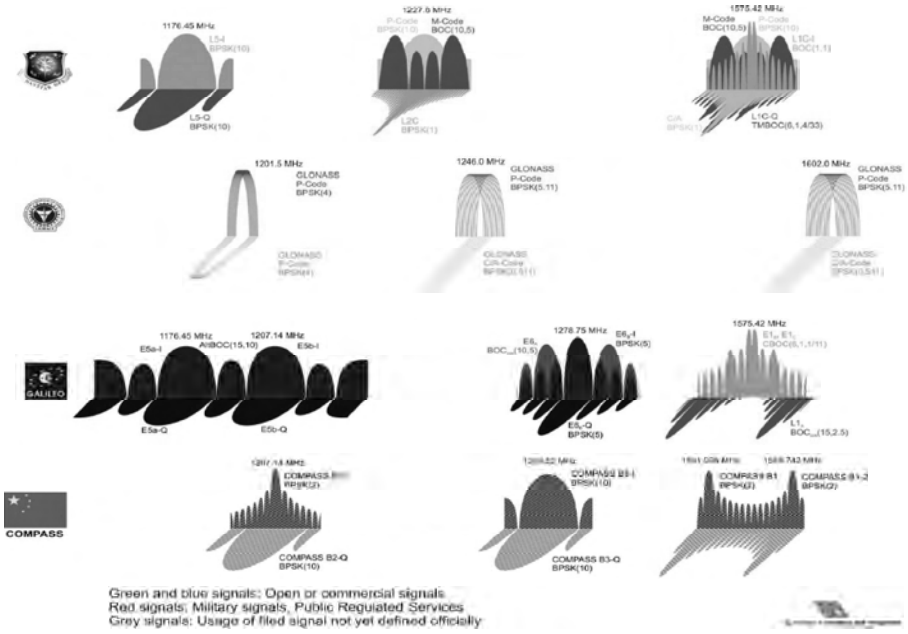

Figure 2. GPS, GLONASS, GALILEO, and Planned Compass Signals

to reduce interference contribution in the L band. On the other hand, the transmission range adopted by the GNSS is due to different reasons: 1) frequencies have to be chosen below 2 GHz, as frequencies above 2 GHz would require beam antennas for the signal reception; 2) the PRN-codes (modulation schemes) require a wide bandwidth for the code modulation on the carrier frequency; therefore it is necessary to adopt frequencies larger than 1 GHz, with the possibility that a larger bandwidth has to be chosen; 3) the chosen frequency should be in a range where the signal propagation is not too influenced by weather phenomena. GPS receivers use the L1 frequency with 1575.42 MHz (GLONASS 1602.0). L1 frequency carries the navigation data as well as the SPS code (standard positioning code). L2 frequency (1227.60 MHz) only carries the P code and is only used by receivers which are designed for PPS timing determination. The L1 component represents a possible signal source to determine accurate satellite positions provided that the overall system gain is able to detect such emission with the standard S/X receiver. The L2 detection could anyway be essential for the determination of the complete parameter set. Most of the today used S/X receivers filter the S band with a minimum usable limit placed at around 2200 MHz, so even considering the large antenna surface of a medium size IVS radio-telescope, signal components of the GNSS emission are probably under the detection threshold. Moreover very few systems having coaxial L/S/X feeds are adopted. A new approach could be considered in case

a new generation of receivers plans to adopt a lower limit closer to the L1 (or L2) signal components, even with a controlled attenuated response.

4. New Opportunities from VLBI2010 Antennas

With VLBI2010, it is expected that phase delays are used, and that delay precision for the radio sources have a target of 1 ps, although systematic effects will make this worse. On the other hand, the GPS signal could be treated quite differently since only the L-band frequency are usable. The new VLBI2010 systems will be able to receive very wide band signals with a lower limit of 2 GHz. This in principle avoids to receive GNSS L1 emission even if it could be considered how the signals will appear in the overall system response, since they will be on the wings of the filters and feed pass-band.

A generic GPS/GLONASS receiver antenna receives the signals coming from the satellites from potentially any direction, so they have a standard gain close to 4-5 dB. The new typical 12 m VLBI2010 antenna dish will have a 47 dB gain at L1 frequency, considering a 50% efficiency. So if the overall gain loss between the antenna and the first amplification stage, including feed and sky frequency filters response, will present an attenuation at 1600 MHz of about 43 dB with respect to the in-band level, the expected SNR obtained pointing on a satellite will be similar to what is achieved in a standard GPS receiver. The related slope, considering a -3 dB level at 2000 MHz would be 10 dB/100 MHz. An additional loss to be taken into account is the circular polarization adopted in the satellite transmitters that produce a further 3 dB attenuation due to the linear polarization scheme adopted in the new receiver system. A more stepped performance could affect the possibility to safely receive the emission coming from the L1 modulated carriers, while it could be required to moderate the effects due to cellular phones and related repeaters operating in the range 1800–1900 MHz.

The condition to have a system able to detect GNSS signals would then come by considering a feed frequency attenuation shape in the lower side of the band that would not exceed the described slope, and the introduction of an additional filter to be included or not in the lower side in order to get better attenuation performance in the L-band, still maintaining the possibility to have it excluded by the chain getting a quite convenient attenuation factor for the detection of the very strong signals coming from the satellite transmitter.

5. Conclusions and Future Developments

In this work we have performed preliminary investigations on the observability of GNSS signals by the VLBI technique, with the main goal to determine GNSS orbits in the same reference system of the VLBI technique. Some characteristics of the GNSS constellations and of the emitted signals have been presented with the objective to evaluate if GNSS signals are detectable by the VLBI technique. Also improvements that the next VLBI2010 antennas could

bring for the observations of the GNSS signals have been considered and it was found that to achieve a full information available a full bandpass starting from around 1.150 GHz should be considered in order to be able to detect the entire GNSS range. Such extension from 2.0 GHz is strongly affected by several potential RFI signals, due to the large number of services operating in such portion of the spectrum. Nevertheless it could be worthwhile to consider such lower range in the feed horn bandwidth and low noise amplifiers, while still keeping a choice to cut it in a further more advanced stage in the receiver. This solution could bring the opportunity to observe GNSS signals with a standard VLBI2010 terminal. Then since the final configurations of the new VLBI2010 antennas are still not established, some observation campaigns could be planned to perform some analysis to estimate different signal strengths, and to establish targets for the system design.

Further investigations are required on the processing of GNSS signal by the VLBI data acquisition system and on the data correlation. The obtainable accuracy of GNSS orbit determinations by the VLBI technique need also to be evaluated. A good accuracy in the GNSS orbit determination by VLBI is very important because the knowledge of the orbits of the different constellations in the same reference system could represent a good link among the different GNSS reference systems and also a good link between GNSS and VLBI.

Acknowledgements

We gratefully acknowledge G.W. Hein, J.A.A. Rodriguez, T. Pany, P. Hartl, authors of the paper 'Envisioning a Future GNSS System of System', Inside GNSS Jan/Feb 2007, for giving permission to publish Fig. 2 of this paper.

References

[1] Altamimi, Z., X. Collilieux, J. Legrand, et al. ITRF2005: A new release of the International Terrestrial Reference Frame based on time series of station positions and Earth Orientation Parameters. J. Geophys. Res., v. 112, B09401, DOI 10.1029/2007JB004949, 2007.

[2] Hein, G.W., J.A.A. Rodriguez, T. Pany, et al. Envisioning a Future GNSS System of System. Inside GNSS, Jan/Feb, 58–67, 2007.

[3] Mac Doran, P.F. Satellite emission interferometric earth surveying series – GPS geodetic system. Bulletin of Geodesy, 53:117–138, 1979.

[4] Thaller, D., M. Krugel, M. Rothacher, et al. Combined Earth orientation parameters based on homogeneous and continuous VLBI and GPS data. Journal of Geodesy, 81:529–541, 2007.

[5] Zhan, X., et al. Spacecraft Tracking with the Chinese VLBI Network. Proceedings of the IV IVS General Meeting 2006, 52–55.

The 5th IVS General Meeting Proceedings, 2008, p. 445–449

VLBI Observation of SELENE (KAGUYA) by VERA and an International Network

Hideo Hanada [1], *Takahiro Iwata* [2], *Nobuyuki Kawano* [1], *Noriyuki Namiki* [3], *Kazuyoshi Asari* [1], *Yoshiaki Ishihara* [1], *Toshiaki Ishikawa* [1], *Fuyuhiko Kikuchi* [1], *Qinghui Liu* [1], *Koji Matsumoto* [1], *Hirotomo Noda* [1], *Seiitsu Tsuruta* [1], *Sander Goossens* [1], *Natalia Petrova* [1], *Sho Sasaki* [1], *Kenzaburo Iwadate* [1], *Takaaki Jike* [1], *Osamu Kameya* [1], *Katsunori Shibata* [1], *Yoshiaki Tamura* [1], *Xiaoyu Hong* [4], *Jinsong Ping* [4], *Yusufu Aili* [5], *Simon Ellingsen* [6], *Wolfgang Schlüter* [7]

[1] *National Astronomical Observatory of Japan, Japan*

[2] *Japan Aerospace Exploration Agency, Japan*

[3] *Kyushu University, Japan*

[4] *Shanhai Astronomical Observatory, Chinese Academy of Science, China*

[5] *Urumqi Observatory, Chinese Academy of Science, China*

[6] *University of Tasmania, Australia*

[7] *Fundamental station Wettzell, Germany*

Abstract. SELENE (KAGUYA) is a Japanese lunar mission which was successfully launched from the Tanegashima Space Center on Sep. 14, 2007. KAGUYA consists of the main orbiter, and two small free-flying subsatellites, called Rstar (OKINA) and Vstar (OUNA). We are observing OKINA and OUNA using differential VLBI observations with the aim of improving the lunar gravity field model. Our observations will particularly improve the accuracy to which the low degree gravitational harmonics and the gravity field near the limb can be measured, and when combined with Doppler measurements will enable three-dimensional information to be extracted. Differential VLBI will be used to accurately measure the trajectories of the satellites, both with the Japanese VERA (VLBI Exploration of Radio Astrometry) telescopes and an array including the international VLBI stations, Shanghai, Urumqi (China), Hobart (Australia), and Wettzell (Germany).

We are using multi-frequency VLBI to determine the angular distance between OKINA and OUNA using three frequencies in S-band, (2212, 2218 and 2287 MHz), and one in X-band, (8456 MHz). Two periods of international ob-

servations, each of one month in duration, with the participation of VERA and the international stations, (in addition to the normal observations by VERA only) are planned for the one year mission period. We are able to measure the phase delay to an accuracy of better than 0.17 rad (10 deg) in X-band in these observations.

1. Introduction

The Japanese lunar explorer SELENE (SElenological and Engineering Explorer) or Kaguya which was launched on Sep. 14, 2007, makes precise observations of the gravitational field of the Moon utilizing both 4-way Doppler observations through a relay satellite (RSAT experiment), and differential VLBI observations of two satellites (VRAD experiment), as well as through the 13 other scientific instruments that are part of the mission [1]. The purpose of these observations is to address the inadequacies in existing data, and hence obtain a highly accurate lunar gravity model. This paper describes the scientific objectives, new technical developments, mission plan, and initial results of VLBI observations of Kaguya.

2. VLBI Observations of Kaguya

VLBI observations are carried out by the Japanese domestic VERA network (4 stations) [2] on a regular basis (8 hours/day, 3 days/week during the mission period of one year), and 2-way and 4-way Doppler measurements are also conducted by the Usuda Station of JAXA (Japan Aerospace Exploration Agency). Since the accuracy of VLBI positioning depends on baseline length, observations with long baselines are desirable. Currently the Shanghai and Urumqi (China), Hobart (Australia), and Wettzell (Germany) stations participate in the international observations to improve the lunar gravity field model through precise orbit determination of Okina and Ouna.

Fig. 1 shows how the VLBI observations contribute to the improvement of the lunar gravity field model [3]. There are three cases: where all the possible Kaguya spacecraft tracking data are included, where VLBI observation is not included, and LP100J. The accuracy of all the coefficients included in the model will be improved by combining VLBI with 2-way and 4-way Doppler measurements. Here we have accounted for the effect of VLBI data on determining the precise orbit of Okina, which is a reference for the 4-way Doppler measurements. By including VLBI data, the coefficients of degrees less than the 33rd harmonic will be improved by about a factor of 2, with the best improvement in the 2nd degree coefficient by a factor 2.6. If through proper force modeling we are able to achieve an arc length of Okina and Ouna longer than 1 day the final accuracy of the Kaguya gravity field will be one order of magnitude better than that of LP100J below approximately degree 30.

VRAD (differential VLBI RADio sources) are on-board two sub-satellites, Okina and Ouna, and are used for differential VLBI observations of the trajectories of the satellites with VERA and the international network. We will apply

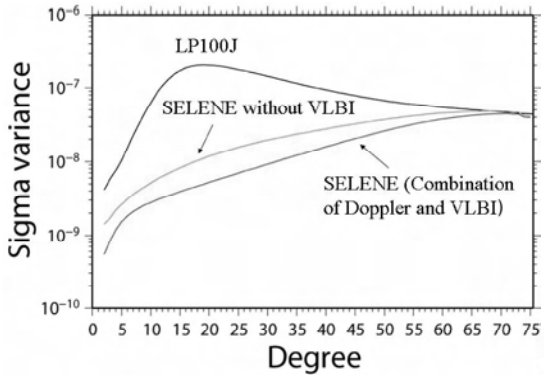

Figure 1. Anticipated coefficient sigma degree variances are shown for the following three cases; LP100J, Kaguya without VLBI observations, Kaguya with VLBI

a multi-frequency VLBI method to measurements of the angular distances between two radio sources in Okina and Ouna using three frequencies in S-band, 2212, 2218 and 2287 MHz, and one in X-band, 8456 MHz [4]. The phase delay will be measured with an accuracy of better than 0.17 radians (10 deg) in X-band, which is equivalent to positioning accuracy of about 20 cm on the Moon with the VLBI network with a baseline length of 2000 km. Kikuchi [5] has shown that the cycle ambiguity can be resolved by combining the same beam VLBI method and the multi frequency VLBI method. In the same beam VLBI method, a ground antenna sees two objects simultaneously when the angular distance between them is less than the angular dimensions of the main beam of the antenna. Liu et al. [6] measured the S-band phase characteristics of the Mizusawa 20 m telescope, one of the VERA network antennas, and confirmed that the phase deviation is smaller than 0.06 rad (3.4 deg).

The international VLBI campaigns for Kaguya are one month long each and take place twice during the 1-year mission period. The basic idea of observation scheduling is to conduct VLBI observations when the orbital plane is in "face-on" configuration in order to add more powerful constraints on orbit determination, which compensates for the loss of line-of-sight sensitivity coming from 2-way Doppler measurements. The "face-on" configuration will take place twice a month and we conduct a 4-day "core observation" for each fortnightly observation chance. The contribution from VLBI is also important to precisely determine the orbit of Okina which serves as a reference for 4-way Doppler observation, playing an important role mainly in "edge-on" configuration. Therefore it is highly desirable to extend the VLBI observation times to the period other than "face-on" configuration, which we refer to as "extended observations".

3. Initial Results

VLBI observations commenced on Nov. 5, 2007 after the initial checkout of Okina and Ouna. In addition to regular VLBI observations using the VERA network, the first international VLBI observations were carried out in Jan. 2008. We had many opportunities to utilize the same-beam VLBI method during the period and have confirmed that the cycle ambiguity of the differential phase delay (DPD) in multi-frequency VLBI (MFV) method can be solved by the same-beam VLBI method. The error of DPD is smaller than 2 ps in a 30 s integration interval (Fig. 2). If the baseline is assumed to be 2000 km, 2 ps corresponds to position sensitivities of 12 cm near the Moon.

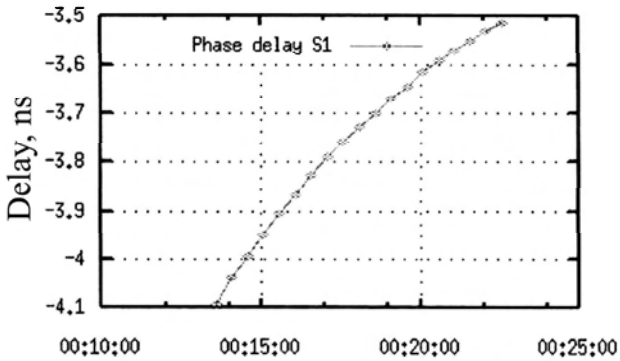

Figure 2. A result of estimation of differential phase delay of S1 for the baseline between Ishigaki and Iriki

4. Summary

We have succeeded in making VLBI observations of Okina/Ouna with VERA and the international network, and confirmed that the receiving, the tracking, and the recording system work well, and that the signals from Okina/Ouna are normal. We have succeeded in correlation of signals from Okina/Ouna, and confirmed that the signals have a S/N high enough to allow resolution of cycle ambiguity with our multi frequency VLBI method. We have succeeded in obtaining phase delays with an accuracy of several in S-band.

Acknowledgements

The authors appreciate the contribution of all engineers of NEC/Toshiba Space Systems Ltd. (NTS), Nippon Antenna Co. Ltd., and Nippi Corporation who diligently developed the onboard instruments and sub-satellites. The authors are grateful to the entire staff of the Kaguya mission as well. The authors also wish to express their gratitude to Dr. Dirk Behrend and Dr. Ya-

suhiro Koyama of the IVS Observing Program Committee for their support and encouragement. The gravity experiments of Kaguya would never have been achieved without a prominent technique and the profound knowledge of Mr. Fumio Fuke who was an engineer of NTS and passed away 2 months after the launch. We express sincere thanks to his contribution and grieve over the loss for Japanese space development.

References

[1] Kato, M., S. Sasaki, K. Tanaka, et al. The Japanese lunar mission SELENE: Science goals and present status. Adv. Space. Res., DOI 10.1016/j.asr.2007.03.049, 2008 (in print).

[2] Kobayashi, H., T. Sasao, N. Kawaguchi, et al. VERA Project. ASP Conference Series, 306, New Technologies in VLBI. Y.C. Minh (ed.), ASP, San Francisco, 2003, 367.

[3] Matsumoto, M., H. Hanada, N. Namiki, et al. A simulation study ofor anticipate accuracy of lunar gravity field model by SELENE tracking data. Adv. Space. Res., DOI 10.1016/j.asr.2007.03.066, 2008 (in print).

[4] Kono, Y., H. Hanada, J. Ping, et al. Precise positioning of spacecraft by multi-frequency VLBI. Earth Planets Space, v. 55, 581–589, 2003.

[5] Kikuchi, F. Differential phase delay estimation by same beam VLBI method. Ph.D. thesis, The Graduate University for Advanced Studies, 83, 2006.

[6] Liu, Q., F. Kikuchi, S. Tsuruta, et al. Effect of phase characteristics of telescope on same-beam differential VLBI. IEEE trans. Antenna Propagation, 55, 1, 466–1, 470, 2007.

The 5th IVS General Meeting Proceedings, 2008, p. 450–454

VLBI and Precise Space Navigation

Vladimir Zharov [1], *Leonid Matveenko* [2]

[1] *Sternberg Astronomical Institute, Moscow State University, Russia*

[2] *Institute for Space Research, Russian Academy of Sciences, Russia*

Abstract. VLBI is one of the most powerful methods for precise positioning of spacecrafts. We discuss one of the first experiments of the VLBI application for tracking of the balloons in the atmosphere of Venus — project "VEGA". Another application is the direct positioning of a space radio telescope: the Radioastron mission. A 10-m radio telescope will be launched into orbit to realize the space-ground interferometer. One of the goals of the mission is precise astrometry on the level of several microarcseconds. Possibility of tracking, prediction of the orbital motion of the Radioastron spacecraft is discussed.

1. Measurements of the Venus Atmosphere by Balloons

Progress in space technology and VLBI method [1] have made it possible to implement classical procedures to investigate gas flows into the Venus atmosphere. It was proposed to release free-flying balloons with a transmitter on board into Venus atmosphere [2]. The measurement of the balloon trajectories was carried out by differential VLBI method [3] of relative to the fly-by spacecrafts (VEGA-1 and VEGA-2). In Jun. 1985, two balloons, with transmitters at 1.6 GHz were released from the VEGA fly-by modules. The power radiated in the Earth's direction was about 5 W and distance about 110×10^6 km.

The VLBI method was used here for the first time for a source which moved along an unpredictable trajectory with high and variable acceleration. These circumstances necessitated more complicated algorithms of signal generation and processing and a large number of radio telescopes (radio interferometers) to observe the balloons simultaneously. Twenty radio telescopes, including the largest instruments, were involved. Two 70-m dishes in Ussuriisk and Evpatoriya were finished just before the start of the experiment [4]. Coherent conversion of signals and time-keeping were accomplished with hydrogen frequency standards. The signals were recorded using MK-2 format. On-line Doppler frequency offset measurements were at the largest antennas master stations.

The differential VLBI method is based on the dependence of the phase of

interference fringes on the coordinates, and fringe rate on the coordinates and the velocity of motion of source relative to the reference source [5]:

$$\begin{aligned}\Delta\Phi &= A\Delta x + B\Delta y + O(\Delta x^2, \Delta y^2),\\ \Delta f &= C\Delta x + D\Delta y + E\dot{\Delta x} + F\dot{\Delta y} + O(\Delta x^2, \Delta y^2),\end{aligned}$$

where $\Delta x, \Delta y, \dot{\Delta x}, \dot{\Delta y}$ are the relative coordinates and velocities of two close objects (in our case, the balloon and the fly-by module) in the view plane.

The phase measurements provide the highest accuracy $< \lambda/D$. To determine the position unambiguously, a priori data on the source position with an accuracy better than $(\lambda/D) \times L$ (L is the distance to the radio source) are essential. In our case $D = 5000$ km the ambiguity zone is 4 km.

There are several methods to resolve the ambiguity. The first one is the fringe rate differential measurements with the longest baseline and than the phase measurements at interferometers with different baselines. Another method is to determine the delay of the broad band emission signal, accuracy determined by $f/\Delta f$. The synthesis of a frequency is provided by two frequencies spaced at 6.5 MHz. The narrow-band filter was carried for increasing the signal-to-noise ratio. The minimum filter band is determined by stability of a signal oscillator and balloon acceleration and is 1 Hz, the $S/N \approx 10$ (in voltage) at largest (master) antennas (Fig. 1) [6]. We received "frequency legend" for slave radio telescopes. The 0.1 mHz corresponds to 1 m/s. In comparative of these two procedures agreement better than 1 μHz for rate and 1° for the phase was achieved. The fly-by trajectory were measured relatively QSO.

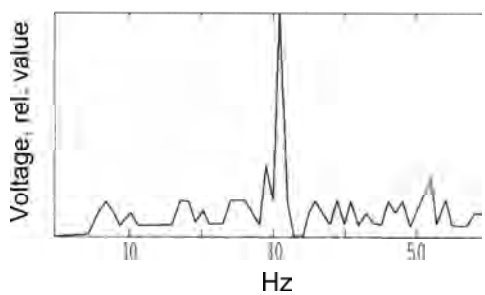

Figure 1. The spectrum of a received signal at Evpatoriya

Balloon-2 launched in the southern hemisphere of the planet led to discovery of gas motion with average velocities of 65.3 m/s and 3.4 m/s in longitude and latitude respectively. Balloon-1, launched in the northern hemisphere, showed that gas motion occur with an average velocity of 68.7 m/s in longitudinal direction, but no wind was detected in the latitudinal direction. The trajectories of the balloons are shown in Fig. 3. The accuracy of phase measurements are 10 km. Balloon-2 drifted from the equator to the North and then moved parallel to the equator. The altitude for the free drift was 53 km.

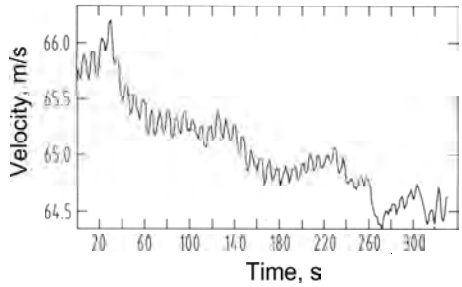

Figure 2. Radial component of velocity of the motion of a transmitter as a function of time

Total visibility times were 34 h and the balloon velocities were $V_1 = 69$ m/s and $V_2 = 67$ m/s.

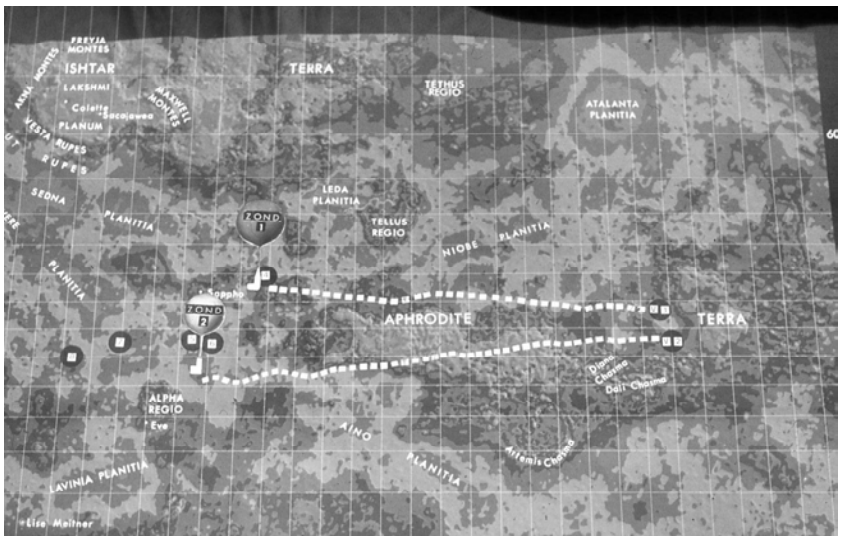

Figure 3. The trajectories of the balloon motions

Variation of frequencies with a period of 7.4 s were detected on many occasions (Fig. 2). These variations occurred more frequently in the southern hemisphere than in the northern one [6]. The peculiarity of balloon-2 determined by trajectory crossing of the Aphrodite mountains. The variability of the signal frequency with 7.4 s period are explanted by pitching of pendulum — the gondola suspended from the balloon by a cord 12 m long.

2. Reconstruction of the Radioastron Orbit Using VLBI Observations

One of the main scientific goals of the Radioastron mission is the study of various astronomical objects with ultra-high angular resolution up to few μas [7]. In order to reach such resolution unstable orbit with high apogee was chosen. Period of satellite rotation around the Earth of about 9.5 days. The perigee radius varies from 10 to 70 thousand km, the apogee radius — from 310 to 390 thousand km.

Accuracy of the reconstructed orbit is determined by the requirements for data processing. Position of the space telescope would be known better than $100 - 300$ m, velocity — 2 mm/s and acceleration 5×10^{-5} mm/s^2.

For more accurate orbit determination the Doppler shift in phase transfer link will be measured by all tracking stations receiving science data stream transmitted from spacecraft.

The goals of simulation were:

- reconstruction of the short orbit arcs (between the thruster's work and spacecraft maneuvers) using Doppler measurements of the radial velocity of spacecraft (RMS error of these measurements is equal to 0.1 mm/s) and;
- reconstruction of the short orbit arcs using VLBI observations of selected radio sources.

Modeling of Doppler measurements of the radial velocity of a spacecraft was calculated for a standard orbit. Then random variations of the coordinates and velocity of this spacecraft, that were in range ± 100 m and ± 1 mm/s, were added. Integrations of the motion equations with Doppler information for many combinations of this noise were made, and comparison with the standard orbit gave us an estimation of accuracy. For one orbital period RMS of position of the spacecraft is less then 3 m, RMS of velocity is < 0.1 mm/s. For short arcs with duration less then < 10 h RMS of position is < 4 cm.

For reconstruction of the short orbit arcs using VLBI observations the NGS-files 95aug22xe, 95aug23xa, 95aug24xa, 95aug25xa, 95aug27xa, 95aug28xa, 95aug29xe, 95aug30xb were selected for modeling. Interval of observation is about period of orbital motion of spacecraft. Radio telescopes GILCREEK, KOKEE, WETTZELL, NRAO85, FORTLEZA, NYALES20, ONSALA60, and WESTFORD worked during period 22-29.08.1995 and HN-VLBA, SC-VLBA, NL-VLBA, ALGOPARK, GGAO7108 during 30.08.1995. It was assumed that after spacecraft maneuvers (1 time per day) 3–5 radio sources were observed. Selected sources are 0804+499 (it was observed more then 10000 times by ground VLBI), 1308+326 (> 40000), 2145+067 (> 35000), 1219+044 (> 8000), 1044+719 (> 15000), 2234+282 (> 35000). The space-ground baseline delays calculated for the standard orbit were corrected (random variations of about 3 ns were added). The clock model for space telescope was unknown and for simplicity it was assumed to be linear function.

Software ARIADNA [8] was used for reduction and analysis of observation. It was shown that observations of radio sources can be used for precise determination of coordinates of the Radioastron spacecraft (< 2 cm); determined position can be used as beginning point for integration of the equations of motion and prediction of orbit.

Simultaneously with orbit determination space-ground VLBI provides high accuracy measurements of coordinates of the selected source. If each of them would be observed 100 times or more during the Radioastron mission we would expect increasing of precision of their position on order of magnitude. The selected sources can be used as fiducial points for new celestial reference frame.

Acknowledgements

We would like to thank IVS GM5 LOC for excellent meeting. One of authors (V.Z.) thanks N. S. Kardashev and Yu. N. Ponomarev for useful discussion.

References

[1] Matveyenko, L.I., N.S. Kardashev, G.B. Sholomitski. Radiofizika, 4, 651, 1965.

[2] Kogan, L.R., V.M. Linkin, L.I. Matveyenko, et al. The Soviet-French Meeting on EOS-Venus Project. Moscow, 1974.

[3] Councelmant III, et al., Moon, 8, 4, 1973.

[4] Matveyenko L.I., R.Z. Sagdeev, V.M. Balebanov, et al. Sov. A.J., 1, 59, 1986.

[5] Kogan, L.R., L.I. Matveyenko, V.I. Kostenko. Space Investigations, 28, 1, 1985.

[6] Sagdeev, R.Z., V.V. Kerzhanovitch, L.R. Kogan, et al. Astron. Astrophys., v. 254, 387–392, 1992.

[7] Kardashev, N.S. Experimental Astronomy, v. 7, 329–343, 1997.

[8] Zharov, V.E. ARIADNA. Private communication.

The 5th IVS General Meeting Proceedings, 2008, p. 455–460

On the Space VLBI Mathematical Model with Nutation Parameters

Erhu Wei [1,2], *Jingnan Liu* [3], *Vincenza Tornatore* [4], *Chuang Shi* [5], *Wei Yan* [1]

[1)] *School of Geodesy and Geomatics, Wuhan University, China*

[2)] *The Key Laboratory of Geospace Environment and Geodesy , Ministry of Education, Wuhan University, China*

[3)] *Wuhan University, China*

[4)] *Politecnico di Milano/DIIAR Rilevamento, Italy*

[5)] *Research Center of GNSS, Wuhan University, China*

Abstract. Space Very Long Baseline Interferometry (SVLBI) is an important space technology for geodesy and geodynamics to a very high accuracy level. At present, the SVLBI mathematical model of geodetic parameters does not consider nutation parameters. In this paper the nutation parameters will be added to the rotation matrix, and the mathematical model of SVLBI observations with the nutation parameters will be derived. Finally, the estimability of parameters in the mathematical model will be analyzed.

1. Introduction

The most important and complicated mission of modern geodesy and geodynamics is definition, realization and interconnection of different reference systems, which include the Conventional Inertial System (CIS) fixed in space and defined by radio sources, the Conventional Terrestrial System (CTS) fixed to the earth and defined by a series of observation stations on the ground, and the Dynamic Reference System defined by the movement of the satellite. At present, Space VLBI (SVLBI) is the unique space technology that can directly connect the three reference frames with high accuracy. SVLBI is often used for other applications in geodesy and geodynamics like determination of geocentric positions of VLBI stations, estimation of the gravity field of the earth, satellite orbit determination.

There have been some studies [1, 4] on the mathematical model to estimate the parameters that can interconnect the reference frames by using SVLBI ob-

servations, but in this mathematical model nutation correction parameters ($\Delta\psi$ and $\Delta\varepsilon$) are not included. In the model there is a rotation matrix which includes Greenwich apparent time correction SG and polar motion corrections ξ,η, which are called earth rotation parameter corrections, ERP's. By using the rotation matrix, the radio source's CIS coordinates can be transformed to CTS. Anyway there are no radio source's true celestial coordinates in actual observations. There are just $J2000.0$ CIS coordinates of the radio source. Nutation parameters are needed to transform CIS to true celestial coordinates.

Along with the development of technology, the long life of deep space exploration satellite makes it possible to observe nutation parameters. The aim of this work is to add nutation parameters to the mathematical model of SVLBI observations. In particular the rotation matrix will be written with nutation correction parameters and the SVLBI observations mathematical model with the nutation correction parameter will be derived. Then, the estimability of parameters in the mathematical model will be analyzed.

2. Mathematical Model

2.1. Rotation Matrix

Actually observation stations are fixed in CTS while the observing radio source is fixed in $J2000.0$ CIS. The satellite can be seen to have true celestial coordinates. To establish the right time delay observation mathematical model it is necessary to transform these different reference systems to the same one. This transformation includes ERP's, nutation and precession parameters [5].

The rotation matrix with ERP corrections has been derived, the precession parameters can be calculated and in this research are considered as constant because the precession cycle is too long to be observed by current SVLBI technology. So the final model just needs to add nutation corrections.

The $J2000.0$ CIS can be transformed to average celestial coordinates at epoch t by precession correction, which can be obtained by astrophysical methods. Then the true celestial coordinates at epoch t can be obtained by nutation correction.

The rigid nutation matrix is expressed as

$$N = R_X(-\varepsilon - \Delta\varepsilon) \cdot R_Z(-\Delta\psi) \cdot R_X(\varepsilon).$$

The elements of the nutation matrix are functions of ε, the mean obliquity of the ecliptic, that can be obtained by astronomic methods and will be considered constant during the derivation, $\Delta\psi$ and $\Delta\varepsilon$ that are respectively the nutation in longitude and nutation in obliquity corrections. The transformation of the $J2000.0$ average position to true position at any epoch can be performed using the nutation rotation matrix. The objective of this paper is to obtain the SVLBI observation mathematical model with nutation correction in longitude and nutation correction in obliquity.

2.2. Mathematical Model of Time Delay Observation

Starting from the mathematical models as found in literature [1, 4], a simple ground-space time delay observation equation with nutation correction, can be expressed as:

$$\begin{aligned} d^I_{ijkl} = -\left\{ \begin{bmatrix} X_j \\ Y_j \\ Z_j \end{bmatrix}^T R_2(-\xi)R_2(-\eta)R_2(\theta_k) - \begin{bmatrix} X^I_K \\ Y^I_K \\ Z^I_K \end{bmatrix}^T \right\} \times \\ \times \left\{ N \begin{bmatrix} \cos\delta_l \cos\alpha_l \\ \cos\alpha_l \sin\alpha_l \\ \sin\alpha_l \end{bmatrix} \right\} + c[\Delta C^I_{0rj} - \Delta C^I_{1rj}(t_k - t_0)]\,, \end{aligned} \tag{1}$$

where X_j, Y_j and Z_j are the CTS coordinates of observation station; X^I_K, Y^I_K and Z^I_K are true celestial coordinates of satellite S^I at epoch t_K; α_l and δ_l are $J2000.0$ CIS right ascension and declination of the radio source, which include precession correction, at epoch t_K; N is the nutation matrix; R is the rotation matrix with ERP's parameters; c is the velocity of light; t_0 is the beginning observing epoch; ΔC^I_{0rj} and ΔC^I_{1rj} are the clock error and clock drift of the reference clock in monitor station and clock P_j at observation station.

The observation station's CTS coordinates and radio source's average celestial coordinates can be transformed to true celestial coordinates by using the equation (1). It is the basic of the derivation of mathematical models.

The expression can be rewritten as the following:

$$\begin{aligned} d^I_{ijkl} = -X_j A1 + Y_j A2 + Z_j A3 + X^I_K A4 + Y^I_K A5 + Z^I_K A6 + \\ + c[\Delta C^I_{0rj} - \Delta C^I_{1rj}(t_k - t_0)]\,, \end{aligned} \tag{2}$$

where $A1$ to $A6$ are the expanding coefficients of ground observations station's coordinates and satellite's coordinates. The following mathematical approximations will be used in the derivation:

$$\begin{aligned} &\cos(\varepsilon + \Delta\varepsilon) \cong \cos\varepsilon \cos\Delta\varepsilon - \sin\Delta\varepsilon \sin\varepsilon, \\ &\sin(\varepsilon + \Delta\varepsilon) \cong \sin\varepsilon \cos\Delta\varepsilon + \sin\Delta\varepsilon \cos\varepsilon. \end{aligned}$$

And the following approximate transformations will also be used because ξ, η, $\Delta\psi$ and $\Delta\varepsilon$ are small:

$$\begin{matrix} \sin\xi \cong \xi, \sin\eta \cong \eta \\ \cos\xi \cong \cos\eta \cong 1 \end{matrix}\,,\ \begin{matrix} \cos(\Delta\psi) \cong 1 \\ \sin(\Delta\psi) \cong \Delta\psi \end{matrix}\,,\ \begin{matrix} \cos(\Delta\varepsilon) \cong 1 \\ \sin(\Delta\varepsilon) \cong \Delta\varepsilon \end{matrix}\,,\ \begin{matrix} \Delta\psi\Delta\psi \cong 0 \\ \Delta\psi\Delta\varepsilon \cong 0 \\ \Delta\varepsilon\Delta\varepsilon \cong 0 \end{matrix}\,,\ \begin{matrix} \xi\eta \cong 0 \\ \xi\xi \cong 0 \\ \eta\eta \cong 0 \end{matrix}\,.$$

So the forms of Ai are:

$$\begin{aligned} A1 = &-\Delta\psi \cos\varepsilon \cos\delta_l \sin(\alpha_l - \theta_k) + \cos\delta_l \cos(\alpha_l - \theta_k) \\ &- \Delta\psi \sin\varepsilon \sin\delta_l \cos\theta_k - \Delta\varepsilon \sin\delta_l \sin\theta_k + \xi \sin\delta_l\,, \\ A2 = &\Delta\psi \cos\varepsilon \cos\delta_l \cos(\alpha_l - \theta_k) + \cos\delta_l \sin(\alpha_l - \theta_k) \\ &+ \Delta\psi \sin\varepsilon \sin\delta_l \sin\theta_k - \Delta\varepsilon \sin\delta_l \cos\theta_k - \eta \sin\delta_l\,, \end{aligned}$$

$$
\begin{aligned}
A3 &= -\xi\cos\delta_l\cos(\alpha_l-\theta_k)+\eta\cos\delta_l\sin(\alpha_l-\theta_k)+\\
&\quad \cos\delta_l(\Delta\psi\cos\alpha_l\sin\varepsilon+\Delta\varepsilon\sin\alpha_l)+\sin\delta_l\,,\\
A4 &= \cos\delta_l(\cos\alpha_l-\Delta\psi\cos\varepsilon\sin\alpha_l)-\Delta\psi\sin\varepsilon\sin\delta_l\,,\\
A5 &= \Delta\psi\cos\varepsilon\cos\alpha_l\cos\delta_l-\Delta\varepsilon\sin\alpha_l+\sin\alpha_l\cos\delta_l\,,\\
A6 &= \Delta\psi\sin\varepsilon\cos\alpha_l\cos\delta_l+\Delta\varepsilon\sin\alpha_l\cos\delta_l+\sin\alpha_l\,.
\end{aligned}
$$

The unknown geodetic parameters will be:
$\{X_j, Y_j, Z_j, X_K^I, Y_K^I, Z_K^I, \Delta\psi, \Delta\varepsilon, \xi, \eta, \theta_k, \alpha_l, \delta_l, \Delta C_{0ij}, \Delta C_{1ij}\}$

2.3. Analysis of Relation Between Parameters

To estimate the unknown parameters of equation (2), this has to be linearized:

$$d(d_{ijkl}^I)=\sum_P C_P dP\,,$$

where C_P are the required partial derivatives from of the time delay with respect to the parameters of interest, indexed by P. They are as follows:

$$C_{X_j}=A1,\quad C_{Y_j}=A2,\quad C_{Z_j}=A3,\quad C_{X_K^I}=A4,\quad C_{Y_K^I}=A5,\quad C_{Z_K^I}=A6,$$

$$
\begin{aligned}
C_{\Delta\psi} &= X_j(-\cos\varepsilon\cos\delta_l\sin(\alpha_l-\theta_k)-\sin\varepsilon\sin\delta_l\cos\theta_k)+\\
&\quad +Y_j(\cos\varepsilon\cos\delta_l\cos(\alpha_l-\theta_k)+\sin\varepsilon\sin\delta_l\sin\theta_k)+Z_j\cos\delta_l\cos\alpha_l\sin\varepsilon+\\
&\quad +X_K^I(-\cos\varepsilon\sin\alpha_l\cos\delta_l-\sin\varepsilon\sin\delta_l)+Y_K^I\cos\varepsilon\cos\alpha_l\cos\delta_l+\\
&\quad +Z_K^I\sin\varepsilon\cos\alpha_l\cos\delta_l\,,
\end{aligned}
$$

$$
\begin{aligned}
C_{\Delta\varepsilon} &= X_j\sin\delta_l\sin\theta_k-Y_j\sin\delta_l\cos\theta_k+Z_j\cos\delta_l\sin\alpha_l\\
&\quad +Y_K^I\sin\alpha_l+Z_K^I\sin\alpha_l\cos\delta_l\,,
\end{aligned}
$$

$$C_\xi = X_j\sin\delta_l-Z_j\cos\delta_l\cos(\alpha_l-\theta_k)\,,$$

$$C_\eta = -Y_j\sin\delta_l+Z_j\cos\delta_l\sin(\alpha_l-\theta_k)\,,$$

$$
\begin{aligned}
C_{\theta_k} &= X_j(\Delta\psi\cos\varepsilon\cos\delta_l\cos(\alpha_l-\theta_k)+\cos\delta_l\sin(\alpha_l-\theta_k)+\\
&\quad +\Delta\psi\sin\varepsilon\sin\delta_l\sin\theta_k-\Delta\varepsilon\sin\delta_l\cos\theta_k)+\\
&\quad +Y_j(\Delta\psi\cos\varepsilon\cos\delta_l\sin(\alpha_l-\theta_k)-\cos\delta_l\cos(\alpha_l-\theta_k)+\\
&\quad +\Delta\psi\sin\varepsilon\sin\delta_l\cos\theta_k+\Delta\varepsilon\sin\delta_l\sin\theta_k)+\\
&\quad +Z_j(-\xi\cos\delta_l\sin(\alpha_l-\theta_k)-\eta\cos\delta_l\cos(\alpha_l-\theta_k))\,,
\end{aligned}
$$

$$
\begin{aligned}
C_{\alpha_l} &= X_j(-\Delta\psi\cos\varepsilon\cos\delta_l\cos(\alpha_l-\theta_k)-\cos\delta_l\sin(\alpha_l-\theta_k))+\\
&\quad +Y_j(-\Delta\psi\cos\varepsilon\cos\delta_l\sin(\alpha_l-\theta_k)+\cos\delta_l\cos(\alpha_l-\theta_k))+\\
&\quad +Z_j(\xi\cos\delta_l\sin(\alpha_l-\theta_k)+\eta\cos\delta_l\cos(\alpha_l-\theta_k)+\\
&\quad +\cos\delta_l(-\Delta\psi\sin\alpha_l\sin\varepsilon+\Delta\varepsilon\cos\alpha_l))+\\
&\quad +X_K^I(\cos\delta_l(-\sin\alpha_l-\Delta\psi\cos\varepsilon\cos\alpha_l))\\
&\quad +Y_K^I(-\Delta\psi\cos\varepsilon\sin\alpha_l\cos\delta_l-\cos\alpha_l(\Delta\varepsilon-\cos\delta_l))\\
&\quad +Z_K^I(-\Delta\psi\sin\varepsilon\sin\alpha_l\cos\delta_l+\cos\alpha_l(\Delta\varepsilon\cos\delta_l+1))\,,
\end{aligned}
$$

$$
\begin{aligned}
C_{\delta_l} = & X_j(-\sin\delta_l(-\Delta\psi\cos\varepsilon\sin(\alpha_l-\theta_k)+\cos(\alpha_l-\theta_k))+ \\
& -\cos\delta_l(\Delta\psi\sin\varepsilon\cos\theta_k-\Delta\varepsilon\sin\theta_k+\xi))+ \\
& +Y_j(-\sin\delta_l(\Delta\psi\cos\varepsilon\cos(\alpha_l-\theta_k)+\sin(\alpha_l-\theta_k))+ \\
& +\cos\delta_l(\Delta\psi\sin\varepsilon\sin\theta_k-\Delta\varepsilon\cos\theta_k-\eta))+ \\
& +Z_j(\sin\delta_l(\xi\cos(\alpha_l-\theta_k)+\eta\sin(\alpha_l-\theta_k)+\Delta\psi\cos\alpha_l\sin\varepsilon+\Delta\varepsilon\sin\alpha_l)+ \\
& +\cos\delta_l)+ \\
& +X_K^I(-\sin\delta_l(\cos\alpha_l-\Delta\psi\cos\varepsilon\sin\alpha_l)-\Delta\psi\sin\varepsilon\cos\delta_l)+ \\
& +Y_K^I(-\sin\delta_l(\Delta\psi\cos\varepsilon\cos\alpha_l-\sin\alpha_l))+ \\
& +Z_K^I(-\sin\delta_l(\Delta\psi\sin\varepsilon\cos\alpha_l+\Delta\varepsilon\sin\alpha_l))\,,
\end{aligned}
$$

$$
C_{\Delta C_{0ij}} = c, \quad C_{\Delta C_{1ij}} = c(t_k - t_0)\,.
$$

So the linear dependencies are as follows:

$$
C_\xi = X_j C_{Z_j} - Z_j C_{X_j} + B_1, \quad C_\eta = Z_j C_{Y_j} - Y_j C_{Z_j} + B_2, \quad C_{\alpha_l} = C_{\theta_k} + B_3,
$$

where B_1 to B_3 are periodic variables. From the derivation above, it is clear that linear dependencies between some parameters are present. These linear dependencies will make the normal equation matrix rank deficient, therefore the normal equation will be singular. It means that not all the parameters can be estimated correctly. The ground station parameters and the earth rotation parameters can not be separated. Further more, an obvious linear dependency exists between α_l and θ_k.

3. Conclusion

Nutation is an important parameter to connect CTS and CIS and it is significant to geodesy and geodynamics. VLBI, especially SVLBI, is a main technology for observing nutation by now. It is important to add nutation correction to SVLBI observation mathematical model.

In this paper, the expansion of the observation equation has been made and the partial derivatives of SVLBI parameters are discussed. From the result of the model derivation, it is clear that linear dependencies between some partial derivative of the SVLBI observation with nutation correction exist. It means that all the parameters except α_l and θ_k can be estimated by the SVLBI ground-space time delay observations. In the future, some mathematical method will be investigated to calculate these parameters.

Acknowledgements

This research is funded by the national '973 Project' of China (No 2006CB-701301), the National Natural Science Foundation of China (No 40774007), and the project of university education and research of Hubei province (No 20053039).

References

[1] Ádám, J. Estimability of Geodetic Parameters from Space VLBI Observables. Report No 406. Dept. of Geodetic Science and Surveying The Ohio State Univ., Columbus, Ohio, 1990.

[2] Capitaine, N., A. Andrei, M. Calabretta, et al. Proposed terminology in fundamental astronomy based on IAU 2000 resolutions. Proc. JD 16, IAU XXVI General Assembly, Highlights of Astronomy, v. 14. Cambridge University Press, DOI 10.1017/S1743921307011490, 2006, 474–475.

[3] Dehant, V., O. de Viron, M. Feissel-Vernier. Investigation of nutation beyond the IAU2000 model. Proc. IVS 3rd General Meeting. N.R. Vandenberg and K.D. Baver (eds.), NASA/CP-2004-212255, 2005, 381–382.

[4] Kulkarni, M.N. A Feasibility Study of Space VLBI for Geodesy and Geodynamics. Report No 420. Dept. of Geodetic Science and Surveying The Ohio State Univ., Columbus, Ohio, 1992.

[5] Li, Z., E. Wei. Space positioning technology and its application. Wuhan University Press, 2006.

[6] Xia, Y. IAU nutation theory. Journal of Nanjing University, v. 28(4), 524–530, 1992.

[7] Huang, S. The Review of Nutation Research. The Progress of Astronomy, v. 15(4), 293–302, 1997.

asuring the Future
2 - 6, 2008 Saint Petersburg Russia

strometry
Russia

Splinter Meeting Report

The 5th IVS General Meeting Proceedings, 2008, p. 465–467

Splinter Meeting Report

Notes of the 9th IVS Analysis Workshop

Axel Nothnagel

Institute of Geodesy and Geoinformation, University of Bonn, Germany

Abstract. At the 9th IVS Analysis Workshop a number of topics were presented and discussed. Here, we address the most important items.

1. Introduction

The 9th IVS Analysis Workshop took place on Mar. 7, 2008, at the Institute of Applied Astronomy, St. Petersburg, Russia. Thanks to the local organizers and especially to Nadia Shuygina the 45 participants of the workshop very much enjoyed a successful day at IAA. On the agenda stood a number of topics which are of importance to the analysis efforts within the IVS.

2. Thermal Expansion of Radio Telescopes

It has long been recognized that modelling of antenna thermal expansion is a critical issue and needs a decision on the reference temperatures for a consistent modelling across the IVS Analysis Centers. Here, a mean temperature is needed for each telescope which can be used as a reference to relate any deviations to. So, a formal decision was called upon in this workshop.

The decision on the reference temperatures had to be made on the basis of several requirements: The choices should be easy to implement and should permit a consistent computation for all telescopes with observations in the IVS archives as well as for any new station to take up operations. On the other hand, the choices should not affect the International Terrestrial Reference Frame (ITRF) and especially its scale. Therefore, a proposal was made to use the GPT model [1] at the epoch when the phase of the annual cycle is zero. Tests have been made to whether the implementation of the model would affect the ITRF with the result that only a few telescopes show height deviations of more than 0.1 mm with most of them being of little importance because they have only be in use for a limited time period [2].

After the IERS had handed over the responsibility for a decision on the reference temperatures to IVS, the final decision was made by the participants

to use this model for computing the reference temperatures. In addition, the participants decided to make the topic of thermal expansion modelling the first chapter of the IVS Conventions. The IVS Analysis Coordinator is charged to set up a web page with the respective information including a description, the reference temperature values for all telescopes existing so far and other helpful information.

3. Nutation

After a brief discussion the participants unanimously decided that the IVS will change to compute the nutation offsets on the basis of the X and Y representation for the determination of the offsets with respect to the IAU2000A model. This means that the coefficients of the datum-free normal equations for nutation will be exported consistently with this paradigm. The time series of the nutation offsets will still be reported in both representations, X/Y and ψ/ε, but then the latter will just be a conversion according to the IERS Conventions 2003 (eq. 23).

While the QUASAR software provides this representation already, the other software packages still have to be adapted. For Calc/Solve it has to be checked whether the P03 precession model has been implemented correctly. In addition, the GSFC group will provide a description of the necessary steps to activate the required changes in Calc/Solve for all other groups using this software. The OCCAM software still has to be modified for the new paradigm. Nevertheless, the new process will be phased in as soon as possible.

4. Data Files of Meteorological Sensors

Meteorological data of VLBI sessions is currently included in the analysis chain by extracting this information for each observation from the log files and entering it into the databases. Through this procedure the time span of the meteorological data is limited to exactly the period of the VLBI observations. Since for some models, such as thermal expansion of the telescopes, it may be necessary to have access to these data also for preceding periods, the current concept is not expandable. In addition, it is desirable to maintain data sets which are independent of the periods of the VLBI observations and consequently can be used by more than one technique.

For these reasons a proposal has been made by Arthur Niell to change the current procedures. The proposal aims at storing all readings of a single sensor in a file which is unrelated to a specific VLBI session but has the time tag and sensor identifier as primary data identification elements. In addition, the files also contain information about calibrations of the sensors and location of the sensor in geocentric X,Y,Z coordinates. Since the participants of the workshop were in favour of this proposal, Arthur Niell will proceed with further steps towards implementation, which, by the way, will also serve the IVS Working Group VLBI Data Structures (WG 4).

5. Miscellaneous

On request of the IERS Analysis Coordinator, Markus Rothacher, a new version of the SINEX format (V3.0) was presented. The participants agreed that they will implement this version as soon as time permits.

At the end of the Analysis Workshop a table of action items was drawn which assigns certain tasks to those colleagues who volunteered to take care of the items. We hope that the action items will be attended to and the tasks will be completed before the next IVS Analysis Workshop which will take place in Bordeaux, France, on invitation of Patrick Charlot of Observatoire de Bordeaux sometime in Spring 2009 in conjunction with the 19th Meeting of the European VLBI Group for Geodesy and Astrometry (EVGA).

References

[1] Boehm, J., R. Heinkelmann, H. Schuh. Short Note: A global model of pressure and temperature for geodetic applications. J. Geod., 81:679-683, DOI:10.1007/s00190-007-0135-3, 2007.

[2] Heinkelmann, R., J. Boehm, H. Schuh. The effect of meteorological input data on the VLBI reference frames. Submitted to Proceedings of GRF2006, 2007.

List of Participants

Artz Tomas	Germany	thomas.artz@uni-bonn.de
Becker Olivier	France	olivier.becker@obspm.fr
Behrend Dirk	USA	Dirk.Behrend@nasa.gov
Berdnikov Anton	Russia	anton_ipa@rambler.ru
Bertarini Alessandra	Germany	abertari@mpifr-bonn.mpg.de
Berzins Karlis	Latvia	kberzins@latnet.lv
Bizouard Christian	France	christian.bizouard@obspm.fr
Boboltz David	USA	dboboltz@usno.navy.mil
Bockmann Sarah	Germany	boeckmann@uni-bonn.de
Boehm Johannes	Austria	johannes.boehm@tuwien.ac.at
Bogdanov Andrey	Russia	bogdanov@isida.ipa.rssi.ru
Bolotin Sergey	Ukraine	bolotin@mao.kiev.ua
Bourda Geraldine	France	Geraldine.Bourda@obs.u-bordeaux1.fr
Campbell Robert	Netherlands	campbell@jive.nl
Capitaine Nicole	France	n.capitaine@obspm.fr
Chalmers Dean	Canada	Dean.Chalmers@nrc-cnrc.gc.ca
Charlot Patrick	France	charlot@obs.u-bordeaux1.fr
Collioud-Marichallot Arnaud	France	Arnaud.Collioud@obs.u-bordeaux1.fr
Colomer Sanmartin Francisco	Spain	F.colomer@oan.es
Colucci Giuseppe	Italy	giuseppe.colucci@telespazio.com
Corey Brian	USA	bcorey@haystack.mit.edu
Engelgardt Gerald Horst	Germany	gerald.engelhardt@bkg.bund.de
Engen Bjorn	Norway	engbjo@statkart.no
Englich Sigrid	Austria	senlich@mars.hg.tuwien.ac.at
Espada Susana Garsia	Spain	s.gespada@oan.es
Fateev Artemiy	Russia	fateev@isida.ipa.rssi.ru
Fedotov Leonid	Russia	flv@ipa.rssi.ru
Fey Alan	USA	afey@usno.navy.mil
Finkelstein Andrey	Russia	amf@ipa.nw.ru
Gayazov Iskander	Russia	gayazov@ipa.nw.ru
Gipson John	USA	John.M.Gipson@nasa.gov
Gnedin Yuri	Russia	gnedin@gao.spb.ru
Gomes Gonsales Jesus	Spain	jggonzalez@fomento.es
Gontier Anne-Marie	France	Anne-Marie.Gontier@obspm.fr
Gordon David	USA	David.Gordon-1@nasa.gov
Gubanov Vadim	Russia	gubanov@ipa.nw.ru
Gurvits Leonid	Netherlands	lgurvits@jive.nl
Haas Rudiger	Sweden	rudiger.haas@chalmers.se
Hanada Hideo	Japan	hanada@miz.nao.ac.jp
Hanssen Rune Ivar	Norway	hanrun@statkart.no

Hase Hayo	Chili	hayo.hase@tigo.cl
Heinkelmann Robert	Austria	rob@mars.hg.tuwien.ac.at
Hugentobler Urs	Germany	urs.hugentobler@bv.tu-muenchen.de
Ichikawa Ryuichi	Japan	richi@nict.go.jp
Il'in Gennady	Russia	igen@ipa.rssi.ru
Ilyasov Yuri	Russia	ilyasov@prao.ru
Ipatov Alexander	Russia	ipatov@ipa.nw.ru
Ivanov Dmitry	Russia	ltf@ipa.rssi.ru
Jacobs Christopher	USA	Christopher.S.Jacobs@jpl.nasa.gov
Jike Takaaki	Japan	jike@miz.nao.ac.jp
Jungho Cho	South Korea	jojh@kasi.re.kr
Kaydanovsky Mikhail	Russia	kmn@ipa.rssi.ru
Kharinov Mikhail	Russia	kharinoff@gmail.com
Kildal Per-Simon	Sweden	per-simon.kildal@chalmers.se
Kim Tuhwan	South Korea	thkim@ajou.ac.kr
Kingham Kerry	USA	kingham.kerry@usno.navy.mil
Koltsov Nikolay	Russia	nec@ipa.rssi.ru
Kovalev Yury	Germany	ykovalev@mpifr-bonn.mpg.de
Koyama Yasuhiro	Japan	koyama@nict.go.jp
Krasinsky George	Russia	kra@ipa.nw.ru
Kudryashova Maria	Austria	mvk@hg.mars.tuwien.ac.at
Kurdubov Sergey	Russia	ksl@ipa.nw.ru
Kurihara Shinobu	Japan	skuri@gsi.go.jp
Kwak Youghee	South Korea	bgirl02@kasi.re.kr
Lambert Sebastien	France	Sebastien.Lambert@obspm.fr
Lanotte Roberto	Italy	roberto.lanotte@telespazio.com
Lavrov Alexey	Russia	lexslavrov@yandex.ru
Lee Chang Hoon	South Korea	chlee@kasi.re.kr
Li Jinling	China	jll@shao.ac.cn
Lobanov Andrei	Germany	alobanov@mpifr-bonn.mpg.de
Ma Chopo	USA	chopo.ma@nasa.gov
MacMillan Daniel	USA	daniel.s.macmillan@nasa.gov
Malkin Zinovy	Russia	malkin@gao.spb.ru
Mardyshkin Vyacheslav	Russia	vvm2@iaa.nw.ru
Marshalov Dmitry	Russia	dam@ipa.rssi.ru
Matsuzaka Shigeru	Japan	shigeru@gsi.go.jp
Matveyenko Leonid	Russia	matveen@iki.rssi.ru
Melnikov Alexey	Russia	melnikov@ipa.nw.ru
Mendes Cerveira Paulo Jorge	Austria	mendes@mars.hg.tuwien.at
Mikhailov Andrey	Russia	agm@ipa.nw.ru
Molotov Igor	Russia	molotov@kiam1.rssi.ru
Mueskens Arno	Germany	mueskeus@mpifr-bonn.mpg.de
Niell Arthur	USA	aniell@haystack.mit.edu
Nilsson Tobias	Sweden	tobias.nilsson@chalmers.se

Nothnagel Axel	Germany	nothnagel@uni-bonn.de
Oh Sejin	South Korea	sjoh@kasi.re.kr
Opseth Per Erik	Norway	ospper@statkart.no
Oyama Tomoaki	Japan	oyamatm@cc.nao.ac.jp
Pany Andrea	Austria	apany@mars.hg.tuwien.ac.at
Pasynok Sergey	Russia	pasynok@imvp.ru
Petrachenko William	Canada	Bill.Petrachenko@nrc.gc.ca
Pitjeva Elena	Russia	evp@ipa.nw.ru
Rahimov Ismail	Russia	rahimov@urania.rtf32s.nw.ru
Rothacher Markus	Germany	rothacher@gfz-potsdam.de
Ruszczyk Chester	USA	chester@haystack.mit.edu
Salnikov Alexander	Russia	ais@ipa.rssi.ru
Schuh Harald	Austria	Harald.schuh@mars.hg.tuwien.at
Shantyr Violetta	Russia	Shantir@ipa.rssi.ru
Shuygina Nadia	Russia	nvf@ipa.nw.ru
Skurikhina Elena	Russia	sea@ipa.nw.ru
Smolentsev Sergey	Russia	smolen@ipa.nw.ru
Souchay Jean	France	Jean.Souchay@obspm.fr
Surkis Igor	Russia	surkis@ipa.nw.ru
Takeuchi Hiroshi	Japan	takeuchi@isas.jaxa.jp
Tesmer Volker	Germany	tesmer@dgfi.badw.de
Thaller Daniela	Germany	thaller@gfz-potsdam.de
Thorandt Volkmar	Germany	volkmar.thorandt@bkg.bund.de
Thornton Deborah	USA	thorton.bruce@usno.navy.mil
Thornton Bruce	USA	thornton.bruce@usno.navy.mil
Titov Oleg	Australia	oleg.titov@ga.gov.au
Tornatore Vincenza	Italy	vincenza.tornatore@polimi.it
Tuccary Gino	Italy	g.tuccari@ira.inaf.it
Volvach Aleksandr	Ukraine	volvach@crao.crimea.ua
Vytnov Alexander	Russia	vytnov@yandex.ru
Wang Ganglia	China	wgl@shao.ac.cn
Wei Erhu	China	ehwei@sgg.whu.edu.cn
Whitney Alan	USA	awhitney@haystack.mit.edu
Wresnik Joerg	Austria	wresnik@mars.hg.tuwien.ac.at
Zhang Bo	China	zb@shao.ac.cn
Zhang Xiuzhong	China	xzhang@shao.ac.cn
Zharov Vladimir	Russia	zharov@sai.msu.ru
Zheng Weimin	China	zhwm@shao.ac.cn
Zimovsky Vladimir	Russia	zim@ipa.rssi.ru